Quantum complexity of symmetry-protected topological phases of matter

Tyler D. Ellison

A dissertation
submitted in partial fulfillment of the
requirements for the degree of

Doctor of Philosophy

University of Washington

2021

Reading Committee:
Lukasz Fidkowski, Chair
Mark Rudner
Subhadeep Gupta

Program Authorized to Offer Degree:
Physics

University of Washington

Abstract

Quantum complexity of symmetry-protected
topological phases of matter

Tyler D. Ellison

Chair of the Supervisory Committee:
Associate Professor Lukasz Fidkowski
Department of Physics

Classical computers have been instrumental to our understanding of quantum phases of matter. However, their ability to simulate quantum many-body systems is fundamentally limited – there are quantum systems that are inherently more challenging to simulate. We study the limitations of classical simulations in the context of symmetry-protected topological (SPT) phases of matter. We identify obstructions to efficiently simulating SPT phases and develop our understanding of their intrinsic quantum information-theoretic structures. More specifically, we define the concepts of a symmetry-protected sign problem and symmetry-protected magic to study the quantum complexity of bosonic SPT phases. We demonstrate that certain SPT phases possess these properties as a consequence of their long-range correlations and anomalous symmetry action at a boundary. We also consider the quantum complexity of fermionic SPT phases by employing bosonization dualities, which map fermionic SPT phases to more familiar bosonic SPT phases. In the process, we develop a bosonization duality within the framework of tensor networks and provide an algorithm for bosonizing a fermionic tensor network state using its local tensors. We then focus on a class of interacting fermionic SPT phases classified by group supercohomology. We construct an exactly solvable Hamiltonian for each two- and three-dimensional supercohomology SPT phase. We also identify explicit finite-depth quantum circuits capable of disentangling the ground states

of our models. We illustrate how the structures of the circuit can give rise to anomalous topological order on the boundary of the three-dimensional models.

TABLE OF CONTENTS

LIST OF FIGURES

Figure Number Page

LIST OF TABLES

ACKNOWLEDGMENTS

It is a true privilege to have the opportunity to pursue a PhD in physics – not only for the luxurious salary, but also for the unparalleled joy that comes from pondering the intricacies of our universe. I am fortunate to have been surrounded by teachers, mentors, collaborators, friends, and family that have helped to make a PhD possible. This dissertation is ultimately a product of their support and encouragement throughout my academic career.

I am especially grateful to my advisor Lukasz Fidkowski for his endless patience in answering naïve questions and readiness to engage in even the most pedantic details of a problem. Lukasz has been overwhelmingly supportive of my academic pursuits and has enabled me to attend conferences and workshops abroad including an extended visit at Perimeter Institute. I wish there was a way to adequately thank Lukasz for his time as my advisor. I can only hope to provide mentorship to the next generation of students as generously as Lukasz.

I would also like to thank my committee members: Mark Rudner, Subhadeep Gupta, Andreas Karch, Laurence Yaffe, David Cobden, and Isabella Novik. Their keen insights and challenging questions have been greatly appreciated in my development as a physicist. In particular, I would like to acknowledge my reading committee members: Mark and Subhadeep, for their time and effort in reviewing this dissertation.

Physics is one unending group project, and I count myself lucky to have been paired with a collection of inspiring collaborators. I have valued the many influential

conversations with my fellow group members: Sujeet Shukla, Joesph Merritt, and Ryan Lanzetta, and I have had the pleasure of forming a longterm collaboration with Yu-An Chen and Nathanan Tantivasadakarn. I have also enjoyed working closely with Timothy H. Hsieh, Kohtaro Kato, and Zi-Wen Liu at Perimeter Institute. My work has been enriched through enlightening discussions with many other members of the community, and I look forward to continuing to learn from and be inspired by my colleagues.

Finally, I am indebted to my family and friends for their unconditional support and refreshing diversions from physics. I have had the fortune of growing up in an environment where education is highly valued and questions about the natural world are encouraged. I owe any academic accomplishments to my parents: Paul and Jenny Ellison, for all of their early mornings preparing me for school and late nights helping me finish homework. I am also beyond grateful to Chennah Heroor and Admiral Snickers for emotionally holding my hand throughout my PhD.

Chapter 1

INTRODUCTION

To begin our discussion of the quantum complexity of symmetry-protected topological phases of matter, let us start by comparing apples and oranges. We ask: how do you tell the difference between an apple and an orange? One reliable way to distinguish between the two (apparently discouraged in grocery stores) is to cut them in half and study the symmetries of a cross section, as pictured in Fig. 1.1. The seeds of an apple form a 5-pointed star, giving the cross sections a 5-fold rotational symmetry. The membranes separating the segments of an orange, on the other hand, typically lead to a 10-fold rotational symmetry of a cross section. Since 5 is not equal to 10, we can tell apples apart from oranges.

Remarkably, the same principles used to tell apples apart from oranges can be used to distinguish between phases of matter. For example, liquids can be differentiated from solids based on their symmetries. Liquids have a continuous translational symmetry, since there is a uniform probability of finding the constituent atoms anywhere within the liquid. Solids, in contrast, have a *discrete* translational symmetry – the atoms are arranged into a crystal and are likely to be found only in discrete locations. In a similar fashion, symmetries can be used to distinguish between non-magnetic (paramagnet) phases and magnetic (ferromagnet) phases. In a non-magnetic phase, the magnetic moments of the atoms are randomly oriented and there is zero net magnetization. The net magnetization has a continuous rotational symmetry, because it is unchanged by rotations of the system. In a magnetic phase, however, the magnetic moments of the atoms are aligned, and the rotational symmetry is broken (see Fig. 1.1).

Symmetries have been a powerful (or fruitful, if you will) tool for distinguishing between

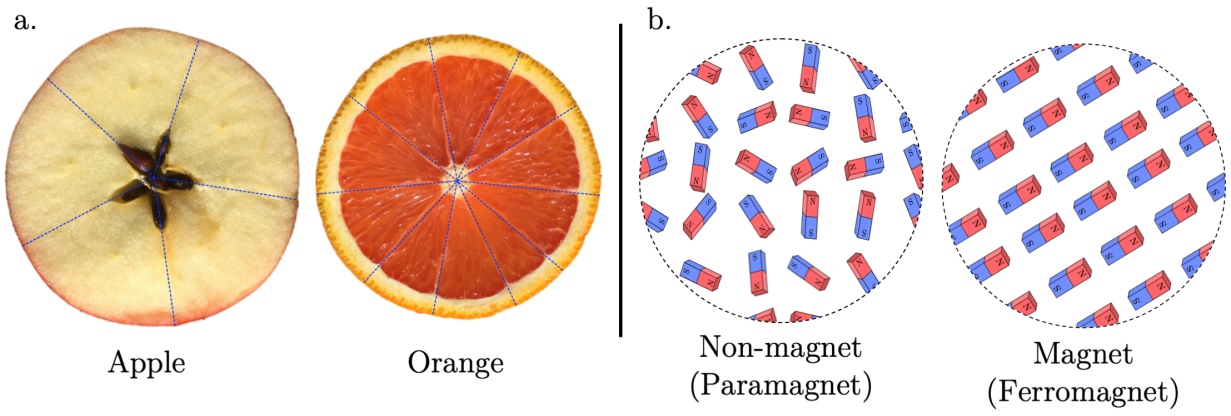

Figure 1.1: a. Apples and oranges can can be distinguished by their symmetries. Apples have a five-fold rotational symmetry, while oranges usually have a ten-fold rotational symmetry. b. Similarly, non-magnetic phases (i.e. paramagnetic phases) can be distinguished from magnetic phases (i.e. ferromagnetic phases) by their symmetries. In a non-magnetic phase, the magnetic moments of the atoms (represented by bar magnets) point in random directions. The net magnetization is zero and is unaffected by any continuous rotation of the system. In a magnetic phase, on the other hand, all of the magnetic moments point in the same direction, breaking the rotational symmetry.

phases of matter. However, there are phases of matter that differ by more subtle, fundamentally quantum mechanical differences. Symmetry-protected topological phases of matter, referred to as SPT phases, are such an example. SPT phases cannot be distinguished by their symmetries alone. Instead, they differ by characteristic patterns of quantum entanglement [1]. We leave a precise definition of "patterns of entanglement" for a more technical discussion in Section 1.2.

For now, we answer the more practical question: how does one distinguish between the distinct patterns of entanglement in SPT phases? To differentiate between liquids and solids one can measure the local density of atoms – the density is peaked at discrete locations in the solid state due to the crystal structure. Likewise, magnetic phases can be distinguished from non-magnetic phases by measuring a local quantity, i.e., the local magnetization. SPT phases, however, cannot be detected by making local measurements in the interior (or bulk)

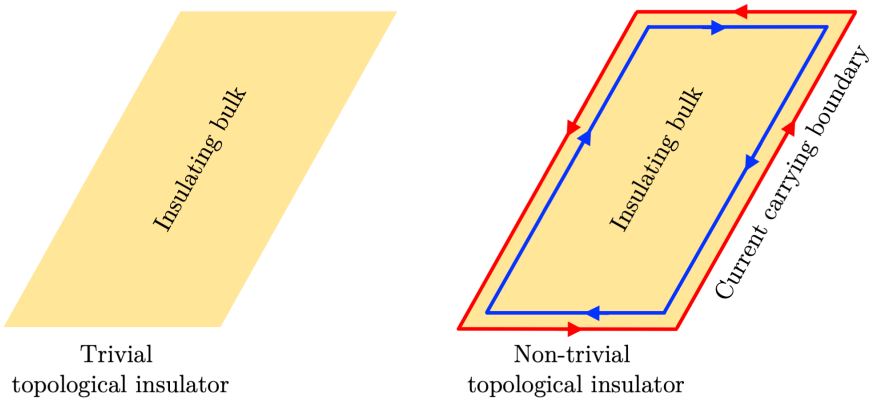

Figure 1.2: There are two types of topological insulators in two dimensions, distinguished by the properties of their boundaries. In the trivial topological insulator phase, the bulk and boundary are insulating. (At least, there is no fundamental obstruction to making the boundary insulating by appropriately trimming the edge.) In the nontrivial topological insulator, the patterns of entanglement in the bulk force the boundary to be a conductor. On the boundary, particles of one type (red) travel counterclockwise, while particles of the other type (blue) travel clockwise. The system is time-reversal symmetric since time-reversal changes the direction of the currents and transforms the two types of particles into one another (red $\leftrightarrow$ blue).

of the system. Observable quantities like the local density and local magnetization are simply unable to detect the differences between the patterns of entanglement. The key to distinguishing between SPT phases is to recognize that the patterns of entanglement in the bulk manifest in exotic behavior at the boundary of the system. The symmetries, along with the properties of the boundary, fully characterize the SPT phase.

To make this point more concrete, we consider a collection of SPT phases with time-reversal symmetry known as topological insulators. There are two distinct types of topological insulators in two dimensions: the trivial topological insulator and the nontrivial topological insulator. They share the same symmetries but, due to the entanglement in the bulk, have notably different properties near the boundary (Fig. 1.2). The trivial topological insulator is insulating both in the bulk and along the edge. The nontrivial topological insulator, in contrast, always conducts current along its boundary. In addition, the current

along the boundary of the nontrivial topological insulator is unusual – the direction of the current depends on subtle properties of the charged particles under time-reversal symmetry. Importantly, the boundary of the nontrivial topological insulator cannot be mimicked in a stand-alone, one-dimensional system. The entanglement within the bulk of the material is necessarily responsible for the exotic behavior on the boundary. This means that the properties of the nontrivial topological insulator cannot be reproduced by simply appending conducting channels (or current carrying wires) to the boundary of a trivial topological insulator.

The strange behavior at the boundary of SPT phases has promising applications to device physics and quantum computing. For one, the flow of particles at the boundary of a nontrivial topological insulator is dissipationless, since the particles are unable to scatter or change directions without breaking the time-reversal symmetry. This property of nontrivial topological insulators could eventually be used to improve the efficiency of certain electronic devices and allow for more reliable transportation of quantum information. There is also potential for using the edge of a nontrivial topological insulator in combination with a superconductor to build a quantum memory – a sort of hard drive for quantum information [2]. SPT phases have also been of interest for measurement-based quantum computation, where quantum information on the boundary of the SPT phase is manipulated by making appropriate measurements in the interior of the system [3].

To take advantage of the exotic behaviors at the boundary of SPT phases, we first need to make progress in constructing SPT phases in experimental settings. The search for experimental realizations of SPT phases is aided by simulating SPT phases on classical and quantum computers. For this reason, it is valuable to have a complete characterization of the "quantumness" of SPT phases. This helps inform us about potential challenges to simulating them efficiently on computers and gives us insight into their inherent quantum informational resources. SPT phases are undeniably quantum mechanical – quantum entanglement in the bulk is essential to the unusual properties exhibited at the boundary. However, some quantum systems are more quantum mechanically complex than others.

The work described in this dissertation explores various measures of the quantum complexity of SPT phases. In Chapter 2, we show that some SPT phases are more challenging to simulate on classical and quantum computers using standard techniques for simulating quantum many-body systems. In the following chapters, we focus on a class of SPT phases called supercohomology SPT phases. Beyond being a mouthful, supercohomology SPT phases are conventionally difficult to simulate. Nonetheless, despite their computational complexity, we develop a coherent description for supercohomology SPT phases and find explicit expressions for their characteristic patterns of quantum entanglement. We then establish a direct connection between the patterns of entanglement in the bulk of supercohomology SPT phases and the strange behaviors at their boundaries.

The remainder of this introduction is devoted to putting the concepts of quantum complexity and SPT phases on more solid footing. We start by introducing the notions of quantum complexity considered in this work. We then carefully define SPT phases and clarify the meaning of "patterns of quantum entanglement". To make the discussion precise, we resort to more technical language. In other words, if you have made it this far into the dissertation, Mom, this is a warning that it may get more challenging to read.

1.1 Quantum complexity of many-body systems

In this work, we interpret quantum complexity as an assessment of our ability to efficiently store and manipulate the quantum information of a state. States with a high degree of quantum complexity are thus more difficult to simulate on classical and quantum computers. It is important to note that there is no "one true" measure of the quantum complexity of a state. In general, the complexity of a task depends on the set of tools being used. For example, it is much easier to keep your feet warm with socks than with a toothbrush. At the same time, toothbrushes are better suited for brushing your teeth than socks.[1] Since there are a variety of methods for simulating quantum many-body systems, there are correspondingly

[1] I am assuming that this is true, but I don't want to get caught with my foot in my mouth.

many ways to assess the quantum complexity of a state. Some quantum states may be more efficiently simulated using one set tools than another. Quantum complexity is thus defined relative to the methods used for simulation.

To help illustrate this point, we consider a system of N qubits. A basis for this system can be labeled by bit strings of length N, where the i^{th} bit denotes the state of the i^{th} qubit. For example, given a bit string $01011\cdots00010$ of length N, the corresponding basis state is:

$$|0,1,0,1,1,\cdots,0,0,0,1,0\rangle. \tag{1.1}$$

An unentangled state, such as this, can be efficiently stored and manipulated on a classical computer, since it only contains N bits of information. However, a generic entangled state of the N qubit system takes the form:

$$|\psi\rangle = \sum_{a_1 a_2 \ldots a_N} A_{a_1 a_2 \ldots a_N} |a_1, a_2, \ldots, a_N\rangle, \tag{1.2}$$

where each a_i is either 0 or 1, and $A_{a_1 a_2 \ldots a_N}$ is a complex number that depends on the bit string $a_1 a_2 \ldots a_N$. The number of possible bit strings, and hence the number of amplitudes $A_{a_1 a_2 \ldots a_N}$, grows like 2^N. Therefore, for a large number of qubits, it highly inefficient to store the state by simply recording each of the amplitudes.

This is the crux of the quantum many-body problem: due to entanglement, the amount of information needed to specify a generic state grows exponentially with the size of the system. If it were possible to efficiently store an arbitrary many-body quantum state for a given system, then it would be possible to solve any associated quantum many-body problem. It is therefore highly desirable to find classes of states that can be efficiently simulated despite the entanglement. Of course, no scheme for simulating states is perfect, and the limitations can be used to define notions of quantum complexity. In what follows, we give a brief description of four methods for simulating quantum states, each of which plays a role in this dissertation: quantum Monte Carlo, the stabilizer formalism, tensor network methods, and

non-interacting fermions.

One of the most effective tools for simulating quantum many-body systems is quantum Monte Carlo. Monte Carlo methods are ubiquitous in physics, and quantum many-body physics is no exception. In quantum Monte Carlo (specifically, path-integral quantum Monte Carlo) the strategy is to view the quantum system as a classical system in one higher dimension. A prerequisite for interpreting a quantum many-body system as a classical system, however, is that the amplitudes $A_{a_1 a_2 \ldots a_N}$ of the ground state have to be real and non-negative. In some cases, there is an obstruction to finding a local basis in which the ground state has real non-negative amplitudes. We refer to this as a sign problem, following Ref. [4]. A sign problem poses an obstacle to efficient simulation by Monte Carlo methods and indicates that the ground state is more quantum mechanically complex than a state with real non-negative amplitudes.

Quantum Monte Carlo methods rely on classical computers, but one could instead consider simulating a quantum state using a quantum computer. Near-term error correcting quantum computers are limited, however. Many of the most promising proposals for fault-tolerant (i.e., error resilient) quantum computers rely on the so-called stabilizer formalism. The stabilizer formalism is able to efficiently simulate only a restricted set of states known as stabilizer states. (For more detail, see Section 2.3.2.) While quantum computers can in principle simulate an arbitrary quantum state, states outside of the stabilizer formalism are computationally more intensive to simulate. Non-stabilizer states are therefore less efficient to simulate on near-term error correcting quantum computers. On the flip side, non-stabilizer states, referred to as magic states, can be used as ancillary states to empower quantum computers [5].

Another strategy for simulating quantum states on classical computers is to use tensor network methods. The goal of tensor network methods is to decompose the amplitudes $A_{a_1 a_2 \ldots a_N}$ into amplitudes that depend on only a few qubits. The amplitudes $A_{a_1 a_2 \ldots a_N}$ can then be recovered by recombining the few-body amplitudes. Tensor network methods are best suited for simulating systems with low levels of entanglement in one dimension, where

they have enabled a complete classification of one-dimensional quantum phases of matter [6]. However, there is active research into developing tensor network methods for higher-dimensional systems [7–9]. One could hope that they will eventually provide a means for efficiently simulating quantum phases of matter in two dimensions as well.

Lastly, we consider simulating quantum states described by non-interacting fermions. Due to the absence of interactions, the quantum many-body problem reduces to solving a single-body problem. For a system of non-interacting fermions, the many-body states are recovered from the single-body states by filling fermions into unoccupied states according to Hund's rule. The free-fermionic states can be specified by an anti-symmetric $N \times N$ matrix called the correlation matrix, where N is the number of fermionic modes. The correlation matrix is a highly efficient way to encode the information of free-fermionic states, and thus non-interacting fermions can be efficiently simulated on classical computers. Furthermore, thanks to the Pauli exclusion principle, non-interacting fermions are able to exhibit a wide range of quantum phases of matter, which includes SPT phases. Given the drastic simplification to solving a single-body problem, SPT phases of non-interacting fermions have been completely classified [10,11]. New tools and techniques are needed to go beyond non-interacting fermions to study systems of strongly-interacting fermions.

The methods for simulating quantum many-body states described above all have their limitations, yielding different notions of the quantum complexity of a state. By studying the quantum complexity of quantum phases of matter, we learn about our limitations in simulating their varied behavior. At the same time, it also informs us about quantum informational resources harbored by the quantum phase of matter. States that fall outside of a given simulation scheme could be used as a resource to aid in simulating a broader class of states. For example, sampling from a state with a sign problem may help improve the applicability of quantum Monte Carlo methods [12]. As for the stabilizer formalism, it has already been established that "non-stabilizerness", or magic, is a necessary ingredient for universal quantum computation in conjunction with the stabilizer formalism. Similarly, interacting fermionic states can be used to promote manipulations of free-fermion states to

universality [13].

A natural place to start in studying the quantum complexity of quantum phases of matter is with SPT phases. The theory of SPT phases has been well-developed and there is a solid understanding of their classification and characterization. They also have relatively low levels of entanglement and can be described by simple, exactly solvable models, thus simplifying the analysis of their quantum complexity. SPT phases have been proposed as resource states for measurement-based quantum computing and their boundaries have applications for quantum computation. It is therefore valuable to have a complete picture of the quantum complexity and the quantum information-theoretic resources inherent to SPT phases.

1.2 Symmetry-protected topological phases of matter

In this section, we provide an abstract definition of SPT phases and argue that distinct SPT phases can be characterized by their patterns of entanglement. The characterization of SPT phases in terms of patterns of entanglement is especially useful for assessing the quantum complexity of SPT phases, as demonstrated in the text. First, however, we comment on the description of SPT phases given at the beginning of the introduction. We described SPT phases as phases of matter that cannot be characterized by their symmetries alone. The more precise statement is that, unlike solid states and magnetic phases, SPT phases do not exhibit spontaneous symmetry breaking. Therefore, they fall outside of the traditional spontaneous symmetry breaking classification of phases of matter. It is also important to note that SPT phases are quantum phases of matter and defined at zero temperature.

At an abstract level, SPT phases are equivalence classes of certain Hamiltonians. We refer to the particular Hamiltonians considered in defining SPT phases as SPT Hamiltonians. An SPT Hamiltonian in D-dimensions with a symmetry G is any Hamiltonian that satisfies the following properties.

(i) **Tensor product Hilbert space:** The Hamiltonian is defined on a tensor product Hilbert space of the form: $\mathcal{H} = \bigotimes_i \mathcal{H}_i$, where each $\mathcal{H}_i$ is a finite-dimensional Hilbert

space. The tensor product structure is motivated by solid-state materials, where the relevant degrees of freedom (d.o.f.) are tightly bound to atoms in a lattice. We interpret i as indexing the sites of a D-dimensional lattice. The site Hilbert spaces $\mathcal{H}_i$ are taken to be finite-dimensional for simplicity. The d.o.f. at each site may be bosons, fermions, or some combination. If they are bosons, then the tensor product is symmetrized, reflecting the commutation relations of bosons. If the d.o.f. are fermions, then the tensor product is anti-symmetrized, capturing the fermionic statistics. We refer to Chapter 3 for more clarification on the structure of the many-body Hilbert space.

(ii) **Local interactions:** The Hamiltonian has exponentially localized interactions. This assumption is primarily to simplify the analysis. However, the exponentially localized interactions can be interpreted as arising from screening effects in solid-state materials. For fermionic systems, we also require that each term in the Hamiltonian is fermion parity even, i.e., it is a product of an even number of creation and annihilation operators. Fermion parity even operators are local in the sense that they commute with fermion parity odd operators at distant sites.

(iii) **Gapped spectrum:** In the limit of large system size, the ground state of the Hamiltonian is separated from the first excited state(s) by a nonzero energy difference. The gap ensures that the system is in the ground state at zero temperature, which implies that all of the information about the phase of matter is encoded in the ground state.

(iv) **Symmetric:** The Hamiltonian has an onsite (or internal) G symmetry. This means that it is represented by an operator of the form: $\bigotimes_i u_i(g)$, for any element $g \in G$ and unitary representation $u_i(g)$ at site i. In this work, all of the symmetries correspond to a finite group and are represented by a unitary operator. We do not consider continuous symmetries, spatial symmetries, or anti-unitary symmetries, although the corresponding SPT phases can be defined similarly..

(v) **Trivial in the absence of symmetry:** The Hamiltonian H can be adiabatically connected to a Hamiltonian with a unique product state ground state while preserving conditions (i)-(iii). In other words, there exists a continuous path of Hamiltonians $H(s)$, with $s \in [0,1]$, satisfying conditions (i)-(iii) such that $H(0) = H$ and $H(1)$ has a unique product state ground state. This condition implies that H has a unique ground state, and precludes spontaneous symmetry breaking. It also implies that SPT Hamiltonians cannot describe quantum Hall phases or phases with anyonic excitations.

With this, we can define SPT phases in D-dimensions protected by a G symmetry (see also Fig. 1.3).

Definition 1 *D-dimensional SPT phases protected by a G symmetry are equivalence classes of G-symmetric SPT Hamiltonians in D-dimensions under the following equivalence relation: two G-symmetric SPT Hamiltonians H_0 and H_1 in D dimensions belong to the same SPT phase if and only if there exists a continuous path of G-symmetric SPT Hamiltonians $H(s)$ in D dimensions, with $s \in [0,1]$, such that $H(0) = H_0$ and $H(1) = H_1$.*

The equivalence relation in the definition of SPT phases partitions the set of SPT Hamiltonians into SPT phases. By definition, a transition between two distinct SPT phases requires leaving the space of G-symmetric SPT Hamiltonians in D-dimensions. This may mean closing the spectral gap or breaking the protecting symmetry, for example. We refer to the SPT phase containing Hamiltonians with a product state ground state as the trivial SPT phase and refer to the others as nontrivial SPT phases.

We are finally in a position where we can clarify the meaning of patterns of entanglement and argue that SPT phases are characterized by their distinct patterns of entanglement. The key observation comes from the quasi-adiabatic theorem described in Ref. [14]. The quasi-adiabatic theorem says that, if two gapped Hamiltonians H_0 and H_1 can be adiabatically connected by a path of Hamiltonians $H(s)$ satisfying conditions (i)-(iii) above, then there exists a local time-dependent Hamiltonian $\tilde{H}(t)$ such that the finite-time evolution of $\tilde{H}(t)$

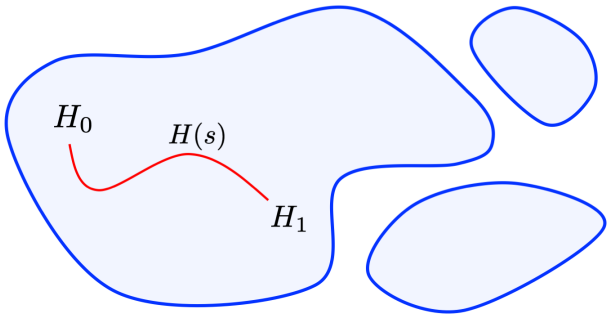

Figure 1.3: SPT phases are defined as equivalence classes of SPT Hamiltonians. Two SPT Hamiltonians H_0 and H_1 belong to the same equivalence class if there is a continuous path of Hamiltonians $H(s)$ (red path) that connects H_0 and H_1. An SPT phase thus corresponds to a path component (a blue region) in the space of SPT Hamiltonians (collection of blue regions).

maps the ground state of H_0 to the ground state of H_1. Explicitly, the ground state of H_0 is mapped to the ground state of H_1 by the unitary operator:

$$\mathcal{U} = \mathcal{T}\left\{e^{-i\int_0^1 dt\tilde{H}(t)}\right\}, \tag{1.3}$$

where $\mathcal{T}$ denotes the time ordering operation. Furthermore, if each Hamiltonian along the path of Hamiltonians $H(s)$ is symmetric, then $\tilde{H}(t)$ is symmetric. The quasi-adiabatic theorem implies that, if two SPT Hamiltonians belong to the same phase, then their ground states can be mapped to one another by the finite-time evolution of a symmetric local Hamiltonian.

The converse of the quasi-adiabatic theorem is also true. If the ground states $|\psi_0\rangle$ and $|\psi_1\rangle$ of two Hamiltonians H_0 and H_1 obeying (i)-(iii) are related by the finite-time evolution of some local Hamiltonian $\tilde{H}(t)$, then there is a path of Hamiltonians satisfying conditions (i)-(iii) that connects H_0 and H_1. This can be seen by defining $\mathcal{U}(s)$ as:

$$\mathcal{U}(s) \equiv \mathcal{T}\left\{e^{-i\int_0^s dt\tilde{H}(t)}\right\}. \tag{1.4}$$

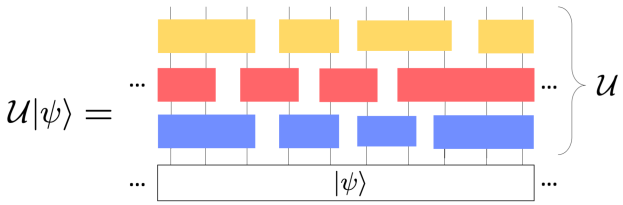

Figure 1.4: Finite-depth quantum circuits (FDQCs) are unitary operators that admit a decomposition into local unitaries as in Eq. (1.6). The FDQC $\mathcal{U}$ is composed of layers (blue, red, yellow, respectively), and each layer is a product of local unitaries (represented by rectangular blocks) with non-overlapping supports.

H_0 and H_1 are adiabatically connected by the path of Hamiltonians:

$$H(s) \equiv \mathcal{U}(s) H_0 \mathcal{U}^\dagger(s), \tag{1.5}$$

which satisfy the conditions (i)-(iii) by the fact that $\mathcal{U}(s)$ is unitary and maps local operators to local operators. Moreover, if $\tilde{H}(t)$ is symmetric for every t, then each Hamiltonian in the path $H(s)$ is symmetric. The converse of the quasi-adiabatic theorem tells us that, if the ground states of two SPT Hamiltonians can be mapped to one another by the finite-time evolution of a symmetric local Hamiltonian, then the two SPT Hamiltonians must belong to the same SPT phase.

Given the quasi-adiabatic theorem and its converse, SPT phases can alternatively be defined as equivalence classes of quantum states [1]. The ground states of two SPT Hamiltonians are equivalent, or belong to the same phase, if and only if there exists a symmetric local Hamiltonian $\tilde{H}(t)$ whose finite-time evolution maps one state to the other. Moving forwards, we refer to the ground states of SPT Hamiltonians as SPT states. We say an SPT state is trivial, or belongs to the trivial SPT phase, if there exists a symmetric local Hamiltonian whose finite-time evolution maps the state onto a product state. Otherwise, we call the SPT state nontrivial, or say that it belongs to a nontrivial SPT phase.

It is often convenient to approximate the finite-time evolution of a Hamiltonian $\tilde{H}(t)$ by

the time evolution of a piece-wise constant Hamiltonian with small time steps. This allows us to approximate the finite-time evolution by a finite-depth quantum circuit (FDQC). FDQCs are unitary operators with a decomposition into local unitary operators, as shown in Fig. 1.4. The general form for a FDQC is:

$$\mathcal{U} = \prod_{\ell}^{d} \prod_{j_\ell} U_{j_\ell}, \tag{1.6}$$

where ℓ indexes the layers of the circuit up to a finite-depth d, and j_ℓ indexes local unitary operators in the ℓ^{th} layer of the circuit with non-overlapping supports.[2] The local unitaries U_{j_ℓ} are sometimes referred to as gates, and they are always assumed to be fermion parity even. Note that, if the finite-time evolution is generated by a symmetric Hamiltonian, then the corresponding FDQC is composed of symmetric gates. Therefore, a convenient working definition for SPT phases is as equivalence classes of SPT states, with the property that two states belong to the same equivalence class if and only if there exists a FDQC composed of symmetric gates that maps one to the other.

The definition of SPT phases at the level of SPT states shows us that SPT phases are characterized by their patterns of entanglement. By condition (v) on SPT Hamiltonians, all SPT states can be (approximately) disentangled by a FDQC. However, nontrivial SPT states have the property that they cannot be disentangled by a FDQC composed of *symmetric* local unitaries. Heuristically, nontrivial SPT states must have entanglement that cannot be removed by making symmetry-preserving local changes to the entanglement. In this sense, nontrivial SPT states have a nontrivial pattern of entanglement. Likewise, SPT states belonging to different SPT phases cannot be mapped to one another by making symmetry-preserving local changes to the entanglement. Therefore, we say that SPT phases can be distinguished by their patterns of entanglement.

In Chapter 2, we provide an example of a nontrivial SPT phase, and prove that the

[2]The support of an operator is the set of sites on which the operator acts non-identically.

corresponding SPT states cannot be disentangled by FDQCs composed of symmetric gates. We also demonstrate that the SPT phases can be distinguished by their anomalous behavior at a boundary. In Chapters 4 and 5, we construct explicit FDQCs capable of disentangling certain fermionic SPT states. In particular, the FDQCs reveal the patterns of entanglement in fermionic SPT phases classified by the mathematical formalism of group supercohomology. In Chapter 5, we then describe how the structures of entanglement in the supercohomology SPT phases can give rise to exotic boundary theories.

1.3 Outline and summary

Here, we outline the remainder of the dissertation by providing brief summaries of Chapters 2-5. We begin with Chapter 2, where we discuss the computational complexity of SPT phases built from bosons. In particular, we introduce the concepts of a symmetry-protected sign problem and symmetry-protected magic. We say a state has a symmetry-protected sign problem if there is an obstruction to finding a symmetry-preserving local change of basis that maps the state to a non-negative state, and we say a state has symmetry-protected magic if there is no FDQC composed of symmetric gates that maps the state to a stabilizer state. We show that certain SPT phases have a symmetry-protected sign problem, by studying the correlations on the boundary of the SPT phases. The symmetry-protected sign problem implies that there is an obstacle to simulation using quantum Monte Carlo methods. We also show that some SPT phases have symmetry-protected magic. Our proof relies on the fact that the patterns of entanglement in the bulk of an SPT phase lead to an anomalous symmetry action at the boundary. The characteristic anomalous symmetry action at the boundary of SPT phases in $D \geq 2$ dimensions prohibits a representation of the system using the stabilizer formalism. We conclude the chapter by discussing potential directions for studying the computational complexity of bosonic quantum phases of matter beyond SPT phases.

In the next chapter, we make a transition to discussing fermionic systems by introducing a two-dimensional tensor network-based bosonization. Bosonization is a duality, or change

of variables, that relates fermionic systems to certain bosonic systems. The Jordan-Wigner duality is an example of a bosonization duality in one dimension. The Jordan-Wigner duality can be applied to higher-dimensional systems but fails to map local operators to local operators. Bosonization dualities that map local operators to local operators, however, have recently been developed for higher-dimensional systems. We build off of the two-dimensional bosonization duality in Ref. [15], and construct a tensor network description of the duality. This allows us to map a fermionic state to the corresponding bosonic state within the tensor network formalism. By using tensor network methods, the bosonization duality can be implemented directly on the local tensors (referred to as local amplitudes in Section 1.1) that compose the fermionic many-body state. Our work also carefully accounts for the Koszul sign, a sign obtained in tensor network decompositions of fermionic states that can muddle the simulation of fermionic systems using tensor networks. Bosonization dualities, such as the one described in Chapter 3, play a crucial role in our analysis of fermionic SPT phases in later chapters.

While SPT phases of non-interacting fermions have been completely classified, the classification and characterization of SPT phases with strongly-interacting fermions have proven more challenging. In Chapters 4 and 5, we construct models for fermionic SPT phases that are beyond the reach of free-fermionic techniques. Despite their complexity as models of strongly-interacting fermions, they are exactly solvable. In particular, we construct exactly solvable models for fermionic SPT phases classified by the framework of group supercohomology. Our strategy for constructing exactly solvable models is to relate the supercohomology fermionic SPT phases to bosonic SPT phases through bosonization. Bosonization allows us to exploit the well-established models for bosonic SPT phases to back out models for the fermionic SPT phases. Starting with the mathematical data that characterizes a nontrivial SPT phase, we build an explicit FDQC that disentangles a representative nontrivial SPT state. In this sense, we uncover the patterns of entanglement characteristic of the supercohomology SPT phases. In Chapter 4, we build models for supercohomology SPT phases in two dimensions. We emphasize the role played by certain combinatorial data known as

spin structure, which appeared as ad hoc choices in previous constructions of fermionic SPT phases. Then, in Chapter 5, we describe the construction of exactly solvable models for supercohomology SPT phases in three dimensions. We also show explicitly how the entanglement in the bulk of our models enables exotic behavior on the boundary.

Chapter 2

COMPUTATIONAL COMPLEXITY OF BOSONIC SPT PHASES

This chapter is based on:
Tyler D. Ellison, Kohtaro Kato, Zi-Wen Liu, and Timothy H. Hsieh. Symmetry-protected sign problem and magic in quantum phases of matter. *arXiv:2010.13803*, October 2020.

We introduce the concepts of a symmetry-protected sign problem and symmetry-protected magic to study the complexity of symmetry-protected topological (SPT) phases of matter. In particular, we say a state has a symmetry-protected sign problem or symmetry-protected magic, if finite-depth quantum circuits composed of symmetric gates are unable to transform the state into a non-negative real wave function or stabilizer state, respectively. We prove that states belonging to certain SPT phases have these properties, as a result of their anomalous symmetry action at a boundary. For example, we find that one-dimensional $\mathbb{Z}_2 \times \mathbb{Z}_2$ SPT states (e.g. cluster state) have a symmetry-protected sign problem, and two-dimensional $\mathbb{Z}_2$ SPT states (e.g. Levin-Gu state) have both a symmetry-protected sign problem and symmetry-protected magic. We also comment on the relation of a symmetry-protected sign problem to the computational wire property of one-dimensional SPT states and speculate about the greater implications of our results for measurement-based quantum computing.

2.1 Introduction

The concept of entanglement is an important tool for diagnosing the complexity of quantum states and has led to a deeper understanding of quantum phases of matter and quantum phase transitions. However, entanglement by itself does not fully capture the quantum complexity of a state – some quantum states can be efficiently simulated by classical systems, despite the

presence of entanglement. This motivates using diagnostics beyond entanglement to assess the quantum complexity of many-body states and to further inform us of the quantum information structures intrinsic to phases of matter. In this chapter, we focus on two means for evaluating the complexity of a state: (i) its 'magic' and (ii) its sign structure.

Magic is an assessment of the extent to which a state can be expressed as a stabilizer state [16]. Since stabilizer states can be efficiently stored and manipulated on classical computers [17], magic can be regarded as a measure of the complexity of a state. The sign structure of a state, on the other hand, relates to the difficulty in expressing a state as a non-negative state – i.e., a state with real non-negative probability amplitudes in a local basis [4, 18]. Complex probability amplitudes are responsible for inherently non-classical phenomena, such as quantum interference, so the sign structure can be used to characterize the quantum nature of a state.

The sign structure of a state is, of course, basis dependent, so to make a meaningful assessment of the complexity of the state, we consider the sign structure modulo local basis changes. Following Ref. [4], we say the wave function has a sign problem if the amplitudes cannot be made non-negative by any local basis transformation. This notion of a sign problem implies that any gapped parent Hamiltonian has a sign problem in the stoquastic sense [4]. Therefore, the sign problem at the level of the wave function also implies that there is an obstacle to efficiently simulating the system using Monte Carlo methods.

While the magic in a many-body state and the notion of a sign problem are promising metrics for the quantum complexity of states, they are notoriously challenging to study analytically and numerically, although substantial progress has been made [4, 12, 16, 19–33]. We therefore propose a simplification by imposing symmetry constraints. In particular, we introduce symmetry-protected magic and a symmetry-protected sign problem. These simplified diagnostics of the complexity of a state allow us to make analytical statements about the structure of quantum information in quantum phases of matter.

More specifically, we consider symmetry-protected topological (SPT) phases of matter, whose properties can be characterized by short-range entangled (SRE) states. Despite the

short-range entanglement, SPT phases are responsible for a rich set of quantum phenomena including the helical edge modes at the boundary of topological insulators [34, 35] and symmetry-protected degeneracies useful for measurement-based quantum computing [36–42]. It is therefore valuable to have a complete understanding of the quantum information structures of SPT phases to be able to both simulate their novel behaviors and harness their resources for quantum computing.

In this work, we contribute to the understanding of the quantum complexity of SPT states, by showing that certain SPT states have symmetry-protected magic and that some possess a symmetry-protected sign problem. The symmetry-protected magic implies that the SPT states have magic that cannot be removed by making local symmetry-preserving changes to the state. This builds on the work of Refs. [43–45], in which particular finely tuned SPT states are shown to have magic. The symmetry-protected sign problem, in contrast, informs us about the sign structure of SPT states and poses an obstruction to finding a non-negative representation through local symmetry-respecting basis changes. To the best of our knowledge, this constitutes the first analytic proof of a (symmetry-protected) sign problem at the level of the wave function. We speculate that our methods for evaluating symmetry-protected sign problems may also be valuable for diagnosing sign problems in the absence of symmetry.

Structure of the chapter

Our main application of symmetry-protected magic and a symmetry-protected sign problem are to SPT states. Therefore, we begin by defining SPT states and SPT phases in Section 2.2.1. For convenience, we work with a definition of SPT phases phrased in terms of finite-depth quantum circuits. Then, in Section 2.2.2, we describe a characteristic feature of SPT phases – the symmetry acts anomalously near a boundary. In the following section, Section 2.2.3, we discuss how the effects of the anomalous symmetry action can be detected using a strange correlator. To illustrate these concepts on a concrete example, we apply them to the 1D cluster state in Section 2.2.4.

We then move on to assess the complexity of SPT states, starting with symmetry-protected magic in Section 2.3. We first review the stabilizer formalism in Section 2.3.1 before defining symmetry-protected magic in Section 2.3.2. Subsequently, in Section 2.3.3, we use the anomalous boundary symmetry action to show that a subset of SPT states (belonging to group cohomology SPT phases in spatial dimensions $D \geq 2$) have symmetry-protected magic.

Next, we turn to the symmetry-protected sign problem in Section 2.4. In Section 2.4.1, we give a precise definition for a symmetry-protected sign problem, and then, in Section 2.4.2, we argue that SPT states in dimensions $D \leq 2$ have a symmetry-protected sign problem relative to local bases where the symmetry is diagonal. The argument relies on the expected "strange correlations" in SPT states. We also provide a second argument in Section 2.4.2 based on the incompatibility between the computational wire property of one-dimensional SPT phases and bounds on measurement-induced entanglement in non-negative wave functions [4].

We conclude by commenting on relations to previous work and by proposing future directions for studying the quantum complexity of topological phases of matter. We also state a number of conjectures, and in particular, we conjecture that states defined on qubits and belonging to the double semion phase have magic that is robust to arbitrary unitary local operations.

2.2 Primer on SPT phases

To begin, we define SPT phases in terms of the circuit complexity of states, following Ref. [1]. We then describe a characteristic property of (non-trivial) SPT phases in Section 2.2.2: the symmetry acts on the system in an anomalous fashion in the presence of a boundary. In certain cases, the effects of the anomalous symmetry action can be detected using strange correlators, which we define in Section 2.2.3. In Section 2.2.4, we illustrate the concepts of the anomalous boundary symmetry action and strange correlators with an example of a well-known SPT state - the 1D cluster state.

2.2.1 Definition of SPT phases

We define SPT states and SPT phases using finite-depth quantum circuits (FDQCs). Recall that a FDQC is any unitary operator that can be written in the form:

$$\mathcal{U} = \prod_{\ell=1}^{d} \Big(\prod_{j_\ell} U_{j_\ell} \Big). \tag{2.1}$$

Here, the first product runs over layers, up to a depth d, and j_ℓ indexes unitary operators U_{j_ℓ} in the layer ℓ. The unitary operators U_{j_ℓ}, referred to as gates, are taken to be local[1] and to have non-overlapping supports within a given layer. We note that the circuit is "finite-depth", if the depth d is both finite and constant in the system size.

To define SPT states in D dimensions, we consider Hilbert spaces of the form:

$$\mathcal{H} = \bigotimes_{i \in \Lambda} \mathcal{H}_i, \tag{2.2}$$

where i labels sites on a lattice Λ embedded in a D dimensional manifold without boundary, and each site hosts a finite-dimensional Hilbert space $\mathcal{H}_i$. For SPT phases protected by a G symmetry, we assume the G symmetry is represented by an *onsite* representation.[2] That is, every g in G is represented by an operator:

$$u(g) = \bigotimes_{i \in \Lambda} u_i(g), \tag{2.3}$$

with each $u_i(g)$ forming a linear representation of G on $\mathcal{H}_i$. With this, an SPT state is any state that satisfies the following three conditions:

- **Short-range entangled:** It can be prepared from a product state by a finite-depth quantum circuit.

[1] Throughout the text, by local, we mean that the support of the operator can be contained in a ball of fixed finite diameter.

[2] Note that, unless otherwise stated, we take the symmetry to be a unitary finite Abelian 0-form symmetry.

- **Symmetric:** It is invariant under the onsite representation of the G symmetry.

- **SPT parent Hamiltonian:** It is the unique ground state of a symmetric local gapped Hamiltonian.

The SPT states are then organized into SPT phases by imposing an equivalence relation. Two SPT states are equivalent, or belong to the same phase, if one can be constructed from the other by a FDQC composed of symmetric gates – with the possible use of ancillary lower-dimensional SPT states. We say an SPT state is trivial if it belongs to the same equivalence class as a product state, whereas a non-trivial SPT state has entanglement that cannot be removed by making symmetry preserving local changes to the state. In other words, a non-trivial SPT state cannot be disentangled by applying a FDQC with symmetric gates.

2.2.2 Anomalous symmetry action at a boundary

Having defined SPT phases, an important question is: what properties characterize an SPT phase? For non-trivial SPT phases, the symmetry action near a boundary is anomalous – i.e., there is an obstruction to finding an *effective* boundary symmetry action that is onsite.[3] In what follows, we give a heuristic description of the effective boundary symmetry action, and we refer to Ref. [46] for more details. In Appendix 2.A, we outline an argument that the obstruction gives a well-defined quantized invariant of the SPT phase.

To describe the effective boundary symmetry action, we first define the boundary Hilbert space. We consider a choice of SPT state along with a parent SPT Hamiltonian on a manifold N without boundary and call the energy gap between the ground state and the first excited state Δ. We then imagine truncating the Hamiltonian to a submanifold M with boundary

[3]Moreover, the effective boundary symmetry action cannot be made onsite through a combination of taking the tensor product with the effective boundary symmetry action of lower-dimensional SPT phases and conjugation by a FDQC.

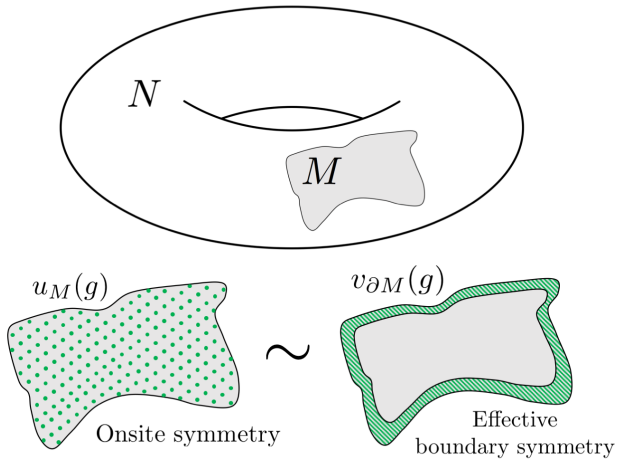

Figure 2.1: To determine the SPT phase associated to a given SPT state, we compute an effective boundary symmetry action. This is done by truncating a corresponding SPT Hamiltonian defined on a closed manifold N to a submanifold M with boundary. In the low-energy Hilbert space of the truncated Hamiltonian, the onsite symmetry action $u_M(g)$ (green dots) on M is equivalent to an effective boundary symmetry action $v_{\partial M}(g)$ (striped green) supported near the boundary of M. The symbol "$\sim$" denotes that $u_M(g)$ and $v_{\partial M}(g)$ are only required to be equivalent in the low-energy Hilbert space. We use the effective boundary symmetry action to show that certain SPT states have symmetry-protected magic in Section 2.3.3.

by removing any terms whose support includes sites outside of M (Fig. 2.1).[4] Furthermore, we use the tensor product structure to restrict the Hilbert space and onsite symmetry to M.

After restricting to M, we expect the spectrum of the truncated Hamiltonian to look qualitatively different – states now possibly lie within the energy window Δ. The boundary Hilbert space is defined as the Hilbert space spanned by the states within the bulk gap Δ. We assume that these low-energy states are similar to the ground state of the un-truncated Hamiltonian in regions far from the boundary.[5] Hence, the low-energy states correspond to excitations localized near the boundary or degenerate ground states.

[4]We assume M is large compared with the Lieb-Robinson length of a FDQC that prepares the ground state of the Hamiltonian on N.

[5]More precisely, the reduced density matrices agree on regions sufficiently far from the boundary. This is the TQO-2 assumption in Refs. [47] and [48].

With this, the effective boundary symmetry action is any unitary linear representation of the G symmetry in the boundary Hilbert space, such that (i) its support is localized[6] near the boundary of M and (ii) its action agrees with the global symmetry on states within the boundary Hilbert space (Fig. 2.1). While the symmetry on M is onsite, the effective boundary symmetry action may be non-onsite.

Ref. [46] showed that certain SPT phases, known as group cohomology phases [49], exhibit an obstruction to an onsite effective boundary symmetry action captured by group cohomology. In particular, in D-dimensions with a G symmetry, the obstruction corresponds to an element of $\mathcal{H}^{D+1}[G, U(1)]$, i.e., the $(D+1)^{\text{th}}$ group cohomology of G with coefficients in $U(1)$. It is believed that $\mathcal{H}^{D+1}[G, U(1)]$ gives a complete classification of (bosonic) SPT phases protected by unitary symmetries in dimensions $D < 4$ [50–52]. We refer to SPT phases characterized by a non-trivial element of $\mathcal{H}^{D+1}[G, U(1)]$ as nontrivial group cohomology phases.

We would like to point out that, according to the Künneth theorem [53], a partial classification of SPT phases protected by a product group $H \times K$ is given by:

$$\mathcal{H}^1[H, \mathcal{H}^D[K, U(1)]]. \tag{2.4}$$

The SPT phases characterized by the group cohomology in Eq. (2.4) are the focus of Proposition 2 in Section 2.3. These SPT phases can be described by decorated domain wall models [54], where the ground state is a superposition of H domain configurations with $(D-1)$-dimensional K SPT states hosted on the domain walls. In Appendix 2.B, we argue that, for some element of H, the corresponding effective boundary symmetry action is implemented by a FDQC that prepares a $(D-1)$-dimensional K SPT state from a product state. The effective boundary symmetry is notably not onsite because the $(D-1)$-dimensional K SPT state is entangled (for $D > 1$).

[6] In particular, we assume the effective boundary symmetry action is supported on M and within a fixed distance from the boundary of M.

2.2.3 Strange correlator

The anomalous symmetry action at a boundary, in the previous section, enforces long-range entanglement in states describing non-trivial SPT phases on a manifold with boundary.[7] This has been shown carefully in one and two spatial dimensions using a tensor network approach [55] and is believed to hold in higher dimensions. We emphasize that on a manifold *without* boundary, the states in an SPT phase are short-range entangled by definition – the long-range entanglement only appears explicitly when a boundary to a trivial SPT phase is exposed.

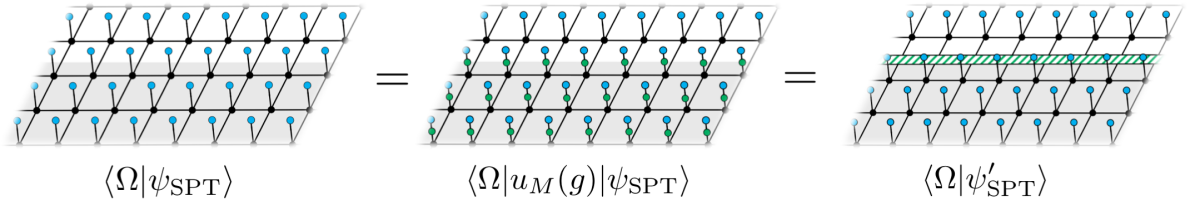

Figure 2.2: The overlap between $\langle\Omega|$ (light blue tensors) and $|\psi_{\mathrm{SPT}}\rangle$ (black tensors) takes the form of a Euclidean partition function for a $(D-1)$-dimensional system, for which, a spacetime configuration corresponds to a set of fixed indices on the virtual bonds. The $(D-1)$-dimensional system defined by $\langle\Omega|\psi_{\mathrm{SPT}}\rangle$ is invariant under an anomalous symmetry if $|\psi_{\mathrm{SPT}}\rangle$ belongs to a non-trivial SPT phase. This can be argued by first using the symmetry of $\langle\Omega|$ to insert the symmetry action $u_M(g)$ (green circles) restricted to a region M (shaded gray). By the arguments in Ref. [56], $u_M(g)$ applied to $|\psi_{\mathrm{SPT}}\rangle$ is equivalent to inserting a certain tensor network operator (striped green) along the virtual bonds on the boundary of M. If $|\psi_{\mathrm{SPT}}\rangle$ is a non-trivial SPT state, then the effective symmetry action on the virtual bonds is anomalous, and the $(D-1)$-dimensional system has an anomalous symmetry. $|\psi'_{\mathrm{SPT}}\rangle$ denotes the state with the tensor network operator applied on the virtual bonds. This motivates the use of strange correlators to prove a symmetry-protected sign problem in certain SPT states (see Section 2.4.2).

One tool that has been developed to probe the long-range entanglement of SPT phases

[7] We note that, by an SPT phase on a manifold with boundary, we have in mind a collection of ground states, where the parent Hamiltonians are truncated SPT Hamiltonians with an arbitrary local symmetric Hamiltonian supported near the boundary.

in the presence of a boundary is the strange correlator [57–60]. The strange correlator takes the general form:

$$\frac{\langle\Omega|\mathcal{O}_i\mathcal{O}_j|\psi_{\mathrm{SPT}}\rangle}{\langle\Omega|\psi_{\mathrm{SPT}}\rangle}, \tag{2.5}$$

where $\langle\Omega|$ is a symmetric product state, $|\psi_{\mathrm{SPT}}\rangle$ is an SPT state on a manifold *without* boundary, and $\mathcal{O}_i$ and $\mathcal{O}_j$ are operators localized near the sites i and j. More specifically, $\mathcal{O}_i$ and $\mathcal{O}_j$ correspond to a strange order parameter, given by a collection of unitary local operators $\{\mathcal{O}_k\}_{k\in\Lambda}$ such that each $\mathcal{O}_k$ has a non-trivial definite charge under the symmetry. That is, for a finite Abelian symmetry G and any $g \in G$, $\mathcal{O}_k$ satisfies:

$$u(g)\mathcal{O}_k u(g)^\dagger = e^{i\kappa(g)}\mathcal{O}_k, \tag{2.6}$$

where $e^{i\kappa(g)}$ forms a non-trivial one dimensional representation of G.

The general expectation is that, for a non-trivial SPT state in either one or two dimensions, there exists a strange order parameter such that the strange correlator in Eq. (2.5) has a power law decay or is constant as the separation between i and j goes to infinity. This is based on numerous examples as well as physical intuition from a tensor network representation of $\langle\Omega|\psi_{\mathrm{SPT}}\rangle$.

Given a tensor network representation of the D-dimensional SPT state $|\psi_{\mathrm{SPT}}\rangle$, we can interpret the overlap $\langle\Omega|\psi_{\mathrm{SPT}}\rangle$ as a partition function for a $(D-1)$-dimensional system, as pictured in Fig. 2.2. The $(D-1)$-dimensional system is invariant under an anomalous symmetry, similar to the anomalous boundary symmetry action of an SPT phase. This can be seen by acting with the symmetry restricted to a subregion M with a boundary. Ref. [56] argued that the symmetry action on M can be replaced with an effective symmetry action on the virtual bonds of the tensor network along the boundary of M (see Fig. 2.2).

For a non-trivial SPT state, the effective symmetry action on the virtual bonds is anomalous, and hence, the $(D-1)$-dimensional partition function $\langle\Omega|\psi_{\mathrm{SPT}}\rangle$ is invariant under an

anomalous symmetry action. This implies that $\langle\Omega|\psi_{\mathrm{SPT}}\rangle$ should be thought of as a partition function for a long-range entangled state, and the strange correlator probes the correlations in this state. Therefore, the strange correlator measures correlations similar to those that arise on the boundary of a state in an SPT phase. (See also Refs. [57] and [58] for a physical interpretation of the strange correlator.)

The use of strange correlators can be rigorously justified for 1D SPT states using the notion of string-order parameters. We illustrate this for the cluster state assuming the working definition of SPT phases, given in Section 2.2.1. We claim that the argument can be generalized straightforwardly to other 1D SPT states.

2.2.4 Example: cluster state

To make the discussion more concrete, we describe the cluster state, an example of a non-trivial 1D SPT state with a $\mathbb{Z}_2 \times \mathbb{Z}_2$ symmetry. The cluster state is defined on a 1D lattice with $2N$ qubits and periodic boundary conditions. We denote the Pauli X and Pauli Z operator at the site i by X_i and Z_i, respectively. The onsite $\mathbb{Z}_2 \times \mathbb{Z}_2$ symmetry is then generated by the operators:

$$u((g,1)) \equiv \prod_j X_{2j}, \quad u((1,g)) \equiv \prod_j X_{2j+1}, \tag{2.7}$$

where we have labeled the elements of $\mathbb{Z}_2 \times \mathbb{Z}_2$ as:

$$\mathbb{Z}_2 \times \mathbb{Z}_2 = \{(1,1),(g,1),(1,g),(g,g)\}. \tag{2.8}$$

The cluster state can be prepared from a product state by the FDQC $\mathcal{U}_{\mathrm{CS}}$ given as:

$$\mathcal{U}_{\mathrm{CS}} \equiv \prod_{\langle i,i+1\rangle} CZ_{i(i+1)}. \tag{2.9}$$

Here, the product is over pairs of neighboring sites, and the control-Z operator $CZ_{i(i+1)}$ is

the two qubit operator whose action on an arbitrary computational basis state $|a\rangle_i|b\rangle_{i+1}$ is:

$$CZ_{i(i+1)}|a\rangle_i|b\rangle_{i+1} = (-1)^{ab}|a\rangle_i|b\rangle_{i+1}, \quad a, b \in \{0, 1\}. \tag{2.10}$$

Explicitly, the cluster state is:

$$|\psi_{\text{CS}}\rangle \equiv \mathcal{U}_{\text{CS}}|+\ldots+\rangle, \tag{2.11}$$

where $|+\ldots+\rangle$ is the simultaneous $+1$ eigenstate of all Pauli X operators.

A parent Hamiltonian for the cluster state is:

$$H_{\text{CS}} \equiv \mathcal{U}_{\text{CS}} \left(-\sum_i X_i \right) \mathcal{U}_{\text{CS}}^\dagger = -\sum_{i=1}^{2N} Z_{i-1} X_i Z_{i+1}. \tag{2.12}$$

H_{CS} is gapped and has a unique ground state given that it has the same spectrum as the paramagnet Hamiltonian: $-\sum_i X_i$. Further, it can be checked that each term of H_{CS} is symmetric. Therefore, H_{CS} is an SPT Hamiltonian.

To see that the ground state is in a non-trivial SPT phase, we introduce a boundary and study the effective symmetry action near the boundary, as described below.

Anomalous boundary symmetry action

In dimension $D = 1$, SPT phases with a G symmetry are classified by $\mathcal{H}^2[G, U(1)]$, where the elements of $\mathcal{H}^2[G, U(1)]$ correspond to projective representations of G [61, 62]. We compute an effective boundary symmetry action for the cluster state model and show that it forms a projective representation of $\mathbb{Z}_2 \times \mathbb{Z}_2$. This is the non-trivial element of $\mathcal{H}^2[\mathbb{Z}_2 \times \mathbb{Z}_2, U(1)] = \mathbb{Z}_2$.

To start, we truncate the Hamiltonian H_{CS} in Eq. (2.12) to a lattice with $2M$ sites and open boundary conditions. This gives us the Hamiltonian H_{CS}^M:

$$H_{\text{CS}}^M \equiv -\sum_{i=2}^{2M-1} Z_{i-1} X_i Z_{i+1}. \tag{2.13}$$

H^M_{CS} has a 4-fold degenerate ground state subspace, which follows from the fact that we have removed the terms associated to the sites $i = 1$ and $i = 2M$. The degenerate ground state subspace of H^M_{CS} defines the boundary Hilbert space.

We now derive an effective boundary symmetry action. The states in the boundary Hilbert space are $+1$ eigenstates of the terms in H^M_{CS}, since the terms are mutually commuting and un-frustrated. Therefore, in the boundary Hilbert space, we have:

$$Z_{i-1}X_iZ_{i+1} \sim 1, \quad \forall i \in \{2, \ldots, 2M-1\}, \tag{2.14}$$

where $\sim$ emphasizes that this holds in the boundary Hilbert space. Using the relation in Eq. (2.14), the generators of the $\mathbb{Z}_2 \times \mathbb{Z}_2$ symmetry can be written in the boundary Hilbert space as:

$$u\big((g,1)\big) \sim Z_1(Z_{2M-1}X_{2M}), \quad u\big((1,g)\big) \sim (X_1Z_2)Z_{2M}. \tag{2.15}$$

We define the right-hand side of the equations in Eq. (2.15) as the operators:

$$v\big((g,1)\big) \equiv Z_1(Z_{2M-1}X_{2M}), \quad v\big((1,g)\big) \equiv (X_1Z_2)Z_{2M}. \tag{2.16}$$

These define a $\mathbb{Z}_2 \times \mathbb{Z}_2$ effective boundary symmetry action, since they form a unitary linear representation of $\mathbb{Z}_2 \times \mathbb{Z}_2$, are localized near the boundary, and, by definition, agree with the global symmetry action in the boundary Hilbert space.

The effective boundary symmetry action generated by the operators in Eq. (2.16) is not onsite – i.e., it is not in the form of a tensor product of linear representations at each site (as defined in Section 2.2.1). Instead, the action at endpoints $i = 1$ and $i = 2M$ are independently projective representations of $\mathbb{Z}_2 \times \mathbb{Z}_2$. For example, at the endpoint $i = 1$, we have:

$$v_{i=1}\big((g,1)\big) \equiv Z_1, \quad v_{i=1}\big((1,g)\big) \equiv X_1Z_2. \tag{2.17}$$

These give a projective representation, as can be seen by the commutation relations between $v_{i=1}((g,1))$ and $v_{i=1}((1,g))$:

$$v_{i=1}((g,1))v_{i=1}((1,g)) = -v_{i=1}((1,g))v_{i=1}((g,1)). \tag{2.18}$$

Thus, the effective boundary symmetry action is anomalous.[8] In Appendix 2.A, we show that the anomalous symmetry action implies that the cluster state cannot be disentangled by a FDQC composed of symmetric gates.

Strange correlator

For the cluster state, we can use the exactly solvable Hamiltonian H_{CS} to identify a suitable strange order parameter. To see this, we consider the product of Hamiltonian terms:

$$\prod_{k=i}^{j-1} Z_{2k}X_{2k+1}Z_{2k+2} = (\prod_{k=i}^{j-1} X_{2k+1})Z_{2i}Z_{2j}. \tag{2.19}$$

This gives us the identity:

$$\langle+\ldots+|\psi_{\text{CS}}\rangle = \langle+\ldots+|(\prod_{k=i}^{j-1} X_{2k+1})Z_{2i}Z_{2j}|\psi_{\text{CS}}\rangle = \langle+\ldots+|Z_{2i}Z_{2j}|\psi_{\text{CS}}\rangle, \tag{2.20}$$

where the first equality comes from the fact that $|\psi_{\text{CS}}\rangle$ is a $+1$ eigenstate of each term of H_{CS}, and the second equality uses that $\langle+\ldots+|$ is a $+1$ eigenstate of every Pauli X operator. From Eq. (2.20), we have:

$$\frac{\langle+\ldots+|Z_{2i}Z_{2j}|\psi_{\text{CS}}\rangle}{\langle+\ldots+|\psi_{\text{CS}}\rangle} = 1, \tag{2.21}$$

for any choice of i and j. By redefining the sites so that the pair of sites $2k-1$ and $2k$ form a single site labeled by k, we can use the set $\{Z_{2k}\}$ as a strange order parameter. Moreover, we

[8] Importantly, the projective representations at the endpoints cannot be made into linear representations by conjugating by a FDQC.

have found a strange order parameter for $|\psi_{\text{CS}}\rangle$ such that the strange correlator is constant in the separation of $2i$ and $2j$, according to Eq. (2.21).

As for other states in the same phase as $|\psi_{\text{CS}}\rangle$, we can use the operator in Eq. (2.19) to identify a strange order parameter for which the strange correlator is constant in the limit $|i-j| \to \infty$. For example, let $|\psi'_{\text{CS}}\rangle$ be the state prepared from $|\psi_{\text{CS}}\rangle$ by the FDQC $\mathcal{U}_{\text{sym}}$ composed of symmetric gates:

$$|\psi'_{\text{CS}}\rangle \equiv \mathcal{U}_{\text{sym}}|\psi_{\text{CS}}\rangle. \tag{2.22}$$

$|\psi'_{\text{CS}}\rangle$ is invariant under the operator:

$$\mathcal{U}_{\text{sym}} \left[(\prod_{k=i}^{j-1} X_{2k+1}) Z_{2i} Z_{2j} \right] \mathcal{U}^{\dagger}_{\text{sym}}. \tag{2.23}$$

Since $\mathcal{U}_{\text{sym}}$ is built from symmetric gates, the operator in Eq. (2.23) is equal to:

$$(\prod_{k=i}^{j-1} X_{2k+1}) \mathcal{O}_i \mathcal{O}_j, \tag{2.24}$$

for some unitary local charged operators $\mathcal{O}_i$ and $\mathcal{O}_j$. Following Eqs. (2.20) and (2.21), we can define a strange order parameter from the collection of $\mathcal{O}_i$ and $\mathcal{O}_j$ for varying endpoints i and j. Thus, every state in the SPT phase (as defined in Section 2.2.1) admits a strange order parameter with a constant strange correlator.

We note that the operators in Eqs. (2.20) and (2.23) are the more familiar string-order parameters that characterize 1D SPT phases. These naturally lead to strange order parameters with a constant strange correlation.

2.3 Symmetry-protected magic

In this section, we introduce symmetry-protected magic and demonstrate that it is a feature of a large class of SPT states. To start, we review the stabilizer formalism and describe how

it can be simulated efficiently on a classical computer. The stabilizer formalism is insufficient for universal quantum computing, but leads to the concept of magic – a resource that can be used to help overcome the limitations of the stabilizer formalism. We then define the notion of symmetry-protected magic and use it to assess the magic in SPT states. In particular, we show that SPT states belonging to group cohomology phases in $D \geq 2$ dimensions have symmetry-protected magic.

2.3.1 Review of the stabilizer formalism

The stabilizer formalism has been instrumental to our understanding of the complexity of quantum phases of matter, as it often provides simple, workable examples. In this section, we give a brief review of the stabilizer formalism to ensure the text is self-contained. We refer to Refs. [16, 63–66] for more thorough reviews.

To make the discussion general, we first define a generalization of Pauli operators to q-dimensional Hilbert spaces, i.e., to qudits. The computational basis states, in this case, are labeled by $j \in \mathbb{Z}_q$, and the usual Pauli Z and Pauli X operators are generalized to:

$$Z \equiv \sum_{j \in \mathbb{Z}_q} e^{\frac{2\pi i}{q} j} |j\rangle\langle j|, \quad X \equiv \sum_{j \in \mathbb{Z}_q} |j+1\rangle\langle j|. \tag{2.25}$$

If q is odd, then the set of Pauli operators on a qudit is generated by products of Z and X, and if q is even, the Pauli operators are generated by Z, X, and the phase i.[9] For systems of more than one qudit, we call a tensor product of Pauli operators a Pauli string. Furthermore, we say a Pauli string is Z-type or X-type if, up to a phase, it consists of only products of Z operators or products of X operators, respectively.

With this, we introduce Clifford unitaries and stabilizer states. A Clifford unitary is any unitary operator that maps Pauli strings to Pauli strings by conjugation. Explicitly, for any

[9] The group generated by the Pauli operators is commonly called the Heisenberg-Weyl group.

Pauli string P, a Clifford unitary U satisfies:

$$UPU^\dagger = Q, \tag{2.26}$$

for some Pauli string Q. A stabilizer state is then any state that can be generated by applying a Clifford unitary to the computational basis state $|0\ldots0\rangle$. Here, $|0\ldots0\rangle$ is the simultaneous $+1$ eigenstate of every Pauli Z operator. Thus, by definition, a stabilizer state $|\psi_{\mathcal{S}}\rangle$ can always be written as:

$$|\psi_{\mathcal{S}}\rangle = U|0\ldots0\rangle, \tag{2.27}$$

for some Clifford unitary U.

At this point, one can define a computational scheme based on applying Clifford unitaries to stabilizer states and making measurements of Pauli strings. However, this restricted set of operations - the stabilizer operations - can be efficiently simulated by a classical computer. This is the statement of the Gottesman–Knill theorem [17] and a consequence of the fact that a stabilizer state can be fully characterized by a stabilizer group, as described below.

Indeed, for every stabilizer state $|\psi_{\mathcal{S}}\rangle$, we can find a group $\mathcal{G}$ of mutually commuting Pauli strings such that $|\psi_{\mathcal{S}}\rangle$ is the unique state satisfying:

$$S|\psi_{\mathcal{S}}\rangle = |\psi_{\mathcal{S}}\rangle, \quad \forall S \in \mathcal{G}. \tag{2.28}$$

We refer to the elements in $\mathcal{G}$ as stabilizers and call the group $\mathcal{G}$ a stabilizer group. We say the stabilizer group $\mathcal{G}$ "stabilizes" or "fixes" $|\psi_{\mathcal{S}}\rangle$ to mean that $|\psi_{\mathcal{S}}\rangle$ is in the simultaneous $+1$ eigenspace of all of the stabilizers. More generally, any group of mutually commuting Pauli strings is a stabilizer group, although it may not fix a unique stabilizer state.

To find a suitable stabilizer group for $|\psi_{\mathcal{S}}\rangle$, we first consider the state $|0\ldots0\rangle$. $|0\ldots0\rangle$ is

uniquely stabilized by the stabilizer group $\mathcal{G}_0$ generated by a Pauli Z operator for each site:

$$\mathcal{G}_0 \equiv \langle Z_i : i \in \text{sites} \rangle. \tag{2.29}$$

From this, we can identify a stabilizer group $\mathcal{G}$ that uniquely fixes $|\psi_{\mathcal{S}}\rangle$. To do so, we conjugate the elements of $\mathcal{G}_0$ by a choice of Clifford unitary U that prepares $|\psi_{\mathcal{S}}\rangle$ from $|0 \ldots 0\rangle$, as in Eq. (2.27):

$$\mathcal{G} \equiv \langle U Z_i U^\dagger : i \in \text{sites} \rangle. \tag{2.30}$$

By construction, the stabilizer group $\mathcal{G}$ in Eq. (2.30) is generated by N Pauli strings, where N is the number of sites. The state can therefore be efficiently specified by a stabilizer group, and moreover, the effects of evolution by a Clifford unitary and measurements of Pauli strings can be determined by appropriately modifying the stabilizer group. We see that the stabilizer operations are no more powerful than a classical computer, and additional ingredients are needed to promote it to a universal set of operations.

Before describing how the stabilizer formalism can be supplemented to achieve universal quantum computation, we remark that the generators of a stabilizer group can be used to build a stabilizer Hamiltonian. More specifically, given a stabilizer group $\mathcal{G}$ that uniquely stabilizes a state $|\psi_{\mathcal{S}}\rangle$, we can construct a Hamiltonian:

$$H_{\mathcal{S}} \equiv -\sum_{S \in \mathcal{S}} S + \text{h.c.}, \tag{2.31}$$

where $\mathcal{S}$ denotes a set of stabilizers that generate $\mathcal{G}$. The unique ground state of $H_{\mathcal{S}}$ is $|\psi_{\mathcal{S}}\rangle$, since it is a $+1$ eigenstate of each $S \in \mathcal{S}$ and is uniquely fixed by $\mathcal{G}$. We note that $H_{\mathcal{S}}$ might not be local.

2.3.2 Definition of symmetry-protected magic

Stabilizer operations, reviewed in the previous section, can be simulated efficiently on a classical computer, but the full power of quantum computation can be recovered by supplementing the stabilizer operations with ancillary non-stabilizer states. In fact, any non-stabilizer (pure) state can be used as ancillary states to promote the stabilizer operations to a universal set of operations. In this context, the non-stabilizer states are referred to as magic states. In a precise sense, the magic of a state (or the "non-stabilizerness") can be treated as a resource, similar to viewing entanglement as a resource. Consequently, resource-theoretical tools have been developed to quantify the amount of magic in a state (see e.g., Refs. [16, 67–70]), however few analytical statements have been made about magic in many-body systems. To make progress in this direction, we define the following coarse measure of the magic to help understand the large-scale structure of magic in a many-body state:

Definition 2 (Long-range magic) *A state $|\psi\rangle$ has long-range magic, if, for any finite-depth quantum circuit $\mathcal{U}$, the state $\mathcal{U}|\psi\rangle$ is a magic state.*

In other words, a state with long-range magic has magic that cannot be removed by any FDQC. In this sense, the state can serve as a robust source of magic. We would like to point out that concepts similar to long-range magic have been recently introduced in Ref. [27] in the context of conformal field theories. We hope to comment on long-range magic in future work, but in the present text we focus on a restricted notion of long-range magic.

In particular, we consider magic that cannot be removed by any FDQC composed of *symmetric* gates. We say such a state has symmetry-protected magic. This is defined more precisely as:

Definition 3 (Symmetry-protected magic) *A state $|\psi\rangle$ has symmetry-protected magic, if, for any finite-depth quantum circuit $\mathcal{U}_{sym}$ composed of symmetric gates, the state $\mathcal{U}_{sym}|\psi\rangle$ is a magic state.*

As a proof of concept, we show that certain SPT states have symmetry-protected magic.

2.3.3 Symmetry-protected magic in SPT states

Our main objective in this section is to show that SPT states, in particular those belonging to non-trivial group cohomology phases in dimensions $D \geq 2$, have symmetry-protected magic. This includes, for example, the $\mathbb{Z}_2$ SPT model introduced in Ref. [71]. We divide our results into two propositions. Proposition 1 applies to SPT states belonging to group cohomology phases protected by a symmetry of the form $\mathbb{Z}_q^m$ (a product of m copies of $\mathbb{Z}_q$) and assumes that the state is defined on a system of q-dimensional qudits. Proposition 2 only applies to a subset of group cohomology phases, but makes no assumption on the dimension of the qudits. In both cases, the proof relies on the anomalous boundary symmetry action characteristic of non-trivial group cohomology SPT phases (see Section 2.2.2). After proving the two propositions, we comment on SPT states that fall outside of our argument – these correspond to SPT phases that can indeed be described efficiently by the stabilizer formalism.

Proposition 1 *Any SPT state belonging to a non-trivial group cohomology phase in $D \geq 2$ dimensions protected by a $G = \mathbb{Z}_q^m$ symmetry has symmetry protected magic, if it is defined on q-dimensional qudits and the symmetry is represented by tensor products of Pauli operators.*

Proof of Proposition 1. We defined SPT phases as collections of SRE states that are equivalent under FDQCs composed of symmetric gates. Therefore, if an SPT state has symmetry-protected magic, it implies that every state in the SPT phase must be a magic state. To prove the proposition, it is then sufficient to show that there are no stabilizer states belonging to non-trivial group cohomology phases in $D \geq 2$ dimensions with a G symmetry represented by Pauli strings.

With this, we proceed by deriving a contradiction. We assume that there is a stabilizer state $|\psi_{\mathcal{S}}\rangle$ belonging to a non-trivial group cohomology phase in $D \geq 2$ dimensions protected by a G symmetry represented by a Pauli string $P(g)$ for every $g \in G$. We argue that this is in conflict with the anomalous boundary symmetry action expected in the non-trivial SPT phase.

The first step is to find a local symmetric stabilizer Hamiltonian whose unique ground state is $|\psi_{\mathcal{S}}\rangle$. Since $|\psi_{\mathcal{S}}\rangle$ is an SPT state, it has a local parent Hamiltonian (albeit possibly non-stabilizer), and it is invariant under the G symmetry, i.e., $P(g)|\psi_{\mathcal{S}}\rangle = |\psi_{\mathcal{S}}\rangle$, for all $g \in G$. In Appendix 2.C, we show that this, in fact, implies that there exists a local symmetric stabilizer Hamiltonian $H_{\mathcal{S}}$ whose unique ground state is $|\psi_{\mathcal{S}}\rangle$ and which commutes with the G symmetry (see Lemma 2).

We can now determine the SPT phase by using $H_{\mathcal{S}}$ to compute the anomalous symmetry action at the boundary (analogous to the calculation of the anomalous boundary symmetry action for the cluster state in Section 2.2.4). For this purpose, we introduce a boundary by truncating the Hamiltonian $H_{\mathcal{S}}$ to a region M with boundary. We define the truncated Hamiltonian $H_{\mathcal{S}}^{M}$ by removing any term whose support is not entirely contained within M.[10] The global symmetry action $P(g)$ can also be restricted to M using that $P(g)$ is a tensor product of linear representations $P_i(g)$ of G:

$$P(g) \equiv \prod_i P_i(g) \to P_M(g) \equiv \prod_{i \in M} P_i(g). \tag{2.32}$$

The truncated Hamiltonian has a G symmetry represented by the operators $P_M(g)$, given above.

Similar to $H_{\mathcal{S}}$, the truncated Hamiltonian is a sum of symmetric commuting stabilizer terms, but unlike $H_{\mathcal{S}}$, it will generically have a ground state degeneracy, and the degenerate ground state subspace forms the boundary Hilbert space. The anomalous behavior of the symmetry, characteristic of the SPT phase, is revealed by the effective symmetry action on the boundary Hilbert space. We recall from Section 2.2.2 that the effective boundary symmetry action is any operator localized near the boundary of M, whose action is equivalent to the symmetry action of $P_M(g)$, within the boundary Hilbert space.

The effective symmetry action at the boundary can be computed by first observing that

[10] To avoid pathologies, we require that M is large compared to the size of the supports of the terms in $H_{\mathcal{S}}$. More precisely, we require $d_M \gg d_S$, where d_M is the diameter of the largest ball inscribing M, and d_S is the minimum diameter such that the support of each stabilizer term fits within a ball of diameter d_S.

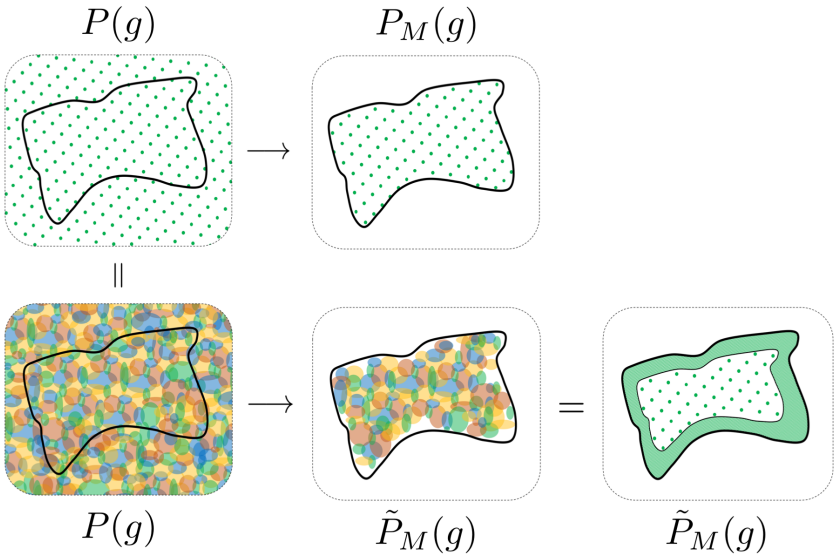

Figure 2.3: We determine the effective boundary symmetry action from $H_{\mathcal{S}}$ by first observing that the global symmetry $P(g)$, for any $g \in G$, can be expressed as a product of terms in $H_{\mathcal{S}}$ (the supports of the stabilizer terms are depicted with colored ovals). The global symmetry action can be restricted to a submanifold M (outlined in black) in two ways. Restricting to M by using the tensor product structure of $P(g)$ results in $P_M(g)$, while restricting to M using the product of stabilizer terms gives $\tilde{P}_M(g)$. $\tilde{P}_M(g)$ acts like the onsite symmetry away from the boundary of M.

the global symmetry action $P(g)$ can be written as a product of the stabilizer terms of the un-truncated Hamiltonian $H_{\mathcal{S}}$. This is because, $H_{\mathcal{S}}$ commutes with $P(g)$ and has a unique ground state. Therefore, $P(g)$ is contained in the stabilizer group generated by the terms of $H_{\mathcal{S}}$ (see Lemma 1 in Appendix 2.C). Consequently, $P(g)$ can be written as:

$$P(g) = \prod_{S_j \in \mathcal{S}_{P(g)}} S_j, \tag{2.33}$$

where $\mathcal{S}_{P(g)}$ is defined as the set of terms in $H_{\mathcal{S}}$ whose product is $P(g)$. By using the expression for $P(g)$ in Eq. (2.33), $P(g)$ can instead be truncated to M by retaining only the

stabilizers S_j whose support $\text{supp}(S_j)$ is entirely contained in M (see Fig. 2.3):

$$\tilde{P}_M(g) \equiv \prod_{\substack{S_j \in \mathcal{S}_{P(g)} \\ \text{supp}(S_j) \subset M}} S_j. \tag{2.34}$$

We note that $\tilde{P}_M(g)$ is a product of terms in $H_{\mathcal{S}}^M$ and as such, acts as the identity on the boundary Hilbert space. This implies, in particular, that $P_M(g)$ is equivalent to $P_M(g)\tilde{P}_M^\dagger(g)$ in the boundary Hilbert space. Further, by comparing Eqs. (2.33) and (2.34), we see that the action of $\tilde{P}_M(g)$ is equivalent to that of $P(g)$ on sites in M greater than a fixed distance from the boundary of M. Therefore, the support of $P_M(g)\tilde{P}_M^\dagger(g)$ is contained in M and localized near the boundary of M. As a result, we can take the effective boundary symmetry action to be:

$$\mathcal{P}(g) \equiv P_M(g)\tilde{P}_M^\dagger(g). \tag{2.35}$$

The effective boundary symmetry action in Eq. (2.35) forms a linear representation of $G = \mathbb{Z}_q^m$ in the boundary Hilbert space. This means that it obeys the group laws of G up to products of stabilizer terms in $H_{\mathcal{S}}^M$. In Appendix 2.D, we show that, assuming the system is defined on q-dimensional qudits, the effective boundary symmetry action can be modified by stabilizers in $H_{\mathcal{S}}^M$ to guarantee that the group relations are satisfied exactly. We denote the modified effective boundary symmetry action by $\mathcal{P}'(g)$.

The characteristic group cohomology class of the SPT order can be deduced from the modified effective boundary symmetry action using the methods of Ref. [46], where the group cohomology class manifests as an obstruction to realizing the effective boundary symmetry action onsite (as a tensor product of linear representations at each site). From the definition of $\mathcal{P}'(g)$ in Appendix 2.D, it can be seen that $\mathcal{P}'(g)$ is a tensor product of Pauli operators:

$$\mathcal{P}'(g) = \prod_k \mathcal{P}'_k(g), \tag{2.36}$$

with the product over sites k in M close to the boundary of M. While $\mathcal{P}'(g)$ forms a linear representation of G in the boundary Hilbert space, the operators $\mathcal{P}'_k(g)$ might only satisfy the group laws projectively. In dimensions $D \geq 2$ this does not pose an obstruction to an onsite representation of the effective boundary symmetry action. The algorithm in Ref. [46] shows that the effective boundary symmetry action in Eq. (2.36) corresponds to the trivial element of $\mathcal{H}^{D+1}[G, U(1)]$ (if $D \geq 2$).

To motivate this conclusion, we argue that any projective representations formed by $\mathcal{P}'_k(g)$ can be resolved by modifying $H_{\mathcal{S}}$ with decoupled 1D SPT Hamiltonians acting on ancillary qudits. Importantly, the 1D SPT Hamiltonians do not change the $D \geq 2$ SPT phase described by $H_{\mathcal{S}}$. Moreover, the 1D SPT Hamiltonians can always be chosen so that their projective effective boundary symmetry actions (see Section 2.2.4, for example) compensate for the projective representations formed by the $\mathcal{P}'_k(g)$. Then by locally redefining the sites, the projective representation from $\mathcal{P}'_k(g)$ and the effective boundary symmetry of the 1D SPT phases form a linear representation on the composite site.

Therefore, the effective boundary symmetry action in Eq. (2.36) is non-anomalous, and by the universality of the anomalous boundary symmetry action (see Appendix 2.A), $|\psi_{\mathcal{S}}\rangle$ cannot be a member of a non-trivial group cohomology SPT phase in $D \geq 2$. This contradicts the initial assumption and implies that there are no stabilizer states in non-trivial group cohomology SPT phases in $D \geq 2$ dimensions protected by a symmetry represented by Pauli strings. Thus, the non-trivial SPT states described in the proposition have symmetry-protected magic. □

Note that Proposition 1 assumes that the SPT state is defined on a system of q-dimensional qudits for a symmetry $\mathbb{Z}_q^m$. For some SPT phases, we expect that the restriction on the dimension of the qudits is necessary. In future work, we hope to comment on a stabilizer model for a non-trivial $\mathbb{Z}_2$ SPT phase in $D = 2$ dimensions defined on a system of 4-dimensional qudits.

On the other hand, there are group cohomology phases for which the restriction on the

dimension of the qudits in Proposition 1 is unnecessary. A stronger statement can be made for SPT phases that can be described by a decorated domain wall model, i.e., the SPT phase is protected by a symmetry of the form $H \times K$ and characterized by an element of $\mathcal{H}^1[H, \mathcal{H}^D[K, U(1)]]$. We formulate this as Proposition 2.

Proposition 2 *Any SPT state belonging to an $H \times K$ SPT phase in $D \geq 2$ dimensions characterized by a non-trivial element of $\mathcal{H}^1[H, \mathcal{H}^D[K, U(1)]]$ has symmetry protected magic, if the symmetry is represented by tensor products of Pauli operators.*

Proof of Proposition 2. We let $|\psi_{\mathcal{S}}\rangle$ be a stabilizer state within an $H \times K$ SPT phase in $D \geq 2$ dimensions. Following the proof of Proposition 1, we identify a local stabilizer parent Hamiltonian $H_{\mathcal{S}}$ for $|\psi_{\mathcal{S}}\rangle$ and define an effective boundary symmetry action as in Eq. (2.35).

We argue that the effective boundary symmetry action of the stabilizer model is unable to reproduce the anomalous symmetry action of an SPT phase characterized by a non-trivial element of $\mathcal{H}^1[H, \mathcal{H}^D[K, U(1)]]$. In Appendix 2.B we prove that, the effective boundary symmetry action for some element of $H \times K$ must be a FDQC that prepares a non-trivial $(D-1)$-dimensional K SPT state from a trivial SPT state. The effective boundary symmetry action of the stabilizer model, however, is a Pauli string for every element of $H \times K$. Pauli strings are insufficient for constructing a non-trivial $(D-1)$-dimensional K SPT state from a trivial SPT state if $D \geq 2$. Therefore, $|\psi_{\mathcal{S}}\rangle$ cannot belong to an SPT phase characterized by a non-trivial element of $\mathcal{H}^1[H, \mathcal{H}^D[K, U(1)]]$. □

The simplest example of an SPT phase that satisfies the conditions of Proposition 2 is a $\mathbb{Z}_2 \times \mathbb{Z}_2 \times \mathbb{Z}_2$ SPT phase in $D = 2$ dimensions. In this case, H and K are equal to $\mathbb{Z}_2$ and $\mathbb{Z}_2 \times \mathbb{Z}_2$, respectively. As argued in Appendix 2.B, the effective boundary symmetry action corresponding to the generator of H prepares a $\mathbb{Z}_2 \times \mathbb{Z}_2$ SPT state from a product state. Proposition 2 tells us that every state belonging to this SPT phase has magic, assuming the symmetry is represented by a Pauli string.

In Propositions 1 and 2, we have shown that a large class of SPT states have symmetry-protected magic. However, there are notable examples of SPT states without symmetry-protected magic. For example, the cluster state, described in Section 2.2.4, is a stabilizer state. In this case, the anomalous boundary symmetry action corresponds to projective representations, and there is no obstruction to forming projective representations with Pauli strings. As another example, the ground state of the 2D CZX-model in Ref. [55] is a stabilizer state, but the onsite symmetry is not represented by a product of Pauli operators.

There are also well-known examples of stabilizer states in non-trivial SPT phases protected by subsystem symmetries (e.g. the 2D cluster state) [72, 73] or protected by higher-form symmetries (e.g. the 3D cluster state) [36, 74–78]. In our argument, we assumed that the protecting symmetry is a 0-form symmetry, i.e., it is supported on a codimension-0 manifold. The assessment of the anomalous nature of the effective boundary symmetry action was specific to 0-form SPT phases. We expect that the proposition can be generalized by accounting for the anomalies associated to subsystem SPT phases and higher-form SPT phases, as described in Refs. [72] and [79]. Evidently, in some cases, the anomalous boundary symmetry action of these SPT phases can be described by Pauli operators.

We have qualified that Propositions 1 and 2 apply to SPT phases classified by group cohomology, but our results may be more general. There are, in fact, known SPT phases in dimensions $D \geq 3$ that are outside of the group cohomology classification – aptly named the beyond cohomology phases [51, 80]. In dimension $D = 3$, there is a beyond cohomology phase protected by time-reversal symmetry that admits a stabilizer representation [81]. However, this SPT phase falls outside of the purview of our argument, since the symmetry is anti-unitary and is not represented by Pauli strings. On the other hand, in $D = 4$, there is a beyond cohomology SPT phase protected by a unitary $\mathbb{Z}_2$ symmetry represented by a Pauli string [82], and we expect the proof of Proposition 1 applies in this case. Indeed, it was recently argued that the effective boundary symmetry action of the SPT phase corresponds to a non-trivial 3D quantum cellular automaton [82, 83]. The operator in Eq. (2.36) is certainly a trivial quantum cellular automaton.

2.4 Symmetry-protected sign problem

The sign problem is a notorious obstacle in efficiently simulating many-body quantum systems using Monte Carlo methods. Often, the sign problem refers to a difficulty in writing the partition function of a quantum system as a classical partition function with non-negative Boltzmann weights. Here, however, our focus is on a sign problem that manifests in the sign structure of a quantum state [4], i.e., in the complex amplitudes of a wave function. Therefore, to get started, we state the sign problem of interest. Then, we define a symmetry-constrained variation of the sign problem, which we call the symmetry-protected sign problem. We illustrate this concept by showing that a subset of SPT states exhibits a symmetry-protected sign problem.

2.4.1 Definition of symmetry-protected sign problem

Complex probability amplitudes are a key feature of quantum states and are essential for describing non-classical phenomena such as quantum interference. For this reason, a non-negative wave function can be regarded as more classical, and indeed, the amplitudes of a non-negative wave function correspond to (the square root of) a classical probability distribution. Whether a state has non-negative amplitudes, however, is basis dependent, i.e., it may be possible to remove a complex sign structure by making a local basis change. This motivates defining the following sign problem at the level of probability amplitudes:

Definition 4 (Sign problem) *A state $|\psi\rangle$ has a sign problem relative to a basis $\{|\alpha\rangle\}$, if, for any finite-depth quantum circuit $\mathcal{U}$, at least one amplitude of the state $\mathcal{U}|\psi\rangle$ in the basis $\{|\alpha\rangle\}$ is outside of the set $\mathbb{R}_{\geq 0}$.*

It is natural to take the basis $\{|\alpha\rangle\}$ to be the computational basis and to interpret the FDQC $\mathcal{U}$ as a local basis change – then, a state has a sign problem if there is no local basis in which

the amplitudes of the state are all non-negative. We make the basis $\{|\alpha\rangle\}$ explicit here to more readily generalize to a symmetry-protected sign problem below.

It remains an open question as to whether any many-body system exhibits a sign problem in the sense above. We note that, in Refs. [12, 30, 31], it is shown that certain topological phases of matter have an obstruction to finding a parent Hamiltonian that is stoquastic - i.e., where the off-diagonal matrix elements of the Hamiltonian are all non-positive [84, 85]. While a stoquastic parent Hamiltonian is sufficient to guarantee that the ground state is non-negative, it is not necessary. Nonetheless, it is natural to conjecture that these same phases of matter exhibit a sign problem related to the sign structure of a ground state wave function.

Notably, SPT states do not have a sign problem. This is because SPT states can be disentangled into a product state by applying a FDQC (see also [86]). However, we consider a symmetry-protected variant of the sign problem, and show that certain SPT states indeed exhibit a *symmetry-protected* sign problem, defined as:

Definition 5 (Symmetry-protected sign problem) *A state $|\psi\rangle$ has a symmetry-protected sign problem relative to a basis $\{|\alpha\rangle\}$, if, for any finite-depth quantum circuit $\mathcal{U}_{sym}$ composed of symmetric gates, at least one amplitude of the state $\mathcal{U}_{sym}|\psi\rangle$ in the basis $\{|\alpha\rangle\}$ is outside of the set $\mathbb{R}_{\geq 0}$.*

In other words, relative to the reference basis $\{|\alpha\rangle\}$, there are no symmetry-preserving local basis changes that make the wave function non-negative. With this simplification of the sign problem to symmetry-preserving basis changes, we are able to show that particular SPT phases have a symmetry-protected sign problem.

2.4.2 Symmetry-protected sign problem for SPT states

In this section, we argue that SPT states in dimensions $D \leq 2$ have a symmetry-protected sign problem in the symmetry-charge basis, where a symmetry-charge basis is a basis of product states in which the symmetry is diagonal [87, 88]. Our proof relies on strange correlators,

defined in Section 2.2.3, and before stating the main proposition, we would like to emphasize:

Remark: Every non-trivial 1D SPT state, as defined in Section 2.2.1, has a strange order parameter with constant strange correlations. This is a consequence of the existence of string order parameters, described in Section 2.2.4. As for higher dimensional SPT phases, it is conjectured that every non-trivial SPT state in 2D has a strange order parameter that has power law decaying or constant strange correlations (see the argument in Section 2.2.3).

Proposition 3 *Let $|\psi_{SPT}\rangle$ be a state belonging to an SPT phase such that, for every state in the SPT phase, there exists a strange order parameter with power law decaying or constant strange correlations. Then $|\psi_{SPT}\rangle$ has a symmetry-protected sign problem relative to product state bases in which the symmetry is represented by products of diagonal Pauli operators.*

Proof of Proposition 3. Without loss of generality, we assume the symmetry is represented by X-type Pauli strings, which are diagonal in the X-basis.

We derive a contradiction by assuming, contrary to the proposition, that $|\psi_{\text{SPT}}\rangle$ *does not* have a symmetry-protected sign problem relative to the X-basis. This means that there is some FDQC $\mathcal{U}_{\text{sym}}$ composed of symmetric gates such that all of the amplitudes of $\mathcal{U}_{\text{sym}}|\psi_{\text{SPT}}\rangle$ are non-negative in the X-basis. We denote $\mathcal{U}_{\text{sym}}|\psi_{\text{SPT}}\rangle$ by $|\varphi_{\text{SPT}}\rangle$, and note that, according to the definition of SPT phases, it belongs to the same SPT phase as $|\psi_{\text{SPT}}\rangle$.

By assumption, there exists a strange order parameter $\{\mathcal{O}_k\}$ for which the strange correlator:

$$\frac{\langle +\ldots+|\mathcal{O}_i\mathcal{O}_j|\varphi_{\text{SPT}}\rangle}{\langle +\ldots+|\varphi_{\text{SPT}}\rangle} \tag{2.37}$$

decays according to a power law or is constant in the separation of i and j.[11]. Here, $|+\ldots+\rangle$

[11]Note that if $|+\ldots+\rangle$ and $|\varphi_{\text{SPT}}\rangle$ are orthogonal, we can always construct a state $|\varphi'_{\text{SPT}}\rangle$ from $|\varphi_{\text{SPT}}\rangle$ by applying pairs of Pauli Z operators, such that $|\varphi'_{\text{SPT}}\rangle$ has a non-zero overlap with $|+\ldots+\rangle$, still belongs to the same phase as $|\psi_{\text{SPT}}\rangle$, and has non-negative amplitudes in the X-basis. (Pauli Z operators are positivity preserving in the X-basis.) Our argument can then be applied to $|\varphi'_{\text{SPT}}\rangle$ instead of $|\varphi_{\text{SPT}}\rangle$.

is the symmetric product state with a +1 eigenvalue under every Pauli X operator.[12] In fact, as shown in Appendix 2.E, the strange order parameter can always be chosen to be a set of Pauli Z strings $\{Q_k^Z\}$. In what follows, we argue that the existence of this strange order parameter is in conflict with the non-negative amplitudes of the SPT state $|\varphi_{\text{SPT}}\rangle$.

To see this, we consider $\{Q_k^Z\}$ as a spontaneous-symmetry breaking order parameter for $|\varphi_{\text{SPT}}\rangle$:[13]

$$\langle\varphi_{\text{SPT}}|Q_i^Z Q_j^Z|\varphi_{\text{SPT}}\rangle. \tag{2.38}$$

We evaluate the correlator by expanding $\langle\varphi_{\text{SPT}}|$ in the X-basis. We label an X-basis state by x and denote the non-negative amplitudes of $\langle\varphi_{\text{SPT}}|$ by $\sqrt{p(x)}$, where $p(x) \in \mathbb{R}_{\geq 0}$. $\langle\varphi_{\text{SPT}}|$ can then be written as:

$$\langle\varphi_{\text{SPT}}| = \sum_x \sqrt{p(x)}\langle x|. \tag{2.39}$$

Inserting this into Eq. (2.38) gives us:

$$\sum_x \sqrt{p(x)}\langle x|Q_i^Z Q_j^Z|\varphi_{\text{SPT}}\rangle = \sqrt{p(+\ldots+)}\langle+\ldots+|Q_i^Z Q_j^Z|\varphi_{\text{SPT}}\rangle + \sum_{x\neq+\ldots+} \sqrt{p(x)}\langle x|Q_i^Z Q_j^Z|\varphi_{\text{SPT}}\rangle. \tag{2.40}$$

The first term on the right-hand side of Eq. (2.40) is proportional to the strange correlator with strange order parameter $\{Q_k^Z\}$. Consequently, it decays slowly with the separation of i and j, i.e., it decays according to a power law or is constant in $|i-j|$. The second term on the right-hand side of Eq. (2.40) is non-negative, because the amplitudes of $|\varphi_{\text{SPT}}\rangle$ are non-negative and Q_i^Z, Q_j^Z preserve non-negativity (in the X-basis).

---

[12] Despite the notation $|+\ldots+\rangle$, the argument holds for systems of qudits.

[13] Note that Q_i^Z and Q_j^Z are charged, so the following matrix elements vanish: $\langle+\ldots+|Q_i^Z|\varphi_{\text{SPT}}\rangle = \langle+\ldots+|Q_j^Z|\varphi_{\text{SPT}}\rangle = 0$.

From Eq. (2.40), we see that $|\varphi_{\text{SPT}}\rangle$ has long-range order. This contradicts the assumption that $|\varphi_{\text{SPT}}\rangle$ is an SPT state with short-range entanglement. Therefore, $|\psi_{\text{SPT}}\rangle$ must have a symmetry-protected sign problem relative to the X-basis, where the symmetry is represented by products of diagonal Pauli operators. □

For a concrete application of Proposition 3, we can consider the cluster state, discussed in Section 2.2.4. The $\mathbb{Z}_2 \times \mathbb{Z}_2$ symmetry of the cluster state is represented by Pauli X operators, and therefore, the cluster state has a symmetry-protected sign problem relative to the X-basis. This is to say, in the symmetry-charge basis, at least one amplitude of the cluster state is outside of $\mathbb{R}_{\geq 0}$, and moreover, there are no symmetry-preserving local basis changes from the X-basis that make all of the amplitudes of the cluster state non-negative.

We note that, although the cluster state has a symmetry-protected sign problem relative to the X-basis, there still exists product state bases in which the amplitudes of the cluster state are non-negative. In particular, the amplitudes of the cluster state are non-negative if the Z-basis is used on even sites and the X-basis is used on odd sites.[14]Proposition 3 does not apply in this case, because, in this basis, the symmetry is not diagonal, and it cannot be mapped to the X-basis by symmetry-preserving local transformations.[15]

To highlight the quantum nature of states with a symmetry-protected sign problem, we would like to describe an alternative proof of Proposition 3 that applies to 1D SPT states. The idea is to make use of the quantum wire property, where, for certain 1D SPT states, measurements in the symmetry-charge basis can be used to generate long-range entanglement [37, 89, 90]. We argue that, if a state can serve as a quantum wire and it is non-negative in the symmetry-charge basis, then it contradicts the results of Ref. [4], in which a bound is set on the entanglement created by making measurements of a non-negative state. More formally, we show the following:

---

[14]In fact, it can be checked that the Hamiltonian is stoquastic in this basis.

[15]Specifically, the bases are related by applying Hadamard gates on the even sites. Hadamard gates do not commute with the symmetry formed by products of Pauli X operators.

Proposition 3′ *Let $|\psi_{SPT}\rangle$ be a state belonging to a 1D SPT phase protected by an Abelian symmetry and corresponding to a maximally non-commutative cohomology class.*[16] *Then $|\psi_{SPT}\rangle$ has a symmetry-protected sign problem relative to product state bases in which the symmetry is represented by products of diagonal unitaries.*

Remark: Here, we make the technical assumption that $|\psi_{\text{SPT}}\rangle$ belongs to an SPT phase labeled by a maximally non-commutative cohomology class to guarantee that $|\psi_{\text{SPT}}\rangle$ exhibits the quantum wire property [89]. We note that we are also working under the assumption that $|\psi_{\text{SPT}}\rangle$ is defined on a lattice with periodic boundary conditions and can be prepared exactly from a product state by a FDQC, as established in Section 2.2.1.

Proof of Proposition 3′. First, we use the results of Ref. [89] to show that long-range entanglement can be generated from measurements of $|\psi_{\text{SPT}}\rangle$. To see this, we consider a matrix product state (MPS) representation of $|\psi_{\text{SPT}}\rangle$:

$|\psi_{\text{SPT}}\rangle =$ 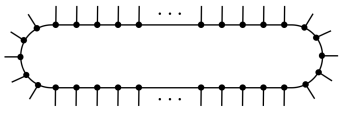 . (2.41)

We then coarse grain the lattice by combining a constant number of neighboring sites into super-sites, such that, for each local tensor of the coarse grained MPS, there exists an isometry W that graphically satisfies:

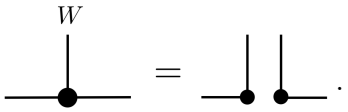

(2.42)

Here, W is an isometry that maps from the d-dimensional physical Hilbert space to a pair of Hilbert spaces of dimension χ_L and χ_R, where χ_L and χ_R are the dimensions of the left and right virtual Hilbert spaces, respectively. Importantly, W disentangles the states in the left

[16] A cohomology class $[\omega] \in \mathcal{H}^2[G, U(1)]$ is maximally non-commutative if for every element $g \in G$ other than the identity, there exists an $h \in G$ such that $\omega(g,h) \neq \omega(h,g)$.

virtual Hilbert space from the states in the right virtual Hilbert space. Heuristically, W_A at the super-site A can be interpreted as first acting with a unitary operator supported on A that locally disentangles $|\psi_{\text{SPT}}\rangle$ and then subsequently removing the unentangled degrees of freedom.

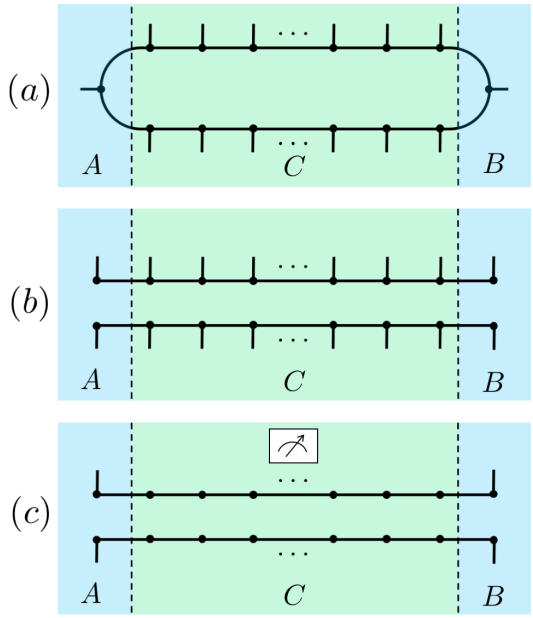

Figure 2.4: (a) We partition the coarse grained MPS into regions A, B, and C by choosing super-sites A and B. (b) Applying the isometry $W_A \otimes W_B$ to $|\psi_{\text{SPT}}\rangle$ splits it into two unentangled MPS: $|\psi^1_{\text{SPT}}\rangle$ and $|\psi^2_{\text{SPT}}\rangle$. (c) The measurement on the super-sites in C fixes the physical indices in the region C according to the measurement outcome $|x\rangle$ and leaves us with the state $|\psi^x_{AB}\rangle$ on $A \cup B$. $|\psi^x_{AB}\rangle$ is entangled between A and B through the virtual bonds, as described in Ref. [89].

The next step is to choose well-separated super-sites A and B and make measurements in the symmetry-charge basis on the complement of $A \cup B$, denoted by C (Fig. 2.4). We claim that measurements in the symmetry-charge basis on C generate entanglement between A and B lower bounded by a value that is independent of the separation of A and B. To show this, we apply the isometry $W_A \otimes W_B$ to $|\psi_{\text{SPT}}\rangle$, with W_A and W_B defined as in Eq. (2.42).

The isometry splits $|\psi_{\text{SPT}}\rangle$ into two independent MPS, as shown in Fig. 2.4:

$$W_A \otimes W_B |\psi_{\text{SPT}}\rangle = |\psi^1_{\text{SPT}}\rangle \otimes |\psi^2_{\text{SPT}}\rangle. \tag{2.43}$$

Note that, after applying the isometry $W_A \otimes W_B$, the degrees of freedom at A and B correspond to the virtual bonds of the MPS, up to local positive diagonal operators (see Cororally 3.12 of Ref. [91]). This is important given that the results of Ref. [89] show that measurements of an SPT state create entanglement at the level of the virtual bonds.

We now measure the sites in C in the symmetry-charge basis and with probability p_x obtain the product state $|x\rangle$ on C. We define $|\psi^x_{AB}\rangle$ to be the state on $A \cup B$ given by fixing the degrees of freedom of $|\psi^1_{\text{SPT}}\rangle \otimes |\psi^2_{\text{SPT}}\rangle$ on C according to the product state $|x\rangle$. By the assumption that $|\psi_{\text{SPT}}\rangle$ belongs to an SPT phase corresponding to a maximally non-commutative cohomology class, Theorem 1 of Ref. [89] tells us that $|\psi^x_{AB}\rangle$ can be written in the form:

$$|\psi^x_{AB}\rangle = \left(|\varphi^1_{\text{junk}}\rangle \otimes U^{x,1}_B |\Phi^1_{\text{max}}\rangle\right) \otimes \left(|\varphi^2_{\text{junk}}\rangle \otimes U^{x,2}_B |\Phi^2_{\text{max}}\rangle\right). \tag{2.44}$$

Here, $|\varphi^1_{\text{junk}}\rangle$,$|\varphi^2_{\text{junk}}\rangle$ are unimportant states that depend on the details of $|\psi_{\text{SPT}}\rangle$, $|\Phi^1_{\text{max}}\rangle$,$|\Phi^2_{\text{max}}\rangle$ are $\sqrt{|G|}$-dimensional maximally entangled states between A and B, and $U^{x,1}_B$,$U^{x,2}_B$ are some unitary operators supported only on B. Note that the first and second lines of Eq. (2.44) correspond to independent contributions from $|\psi^1_{\text{SPT}}\rangle$ and $|\psi^2_{\text{SPT}}\rangle$. For any measurement outcome $|x\rangle$, the entanglement entropy of $|\psi^x_{AB}\rangle$ between A and B is therefore bounded below as:

$$S\left(\rho^x_A\right) \geq 2 \log_2 \sqrt{|G|}, \tag{2.45}$$

with ρ^x_A denoting the reduced density matrix of $|\psi^x_{AB}\rangle$ on A. Since $W_A \otimes W_B$ has no affect on the entanglement generated between A and B, we see that making measurements of $|\psi_{\text{SPT}}\rangle$ on C induces entanglement between A and B with a constant lower bound, as claimed.

On the other hand, Proposition 4.1 of Ref. [4] implies that, if $|\psi_{\mathrm{SPT}}\rangle$ is non-negative in the symmetry-charge basis, then the average entanglement entropy after the measurements is bounded from above as:

$$\sum_x p_x S\left(\rho_A^x\right) \leq f(L), \tag{2.46}$$

where L is the distance between the super-sites A and B, and $f(L)$ is a function that decays rapidly to zero (faster than any polynomial). For a sufficiently large L, the bound in Eq. (2.46) conflicts with Eq. (2.45).

Therefore, $|\psi_{\mathrm{SPT}}\rangle$ cannot be non-negative in the symmetry-charge basis. Furthermore, the argument applies to any state constructed from $|\psi_{\mathrm{SPT}}\rangle$ by a FDQC composed of symmetric gates, since the quantum wire property is shared by states in the same phase. We can thus conclude that $|\psi_{\mathrm{SPT}}\rangle$ has a symmetry-protected sign problem relative to the symmetry-charge basis. □

2.5 Discussion

We have introduced the concepts of symmetry-protected magic and a symmetry-protected sign problem to facilitate the study of many-body magic and the sign structure of wave functions. We have applied these concepts to SPT states to assess their quantum complexity. Using the universal properties of certain non-trivial group cohomology phases in $D \geq 2$ dimensions, we showed that the corresponding SPT states have symmetry-protected magic, assuming the symmetry is represented by products of Pauli operators. This implies that there is no stabilizer state representative in these SPT phases. We also argued that SPT states in dimensions $D \leq 2$ have a symmetry-protected sign problem in bases where the symmetry is diagonal. Consequently, in this basis, there is an obstruction to a description of the SPT phase by a non-negative wave function.

By imposing symmetry constraints, we were able to make analytic statements about the complexity of quantum states, including the first verification of a sign problem at the level of probability amplitudes. We note that a restriction to symmetric systems has also

been beneficial for studying the No Low-energy Trivial States conjecture in Ref. [92]. We anticipate that, moving forwards, symmetry constraints will be a valuable tool for addressing outstanding quantum information problems.

We would like to emphasize that our assessment of the symmetry-protected magic in SPT phases applies to systems with even-dimensional qudits. This is noteworthy given that magic is more easily quantified and better understood in systems of qudits with odd dimensions (and especially odd prime dimensions), thanks to the discrete Wigner formalism [93, 94]. The associated discrete Wigner function maps states to quasi-probabilities, and for systems of odd dimensional qudits, the negative quasi-probabilities can be used to define a measure of the amount of magic in the state [16].

In the case that the qudits are odd-dimensional, symmetry-protected magic can be interpreted as a sign problem, which manifests through the quasi-probability distribution of the discrete Wigner function (known as the discrete Hudson's theorem) [94]. Symmetry-protected magic says that the signs in the quasi-probability distribution cannot be removed by making symmetry preserving unitary local changes to the state. We point out that this sign problem has appeared in the simulation of random quantum circuits as in Ref. [95].

Our work therefore deals with two different notions of a sign problem – one relates to the quasi-probability distribution of a discrete Wigner function, while the other corresponds to the complex probability amplitudes of a state. It should be noted that these are distinct from the usual notion of a sign problem related to the "stoquasticity" of a Hamiltonian and discussed in the context of simulating quantum systems by Monte Carlo methods. However, a sign problem at the level of the amplitudes of a wave function, in fact, implies that any gapped parent Hamiltonian suffers from a sign problem in the stoquastic sense (see Ref. [4] and Appendix A of Ref. [12]).

To conclude, we would like to further comment on related work, make a few conjectures, and discuss some promising directions for future work.

Symmetry-protected magic

Propositions 1 and 2 show that stabilizer operations are insufficient for simulating certain SPT states. It is important to note that this also implies that those SPT states can be used as a source of magic for quantum computing. It would be interesting if a quantized universal property of the corresponding SPT phases - say, their responses to probing with symmetry defects - could be exploited to reliably produce a standard magic state (e.g. a CCZ state), independent of the microscopic details of the systems. We also speculate that there is a series of adaptive measurements that produces a standard magic state on a large length scale, similar to how a series of local measurements of 1D SPT states can create entanglement between distant sites [90].

It is also interesting to consider the implications of our work for the use of group cohomology SPT states as resources for measurement-based quantum computing (MBQC). Remarkable progress has been made in identifying computationally universal phases of matter protected by subsystem symmetries [38, 39], but much remains to be understood about the MBQC utility of SPT phases with global (0-form) symmetries. In Refs. [43] and [44], it was recognized that a particular "fixed point" wave function in a $2D$ $\mathbb{Z}_2 \times \mathbb{Z}_2 \times \mathbb{Z}_2$ group cohomology SPT phase harbors magic. Furthermore, it was shown that the state can be used as a resource for universal MBQC using only Pauli measurements. It is natural to wonder whether the entire phase can be used for universal MBQC with Pauli measurements. Our results are consistent with this conjecture and suggest that other group cohomology SPT states may be able to serve as universal resources as well. For a related discussion on the quantification of magic, see Ref. [29].

According to Propositions 1 and 2, certain SPT states must be non-stabilizer and, as such, cannot be prepared from $|0 \dots 0\rangle$ by a Clifford unitary. Inspired by Ref. [45], we speculate that the higher levels of the Clifford hierarchy may also be useful for understanding the complexity of SPT states. The Clifford unitaries form the second level of the hierarchy $\mathcal{C}_2$,

and the higher levels of the hierarchy are obtained recursively as:

$$\mathcal{C}_{D+1} \equiv \left\{U : UPU^\dagger \in \mathcal{C}_D, \forall P \in \mathcal{C}_1\right\}, \tag{2.47}$$

where $\mathcal{C}_1$ denotes the set of Pauli strings. The results of Ref. [45] imply that particular finely tuned SPT states in D-dimensions cannot be prepared from $|0\ldots0\rangle$ by any FDQC belonging to the D^{th} level of the hierarchy. It may be interesting to study the extent to which this applies to other states in the SPT phase.

In this chapter, we focused on the magic in quantum phases characterized by SRE states, but an important avenue for future work is to study magic in systems with long-range entanglement, such as in conformal field theories (CFTs) and intrinsic topological orders. Refs. [27] and [28] have made the first steps in numerically studying the emergence of magic at a critical point, and Ref. [27] conjectured that CFTs generically have magic at large length scales, detectable by correlations.

Regarding the magic inherent in topologically ordered phases, Ref. [96] provided a classification of systems in 2D that can be described by a local stabilizer Hamiltonian, assuming the stabilizer Hamiltonian is translationally invariant and defined on a Hilbert space built of prime dimensional qudits. These results place important restrictions on the phases of matter that admit a representation by a stabilizer state. However, more work is needed to lift the assumptions and better understand long-range magic (Definition 2) in phases with intrinsic topological order. We conjecture that states defined on qubits in the double semion phase, for example, have long-range magic, and we look forward to commenting further on this conjecture in upcoming work.

Symmetry-protected sign problem

We argued that non-trivial SPT states in dimensions $D \leq 2$ have a symmetry-protected sign problem relative to the symmetry-charge basis, where the symmetry is diagonal. It is unclear whether these SPT states have a symmetry-protected sign problem relative to other

bases, as our techniques are specialized for the symmetry-charge basis. For instance, does the cluster state have a symmetry-protected sign problem relative to the Z-basis? A complete characterization of the symmetry-protected sign problems might lead to new tools useful for tackling the sign problem in the absence of symmetry constraints. New techniques are also needed to study the symmetry-protected sign problem in SPT states in dimensions $D \geq 3$, since the strange correlations may no longer be a reliable way to diagnose the SPT order.

In Section 2.3.3, we also argued that the quantum wire property of non-trivial 1D SPT states is incompatible with a non-negative wave function in the symmetry-charge basis. This suggests a potential operational consequence of a symmetry-protected sign problem. In particular, for non-trivial 1D SPT states, entanglement can be generated between any two regions by making measurements on the complement in the symmetry-charge basis. We speculate that, more generally, a symmetry-protected sign problem relative to a basis $|\{\alpha\}\rangle$ implies that measurements in the $|\{\alpha\}\rangle$ basis can be used to create entanglement between distant regions. In any event, further work is needed to build off of the results of Ref. [4] and to fully understand the connection between the sign structure of a quantum state and its localizable entanglement [97].

Appendices

2.A Universality of the anomalous symmetry action

In Section 2.2.2, we stated that group cohomology SPT phases can be characterized by anomalies – i.e., obstructions to finding an effective boundary symmetry action that is on-site.[17] The calculation of the anomaly, as described in Section 2.2.2, (seemingly) depends on the following choices: (i) a representative SPT state, (ii) a parent SPT Hamiltonian for the SPT state, and (iii) an effective boundary symmetry action derived from the parent Hamiltonian. Following Appendix C of Ref. [46], we sketch an argument below that the

[17] More specifically, the obstructions are to finding an effective boundary symmetry action that is onsite up to taking tensor products with effective actions of lower-dimensional SPT phases and by conjugating the effective symmetry action with a FDQC.

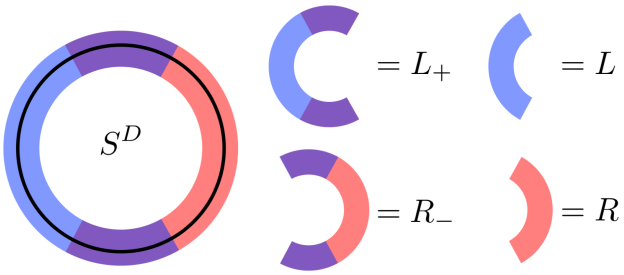

Figure 2.5: $|\psi_1\rangle$ and $|\psi_2\rangle$ are defined on a D-sphere S^D. We partition S^D into overlapping regions L_+ (union of blue and purple) and R_- (union of red and purple). L_+ contains the subregion L (blue), and R_- contains the subregion R (red).

computation of the anomaly ultimately does not depend on these choices. In other words, we argue that the anomaly is well-defined as an invariant of the SPT phase. The strategy is to study the anomaly at the interface between two different possible choices of (i), (ii), and (iii). To simplify the discussion, we assume that the parent Hamiltonians are un-frustrated. (This is sufficient for our purposes.) We expect that the argument can be generalized to show that the anomaly is well-defined for any choice of parent SPT Hamiltonian.

We consider two states $|\psi_1\rangle$ and $|\psi_2\rangle$ belonging to the same D-dimensional SPT phase along with a choice of corresponding SPT Hamiltonians H_1 and H_2. For concreteness, we take $|\psi_1\rangle$ and $|\psi_2\rangle$ to be defined on a D-sphere S^D. Since $|\psi_1\rangle$ and $|\psi_2\rangle$ are in the same phase, there exists a FDQC $\mathcal{U}_{\text{sym}}$ composed of symmetric gates such that:

$$\mathcal{U}_{\text{sym}}|\psi_2\rangle = |\psi_1\rangle. \tag{2.48}$$

We can then construct the SPT Hamiltonian $\tilde{H}_2$, defined as:

$$\tilde{H}_2 \equiv \mathcal{U}_{\text{sym}} H_2 \mathcal{U}_{\text{sym}}^\dagger, \tag{2.49}$$

which has the unique ground state $|\psi_1\rangle$.

Now, we combine terms from H_1 and $\tilde{H}_2$ to form a new SPT Hamiltonian H on S^D whose

ground state is also $|\psi_1\rangle$. Roughly speaking, H is comprised of the terms in H_1 on the left half of the sphere and the terms in $\tilde{H}_2$ on the right half. More specifically, we divide the D-sphere into two overlapping regions L_+ and R_-, as shown in Fig. 2.5. L_+ and R_- cover the D-sphere, and their intersection is a thickened $(D-1)$-sphere. We take the "width" of the intersection to be large compared with the Lieb-Robinson length of some (arbitrary) FDQC that prepares $|\psi_1\rangle$. To construct H, we truncate H_1 to L_+, to define $H_1^{L_+}$, and we truncate $\tilde{H}_2$ to R_-, to define $\tilde{H}_2^{R_-}$. The SPT Hamiltonian H is then:

$$H \equiv H_1^{L_+} + \tilde{H}_2^{R_-}, \tag{2.50}$$

with the unique ground state $|\psi_1\rangle$. The fact that $|\psi_1\rangle$ is the ground state follows from the assumption that H_1 and H_2 are un-frustrated.

Next, we study the possible anomaly at the interface between H_1 and $\tilde{H}_2$. In particular, we introduce a boundary by truncating H to the region $L \cup R$, where L and R are defined as:

$$L \equiv L_+ - L_+ \cap R_-, \quad R \equiv R_- - L_+ \cap R_-, \tag{2.51}$$

as depicted in Fig. 2.5. In other words, we remove any term in H that is supported (in part) on the overlap between L_+ and R_-. We are left with the truncated Hamiltonian $H^{L\cup R}$:

$$H^{L\cup R} \equiv H_1^L + \tilde{H}_2^R, \tag{2.52}$$

where H_1^L is the truncation of H_1 to L and $\tilde{H}_2^R$ is the truncation of $\tilde{H}_2$ to R. Importantly, we consider $H^{L\cup R}$ as a Hamiltonian on the full Hilbert space of S^D.

The boundary Hilbert space of $H^{L\cup R}$ can be decomposed into a tensor product of the following three Hilbert spaces: (i) the low-energy Hilbert space of H_1^L on L, (ii) the full Hilbert space on the intersection $L_+ \cap R_-$, and (iii) the low-energy Hilbert space of $\tilde{H}_2^R$ on R. Accordingly, we can construct an effective symmetry action near the boundary of $L \cup R$ by

multiplying an effective action on L, an onsite symmetry on $L_+ \cap R_-$, and an effective action on R. More explicitly, we can choose the effective boundary symmetry action representing $g \in G$ to be $v^L(g)$ on L and $v^R(g)$ on R, so that an effective boundary symmetry action $v(g)$ on $L \cup R$ is:

$$v(g) \equiv v^L(g) \left(\prod_{i \in L_+ \cap R_-} u_i(g) \right) v^R(g). \tag{2.53}$$

We note that the effective boundary symmetry action in Eq. (2.53) is localized near $L_+ \cap R_-$.

The algorithm defined in Ref. [46] can now be applied to $v(g)$ to identify potential obstructions to making $v(g)$ onsite. The obstruction corresponds to an element $[\omega] \in \mathcal{H}^{D+1}[G, U(1)]$, and one can show that it can be divided into a contribution $[\omega^L] \in \mathcal{H}^{D+1}[G, U(1)]$ from $v^L(g)$ and a contribution $[\omega^R] \in \mathcal{H}^{D+1}[G, U(1)]$ from $v^R(g)$, so that:

$$[\omega] = [\omega^L] \cdot [\omega^R]. \tag{2.54}$$

The last step is to argue that $[\omega]$ calculated from $v(g)$ using the procedure in Ref. [46] must correspond to the trivial class in $\mathcal{H}^{D+1}[G, U(1)]$. Therefore, regardless of the choices made in determining $v^L(g)$ and $v^R(g)$, we have $[\omega^L] = [\omega^R]^{-1}$. This constraint implies that the anomaly is well-defined, since $v^L(g)$ and $v^R(g)$ can be chosen independently. For simplicity, we show that $[\omega]$ is the trivial class for only the 1D case. We note that the 2D case can be found in Appendix C of Ref. [46], and we fully expect that the argument can be generalized straightforwardly to higher dimensions.

To show that $[\omega]$ must be trivial in the 1D case, we consider the state $|\psi_1\rangle$. Since $|\psi_1\rangle$ belongs to the boundary Hilbert space of $H^{L \cup R}$, the symmetry action $u(g)$, for any $g \in G$, can be replaced by $v(g)$ when acting on $|\psi_1\rangle$. Therefore, we have the equality:

$$v(g)|\psi_1\rangle = |\psi_1\rangle, \quad \forall g \in G. \tag{2.55}$$

In 1D, the support of $v(g)$ can be partitioned into two connected components, which we label as A and B. Consequently, $v(g)$ can be split[18] into an operator $v_A(g)$ supported on A and $v_B(g)$ supported on B. From Eq. (2.55), we have:

$$v_A(g)v_B(g)|\psi_1\rangle = |\psi_1\rangle, \quad \forall g \in G. \tag{2.56}$$

Furthermore, we can always define $v_A(g)$ and $v_B(g)$ so that:

$$v_A(g)|\psi_1\rangle = |\psi_1\rangle, \quad \forall g \in G. \tag{2.57}$$

It follows that $v_A(g)$ forms a linear representation of G on $|\psi_1\rangle$:

$$v_A(g)v_A(h)|\psi_1\rangle = |\psi_1\rangle = v_A(gh)|\psi_1\rangle, \quad \forall g, h \in G. \tag{2.58}$$

Since $v_A(g)$ forms a trivial projective representation (i.e., a linear representation), the associated element of $\mathcal{H}^2[G, U(1)]$ must be the trivial class.

2.A.1 Cluster state example

Using the ideas above, we argue that the cluster state belongs to a non-trivial SPT phase. In particular, the projective representation satisfied by the effective boundary symmetry action poses an obstruction to finding a FDQC with symmetric gates that can disentangle the cluster state. We show this by deriving a contradiction.

Suppose that $|\psi_{\text{CS}}\rangle$ can be disentangled by a FDQC $\mathcal{U}_{\text{sym}}$ composed of symmetric gates:

$$\mathcal{U}_{\text{sym}}|\psi_{\text{CS}}\rangle = |+\ldots+\rangle. \tag{2.59}$$

Then the Hamiltonian $\tilde{H}_{\text{CS}} \equiv \mathcal{U}_{\text{sym}} H_{\text{CS}} \mathcal{U}_{\text{sym}}^\dagger$ has the unique product state ground state $|+\ldots+\rangle$. Further, we can identify an effective boundary symmetry action for $\tilde{H}_{\text{CS}}$ by

[18] The operator can be split unambiguously up to a g dependent phase.

conjugating the effective action computed using H_{CS} [copied from Eq. (2.16)]:

$$\begin{aligned} v((g,1)) &= Z_1(Z_{2M-1}X_{2M}), \\ v((1,g)) &= (X_1Z_2)Z_{2M}, \end{aligned} \tag{2.60}$$

by the FDQC $\mathcal{U}_{\text{sym}}$:

$$\begin{aligned} \tilde{v}((g,1)) &\equiv \mathcal{U}_{\text{sym}} v((g,1)) \mathcal{U}_{\text{sym}}^\dagger, \\ \tilde{v}((1,g)) &\equiv \mathcal{U}_{\text{sym}} v((1,g)) \mathcal{U}_{\text{sym}}^\dagger. \end{aligned} \tag{2.61}$$

Similar to the effective action in Eq. (2.60), when $\tilde{v}((g,1))$ and $\tilde{v}((1,g))$ are restricted to a region near either the endpoint 1 or $2M$, they form a projective representation of $\mathbb{Z}_2 \times \mathbb{Z}_2$, corresponding to the non-trivial element of $\mathcal{H}^2[\mathbb{Z}_2 \times \mathbb{Z}_2, U(1)]$.

We compare $\tilde{H}_{\text{CS}}$ to the paramagnet SPT Hamiltonian H_0:

$$H_0 \equiv -\sum_i X_i, \tag{2.62}$$

which also has $|+\ldots+\rangle$ as its unique ground state. An effective boundary symmetry action computed with respect to H_0 is given by:

$$\begin{aligned} v^0((g,1)) &\equiv X_2 X_{2M} \\ v^0((1,g)) &\equiv X_1 X_{2M-1}. \end{aligned} \tag{2.63}$$

The restrictions of $v^0((g,1))$ and $v^0((1,g))$ to an endpoint forms a linear representation of $\mathbb{Z}_2 \times \mathbb{Z}_2$, corresponding to the trivial element of $\mathcal{H}^2[\mathbb{Z}_2 \times \mathbb{Z}_2, U(1)]$.

We see that the quantized invariant for the SPT phase containing $|+\ldots+\rangle$ computed using $\tilde{H}_{\text{CS}}$ differs from the quantized invariant computed using H_0. This contradicts the fact the anomaly is well-defined. Therefore, the cluster state $|\psi_{\text{CS}}\rangle$ cannot be disentangled using a FDQC composed of symmetric gates.

2.B Decorated domain wall models

In this section, we define decorated domain wall models corresponding to $H \times K$ SPT phases characterized by an element of $\mathcal{H}^1[H, \mathcal{H}^D[K, U(1)]]$. To illustrate the construction, we consider an example of a 1D SPT phase protected by a $\mathbb{Z}_2 \times \mathbb{Z}_2$ symmetry. We then demonstrate that the decorated domain wall models have an effective boundary symmetry action that prepares a $(D-1)$-dimensional K SPT state from a trivial SPT state. This property of the decorated domain wall models allows us to complete the proof of Proposition 2.

2.B.1 *Review of* $\mathcal{H}^1[H, \mathcal{H}^D[K, U(1)]]$

Our decorated domain wall models are constructed directly from the data of the group cohomology group $\mathcal{H}^1[H, \mathcal{H}^D[K, U(1)]]$. Therefore, before describing the decorated domain wall models, we review the essential details of $\mathcal{H}^1[H, \mathcal{H}^D[K, U(1)]]$. We refer to Ref. [49] for more information on group cohomology.

We start by reviewing the relevant data of the group cohomology $\mathcal{H}^D[K, U(1)]$. The elements of $\mathcal{H}^D[K, U(1)]$ can be labeled by functions from K^{D+1} to $U(1)$ satisfying certain constraints. More specifically, an element $[\nu]$ in $\mathcal{H}^D[K, U(1)]$ is labeled by a function $\nu : K^{D+1} \to U(1)$ that is closed and homogeneous. By closed, we mean that ν satisfies the condition:

$$\prod_{i=0}^{D} \nu(k_0, \ldots, \widehat{k_i}, \ldots, k_{D+1})^{(-1)^i} = 1, \tag{2.64}$$

where $\widehat{k_i}$ denotes that k_i is omitted. By homogeneous, we mean that ν satisfies:

$$\nu(k_0, \ldots, k_D) = \nu(kk_0, \ldots, kk_D), \tag{2.65}$$

for all $k \in K$.

The elements of $\mathcal{H}^D[K, U(1)]$ form a finite Abelian group under multiplication with the

product of $[\nu]$ and $[\nu']$ in $\mathcal{H}^D[K, U(1)]$ given by:

$$[\nu] \cdot [\nu'] = [\nu\nu']. \tag{2.66}$$

Accordingly, the group $\mathcal{H}^D[K, U(1)]$ takes the general form:

$$\mathcal{H}^D[K, U(1)] = \prod_{j=1}^{p} \mathbb{Z}_{n_j}, \tag{2.67}$$

where p gives the number of generators of $\mathcal{H}^D[K, U(1)]$. We label the j^{th} generator of the cohomology by the function ν_j.

With this, we can describe the data of the group cohomology $\mathcal{H}^1[H, \mathcal{H}^D[K, U(1)]]$. The elements of the group $\mathcal{H}^1[H, \mathcal{H}^D[K, U(1)]]$ can be labeled by functions of the form:

$$\eta \equiv \prod_{j=1}^{p} \nu_j^{\phi_j} : K^{D+1} \times H^2 \to U(1). \tag{2.68}$$

Here, ϕ_j is a function from H^2 to $\mathbb{Z}_{n_j}$ that is closed and homogeneous. In this case, closed means that ϕ_j satisfies:

$$\phi_j(h_1, h_2) - \phi_j(h_0, h_2) + \phi_j(h_0, h_1) = 0, \tag{2.69}$$

and homogeneous means that ϕ_j satisfies:

$$\phi_j(h_0, h_1) = \phi_j(hh_0, hh_1), \quad \forall h \in H. \tag{2.70}$$

Explicitly, η evaluated on the group elements $k_0, \ldots, k_D$ in K and h_0, h_1 in H is:

$$\eta(k_0, \ldots, k_D; h_0, h_1) = \prod_{j=1}^{p} \nu_j(k_0, \ldots, k_D)^{\phi_j(h_0, h_1)}. \tag{2.71}$$

In the next section, we show that the function η above can be used to construct a model

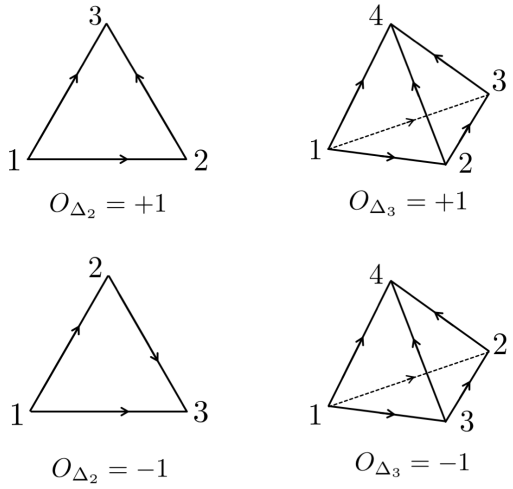

Figure 2.6: The branching structure induces an ordering of the vertices of a simplex according to the number of edges pointing towards a vertex. It also defines an orientation of d-simplices in a d-manifold relative to the orientation of the manifold. We denote the $\{\pm 1\}$-valued orientation of a d-simplex Δ_d by O_{Δ_d}.

belonging to the SPT phase characterized by $[\eta] \in \mathcal{H}^1[H, \mathcal{H}^D[K, U(1)]]$.

2.B.2 Construction of the decorated domain wall models

We define our decorated domain wall models on an arbitrary triangulation of an orientable closed D-dimensional manifold N. The triangulation specifies a decomposition of N into simplices (e.g., vertices, edges, faces, etc.), and we denote d-dimensional simplices (d-simplices) by Δ_d. We also require that the triangulation is equipped with a branching structure, i.e., an assignment of an orientation to each edge so that there are no cycles around any face. The branching structure defines a local ordering of the vertices and an orientation of the d-simplices (for $d \geq 1$), as shown in Fig. 2.6. We occasionally write a d-simplex in terms of its vertices, such as: $\Delta_d = \langle 1, \ldots, d \rangle$, where the vertices $1, \ldots, d$ are ordered according to the branching structure.

To construct a model for an SPT phase protected by $H \times K$ symmetry, we place an $|H|$-dimensional qudit at each D-simplex and a $|K|$-dimensional qudit at each vertex. We

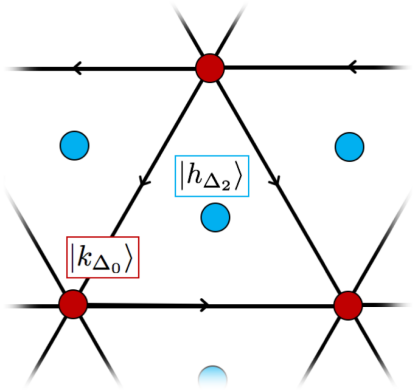

Figure 2.7: In 2D, the decorated domain wall model for an $H \times K$ SPT phase is defined on a triangulation of a 2D lattice with an $|H|$-dimensional Hilbert space (blue) at each 2-simplex and a $|K|$-dimensional Hilbert space (red) at each vertex. A product state basis for the total Hilbert space is given by states labeled by $(H \times K)$-configurations $\{h_{\Delta_2}\}, \{k_{\Delta_0}\}$. For the basis state $|\{h_{\Delta_2}\}, \{k_{\Delta_0}\}\rangle$, the state at the 2-simplex Δ_2 is $|h_{\Delta_2}\rangle$ and the state at the vertex Δ_0 is $|k_{\Delta_0}\rangle$.

label the basis states of a qudit at a D-simplex by elements of H and the basis states of a qudit at a vertex by elements of K. A basis for the full Hilbert space is then given by product states of the form $|\{h_{\Delta_D}\}, \{k_{\Delta_0}\}\rangle$, where the state at Δ_D is $|h_{\Delta_D}\rangle$ and the state at Δ_0 is $|k_{\Delta_0}\rangle$ (Fig. 2.7). Furthermore, we define the $H \times K$ symmetry to act as left multiplication, so for any element $(h, k) \in H \times K$, the onsite symmetry action $u\big((h, k)\big)$ is defined by:

$$u\big((h, k)\big)|\{h_{\Delta_D}\}, \{k_{\Delta_0}\}\rangle = |\{hh_{\Delta_D}\}, \{kk_{\Delta_0}\}\rangle. \tag{2.72}$$

Next, we introduce an $H \times K$ paramagnet Hamiltonian with a ground state in the trivial SPT phase. We construct the decorated domain wall models starting with the paramagnet Hamiltonian. The paramagnet Hamiltonian is:

$$H_0 \equiv -\sum_{\Delta_D} \Pi_{\Delta_D} - \sum_{\Delta_0} \Pi_{\Delta_0}, \tag{2.73}$$

where Π_{Δ_D} and Π_{Δ_0} are projectors onto symmetric states at Δ_D and Δ_0 (tensored with the identity on all other sites):

$$\Pi_{\Delta_D} \equiv \frac{1}{|H|}\left(\sum_{h_{\Delta_D}} |h_{\Delta_D}\rangle\right)\left(\sum_{h_{\Delta_D}} \langle h_{\Delta_D}|\right), \tag{2.74}$$

$$\Pi_{\Delta_0} \equiv \frac{1}{|K|}\left(\sum_{k_{\Delta_0}} |k_{\Delta_0}\rangle\right)\left(\sum_{k_{\Delta_0}} \langle k_{\Delta_0}|\right). \tag{2.75}$$

The ground state of H_0 is the symmetric product state:

$$|\psi_0\rangle \equiv \sum_{\{h_{\Delta_D}\},\{k_{\Delta_0}\}} |\{h_{\Delta_D}\},\{k_{\Delta_0}\}\rangle, \tag{2.76}$$

with the sum over $\{h_{\Delta_D}\}$ and $\{k_{\Delta_0}\}$ configurations and with the normalization suppressed. To simplify the notation, we use $\mathcal{C}$ to denote a configuration of $\{h_{\Delta_D}\}$ and $\{k_{\Delta_0}\}$. $|\psi_0\rangle$ can then be written as:

$$|\psi_0\rangle = \sum_{\mathcal{C}} |\mathcal{C}\rangle. \tag{2.77}$$

The decorated domain wall models are constructed from the $H \times K$ paramagnet Hamiltonian by conjugating with a FDQC $\mathcal{U}_\eta$. The FDQC is built from a choice of η in Eq. (2.68) and takes the form:

$$\mathcal{U}_\eta \equiv \prod_{\Delta_{D-1}} U_{\Delta_{D-1}}, \tag{2.78}$$

where $U_{\Delta_{D-1}}$ are the local gates:

$$U_{\Delta_{D-1}} \equiv \sum_{\mathcal{C}} \bar{\eta}_{\mathcal{C}}(\Delta_{D-1})|\mathcal{C}\rangle\langle\mathcal{C}|. \tag{2.79}$$

Here, $\bar{\eta}_{\mathcal{C}}(\Delta_{D-1})$ is a $U(1)$-valued phase that depends on the configuration $\mathcal{C}$ in the vicinity of

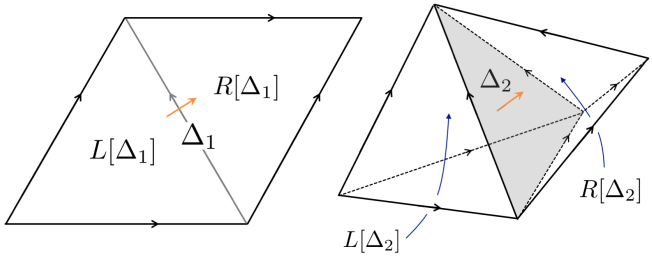

Figure 2.8: The D-simplices $L[\Delta_{D-1}]$ and $R[\Delta_{D-1}]$ are the two D-simplices that neighbor the $(D-1)$-simplex Δ_{D-1}. The normal vector of Δ_{D-1} (orange) is determined by the orientation of Δ_{D-1} (Fig. 2.6) and points from $L[\Delta_{D-1}]$ to $R[\Delta_{D-1}]$.

Δ_{D-1}. For a $(D-1)$-simplex $\Delta_{D-1} = \langle 1, \ldots, D-1 \rangle$, $\bar{\eta}_{\mathcal{C}}(\Delta_{D-1})$ is explicitly:

$$\begin{aligned} \bar{\eta}_{\mathcal{C}}(\Delta_{D-1}) &\equiv \eta(1, k_1, \ldots, k_{D-1}; h_{L[\Delta_{D-1}]}, h_{R[\Delta_{D-1}]}) \\ &= \prod_{j=1}^{p} \nu_j(1, k_1, \ldots, k_{D-1})^{\phi_j\left(h_{L[\Delta_{D-1}]}, h_{R[\Delta_{D-1}]}\right)}, \end{aligned} \tag{2.80}$$

where $k_1, \ldots, k_{D-1}$ are the K labels at the vertices of Δ_{D-1} in the configuration $\mathcal{C}$, and $L[\Delta_{D-1}]$ and $R[\Delta_{D-1}]$ are the D-simplices on either side of Δ_{D-1} as depicted in Fig. 2.8.

We are now able to define the decorated domain wall Hamiltonian H_η corresponding to the element $[\eta]$ in the group cohomology $\mathcal{H}^1[H, \mathcal{H}^D[K, U(1)]]$. We define H_η to be the Hamiltonian:

$$H_\eta \equiv \mathcal{U}_\eta^\dagger H_0 \mathcal{U}_\eta. \tag{2.81}$$

H_η is local due to the finite Lieb-Robinson length of $\mathcal{U}_\eta$, and it is symmetric due to the fact that $\mathcal{U}_\eta$ commutes with the global symmetry $u((h,k))$, for every (h,k) in $H \times K$. The symmetry of $\mathcal{U}_\eta$ can be checked by using that ν_j and ϕ_j are closed and homogeneous for every j. Note that the local gates $U_{\Delta_{D-1}}$ are not symmetric for non-trivial η, however. The ground state of H_η can be constructed by applying $\mathcal{U}_\eta$ to the ground state of H_0; this defines:

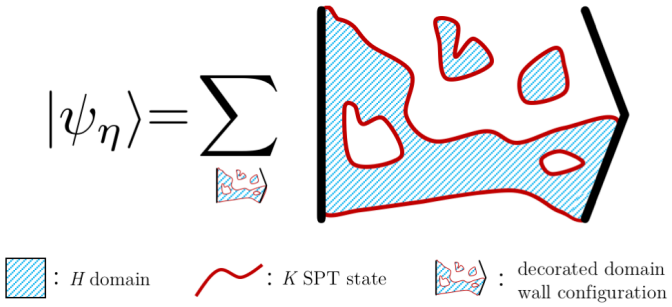

Figure 2.9: The ground state $|\psi_\eta\rangle$ is a superposition of decorated domain wall configurations, where H domains (blue) are decorated with K SPT states (red) along the domain walls.

$$|\psi_\eta\rangle \equiv \mathcal{U}_\eta|\psi_0\rangle = \sum_{\mathcal{C}} \prod_{\Delta_{D-1}} \bar{\eta}_{\mathcal{C}}(\Delta_{D-1})|\mathcal{C}\rangle. \tag{2.82}$$

The ground state $|\psi_\eta\rangle$ can be understood in terms of H domain walls decorated by $(D-1)$-dimensional K SPT states. To see this, we expand the amplitude in Eq. (2.82) using the expression for $\bar{\eta}_{\mathcal{C}}(\Delta_{D-1})$ in Eq. (2.80). The amplitude corresponding to the configuration $\mathcal{C}$ is:

$$\prod_{\Delta_{D-1}} \prod_{j=1}^{p} \nu_j(1, k_1, \ldots, k_{D-1})^{\phi_j\left(h_{L[\Delta_{D-1}]}, h_{R[\Delta_{D-1}]}\right)}. \tag{2.83}$$

The functions ϕ_j count the H domain walls between the D-simplices $L[\Delta_{D-1}]$ and $R[\Delta_{D-1}]$ bordering Δ_{D-1}. Factors of ν_j are assigned to the $(D-1)$-simplices according to the number of H domain walls. The product of ν_j along an H domain wall gives a $(D-1)$-dimensional K SPT state defined in Ref. [49]. The ground state $|\psi_\eta\rangle$ is depicted in Fig. 2.9.

2.B.3 Cluster state example

To make the construction of the decorated domain wall models less abstract, we consider a 1D example with a $\mathbb{Z}_2 \times \mathbb{Z}_2$ symmetry. We show that the decorated domain wall model reproduces the cluster state model in Section 2.2.4.

For $D = 1$ with a $\mathbb{Z}_2 \times \mathbb{Z}_2$ symmetry, the decorated domain wall model is characterized by an element of the group cohomology $\mathcal{H}^1[\mathbb{Z}_2, \mathcal{H}^1[\mathbb{Z}_2, U(1)]]$. In this case, $\mathcal{H}^1[\mathbb{Z}_2, U(1)]$ forms a $\mathbb{Z}_2$ group, and the generator can be represented by the function $\nu : \mathbb{Z}_2^2 \to U(1)$ defined by:

$$\nu(k_0, k_1) = (-1)^{k_0 + k_1}. \tag{2.84}$$

The non-trivial element of the group cohomology group $\mathcal{H}^1[\mathbb{Z}_2, \mathcal{H}^1[\mathbb{Z}_2, U(1)]] = \mathbb{Z}_2$ can be labeled by the function:

$$\eta = \nu^\phi : \mathbb{Z}_2^2 \times \mathbb{Z}_2^2 \to U(1), \tag{2.85}$$

where $\phi : \mathbb{Z}_2^2 \to \mathbb{Z}_2$ is:

$$\phi(h_0, h_1) = h_0 + h_1. \tag{2.86}$$

More explicitly, η is defined by:

$$\eta(k_0, k_1; h_0, h_1) = \nu(k_0, k_1)^{\phi(h_0, h_1)} = (-1)^{(k_0 + k_1)(h_0 + h_1)}. \tag{2.87}$$

We can now build the decorated domain wall model on a periodic 1D lattice with a qubit at each edge Δ_1 and at each vertex Δ_0. To make contact with the cluster state model in Section 2.2.4, we label edges by even integers ($\Delta_1 = 2j$) and vertices by odd integers ($\Delta_0 = 2j + 1$). The symmetry action corresponding to (h, k) in $\mathbb{Z}_2 \times \mathbb{Z}_2$ is:

$$u\big((h, k)\big)|\{h_{2j}\}, \{k_{2j+1}\}\rangle = |\{h + h_{2j}\}, \{k + k_{2j+1}\}\rangle, \tag{2.88}$$

where the addition is modulo 2. This can be represented by the product of Pauli X operators:

$$u((h,k)) = \Big(\prod_j X_{2j}\Big)^h \Big(\prod_j X_{2j+1}\Big)^k, \tag{2.89}$$

in agreement with the symmetry action in Section 2.2.4.

We construct the Hamiltonian for the decorated domain wall model starting with the $\mathbb{Z}_2 \times \mathbb{Z}_2$ paramagnet Hamiltonian H_0:

$$H_0 = -\sum_i X_i. \tag{2.90}$$

Note that the paramagnet Hamiltonian above only differs from the Hamiltonian described in Eq. (2.73) by a constant shift of energy. The ground state of the paramagnet Hamiltonian is the product state:

$$|\psi_0\rangle = \sum_{\mathcal{C}} |\mathcal{C}\rangle = |+\cdots+\rangle. \tag{2.91}$$

The last step in the construction is to conjugate H_0 by the FDQC $\mathcal{U}_\eta$. Here, $\mathcal{U}_\eta$ is given by:

$$\mathcal{U}_\eta = \prod_j \sum_{\mathcal{C}} (-1)^{k_{2j+1}(h_{2j}+h_{2j+2})} |\mathcal{C}\rangle\langle\mathcal{C}|, \tag{2.92}$$

which can be written using Pauli Z operators as:

$$\mathcal{U}_\eta = \prod_j Z_{2j+1}^{\frac{1}{2}(1-Z_{2j}Z_{2j+2})}. \tag{2.93}$$

The exponent in Eq. (2.93) detects domain walls between the sites $2j$ and $2j+2$. The operator Z_{2j+1} then creates a charge at $2j+1$ if there is a domain wall between the neighboring even sites. The charge can be interpreted as a non-trivial 0-dimensional SPT state.

U_η can equivalently be expressed as a product of control Z operators:

$$\mathcal{U}_\eta = \prod_j CZ_{2j(2j+1)} CZ_{(2j+1)(2j+2)} = \prod_i CZ_{i(i+1)}. \tag{2.94}$$

In this form, one can see that $\mathcal{U}_\eta$ is precisely the FDQC $\mathcal{U}_{\text{CS}}$ from Section 2.2.4. Furthermore, the Hamiltonian $H_\eta = \mathcal{U}_\eta H_0 \mathcal{U}_\eta^\dagger$ is the same as the cluster state Hamiltonian H_{CS} in Eq. (2.12).

2.B.4 Effective boundary symmetry action of the decorated domain wall models

Our decorated domain wall models are designed so that the effective boundary symmetry action corresponding to some element $(h, 1)$ in $H \times K$ is a FDQC that prepares a non-trivial K SPT state from a trivial SPT state. In fact, the effective boundary symmetry action prepares the representative group cohomology K SPT states constructed in Ref. [49]. For simplicity, we assume that H is Abelian. The computation can be generalized to non-Abelian symmetries straightforwardly.

As described in Section 2.2.2, the first step in computing the effective boundary symmetry action is to define the boundary Hilbert space. To do so, we truncate the Hamiltonian H_η to a manifold M with boundary by removing any terms in H_η that are supported on sites outside of M. The boundary Hilbert space $\mathcal{H}_\eta^{\text{low}}$ is then the low-energy Hilbert space of the truncated Hamiltonian H_η^M.

We also define a truncation of the FDQC $\mathcal{U}_\eta$ to M. $\mathcal{U}_\eta$ is truncated by removing all of the gates supported on sites outside of M. This gives the FDQC:

$$\mathcal{U}_\eta^M \equiv \prod_{\Delta_{D-1} \in M \setminus \partial M} U_{\Delta_{D-1}}, \tag{2.95}$$

where the product is over $(D-1)$-simplices in M that do not belong to the boundary of M. Importantly, for any state $|\psi_{\text{low}}\rangle$ in the low-energy Hilbert space of H_η^M, the FDQC $(\mathcal{U}_\eta^M)^\dagger$ disentangles $|\psi_{\text{low}}\rangle$ away from the boundary of M. More specifically, the action of $(\mathcal{U}_\eta^M)^\dagger$ on

$|\psi_{\text{low}}\rangle$ is:

$$(\mathcal{U}_\eta^M)^\dagger|\psi_{\text{low}}\rangle = |\psi\rangle_{M\setminus M_\circ} \otimes |\psi_{\text{prod}}\rangle_{M_\circ}. \tag{2.96}$$

Here, $M_\circ$ is a submanifold of M that contains the sites greater than two Lieb-Robinson lengths from the boundary of M but does not contain any sites within one Lieb-Robinson length of the boundary. Furthermore, in Eq. (2.96) $|\psi\rangle_{M\setminus M_\circ}$ is some state defined on the sites in M outside of $M_\circ$, and $|\psi_{\text{prod}}\rangle$ is a symmetric product state on the sites in $M_\circ$. Eq. (2.96) agrees with the intuition that states in the boundary Hilbert space resemble the ground state of H_η far away from the boundary of M.

We now define the effective boundary symmetry action corresponding to (h,k) in $H\times K$ to be:

$$v\big((h,k)\big) \equiv u_M\big((h,k)\big)\mathcal{U}_\eta^M u_{M_\circ}^\dagger\big((h,k)\big)(\mathcal{U}_\eta^M)^\dagger, \tag{2.97}$$

where $u_M\big((h,k)\big)$ and $u_{M_\circ}^\dagger\big((h,k)\big)$ are the onsite symmetry actions restricted to M and $M_\circ$, respectively. To show that this is an appropriate choice for the effective boundary symmetry action, we consider acting with $v\big((h,k)\big)$ on an arbitrary state $|\psi_{\text{low}}\rangle$ in the boundary Hilbert space:

$$v\big((h,k)\big)|\psi_{\text{low}}\rangle = u_M\big((h,k)\big)\mathcal{U}_\eta^M u_{M_\circ}^\dagger\big((h,k)\big)(\mathcal{U}_\eta^M)^\dagger|\psi_{\text{low}}\rangle. \tag{2.98}$$

Using Eq. (2.96) and that $|\psi_{\text{prod}}\rangle_{M_\circ}$ is symmetric, we find:

$$v\big((h,k)\big)|\psi_{\text{low}}\rangle = u_M\big((h,k)\big)\mathcal{U}_\eta^M\Big(|\psi\rangle_{M\setminus M_\circ} \otimes |\psi_{\text{prod}}\rangle_{M_\circ}\Big) = u_M\big((h,k)\big)|\psi_{\text{low}}\rangle. \tag{2.99}$$

Therefore, the action of $v\big((h,k)\big)$ on states in the boundary Hilbert space is the same as the action of $u_M\big((h,k)\big)$. This implies that $v\big((h,k)\big)$ forms a linear representation of the symmetry on the boundary Hilbert space. The support of $v\big((h,k)\big)$ is also localized to the

boundary of M. This is because $\mathcal{U}_\eta$ is symmetric, and $\mathcal{U}_\eta^M$ commutes with $u_{M_\circ}^\dagger((h,k))$ up to an operator supported within three Lieb-Robinson lengths of the boundary of M.

Finally, we compute the effective boundary symmetry action for an element $(h,1)$ in $H \times K$ using Eq. (2.97). We start by conjugating $\mathcal{U}_\eta^M$ by the symmetry action restricted to $M_\circ$:

$$u_{M_\circ}((h,1))\mathcal{U}_\eta^M u_{M_\circ}^\dagger((h,1)). \tag{2.100}$$

The FDQC $\mathcal{U}_\eta^M$ only depends on the $|H|$-dimensional qudits through the functions ϕ_j in Eq. (2.80). Given that each ϕ_j is homogeneous [Eq. (2.70)], $\mathcal{U}_\eta^M$ is only affected by the symmetry action near the boundary of $M_\circ$. In particular, one can use that ϕ_j is closed [Eq. (2.69)] to show:

$$u_{M_\circ}((h,1))\mathcal{U}_\eta^M u_{M_\circ}^\dagger((h,1)) = \mathcal{V}((h,1))\mathcal{U}_\eta^M, \tag{2.101}$$

where $\mathcal{V}((h,1))$ is the operator:

$$\mathcal{V}((h,1)) = \prod_{\Delta_{D-1}\in\partial M_\circ} \sum_{\mathcal{C}} \bar{\eta}_{\mathcal{C}}^{(h)}(\Delta_{D-1})^{O_{\Delta_{D-1}}} |\mathcal{C}\rangle\langle\mathcal{C}|. \tag{2.102}$$

In the expression above, the product is over $(D-1)$-simplices in the boundary of $M_\circ$, $O_{\Delta_{D-1}}$ is the $\{\pm 1\}$-valued orientation of the simplex Δ_{D-1} relative to the boundary of $M_\circ$, and for $\Delta_{D-1} = \langle 1, \ldots, D-1\rangle$, $\bar{\eta}_{\mathcal{C}}^{(h)}(\Delta_{D-1})$ is the $U(1)$ phase:

$$\bar{\eta}_{\mathcal{C}}^{(h)}(\Delta_{D-1}) \equiv \prod_{j=1}^{p} \nu_j(1, k_1, \ldots, k_{D-1})^{\phi_j(1,h)}. \tag{2.103}$$

If $\phi_j(1,h)$ is non-trivial, then $\mathcal{V}((h,1))$ is precisely the FDQC described in Ref. [49] that prepares a K SPT state characterized by the element of $H^D[K, U(1)]$ labeled by ν_j.

To finish the calculation of the effective boundary symmetry action, we substitute Eq. (2.101)

into Eq. (2.97). This gives us:

$$v\big((h,1)\big) = u_{M\setminus M_\circ}\big((h,1)\big)\mathcal{V}\big((h,1)\big), \tag{2.104}$$

where $u_{M\setminus M_\circ}\big((h,1)\big)$ is the restriction of the onsite symmetry to the sites in M that are outside of $M_\circ$. We now see that, for any $(h,1)$ in $H\times K$ for which $\phi_j(1,h)$ is non-trivial, the effective boundary symmetry action prepares a $(D-1)$-dimensional K SPT state corresponding to ν_j along the boundary of $M_\circ$. If the decorated domain wall model corresponds to a non-trivial element of the group cohomology $\mathcal{H}^1[H,\mathcal{H}^D[K,U(1)]]$ then $\phi_j(1,h)$ is non-trivial for some group element $(h,1)$ and ν_j characterizes a non-trivial K SPT phase.

2.B.5 Completing the proof of Proposition 2

Thus far, we have shown that the decorated domain wall models characterized by a non-trivial element of the group cohomology $\mathcal{H}^1[H,\mathcal{H}^D[K,U(1)]]$ have an effective boundary symmetry action that prepares a non-trivial SPT state in $(D-1)$-dimensions. We now use the decorated domain wall models to complete the proof of Proposition 2. In particular, we argue that a stabilizer state $|\psi_{\mathcal{S}}\rangle$ in dimension $D\geq 2$ cannot belong to the same SPT phase as a non-trivial decorated domain wall model (assuming the symmetry is represented by a product of Pauli operators). The key observation is that the effective boundary symmetry action of the stabilizer model cannot prepare a non-trivial $(D-1)$-dimensional K SPT state for $D\geq 2$.

To derive a contradiction, suppose $|\psi_{\mathcal{S}}\rangle$ belongs to the same SPT phase as the ground state $|\psi_\eta\rangle$ of a non-trivial decorated domain wall model. Then there exists a FDQC $\mathcal{U}_{\text{sym}}$ composed of symmetric gates with the property:

$$\mathcal{U}_{\text{sym}}|\psi_{\mathcal{S}}\rangle = |\psi_\eta\rangle. \tag{2.105}$$

With this, we can define a Hamiltonian $\widetilde{H}_\eta$ as:

$$\widetilde{H}_\eta \equiv \mathcal{U}_{\text{sym}} H_{\mathcal{S}} \mathcal{U}_{\text{sym}}^\dagger, \tag{2.106}$$

where $H_{\mathcal{S}}$ is the local stabilizer parent Hamiltonian for $|\psi_{\mathcal{S}}\rangle$. Notably, $\widetilde{H}_\eta$ has the same ground state as the decorated domain wall Hamiltonian H_η. In what follows, we use $\widetilde{H}_\eta$ to compute an alternative effective boundary symmetry action $\widetilde{\mathcal{V}}\big((h,k)\big)$ for the decorated domain wall model. We then show that $\widetilde{\mathcal{V}}\big((h,k)\big)$ is inconsistent with the effective boundary symmetry action $\mathcal{V}\big((h,k)\big)$ derived using H_η.

The first step in deriving an effective boundary symmetry action for the decorated domain wall model using $\widetilde{H}_\eta$ is to truncate $\widetilde{H}_\eta$ and define the corresponding boundary Hilbert space. Given a manifold with boundary M, we truncate $\widetilde{H}_\eta$ to the submanifold $M_\circ$, with $M_\circ$ defined below Eq. (2.96). By truncating to $M_\circ$, we ensure that the low-energy Hilbert space $\widetilde{\mathcal{H}}_\eta^{\text{low}}$ of the truncated Hamiltonian $\widetilde{H}_\eta^{M_\circ}$ contains the low-energy Hilbert space $\mathcal{H}_\eta^{\text{low}}$ of the Hamiltonian H_η^M, i.e., $\mathcal{H}_\eta^{\text{low}} \subset \widetilde{\mathcal{H}}_\eta^{\text{low}}$. Therefore, any effective boundary symmetry action defined on $\widetilde{\mathcal{H}}_\eta^{\text{low}}$ gives an effective boundary symmetry action on $\mathcal{H}_\eta^{\text{low}}$.

Recall that, in the proof of Proposition 1, we argued that an effective boundary symmetry action for $|\psi_{\mathcal{S}}\rangle$ with a local stabilizer parent Hamiltonian $H_{\mathcal{S}}$ is given by a tensor product of Pauli operators denoted as $\mathcal{P}\big((h,k)\big)$. Using $\mathcal{P}\big((h,k)\big)$ constructed on the submanifold $M_\circ$, we define $\widetilde{\mathcal{V}}\big((h,k)\big)$ as:

$$\widetilde{\mathcal{V}}\big((h,k)\big) \equiv \mathcal{U}_{\text{sym}} \mathcal{P}\big((h,k)\big) \mathcal{U}_{\text{sym}}^\dagger. \tag{2.107}$$

$\widetilde{\mathcal{V}}\big((h,k)\big)$ gives an effective boundary symmetry action on $\widetilde{\mathcal{H}}_\eta^{\text{low}}$, and thus, it gives an effective boundary symmetry action on the boundary Hilbert space $\mathcal{H}_\eta^{\text{low}}$. This means that, for any $(h,k) \in H \times K$ and any state $|\psi_{\text{low}}\rangle \in \mathcal{H}_\eta^{\text{low}}$, we have:

$$\mathcal{V}\big((h,k)\big)|\psi_{\text{low}}\rangle = \widetilde{\mathcal{V}}\big((h,k)\big)|\psi_{\text{low}}\rangle. \tag{2.108}$$

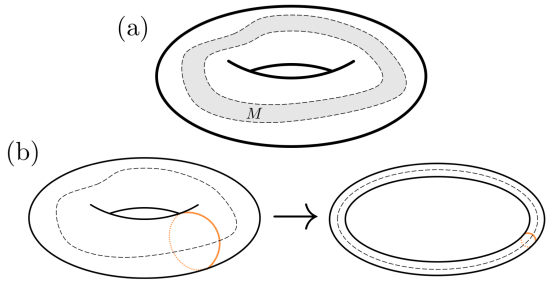

Figure 2.10: (a) The submanifold M of the torus is topologically equivalent to a thickened 1-dimensional torus, and the boundary of M has two components (dashed lines). (b) We compactify the 2-dimensional torus to a (quasi) 1-dimensional torus by making the meridian of the torus (orange) finite. Note that the component of the boundary of M (dashed line) forms a non-contractible submanifold of the compactified torus.

We argue below that Eq. (2.108) leads to a contradiction. The main idea is that $\mathcal{V}((h,k))$ prepares a non-trivial K SPT state, while $\widetilde{\mathcal{V}}((h,k))$ is unable to prepare a non-trivial $(D-1)$-dimensional K SPT state from a trivial SPT state. To make this explicit, we use dimensional reduction, as described in Ref. [98].

We consider the decorated domain wall model on a D-dimensional torus T^D. We then construct a submanifold M with boundary, by thickening a non-contractible $(D-1)$-dimensional torus embedded in T^D (see Fig. 2.10 for an example). The boundary of M has two components, each of which is topologically equivalent to a $(D-1)$-dimensional torus. We truncate to the submanifold M in the usual way and define the effective boundary symmetry actions $\mathcal{V}((h,k))$ and $\widetilde{\mathcal{V}}((h,k))$. Since the boundary of M has two disconnected components, the effective boundary symmetry actions split as:

$$\begin{aligned}\mathcal{V}((h,k)) &= \mathcal{V}_a((h,k))\mathcal{V}_b((h,k)) \\ \widetilde{\mathcal{V}}((h,k)) &= \widetilde{\mathcal{V}}_a((h,k))\widetilde{\mathcal{V}}_b((h,k)),\end{aligned} \tag{2.109}$$

where a and b denote the two components of the boundary of M.

We focus on the operators $\mathcal{V}_a((h,k))$ and $\widetilde{\mathcal{V}}_a((h,k))$. These create a symmetry branch cut (or symmetry defect [99]) along a, and can intepreted as inserting symmetry flux through

the D-torus. It is important to note that, for some group element $(h,1)$, $\mathcal{V}_a((h,1))$ prepares a non-trivial $(D-1)$-dimensional K SPT state on the non-contractible submanifold a. Also note that, for every (h,k) in $H\times K$, $\widetilde{\mathcal{V}}_a((h,k))$ takes the form of a tensor product of Pauli operators $\mathcal{P}_a((h,k))$ conjugated by $\mathcal{U}_{\text{sym}}$, as in Eq. (2.107):

$$\widetilde{\mathcal{V}}_a((h,k)) = \mathcal{U}_{\text{sym}}\mathcal{P}_a((h,k))\mathcal{U}_{\text{sym}}^\dagger. \tag{2.110}$$

Assuming the components a and b are well separated in terms of the Lieb-Robinson length of $\mathcal{U}_\eta$, the action of $\mathcal{V}_a((h,k))$ and $\widetilde{\mathcal{V}}_a((h,k))$ agree on any state belonging to $\mathcal{H}_\eta^{\text{low}}$:

$$\mathcal{V}_a((h,k))|\psi_{\text{low}}\rangle = \widetilde{\mathcal{V}}_a((h,k))|\psi_{\text{low}}\rangle. \tag{2.111}$$

In particular, the ground state $|\psi_\eta\rangle$ on T^D is in the low-energy Hilbert space $\mathcal{H}_\eta^{\text{low}}$, so the operators satisfy:

$$\mathcal{V}_a((h,k))|\psi_\eta\rangle = \widetilde{\mathcal{V}}_a((h,k))|\psi_\eta\rangle. \tag{2.112}$$

Finally, we consider a compactification of T^D to a (quasi) $(D-1)$-dimensional torus T^{D-1} by making one of the directions in T^D finite, as shown in Fig. 2.10. In particular, we compactify T^D to T^{D-1} in such a way that a forms a non-contractible submanifold of T^{D-1}. The equality in Eq. (2.112) also holds on the $(D-1)$-dimensional torus.

On the $(D-1)$-dimensional torus, we can argue that Eq. (2.112) gives a contradiction. It can be checked using the methods of Ref. [46] that $\mathcal{V}_a((h,1))$ prepares a non-trivial $(D-1)$-dimensional K SPT state for some choice of h, while $\widetilde{\mathcal{V}}_a((h,1))$ cannot change the $(D-1)$-dimensional SPT phase of the compactified state $|\psi_\eta\rangle$ for any h. The latter is made explicit by writing $\widetilde{\mathcal{V}}_a((h,1))$ as:

$$\widetilde{\mathcal{V}}_a((h,1)) = \mathcal{U}_{\text{sym}}\mathcal{P}_a((h,1))\mathcal{U}_{\text{sym}}^\dagger. \tag{2.113}$$

Since $\mathcal{U}_{\text{sym}}$ and $\mathcal{U}_{\text{sym}}^\dagger$ are FDQCs composed of symmetric gates, they do not change the SPT phase. Furthermore, the tensor product of Pauli operators $\mathcal{P}_a\big((h,1)\big)$ is able to create charges, but it is unable change the SPT phase of a $(D-1)$-dimensional SPT state, for $D \geq 2$. Therefore, the states $\mathcal{V}_a\big((h,1)\big)|\psi_\eta\rangle$ and $\widetilde{\mathcal{V}}_a\big((h,1)\big)|\psi_\eta\rangle$ belong to distinct K SPT phases for some $h \in H$.

We have shown that Eq. (2.112) is inconsistent. This implies that the stabilizer state $|\psi_{\mathcal{S}}\rangle$ cannot belong to the same phase as the ground state $|\psi_\eta\rangle$ of a non-trivial decorated domain wall model, assuming the symmetry is represented by a Pauli string. In other words, the stabilizer state must belong to an SPT phase characterized by the trivial element of $\mathcal{H}^1[H, \mathcal{H}^D[K, U(1)]]$. This completes the proof of Proposition 2.

2.C Existence of a local stabilizer parent Hamiltonian

In the proof of Proposition 1, we claimed that a stabilizer SPT state admits a local symmetric stabilizer Hamiltonian. Here, we justify this claim. We start by proving a lemma regarding the stabilizer group $\mathcal{G}$, defined in Eq. (2.30).

Lemma 1 *Let $\mathcal{G}$ be the stabilizer group defined as:*

$$\mathcal{G} \equiv \langle U Z_i U^\dagger : i \in \textit{sites} \rangle, \tag{2.114}$$

which uniquely fixes the stabilizer state $|\psi_{\mathcal{S}}\rangle$ constructed from $|0\ldots0\rangle$ by the Clifford unitary U. Then, if a Pauli string P satisfies one of the following, P is contained in $\mathcal{G}$:

(i) P commutes with every element of $\mathcal{G}$

(ii) P stabilizes $|\psi_{\mathcal{S}}\rangle$, i.e., $P|\psi_{\mathcal{S}}\rangle = |\psi_{\mathcal{S}}\rangle$.

Proof of Lemma 1: We make use of the fact that $\mathcal{G}$ can be constructed by conjugating the generators of the stabilizer group $\mathcal{G}_0$ by the Clifford unitary U, where $\mathcal{G}_0$ is:

$$\mathcal{G}_0 \equiv \langle Z_i : i \in \text{sites} \rangle. \tag{2.115}$$

If the Pauli string P satisfies (i), then $U^\dagger PU$ is a Pauli string that commutes with every element of $\mathcal{G}_0$. Any Pauli string that commutes with $\mathcal{G}_0$ must be a product of Pauli Z operators. This implies that P is a product of Pauli strings of the form $UZ_iU^\dagger$. Hence, P belongs to $\mathcal{G}$.

If the Pauli string P satisfies (ii), then $U^\dagger PU$ is a Pauli string that leaves $|0\dots0\rangle$ invariant: $U^\dagger PU|0\dots0\rangle = |0\dots0\rangle$. The only Pauli strings that leave $|0\dots0\rangle$ invariant are products of Pauli Z operators. Therefore, $U^\dagger PU$ is a product of Pauli Z operators, and P is a product of elements in $\mathcal{G}$. □

Now, we can prove the following statement about the existence of a local symmetric stabilizer Hamiltonian.

Lemma 2 *Let $|\psi_{\mathcal{S}}\rangle$ be a stabilizer state which is a unique ground state of a geometrically local Hamiltonian H_{loc}.*[19] *Then, there exists a local stabilizer Hamiltonian $H_{\mathcal{S}}$ such that $|\psi_{\mathcal{S}}\rangle$ is the unique ground state of $H_{\mathcal{S}}$. Furthermore, if $|\psi_{\mathcal{S}}\rangle$ is invariant under a Pauli string P, i.e., $P|\psi_{\mathcal{S}}\rangle = |\psi_{\mathcal{S}}\rangle$, then $H_{\mathcal{S}}$ commutes with P.*

Proof of Lemma 2. Since $|\psi_{\mathcal{S}}\rangle$ is a stabilizer state, there is a stabilizer group $\mathcal{G}$ that uniquely fixes $|\psi_{\mathcal{S}}\rangle$, such as the stabilizer group in Lemma 1. We claim that the generators of $\mathcal{G}$ can always be chosen to be geometrically local. To see this, we imagine minimizing the largest support of the generators over all possible choices for generators of $\mathcal{G}$. We let d_S denote the minimum length such that each stabilizer term can be contained in a ball of diameter d_S. We argue that d_S is constant, i.e., independent of the system size.

If there exists a generator S that is not contained in a constant size ball, then there is a stabilizer state $|\phi_{\mathcal{S}}\rangle$ that has a $+1$ eigenvalue for all the generators except S, for which the eigenvalue is some root of unity (not equal to $+1$). $|\psi_{\mathcal{S}}\rangle$ and $|\phi_{\mathcal{S}}\rangle$ are orthogonal, and yet they have the same reduced density matrices on any constant-size region. The latter follows

[19] We recall that a geometrically local Hamiltonian is a sum of terms such that the support of each term can be contained within a ball of fixed finite diameter.

from the fact that S is not contained in any constant-size region and that the reduced density matrices of stabilizer states on a region M depend solely on the stabilizer group elements whose support is contained in M [100, 101]. (Note that if there is another generator T such that ST is supported in a constant-sized region M, then we can use ST as a generator instead of S. This contradicts the assumption that we have minimized the maximum support of the generators.)

Since $|\psi_{\mathcal{S}}\rangle$ and $|\phi_{\mathcal{S}}\rangle$ have the same reduced density matrices on constant-sized regions, $|\phi_{\mathcal{S}}\rangle$ gives another ground state of H_{loc}. This conflicts with the assumption that H_{loc} has a unique ground state. Thus, the support of S must be contained in a constant-size ball, and d_S can be chosen independent of the system size. Therefore, it is possible to find a set of generators for $\mathcal{G}$, which are geometrically local. We define $H_{\mathcal{S}}$ to be the negative sum of the local generators (with their Hermitian conjugates). $|\psi_{\mathcal{S}}\rangle$ is the unique ground state of $H_{\mathcal{S}}$, since the terms of $H_{\mathcal{S}}$ span $\mathcal{G}$.

Lastly, if $|\psi_{\mathcal{S}}\rangle$ is invariant under a Pauli operator P, then P is an element of $\mathcal{G}$, assuming $\mathcal{G}$ is the stabilizer group in Lemma 1. This follows directly from Lemma 1. Since $\mathcal{G}$ is a commuting group, P commutes with $H_{\mathcal{S}}$. □

2.D Modified effective boundary symmetry action

To prove Proposition 1, we derived an effective boundary symmetry action $\mathcal{P}(g)$ for the stabilizer state $|\psi_{\mathcal{S}}\rangle$ using a stabilizer parent Hamiltonian $H_{\mathcal{S}}$. While the effective boundary symmetry action forms a linear representation of the $G = \mathbb{Z}_q^m$ symmetry in the boundary Hilbert space, it is only guaranteed to satisfy the group laws of G up to products of stabilizer terms belonging to the truncated Hamiltonian $H_{\mathcal{S}}^M$. Here, we complete the proof of Proposition 1 by showing that the effective boundary symmetry action can be modified so that is satisfies the group laws exactly. This assumes that the state $|\psi_{\mathcal{S}}\rangle$ is defined on a Hilbert space composed of q-dimensional qudits.

To begin, we verify that the effective boundary symmetry action satisfies the group laws up to elements of $\mathcal{G}^M$, where $\mathcal{G}^M$ is the stabilizer group generated by the terms in $H_{\mathcal{S}}^M$. Recall

that the effective boundary symmetry action derived in the proof of Proposition 1 is:

$$\mathcal{P}(g) = P_M(g)\tilde{P}_M^\dagger(g), \tag{2.116}$$

where g is in G, $P_M(g)$ is the restriction of the onsite symmetry to M, and $\tilde{P}_M^\dagger(g)$ belongs to $\mathcal{G}^M$. The product of $\mathcal{P}(g)$ and $\mathcal{P}(h)$ for arbitrary elements g, h in G is then:

$$\mathcal{P}(g)\mathcal{P}(h) = \left[P_M(g)\tilde{P}_M^\dagger(g)\right]\left[P_M(h)\tilde{P}_M^\dagger(h)\right]. \tag{2.117}$$

This can be simplified by commuting $\tilde{P}_M^\dagger(g)$ past $P_M(h)$. These commute because $P_M(h)$ is the onsite symmetry action restricted to M, and $\tilde{P}_M^\dagger(g)$ is a product of symmetric stabilizer terms whose supports are contained in M. This gives us:

$$\mathcal{P}(g)\mathcal{P}(h) = P_M(gh)\tilde{P}_M^\dagger(g)\tilde{P}_M^\dagger(h). \tag{2.118}$$

The product $\tilde{P}_M^\dagger(g)\tilde{P}_M^\dagger(h)$ agrees with $\tilde{P}_M^\dagger(gh)$ away from the boundary of M [see the definition in Eq. (2.34)]. Moreover, it only differs from $\tilde{P}_M^\dagger(gh)$ by elements of $\mathcal{G}^M$ that are supported near the boundary of M. We define $S(g,h)$ to be the product of stabilizer terms in $\mathcal{G}^M$ near the boundary of M such that:

$$\tilde{P}_M^\dagger(g)\tilde{P}_M^\dagger(h) = S(g,h)\tilde{P}_M^\dagger(gh). \tag{2.119}$$

Substituting Eq. (2.119) into Eq. (2.118), we arrive at:

$$\mathcal{P}(g)\mathcal{P}(h) = S(g,h)\mathcal{P}(gh), \tag{2.120}$$

which implies that the effective boundary symmetry action obeys the group laws up to elements of $\mathcal{G}^M$ supported near the boundary of M.

We note that the operators in Eq. (2.119) are mutually commuting. This is a consequence

of the fact that, for any $g \in G$, $\tilde{P}_M^\dagger(g)$ is a product of symmetric stabilizer terms whose supports are contained in M. We also point out that the effective boundary symmetry action $\mathcal{P}(1)$, corresponding to the identity in G, can be taken to be the identity. This implies that $S(g,1) = S(1,g) = 1$, for any $g \in G$.

The extra stabilizer terms $S(g,h)$ in Eq. (2.120) can be eliminated by modifying the effective boundary symmetry action. In particular, we are free to modify $\mathcal{P}(g)$ by any product of stabilizers in $H_{\mathcal{S}}^M$ supported near the boundary of M. We define $\mathcal{P}'(g)$ to be the effective boundary symmetry action modified by stabilizer terms $T(g)$, i.e.:

$$\mathcal{P}'(g) = T(g)\mathcal{P}(g). \tag{2.121}$$

In what follows, we describe a particular choice of $T(g)$ for every $g \in G$ such that the modified effective boundary symmetry action $\mathcal{P}'(g)$ satisfies the group laws exactly.

To specify our choice of $T(g)$, we introduce some notation for the elements of $G = \mathbb{Z}_q^m$. We denote the m generators of $\mathbb{Z}_q^m$ as $a_1, \ldots, a_m$, and the product of two generators a_i, a_j as $a_i a_j$. A general element g of $\mathbb{Z}_q^m$ can then be written as:

$$g = a_1^{g_1} a_2^{g_2} \cdots a_m^{g_m}, \tag{2.122}$$

where $g_1, \ldots, g_m$ are integers belonging to $\{0, \ldots, q-1\}$.

With this, we take $T(a_1^{g_1} a_2^{g_2} \cdots a_m^{g_m})$ to be the product of stabilizer terms given by:

$$T(a_1^{g_1} a_2^{g_2} \cdots a_m^{g_m}) = \prod_{\substack{i=1 \\ g_i \neq 0}}^{m} \prod_{k_i=1}^{g_i} S(a_{i-1}^{g_{i-1}} a_i^{k_i}, a_i^{g_i - k_i} a_{i+1}^{g_{i+1}} \cdots a_m^{g_m}). \tag{2.123}$$

To build intuition for the expression above, we consider $T(g)$, where g is either a generator of $\mathbb{Z}_q^m$ or a product of two generators. When g is any generator a_i, we have $T(a_i) = 1$, since $S(h,1)$ is the identity for any $h \in \mathbb{Z}_q^m$. If g is $a_i a_j \neq 1$, then $T(a_i a_j)$ is equal to $S(a_i, a_j)$. We

see that this implies that $\mathcal{P}'(a_i a_j)$ is equal to the product of $\mathcal{P}'(a_i)$ and $\mathcal{P}'(a_j)$:

$$\mathcal{P}'(a_i a_j) = S(a_i, a_j)\mathcal{P}(a_i a_j) = \mathcal{P}(a_i)\mathcal{P}(a_j) = \mathcal{P}'(a_i)\mathcal{P}'(a_j). \tag{2.124}$$

More generally, the product in Eq. (2.123) is designed so that $\mathcal{P}'(a_1^{g_1} a_2^{g_2} \cdots a_m^{g_m})$ satisfies:

$$\mathcal{P}'(a_1^{g_1} a_2^{g_2} \cdots a_m^{g_m}) = \mathcal{P}'(a_1)^{g_1}\mathcal{P}'(a_2)^{g_2} \cdots \mathcal{P}'(a_m)^{g_m}. \tag{2.125}$$

We now compute the group laws for the modified effective boundary symmetry actions defined using the choice of $T(g)$ in Eq. (2.123). The product of $\mathcal{P}'(g)$ and $\mathcal{P}'(h)$ for general group elements $g = a_1^{g_1} a_2^{g_2} \cdots a_m^{g_m}$ and $h = a_1^{h_1} a_2^{h_2} \cdots a_m^{h_m}$ is:

$$\mathcal{P}'(g)\mathcal{P}'(h) = \left[\mathcal{P}'(a_1)^{g_1}\mathcal{P}'(a_2)^{g_2} \cdots \mathcal{P}'(a_m)^{g_m}\right]\left[\mathcal{P}'(a_1)^{h_1}\mathcal{P}'(a_2)^{h_2} \cdots \mathcal{P}'(a_m)^{h_m}\right], \tag{2.126}$$

where we have used the identity in Eq. (2.125). Since the operators on the right hand side of Eq. (2.126) are mutually commuting, we can write $\mathcal{P}'(g)\mathcal{P}'(h)$ as:

$$\mathcal{P}'(g)\mathcal{P}'(h) = \mathcal{P}'(a_1)^{g_1+h_1}\mathcal{P}'(a_2)^{g_2+h_2} \cdots \mathcal{P}'(a_m)^{g_m+h_m}. \tag{2.127}$$

We evaluate the expression in Eq. (2.127) further by writing $g_i + h_i$ as:

$$g_i + h_i = (g_i + h_i - [g_i + h_i]_q) + [g_i + h_i]_q = n_i q + [g_i + h_i]_q, \tag{2.128}$$

where $[\cdot]_q$ denotes addition modulo q, and $n_i q$ is an integer multiple of q. Substituting Eq. (2.128) into Eq. (2.127), we find:

$$\begin{aligned}\mathcal{P}'(g)\mathcal{P}'(h) = \mathcal{P}'(a_1)^{n_1 q}\mathcal{P}'(a_2)^{n_2 q} \cdots \mathcal{P}'(a_m)^{n_m q} \\ \times \mathcal{P}'(a_1)^{[g_1+h_1]_q}\mathcal{P}'(a_2)^{[g_2+h_2]_q} \cdots \mathcal{P}'(a_m)^{[g_m+h_m]_q}.\end{aligned} \tag{2.129}$$

According to Eq. (2.125), this is equivalent to:

$$\mathcal{P}'(g)\mathcal{P}'(h) = \mathcal{P}'(a_1)^{n_1 q}\mathcal{P}'(a_2)^{n_2 q}\cdots\mathcal{P}'(a_m)^{n_m q}\mathcal{P}'(gh). \tag{2.130}$$

Lastly, we argue that the pre-factor on the right hand side of Eq. (2.130) is the identity. To see this, we expand each factor of $\mathcal{P}'(a_i)$ using the definition of $\mathcal{P}(g)$ in Eq. (2.116) and use that $P_M(g)$ forms a linear representation of $\mathbb{Z}_q^m$:

$$\mathcal{P}'(a_1)^{n_1 q}\mathcal{P}'(a_2)^{n_2 q}\cdots\mathcal{P}'(a_m)^{n_m q} = \tilde{P}_M^\dagger(a_1)^{n_1 q}\tilde{P}_M^\dagger(a_2)^{n_2 q}\cdots\tilde{P}_M^\dagger(a_m)^{n_m q} \tag{2.131}$$

Since the system is defined on q-dimensional qudits, any product of stabilizer terms raised to the power of q, such as $\tilde{P}_M^\dagger(a_i)^{n_i q}$, must be the identity. Therefore, we have:

$$\mathcal{P}'(a_1)^{n_1 q}\mathcal{P}'(a_2)^{n_2 q}\cdots\mathcal{P}'(a_m)^{n_m q} = 1, \tag{2.132}$$

and according to Eq. (2.130), the modified effective boundary symmetry action satisfies the group laws exactly:

$$\mathcal{P}'(g)\mathcal{P}'(h) = \mathcal{P}'(gh), \quad \forall g, h \in G. \tag{2.133}$$

2.E Simplified strange order parameter

In this appendix, we show that the strange order parameters used in the proof of Proposition 3 can always be chosen to be Z-type Pauli strings.

Lemma 3 *Let $\{\mathcal{O}_k\}$ be a strange order parameter such that the strange correlator:*

$$\frac{\langle +\ldots+|\mathcal{O}_i\mathcal{O}_j|\varphi_{SPT}\rangle}{\langle +\ldots+|\varphi_{SPT}\rangle}, \tag{2.134}$$

decays slowly, i.e., it decays as a power law or is constant in the separation of i and j. Then, there exists a strange order parameter formed by Z-type Pauli string operators $\{Q_k^Z\}$ that

decays slowly in $|i-j|$.

Proof of Lemma 3: The strange order parameter $\{\mathcal{O}_k\}$ can be simplified by commuting the Pauli X operators in $\mathcal{O}_i$ and $\mathcal{O}_j$ to act on $\langle+\ldots+|$ in Eq. (2.134). This leaves us with:

$$\frac{\langle+\ldots+|\mathcal{O}_i\mathcal{O}_j|\varphi_{\text{SPT}}\rangle}{\langle+\ldots+|\varphi_{\text{SPT}}\rangle} = \frac{\langle+\ldots+|\mathcal{Z}_i\mathcal{Z}_j|\varphi_{\text{SPT}}\rangle}{\langle+\ldots+|\varphi_{\text{SPT}}\rangle}, \tag{2.135}$$

where $\mathcal{Z}_i$ and $\mathcal{Z}_j$ are charged operators generated by sums of Z-type Pauli strings. To be explicit, $\mathcal{Z}_i$ and $\mathcal{Z}_j$ can be written as:

$$\mathcal{Z}_i = \sum_{P^Z} C^i_{P^Z} P^Z, \quad \mathcal{Z}_j = \sum_{P^Z} C^j_{P^Z} P^Z, \tag{2.136}$$

where the sums are over all Z-type Pauli strings P^Z, and $C^i_{P^Z}$ and $C^j_{P^Z}$ are some complex valued coefficients. Note that due to the locality of the $\mathcal{O}_i$ and $\mathcal{O}_j$, $\mathcal{Z}_i$ and $\mathcal{Z}_j$ are localized near i and j, respectively, and consequently, there are only finitely many non-zero coefficients $C^i_{P^Z}$ and $C^j_{P^Z}$. Furthermore, the unitarity of $\mathcal{O}_i$ and $\mathcal{O}_j$, implies $|C^i_{P^Z}|, |C^j_{P^Z}| \leq 1$ for every P^Z. We also note that neither $\mathcal{Z}_i$ nor $\mathcal{Z}_j$ is the identity, since $\mathcal{O}_i$ and $\mathcal{O}_j$ are charged.

With this, we can expand the right-hand side of Eq. (2.135) as:

$$\sum_{P_i^Z}\sum_{P_j^Z} C^i_{P_i^Z} C^j_{P_j^Z} \frac{\langle+\ldots+|P_i^Z P_j^Z|\varphi_{\text{SPT}}\rangle}{\langle+\ldots+|\varphi_{\text{SPT}}\rangle}. \tag{2.137}$$

Given that the strange correlator in Eq. (2.134) decays slowly in $|i-j|$, the expression above also decays slowly in $|i-j|$. Furthermore, since there are finitely many non-zero coefficients $C^i_{P_i^Z}, C^j_{P_j^Z}$, all of which are bounded from above, there must be a choice of P_i^Z and P_j^Z such that the expression:

$$\frac{\langle+\ldots+|P_i^Z P_j^Z|\varphi_{\text{SPT}}\rangle}{\langle+\ldots+|\varphi_{\text{SPT}}\rangle} \tag{2.138}$$

decays slowly with the separation of i and j. Let us denote this choice of P_i^Z and P_j^Z by Q_i^Z

and Q_j^Z. The set $\{Q_k^Z\}$ forms a strange order parameter for $|\varphi_{\text{SPT}}\rangle$ with strange correlations that decay slowly in the separation of i and j. $\square$

Chapter 3

TENSOR NETWORK APPROACH TO BOSONIZATION

This chapter is based on:
Sujeet K. Shukla, Tyler D. Ellison, and Lukasz Fidkowski. Tensor network approach to two-dimensional bosonization. Phys. Rev. B, 101:155105, Apr 2020.

We present a 2D bosonization duality using the language of tensor networks. Specifically, we construct a tensor network operator (TNO) that implements an exact 2D bosonization duality. The primary benefit of the TNO is that it allows for bosonization at the level of quantum states. Thus, we use the TNO to provide an explicit algorithm for bosonizing fermionic projected entangled pair states (fPEPs). A key step in the algorithm is to account for a choice of spin-structure, encoded in a set of bonds of the bosonized fPEPS. This enables our tensor network approach to bosonization to be applied to systems on arbitrary triangulations of orientable 2D manifolds.

3.1 Introduction

The Jordan-Wigner transformation is a well established example of a bosonization duality – it maps a system of spinless complex fermions to a system of spins [102]. The duality has led to many fruitful applications to one dimensional systems, where it equates 1D fermionic models and spin chains. However, while the Jordan-Wigner transformation is a powerful tool in one dimension, there are challenges to applying it to higher dimensional systems. To implement the Jordan-Wigner transformation in dimensions greater than one, the duality is applied along a 1D path which snakes through the fermionic system. In general, this yields a transformation that maps local fermionic Hamiltonians to *non*-local bosonic Hamiltonians.

Generalizations of the Jordan Wigner transformation to two dimensions have since overcome this obstacle and indeed map local fermionic Hamiltonians to local bosonic Hamilto-

nians [15, 103–105]. Similar to the one dimensional Jordan-Wigner transformation, these two dimensional bosonization dualities are expressed at the level of operators. That is, they define a mapping of operators, where operators that act on fermionic degrees of freedom are mapped to operators that act on spins. Such a mapping of operators[1] necessarily comes from conjugating by some unitary operator on the Hilbert space [106]. However, finding the explicit form of this unitary, and thereby obtaining the action of the duality at the level of quantum states, is challenging.

In this chapter, we formulate a two dimensional bosonization duality at the level of quantum states. Specifically, we identify a tensor network representation of the duality in Ref. [15]. This is to say, we construct a tensor network operator (TNO) which, by conjugation, maps operators according to the transformation in Ref. [15]. Moreover, the TNO may be applied directly to fermionic tensor network states to map them to bosonic states. Further, we show that bosonized fermionic projected entangled pair states (fPEPS) may be written explicitly as bosonic projected entangled pair states (bPEPS).

The TNO inherits two of the main features of the transformation detailed in Ref. [15]. First, the mapping of operators in Ref. [15] makes the physical interpretation of two dimensional bosonization transparent – fermionic excitations are mapped to *emergent* fermions in a $\mathbb{Z}_2$ gauge theory. Operators that create pairs of fermions are explicitly mapped to operators that create pairs of emergent fermions, which are interpreted as bound states of a bosonic gauge charge and flux. The gauge constraint on the bosonic side of the duality expressly prohibits unbound charge and flux excitations. Consequently, our TNO clearly maps the subspace of states with an even number of fermions to a constrained Hilbert space with a basis given by configurations of emergent fermions. Second, the bosonization duality of Ref. [15] carefully accounts for spin-structure – a mathematical input necessary for bosonization dualities – while in other treatments, spin-structure is hidden in seemingly arbitrary choices. In our construction, a choice of spin-structure is then specified by a certain set of bonds in

[1] This is technically a C^* algebra automorphism.

the TNO. Importantly, keeping track of the spin-structure allows us to establish our tensor network bosonization for fermionic systems on arbitrary triangulations of closed, orientable 2D manifolds.

For context, our approach to bosonization is analogous to a method employed in Ref. [107] for gauging symmetries at the level of quantum states. In Ref. [107], a TNO is used to map a state with a global symmetry to a state with the corresponding gauge symmetry. Indeed, symmetries may be gauged by using a duality [71], and the TNOs in Ref. [107] can be understood as a tensor network representation of the duality corresponding to gauging the symmetry. We note that, using the methods of Ref. [107] to gauge the fermion parity symmetry in a fermionic system, one obtains a TNO that is closely related to our bosonization TNO. However, unlike the bosonization TNO, the TNO corresponding to gauging fermion parity maps to a system with fermionic degrees of freedom (although, see [108]). The inverse (or Hermitian conjugate) of our bosonization TNO (this maps a bosonic state to a fermionic state) can be understood as "un-gauging" fermion parity or "fermion condensation" [109–111].

We emphasize that our bosonization duality is distinct from the efforts to express fermionic tensor networks in terms of bosonic tensor networks. Refs. [112–114] develop strategies for rewriting fermionic tensor network states as bosonic tensor network states. However, these do not change the state – only its tensor network representation. The bosonization duality, in contrast, maps unentangled fermionic states to long-range entangled bosonic states. Nonetheless, our bosonization duality may prove useful for analyzing fermionic states, since expectation values of local fermionic operators can be recovered by computing the expectation value of the transformed operators in the bosonized tensor network state. Furthermore, our bosonization duality and the subsequent rewriting as an explicit bosonic tensor network state preserves the locality of the tensor network and only increases the bond dimension by a factor of 2.

The remainder of the chapter is structured as follows. We begin by introducing the formalism of $\mathbb{Z}_2$-graded Hilbert spaces and $\mathbb{Z}_2$-graded tensor networks. We find the language

of $\mathbb{Z}_2$-graded tensor networks especially convenient for expressing our bosonization TNO, and we use the notation established in section 3.2 throughout the text. We encourage readers that are familiar with the formalism of $\mathbb{Z}_2$-grading to briefly skim section 3.2 to simply acquaint themselves with our notation. Before constructing the bosonization TNO, we review the 2D bosonization duality of Ref. [15], in section 3.3.1. Subsequently, in section 3.3.2 we construct the TNO that implements this 2D bosonization duality at the level of states. After applying the bosonization TNO to a fermionic tensor network state, the resulting state is not explicitly a bosonic tensor network state. Therefore, section 3.4 is devoted to describing an algorithmic procedure for "removing the grading" and rewriting a bosonized fPEPS as a bPEPS. The procedure involves summing over inequivalent spin-structures, discussed in section 3.4.4. Lastly, we note that we describe a tensor network representation of 1D bosonization in Appendices 3.C and 3.D.

3.2 $\mathbb{Z}_2$-graded tensor networks

Our bosonization TNO is naturally expressed in terms of $\mathbb{Z}_2$-graded tensor networks. Therefore, the purpose of this section is to give a concise introduction to $\mathbb{Z}_2$-graded tensor networks and establish the notation used throughout the text. For a similar exposition of $\mathbb{Z}_2$-graded tensor networks, one can consult Refs. [115, 116]. We start by defining $\mathbb{Z}_2$-graded Hilbert spaces and $\mathbb{Z}_2$-graded tensors. Then, we introduce the contraction map to "glue" together $\mathbb{Z}_2$-graded tensors. The contraction map allows us to define a linear action of tensors on each other and to form $\mathbb{Z}_2$-graded tensor networks. Accordingly, we describe a representation of a fermionic operator algebra in terms of $\mathbb{Z}_2$-graded tensors and present a diagrammatic representation for $\mathbb{Z}_2$-graded tensor networks.

3.2.1 $\mathbb{Z}_2$-graded Hilbert spaces

A $\mathbb{Z}_2$-graded Hilbert space is a Hilbert space $\mathcal{H}$ with a natural direct sum decomposition: $\mathcal{H} = \mathcal{H}^0 \bigoplus \mathcal{H}^1$. A vector $|j) \in \mathcal{H}$ lying solely in either $\mathcal{H}^0$ or $\mathcal{H}^1$ has a $\{0, 1\}$ valued *grading* denoted as $|j|$, where $|j| = 0$ if $|j) \in \mathcal{H}^0$ and $|j| = 1$ if $|j) \in \mathcal{H}^1$. (We use round brackets

for vectors in $\mathbb{Z}_2$-graded Hilbert spaces.) In the context of fermionic systems, we consider $\mathcal{H}^0$ to be the subspace spanned by states with an even number of fermions and $\mathcal{H}^1$ to be the subspace spanned by states with an odd number of fermions. Thus, the grading of a vector and its fermion parity coincide. For this reason, we use grading and parity interchangeably. Further, we refer to vectors with a definite parity as homogeneous vectors, and we call states formed from a superposition of both even and odd parity vectors inhomogeneous.

To capture the physics of a many-body fermionic system, we will need a generalization of the usual tensor product – the graded tensor product $\hat{\otimes}$. For graded Hilbert spaces $\mathcal{H}_a$ and $\mathcal{H}_b$, we define the graded tensor product space $\mathcal{H}_a\hat{\otimes}\mathcal{H}_b$ to be the quotient space:

$$\mathcal{H}_a\hat{\otimes}\mathcal{H}_b \equiv \frac{(\mathcal{H}_a \otimes \mathcal{H}_b)\bigoplus(\mathcal{H}_b \otimes \mathcal{H}_a)}{\sim}. \tag{3.1}$$

Here, $\otimes$ is the usual (unsymmetrized) tensor product of Hilbert spaces, and $\sim$ denotes the relation:

$$|j)_a \otimes |k)_b \sim (-1)^{|j||k|}|k)_b \otimes |j)_a \tag{3.2}$$

for $|j)_a \in \mathcal{H}_a$ and $|k)_b \in \mathcal{H}_b$ both with definite grading. The Hilbert space $\mathcal{H}_a\hat{\otimes}\mathcal{H}_b$ is itself a graded Hilbert space with the equivalence class $|j)_a\hat{\otimes}|k)_b \in \mathcal{H}_a\hat{\otimes}\mathcal{H}_b$ having a grading of $|j| + |k|$ mod 2. As a consequence of Eq. (3.2), we have:

$$|j)_a\hat{\otimes}|k)_b = (-1)^{|j||k|}|k)_b\hat{\otimes}|j)_a. \tag{3.3}$$

This property of the graded tensor product is key to describing fermions, as it encodes the exchange statistics of the fermions. One can see that the graded tensor product captures the familiar notion of a fermionic Fock space by representing the equivalence class $|j)_a\hat{\otimes}|k)_b$ by the vector $\frac{1}{2}\Big(|j)_a \otimes |k)_b + (-1)^{|j||k|}|k)_b \otimes |j)_a\Big)$. When $|j)_a$ and $|k)_b$ are both fermion parity odd, we have an anti-symmetric combination – the Slater determinant.

Before moving on to describe $\mathbb{Z}_2$-graded tensors, we would like to note that Hilbert spaces for bosonic systems also fit into the framework of $\mathbb{Z}_2$-graded Hilbert spaces. A bosonic Hilbert space can be understood as a $\mathbb{Z}_2$-graded Hilbert space for which $\mathcal{H}^1$, the space of vectors with odd grading, is empty, leaving $\mathcal{H} = \mathcal{H}^0$. The graded tensor product between two bosonic Hilbert spaces reduces to the symmetrized tensor product between the Hilbert spaces, as is standard in tensor networks for bosonic systems. In a slight abuse of notation, we will denote vectors $|j\rangle$ in bosonic Hilbert spaces with angled brackets. In what follows, we will freely take graded tensor products of states in bosonic Hilbert spaces and states in fermionic Hilbert spaces, and the angled brackets are to remind us that those vectors necessarily have trivial grading.

3.2.2 $\mathbb{Z}_2$-graded tensors

A rank N $\mathbb{Z}_2$-graded tensor T is an element of the graded tensor product of N $\mathbb{Z}_2$-graded Hilbert spaces, i.e., $\mathsf{T} \in \mathcal{H}_1 \hat{\otimes} \ldots \hat{\otimes} \mathcal{H}_N$. Similar to tensors used to study bosonic systems, $\mathbb{Z}_2$-graded tensors admit a convenient graphical representation. Let us consider a specific example with $N = 4$ for illustration:

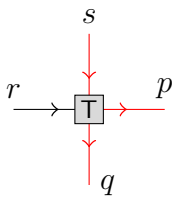

$$\equiv \sum_{a,b,c,d} T_{abcd} |a)_p |b)_q \langle c|_r (d|_s. \tag{3.4}$$

On the left hand side of Eq. (3.4), we have a diagrammatic representation of the tensor $\mathsf{T} \in \mathcal{H}_p \hat{\otimes} \mathcal{H}_q \hat{\otimes} \mathcal{H}_r^* \hat{\otimes} \mathcal{H}_s^*$, where $\mathcal{H}^*$ is the dual Hilbert space of $\mathcal{H}$. In the diagram, the characters at the end of the legs label the Hilbert spaces, and the orientation of the leg indicates whether we consider the Hilbert space to be a dual Hilbert space. (Legs oriented towards the node correspond to a dual Hilbert space.) Further, we have used red legs for $\mathbb{Z}_2$-graded Hilbert spaces and black legs for bosonic Hilbert spaces.

The right hand side of Eq. (3.4) is the tensor component form of T with *component values*

T_{abcd}. Note that we have suppressed the $\hat{\otimes}$ between vectors, and as previously mentioned, we use angled brackets for vectors which necessarily have trivial grading [$\langle c|_r$ in Eq. (3.4)]. Thus, the vector $|a)_p|b)_q\langle c|_r(d|_s$ has a grading of $|a|+|b|+|d|$ mod 2. Since the graded tensor product of Hilbert spaces is a graded Hilbert space, a tensor can be either homogeneous or inhomogeneous. A homogeneous tensor has nonzero component values only for vectors sharing the same parity, and otherwise, the tensor is inhomogeneous.

It is important to note that the tensor T is independent of the ordering of vectors in Eq. (3.4), but the component values (T_{abcd}) can depend on the ordering. For example, if we swap the order of $|a)_p$ and $|b)_q$, we get:

$$\mathsf{T} = \sum_{a,b,c,d} T_{abcd}(-1)^{|a||b|}|b)_q|a)_p\langle c|_r(d|_s. \tag{3.5}$$

Hence, the tensor components have an additional sign $(-1)^{|a||b|}$ with the new choice of ordering. The ordering should therefore be interpreted as a particular choice of orthonormal basis with which to express the tensor. We will often refer to the choice of ordering of the vectors in the component form of a tensor as a choice of *internal ordering*.

3.2.3 Contraction map and tensor action

To form tensor networks, we require a map to "glue" together tensors. To this end, we define the *contraction map*:

$$\begin{aligned} \mathcal{C} : \mathcal{H}^* \hat{\otimes} \mathcal{H} &\to \mathbb{C}eqs \\ (j|\hat{\otimes}|k) &\mapsto (j|k) = \delta_{jk}. \end{aligned} \tag{3.6}$$

Notice that a reordering of vectors may be necessary before evaluating $\mathcal{C}$. For example:

$$\mathcal{C}\big[|k)\hat{\otimes}(j|\big] = \mathcal{C}\big[(-1)^{|j||k|}(j|\hat{\otimes}|k)\big] = (-1)^{|j||k|}\delta_{jk}. \tag{3.7}$$

Interpreting $\mathcal{C}\big[|k)\hat{\otimes}(j|\big]$ as $\mathrm{tr}[|k)\hat{\otimes}(j|]$, we see that it differs from the usual trace by a sign, $(-1)^{|j||k|}$. This phase is referred to as the *supertrace sign*.

In general, the indices to be contracted need not be next to each other in an algebraic expression. For this reason, we introduce the superscript notation:

$$|k)^{\mathcal{C}}\hat{\otimes}(j|^{\mathcal{C}} \equiv \mathcal{C}\big[|k)\hat{\otimes}(j|\big]. \tag{3.8}$$

A dual vector and a vector with matching superscripts $\mathcal{C}$ are to first be reordered then contracted with the map $\mathcal{C}$.

We now provide examples to illustrate the contraction of $\mathbb{Z}_2$-graded tensors. We consider the following three even parity tensors to guide the discussion:

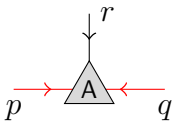

$$\equiv \sum_{a,b,c} A_{abc}(a|_q\langle b|_r(c|_p \tag{3.9}$$

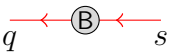

$$\equiv \sum_{d,e} B_{de}|d)_q(e|_s \tag{3.10}$$

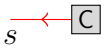

$$\equiv \sum_{f} C_f|f)_s eqs. \tag{3.11}$$

First, we contract the s leg of B with the s leg of C. The resulting tensor is denoted as $\mathsf{B}\cdot\mathsf{C}$:

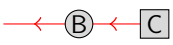

$$\equiv \mathcal{C}_s\left[\mathsf{B}\hat{\otimes}\mathsf{C}\right] = \sum_{d,e} B_{de}|d)_q(e|_s^{\mathcal{C}} \sum_{f} C_f|f)_s^{\mathcal{C}} = \sum_{d,e} B_{de}C_e|d)_q \equiv \mathsf{B}\cdot\mathsf{C}, \tag{3.12}$$

where $\mathcal{C}_s\left[\cdots\right]$ refers to contraction of the s index. Notice that C is a $\mathbb{Z}_2$-graded vector, and B is a $\mathbb{Z}_2$-graded matrix. We see that B acts on C by contraction and gives a new vector, $\mathsf{B}\cdot\mathsf{C}$. Hence B can represent linear operators on $\mathbb{Z}_2$-graded vector spaces.

Second, we contract A with $\mathsf{B}\cdot\mathsf{C}$ by contracting the q leg of A with that of $\mathsf{B}\cdot\mathsf{C}$ to produce

a new tensor $\mathsf{A}\cdot\mathsf{B}\cdot\mathsf{C}$:

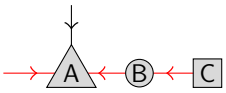

$$\equiv \mathcal{C}_q\left[\mathsf{A}\hat{\otimes}\mathsf{B}\cdot\mathsf{C}\right] = \sum_{a,b,c} A_{abc}(a|_q^{\mathcal{C}}\langle b|_r(c|_p \sum_{d,e} B_{de}C_e|d)_q^{\mathcal{C}}$$
$$= \sum_{a,b,c,e} (-1)^{|a||c|} A_{abc}B_{ae}C_e\langle b|_r(c|_p \equiv \mathsf{A}\cdot\mathsf{B}\cdot\mathsf{C}. \quad (3.13)$$

Note that the sign $(-1)^{|a||c|}$ comes from moving $(a|_q$ past $\langle b|_r(c|_p$ in order to perform the contraction. We can say that A acted on $\mathsf{B}\cdot\mathsf{C}$ by contraction to produce a tensor $\mathsf{A}\cdot\mathsf{B}\cdot\mathsf{C}$.

In general, contraction of any two tensors can be interpreted in this way: a tensor T *acts* on another tensor S by contraction to produce a tensor $\mathsf{T}\cdot\mathsf{S}$. Letting *ind* be the set of indices contracted between T and S, we have:

$$\mathsf{T}\cdot\mathsf{S} = \mathcal{C}_{ind}[\mathsf{T}\hat{\otimes}\mathsf{S}], \quad (3.14)$$

where $\mathcal{C}_{ind}[...]$ refers to contraction over the indices in the set *ind*. Note that, since $\mathsf{T}\cdot\mathsf{S}$ depends on the set *ind*, we should ideally write it as $\mathsf{T}\cdot_{ind}\mathsf{S}$. However, the set *ind* is typically clear from context, so we omit the subscript for notational convenience.

3.2.4 $\mathbb{Z}_2$-graded representation of a fermionic operator algebra

Now that we have defined tensors' linear action via contraction, we establish a representation for the fermionic operator algebra of a spinless complex fermion using $\mathbb{Z}_2$-graded tensors. The representation is essential for the construction of the bosonization TNO, since the bosonization TNO maps fermionic operators represented by $\mathbb{Z}_2$-graded tensors to bosonic operators.

The operator algebra of a spinless complex fermion at a site p is generated by the familiar fermionic creation and annihilation operators: $c_p^\dagger$, c_p. However, it is often convenient to

instead work with a generating set formed by the two *Majorana operators*:

$$\gamma_p = c_p^\dagger + c_p \quad \text{and} \quad \bar{\gamma}_p = i(c_p^\dagger - c_p). \tag{3.15}$$

These are Hermitian, unitary operators:

$$\gamma_p^\dagger = \gamma_p, \quad \bar{\gamma}_p^\dagger = \bar{\gamma}_p, \quad \gamma_p^2 = \bar{\gamma}_p^2 = 1, \tag{3.16}$$

and they satisfy the following commutation relations:

$$\begin{aligned} \{\gamma_p, \bar{\gamma}_{p'}\} =& 0 \\ \{\gamma_p, \gamma_{p'}\} =& \{\bar{\gamma}_p, \bar{\gamma}_{p'}\} = 2\delta_{p,p'}, \end{aligned} \tag{3.17}$$

where braces denote the anti-commutator and $\delta_{p,p'}$ is the Kronecker delta function. Furthermore, the *fermion parity operator* P_p is given by:

$$P_p = (-1)^{c_p^\dagger c_p} = -i\gamma_p\bar{\gamma}_p. \tag{3.18}$$

We now show that γ_p, $\bar{\gamma}_p$ and P_p can be represented as rank-2 $\mathbb{Z}_2$-graded tensors. Letting $|1)$ and $|0)$ represent the fermion occupied and unoccupied states respectively, then the creation and annihilation operators have the following canonical representations:

$$\begin{aligned} c_p|1)_p = |0)_p,\ c_p|0)_p = 0 \\ c_p^\dagger|1)_p = 0,\ c_p^\dagger|0)_p = |1)_p. \end{aligned} \tag{3.19}$$

Using Eq. (3.15), this leads to the following representation of Majorana operators:

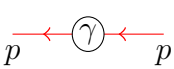

$$\equiv |1)_p(0|_p + |0)_p(1|_p = \sum_a |a+1)_p(a|_p \tag{3.20}$$

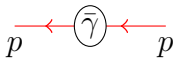

$$\equiv i|1)_p(0|_p - i|0)_p(1|_p = \sum_a (-1)^a i|a+1)_p(a|_p. \tag{3.21}$$

Here, and throughout the chapter, indices are assumed to take binary values, unless stated otherwise. Thus, $\sum_a \equiv \sum_{a=0}^{1}$, and $(a+1) \equiv (a+1) \bmod 2$, etc. In Appendix 3.A, we show that the algebraic properties of the Majorana operators are indeed satisfied by the tensor representations in Eqs. (3.20) and (3.21). Furthermore, using Eq. (3.18), fermion parity P can be represented as:

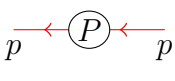

$$\equiv \sum_a (-1)^a |a)_p(a|_p = |0)_p(0|_p - |1)_p(1|_p. \tag{3.22}$$

Eq. (3.22) agrees with the intuition that the $\mathbb{Z}_2$-grading of a vector corresponds to the fermion parity of the state.

3.2.5 $\mathbb{Z}_2$-graded tensor network diagrams

To establish a general theory of $\mathbb{Z}_2$-graded tensor networks, we need to make sure that tensor diagrams can unambiguously represent the algebraic values. For example, given the tensor network diagram:

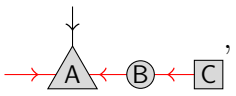

, (3.23)

how do we know whether it represents the tensor $\mathsf{A}\cdot\mathsf{B}\cdot\mathsf{C}$ or $\mathsf{B}\cdot\mathsf{C}\cdot\mathsf{A}$, or any other order of action of tensors A, B, and C? Unlike bosonic tensors, $\mathbb{Z}_2$-graded tensors do not commute with each other, and hence, in general, $\mathsf{A}\cdot\mathsf{B}\cdot\mathsf{C}$ and $\mathsf{B}\cdot\mathsf{C}\cdot\mathsf{A}$ are different tensors. If T and S are homogeneous tensors, then the commutation relation of graded tensor products in Eq. (3.3) implies the following commutation relation:

$$\mathsf{T}\cdot\mathsf{S} = (-1)^{|\mathsf{T}||\mathsf{S}|}\mathsf{S}\cdot\mathsf{T}. \tag{3.24}$$

In particular, as long as only one tensor is odd, we have $\mathsf{T}\cdot\mathsf{S} = \mathsf{S}\cdot\mathsf{T}$, and the order of action of these tensors does not matter. Extending this argument, we see that for a set of homogeneous tensors $\{\mathsf{A}, \mathsf{B}, \mathsf{C}, \ldots\}$, as long as at most one tensor is odd, the order of contraction does not matter.

What happens when more than one odd tensor appears in a TN? An example of such a tensor network is given in the following diagram, where we assume A is an even tensor:

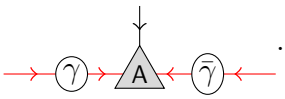

(3.25)

How should this tensor network diagram be read algebraically? For instance, it could represent either $\gamma\cdot\mathsf{A}\cdot\bar{\gamma}$ or $\bar{\gamma}\cdot\gamma\cdot\mathsf{A}$, among other possibilities. This is problematic because, according to Eq. (3.24), $\gamma\cdot\mathsf{A}\cdot\bar{\gamma} = -\bar{\gamma}\cdot\gamma\cdot\mathsf{A}$. Hence, the algebraic value of the this tensor network diagram is ill defined.

To remove this ambiguity, we need to indicate the order in which γ and $\bar{\gamma}$ are applied. We do this by adopting the following simple notation: if two or more odd tensors appear in a diagram, we place numbers next to their nodes to indicate their relative order. For example, $\gamma\cdot A\cdot\bar{\gamma}$ and $\bar{\gamma}\cdot\gamma\cdot\mathsf{A}$ are then respectively represented by the following diagrams:

$\gamma\cdot A\cdot\bar{\gamma} \equiv$

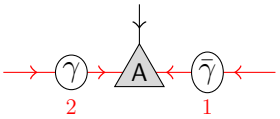

(3.26)

$\bar{\gamma}\cdot\gamma\cdot A \equiv$

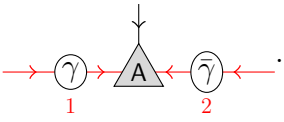

(3.27)

In fact, the first diagram can also represent any tensor network in which $\bar{\gamma}$ is applied *before* γ, so it can also represent $\gamma\cdot\bar{\gamma}\cdot A$ or $A\cdot\gamma\cdot\bar{\gamma}$. Similarly, the second diagram can also represent $\bar{\gamma}\cdot A\cdot\gamma$ and $A\cdot\bar{\gamma}\cdot\gamma$ (recall that we assume A is an even tensor).

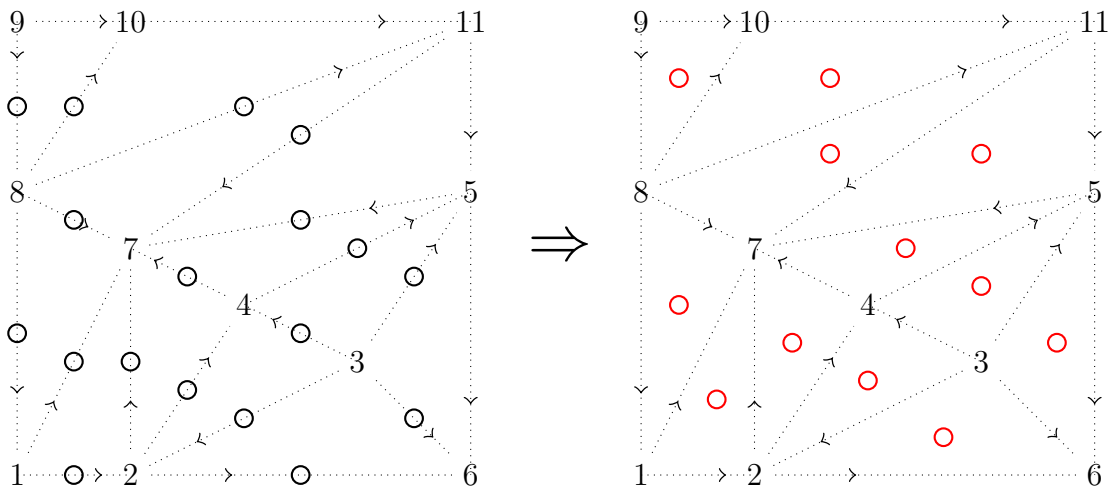

Figure 3.1: The bosonization duality maps a system of spinless complex fermions to a system of spin-1/2 degrees of freedom. The bottom picture shows the fermionic degrees of freedom (red circles) at each triangular face f. The top picture shows the spin-1/2 bosonic degrees of freedom (black circles) on each edge e.

3.3 Tensor network bosonization duality in 2D

In this section, we use the formalism of $\mathbb{Z}_2$-graded tensor networks to construct a TNO that implements the exact 2D bosonization duality of Ref. [15]. We start by reviewing the operator-level duality, and then show that it can be naturally represented by a TNO, which we refer to as the bosonization TNO. The TNO representation allows us to easily compute the action of bosonization on quantum states (as opposed to just the action on operators). In particular, in Section 3.4, we use the bosonization TNO to map fermionic tensor network states to bosonic tensor network states.

3.3.1 Review of the operator-level bosonization duality

To begin, we describe the lattice on which the duality is defined and set some notation. The duality in Ref. [15] can be defined on an arbitrary triangulation of a 2D manifold with boundary [109, 117]. It is also required that the lattice has a branching structure, i.e. each edge has an orientation (see Fig. 3.1) such that the edges around any triangle do not form

a cycle. The branching structure yields an ordering of the vertices around a triangle and allows us to define an orientation of each triangle relative to the orientation of the underlying oriented manifold. We denote the ordered vertices of the triangular face f as f_0, f_1 and f_2, where f_j is the j-vertex of the triangle, and j refers to the number of edges of the triangle f that point toward f_j. We adopt the convention that a triangle is positively oriented if f_0, f_1 and f_2 appear in counter-clockwise order, and otherwise it is negatively oriented. Further, we label the edges of f by f_{01}, f_{12}, and f_{02}, such that f_{jk} is the edge pointing from f_j to f_k. We also find it convenient to denote the endpoints of the edge e as e_0 and e_1, with e pointing from e_0 to e_1.

Let us illustrate the notation above using examples from Fig. 3.1. (Note that the vertices in Fig. 3.1 are labeled with integers arbitrarily simply to guide the discussion. They do not denote a global ordering of the vertices.) If $f = \langle 3, 2, 4\rangle$ then $f_0 = \langle 3\rangle$, $f_1 = \langle 2\rangle$, $f_2 = \langle 4\rangle$ and $f_{01} = \langle 3, 2\rangle$, $f_{12} = \langle 2, 4\rangle$, $f_{02} = \langle 3, 4\rangle$. Further, if $e = \langle 2, 4\rangle$, then $e_0 = 2$, $e_1 = 4$. The triangle $\langle 8, 1, 7\rangle$ is positively oriented while $\langle 3, 2, 4\rangle$ is negatively oriented.

We are now in a position to describe the fermionic degrees of freedom on the lattice and the corresponding operator algebra mapped by the bosonization duality. Each triangle f hosts a spinless complex fermion, and as explained in Section 3.2.4, its operator algebra is generated by Majorana operators, γ_f and $\bar{\gamma}_f$. The total fermionic algebra is generated by the set of $\gamma_f, \bar{\gamma}_f$ for all triangles f.

The bosonization duality is defined on a subset of the full fermionic operator algebra to ensure that the duality maps local operators to local operators. Specifically, the duality is defined on the subalgebra of even operators $\mathcal{E}$, i.e., the operators that commute with the global fermion parity operator $\prod_f P_f$, where

$$P_f = -i\gamma_f\bar{\gamma}_f \tag{3.28}$$

is the fermion parity operator at f. $\mathcal{E}$ is generated by fermion parity P_f at each triangle f,

and *hopping operators* S_e at each edge e defined as:

$$S_e = i(-1)^{\eta_e}\gamma_{L_e}\bar{\gamma}_{R_e}. \tag{3.29}$$

Here, L_e and R_e denote the triangle to the left and right of the edge e, respectively. For example, in Fig. 3.1, we have $L_{\langle 2,4\rangle} = \langle 2,4,7\rangle$ and $R_{\langle 2,4\rangle} = \langle 3,2,4\rangle$. $(-1)^{\eta_e}$ is a sign that comes from a choice of the so-called *spin-structure* η [109]. We postpone a detailed discussion of spin-structure until Section 3.4.4 below. For now, η should be understood as a chosen set of edges with η_e defined as:

$$\eta_e = \begin{cases} 1 & \text{if } e \in \eta \\ 0 & \text{otherwise.} \end{cases} \tag{3.30}$$

As we will explain below, η is dependent upon the branching structure, and roughly speaking, ensures that the bosonization duality is uniform across the 2D manifold.

We now discuss the relations satisfied by the generators of the even algebra $\mathcal{E}$. First, all parity operators commute with each other: $P_f P_{f'} = P_{f'} P_f$, for all f, f'. However, not all hopping operators commute with each other. Instead, they satisfy the following commutation relations:

$$S_e S_{e'} = (-1)^{\delta_{L_e,L_{e'}}}(-1)^{\delta_{R_e,R_{e'}}} S_{e'} S_e. \tag{3.31}$$

That is, two hopping operators anticommute if and only if they have a common triangle to the left or to the right. For example, in Fig. 3.1, $S_{\langle 2,4\rangle}$ and $S_{\langle 3,2\rangle}$ anti-commute because they have a common triangle to the right: $R_{\langle 2,4\rangle} = R_{\langle 3,2\rangle} = \langle 324\rangle$. However, $S_{\langle 2,4\rangle}$ and $S_{\langle 3,4\rangle}$ commute because they do not have a common right or left triangle. Parity operators and

hopping operators anti-commute if they share a triangle:

$$S_e P_f = (-1)^{\delta_{e\subset f}} P_f S_e, \tag{3.32}$$

otherwise they commute. ($\delta_{e\subset f} = 1$ if edge e is part of the triangle, otherwise it is 0.) Furthermore, the fermion parity operators and hopping operators are not independent, since for each vertex v, they satisfy the relation [109]:

$$\prod_{e:e_0=v} S_e \prod_{e:e_1=v} S_e \prod_{f:f_0,f_2=v} P_f = 1. \tag{3.33}$$

In equation (3.33), the first product is over all edges e for which the e_0 vertex is v, the second product is over all edges e for which v is the e_1 vertex, and the last product is over all triangles for which v is either a 0-vertex or a 2-vertex. Note that the sign of $(-1)^{\eta_e}$ in the definition of the hoping operator [Eq. (3.29)] is crucial to obtain 1 on the right hand side of Eq. (3.33). This completes our description of the algebra $\mathcal{E}$ on the fermionic side of the duality[2], and we move on to describe the bosonic side of the duality.

On the bosonic side of the duality, as shown in Fig. 3.1, we have a spin-1/2 degree of freedom at each edge e. The operator algebra at e is generated by the Pauli operators X_e and Z_e, and the full bosonic algebra is generated by the set containing X_e and Z_e for all edges e. The bosonization duality maps to just a subalgebra of the full bosonic algebra, where the subalgebra is defined by a certain $\mathbb{Z}_2$ gauge constraint. The explicit form for the gauge constraint will emerge naturally from the mapping of operators described below.

The bosonization duality $\mathfrak{D}$, is a homomorphism from the algebra of fermion parity even operators $\mathcal{E}$ to a particular bosonic subalgebra. $\mathfrak{D}$ is defined by its action on the generators of $\mathcal{E}$, P_f and S_e. It maps fermion parity P_f to an operator that measures the $\mathbb{Z}_2$ flux at

[2]For each non-contractible cycle of the manifold there is an additional relation between the parity operators and hopping operators. These relations correspond to a certain product of S_e and P_f along the cycle. With an appropriate choice of η we are in the $+1$ sector of these relations. See [117] for more detail.

triangle f, namely:

$$W_f \equiv Z_{f_{01}} Z_{f_{12}} Z_{f_{02}}. \tag{3.34}$$

Since S_e and P_f anticommute whenever e borders f, a natural first guess for the image of S_e under $\mathfrak{D}$ is the operator X_e. X_e creates a pair of $\mathbb{Z}_2$ fluxes and hence anti-commutes with the operator that measures flux on a neighboring triangle. However, mapping S_e to X_e does not preserve the commutation relations with the other hopping operators. To remedy this, we dress X_e with Pauli Z operators:

$$U_e \equiv X_e \prod_{f \in \{L_e, R_e\}} Z_{f_{01}}^{\delta_{e,f_{12}}}. \tag{3.35}$$

In words, the expression in Eq. (4.35) says that if e is the f_{12} edge of the triangle to the left, then we include a factor of $Z_{f_{01}}$ on the f_{01} edge of that triangle. Likewise, if e is the f_{12} edge of the triangle to the right, then we include a factor of $Z_{f_{01}}$ on the f_{01} edge of that triangle. For example, looking at Fig. 3.1, we have $U_{\langle 3,4\rangle} = X_{\langle 3,4\rangle}$, $U_{\langle 2,4\rangle} = X_{\langle 2,4\rangle} Z_{\langle 3,2\rangle}$, $U_{\langle 5,7\rangle} = X_{\langle 2,7\rangle} Z_{\langle 4,5\rangle} Z_{\langle 11,5\rangle}$, etc.

Lastly, we must check that the relation in Eq. (3.32) is preserved by the bosonization duality. For each vertex v, we find:

$$\prod_{e:e_0=v} U_e \prod_{e:e_1=v} U_e \prod_{f:f_0,f_2=v} W_f = G_v, \tag{3.36}$$

where G_v is equal to:

$$G_v = \prod_{e \supset v} X_e \prod_{f:f_0=v} W_f. \tag{3.37}$$

The first product in Eq. (3.37) is over all edges e connected to v. Thus, to preserve the relation (3.32), we need to impose the gauge constraint $G_v = 1$ for all v.

Denoting by $\mathcal{G}$ the bosonic subalgebra generated by the set of W_f and U_e with the gauge constraint $G_v = 1$ for all v, we see that the 2D bosonization duality $\mathfrak{D}$ is a bijective map from $\mathcal{E}$ to $\mathcal{G}$ defined by:

$$\begin{aligned} \mathfrak{D}(P_f) &= W_f, \\ \mathfrak{D}(S_e) &= U_e. \end{aligned} \tag{3.38}$$

The choice of spin-structure η ensures that the gauge constraint on the bosonic side of the duality is $G_v = 1$ at every vertex v. In Section 3.4, we detail a prescription for choosing a suitable spin structure η.

3.3.2 TNO representation of the 2D duality

Having reviewed both $\mathbb{Z}_2$-graded tensor networks and the operator-level 2D bosonization duality, we can now describe one of our main results – a realization of 2D bosonization at the level of quantum states. To accomplish this, we represent the bosonization duality $\mathfrak{D}$ in Eq. (3.38) using a TNO, D. We say that a TNO D represents the duality $\mathfrak{D}$, if it satisfies:

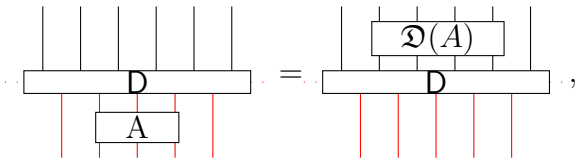

(3.39)

for all fermion parity even operators $A \in \mathcal{E}$. Algebraically, this is:

$$\mathsf{D} \cdot A = \mathfrak{D}(A) \cdot \mathsf{D}. \tag{3.40}$$

In Eq. (3.40), we have used the operation $\cdot$ defined in Section 3.2.3 for the contraction of $\mathbb{Z}_2$-graded tensors. For Eq. (3.40) to hold, it suffices to show that D satisfies Eq. (3.40) for the generators of $\mathcal{E}$, since for any $A, B, C \in \mathcal{E}$ we have:

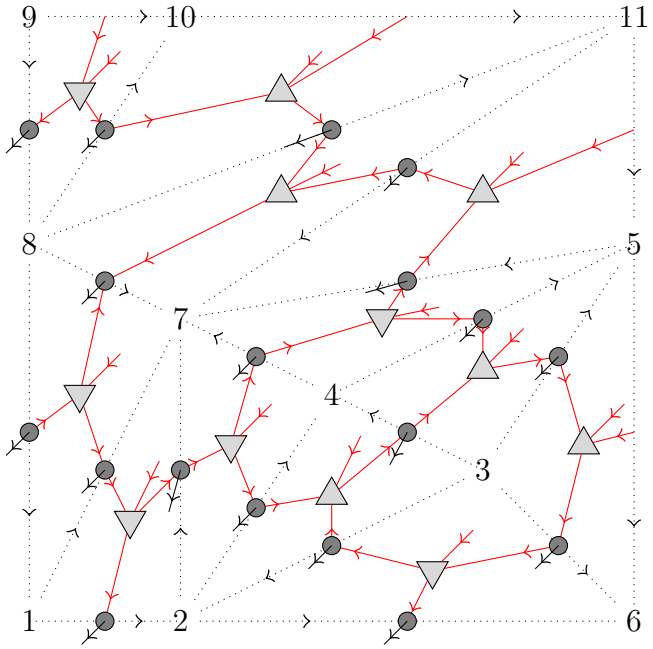

Figure 3.2: TNO representation of the bosonization duality on a general triangulation of a 2D torus. The TNO is constructed from three types of tensors: F on positive triangles (downward pointing triangular nodes), $\bar{\mathsf{F}}$ on negative triangles (upward pointing triangular nodes), and B_η on edges (circular nodes). The TNO is a map from the fermionic legs (red legs, pointing towards the triangular nodes from behind) of F and $\bar{\mathsf{F}}$ tensors to the bosonic legs of B_η (black legs, pointing out of the page).

$$\begin{aligned}\mathsf{D}\cdot(AB+C) = \mathsf{D}\cdot AB + \mathsf{D}\cdot C = \mathfrak{D}(A)\cdot\mathsf{D}\cdot B + \mathfrak{D}(C)\cdot\mathsf{D} \\ = \mathfrak{D}(A)\mathfrak{D}(B)\cdot\mathsf{D} + \mathfrak{D}(C)\cdot\mathsf{D} = \mathfrak{D}(AB+C)\cdot\mathsf{D}\end{aligned} \tag{3.41}$$

Hence, we need only find a D that satisfies:

$$\mathsf{D}\cdot P_f = W_f\cdot\mathsf{D} \tag{3.42a}$$

$$\mathsf{D}\cdot S_e = U_e\cdot\mathsf{D}, \tag{3.42b}$$

for all triangles f and edges e. To this end, we propose the TNO ansatz for D shown in Fig. 3.2.

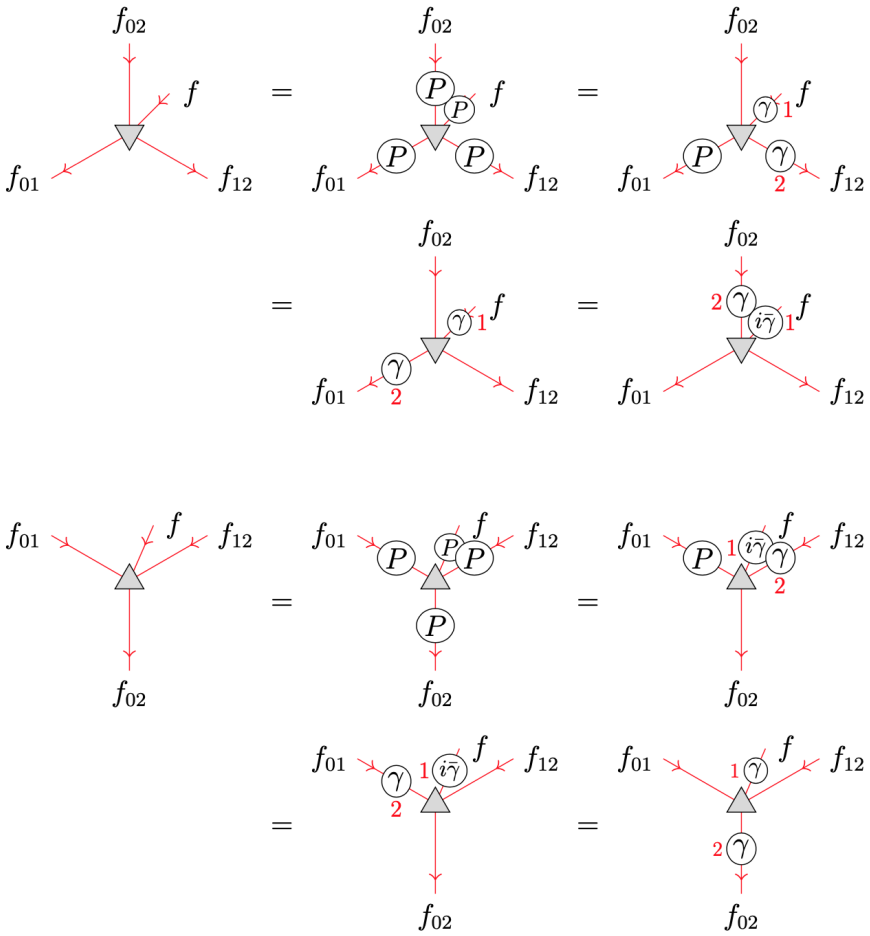

Figure 3.3: Graphical representation of the symmetries in Eqs. (3.51) and (3.53) for the tensors $\mathsf{F}[f]$ (downward pointing triangular nodes), $\bar{\mathsf{F}}[f]$ (upward pointing triangular nodes).

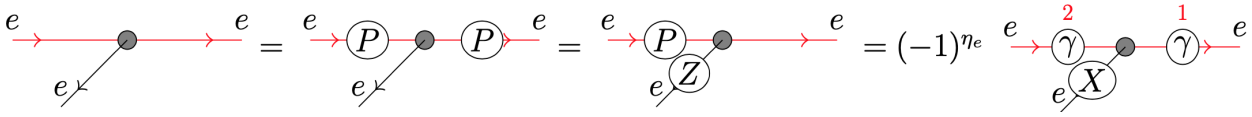

Figure 3.4: Graphical representation of the symmetry in Eq. (3.55) for the tensor $\mathsf{B}_\eta[e]$ (circular nodes).

The ansatz depicted in Fig. 3.2 is created by contracting together three kinds of tensors: tensors $\mathsf{F}[f]$ on positivly oriented triangles, tensors $\bar{\mathsf{F}}[f]$ on negativly oriented triangles, and tensors $\mathsf{B}_\eta[e]$ on edges. In explicit component form, the tensors $\mathsf{F}[f]$ and $\bar{\mathsf{F}}[f]$ are:

$$\begin{aligned}\mathsf{F}[f] &\equiv \sum_{j,a,b,c} F^{j}_{a,b,c}|c)_{f_{01}}|a)_{f_{12}}(b|_{f_{02}}(j|_{f}\\ \bar{\mathsf{F}}[f] &\equiv \sum_{j,a,b,c} \bar{F}^{j}_{a,b,c}|b)_{f_{02}}(a|_{f_{12}}(c|_{f_{01}}(j|_{f},\end{aligned} \tag{3.43}$$

where all sums are over binary values. Diagrammatically, we represent $\mathsf{F}[f]$ and $\bar{\mathsf{F}}[f]$ respectively as:

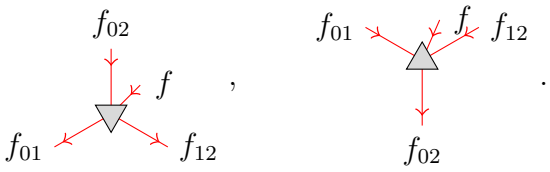

(3.44)

The legs labeled by f are the physical legs and extend into the page. These legs contract with fermionic operators or a fermionic tensor network state when the TNO is applied.

The tensor $\mathsf{B}_\eta[e]$ at each edge is obtained by making a spin-structure dependent modification to a tensor $\mathsf{B}[e]$. $\mathsf{B}[e]$ has the component form:

$$\mathsf{B}[e] = \sum_{j,a,b} B^{j}_{a,b}|a)_e|j\rangle_e(b|_e, \tag{3.45}$$

while the component form of $\mathsf{B}_\eta[e]$ is:

$$\begin{aligned}\mathsf{B}_\eta[e] =& Z_e^{\eta_e}\bullet\mathsf{B}\\ =& \sum_{j,a,b}(-1)^{j\eta_e}B^{j}_{a,b}|a)_e|j\rangle_e(b|_e,\end{aligned} \tag{3.46}$$

which is pictorially represented as:

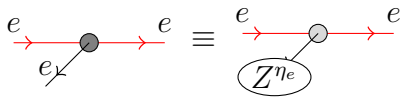

(3.47)

The darker node on the left hand side represents B_η, and the lighter node on the right hand side represents B. The physical legs are bosonic Hilbert spaces depicted in black and pointing out of the page. D is formed by gluing together the three tensors as dictated by the diagram (3.2), using the contraction map defined in Section 3.2.

Now, we view the constraints in Eqs. (3.42a) and (3.42b) as symmetries of the tensor D, and search for constraints on the local tensors F, $\bar{\mathsf{F}}$, and B that ensure these symmetries. To build intuition, we consider an example using bosonic tensors. Suppose the tensor $\mathsf{A} \cdot \mathsf{B}$ composed of the bosonic tensors A and B has the following symmetry:

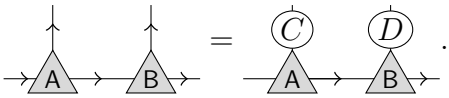

(3.48)

A sufficient condition, for $\mathsf{A} \cdot \mathsf{B}$ to satisfy Eq. (3.48), is that the local tensors A and B have the symmetries:

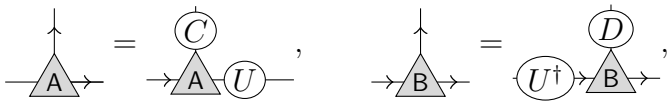

(3.49)

for some unitary operator U. This is because the contraction of A and B then satisfies:

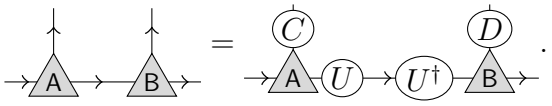

(3.50)

Since U and $U^\dagger$ on the virtual legs cancel, we obtain the symmetry in Eq. (3.48).

Additional symmetries of $\mathsf{A} \cdot \mathsf{B}$ require further constraints on the local tensors A and B. To determine a non-trivial solution for A and B, the symmetries of the local tensors need to be compatible. For example, if the symmetries $S_1 \cdot \mathsf{A} = \mathsf{A}$ and $S_2 \cdot \mathsf{A} = \mathsf{A}$ anticommute, i.e.,

$S_1 \cdot S_2 \cdot \mathsf{A} = -S_2 \cdot S_1 \cdot \mathsf{A}$, then A is forced to be 0.

Using the principles illustrated in the example above, we identified symmetries of F, $\bar{\mathsf{F}}$, and B that yield the constraints of D in Eqs.(3.42a) and (3.42b). The symmetries of the local tensors are depicted in Figs. 3.3 and 3.4. Algebraically, we write the symmetries for $\mathsf{F}[f]$ and $\bar{\mathsf{F}}[f]$ as:

$$\mathsf{F} = P_{f_{01}} \cdot P_{f_{12}} \cdot \mathsf{F} \cdot P_{f_{02}} \cdot P_f = P_{f_{01}} \cdot \gamma_{f_{12}} \cdot \mathsf{F} \cdot \gamma_f \tag{3.51}$$

$$= \gamma_{f_{01}} \cdot \mathsf{F} \cdot \gamma_f = \mathsf{F} \cdot \gamma_{f_{02}} \cdot i\bar{\gamma}_f \tag{3.52}$$

$$\bar{\mathsf{F}} = P_{f_{02}} \cdot \bar{\mathsf{F}} \cdot P_{f_{01}} \cdot P_{f_{12}} \cdot P_f = \bar{\mathsf{F}} \cdot \gamma_{f_{12}} \cdot P_{f_{01}} \cdot i\bar{\gamma}_f \tag{3.53}$$

$$= \bar{\mathsf{F}} \cdot \gamma_{f_{01}} \cdot i\bar{\gamma}_f = \gamma_{f_{02}} \cdot \bar{\mathsf{F}} \cdot \gamma_f \tag{3.54}$$

and the symmetries for $\mathsf{B}[e]$ can be written as:

$$\mathsf{B}_\eta = P_e \cdot \mathsf{B}_\eta \cdot P_e = P_e \cdot Z_e \cdot \mathsf{B}_\eta = (-1)^{\eta_e} \gamma_e \cdot X_e \cdot \mathsf{B}_\eta \cdot \gamma_e, \tag{3.55}$$

where the contractions in Eqs. (3.51), (3.53), and (3.55) should be read in conjunction with the diagrams in Figs. 3.3 and 3.4. We note that the first symmetry of each tensor implies that it is fermion parity even.

To see how the symmetries of the local tensors ensure that D satisfies the relations in Eqs. (3.42a) and (3.42b) we use the graphical representations of the symmetries shown in Figs. 3.3 and 3.3. For example, consider the action of the TNO on the parity operator at face f:

$\mathsf{D} \cdot P_f =$ 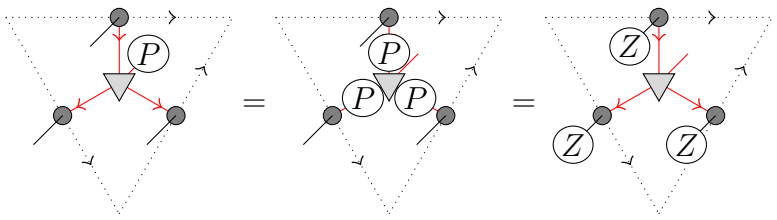 $= W_f \cdot \mathsf{D}.$ (3.56)

Here, we have applied the symmetries of $\mathsf{F}[f]$ and B in succession to show that D satisfies

Eq. (3.42a). Similarly, for a hopping operator we have:

$\mathsf{D}\cdot S_e = (-1)^{\eta_e}$ 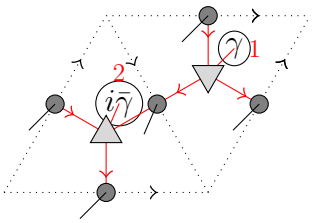 $= (-1)^{\eta_e}$ 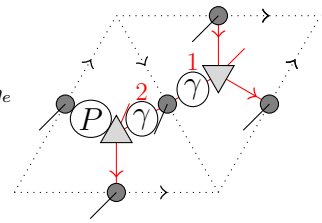

$=$ 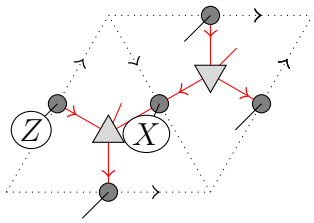 $= U_e\cdot\mathsf{D}.$ (3.57)

Thus, D satisfies (3.42b) as well. This implies that D formed from F, $\bar{\mathsf{F}}$, and B_η is indeed a representation of the operator-level duality of Ref. [15].

The tensors F, $\bar{\mathsf{F}}$, and B_η can be computed explicitly using their symmetries in Figs. 3.3 and 3.3. This is because the symmetries are independent, commute with each other, and square to the identity. Hence for F and $\bar{\mathsf{F}}$, they form a $\mathbb{Z}_2^5$ symmetry group, and for B they form a $\mathbb{Z}_2^3$ symmetry group. Since F and $\bar{\mathsf{F}}$ belong to 2^5 dimensional spaces, and B belongs to a 2^3 dimensional space, their symmetries fix their values uniquely up to a normalization factor. With this, we compute the local tensors to be:

$$\begin{aligned}
\mathsf{F}[f] &\propto \sum_{a,b,c} |c)_{f_{01}} |a)_{f_{12}} (b|_{f_{02}} (a+b+c|_f \\
\bar{\mathsf{F}}[f] &\propto \sum_{a,b,c} |b)_{f_{02}} (c|_{f_{01}} (a|_{f_{12}} (a+b+c|_f \\
\mathsf{B}[e] &\propto \sum_{a} |a)_e |a\rangle_e (a|_e .
\end{aligned} \tag{3.58}$$

Remember that all indices take values in $\{0,1\}$, and $a+b+c \equiv a+b+c \bmod 2$.

3.3.3 Bosonization of quantum states

We are now able to define the bosonization of quantum states, wherein a fermionic state is bosonized by simply applying the bosonization TNO. Before providing a simple example, we comment on constraints of the state-level duality that arise from the symmetries of D. In particular, we show that fermion parity odd states belong to the kernel of D and that D maps to bosonic states satisfying the constraint $G_v = 1$ for all v. Hence, fermion parity even states are mapped to bosonic states in a certain $\mathbb{Z}_2$ gauge theory.

To show that fermion parity odd states are in the kernel of the bosonization TNO, we use that $\prod_f W_f = 1$ on a closed manifold. This leads to:

$$\mathsf{D} = \prod_f W_f \bullet \mathsf{D} = \mathsf{D} \bullet \prod_f P_f. \tag{3.59}$$

When D is applied to a fermionic state $|\psi_f)$, Eq. (3.59) implies:

$$\mathsf{D}|\psi_f) = \mathsf{D} \bullet \prod_f P_f |\psi_f). \tag{3.60}$$

Thus, if $|\psi_f)$ is fermion parity odd, we have: $\prod_f P_f|\psi_f) = -|\psi_f)$, and it must be that $\mathsf{D}|\psi_f) = 0$.

The constraints on the image of D can be determined using the relation in Eq. (3.33). We see that:

$$\mathsf{D} = \mathsf{D} \bullet \left(\prod_{e:e_0=v} S_e \prod_{e:e_1=v} S_e \prod_{f:f_0,f_2=v} P_f \right) = \left(\prod_{e:e_0=v} U_e \prod_{e:e_1=v} U_e \prod_{f:f_0,f_2=v} W_f \right) \bullet \mathsf{D} = G_v \bullet \mathsf{D}. \tag{3.61}$$

Hence, for any bosonic state $\langle \psi_b|$:

$$\langle \psi_b|\mathsf{D} = \langle \psi_b| G_v \bullet \mathsf{D}, \tag{3.62}$$

which implies that D projects to the $G_v = 1$ subspace for each vertex v.

Now, we give a first example of the state-level duality and use the symmetries of D to show that the bosonization of an atomic insulator state yields a ground state of the toric code (a deconfined $\mathbb{Z}_2$ gauge theory). The atomic insulator state $|\psi_{AI})$ is the unique ground state of the Hamiltonian: $H_{AI} = -\sum_f P_f$. H_{AI} is certainly unfrustrated, so $|\psi_{AI})$ satisfies $P_f|\psi_{AI}) = |\psi_{AI})$ for all f. Applying D to $|\psi_{AI})$, we find:

$$\mathsf{D}|\psi_{AI}) = \mathsf{D}\cdot P_f|\psi_{AI}) = W_f\cdot\mathsf{D}|\psi_{AI}),\ \forall f. \tag{3.63}$$

Therefore, the bosonized state $\mathsf{D}|\psi_{AI})$ is in the $+1$ eigenspace of W_f for all f. Given the constraint on the image of D, the bosonized state is also in the $+1$ eigenspace of G_v for all v. Hence, $\mathsf{D}|\psi_{AI})$ is a ground state of the unfrustrated Hamiltonian $H = -\sum_v G_v - \sum_f W_f$. Recalling the definition of G_v defined in Eq. (3.37):

$$G_v = \prod_{e\supset v} X_e \prod_{f:f_0=v} W_f, \tag{3.64}$$

we see that the G_v terms in H can be replaced by $\prod_{e\supset v} X_e$ without changing the ground states. ($G_v = \prod_{e\supset v} X_e$ in the subspace where $W_f = 1$.) Thus, $\mathsf{D}|\psi_{AI})$ is a ground state of the toric code Hamiltonian $H_{TC} = -\sum_v \prod_{e\supset v} X_e - \sum_f W_f$.

To gain intuition for the mapping, we consider acting with D on a state with non-trivial fermion occupancy. In particular, we apply a hopping operator S_e at edge e to the atomic insulator state $|\psi_{AI})$ to obtain a state with fermions at the two faces neighboring e. The image of $S_e|\psi_{AI})$ under D is:

$$\mathsf{D}\cdot S_e|\psi_{AI}) = U_e\cdot\mathsf{D}|\psi_{AI}) = U_e|\psi_{TC}\rangle. \tag{3.65}$$

U_e (defined in Eq.(4.35)) creates a $\mathbb{Z}_2$ flux (-1 eigenvalue of W_f) at each face bordering the edge e and moves $\mathbb{Z}_2$ charges (-1 eigenvalue of $\prod_{e\supset v} X_e$) to the 0-vertices of L_e and R_e. A $\mathbb{Z}_2$ flux bound to a $\mathbb{Z}_2$ charge has fermionic statistics – it is an *emergent* fermion. Therefore,

physical fermions are mapped to emergent fermions in the $\mathbb{Z}_2$ gauge theory. The gauge constraint $G_v = 1$, $\forall v$ removes ambiguity in this mapping, since it enforces that charges are bound to fluxes, with the charges located at the 0-vertex of the corresponding triangle.

Any fermion parity even state can be created from $|\psi_{AI})$ by applying operators in $\mathcal{E}$. Hence, one strategy for mapping an arbitrary even fermion parity state $|\psi_f)$ is to identify an even operator $\mathcal{O}\big(\{S_e\}_e, \{P_f\}_f\big)$, written here explicitly in terms of the generators of $\mathcal{E}$, such that:

$$|\psi_f) = \mathcal{O}\big(\{S_e\}_e, \{P_f\}_f\big)|\psi_{AI}). \tag{3.66}$$

Then, the duality maps:

$$|\psi_f) \to \mathcal{O}\big(\{U_e\}_e, \{W_f\}_f\big)|\psi_{TC}). \tag{3.67}$$

In general, it may be challenging to find an operator, expressed in terms of the generators of $\mathcal{E}$, that creates $|\psi_f)$ from $|\psi_{AI})$. Moreover, the analysis of bosonizing states, thus far, has only required the operator-level bosonization duality. In the next section, we illustrate the true potential of the bosonization TNO. Given a fermion parity even state $|\psi_f)$ constructed from the contraction of local tensors, we show that $|\psi_f)$ can be bosonized by using D to modify each of the local tensors. The resulting state can then be written as a bosonic tensor network state.

3.4 Bosonization of fPEPS

In the previous section, we introduced the bosonization of a fermionic state $|\psi_f)$ as the action of the bosonization TNO D on $|\psi_f)$. As we now show, the TNO is especially useful when the fermionic $|\psi_f)$ is represented as a fermionic tensor network state. While the action of D on the fermionic tensor network state $|\psi_f)$ indeed yields a bosonic state $\mathsf{D}|\psi_f) = |\psi_b\rangle$, $|\psi_b\rangle$ is not manifestly a bosonic tensor network state. This is due, in part, to the $\mathbb{Z}_2$-graded virtual legs

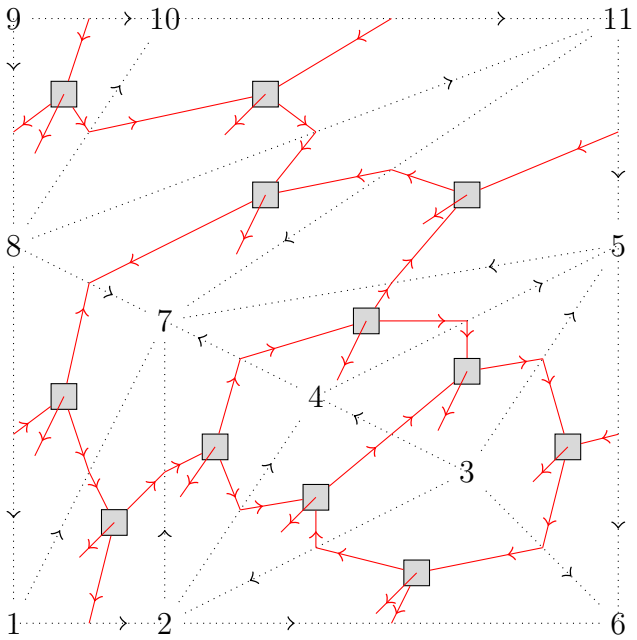

Figure 3.5: An example fPEPS on an arbitrarily triangulated torus. The square nodes represent the tensors T and $\bar{\mathsf{T}}$ in Eqs. (3.68) and (3.69). The legs affixed to the center of the square nodes and pointing out of the page are the physical legs of the fPEPS. All other legs are contracted with a leg of a neighboring tensor.

of the bosonization TNO. However, if $|\psi_f)$ is in the form of a fermionic projected entangled pair state (fPEPS) (see Fig. 3.5 for an example), we can explicitly rewrite $|\psi_b\rangle$ as a bosonic projected entangled pair state (bPEPS). In this section, we give a detailed algorithm for converting bosonized fPEPS into bPEPS, which is well defined on arbitrary triangulations of orientable 2D manifolds without boundary.

3.4.1 Contracting the bosonization TNO with an fPEPS

An fPEPS on a triangulated manifold is built from $\mathbb{Z}_2$-graded tensors $\mathsf{T}[f']$ on positively oriented triangles and $\bar{\mathsf{T}}[f']$ on negatively oriented triangles.

Assuming that the tensors are fermion parity even, they can be written in component form as:

$$\begin{aligned}\mathsf{T}[f'] &\equiv \sum_{a,b,c} T^{(f')}_{abc} |c)_{f'_{01}} |a)_{f'_{12}} (b|_{f'_{02}} (a+b+c|_{f'} \\ \bar{\mathsf{T}}[f'] &\equiv \sum_{a,b,c} \bar{T}^{(f')}_{abc} |b)_{f'_{02}} (a|_{f'_{12}} (c|_{f'_{01}} (a+b+c|_{f'},\end{aligned} \tag{3.68}$$

where for generality, the tensor components are position dependent. $\mathsf{T}[f']$ and $\bar{\mathsf{T}}[f']$ can then be represented, respectively, as follows:

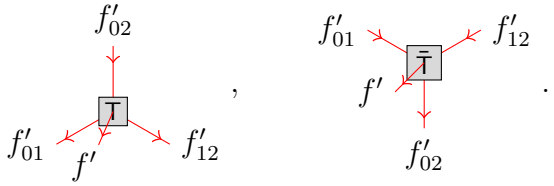

(3.69)

Fig. 3.5 shows an fPEPS formed from contracting $\mathsf{T}[f']$ and $\bar{\mathsf{T}}[f']$ on an arbitrary triangulation of a torus.

In general, one can insert matrix product operators (MPO) before closing an fPEPS on a closed manifold. Though we believe our construction can be extended to such cases, in the interest of brevity and clarity, we restrict the discussion to fPEPS without any MPO

insertions.

To apply D to an fPEPS $|\psi_f)$, we contract the physical indices of F tensors with those of the T tensors, and likewise, we contract $\bar{\mathsf{F}}$ tensors with $\bar{\mathsf{T}}$ tensors. Thus, the first step in bosonizing an fPEPS is to calculate the tensors $\mathsf{M_f} = \mathsf{F}\cdot\mathsf{T}$ for positively oriented triangles and the tensors $\bar{\mathsf{M}}_\mathsf{f} = \bar{\mathsf{F}}\cdot\bar{\mathsf{T}}$ for negatively oriented triangles. Graphically, $\mathsf{M_f}$ and $\bar{\mathsf{M}}_\mathsf{f}$ can be drawn, respectively, as:

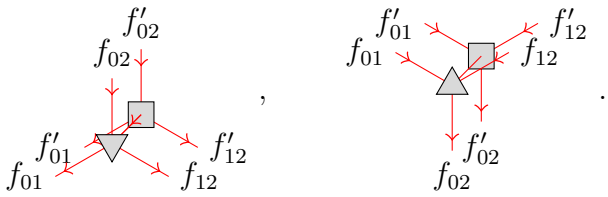

(3.70)

The bosonized state $|\psi_b\rangle$ is a tensor network state (in fact an fPEPS) generated by tensors $\mathsf{M_f}$, $\bar{\mathsf{M}}_\mathsf{f}$, as well as $\mathsf{B}_\eta[e]$ on edges. Since there are two layers of virtual legs to be contracted, we refer to them as the "state layer" and the "TNO layer". Note that $\mathsf{M_f}$ and $\bar{\mathsf{M}}_\mathsf{f}$ tensors have virtual legs on both layers, but $\mathsf{B}_\eta[e]$ is only on the TNO layer.

While $|\psi_b\rangle$ is a tensor network state and an fPEPS, it is not generically a bPEPS, as there are fermionic virtual indices remaining. The challenge is then to re-express $|\psi_b\rangle$ as a bPEPS, or, in a sense, to convert the fermionic virtual legs to bosonic virtual legs. We accomplish this by systematically accounting for the signs accrued in contracting the fermionic virtual legs – the so-called *Koszul signs*. To make our strategy clear, we first discuss Koszul signs and introduce the idea of a *removable grading*. These concepts play a key role in the rest of this section, so we describe them in generality before returning to the problem of converting the fermionic virtual legs of $|\psi_b\rangle$ to bosonic virtual legs.

3.4.2 Koszul signs and removable grading

The bosonized fPEPS encodes a bosonic quantum state $|\psi_b\rangle = \sum_{\{\phi\}} C_\phi |\phi\rangle$, where the collection of $|\phi\rangle$ form a complete set of product states. The coefficients C_ϕ can be recovered from the bosonized fPEPS by fixing the physical indices according to $|\phi\rangle$ and summing over

the virtual indices. Given the $\mathbb{Z}_2$-grading of the virtual legs, there are signs picked up upon re-ordering and contracting the $\mathbb{Z}_2$-graded vectors, which can contribute to the coefficient C_ϕ. A natural question is whether the grading of a virtual index is essential to the tensor network, i.e., if the grading of a particular virtual index is removed, does the value of the bosonized fPEPS change?

For illustration, consider the two simple graded tensors:

$$\mathsf{A} = \sum_{a,a'} A_{aa'}(a'|_s(a|_t, \quad \mathsf{B} = \sum_{b,b'} B_{bb'}|b')_s|b)_t. \tag{3.71}$$

(We can think of s and t as indices corresponding to the state and TNO layers, respectively.) We want to calculate the tensor network (which is a scalar in this case) $\mathsf{A}\cdot\mathsf{B}$. Let us describe the contraction of these tensors as a two step process. In the first step, we contract the basis tensors:

$$(a'|_s(a|_t\cdot|b')_s|b)_t = (-1)^{|b'||a|}\delta_{ab}\delta_{a'b'}, \tag{3.72}$$

and in the second step, we calculate the components:

$$\sum_{a,a,b,b'} (-1)^{|b'||a|}\delta_{ab}\delta_{a'b'}A_{aa'}B_{bb'} = \sum_{a,a'}(-1)^{|a'||a|}A_{aa'}B_{aa'}. \tag{3.73}$$

Notice that we produce an additional sign of $(-1)^{|b'||a|}$ in the basis contraction step due to the graded nature of indices. This is the key difference between virtual indices of fermionic and bosonic tensor networks – bosonic indices do not produce any additional signs in basis contraction. We refer to these additional signs of basis contractions as Koszul signs. The point is that the grading of a virtual index contributes to the fPEPS only through possible Koszul signs. Therefore, we can remove the grading of a virtual index as long as we properly account for the Koszul signs.

Sometimes this can be done simply by picking a specific internal ordering for the fermionic

tensors and interpreting their components, with respect to this ordering, as components of purely bosonic tensors. We say that the grading of the virtual indices in the original fermionic tensor network can be removed, if the contraction of this new bosonic tensor network is the same as that of the original fermionic tensor network. When we have some a priori internal ordering for the fermionic tensors in mind already – one that does produce Koszul signs – then we can refer to this process as *changing the internal ordering* to eliminate the Koszul signs. For example, consider changing the internal ordering of A to $\mathsf{A} = \sum_{a,a'} A_{aa'}(-1)^{|a'||a|}(a|_t(a'|_s$. Now, there is no Koszul sign in the basis contraction: $(a|_t(a'|_s \cdot |b')_s|b)_t = \delta_{a,b}\delta_{a',b'}$. Removing the grading from A and B yields:

$$\mathsf{A}_\mathsf{b} = \sum_{a,a'} A_{aa'}(-1)^{|a'||a|}\langle a|_t\langle a'|_s, \quad \mathsf{B}_\mathsf{b} = \sum_{b,b'} B_{bb'}|b'\rangle_s|b\rangle_t. \tag{3.74}$$

A_b and B_b are purely bosonic tensors, and they produce the same tensor network: $\mathsf{A}_\mathsf{b}\cdot\mathsf{B}_\mathsf{b} = \mathsf{A}\cdot\mathsf{B}$. Note that the grading is removable for only particular choices of the internal ordering.

In other cases, the Koszul signs can be accounted for with a removal of the grading, followed by an insertion of additional operators into the tensor network. To see an example of this, consider the two even tensors $\mathsf{A} = \sum_a A_a|a)_p(a|_q$ and $\mathsf{B} = \sum_b B_b|b)_q(b|_p$. We then aim to compute the tensor network (a scalar) $\mathrm{tr}\,[\mathsf{A}\cdot\mathsf{B}]$, where the $\cdot$ denotes the contraction of the q leg and the trace over the p index is to emphasize that we are contracting the first index with the last index to close the loop. Contracting the basis tensors yields:

$$\mathrm{tr}\,[|a)_p(a|_q\cdot|b)_q(b|_p] = \delta_{ab}\mathrm{tr}\,[|a)_p(b|_p] = (-1)^{|a|}\delta_{ab}. \tag{3.75}$$

The grading of the q vector did not produce a sign, so it can be removed without affecting the tensor network. However, if we try to remove the grading of the p vector as well, the sign $(-1)^{|a|}$ is no longer accounted for. One way to reproduce the sign $(-1)^{|a|}$ is to insert a $Z = \sum_c (-1)^{|c|}|c\rangle\langle c|$ operator on leg p after removing the grading. That is, grading removal

gives bosonic tensors $\mathsf{A_b} = \sum_a A_a|a\rangle_p\langle a|_q$ and $\mathsf{B_b} = \sum_b B_b|b\rangle_q\langle b|_p$, which satisfy:

$$\mathrm{tr}\left[\mathsf{A_b}{\scriptstyle\bullet}\mathsf{B_b}{\scriptstyle\bullet}Z_p\right] = \sum_{a,b,c}(-1)^{|c|}A_aB_b\mathrm{tr}\left[|a\rangle_p\langle a|_q{\scriptstyle\bullet}|b\rangle_q\langle b|_p{\scriptstyle\bullet}|c\rangle_p\langle c|_p\right] = \mathrm{tr}\left[\mathsf{A}{\scriptstyle\bullet}\mathsf{B}\right] \tag{3.76}$$

When the grading of a virtual index can be accounted for by inserting an additional operator O on un-graded indices, we will say that the grading is "removable with O-insertion".

3.4.3 Koszul signs in the bosonized fPEPS

We now return to the problem of re-writing the bosonized fPEPS as an explicit bPEPS. We will find that, for a particular internal ordering, the grading of the virtual legs in the bosonized fPEPS is removable with $(Z_t \otimes Z_s)^{\eta_e}$-insertion. Here, Z_t is a Pauli Z operator acting in the TNO layer, and Z_s is a Pauli Z operator acting in the state layer. In other words, the state represented by the bosonized fPEPS may be equivalently represented by the bPEPS obtained by removing the grading of the virtual legs (assuming a certain internal ordering) and applying $(Z_t \otimes Z_s)^{\eta_e}$ before contracting the tensors at each edge. To show this, we will compute the Koszul signs explicitly. We will see that the Koszul signs have a nice geometric interpretation in terms of the branching structure of the triangulated manifold.

Simplifying the Koszul sign calculation

We begin by simplifying the problem. First, $\mathsf{B}_\eta = Z^{\eta_e}{\scriptstyle\bullet}\mathsf{B}$ does not contribute to any Koszul signs, since B_η can always be contracted with one of its neighboring $\mathsf{M_f}$ or $\bar{\mathsf{M}}_\mathsf{f}$ tensors without any change of internal ordering. This is possible due to the even parity of B_η and its simple, two-virtual-leg form $\mathsf{B}_\eta = \sum_a (-1)^{a\eta_e}|a)_e|a\rangle_e(a|_e$. Therefore, the Koszul signs accrued in contracting the tensors $\mathsf{M_f}$, $\bar{\mathsf{M}}_\mathsf{f}$, and B_η are equivalent to the Koszul signs from directly contracting the $\mathsf{M_f}$ and $\bar{\mathsf{M}}_\mathsf{f}$ tensors without B_η.

We continue to simplify the calculation of the Koszul signs by reducing $\mathsf{M_f}$ and $\bar{\mathsf{M}}_\mathsf{f}$ from two layers of fermionic virtual legs as in Eq. (3.70) to a single layer of fermionic virtual legs. The first step is to choose the following internal ordering for the tensors $\mathsf{M_f}$ and $\bar{\mathsf{M}}_\mathsf{f}$,

respectively:

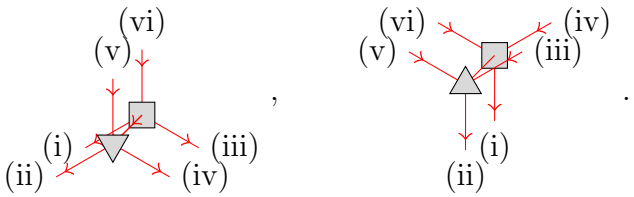

(3.77)

Notice that for outward pointing legs (ket vectors), the state layer index comes before the TNO layer index, while for inward pointing legs (bra vectors), the order is reversed. Letting $|a')_s$ and $|a)_t$ be the state and TNO layer vectors, respectively, then with the ordering in Eq. (3.77), we have $(a|_t(a'|_s \bullet |a')_s|a)_t = 1$, and no Koszul sign is produced between a' and a. Therefore, we can combine the legs and consider a composite index (a', a) with tensors written in terms of $|a', a)_{st}$ and $(a', a|_{st}$. The Hilbert space of the composite leg corresponds to the Hilbert space of two spinless fermions. This is isomorphic to a single spinless fermion and a spin-1/2 under the isomorphism:

$$|a', a) \leftrightarrow |a + a')|a\rangle. \tag{3.78}$$

Since the spin-1/2 degree of freedom does not affect the Koszul signs, we may disregard it for the present computation.

In summary, we have reduced the calculation of the Koszul signs of the bosonized fPEPS to a calculation of the Koszul signs obtained in the contraction of single layer tensors with internal orderings inherited from Eq. (3.77) and pictured below:

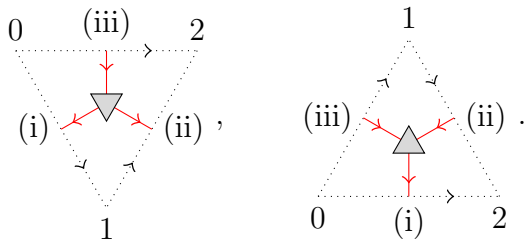

(3.79)

In Eq. (3.79), we have again used triangular nodes, but these tensors should not be confused with the four legged F and $\bar{\mathsf{F}}$ tensors. It should be noted that similar simplifications can be performed for the contraction (inner product) of any two fPEPS (built from fermion parity even local tensors). Consequently, the calculation of the Koszul signs below holds more generally than the application at hand – turning a bosonized fPEPS into a bPEPS.

Contraction of basis tensors

As mentioned in Section 3.4.2, the contraction of tensors can be performed in two steps: (i) the basis tensors are contracted, and (ii) the components are calculated. The Koszul signs arise only in the first step. Therefore, to calculate the Koszul signs, we focus on the contraction of basis tensors with the ordering in Eq. (3.79). We denote the set of basis tensors at a positively oriented face f as $\mathcal{Q}[f]$ and the set of basis tensors at a negatively oriented face f as $\bar{\mathcal{Q}}[f]$. Explicitly, we have:

$$\begin{aligned}\mathcal{Q}[f] =&\{|a+b)_{f_{01}}|a)_{f_{12}}(b|_{f_{02}},\ a,b=0,1\}\\ \bar{\mathcal{Q}}[f] =&\{|b)_{f_{02}}(a|_{f_{12}}(a+b|_{f_{01}},\ a,b=0,1\}.\end{aligned} \tag{3.80}$$

Note that the tensors in $\mathcal{Q}[f]$ and $\bar{\mathcal{Q}}[f]$ are fermion parity even by construction. M_f and $\bar{\mathsf{M}}_\mathsf{f}$ are fermion parity even, so their component value for any fermion parity odd basis tensor is necessarily zero. Thus, we can disregard fermion parity odd basis tensors in computing the Koszul signs.

We now analyze the contraction of basis tensors in Eq. (3.80). For each triangle, we have an independently chosen element of either $\mathcal{Q}[f]$ or $\bar{\mathcal{Q}}[f]$ (depending on the orientation of f). The resulting product of basis tensors evaluates to 0, -1, or 1. If an odd vector $|1)$ is paired with an even vector $|0)$ at any edge, then the product is 0. (This is simply the statement that $(0|1) = (1|0) = 0$.) Thus, the configurations of basis tensors that evaluate to a nonzero value must have odd legs paired at edges. Since the elements of $\mathcal{Q}[f]$ and $\bar{\mathcal{Q}}[f]$ have even fermion parity (an even number of odd legs), this implies that the odd legs form closed loops

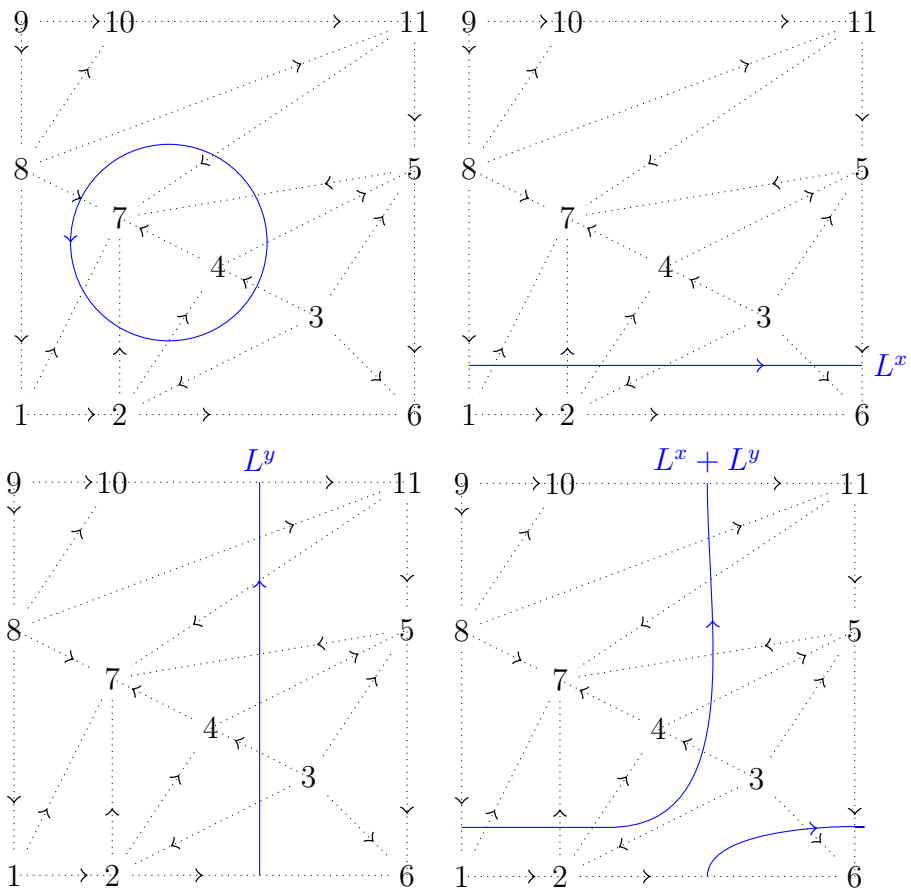

Figure 3.6: Examples of 1-cochains. Edges intersected by the blue line have coefficient $g_e = 1$, while all other edges have $g_e = 0$. The top left picture is an example of a contractible 1-cocycle. The other three pictures are representative 1-cocycles of the three non-trivial classes.

(on the dual lattice) for any configuration that gives a nonzero value.

The computation of the Koszul signs then distills down to calculating the ± 1 valued contraction of configurations with closed loops of $|1)$ states at edges. To formalize the problem, we define g_e as the $\{0, 1\}$ valued index at the edge e, and $\hat{\sigma}(\{g_e\}) = \pm 1$ as the sign obtained by evaluating the tensor contractions corresponding to the configuration $\{g_e\}$.

Basis contraction and cohomology

To make our arguments precise, we find it convenient to describe configurations of odd edges using the language of cohomology. To this end, we define a 0-*cochain* as a sum $\sum_v g_v \mathbf{v}$, where $\mathbf{v}$ is a $\mathbb{Z}_2$-valued function of vertices such that $\mathbf{v}$ evaluates to 1 on the vertex v and 0 otherwise, and g_v are coefficients in $\mathbb{Z}_2$. Similarly, 1-*cochains* and 2-*cochains* may be defined as sums $\sum_e g_e \mathbf{e}$ and $\sum_f g_f \mathbf{f}$, respectively. A configuration of odd edges $\{g_e\}$ then naturally corresponds to the 1-cochain $\sum_e g_e \mathbf{e}$. Furthermore, j-cochains can be added by combining the coefficients component wise, i.e., $\sum_e g_e \mathbf{e} + \sum_e g'_e \mathbf{e} = \sum_e (g_e + g'_e)\mathbf{e}$.

The *coboundary operator* δ from j-cochains to $j+1$-cochains is defined by:

$$\delta \mathbf{v} = \sum_{e \supset v} \mathbf{e}, \qquad \delta \mathbf{e} = \sum_{f \supset e} \mathbf{f}, \tag{3.81}$$

where the sum on the left is over all edges sharing the vertex v and the sum on the right is over the two faces bordering the edge e. For example, in Fig. 3.6:

$$\begin{aligned} \delta\langle \mathbf{4} \rangle &= \langle \mathbf{2}, \mathbf{4} \rangle + \langle \mathbf{3}, \mathbf{4} \rangle + \langle \mathbf{4}, \mathbf{5} \rangle + \langle \mathbf{4}, \mathbf{7} \rangle \\ \delta\langle \mathbf{4}, \mathbf{7} \rangle &= \langle \mathbf{2}, \mathbf{4}, \mathbf{7} \rangle + \langle \mathbf{4}, \mathbf{5}, \mathbf{7} \rangle \end{aligned} \tag{3.82}$$

We call a cochain C *closed* if $\delta C = 0$. Note that each of the 1-cochains depicted in Fig. 3.6, for example, are closed. More generally, a closed 1-cochain, or 1-cocycle, can be thought of as a sum of loops along the dual lattice. As such, the configurations $\{g_e\}$, obtained from basis contraction, are examples of 1-cocycles.

A 1-cochain C is called a 1-*coboundary* if there exists a 0-cochain R such that $C = \delta R$. δ can be understood as a boundary operator on the dual lattice, so intuitively, a 1-coboundary is a boundary of a region on the dual lattice. For example, the top left picture of Fig. 3.6 depicts a 1-coboundary – it is equal to δR for $R = \langle \mathbf{7} \rangle + \langle \mathbf{4} \rangle$. In general, 1-coboundaries are sums of contractible loops, which are generated by small loops $L_v \equiv \delta \mathbf{v}$ enclosing a single vertex. A configuration L with a single, contractible loop is a 1-coboundary of a 0-cochain R

containing vertices enclosed by the loop, i.e., $L = \sum_{v \in L} L_v$ with the sum being over vertices v enclosed by L. Some loops of odd edges such as the 1-cocycles L^x, L^y, and $L^x + L^y$ in Fig. 3.6, are *non-contractible*. These are 1-cocycles that cannot be written as δR for any 0-cochain R.

We can further define an equivalence of 1-cocycles where $C_1 \sim C_2$ if there exists a 0-cochain R such that $C_1 = C_2 + \delta R$. In other words, two 1-cocycles are equivalent if one can be constructed from the other by appending, or adding contractible loops. Hence, all 1-coboundaries belong to the same equivalence class – the class of trivial 1-cocycles. For a torus, it is well known that there are four inequivalent classes of 1-cocycles. These may be represented by L^x, L^y, $L^x + L^y$, and δR for a 0-cochain R. Therefore, an arbitrary 1-cocycle on a torus can be expressed as:

$$C = g_x L^x + g_y L^y + \sum_v g_v L_v, \tag{3.83}$$

for some choice of $g_x, g_y, g_v \in \mathbb{Z}_2$.

Koszul signs from a single loop

Given that a 1-cocycle can be decomposed in terms of constituent loops, as in Eq. (3.83), we begin by calculating the Koszul sign $\hat{\sigma}(L)$ for configurations L with a single loop of odd edges along the path L in the dual lattice. To propose an exact value for $\hat{\sigma}(L)$, we introduce the following notation. We assign a direction to the path L so that, with respect to a global orientation of the 2D manifold, the loop has a "left side" and a "right side".[3] L overlaps with a triangle f at two edges, and we call the common vertex of these two edges f_L. There are six possibilities for f_L: it can be a 0-, 1-, or 2-vertex of the triangle f, and it can lie to the left or to the right of the loop. We let $\bar{l}_L$ and $\bar{r}_L$ be the sets of f_L for which f_L is a

[3]More formally, let v_1 be the unit tangent vector along L, in the direction of L. Then we say that the unit normal vector v_2 points to the "left" side of L if $v_1 \wedge v_2$ is equal to the orientation of the underlying 2D manifold.

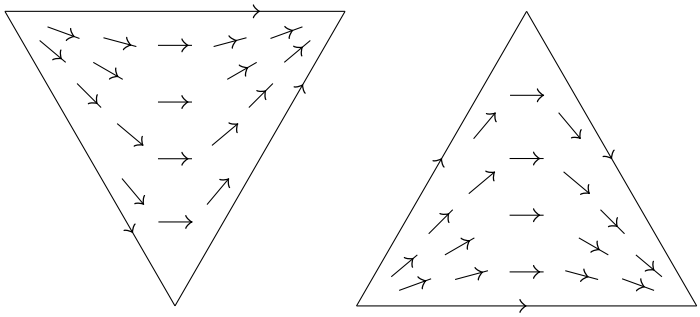

Figure 3.7: The branching structure is interpolated into the interior of each triangle to form the continuous, non-vanishing vector field $\mathcal{V}$.

1-vertex of f and is to the left or right of L, respectively. We use $n(\bar{l}_L)$ and $n(\bar{r}_L)$ to denote the cardinality of $\bar{l}_L$ and $\bar{r}_L$. Then we have:

Proposition 4

$$\hat{\sigma}(L) = -(-1)^{\frac{1}{2}(n(\bar{l}_L)-n(\bar{r}_L))}. \tag{3.84}$$

Proof of Proposition 4. See Appendix 3.B. □

Winding number and Koszul signs

$\hat{\sigma}(L)$ is closely related to the winding number of a certain vector field along the oriented path L. In particular, $\hat{\sigma}(L)$ can be computed from the continuous, non-vanishing vector field $\mathcal{V}$ obtained from the branching structure by interpolating it into the interior of the triangles, as shown in Fig. 3.7 (see Ref. [118]). To calculate the winding number of $\mathcal{V}$ along L we define $\hat{n}$ to be the left pointing unit normal vector of the loop L and $\hat{v}$ to be the local vector of $\mathcal{V}$. Then, we integrate the derivate of the angle $\theta = \cos^{-1}(\hat{v} \cdot \hat{n})$ between $\hat{n}$ and $\hat{v}$ along L. Given that θ is continuous, the change in θ around L must be $2\pi m$, where m is an integer. m gives the winding number of $\mathcal{V}$ along L, which we denote as $w(L)$.[4] For definiteness, we

[4]Note that the definition of winding number here is the winding number of the vector field relative to the normal vector of the loop L. We emphasize that this differs by a sign from a notion of the winding number of a vector field sometimes used in physics.

choose clockwise rotation to be positive.

Proposition 5

$$w(L) = \frac{1}{2}\big(n(\bar{l}_L) - n(\bar{r}_L)\big). \tag{3.85}$$

Equivalently,

$$\hat{\sigma}(L) = -(-1)^{w(L)}. \tag{3.86}$$

Proof of Proposition 5. We consider the ways in which L can pass through triangles and in each case, identify the change in $\theta = \cos^{-1}(\hat{v} \cdot \hat{n})$. When f_L is a 0- or 2-vertex, the total change in θ is 0. This is illustrated in the following example, where f_L is a 2-vertex:

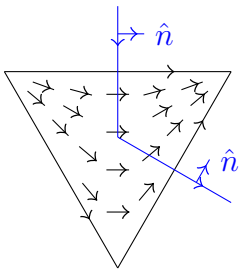

. (3.87)

The change in θ through the triangle above is 0, since the vector field is nearly parallel to $\hat{n}$ along the path. A similar argument applies whenever f_L is a 0- or 2-vertex. Thus, the only crossings that can contribute to the winding number are when f_L is a 1-vertex.

We first examine the case where f_L is a 1-vertex to the left of L, i.e., $f_L \in \bar{l}_L$. There are two such crossings:

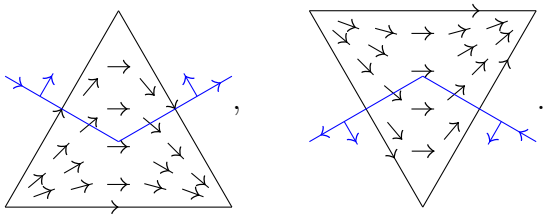

, . (3.88)

(Note the triangle on the left is negatively oriented while the triangle on the right is positively oriented.) For both crossings, moving along L, the vector field rotates clockwise relative to $\hat{n}$, and θ changes by $+\pi$. If instead, f_L is to the right of L then the corresponding crossings are:

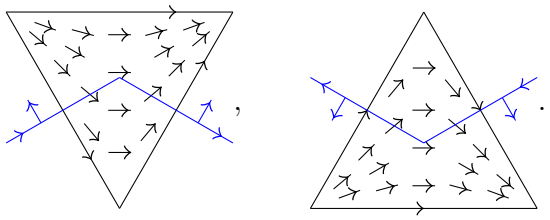

(3.89)

We see that, in this case, the vector field winds counterclockwise along L, and θ changes by $-\pi$.

In conclusion, whenever f_L belongs to $\bar{l}_L$, θ changes by π, and when f_L is in $\bar{r}_L$, θ changes by $-\pi$. Accordingly, the winding number along L, with respect to $\hat{n}$, is:

$$w(L) = \sum_{f_L} \left(\frac{1}{2}\delta_{f_L \in \bar{l}_L} - \frac{1}{2}\delta_{f_L \in \bar{r}_L} \right) = \frac{1}{2}\big(n(\bar{l}_L) - n(\bar{r}_L)\big), \tag{3.90}$$

where $\delta_{f_L \in \bar{l}_L}$ and $\frac{1}{2}\delta_{f_L \in \bar{r}_L}$ are indicator functions for the sets $\bar{l}_L$ and $\bar{r}_L$, respectively. □

In Refs. [118, 119], it is argued that a function on loops of the form $-(-1)^{w(L)}$, such as $\hat{\sigma}(L)$, gives a *quadratic refinement of the intersection pairing*. This is to say that, as a consequence of Prop. 5, $\hat{\sigma}$ satisfies:

$$\hat{\sigma}(L_1 + L_2) = (-1)^{\langle L_1, L_2 \rangle} \hat{\sigma}(L_1)\hat{\sigma}(L_2), \tag{3.91}$$

where $\langle L_1, L_2 \rangle$ is the intersection number (mod 2) of L_1 and L_2. For example, the non-contractible cycles L^x and L^y on a torus in Fig. 3.6 have an intersection number $\langle L^x, L^y \rangle = 1 \bmod 2$. Therefore, by Eq. (3.91), we have: $\hat{\sigma}(L^x + L^y) = -\hat{\sigma}(L^x)\hat{\sigma}(L^y)$.

Importantly, Eq. (3.91) allows us to relate the sign $\hat{\sigma}(C)$ for a general configuration

$C = \sum_i L_i$ to the signs $\hat{\sigma}(L_i)$ of constituent loops. For a single contractible loop L, which can be decomposed into a sum of loops $L = \sum_{v \in L} L_v$, the sign $\hat{\sigma}(L)$ can be written as [using Eq. (3.91):

$$\hat{\sigma}(L) = \prod_{v \in L} \hat{\sigma}(L_v). \tag{3.92}$$

The product in Eq. (3.92) is over vertices enclosed by the loop L.

We call a vertex v *singular* if the loop L_v, enclosing only v, is such that $\hat{\sigma}(L_v) = -1$. Referring to Eq. (3.92), the sign $\hat{\sigma}(L)$ for a contractible loop L can be computed by simply counting the singular vertices enclosed by L. Explicitly, $\hat{\sigma}(L)$ for a contractible loop L is:

$$\hat{\sigma}(L) = (-1)^{n_{sv}(L)}, \tag{3.93}$$

where $n_{sv}(L)$ is the number of singular vertices enclosed by the loop L. This is a manifestation of Stokes' theorem for the winding number of the vector field along L. We note that, using Prop. 4, a vertex v is singular if it is the 1-vertex of $4m$ triangles, for an integer m. Alternatively, using Prop. 5, v is singular if $-(-1)^{w(L_v)} = -1$.

3.4.4 Removing grading and choosing spin-structure

The function $\hat{\sigma}$ captures the Koszul signs accrued in the contraction of the fermionic virtual legs of the bosonized fPEPS. The goal of this section is to replace the $\mathbb{Z}_2$-graded virtual legs of the bosonized fPEPS with un-graded legs and simulate the Koszul signs given by $\hat{\sigma}$ by inserting Pauli Z operators on certain bosonic virtual legs.

More specifically, we first convert the fermionic virtual legs to bosonic virtual legs, i.e., with the internal ordering fixed, we map a fermion parity even state $|0)$ to an up spin $|0\rangle$ (in the Z basis) and a fermion parity odd state $|1)$ to a down spin $|1\rangle$. The bosonic virtual legs fail to replicate the Koszul signs that were obtained by contracting the fermionic virtual legs. Thus, second, we fix this by choosing a set of edges η (a choice of spin-structure) and

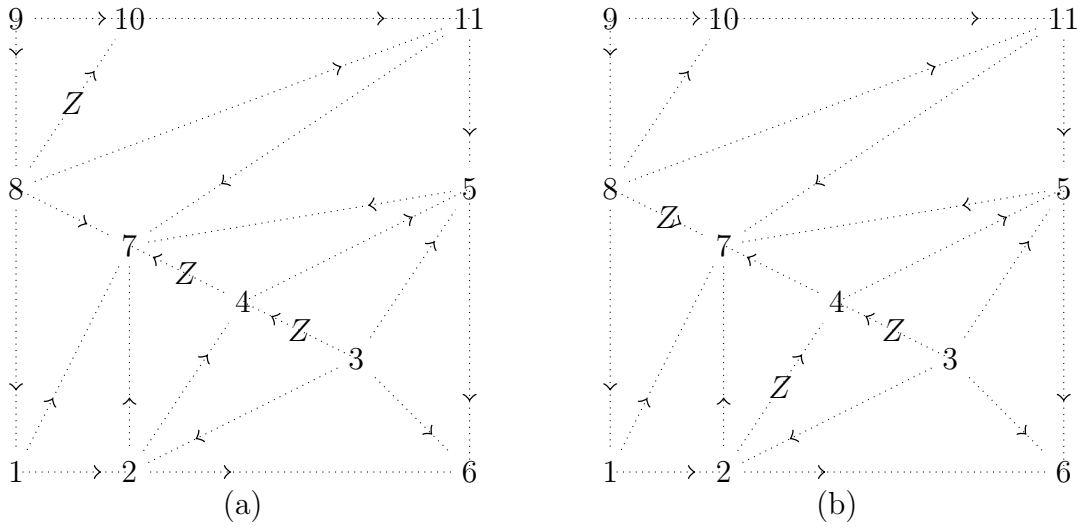

Figure 3.8: An arbitrary triangulation of a torus with the four singular vertices: $\langle 3\rangle$, $\langle 7\rangle$, $\langle 5 = 8\rangle$, $\langle 2 = 10\rangle$, $\langle 2 = 11\rangle$. (a) Z-operators placed at edges corresponding to the spin-structure $\eta = \{\langle 3, 4\rangle, \langle 4, 7\rangle, \langle 8, 10\rangle\}$. (b) Z-operators placed at edges for an alternative choice of spin-structure $\eta = \{\langle 3, 4\rangle, \langle 4, 2\rangle, \langle 7, 8\rangle\}$.

including an extra Z operator on edges $e \in \eta$ before contraction. When down spins $|1\rangle$ contract on an edge $e \in \eta$, the extra Pauli Z operator results in a sign -1. We need to choose η so that the contraction of a configuration C of loops of down spins $|1\rangle$ yields the sign $\hat{\sigma}(C)$.

We begin by accounting for the Koszul signs $\hat{\sigma}(L)$ accrued by contractible loops L. Next, we discuss a matrix product operator (MPO) which captures the Koszul signs from non-contractible loops. We focus on the case when the manifold is a torus and only outline the procedure for more general 2D manifolds.

Reproducing Koszul signs for contractible loops

Our strategy for accounting for $\hat{\sigma}(L)$, when L is a contractible loop is to 'pair-up' the singular vertices and construct the set η from edges that connect the two singular vertices in each pair. More precisely, Stokes' theorem guarantees an even number of singular vertices on a

closed manifold, so we can always find a set of edges η such that the boundary of η gives the set of singular vertices. Here, the boundary of η is defined as the set of vertices that are endpoints of an odd number of edges in η. Intuitively, η can then be understood as 'pairing-up' singular vertices with each other through arbitrary paths. Fig. 3.8 provides an example of choosing η on a torus.

To replicate the sign $\hat{\sigma}(L)$, we insert Z operators on all edges in η (see Fig. 3.8). Now, in evaluating a configuration with a single loop L of down spins $|1\rangle$, we incur the sign:

$$\sigma_\eta(L) \equiv (-1)^{n(L,\eta)}, \tag{3.94}$$

where $n(L,\eta)$ denotes the number of common edges (or crossings) between the loop L and the edges in η. Given our construction of η, $n(L,\eta)$ is equal (mod 2) to the number of singular vertices enclosed in L. Therefore, for any contractible loop L:

$$\sigma_\eta(L) = (-1)^{n_{sv}(L)}, \tag{3.95}$$

in agreement with Eq. (3.93). Consequently, for any 1-cocycle C and 0-cochain R, we have:

$$\sigma_\eta(C+\delta R) = \sigma_\eta(C)\sigma_\eta(\delta R) = \sigma_\eta(C)\prod_{v\subset R}\sigma_\eta(L_v). \tag{3.96}$$

The product $\prod_{v\subset R}$ is over all vertices such that the coefficient of $\mathbf{v}$ in R is nontrivial.

We note that a choice of η can be modified by including any set of edges forming a contractible loop. We call two sets η and η' equivalent spin-structures, if one can be obtained from the other by appending contractible loops of edges.

Reproducing Koszul signs for non-contractible loops

$\sigma_\eta(C)$ simulates $\hat{\sigma}(C)$ for trivial 1-cocycles C. This is sufficient to account for Koszul signs when the fermionic system is defined on a sphere or an infinite plane. However, $\sigma_\eta(C)$ does

not capture the sign $\hat{\sigma}(C)$ when C is a non-trivial 1-cocycle. To account for the Koszul signs on a torus or higher genus manifolds, we insert MPOs along non-contractible loops to perform a certain sum over inequivalent spin-structures. In the following, we describe the case of a torus in detail and only sketch the generalization to higher genus manifolds.

To start, we consider a particular triangulation of a torus without any singular vertices, as shown in Fig. 3.9(a-c). Since there are no singular vertices, $\hat{\sigma}(L) = 1$ for any contractible loop L. For non-contractible loops, however, the Koszul signs are non-trivial. To see this, we let L^x and L^y be distinct non-contractible loops lying parallel to the x-axis and y-axis, respectively. The specific choices of L^x and L^y do not matter, because contractible loops can freely be appended without changing $\hat{\sigma}(L^x)$ and $\hat{\sigma}(L^y)$. This follows from Eq. (3.91) and the fact that there are no singular vertices. Now, using either Prop. 4 or Prop. 5, one finds:

$$\hat{\sigma}(L^x) = \hat{\sigma}(L^y) = \hat{\sigma}(L^x + L^y) = -1. \tag{3.97}$$

Hence, after converting the $\mathbb{Z}_2$-graded virtual legs to bosonic virtual legs, a modification is necessary to simulate the sign in Eq. (3.97). A possible solution is to insert Pauli Z operators along non-contractible loops. Naively, we can insert Z operators along only the x-axis [Fig. 3.9(a)], only the y-axis [Fig. 3.9(b)], or both the x-axis and the y-axis [Fig. 3.9(c)]. We find that all of these options fail to reproduce the sign in Eq. (3.97). The solution is a certain superposition of these options, which can be expressed using an MPO. Before describing this MPO, we develop some notation and discuss the effects of inserting Z operators along the axes.

First, we define the spin-structure η^x, which contains the edges along the x-axis. The product of Z operators applied along the edges in η^x can be expressed as $\prod_e Z_e^{\eta^x}$, where, in this expression, η^x is the indicator function for the set η^x. The operator $\prod_e Z_e^{\eta^x}$ is pictured in Fig. 3.9(a). Then, letting $\sigma_{\eta^x}(L)$ be the sign obtained in contracting a configuration of

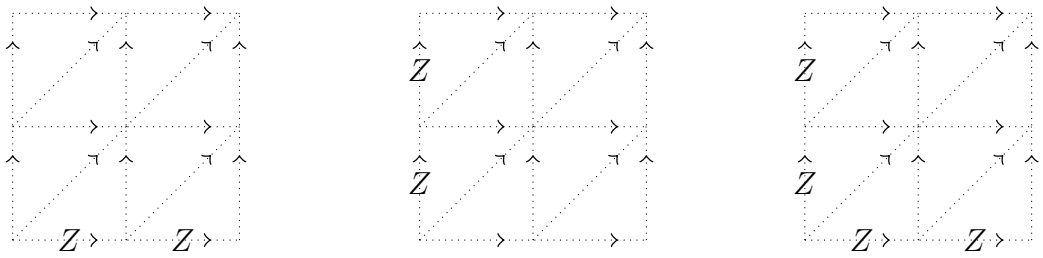

$\prod_e Z^{\eta^x}$ (a) $\prod_e Z^{\eta^y}$ (b) $\prod_e Z^{\eta^{xy}}$ (c)

Figure 3.9: Triangulation of a torus without any singular vertices, but with Z-operators placed along (a) the x-axis (b) the y-axis (c) both the x-axis and the y-axis.

down spins along L with the added operator $\prod_e Z_e^{\eta^x}$, we have:

$$\sigma_{\eta^x}(L^x) = 1, \quad \sigma_{\eta^x}(L^y) = -1, \quad \sigma_{\eta^x}(L^x + L^y) = -1. \tag{3.98}$$

Next, we define the spin-structures η^y and η^{xy} similarly. η^y is the set of edges along the y-axis and corresponds to the insertion of the operator $\prod_e Z_e^{\eta^y}$, depicted in Fig. 3.9(b). In this case, the sign accrued in contracting the bosonic legs is:

$$\sigma_{\eta^y}(L^x) = -1, \quad \sigma_{\eta^y}(L^y) = 1, \quad \sigma_{\eta^y}(L^x + L^y) = -1. \tag{3.99}$$

If we instead insert Z operators along both the x-axis and y-axis, as in Fig. 3.9(c), and define η^{xy} as the union of η^x and η^y, we obtain the signs:

$$\sigma_{\eta^{xy}}(L^x) = -1, \quad \sigma_{\eta^{xy}}(L^y) = -1, \quad \sigma_{\eta^{xy}}(L^x + L^y) = 1. \tag{3.100}$$

In each case above [Eqs. (3.98)-(3.100)], the operator insertion fails to replicate the sign in

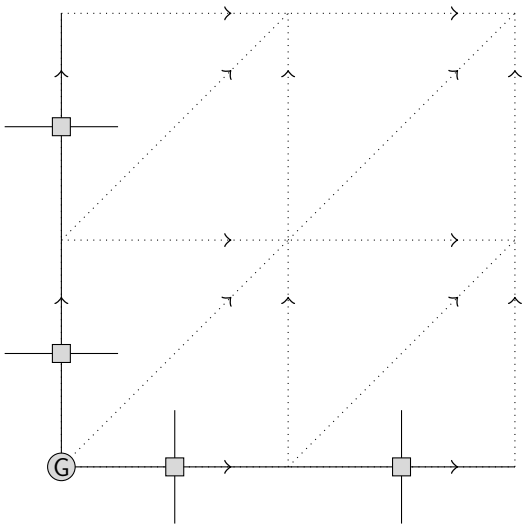

Figure 3.10: Triangulation of a torus without any singular vertices, and with the MPOs generated by W (square nodes) and G (circular nodes). The MPOs generated by W wrap around both the x-axis and the y-axis and the G tensor is placed at their intersection.

Eq. (3.97). However, the sign in Eq. (3.97) can be simulated using the following superposition of operators:

$$\frac{1}{2}\left(-1+\prod_e Z_e^{\eta^x}+\prod_e Z_e^{\eta^y}+\prod_e Z_e^{\eta^{xy}}\right). \tag{3.101}$$

Explicitly, the sign obtained in contracting an arbitrary loop of down spins L is then:

$$\frac{1}{2}\big(-1+\sigma_{\eta^x}(L)+\sigma_{\eta^y}(L)+\sigma_{\eta^{xy}}(L)\big). \tag{3.102}$$

One can check that, for loops L^x, L^y, and L^x+L^y, the sign given by Eq. (3.102) matches the sign in Eq. (3.97). Furthermore, the sign in Eq. (3.102) agrees with $\hat{\sigma}$ on all loops.

The operator in Eq. (3.101) can be represented using MPOs. We start by considering an MPO of the form:

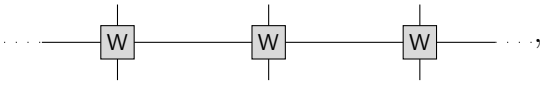

(3.103)

generated by the local tensors W, given by:

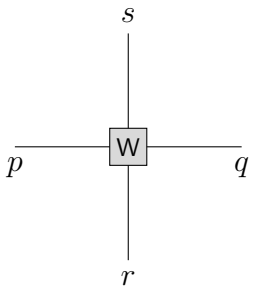

$$= \sum_{a,b} (-1)^{(a)(b)} |a\rangle_p |b\rangle_r \langle b|_s \langle a|_q = |0\rangle I \langle 0| + |1\rangle Z \langle 1|. \tag{3.104}$$

When the virtual (horizontal) legs take value 0, W acts as the identity, and when they take value 1, W acts as a Z operator. Therefore, W generates a controlled Z operator of the form $\ldots III \ldots + \ldots ZZZ \ldots$.

If we insert this MPO on the virtual level of the bosonic tensor network, say, along the x-axis, it is equivalent to inserting the operator $1 + \prod_e Z_e^{\eta^x}$. Similarly, inserting it along the y-axis is equal to the operator $1 + \prod_e Z_e^{\eta^y}$. If we insert the MPO along both the x-axis and the y-axis they cross as a single vertex, and we link the MPOs together at their intersection using another tensor G (see Fig. 3.10). We take G to be:

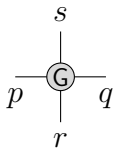

$$\begin{aligned} &= \frac{1}{2} \sum_{a,b} (-1)^{(a+1)(b+1)} |a\rangle_p |b\rangle_r \langle b|_s \langle a|_q \\ &= -\frac{1}{2} |0\rangle_p |0\rangle_r \langle 0|_s \langle 0|_q + \frac{1}{2} |0\rangle_p |1\rangle_r \langle 1|_s \langle 0|_q \\ &\quad + \frac{1}{2} |1\rangle_p |0\rangle_r \langle 0|_s \langle 1|_q + \frac{1}{2} |1\rangle_p |1\rangle_r \langle 1|_s \langle 1|_q. \end{aligned} \tag{3.105}$$

Now, when virtual legs of the MPOs in both the x and y direction take value 0, G is $-\frac{1}{2}$, and otherwise it is $\frac{1}{2}$. Thus, the total MPO produces the superposition of operators:

$$\frac{1}{2} \left(-1 + \prod_e Z_e^{\eta^x} + \prod_e Z_e^{\eta^y} + \prod_e Z_e^{\eta^x} \prod_e Z_e^{\eta^y} \right). \tag{3.106}$$

Recalling that η^{xy} is the union of η^x and η^y, we see that the operator above is equivalent

to the operator in Eq. (3.101). The Koszul signs, therefore, can be accounted for using the MPO generated by W and G, pictured in Fig. 3.10.

In effect, the MPO implements a sum over inequivalent spin-structures to capture the Koszul signs of non-contractible loops. The tensor G dictates the particular sum over spin-structures and, in general, depends on the branching structure. To see this, we next consider a general triangulation of a torus, where we must incorporate σ_η, accounting for singular vertices, with the sum over inequivalent spin-structures given by the MPO.

General triangulation of a torus

Thus far, we have argued that we can account for Koszul signs in the following two cases: (i) trivial 1-cocycles formed from contractible loops of $|1)$ states and (ii) non-contractible loops formed by $|1)$ states in the absence of singular vertices. To reproduce the Koszul signs from contraction on a general triangulation of a torus, we then must be able to simulate the Koszul signs from non-contractible loops in the presence of singular vertices. We will find that we require a branching structure dependent choice of the tensor G to obtain an appropriate sum over inequivalent spin-structures.

The first step is to account for the Koszul signs of contractible loops, as in 3.4.4. That is, we choose a set of edges η such that the edges in η pair up the singular vertices and insert Z operators at the edges in η. The sign from evaluating a loop L of down spins is then $\sigma_\eta(L)$ as in Eqs. (3.94) and (3.95).

After choosing η we can account for the Koszul signs from non-contractible loops. As before, we choose representative non-contractible loops L^x and L^y lying parallel to the x- and y-axis, respectively, such as those in Fig. 3.6. However, unlike the case with no singular vertices, the choice of L^x and L^y matters. For example, the sign $\hat{\sigma}(L^x)$ changes if L^x is shifted across a singular vertex. Likewise the sign of $\sigma_\eta(L^x)$ changes if L^x is shifted across a singular vertex. Therefore, to remove the ambiguity, we define the $\{0,1\}$ valued α_x and α_y

by:

$$(-1)^{\alpha_x} \equiv \hat{\sigma}(L^x)/\sigma_\eta(L^x) \tag{3.107}$$

$$(-1)^{\alpha_y} \equiv \hat{\sigma}(L^y)/\sigma_\eta(L^y) \tag{3.108}$$

$$(-1)^{\alpha_x+\alpha_y+1} = \hat{\sigma}(L^x + L^y)/\sigma_\eta(L^x + L^y). \tag{3.109}$$

We emphasize that the expressions above are independent of the particular choice of representative non-contractible loops L^x and L^y, using Eqs. (3.91) and (3.96).

We now only need to reproduce the signs on the left side of Eqs. (3.107), (3.108), and (3.109) for non-contractible loops using the MPO generated by W and G. A superposition of operators that yields these signs from contracting bosonic legs is:

$$\frac{1}{2}(-1)^{\alpha_x\alpha_y}\left(1 + (-1)^{\alpha_y}\prod_e Z_e^{\eta^x} + (-1)^{\alpha_x}\prod_e Z_e^{\eta^y} + (-1)^{\alpha_x+\alpha_y}\prod_e Z_e^{\eta^{xy}}\right). \tag{3.110}$$

It can be shown that this operator is generated by W and G with the components of G given by:

$$G_{ab} = \frac{1}{2}(-1)^{(\alpha_y+a)(\alpha_x+b)}. \tag{3.111}$$

For the special case of the triangulation in Fig. 3.9, $\alpha_x = \alpha_y = 1$ and Eq. (3.111) gives $G_{ab} = \frac{1}{2}(-1)^{(a+1)(b+1)}$, which matches our previous result. Given the spin structure in Fig. 3.13, $\alpha_x = \alpha_y = 0$. Thus, in this case, to capture the Koszul signs from non-contractible loops, the components of G should be $G_{ab} = \frac{1}{2}(-1)^{ab}$.

Higher genus manifolds

We briefly describe how our results can be extended to higher genus manifolds. We exploit the fact that any 2D oriented manifold M with genus g is topologically equivalent to a manifold constructed from the connected sum $\#$ of a sphere with g torii: $M \simeq S^2\#T^2\#\cdots\#T^2$.

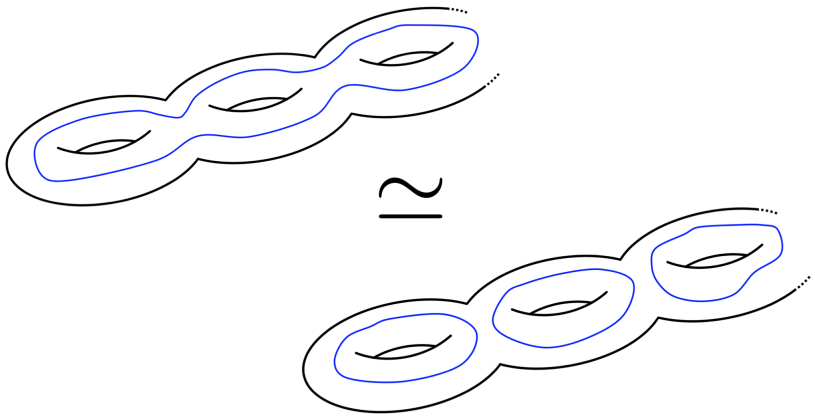

Figure 3.11: A cocycle on a genus g manifold is cohomologous to a $\mathbb{Z}_2$ sum of cocycles on the component torii. The non-trivial cocycles on independent torii on the right hand side have a trivial intersection number.

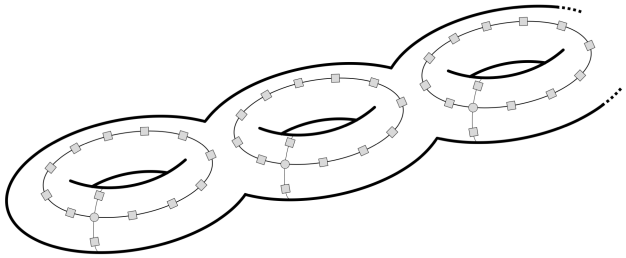

Figure 3.12: MPOs generated by W and G are inserted on each component torii. The G tensor may differ between the torii.

Furthermore, given a decomposition of M into a connected sum of a sphere and torii, any cocycle C can be written as:

$$C = \sum_{j=1}^{g} a_{j,x} L^{j,x} + \sum_{j=1}^{g} a_{j,y} L^{j,y} + \delta R. \tag{3.112}$$

Here, $L^{j,x}$ and $L^{j,y}$ denote generators of the non-trivial cocycles around the j^{th} torus in the connected sum decomposition, and δR gives a trivial cococyle. According to Eq. (3.112), any cocycle C is cohomologous to one of the form [see Fig. 3.11]:

$$\sum_{j=1}^{g} a_{j,x} L^{j,x} + \sum_{j=1}^{g} a_{j,y} L^{j,y}. \tag{3.113}$$

With this, we can now describe how to account for the Koszul signs from contraction on a genus g manifold. As before, the Koszul signs from contractible loops can be taken care of by making a choice of η and inserting Pauli Z operators along the edges in η. As for non-trivial cocycles, we first decompose the cocycle as in Eq. (3.112). Then, we identify the cohomologous cocycle given in Eq. (3.113), which differs by a trivial cocycle. (The difference in the Koszul sign between the cohomologous cocycles is already accounted for by the choice of η.) Using that the Koszul sign corresponds to a quadratic refinement of the intersection pairing [Eq. (3.91)], the computation of the Koszul signs for a cocycle in the form of Eq. (3.113) reduces to a computation of the Koszul signs for the loops $L^{j,x}$ and $L^{j,y}$. This is because loops belonging to different torii have trivial intersection number:

$$\langle L^{x,j}, L^{x,k} \rangle = \langle L^{x,j}, L^{x,k} \rangle = \langle L^{x,j}, L^{x,k} \rangle = 0 \bmod 2, \tag{3.114}$$

for all $j \neq k$. Therefore, the problem is reduced to that of g independent arbitrarily triangulated torii. The Koszul signs of non-contractible loops can be accounted for by inserting MPOs generated by W and G as in Fig. 3.12. A similar strategy as in Section 3.4.4 can be used to choose G at each intersection of the MPOs.

Grading removal for the bosonized fPEPS

Now, we return to the original problem of writing bosonized fPEPS as bPEPS. To compute the Koszul signs, we worked with a single layer of fermionic virtual legs, while a bosonized fPEPS has both the state layer and TNO layer of fermionic virtual legs. Therefore, we need to translate our results for accounting for Koszul signs back to the case of two layers of virtual legs.

To simplify the calculation of the Koszul sign, we noticed that [Eq.(3.78)], with the chosen ordering of the fermionic virtual legs, the pair of virtual legs $|a)_t|a')_s$ could be mapped to a spinless fermionic degree of freedom and a spin-1/2 via the isomorphism:

$$|a)_t|a')_s \to |a+a')|a\rangle. \tag{3.115}$$

Then, we worked only with the fermionic leg. Ultimately, we converted the fermionic legs $|a+a')$ to bosonic legs $|a+a'\rangle$ with the addition of Z operators on certain edges. A Z operator acting on $|a+a'\rangle$ correponds to acting with a parity operator on $|a+a')$ or the operator $P_s \otimes P_t$ on $|a)_t|a')_s$. Therefore, to replace the two layers of fermionic legs with two layers of bosonic legs: $|a)_t|a')_s \to |a\rangle_t|a'\rangle_s$, we see that we need to apply operators $Z_t \otimes Z_s$ at edges to account for Koszul signs.

In summary, we convert the two layers of fermionic legs (with the fixed internal ordering) to bosonic legs. Then, we insert $(Z_t \otimes Z_s)^{\eta_e}$ at every edge to account for the Koszul signs from contractible loops. To account for the Koszul signs from non-contractible loops, we modify the MPO so that W in Eq. (3.104) is: $|0\rangle(I_t \otimes I_s)\langle 0| + |1\rangle(Z_t \otimes Z_s)\langle 1|$.

3.4.5 Algorithm for bosonizing an fPEPS

The following gives an algorithm for bosonizing an fPEPS on a torus and writing it explicitly as a bPEPS.

1. Given a triangulated 2D manifold with branching structure, determine the singular

vertices. Singular vertices are those that are 1-vertices of $4m$ number of triangles. Pair singular vertices along convenient paths. The edges along these paths are the elements of η.

2. Construct the tensors $\mathsf{M_f} = \mathsf{F}\bullet\mathsf{T}$ and $\bar{\mathsf{M}}_\mathsf{f} = \bar{\mathsf{F}}\bullet\bar{\mathsf{T}}$. Rearrange the virtual indices to match the order shown in Eq. (3.77). Remove the grading of the virtual indices of $\mathsf{M_f}$, $\bar{\mathsf{M}}_\mathsf{f}$, and B_η. The resulting tensors are $\mathsf{M_b}$, $\bar{\mathsf{M}}_\mathsf{b}$, and $\mathsf{B_b}$, respectively.

3. Choose convenient generators of the non-contractible loops parallel to the x-axis and y-axis, say L^x and L^y, and calculate $(-1)^{\alpha_x} = \hat{\sigma}(L^x)/\sigma_\eta(L^x)$ and $(-1)^{\alpha_y} = \hat{\sigma}(L^y)/\sigma_\eta(L^y)$. Determine the tensor G using Eq. (3.111).

4. Insert factors of $Z_t \otimes Z_s$ on virtual legs corresponding to the edges in η. Insert tensors W along convenient generators of non-contractible loops parallel to the x- and y-axes, and glue the MPOs at their intersection with the G tensor calculated in the previous step. Finally, contract $\mathsf{M_b}$, $\bar{\mathsf{M}}_\mathsf{b}$, and $\mathsf{B_b}$ with the inserted factors of $Z_t \otimes Z_s$ and the MPO generated by W and G.

3.4.6 Example of bosonizing an fPEPS

As an example, we bosonize the atomic insulator state $|\psi_{AI}\rangle$ on a 2D torus, triangulated as shown in Fig. 3.13. The tensor network representation has a vacuum tensor everywhere: $T_{000} = 1, \bar{T}_{000} = 1$ and all other components zero.

Step 1: The singular vertices are $\langle 3\rangle$, $\langle 7\rangle$, $\langle 8\rangle$ and $\langle 10\rangle$. We pair them along the paths shown in Fig. 3.13, so the spin structure η is $\eta = \{\langle 3,4\rangle, \langle 4,7\rangle, \langle 8,10\rangle\}$.

Step 2: We compute the tensors $\mathsf{M_f}$, $\bar{\mathsf{M}}_\mathsf{f}$, and B_η, order the legs according to Eq. (3.77), and

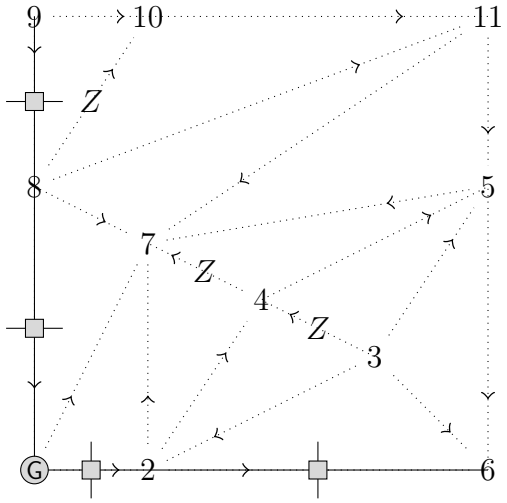

Figure 3.13: Choice of spin structure $\eta = \{\langle 3,4\rangle, \langle 4,7\rangle, \langle 8,10\rangle\}$ and placement of the MPO generated by W and G. The Z^{η_e} operators shown represent the $(Z_t \otimes Z_s)^{\eta_e}$-operators that are inserted in the example of Section 3.4.6.

replace the fermionic legs with bosonic legs to obtain:

$$\begin{aligned}
\mathsf{M}_\mathsf{b} &= \sum_{a,b,c} \delta_{a+b+c,0} |c\rangle_{f_{01}} |0\rangle_{f'_{01}} |a\rangle_{f_{12}} |0\rangle_{f'_{12}} \langle 0|_{f'_{02}} \langle b|_{f_{02}} \\
\bar{\mathsf{M}}_\mathsf{b} &= \sum_{a,b,c} \delta_{a+b+c,0} |b\rangle_{f_{02}} |0\rangle_{f'_{02}} \langle 0|_{f'_{12}} \langle a|_{f_{12}} \langle 0|_{f'_{01}} \langle c|_{f_{01}} \\
\mathsf{B}_\mathsf{b} &= \sum_a Z_e^{\eta_e} |a\rangle_e |a\rangle_e \langle a|_e .
\end{aligned} \tag{3.116}$$

Step 3: We use L^x in the upper right corner of Fig. 3.6 to calculate:

$$(-1)^{\alpha_x} = \hat{\sigma}(L^x)/\sigma_\eta(L^x) = 1, \tag{3.117}$$

and we use L^y in the lower left corner of Fig. 3.6 to calculate:

$$(-1)^{\alpha_y} = \hat{\sigma}(L^y)/\sigma_\eta(L^y) = 1. \tag{3.118}$$

$\alpha_x = \alpha_y = 0$, so G has components $G_{ab} = (-1)^{ab}$.

Step 4: We insert the operator $(Z_t \otimes Z_s)^{\eta_e}$ at each edge and insert the MPO generated by W and G as in Fig. 3.13. The state layer has only 0 indices, so the factors of Z_s do not affect the state. We freely remove all of the state layer indices. The factors of $Z_t^{\eta_e}$ cancel with the factor of $Z_e^{\eta_e}$ in the definition of B_b in Eq. 3.116.

The result is a bPEPS generated by the tensors:

$$\begin{aligned} \mathsf{M}_\mathsf{b} &= \sum_{a,b} |a+b\rangle_{f_{01}} |a\rangle_{f_{12}} \langle b|_{f_{02}} \\ \bar{\mathsf{M}}_\mathsf{b} &= \sum_{a,b} |b\rangle_{f_{02}} \langle a|_{f_{12}} \langle a+b|_{f_{01}} \\ \mathsf{B}_\mathsf{b} &= \sum_{a} |a\rangle_e |a\rangle_e \langle a|_e, \end{aligned} \tag{3.119}$$

with the MPO generated by W and G inserted along the x- and y-axes (Fig. 3.13). The bPEPS is in a ground state of Kitaev's toric code Hamiltonian. One way to see this is to notice that M_b and $\bar{\mathsf{M}}_\mathsf{b}$ have the MPO symmetries:

$$\begin{aligned} Z_{f_{01}} Z_{f_{12}} Z_{f_{02}} \cdot \mathsf{M}_\mathsf{b} &= \mathsf{M}_\mathsf{b} \\ Z_{f_{01}} Z_{f_{12}} Z_{f_{02}} \cdot \bar{\mathsf{M}}_\mathsf{b} &= \bar{\mathsf{M}}_\mathsf{b}, \end{aligned} \tag{3.120}$$

indicative of the toric code phase. Moreover, the symmetry implies that M_b and $\bar{\mathsf{M}}_\mathsf{b}$ have an even number of down spins. Since B_b copies the virtual legs to the physical leg, the ground state is a superposition of all loops (on the dual lattice) of down spins. The tensor G dictates the particular toric code ground state. For the branching structure in Fig. 3.13, the ground state is an equal amplitude superposition of all loops (on the dual lattice) of down spins acted on by the following operator:

$$\frac{1}{2}\left(1 - \prod_e Z_e^{\eta^x} - \prod_e Z_e^{\eta^y} + \prod_e Z^{\eta^{xy}}\right). \tag{3.121}$$

While the example of an atomic insulator state is rather simple, we expect the algorithm to extend naturally to more complicated problems.

3.5 Discussion

Tensor networks provide a powerful framework for studying quantum many-body systems. Their simple parameterization allows for efficient numerical computations, and their diagrammatic representation elucidates the structure of entanglement in quantum states. More abstractly, tensor networks provide a uniform language for discussing quantum many-body systems. Here, we have extended the formalism of tensor networks to exact bosonization dualities. In particular, we have constructed a TNO that implements the two dimensional bosonization duality first discussed in Ref. [15]. Furthermore, our bosonization TNO can be applied directly to fermionic tensor network states, thus defining bosonization at the level of quantum states.

A critical step of our bosonization procedure is to express the bosonized state as an explicit bosonic tensor network. To this end, we described how to account for Koszul signs accrued in contracting fermionic tensor networks, and we constructed matrix product operators to be placed along non-trivial cycles for this purpose. As a result, our bosonization duality at the level of states can be applied to fermionic systems on arbitrary triangulations of 2D manifolds without a boundary.

We would also like to emphasize that the calculation of Koszul signs in Section 3.4 has potential for applications outside of the bosonization of fPEPS. In fact, the calculation applies to the contraction of *any*[5] 2D fPEPS generated by fermion parity even local tensors and without fermionic physical legs. In particular, it may be useful for efficiently evaluating the overlap between two fPEPS. Explicitly, one can use the technology developed in Section 3.4 to replace the fermionic virtual legs with bosonic virtual legs and account for the Koszul signs. Notably, for a regular triangular lattice or square lattice, our results show that the

[5]Assuming the 2D fPEPS is defined on a triangulation of an orientable 2D manifold.

fermionic virtual legs can freely be replaced with bosonic virtual legs as long as the MPO generated by W and G is inserted before closing the tensor network on a manifold with non-trivial genus.

Directions for future work include generalizing our bosonization duality, identifying tensor network representations of wider classes of dualities, and utilizing the bosonization TNO to study fermionic systems. A natural generalization is to develop a 3D bosonization duality at the level of quantum states. Recently, [120] presented a bosonization duality in 3D, and we expect that this duality admits a tensor network representation. Formulating a TNO for the 3D duality might also make it clear how to bosonize in dimensions greater than three. Another possible generalization is to extend our bosonization duality to manifolds with boundaries.

It would be interesting to construct tensor network representations for other operator-level dualities. Ref. [117] describes a duality for parafermionization in 2D, in which a system of constrained spins is dual to a system of parafermions. Formulating a corresponding TNO would require a careful understanding of paraspin-structure – a generalization of spin-structure to parafermions. We also expect that recently developed dualities for gauging subsytem symmetries can be naturally formulated in terms of tensor networks [121]. Further, it would be nice to interpret the results of Ref. [122] using tensor networks.

We anticipate that our bosonization procedure will be useful for studying fermionic topological orders. Beginning with a fermionic tensor network state, one can apply the bosonization procedure outlined in the text and subsequently analyze the topological order of the bosonic state using the myriad of techniques developed to study bosonic topological orders. In addition, MPO symmetries of the fermionic state can be tracked through the bosonization procedure to obtain the MPO symmetries of the bosonic system.

Going the other direction, the Hermitian conjugate of the bosonization TNO can be applied to a bosonic state to obtain a fermionic tensor network state. Two dimensional (non-chiral) bosonic topological orders have been well studied using tensor networks, so we can use the known tensor network representations of fixed point states to construct fixed point

states for fermionic topological phases. Furthermore, the MPO symmetries of the bosonic system descend to MPO symmetries of the fermionic system. While fixed point states for intrinsic fermionic topological orders and fermionic symmetry protected topological phases were identified in Refs. [115,116], our bosonization procedure gives a means for constructing and studying fixed point states for fermionic symmetry-enriched topological orders as well.

Appendices

3.A $\mathbb{Z}_2$-graded tensor representation of Majorana operators

In this appendix, we show that the tensors introduced in section 3.2 and rewritten here:

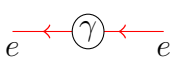

$$= \sum_a |a+1)_e (a|_e \tag{3.122}$$

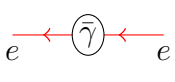

$$= \sum_a (-1)^a i |a+1)_e (a|_e, \tag{3.123}$$

are indeed good representations of Majorana operators. To do so, we explicitly show that the algebraic relations of the Majorana tensors match those of the Majorana operators introduced in section 3.2.4.

We begin by analyzing the algebra at a single site e. To this end, we apply the Majorana tensors to an arbitrary state A at site e:

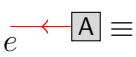

$$\equiv \sum_a A_a |a)_e. \tag{3.124}$$

According to section 3.2.4, at site e, $\gamma_e^2 = \bar{\gamma}_e^2 = 1$. Applying a single γ tensor to A, we find:

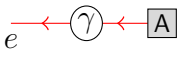

$$\equiv \sum_b |b+1)_e (b|_e^{\mathcal{C}} \sum_a A_a |a)_e^{\mathcal{C}} = \sum_a A_a |a+1)_e. \tag{3.125}$$

Then, acting with another γ on $\gamma\mathsf{A}$ gives:

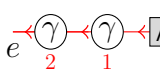

$$\equiv \sum_b |b+1)_e (b|_e^{\mathcal{C}} \sum_a A_a |a+1)_e^{\mathcal{C}} = \sum_a A_a |a)_e. \tag{3.126}$$

Since A was arbitrary, we see that γ contracted in succession with another γ acts as the identity. The relation $\bar{\gamma}_e^2 = 1$, can be shown similarly.

Next, we show that the relation $\bar{\gamma}_e \gamma_e = -\gamma_e \bar{\gamma}_e$ is represented by the Majorana tensors. $\bar{\gamma}\gamma\mathsf{A}$ is:

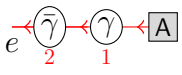

$$\equiv \sum_c (-1)^c i|c+1)_e (c|_e^{\mathcal{C}_2} \sum_b |b+1)_e^{\mathcal{C}_2} (b|_e^{\mathcal{C}_1} \sum_a A_a |a)_e^{\mathcal{C}_1} = -\sum_a (-1)^a i|a)_e, \tag{3.127}$$

while $\gamma\bar{\gamma}\mathsf{A}$ is:

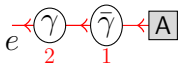

$$\equiv \sum_b |b+1)_e (b|_e^{\mathcal{C}_2} \sum_c (-1)^c i|c+1)_e^{\mathcal{C}_2} (c|_e^{\mathcal{C}_1} \sum_a A_a |a)_e^{\mathcal{C}_1} = \sum_a (-1)^a i|a)_e. \tag{3.128}$$

Comparing (3.127) and (3.128), we see that the tensors γ and $\bar{\gamma}$ capture the relation $\gamma_e \bar{\gamma}_e = -\bar{\gamma}_e \gamma_e$. It is important to note that in going from (3.127) to (3.128), the contractions are different. The difference in sign is not simply due to the odd grading of γ and $\bar{\gamma}$.

Now, we consider the algebraic relations of Majorana operators at different sites. Majorana operators acting at different sites anti-commute, so we must show that switching the order of contraction, for Majorana tensors applied to different legs yields a sign. This property follows from the odd grading of the Majorana tensors. We write an arbitrary state $|\psi)$ with N two dimensional fermionic site Hilbert spaces as:

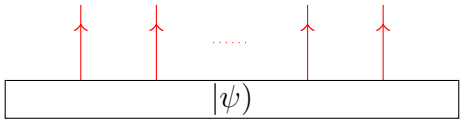

$$= \sum_{a_1,\ldots,a_N} \Psi_{a_1,\ldots,a_N} |a_1)_{e^1} \ldots |a_N)_{e^N}. \tag{3.129}$$

First acting with γ at site e^j and second acting with γ at site e^i, we have:

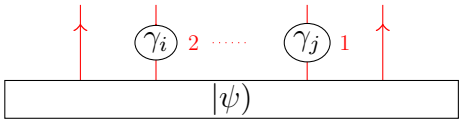

(3.130)

$$\equiv \left(\sum_c |c+1)_{e^i}(c|^{\mathcal{C}_2}_{e^i}\right)\left(\sum_b |b+1)_{e^j}(b|^{\mathcal{C}_1}_{e^j}\right)\sum_{a_1,\ldots,a_N}\Psi_{a_1,\ldots,a_N}|a_1)_{e^1}\ldots|a_i)^{\mathcal{C}_1}_{e^i}\ldots|a_j)^{\mathcal{C}_2}_{e^j}\ldots|a_N)_{e^N} \tag{3.131}$$

$$= \sum_{a_1,\ldots,a_N}\Psi'_{a_1,\ldots,a_N}|a_1)_{e^1}\ldots\left(\sum_c |c+1)_{e^i}(c|^{\mathcal{C}_2}_{e^i}\right)|a_i)^{\mathcal{C}_2}_{e^i}\ldots\left(\sum_b |b+1)_{e^j}(b|^{\mathcal{C}_1}_{e^j}\right)|a_j)^{\mathcal{C}_1}_{e^j}\ldots|a_N)_{e^N} \tag{3.132}$$

$$= \sum_{a_1,\ldots,a_N}\Psi'_{a_1,\ldots,a_N}|a_1)_{e^1}\ldots\left(\sum_c |c+1)_{e^i}(c|^{\mathcal{C}_1}_{e^i}\right)|a_i)^{\mathcal{C}_1}_{e^i}\ldots\left(\sum_b |b+1)_{e^j}(b|^{\mathcal{C}_2}_{e^j}\right)|a_j)^{\mathcal{C}_2}_{e^j}\ldots|a_N)_{e^N} \tag{3.133}$$

$$= \left(\sum_c |c+1)_{e^i}(c|^{\mathcal{C}_1}_{e^i}\right)\left(\sum_b |b+1)_{e^j}(b|^{\mathcal{C}_2}_{e^j}\right)\sum_{a_1,\ldots,a_N}\Psi_{a_1,\ldots,a_N}|a_1)_{e^1}\ldots|a_i)^{\mathcal{C}_1}_{e^i}\ldots|a_j)^{\mathcal{C}_2}_{e^j}\ldots|a_N)_{e^N} \tag{3.134}$$

$$= -\left(\sum_b |b+1)_{e^j}(b|^{\mathcal{C}_2}_{e^j}\right)\left(\sum_c |c+1)_{e^i}(c|^{\mathcal{C}_1}_{e^i}\right)\sum_{a_1,\ldots,a_N}\Psi_{a_1,\ldots,a_N}|a_1)_{e^1}\ldots|a_i)^{\mathcal{C}_1}_{e^i}\ldots|a_j)^{\mathcal{C}_2}_{e^j}\ldots|a_N)_{e^N} \tag{3.135}$$

$=-$

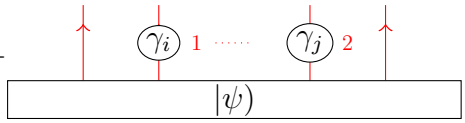

(3.136)

In (3.132), we have absorbed the signs from moving the Majorana tensors past odd vectors into the coefficient Ψ'. After moving the Majorana tensors, the ordering of the contractions are switched [line (3.133)]. Lastly, we have moved the Majorana tensors to the left and interchanged their order [(3.134) and (3.135)]. The contraction $\mathcal{C}_1$ is then to the right of $\mathcal{C}_2$, and we can read line (3.135) as first a γ acts on site e^i then a γ acts on site e^j. We thus have that γ tensors acting on different sites anti-commute. Looking at (3.130) and (3.135),

we see that the difference in sign is purely a consequence of the odd parity of γ. Indeed, more generally, γ tensors acting on different legs of an arbitrary tensor will anti-commute. An analogous calculation for $\bar{\gamma}$ tensors or a mixture of γ and $\bar{\gamma}$ tensors shows that they anti-commute when acting on different legs.

3.B Calculation of the Koszul sign for a single loop

Here, we provide a proof of Prop. 4. We choose an arbitrary edge of the loop L to be e^0 and label the j^{th} edge of the path as e^j. Starting with the triangle following e^0, along the orientation of L, we denote the j^{th} triangle on the path as f^j. For each triangle f^j, we have a specific basis tensor $\mathsf{Q}^L_{f^j}$ from the set $\mathcal{Q}[f]$ or $\bar{\mathcal{Q}}[f]$ [see Eq. (3.80)] depending on the orientation of f^j. The sign to be calculated is then:

$$\hat{\sigma}(L) = \mathrm{tr}\left[\mathsf{Q}^L_{f^0} \cdot \mathsf{Q}^L_{f^1} \cdot \ldots \cdot \mathsf{Q}^L_{f^n}\right]. \tag{3.137}$$

As already mentioned, there are six possible ways for the loop to cross a triangle. We list the six possible crossings of a positive triangle and its associated basis tensors Q^L_f (ignoring legs with even parity):

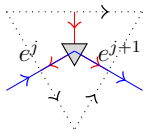

$$\equiv |1)_{e^j}|1)_{e^{j+1}} = -i|1)_{e^j}\left[i|1)_{e^{j+1}}\right],$$

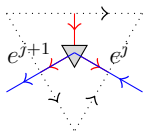

$$\equiv -|1)_{e^j}|1)_{e^{j+1}} = i|1)_{e^j}\left[i|1)_{e^{j+1}}\right]$$

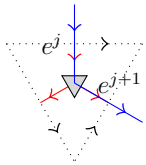

$$\equiv |1)_{e^{j+1}}(1|_{e^j} = \left[i(1|_{e^j}\right]\left[i|1)_{e^{j+1}}\right],$$

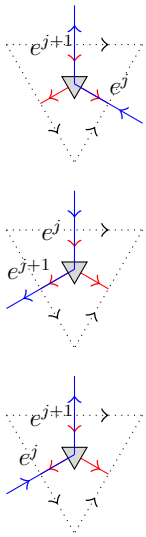

(3.138)

The blue arrows denote the loop L, which enters at edge e^j and exists from edge e^{j+1}. Notice that when the loop goes around a 0-vertex or a 2-vertex (bottom four pictures), both edges point to the same side of L, but when the loop goes around a 1-vertex (top two pictures), a right-left transition of edge directions occurs. The relation between the diagrams and the tensors can be summarized as follows:

(i) Edges e^j pointing to the *right* of L contribute $(1|_{e^j}$ to the tensor Q^L_{fj-1} and $|1)_{e^j}$ to the tensor Q^L_{fj}.

(ii) Edges e^j pointing to the *left* of L contribute $i|1)_{e^j}$ to the tensor Q^L_{fj-1} and $i(1|_{e^j}$ to the tensor Q^L_{fj}.

(iii) If f_L is an 1-vertex, then we accrue an additional phase $i^{\delta_{f_L\in\bar{l}_L}}i^{-\delta_{f_L\in\bar{r}_L}}$, where $\delta_{f_L\in\bar{l}_L}=1$ if $f_L\in\bar{l}_L$ and $\delta_{f_L\in\bar{l}_L}=0$ otherwise. $\delta_{f_L\in\bar{r}_L}$ is defined similarly. Therefore, if f_L is a 1-vertex, we accrue a phase i, if it lies to the left of L or a phase $-i$, if it lies to the right of L.

Negatively oriented triangles also have 6 possible crossings. It can be checked that the same rules as in (i)-(iii) above apply to negative triangles. For example, consider the following

crossing on a negative triangle:

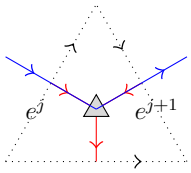

$$\equiv (1|_{e^{j+1}}(1|_{e^j}, \tag{3.139}$$

where the RHS is an element of (3.80) (ignoring even parity legs). Now, we verify that the rules (i)-(iii) yield the RHS of Eq. (3.139). Rule (ii) implies e^j contributes $i(1|_{e^j}$, rule (i) implies edge e^{j+1} contributes $(1|_{e^{j+1}}$, and finally, rule (iii) implies that the f_L vertex contributes an i phase. Putting it together, we get the tensor $i(1|_{e^j}(1|_{e^{j+1}}i = (1|_{e^{j+1}}(1|_{e^j}$, which is indeed the RHS of Eq. (3.139). The other five cases of crossing across negatively oriented triangles can be checked similarly.

With this, we calculate the sign in Eq. (3.137). We consider the contraction of tensors Q^L_{fj-1} and Q^L_{fj} at the edge e^j. If e^j points to the the right of L, then, according to rule (i), Q^L_{fj-1} has $(1|_{e^j}$ and Q^L_{fj} has $|1)_{e^j}$. No Koszul sign is produced in contraction at e^j because $(1|_{e^j}\cdot|1)_{e^j} = 1$. Similarly, if e^j points to the the left of L, then, according to rule (ii), Q^L_{fj-1} has $i|1)_{e^j}$ and Q^L_{fj} has $i(1|_{e^j}$, and again no Koszul sign is produced: $i|1)_{e^j}\cdot i(1|_{e^j} = 1$. The remaining sources of signs are triangles that contribute a sign $i^{\delta_{f_L\in\bar{l}_L}}i^{-\delta_{f_L\in\bar{r}_L}}$ according to rule (iii), and the overall -1 supertrace sign that comes from contracting the first and last indices in Eq. (3.137). Therefore, the total sign is:

$$\hat{\sigma}(L) = -\prod_{f_L} i^{\delta_{f_L\in\bar{l}_L}}i^{-\delta_{f_L\in\bar{r}_L}} = -i^{(n(\bar{l}_L)-n(\bar{r}_L))} = -(-1)^{\frac{1}{2}(n(\bar{l}_L)-n(\bar{r}_L))}. \tag{3.140}$$

Note that $\hat{\sigma}(C)$ is always ± 1, because the total number of transition points $n(\bar{l}_L) + n(\bar{r}_L)$ has to be even. This implies $n(\bar{l}_L) - n(\bar{r}_L)$ is even as well.

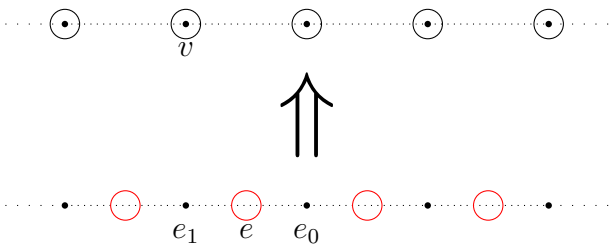

Figure 3.14: The bosonization duality is a map from a fermionic system to a bosonic system. In the fermionic system there is a spinless complex fermion degree of freedom (red circles) at each edge e. In the bosonic system there is a spin-1/2 at each vertex v.

3.C Tensor Network Bosonization in 1D

For completeness, we give a detailed description of the TNO representation of bosonization in 1D. To start, we present 1D bosonization as a map of local fermionic operators to local bosonic operators.

3.C.1 Review of 1D bosonization

On the fermionic side of the duality, we consider a one dimensional lattice with a spinless complex fermion at each edge, as pictured in Fig. 3.14. The complex fermion at edge e may be described using the familiar fermionic creation and annihilation operators: $c_e^\dagger$, c_e. These generate the full fermionic operator algebra at e. However, it will be convenient to instead work with Majorana operators, $\gamma_e, \bar{\gamma}_e$, as discussed in section 3.2.4.

To ensure the bosonization duality maps local operators to local operators, we define the duality on a subset of the full fermionic operator algebra - the subalgebra of fermion parity even operators $\mathcal{E}$. The fermion parity even operators are those that commute with the global fermion parity operator $\prod_e P_e$, where P_e is the fermion parity at the edge e. $\mathcal{E}$ can be generated by two types of operators: fermion parity P_e at each edge and the hopping operators S_v at each vertex v. The hopping operators transfer fermion parity between edges

and are defined by:

$$S_v \equiv i\gamma_{L_v}\bar{\gamma}_{R_v}, \tag{3.141}$$

with L_v and R_v the edge to the left and right of vertex v, respectively. The hopping operators are mutually commuting and commute with all parity operators besides the neighboring two, i.e.:

$$S_v P_e = (-1)^{\delta_{v\subset e}} P_e S_v, \tag{3.142}$$

where $\delta_{v\subset e} = 1$ if vertex v is at one of the endpoints of the edge e and $\delta_{v\subset e} = 0$ otherwise. With open boundary conditions, the set of fermion parity operators and hopping operators are independent. However on a closed manifold they satisfy the relation:

$$\prod_v S_v \prod_e P_e = -1 \tag{3.143}$$

On the bosonic side of the duality we have a spin-1/2 at each vertex (see Fig. 3.14). The operator algebra of the spin-1/2 at vertex v can be generated by the Pauli operators: X_v, Z_v. Thus, the set of X_v and Z_v for all vertices generates the full bosonic operator algebra, which we denote as $\mathcal{A}$.

We now define the duality map $\mathfrak{D} : \mathcal{E} \to \mathcal{A}$ on the generators of $\mathcal{E}$:

$$\begin{aligned} \mathfrak{D}(P_e) &= Z_{e_0} Z_{e_1} \\ \mathfrak{D}(S_v) &= X_v. \end{aligned} \tag{3.144}$$

where e_0 and e_1 denote the vertices at the endpoints of e such that e points from e_0 to e_1 (Fig. 3.14). $\mathfrak{D}$ is an injective homomorphism from $\mathcal{E}$ to $\mathcal{A}$ so that for $A_1, A_2 \in \mathcal{E}$:

$$\mathfrak{D}(A_1 + A_2) = \mathfrak{D}(A_1) + \mathfrak{D}(A_2)$$

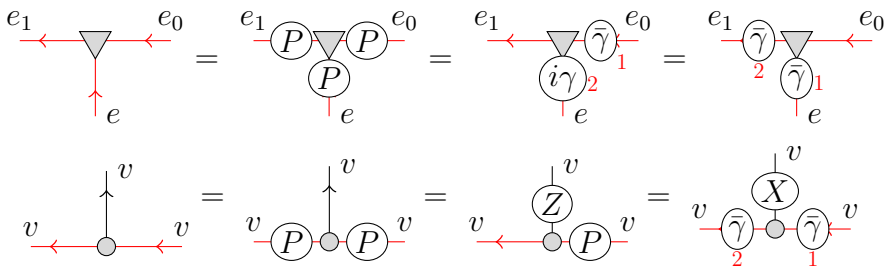

Figure 3.15: Diagrammatic representation of the symmetries of F (first line) and B (second line) written algebraically in Eqs. (3.152a) and (3.152b).

$$\mathfrak{D}(A_1 A_2) = \mathfrak{D}(A_1)\mathfrak{D}(A_2). \tag{3.145}$$

One can check that $\mathfrak{D}$ preserves the commutation relations in (3.142).

Note that the bosonization duality in Eq. (3.144) is not the usual Jordan-Wigner transformation, defined, for example, in Ref. [123]. $\mathfrak{D}$ is instead the composition of the familiar Jordan-Wigner transformation (restricted to $\mathcal{E}$) with the Kramers-Wannier duality. We have chosen the duality $\mathfrak{D}$ to define bosonization, because it is locality preserving and more naturally relates to the 2D bosonization in section 3.3.

To translate the operator duality defined in (3.144) to a TNO, we employ the formalism of $\mathbb{Z}_2$-graded Hilbert spaces and graded tensor products.

3.C.2 TNO representation of the duality

We now give a tensor network operator (TNO) representation D of the bosonization duality $\mathfrak{D}$ in Eq. (3.144). We begin with the following TNO ansatz:

$\mathsf{D} =$ 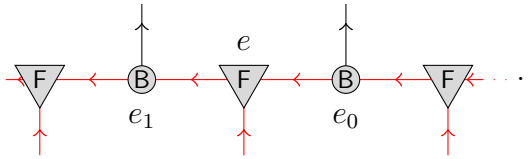

. (3.146)

For now, we leave the boundary conditions of D unspecified – they will enter the construction later.

D is constructed by gluing together two kinds of local tensors, F (triangular nodes) and B (circular nodes), as pictured in (3.146). An F tensor is placed at each edge e and is represented as follows:

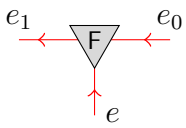

$$\equiv \sum_{j,a,b} F^j_{a,b} |a)_{e_1} (j|_e (b|_{e_0}. \tag{3.147}$$

At each vertex v, we place a tensor B:

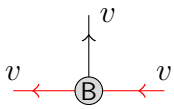

$$\equiv \sum_{j,a,b} B^j_{a,b} |a)_v |j\rangle_v (b|_v. \tag{3.148}$$

Notice that in Eq. (3.147), we have three distinct Hilbert spaces labeled by the same site – one fermionic space (to which $|a)_v$ belongs), one dual fermionic space (to which $(a|_v$ belongs) and one bosonic space (to which $|j\rangle_v$ belongs).

To implement the duality map $\mathfrak{D}$ of Eq. (3.144), we need to choose tensors F and B such that the following relations hold for all even operators $A \in \mathcal{E}$:

$$\mathsf{D} \cdot A = \mathfrak{D}(A) \cdot \mathsf{D}, \tag{3.149}$$

or diagrammatically:

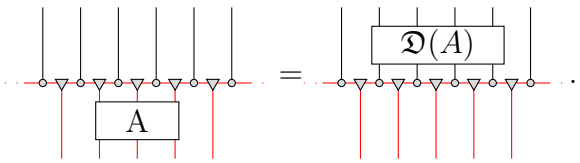

(3.150)

Note that, we need only show that the relations are satisfied for P_e and S_v – the generators

of $\mathcal{E}$. That is, we need to show that:

$$\mathsf{D}\cdot P_e = \mathfrak{D}(P_e)\cdot\mathsf{D} = Z_{e_0}Z_{e_1}\cdot\mathsf{D} \tag{3.151a}$$

$$\mathsf{D}\cdot S_v = \mathfrak{D}(S_v)\cdot\mathsf{D} = X_v\cdot\mathsf{D}. \tag{3.151b}$$

We can look at these constraints as symmetries of the tensor D, which can be reduced to symmetries of local tensors F and B. We claim that D satisfies (3.151a) and (3.151b) if F and B have the following symmetries:

$$\mathsf{F} = P_{e_1}\cdot\mathsf{F}\cdot P_{e_0}\cdot P_e = \mathsf{F}\cdot i\gamma_e\cdot\bar{\gamma}_{e_0} = \bar{\gamma}_{e_1}\cdot\mathsf{F}\cdot\bar{\gamma}_e \tag{3.152a}$$

$$\mathsf{B} = P_v\cdot\mathsf{B}\cdot P_v = Z_v\cdot\mathsf{B}\cdot P_v = \bar{\gamma}_v\cdot X_v\cdot\mathsf{B}. \tag{3.152b}$$

These symmetries are represented graphically in Fig. 3.15.

Using the diagrammatic representation of the symmetries, we can illustrate that D obeys (3.151a) and (3.151b). By successive applications of the symmetries in Fig. 3.15, we have:

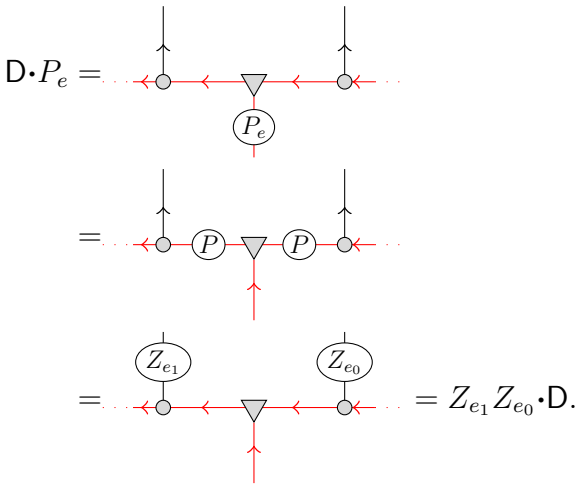

(3.153)

Similarly, for the hopping operator, we have:

$$\mathsf{D}\cdot S_v = \mathsf{D}\cdot i\gamma_{L_v}\bar{\gamma}_{R_v}$$

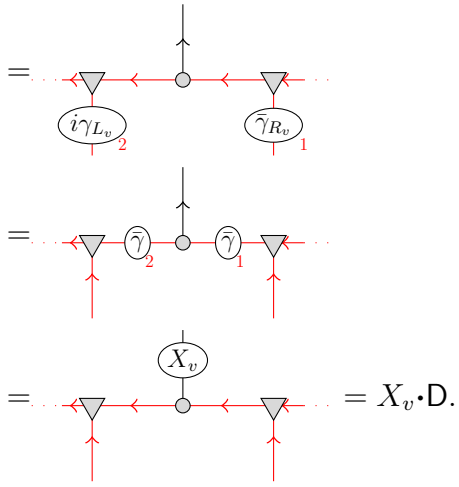

$$= X_v\cdot\mathsf{D}. \tag{3.154}$$

Hence, D is a good representation of the operator duality $\mathfrak{D}$.

Furthermore, we can use the symmetries of F and B to compute their explicit component form. Notice that the three symmetries of F are independent, commute with each other, and square to the identity. Thus, they generate a $\mathbb{Z}_2^3 = \mathbb{Z}_2 \times \mathbb{Z}_2 \times \mathbb{Z}_2$ symmetry group. Similarly, the three symmetries of B form a $\mathbb{Z}_2^3$ group. Since both tensors are vectors in a $2^3 = 8$ dimensional Hilbert space, the symmetries fix the tensors completely (up to a normalization). The explicit tensors can then be calculated by projecting the vaccuum tensor onto the symmetric subspace:

$$\mathsf{F} \propto \sum_{a,b,c} (\bar{\gamma}_{e_1}\bar{\gamma}_e)^a (i\gamma_e)^b P^c_{e_1}|0)_{e_1}(0|_e(0|_{e_0} P^c_e P^c_{e_0}\gamma^b_{e_0} = \sum_{a,b} |a)_{e_1}(a+b|_e(b|_{e_0}. \tag{3.155}$$

Applying the same strategy to compute B, we find:

$$\mathsf{B} \propto \sum_a |a)_v|a\rangle_v(a|_v. \tag{3.156}$$

Thus far, we have constructed a TNO that implements a map of local operators to local

operators. In the next subsection, we will illustrate one of the key advantages of the TNO representation of the bosonization duality. That is, we will see that D may be applied to fermionic tensor network states to map them to bosonic tensor network states.

3.D Bosonization of fermionic matrix product states

We now show that certain fermionic matrix product states (fMPS) can be directly bosonized using the bosonization TNO, D, defined in the previous subsection. In particular, we will describe the bosonization procedure for fMPS of the form:

$|\psi) =$ 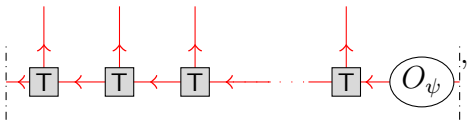

, (3.157)

where T is a fermion parity even tensor and O_ψ is an operator with definite parity. O_ψ is inserted before closing the fermionic matrix product state to dictate the parity of the state and the boundary conditions. We will use vertical dash-dotted lines to denote closing the boundary (or taking the trace, algebraically). Unless otherwise stated, we assume the Hilbert spaces are two dimensional. Algebraically, $|\psi)$ can be written as:

$$|\psi) = \sum_{j_0,\ldots,j_N} \mathrm{tr}\left[T^{j_0}T^{j_1}\ldots T^{j_N}O_\psi\right] |j_0)_{e^0}|j_1)_{e^1}\ldots|j_N)_{e^N}, \tag{3.158}$$

where e^k denotes the edge connecting the $k-1$ vertex and the k vertex. The first step in bosonizing $|\psi)$ is to close D with an operator O_D:

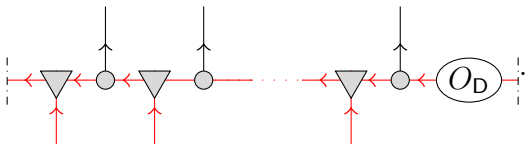

(3.159)

As we will show now, the choice of O_D determines both the subspace of the fermionic Hilbert space mapped non-trivially by the duality as well as the subspace of the bosonic Hilbert space in the image of the duality.

3.D.1 Boundary conditions in 1D

Here, we discuss how the choice of $\mathsf{O_D}$ affects the duality. With $\mathsf{O_D}$ parameterized as $\mathsf{O_D} = (-i\bar{\gamma})^\alpha P^\beta$ and $\alpha, \beta \in \{0, 1\}$, we will show that α determines the parity of the fermionic states that are mapped to non-trivial bosonic states and β dictates the image of the duality. Specifically, for $\alpha = 0(1)$, the subspace of states with even (odd) parity are mapped to the subspace of bosonic states invariant under the operator $(-1)^{\beta+1}\prod_v X_v$.

To begin, we note that the choice of $\mathsf{O_D}$ does not affect the duality away from the boundary. Away from the boundary, the graphical calculation in (3.153) and (3.154) is unchanged by the choice of $\mathsf{O_D}$. For a chain with $N+1$ sites, we constrain $\mathsf{O_D}$ by considering the image of the fermion parity operator P_{e^0} and the hopping operator S_N. (Recall that we have defined e^k as the edge connecting vertices $k-1$ and k, so e^0 connects 0 and N.) We will also require that, similar to the case away from the boundary, D maps local operators near the boundary to local operators.

Now, we consider acting on P_{e^0} with D. The diagrammatic calculation yields:

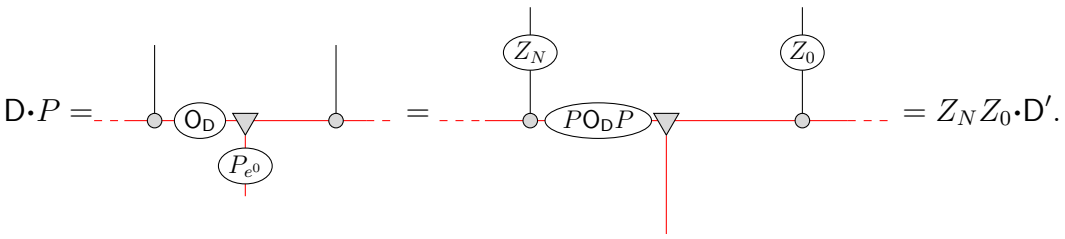

(3.160)

Note that the operator Z_N is required to ensure that the commutation relations between P_{e^0} and S_N are preserved by the duality. In the last line of (3.160), D' is the same as D but with $\mathsf{O_D}$ replaced by $P\mathsf{O_D}P$. The bosonization TNO should be left unmodified, so we require that $\mathsf{D}' \propto \mathsf{D}$. This means that $P\mathsf{O_D}P = c\mathsf{O_D}$ for some $c \in \mathbb{C}$, and we have:

$$\mathsf{D} = \mathsf{D}\cdot P_{e^0}^2 = c^2\mathsf{D}. \tag{3.161}$$

Therefore, c must be ± 1, or $P\mathsf{O_D}P = \pm\mathsf{O_D}$. We then see that $\mathsf{O_D}$ must have definite fermion

parity, so it can be parameterized as $\mathsf{O_D} = (-i\bar{\gamma})^\alpha P^\beta$ with $\alpha, \beta \in \{0, 1\}$.

Next, we act on the hopping operator S_N with D:

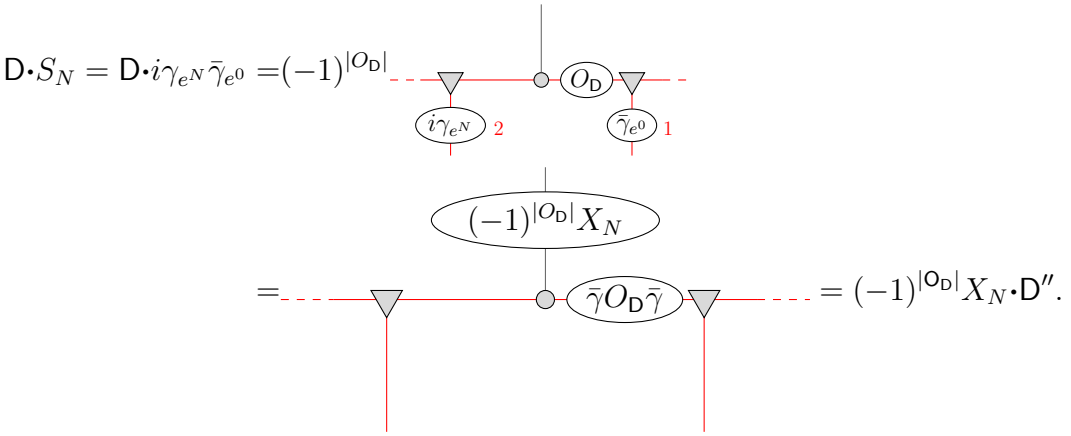

(3.162)

The factor of $(-1)^{|\mathsf{O_D}|}$ is a consequence of moving $i\gamma_{e^N}$ past $\mathsf{O_D}$. In the last line of (3.162), $\mathsf{D''}$ is the same as D except with $\mathsf{O_D}$ replaced by $\bar{\gamma}\mathsf{O_D}\bar{\gamma}$. To obtain a relation as in (3.149), we require that $\mathsf{D''} \propto \mathsf{D}$. Assuming $\bar{\gamma}\mathsf{O_D}\bar{\gamma} = a\mathsf{O_D}$ for $a \in \mathbb{C}$, we obtain:

$$\mathsf{D} = \mathsf{D}{\cdot}S_N^2 = a^2\mathsf{D}, \tag{3.163}$$

and thus, $a = \pm 1$.

We are now able to discuss the affect of $\mathsf{O_D}$ on the mapping of states. We define $\mathsf{D}_{\alpha\beta}$ to be the TNO formed by closing D with $\mathsf{O_D}$ parameterized by $\mathsf{O_D} = (-i\bar{\gamma})^\alpha (P)^\beta$. Then, (3.160) and (3.162) are summarized by:

$$\mathsf{D}_{\alpha\beta}{\cdot}P_{e^0} = (-1)^\alpha Z_N Z_0 {\cdot}\mathsf{D}_{\alpha\beta} \tag{3.164}$$

$$\mathsf{D}_{\alpha\beta}{\cdot}S_N = (-1)^{\alpha+\beta} X_N {\cdot}\mathsf{D}_{\alpha\beta}. \tag{3.165}$$

Acting on global fermion parity with $\mathsf{D}_{\alpha\beta}$, we find:

$$\mathsf{D}_{\alpha\beta}\cdot\prod_e P_e = (-1)^\alpha \left(\prod_e Z_{e_0}Z_{e_1}\right)\cdot\mathsf{D}_{\alpha\beta} = (-1)^\alpha \mathsf{D}_{\alpha\beta}. \tag{3.166}$$

This implies that $\mathsf{D}_{\alpha\beta}$ maps fermionic states $|\psi)$ with $|\psi| \neq \alpha$ to zero. Explicitly, we have:

$$\mathsf{D}_{\alpha\beta}|\psi) = (-1)^{|\psi|}\mathsf{D}_{\alpha\beta}\cdot\prod_e P_e|\psi) = (-1)^{|\psi|+\alpha}\mathsf{D}_{\alpha\beta}|\psi). \tag{3.167}$$

Therefore, $\mathsf{D}_{\alpha\beta}|\psi) = 0$ whenever $|\psi| \neq \alpha$. To bosonize an even state, α should be equal to 0, and accordingly, O_D is proportional to I or P. For an odd state, one should use $\alpha = 1$, in which case, O_D is proportional to $-i\bar{\gamma}$ or γ.

To understand the role of the β parameter, we act on $\mathsf{D}_{\alpha\beta}$ with $\prod_v X_v$:

$$\prod_v X_v\cdot\mathsf{D}_{\alpha\beta} = (-1)^{\alpha+\beta}\mathsf{D}_{\alpha\beta}\cdot\prod_v S_v. \tag{3.168}$$

Now we use a global relation of the fermionic operator algebra. It can be checked that:

$$\prod_v S_v = -\prod_e P_e. \tag{3.169}$$

Hence, continuing the calculation from (3.168):

$$\prod_v X_v\cdot\mathsf{D}_{\alpha\beta} = (-1)^{\alpha+\beta+1}\mathsf{D}_{\alpha\beta}\cdot\prod_e P_e = (-1)^{\beta+1}\mathsf{D}_{\alpha\beta}. \tag{3.170}$$

This means that the duality maps a fermionic state $|\psi)$ to the $(-1)^{\beta+1}$ eigenspace of $\prod_v X_v$, as can be seen from the following:

$$\prod_v X_v\cdot\mathsf{D}_{\alpha\beta}|\psi) = (-1)^{\beta+1}\mathsf{D}_{\alpha\beta}|\psi). \tag{3.171}$$

We have thus shown that O_D can be parameterized by $\mathsf{O}_\mathsf{D} = (-i\bar{\gamma})^\alpha P^\beta$ with $\alpha, \beta \in \{0, 1\}$,

and that D closed with $\mathsf{O_D}$ gives a map from the $(-1)^\alpha$ eigenspace of $\prod_e P_e$ to the $(-1)^{\beta+1}$ eigenspace of $\prod_v X_v$.

3.D.2 Converting virtual indices to bosonic indices

The second step is to contract D with $|\psi)$ to form $|\psi_{\text{bos}}\rangle$:

$|\psi_{\text{bos}}\rangle =$ 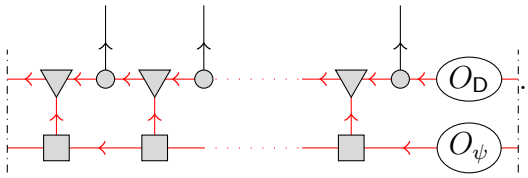

. (3.172)

We can then see that $|\psi_{\text{bos}}\rangle$ is built from the local tensors $\mathsf{M_f} \equiv \mathsf{T{\cdot}F{\cdot}B}$:

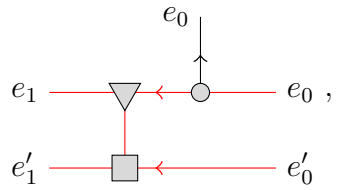

(3.173)

and the tensor network is closed with the operator $\mathsf{O_f} \equiv O_\psi O_{\mathsf{D}}$:

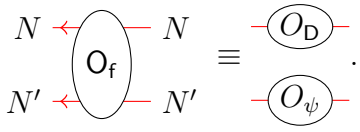

. (3.174)

The state $|\psi_{\text{bos}}\rangle$ formed by contracting together $\mathsf{M_f}$ and closing with $\mathsf{O_f}$ is indeed a bosonic state. However, it is not manifestly a bosonic matrix product state (bMPS), since the virtual legs may have nontrivial grading.

In the third and final step of the bosonization procedure, we write $|\psi_{\text{bos}}\rangle$ as a bonafide bMPS – constructed from a local tensor with bosonic virtual legs. As suggested in section 3.4.2, we do so by choosing a particular internal ordering of the virtual legs of $\mathsf{M_f}$ and $\mathsf{O_f}$, in which they become convertible to bosonic indices. We start by writing $\mathsf{M_f}$ and $\mathsf{O_f}$ in tensor

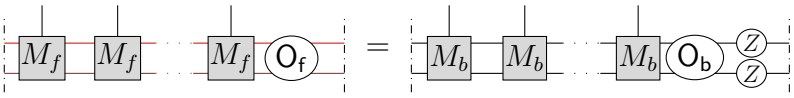

Figure 3.16: With the internal ordering chosen in (3.176) and (3.178), the virtual legs of $\mathsf{M_f}$ and $\mathsf{O_f}$ can be replaced with un-graded virtual legs. The supertrace sign produced between the first and last indices on both layers is accounted for by inserting the operator $Z_N \otimes Z_{N'}$ before closing the state generated by $\mathsf{M_b}$ and $\mathsf{O_b}$.

component form. In tensor component form, a generic $\mathsf{M_f}$ is:

$$\mathsf{M_f} = \sum_{\substack{j,a',a,\\ b,b'=0}} (M_f)^{j}_{aa',b'b} |a')_{e_1'} |a)_{e_1} |j\rangle_{e_0} (b|_{e_0} (b'|_{e_0'}, \tag{3.175}$$

where the components of $\mathsf{M_f}$ can of course be expressed in terms of the components of F, B, and T. Note that we have chosen a specific ordering of the vectors in $\mathsf{M_f}$. Schematically, the vectors are ordered as:

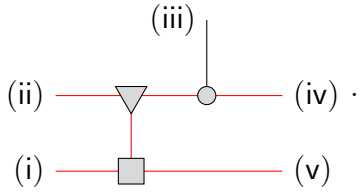

(3.176)

Next, we write a generic $\mathsf{O_f}$ in tensor component form:

$$\mathsf{O_f} = \sum_{a',b',a,b} (O_f)_{a',b',a,b} |a')_{N'} |a)_{N} (b|_{N} (b'|_{N'}, \tag{3.177}$$

where we have intentionally ordered the graded vectors according to the diagram:

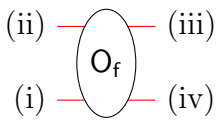

(3.178)

It may be checked that with the special choices of ordering in (3.176), we do not produce

any Koszul signs while contracting the $\mathsf{M_f}$ with each other. Therefore, as suggested in section (3.4.2), we can simply replace all fermionic virtual legs shared by two $\mathsf{M_f}$ tensors with bosonic legs. Similarly, with the choice of ordering in (3.178), no sign is produced in the contraction of $\mathsf{M_f}$ with $\mathsf{O_f}$, so their common indices can also be replaced with bosonic indices. However, a Koszul sign *is* produced in the trace operation (contraction of first and last indices) due to the supertrace phase [see (3.7)]. However, these indices are convertible to bosonic indices with $(Z_N \otimes Z_{N'})$-insertion (see section 3.4.2). That is, we can replace them with bosonic indices as long as we insert an operator $Z_N \otimes Z_{N'}$ (one Z on each of the two virtual indices) before closing the MPS.

We denote the bosonic tensor obtained by replacing the fermionic virtual legs of $\mathsf{M_f}$ as $\mathsf{M_b}$, and similarly, we denote the bosonic tensor obtained by replacing the fermionic virtual legs of $\mathsf{O_f}$ as $\mathsf{O_b}$. Then, the state generated by $\mathsf{M_f}$ and $\mathsf{O_f}$ and the state generated by $\mathsf{M_b}$ with $\mathsf{O_b}$ and $Z_N \otimes Z_{N'}$ is the same state (see Fig. 3.16). It is convenient to further absorb the Z factors into the definition of $\mathsf{O_b}$. With this, the bMPS is generated by the tensors:

$$\mathsf{M_b} = \sum_{\substack{j,a',a\\,b,b'=0}} (M_f)^{j}_{aa',b'b} |a'\rangle_{e_0'} |a\rangle_{e_0} |j\rangle_{e_1} \langle b|_{e_1} \langle b'|_{e_1'} \tag{3.179}$$

$$\mathsf{O_b} = \sum_{a',b',a,b} (O_f)_{a',b',a,b} (-1)^{b+b'} |a'\rangle_{N'} |a\rangle_{N} \langle b|_{N} \langle b'|_{N'}, \tag{3.180}$$

where the phase $(-1)^{b+b'}$ comes from the application of $Z_N \otimes Z_{N'}$. Now, contracting $\mathsf{M_b}$ and closing the tensor network with the bosonic tensor $\mathsf{O_b}$ yields $|\psi_{\text{bos}}\rangle$, and in this way, $|\psi_{\text{bos}}\rangle$ is expressly a bMPS. Thus, we have successfully mapped the fMPS $|\psi)$ to the bMPS $|\psi_{\text{bos}}\rangle$.

In summary, bosonization of a fMPS defined by a tensor T and operator O_ψ as in Eq. (3.158) proceeds in three steps.

1. Choose an operator $O_{\mathsf{D}} = (-i\bar{\gamma})^\alpha P^\beta$ with $\alpha, \beta \in \{0, 1\}$ with which to close the bosonization TNO.

2. Construct $\mathsf{M_f}$ by contracting T, F, and B. Form $\mathsf{O_f}$ by combining O_ψ and O_{D}.

3. Rearrange the vectors in $\mathsf{M_f}$ and $\mathsf{O_f}$ to match the ordering in (3.176) and (3.178), respectively. Form $\mathsf{M_b}$ and $\mathsf{O_b}$ from $\mathsf{M_f}$ and $\mathsf{O_f}$ by taking the graded vectors to have trivial grading and modifying the components $(O_f)_{a',b',a,b}$ of $\mathsf{O_f}$ by $(-1)^{b+b'}$ to account for the supertrace.

In the next subsection, we provide explicit examples of the tensor network bosonization steps above.

3.D.3 Examples

We will illustrate the tensor network bosonization procedure of the previous section on two examples – a trivial atomic insulating state and the nontrivial ground state of the Kitaev chain. To motivate the TNO duality, we also analyze the examples at the operator level using the duality of section 3.C.1.

Example 1: The trivial atomic insulating state is the ground state of the Hamiltonian $H_{\text{triv}} = -\sum_e P_e$. It has zero fermion occupancy at each site and can be expressed in the form:

$$|\psi_{\text{triv}}) = \sum_{j_0,\ldots,j_N} \text{tr}\left[T^{j_0}\ldots T^{j_N} O_\psi\right] |j_1)_{e^0}\ldots|j_N)_{e^N}. \tag{3.181}$$

with T being the trivial tensor:

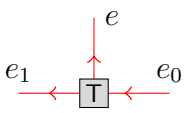

$$= |0)_{e_1}|0)_e(0|_{e_0}, \tag{3.182}$$

and O_ψ equal to the parity operator P.

Using the 1D operator duality in section 3.C.1 [Eq. (3.144)], we see that H_{triv} is mapped to the spontaneous symmetry breaking Hamiltonian $H_{SSB} = -\sum_e Z_{e^1} Z_{e^0}$. In accordance, we will see that the bosonization TNO maps the ground state of H_{triv} to a ground state of H_{SSB}.

The first step of the tensor network bosonization procedure is to choose an operator O_{D} with which to close the bosonization TNO. For simplicity, let us choose O_{D} to be fermion parity P. This choice of O_{D} gives a map from the set of fermion parity even states to the set of states symmetric under $\prod_v X_v$ (Appendix 3.D.1).

Next, we construct the tensor $\mathsf{M_f}$ and the operator $\mathsf{O_f}$. $\mathsf{M_f}$ is obtained by contracting T, F, and B as in (3.173):

$$\begin{aligned}\mathsf{M_f} = \mathsf{T}\cdot\mathsf{F}\cdot\mathsf{B} &= |0)_{e_1'}|0)^{\mathcal{C}_1}_{e'}(0|_{e_0'}\sum_{a,b}|a)_{e_1}(a+b|^{\mathcal{C}_1}_{e}(b|^{\mathcal{C}_2}_{e_0}\sum_{c}|c)^{\mathcal{C}_2}_{e_0}|c\rangle_{e_0}(c|_{e_0} \\ &= \sum_{a}|0)_{e_1'}(0|_{e_0'}|a)_{e_1}|a\rangle_{e_0}(a|_{e_0} = \sum_{a}|0)_{e_1'}|a)_{e_1}|a\rangle_{e_0}(a|_{e_0}(0|_{e_0'},\end{aligned} \tag{3.183}$$

and $\mathsf{O_f}$ is simply

$$\mathsf{O_f} = \left(\sum_{b'}(-1)^{b'}|b')_{N'}(b'|_{0'}\right)\left(\sum_{b}(-1)^{b}|b)_{N}(b|_{0}\right). \tag{3.184}$$

Then, we rearrange the order of the graded vectors in $\mathsf{M_f}$ and $\mathsf{O_f}$ according to (3.176) and (3.178). In the final step of the tensor network bosonization procedure, we construct $\mathsf{M_b}$ and $\mathsf{O_b}$ by removing the grading and appropriately accounting for the supertrace. Following these steps, $\mathsf{M_b}$ is:

$$\mathsf{M_b} = \sum_{a}|0\rangle_{e_0'}|a\rangle_{e_0}|a\rangle_{e_1}\langle a|_{e_1}\langle 0|_{e_1'}, \tag{3.185}$$

and re-ordering the vectors of $\mathsf{O_f}$ and accounting for the supertrace gives:

$$\mathsf{O_b} = \sum_{b',b}|b'\rangle_{e_0'}|b\rangle_{e_0}\langle b|_{e_1}\langle b'|_{e_1'}. \tag{3.186}$$

The bosonized state is constructed by gluing together $\mathsf{M_b}$ and closing the tensor network with $\mathsf{O_b}$. To see that $\mathsf{M_b}$ generates the ground state of H_{SSB}, we first notice that, for $\mathsf{M_b}$ in Eq. (3.185), the e_0' and e_1' indices do not affect the bosonized state. Therefore, $\mathsf{M_b}$ and $\mathsf{O_b}$

can be reduced to:

$$\tilde{\mathsf{M}}_{\mathsf{b}} = \sum_a |a\rangle_{e_0}|a\rangle_{e_1}\langle a|_{e_1} \tag{3.187}$$

$$\tilde{\mathsf{O}}_{\mathsf{b}} = \sum_b |b\rangle_{e_0}\langle b|_{e_1}. \tag{3.188}$$

$\tilde{\mathsf{M}}_{\mathsf{b}}$ generates the state:

$$|\psi_{\text{bos}}\rangle = |00\ldots\rangle + |11\ldots\rangle, \tag{3.189}$$

which is the ground state of H_{SSB}. Therefore, M_{b} also generates the ground state of H_{SSB}.

Example 2: Now, we turn to the example of the non-trivial ground state $|\psi_{\text{K}})$ of the Kitaev chain. $|\psi_{\text{K}})$ is the ground state of the Hamiltonian $H_{\text{K}} = -\sum_v S_v$, and it can be written as a fMPS with [115]:

$$\mathsf{T} = \sum_{a,b} (-1)^{a(a+b)} |a)_{e_1'} |a+b)_e (b|_{e_0'}, \tag{3.190}$$

and $O_\psi = -i\bar{\gamma}$.

The operator duality $\mathfrak{D}$ maps H_{K} to the paramagnet Hamiltonian $H_{\text{para}} = -\sum_v X_v$, so the bosonization TNO should transform $|\psi_{\text{K}})$ to the paramagnet ground state $|\psi_{\text{para}}) = |++\ldots\rangle$, where $|+\rangle = \frac{1}{\sqrt{2}}(|0\rangle + |1\rangle)$.

Following the three steps outlined in the previous section, we first choose O_{D}. Since O_ψ is fermion parity odd, we choose $O_{\mathsf{D}} = (-i\bar{\gamma})P = \gamma$. First, we compute M_{f} by contracting

T, F, and B:

$$\begin{aligned}\mathsf{M_f} =& \mathsf{T}\cdot\mathsf{F}\cdot\mathsf{B}\\ =&\left[\sum_{a',b'}(-1)^{|b'|(|a'|+|b'|)}|a')_{e'_0}|a'+b')^{\mathcal{C}_1}_{e'}(b'|_{e'_1}\right]\left[\sum_{a,b}|a)_{e_0}(a+b|^{\mathcal{C}_1}_{e}(b|^{\mathcal{C}_2}_{e_1}\right]\left[\sum_{c}|c)^{\mathcal{C}_2}_{e_1}|c\rangle_{e_1}(c|_{e_1}\right]\\ =&\sum_{a,b,a',b'}(-1)^{(b'+b)(a'+b')}\delta_{a+b,a'+b'}|a')_{e'_0}|a)_{e_0}|b\rangle_{e_1}(b|_{e_1}(b'|_{e'_1}\end{aligned}$$

Next, we remove the grading of the vectors in $\mathsf{M_f}$ and $\mathsf{O_f} = -i\bar{\gamma}$ and account for the supertrace to form $\mathsf{M_b}$ and $\mathsf{O_b}$:

$$\mathsf{M_b} = \sum_{\substack{a,b\\a',b'}}(-1)^{(a'+b)(a'+b')}\delta_{a+b,a'+b'}|a'\rangle_{e'_0}|a\rangle_{e_0}|b\rangle_{e_1}\langle b|_{e_1}\langle b'|_{e'_1} \tag{3.191}$$

$$\mathsf{O_b} = \sum_{b,b'}(-1)^{b+b'}|b'\rangle_{N'}|b\rangle_{N}\langle b+1|_0\langle b'+1|_{0'}. \tag{3.192}$$

Explicitly, we have:

$$\mathsf{M_b} = \big(|00\rangle - |11\rangle\big)\big(|0\rangle\langle 00| - |1\rangle\langle 11|\big) + \big(|10\rangle + |01\rangle\big)\big(|0\rangle\langle 10| + |1\rangle\langle 01|\big) \tag{3.193}$$

$$\mathsf{O_b} = |00\rangle\langle 11| + |11\rangle\langle 00| - |01\rangle\langle 10| - |10\rangle\langle 01|. \tag{3.194}$$

Defining $|v_0\rangle = |00\rangle - |11\rangle$ and $|v_1\rangle = |10\rangle + |01\rangle$ and the corresponding projectors: $P_j = |v_j\rangle\langle v_j|$, $j = 0, 1$, then $\mathsf{M_b}$ satisfies $\mathsf{M_b}P_j = P_j\mathsf{M_b}P_j$. The boundary operator also satisfies $P_j\mathsf{O_b} = P_j\mathsf{O_b}P_j$. Thus, there are two canonical blocks:

$$\begin{aligned}P_j\mathsf{M_b}P_j &= |v_j\rangle(|+\rangle)\langle v_j| \quad j = 0, 1\\ \langle v_j|\mathsf{O_b}|v_j\rangle &= -1,\end{aligned} \tag{3.195}$$

where $|+\rangle = |0\rangle + |1\rangle$. Both blocks give the same state: $-|+\rangle^{\otimes N}$.

Chapter 4

DISENTANGLING INTERACTING FERMIONIC SPT PHASES IN TWO DIMENSIONS

This chapter is based on:
Tyler D. Ellison and Lukasz Fidkowski. Disentangling interacting symmetry-protected phases of fermions in two dimensions. Phys. Rev. X, 9:011016, Jan 2019.

We construct fixed point lattice models for group supercohomology symmetry protected topological (SPT) phases of fermions in $2+1$D. A key feature of our approach is to construct finite depth circuits of local unitaries that explicitly build the ground states from a tensor product state. We then recover the classification of fermionic SPT phases, including the group structure under stacking, from the algebraic composition rules of these circuits. Furthermore, we show that the circuits are symmetric, implying that the group supercohomology phases can be many body localized. Our strategy involves first building an auxiliary bosonic model, and then fermionizing it using the duality of Ref. [15]. One benefit of this approach is that it clearly disentangles the role of the algebraic group supercohomology data, which is used to build the auxiliary bosonic model, from that of the spin structure, which is combinatorially encoded in the lattice and enters only in the fermionization step. In particular this allows us to study our models on 2d spatial manifolds of any topology, and to define a lattice-level procedure for ungauging fermion parity.

4.1 Introduction

A major goal in understanding symmetry protected topological (SPT) phases is their classification, i.e. the identification and enumeration of the possible phases. Essential to a classification scheme is the construction of microscopic models for each phase, as well as the identification of quantized many-body invariants which discriminate between the different

phases. For bosonic SPT phases in 2+1D with unitary onsite symmetries, the classification is well understood in terms of the framework of group cohomology theory. The algebraic data of group cohomology is used both in the construction of exactly solvable lattice models [49] and in the identification of quantized invariants, where group cohomology classes appear in the universal statistics of the symmetry flux excitations [71].

In contrast, despite much recent progress [116, 124–129], the classification of fermionic SPT phases is not as well understood. A mathematical structure analogous to group cohomology - termed group supercohomology - was introduced in the pioneering work of Ref. [126] to describe a subset of fermionic SPT phases. However, group supercohomology has yet to be as directly connected to explicit lattice Hamiltonians or to universal quantized observables. While certain lattice fermionic Hamiltonians were, in fact, written down in terms of group supercohomology data in Ref. [126], these intricate constructions rely on seemingly arbitrary choices and cannot straightforwardly be put on spatial manifolds of general topology. In a space-time path integral formalism, these arbitrary choices have since been interpreted as choices of spin structure [125] – now understood to be a crucial ingredient in constructing fixed point fermionic SPT models. Progress has been made in incorporating spin structures directly in a Hamiltonian formalism [130–132], in particular in Ref. [129], where ground state wavefunctions incorporating spin structure were defined implicitly in terms of constraints that involve different lattice structures related by local deformations. However, there is still no general prescription for turning group supercohomology data and a choice of spin structure into a fermionic Hamiltonian on a fixed lattice in a general spatial geometry.

Group supercohomology classes have also not yet been directly connected to quantized many-body invariants of gapped, lattice Hamiltonians. It has been shown [133], that the supercohomology data can be interpreted as quantized topological terms in the effective space-time action for a combination of the global symmetry and fermion parity gauge fields. That being the case, these space-time observables should in principle be encoded in the joint braiding statistics of symmetry and fermion parity fluxes, but such statistics have only

been studied in the continuum [128, 134]. For bosonic SPT phases, the underlying group cohomology data can be extracted using a well defined lattice minimal coupling gauging procedure that maps the SPT system to a system with topological order. An analogous lattice Hamiltonian procedure has so far been missing on the fermionic side - making it difficult to argue that group supercohomology classes are quantized invariants of lattice fermionic SPT Hamiltonians.

In this chapter, we solve both of these problems in the case of 2+1 dimensions and finite unitary on-site symmetry $G \times \mathbb{Z}_2^{\mathrm{f}}$, where $\mathbb{Z}_2^{\mathrm{f}}$ is fermion parity. Specifically, we accomplish the following:

(1) We construct a representative fermionic lattice SPT Hamiltonian for every choice of group supercohomology data, 2d oriented spatial manifold M, and spin structure on M. Moreover, we write down an explicit finite depth quantum circuit of local unitaries that constructs its ground state from a trivial product state.

(2) Using these finite depth circuits, we recover the group structure of our SPT phases under stacking. We also find that two different sets of group supercohomology data can lead to circuits that differ only by a product of symmetric local unitaries, and hence define the same phase. This leads to a natural equivalence relation on group supercohomology data, which matches that of previous works. Conversely, we prove that for inequivalent group supercohomology data, the corresponding Hamiltonians are in distinct phases.

A choice of group supercohomology data is encoded in a pair (n, ν), where n and ν are certain $\mathbb{Z}_2$ and $U(1)$-valued functions of G variables, respectively (defined precisely in section 4.2.1 below). Given the data (n, ν), the construction of our fermionic lattice SPT Hamiltonian, inspired by the work of Ref. [124], proceeds in 3 steps.

(i) We use n and ν to construct an auxiliary *bosonic* SPT Hamiltonian with enlarged symmetry group $\tilde{G}$, where $\tilde{G}$ is the extension of G by $\mathbb{Z}_2$ determined by n. $\tilde{G}$ contains $\mathbb{Z}_2$ as a subgroup and G as a quotient: $G = \tilde{G}/\mathbb{Z}_2$, so the auxiliary bosonic SPT model has a global $\mathbb{Z}_2$ symmetry but is not in general G-symmetric. Being a group cohomology bosonic SPT,

it can be put on any spatial manifold M with a triangulation and branching structure [49].

(ii) We gauge the $\mathbb{Z}_2 \subset \tilde{G}$ by minimally coupling the auxiliary bosonic SPT to a $\mathbb{Z}_2$ lattice gauge field and imposing a Gauss's law constraint. By choosing an appropriate basis of gauge invariant operators, this gauge theory can be interpreted as an unconstrained bosonic model - which we refer to as the 'shadow' model following Ref. [124] - with global symmetry $G = \tilde{G}/\mathbb{Z}_2$ and toric code topological order. Specifically, the shadow model has generalized G-spin vertex degrees of freedom, which transform under the G symmetry in the standard way, and spin-$\frac{1}{2}$ link degrees of freedom, which encode a toric code topological order.

(iii) Finally, we obtain our fermionic SPT by applying the fermionization duality of Ref. [15] (reviewed below) to trade the bosonic spin-$\frac{1}{2}$ link degrees of freedom in the shadow model for spinless complex fermions located on the triangular faces. The underlying idea behind this fermionization is to represent the fermion as the bound state of a toric code charge and flux excitation [104, 135]. The fermionization procedure is not unique, however, as it requires a choice of spin structure. Spin structure enters our construction only here, encoded combinatorially in a certain subset of links $\mathcal{E}$. This step can be thought of as effectively 'un-gauging' fermion parity symmetry [111], resulting in a model defined in a fermionic Fock space.

This three-step construction highlights one important advantage of our approach: it clearly disentangles the roles of group supercohomology data and spin structure in fermionic SPT models. One needs just the group supercohomology data to construct the bosonic shadow model (steps (i) and (ii)), whereas the spin structure enters only in the fermionization duality that maps this shadow model to the desired fermionic SPT (step (iii)).

A key part of our approach is the construction of finite depth quantum circuits of local unitaries[1] [1], which build the fermionic SPT ground states from a trivial product state. Access

[1]A finite depth quantum circuit of local unitaries is a unitary operator that can be expressed in the form $\left(\prod_j U_{n,j}\right) \cdots \left(\prod_j U_{1,j}\right)$ where the unitaries $U_{i,j}$ satisfy the following properties. First, each $U_{i,j}$ acts as the identity everywhere except on spins located in a disk of finite radius. In this sense, $U_{i,j}$ is a local unitary. Furthermore, for each $j \neq k$, $U_{i,j}$ has non-overlapping support with $U_{i,k}$. The collection of unitaries sharing the first index define a 'layer' of the quantum circuit. That is, $\prod_j U_{i,j}$ is the i^{th} layer of the quantum circuit.

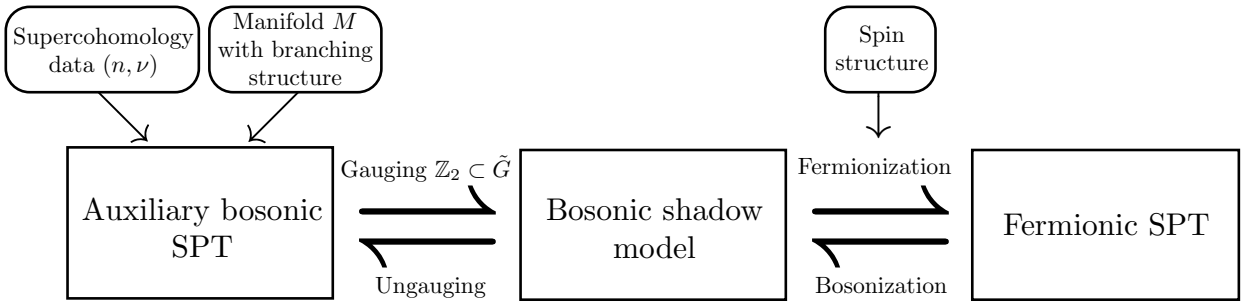

Figure 4.1: Our construction of a fermionic SPT Hamiltonian begins with the input of supercohomology data and a choice of manifold M with branching structure. This data is used to build an auxiliary bosonic SPT protected by a $\tilde{G}$ symmetry. Then we gauge the $\mathbb{Z}_2$ subgroup of $\tilde{G}$ to obtain the bosonic shadow model - a G symmetry enriched toric code. Finally, with a choice of spin structure, we fermionize the bosonic shadow model to arrive at the G protected fermionic SPT.

to these finite depth circuits has several benefits. First, they give us explicit representations of the corresponding ground states in terms of G domain models decorated with fermions (as opposed to ground state wave functions that are only defined implicitly via constraints). Second, we show that composing these circuits is equivalent to stacking the corresponding fermionic SPT phases, allowing us to extract the stacking group law for supercohomology data just by multiplying circuits. Third, we show that equivalent group supercohomology data gives rise to circuits that differ by a product of symmetric local unitaries, and hence correspond to the same phase. Conversely, by bosonizing our models and using well established classification results for bosonic symmetry enriched toric code phases [130, 136, 137], we show that inequivalent group supercohomology data always lead to inequivalent phases.

An intriguing feature of the finite depth circuit that builds our supercohomology fermionic SPT ground state is that, as a unitary operator, it is G-symmetric. This is despite the fact that, when the SPT phase in question is nontrivial, the local unitaries that make it

---

'Finite depth' means that the number of layers remains finite in the thermodynamic limit of large system size.

up cannot all be individually G-symmetric. This is a property that the supercohomology models share with bosonic group cohomology models, but not with the so-called 'beyond group cohomology' models (see *e.g.* appendix C of Ref. [138]). One consequence of this property is that the supercohomology phases can be many-body localized [139–145]. This is done by disordering the couplings in a trivial commuting projector parent Hamiltonian for the trivial product state and then conjugating by the circuit.

The rest of this chapter is structured as follows. In section 4.2, we focus on the construction of the bosonic shadow model described in steps (i) and (ii) above. In section 4.3, we review the bosonization duality of Ref. [15] and complete step (iii) of our construction. In section 4.4, we study the group structure of fermionic SPT phases using the finite depth circuits that build their ground states. In particular, we derive a notion of equivalence of group supercohomology data (in agreement with Ref. [124, 128, 129]) such that equivalent data gives rise to models in the same phase and inequivalent data necessarily yields inequivalent phases. We conclude in section 4.5 with some comments about many-body localizability for our models, possible future extensions of our work, and comparisons with other work. Throughout the chapter we illustrate our results for the simple case of $G = \mathbb{Z}_2$ (i.e. total symmetry $\mathbb{Z}_2 \times \mathbb{Z}_2^{\mathrm{f}}$). In Appendices 4.A-4.F, we provide detailed derivations of the results in this chapter.

As we were completing this work, we learned of a related preprint by N. Tantivasadakarn and A. Vishwanath [146], which also constructs a many-body localizable model for the $\mathbb{Z}_2 \times \mathbb{Z}_2^{\mathrm{f}}$ group supercohomology SPT.

4.2 Bosonic shadow model from group supercohomology data

In this section we will show how to use group supercohomology data associated to a finite group G to construct a purely bosonic Hamiltonian lattice model, which, in agreement with Ref. [124], we refer to as the shadow model. The model is defined on a triangulation of a 2d manifold - i.e. a planar graph consisting of vertices p and links $\langle pq \rangle$, all of whose faces

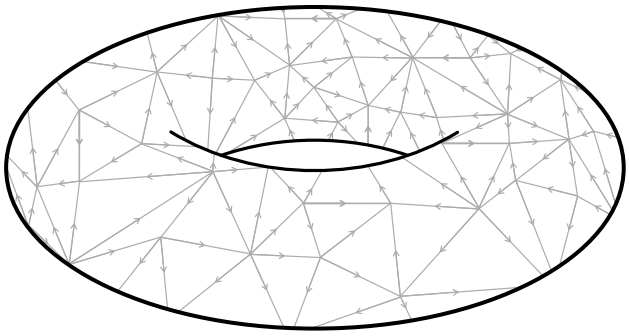

Figure 4.2: All of the models constructed in this chapter may be defined on an arbitrary triangulation of an orientable 2d manifold with a branching structure. Note that a triangulation is a planar graph in which all faces are triangular. Also, recall that a branching structure is an assignment of an orientation to each link such that there are no cycles around any of the triangles.

are triangular - with branching structure (FIG. 4.2). Recall that a branching structure is an assignment of an orientation to each link with the property that there are no cycles around any triangle. The notation $\langle pq \rangle$ always denotes a link oriented from p to q. The Hilbert space will consist of generalized G-spin degrees of freedom $|g_p\rangle$ at vertices p and spin-$\frac{1}{2}$ degrees of freedom on links $\langle pq \rangle$, with Pauli algebra generated by $\hat{X}_{pq}, \hat{Z}_{pq}$ (see FIG. 4.3).

Before delving into the construction of the shadow model Hamiltonian, let us first provide some intuition for why a bosonic model built on such a Hilbert space can encode the physics of a fermionic SPT. This intuition is based on interpreting the spin-$\frac{1}{2}$ link degrees of freedom as the Hilbert space of the usual commuting projector toric code Hamiltonian:

$$\hat{H}^{\text{t.c.}} = -\sum_{p} \prod_{\langle st \rangle \ni p} \hat{X}_{st} - \sum_{\langle pqr \rangle} \hat{Z}_{pq} \hat{Z}_{qr} \hat{Z}_{pr}, \tag{4.1}$$

where the product in the first sum above is over all oriented links $\langle st \rangle$ that contain the vertex p (i.e. either $s = p$ or $t = p$). A basis for this toric code Hilbert space can be obtained by specifying, for each basis state, the locations of all the vertex ('e') and triangular plaquette ('m') excitations, which are violations of the first and second terms in (4.1), respectively.

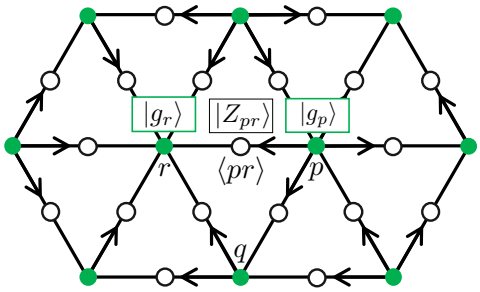

Figure 4.3: The bosonic shadow model is defined on a Hilbert space with generalized G-spin degrees of freedom at vertices and spin-$\frac{1}{2}$ degrees of freedom on links. This gives the total Hilbert space: $\left(\bigotimes_p \mathbb{C}_p^{|G|}\right) \otimes \left(\bigotimes_{\langle pq\rangle} \mathbb{C}_{pq}^2\right)$. A basis is given by configuration states $|\{g_p\},\{Z_{pq}\}\rangle$, i.e. product states for which $g_p \in G$ is chosen for each vertex p and $Z_{pq} = \pm 1$ is chosen for each link $\langle pq\rangle$.

The key idea is that the bound state of an e and an m excitation is a fermion, so a fermionic Hilbert space can effectively be constructed by restricting to the subspace where all of the e excitations have been bound up with m excitations into fermions.

Because the e excitations live on vertices and the m excitations live on plaquettes, there is some arbitrariness in defining their fermionic bound state. This arbitrariness can be resolved by using the branching structure. Following Ref. [15], we define a fermion on triangle $\langle pqr\rangle$ to be the bound state of an m excitation on $\langle pqr\rangle$ with an e excitation on its first vertex p. Here the ordering p, q, r of the vertices is specified uniquely by the branching structure (see FIG 4.4). The condition that all the e excitations have been bound up with m excitations into fermions in this way can then be stated as follows. At each vertex p, the $\mathbb{Z}_2$ charge (i.e. number of e excitations modulo 2) measured at p must be equal to the total $\mathbb{Z}_2$ flux (i.e. number of m excitations modulo 2) on all triangles $\langle pqr\rangle$ for which p is the first vertex according to the branching structure. Defining

$$\hat{W}_{pqr} \equiv \hat{Z}_{pq}\hat{Z}_{qr}\hat{Z}_{pr} \tag{4.2}$$

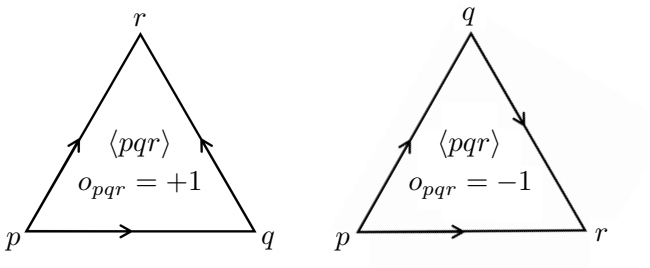

Figure 4.4: The vertices around a triangle are ordered by the number of links pointing towards the vertex. o_{pqr} is -1 or $+1$ depending on the orientation of the triangle relative to a choice of orientation for the manifold.

to be the operator that measures the $\mathbb{Z}_2$ flux on $\langle pqr \rangle$, this is then just the condition that the state be in the $+1$ eigenspace of each operator

$$\hat{G}_p \equiv \prod_{\substack{\langle tqr \rangle \\ t=p}} \hat{W}_{tqr} \prod_{\langle st \rangle \ni p} \hat{X}_{st}. \tag{4.3}$$

The first product above is over all triangles whose first vertex is p. We thus expect that the shadow model Hamiltonian will commute with all of the $\hat{G}_p$ and that its ground states will lie in the $+1$ eigenspace of each $\hat{G}_p$. Because of the second product in (4.3), $\hat{G}_p$ resembles a Gauss's law constraint. In accordance with Ref. [15], we will refer to it as a 'modified Gauss's law'.

Our construction of the shadow model Hamiltonian proceeds in two steps. First, we use group supercohomology data to construct an auxiliary bosonic SPT, with an enlarged symmetry group $\tilde{G}$ equal to a certain $\mathbb{Z}_2$ extension of G. Second, we gauge the global $\mathbb{Z}_2$ subgroup of $\tilde{G}$ in this auxiliary bosonic SPT to end up with our desired bosonic shadow model. Again, we emphasize that because all of these constructions are bosonic, the spin structure does not enter into them at all. To begin, we briefly review group supercohomology.

4.2.1 Group supercohomology data

For a finite group G, group supercohomology data consists of a pair (n, ν), where $n : G \times G \times G \to \mathbb{Z}_2$ is a $\mathbb{Z}_2$ valued function of 3 group variables, and $\nu : G \times G \times G \times G \to U(1)$ is a $U(1)$ valued function of 4 group variables, satisfying the following two properties:

1) n is a homogeneous cocycle, where homogeneity means

$$n(gg_0, gg_1, gg_2) = n(g_0, g_1, g_2) \tag{4.4}$$

for all g, and the cocycle property is [2]

$$\delta n = 0. \tag{4.7}$$

2) ν is homogeneous, i.e.

$$\nu(gg_0, gg_1, gg_2, gg_3) = \nu(g_0, g_1, g_2, g_3), \tag{4.8}$$

for all g and satisfies

$$\delta\nu(g_0, g_1, g_2, g_3, g_4) = (-1)^{n(g_0,g_1,g_2)n(g_2,g_3,g_4)}. \tag{4.9}$$

Just as for ordinary group cocycles, there is an equivalence relation on group supercohomol-

---

[2] Let h be a map from G^k to $\mathbb{Z}_2$. The coboundary of h is given by

$$\delta h(g_0, ..., g_k) = \sum_{j=0}^{k} (-1)^j h(g_0, ..., \widehat{g_j}, ..., g_k) \tag{4.5}$$

where $\widehat{g_j}$ means that g_j is omitted. Let f be a map from G^k to $U(1)$. Then the coboundary of f is given by

$$\delta f(g_0, ..., g_k) = \prod_{j=0}^{k} f(g_0, ..., \widehat{g_j}, ..., g_k)^{(-1)^j}. \tag{4.6}$$

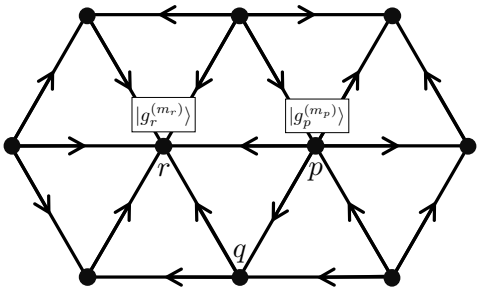

Figure 4.5: The auxiliary bosonic SPT has $\tilde{G}$ degrees of freedom at each vertex. Specifically, at each vertex, we attach a Hilbert space $\mathbb{C}^{|\tilde{G}|}$ with a basis labeled by elements of $\tilde{G}$. A natural basis for the total Hilbert space $\bigotimes_p \mathbb{C}_p^{|\tilde{G}|}$ is then a set of product states for which at each vertex an element of $\tilde{G}$ is chosen. We refer to this basis of product states as the configuration basis. An arbitrary element of the configuration basis may be written as $\left|\left\{g_p^{(m_p)}\right\}\right\rangle$.

ogy data. Rather than defining it now, we will postpone the discussion of this equivalence relation to section 4.4.3, where we identify it through physical arguments. Group supercohomology classes will then be defined as equivalence classes of group supercohomology data modulo this relation.

For convenience, in our constructions below, we will always take n to be a normalized cocycle. This is to say, we choose n such that

$$n(g,g,h) = n(g,h,h) = 0 \tag{4.10}$$

for all g, h. There is no loss of generality in restricting to normalized cocycles, because each equivalence class of group supercohomology data has a representative (n,ν) with n normalized.

4.2.2 Auxiliary bosonic SPT

The auxiliary bosonic SPT is again defined on a triangulation of an orientable two dimensional spatial manifold M together with a branching structure. The symmetry group $\tilde{G}$ of

the auxiliary bosonic SPT is the $\mathbb{Z}_2$ extension of G determined by n. Explicitly, $\tilde{G}$ consists of $2|G|$ elements $g^{(m)}$, where $g \in G$ and $m \in \mathbb{Z}_2 = \{0, 1\}$, obeying the group law:

$$g^{(m)} h^{(\ell)} = (gh)^{(m+\ell+n(1,g,gh))}. \tag{4.11}$$

The degrees of freedom in the auxiliary model are generalized $\tilde{G}$-spins $\left|g_p^{(m_p)}\right\rangle$ living on the vertices of the triangulation, and the standard bosonic SPT construction of Ref. [49] allows us to write down the following SPT ground state wave function in the $\left\{g_p^{(m_p)}\right\}$ configuration basis:

$$\Psi_{\mathrm{SPT}}\left(\left\{g_p^{(m_p)}\right\}\right) = \left\langle \left\{g_p^{(m_p)}\right\} \middle| \Psi_{\mathrm{SPT}} \right\rangle = \prod_{\langle pqr \rangle} \alpha\left(g_p^{(m_p)}, g_q^{(m_q)}, g_r^{(m_r)}, 1\right)^{o_{pqr}}. \tag{4.12}$$

Here, as below, we do not keep track of the irrelevant overall normalization factor of the ground state wave function. The product in (4.12) is over ordered triangles $\langle pqr \rangle$, with the ordering determined by the branching structure. o_{pqr} is $+1$ if the orientation of the triangle $\langle pqr \rangle$ is aligned with the orientation of the manifold and -1 otherwise (see FIG. 4.4). Finally, α is defined in terms of the group supercohomology data as [124]:

$$\alpha\left(g_0^{(m_0)}, g_1^{(m_1)}, g_2^{(m_2)}, g_3^{(m_3)}\right) \equiv \nu(g_0, g_1, g_2, g_3)(-1)^{\epsilon\left(\left(g_0^{(m_0)}\right)^{-1} g_1^{(m_1)}\right) n(g_1, g_2, g_3)}, \tag{4.13}$$

where we have defined the projector

$$\epsilon\left(g^{(m)}\right) \equiv m. \tag{4.14}$$

One can explicitly verify that α is homogenous and a cocycle ($\delta\alpha = 0$) by using equations (4.4) and (4.8) along with the group law (4.11) of $\tilde{G}$, as well as the normalization property (4.10). Thus (4.12) is a bosonic SPT ground state. The seemingly complicated cocycle α is designed to produce a shadow model wave function that lies in the $\hat{G}_p = +1$ Hilbert space, as we will see in the next subsection.

4.2.3 Bosonic shadow model wave function

We now construct the bosonic shadow model by gauging the $\mathbb{Z}_2$ subgroup of $\tilde{G}$ in the auxiliary bosonic SPT. This is done in the standard way by introducing a lattice $\mathbb{Z}_2$ gauge field $\mu^z_{pq} = \pm 1$ and performing the usual minimal coupling procedure [71], so we relegate the details to Appendix 4.A. A complete set of commuting gauge invariant observables in the resulting gauge theory is given by $\{g_p, Z_{pq}\}$, where g_p is the G component of the $\tilde{G}$ degree of freedom $g_p^{(m_p)}$ at vertex p, and

$$Z_{pq} = \mu^z_{pq}(-1)^{\epsilon\left(\left(g_p^{(m_p)}\right)^{-1} g_q^{(m_q)}\right)} \tag{4.15}$$

can be thought of as the $\mathbb{Z}_2$ part of the lattice gauge covariant derivative of the $\tilde{G}$ 'matter' fields. We explicitly demonstrate in Appendix 4.A that this gauge theory Hilbert space is isomorphic, via a duality transformation, to the unconstrained Hilbert space of generalized G-spin degrees of freedom $|g_p\rangle$ at vertices p and spin-1/2 degrees of freedom on links $\langle pq\rangle$, with Pauli algebra generated by $\hat{X}_{pq}, \hat{Z}_{pq}$.

A ground state wave function Ψ_{b} of the gauged theory can be obtained by setting the amplitude $\Psi_{\mathrm{b}}(\{g_p, Z_{pq}\})$ of any configuration $\{g_p, Z_{pq}\}$ equal to $\Psi_{\mathrm{SPT}}\left(\left\{g_p^{(m_p)}\right\}\right)$ if there exists $\left\{g_p^{(m_p)}\right\}$ for which

$$Z_{pq} = (-1)^{\epsilon\left(\left(g_p^{(m_p)}\right)^{-1} g_q^{(m_q)}\right)} = (-1)^{m_p + m_q + n(1, g_p, g_q)} \tag{4.16}$$

and zero otherwise (see FIG. 4.6 and 4.7 for an example). Such $\left\{g_p^{(m_p)}\right\}$, if it exists, is ambiguous only up to a global $\mathbb{Z}_2$ transformation, i.e. a shift $m_p \to m_p + 1$,[3] and since Ψ_{SPT} is invariant under this shift, Ψ_{b} is well defined. Explicitly,

$$\Psi_{\mathrm{b}}\left(\{g_p, Z_{pq}\}\right) = \prod_{\langle pqr\rangle} \nu(g_p, g_q, g_r, 1)^{o_{pqr}} Z_{pq}^{n(g_q, g_r, 1)}$$

[3]Here we use the fact that n is a normalized 2-cocycle.

$$\times \left(\prod_{\langle pqr \rangle} \delta_{Z_{pq} Z_{qr} Z_{pr}, (-1)^{n(g_p, g_q, g_r)}} \right) h(\{Z_{pq}(-1)^{n(1, g_p, g_q)}\}), \quad (4.17)$$

as can be verified by observing that we recover the auxiliary bosonic SPT ground state wave function amplitude by inserting (4.16) in (4.17). Again, we do not keep track of the irrelevant overall normalization of the wave function. The function $h(\{Z_{pq}(-1)^{n(1,g_p,g_q)}\}) = 0, 1$ is a constraint that enforces trivial μ^z-holonomy around each topologically nontrivial cycle in the geometry. Specifically, it is equal to a product of delta functions over all nontrivial cycles, which enforce the constraint that the product of $Z_{pq}(-1)^{n(1,g_p,g_q)}$ along the links of the cycle is equal to 1. These holonomy constraints, together with the delta functions in (4.17), ensure that the amplitude of a given configuration $\{g_p, Z_{pq}\}$ is nonzero if and only if there exists $\left\{g_p^{(m_p)}\right\}$ satisfying (4.16). Once we write down a parent Hamiltonian for Ψ_{b}, we will have other ground states, which will all be of the form (4.17) except with nontrivial holonomy constraints.

Because it comes from gauging a global $\mathbb{Z}_2$ symmetry in a short range entangled state, the shadow model wave function Ψ_{b} describes a toric code topological order. Furthermore, since Ψ_{SPT} is $\tilde{G}$ symmetric, Ψ_{b} is G symmetric, and hence the shadow model wave function describes a G-symmetry enriched toric code. One can also explicitly check that

$$\hat{G}_p |\Psi_{\mathrm{b}}\rangle = |\Psi_{\mathrm{b}}\rangle \quad (4.18)$$

for all p, so that $|\Psi_{\mathrm{b}}\rangle$ contains only fermion excitations, without any unbound e excitations or m excitations, in the sense defined above. We will also verify (4.18) below by writing down a finite depth circuit of local unitaries which commutes with all of the $\hat{G}_p$, and constructs Ψ_{b} from a state which trivially lies in the $\hat{G}_p = +1$ eigenspace of each $\hat{G}_p$.

4.2.4 Bosonic shadow model Hamiltonian from a finite depth circuit

Our ultimate aim is to use the fermionization duality of Ref. [15] to turn the bosonic shadow model wave function into the ground state of a fermionic SPT. However, as this fermionization duality is defined at the level of local operators, we must first write down a local parent Hamiltonian for $|\Psi_{\mathrm{b}}\rangle$ on which we can apply the duality.

One way to obtain such a parent Hamiltonian is to simply start with the form of the bosonic $\tilde{G}$ SPT parent Hamiltonian written down in Ref. [49] and directly couple it to a lattice $\mathbb{Z}_2$ gauge field. We outline this approach in Appendix 4.A, but for our purposes, we will find it more useful to construct a different parent Hamiltonian for $|\Psi_{\mathrm{b}}\rangle$.

Our choice of parent Hamiltonian is based on the insight that $|\Psi_{\mathrm{b}}\rangle$, as defined by the wavefunction in (4.17), can be obtained by applying an appropriate finite depth circuit of local unitaries to a ground state of the following Hamiltonian, which describes a trivial generalized G-spin paramagnet and a decoupled copy of the toric code:

$$\hat{H}^0_{\mathrm{b}} = -\sum_p \hat{P}^{\mathrm{sym}}_p - \sum_p \prod_{\langle st\rangle \ni p} \hat{X}_{st} - \sum_{\langle pqr\rangle} \hat{W}_{pqr}. \tag{4.19}$$

Here, $\hat{P}^{\mathrm{sym}}_p$ is the projector onto the symmetric state $\frac{1}{\sqrt{|G|}}\sum_{g_p\in G}|g_p\rangle$ at vertex p tensored with the identity on the remaining sites, and $\hat{W}_{pqr}$, which was defined in (4.2), measures the $\mathbb{Z}_2$ flux on $\langle pqr\rangle$. One ground state of (4.19) is

$$\Psi_{\mathrm{t.c.}}(\{g_p, Z_{pq}\}) = \left(\prod_{\langle pqr\rangle} \delta_{Z_{pq}Z_{qr}Z_{pr},1}\right) h(\{Z_{pq}\}), \tag{4.20}$$

where the holonomy constraint $h(\{Z_{pq}\})$ was defined below (4.17).

We now claim that

$$|\Psi_{\mathrm{b}}\rangle = \hat{U}_{\mathrm{b}}|\Psi_{\mathrm{t.c.}}\rangle, \tag{4.21}$$

where $\hat{U}_{\mathrm{b}}$ is the following finite depth circuit of local unitaries:

$$\hat{U}_{\mathrm{b}} = \prod_{\langle pqr\rangle} \left(\hat{\nu}_{pqr}^{o_{pqr}} \hat{Z}_{pq}^{\hat{n}_{qr}} \right) \prod_{\langle pq\rangle} \hat{X}_{pq}^{\hat{n}_{pq}} \prod_{\langle pqr\rangle} \hat{W}_{pqr}^{\hat{n}_{pr}}. \tag{4.22}$$

Here, $\hat{n}_{pq}$ is the operator defined by

$$\hat{n}_{pq} \, |\{g_t\}\rangle = n(g_p, g_q, 1) |\{g_t\}\rangle, \tag{4.23}$$

and $\hat{\nu}_{pqr}^{o_{pqr}}$ is given by

$$\hat{\nu}_{pqr}^{o_{pqr}} |\{g_t\}\rangle = \nu(g_p, g_q, g_r, 1)^{o_{pqr}} |\{g_t\}\rangle. \tag{4.24}$$

To see that $|\Psi_{\mathrm{b}}\rangle = \hat{U}_{\mathrm{b}} |\Psi_{\mathrm{t.c.}}\rangle$, first note that the all of the configurations appearing with non-zero amplitude in $|\Psi_{\mathrm{t.c.}}\rangle$ have trivial $\mathbb{Z}_2$-flux through all triangles, while the states in (4.17) have nontrivial $\mathbb{Z}_2$-flux at triangles $\langle pqr\rangle$ for which $(-1)^{n(g_p,g_q,g_r)} = -1$. This difference is remedied by the term $\prod_{\langle pq\rangle} \hat{X}_{pq}^{\hat{n}_{pq}}$ in (4.22). The cocycle condition $\delta n = 0$ guarantees that the nontrivial $\mathbb{Z}_2$-fluxes are put into the correct positions by this term. Second, the term $\prod_{\langle pqr\rangle} \hat{\nu}_{pqr}^{o_{pqr}} \hat{Z}_{pq}^{\hat{n}_{qr}}$ is simply to ensure that the phases assigned to configurations match those in $|\Psi_{\mathrm{b}}\rangle$.

It is proved in Appendix 4.B that $\hat{U}_{\mathrm{b}}$ is nearly G-symmetric - conjugating it by any global symmetry generator yields $\hat{U}_{\mathrm{b}}$ multiplied by a product of some $\hat{G}_p$ operators. This property of $\hat{U}_{\mathrm{b}}$ in particular relies on the term $\prod_{\langle pqr\rangle} \hat{W}_{pqr}^{\hat{n}_{pr}}$ in (4.22), which may have seemed unnecessary at first since it acts trivially on the toric code ground states.

Together with the manifest G and $\hat{G}_p$ invariance of $\hat{H}_{\mathrm{b}}^0$, this property of $\hat{U}_{\mathrm{b}}$ implies that

$$\hat{H}_{\mathrm{b}} = \hat{U}_{\mathrm{b}} \hat{H}_{\mathrm{b}}^0 \hat{U}_{\mathrm{b}}^\dagger, \tag{4.25}$$

is a G-symmetric parent Hamiltonian for $|\Psi_{\mathrm{b}}\rangle$. We will see in section 4.3.4 that $\hat{U}_{\mathrm{b}}$ also commutes with all $\hat{G}_p$, so that the $\hat{H}_{\mathrm{b}}$ does as well. We have thus constructed, using group

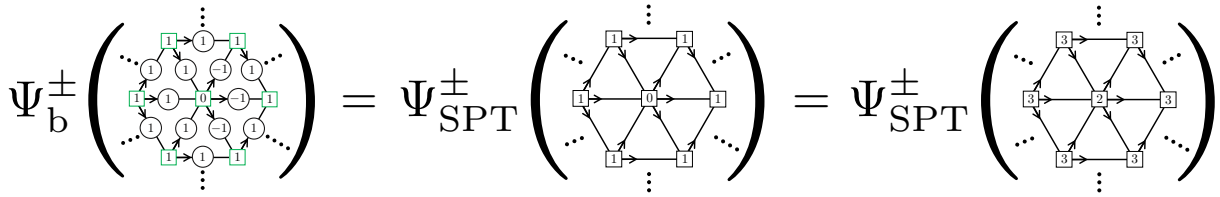

Figure 4.6: Pictured above is an example of the amplitude $\Psi_{\mathrm{b}}^{\pm}(\{g_p\},\{Z_{pq}\})$ for the $G = \mathbb{Z}_2$ case with nontrivial n, defined in (4.30). Here, the argument of $\Psi_{\mathrm{b}}^{\pm}$ is a particular configuration with a single $|0\rangle$ vertex and all other vertices in the $|1\rangle$ state. The link degrees of freedom are $|1\rangle$ everywhere besides the three $|-1\rangle$ valued links illustrated in the figure. The ellipses denote the fact that $\Psi_{\mathrm{b}}^{\pm}$ is dependent on the global configuration despite the fact that we have only shown a local portion of the configuration. The amplitude $\Psi_{\mathrm{b}}^{\pm}(\{g_p\},\{Z_{pq}\})$ is equivalent to $\Psi_{\mathrm{SPT}}^{\pm}\left(\left\{g_p^{(m_p)}\right\}\right)$ if there exists $\left\{g_p^{(m_p)}\right\}$ such that $Z_{pq} = (-1)^{\epsilon\left(\left(g_p^{(m_p)}\right)^{-1} g_q^{(m_q)}\right)}$ for all $\langle pq\rangle$. In this example, with $\tilde{G} = \mathbb{Z}_4$, $\epsilon(0) = \epsilon(3) = 0$, and $\epsilon(1) = \epsilon(2) = 1$, two such configurations exist. One has a single $|0\rangle$ vertex with all other vertices $|1\rangle$ while the other has a single $|2\rangle$ vertex with all other vertices $|3\rangle$. These two configurations differ by the square of the $\mathbb{Z}_4$ global symmetry generator, so due to the fact that $\Psi_{\mathrm{SPT}}^{\pm}\left(\left\{g_p^{(m_p)}\right\}\right)$ is $\mathbb{Z}_4$-symmetric, they give the same amplitude.

supercohomology data, a bosonic shadow model Hamiltonian that commutes with all of the $\hat{G}_p$, and whose ground states all satisfy $\hat{G}_p = +1$. This bosonic shadow model describes a G-symmetry enriched toric code phase.

4.2.5 Example: $G = \mathbb{Z}_2$

Let us describe the above constructions for the simplest nontrivial examples of supercohomology phases, which occur for $G = \mathbb{Z}_2$ (i.e. total symmetry group $\mathbb{Z}_2 \times \mathbb{Z}_2^{\mathrm{f}}$). In contrast to the case of general G, where we used multiplicative notation for the group law, in the case $G = \mathbb{Z}_2$, we will use additive notation and denote $\mathbb{Z}_2$ elements by $s = 0, 1$.

For $G = \mathbb{Z}_2$, there are four inequivalent supercohomology classes. Two of these have trivial n and correspond to the trivial phase and the purely bosonic $\mathbb{Z}_2$ SPT. The other two

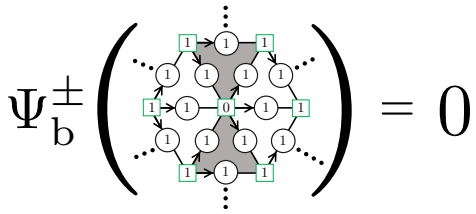

Figure 4.7: Here we show the evaluation of $\Psi_{\mathrm{b}}^{\pm}$ on a specific configuration with one vertex in the $|0\rangle$ state and all other vertices, including those not pictured, in the $|1\rangle$ state along with $|1\rangle$ states at every link Hilbert space. The amplitude of this configuration is zero because there is no configuration $\left\{g_p^{(m_p)}\right\}$ such that (4.16) is satisfied. This can be seen by the fact that the product of Z_{pq} around either one of the two shaded triangles is 1 while the product of $(-1)^{\epsilon\left(\left(g_p^{(m_p)}\right)^{-1} g_q^{(m_q)}\right)}$ around either of these triangles is $(-1)^{n(g_p,g_q,g_r)} = -1$.

both have the same nontrivial n:

$$n(s_0,s_1,s_2) = \begin{cases} 1 & (s_0,s_1,s_2) = (0,1,0) \\ 1 & (s_0,s_1,s_2) = (1,0,1) \\ 0 & \text{otherwise,} \end{cases} \tag{4.26}$$

but different ν:

$$\nu_{\pm}(s_0,s_1,s_2,s_3) = \begin{cases} \pm i & (s_0,s_1,s_2,s_3) = (1,0,1,0) \\ \pm i & (s_0,s_1,s_2,s_3) = (0,1,0,1) \\ 1 & \text{otherwise.} \end{cases} \tag{4.27}$$

This data defines two possible phases according to the choice of sign in (4.27), which turn out to be the index 2 and 6 members of the $\mathbb{Z}_8$ interacting classification in this symmetry class [147–149]. The $\mathbb{Z}_2$ extension of $G = \mathbb{Z}_2$ defined by n is $\tilde{G} = \mathbb{Z}_4$, and ϵ is $\epsilon(0) = \epsilon(3) = 0$, $\epsilon(1) = \epsilon(2) = 1$. Explicitly computing the cocycle α defined in (4.13), we obtain

$$\alpha_{\pm}(\tilde{s}_0,\tilde{s}_1,\tilde{s}_2,\tilde{s}_3) = (\pm i)^{(\tilde{s}_0-\tilde{s}_1)(\overline{\tilde{s}_1-\tilde{s}_2})(\overline{\tilde{s}_2-\tilde{s}_3})}, \tag{4.28}$$

where $\tilde{s} \in \mathbb{Z}_4$ and the overline denotes reduction modulo 2.

The corresponding auxiliary $\mathbb{Z}_4$ SPT wave function is:

$$\Psi^{\pm}_{\mathrm{SPT}}(\{\tilde{s}_p\}) = \prod_{\langle pqr\rangle} \alpha_{\pm}(\tilde{s}_p, \tilde{s}_q, \tilde{s}_r, 0)^{o_{pqr}}. \tag{4.29}$$

The bosonic shadow Hilbert space has $\mathbb{Z}_2$ degrees of freedom $s_p = 0, 1$ on vertices p and spin-$\frac{1}{2}$ degrees of freedom $Z_{pq} = \pm 1$ on links $\langle pq\rangle$. The shadow model ground states are (see FIG. 4.6 and 4.7)

$$\Psi^{\pm}_{\mathrm{b}}(\{s_p\}, \{Z_{pq}\}) = \prod_{\langle pqr\rangle} \nu_{\pm}\left(s_p, s_q, s_r, 0\right)^{o_{pqr}} Z_{pq}^{n(s_q, s_r, 0)} \times \left(\prod_{\langle pqr\rangle} \delta_{Z_{pq}Z_{qr}Z_{pr}, (-1)^{n(s_p, s_q, s_r)}}\right) h(\{Z_{pq}(-1)^{n(1, s_p, s_q)}\}). \tag{4.30}$$

Here, $h(\{Z_{pq}\}) = 0, 1$ is a function that projects onto a choice of holonomy of the $\mathbb{Z}_2$ gauge field.

Using the explicit form of the supercohomology data $n(s_p, s_q, 0) = (1 - s_p)s_q$ and $\nu_{\pm}(s_p, s_q, s_r, 0) = (\pm i)^{s_p(1-s_q)s_r}$, we see that the circuit (4.22) becomes

$$\hat{U}^{\pm}_{\mathrm{b}} = \prod_{\langle pqr\rangle} (\pm i)^{o_{pqr}\hat{s}_p(1-\hat{s}_q)\hat{s}_r} \hat{Z}_{pq}^{(1-\hat{s}_q)\hat{s}_r} \times \prod_{\langle pq\rangle} \hat{X}_{pq}^{(1-\hat{s}_p)\hat{s}_q} \prod_{\langle pqr\rangle} \hat{W}_{pqr}^{(1-\hat{s}_p)\hat{s}_r}. \tag{4.31}$$

From this circuit, we obtain the Hamiltonian

$$\hat{H}^{\pm}_{\mathrm{b}} = \hat{U}^{\pm}_{\mathrm{b}} \hat{H}^{0}_{\mathrm{b}} (\hat{U}^{\pm}_{\mathrm{b}})^{\dagger} \tag{4.32}$$

for the gauged model.

For completeness, we note that the global $\mathbb{Z}_2$ symmetry generator in the gauged model

acts by

$$|\{s_p, Z_{pq}\}\rangle \to |\{1 - s_p, Z_{pq}\}\rangle. \tag{4.33}$$

This is just the descendant of the $\mathbb{Z}_4$ generator in the $\mathbb{Z}_4$ SPT.

4.3 Fermionizing the shadow model

In the previous section, we used the supercohomology data to construct a bosonic shadow model $\hat{H}_{\mathrm{b}}$ on a Hilbert space consisting of generalized G-spin degrees of freedom on vertices p and spin-$\frac{1}{2}$ degrees of freedom on links $\langle pq \rangle$. In this section, we describe how this bosonic model may be fermionized, i.e. rewritten in terms of local fermionic operators. This fermionization is effectively a procedure for 'un-gauging' fermion parity symmetry. Equivalently, it can be viewed as a prescription for a lattice level fermion condensation (see Appendix 4.D for further detail). We emphasize that this is the only point at which a choice of spin structure enters the construction.

Focusing just on the spin-$\frac{1}{2}$ link degrees of freedom, we utilize the fermionization prescription developed in Ref. [15], reviewed in the next three subsections, which provides an exact duality between the local operator algebra of a bosonic model and that of a fermionic model. To define this duality, one must specify some combinatorial data, which we show amounts to a choice of spin structure for the spatial manifold M. We will first define the local bosonic and fermionic operator algebras $\mathcal{A}_{\mathrm{bos}}$ and $\mathcal{A}_{\mathrm{fer}}$, respectively, and then construct the spin-structure dependent duality between them. Finally, we apply this duality to $\hat{H}_{\mathrm{b}}$ to produce our fermionic Hamiltonian $\hat{H}_{\mathrm{f}}$ and demonstrate that it describes an SPT.

4.3.1 Bosonic operator algebra $\mathcal{A}_{bos}$

On the bosonic side, we consider the spin-$\frac{1}{2}$ degrees of freedom living on links, with Pauli algebra generated by $\hat{X}_{pq}$ and $\hat{Z}_{pq}$. $\mathcal{A}_{\mathrm{bos}}$ is defined as the operator algebra generated by the

subset of local operators that commute with all the $\hat{G}_p$ defined in (4.3):

$$\hat{G}_p = \prod_{\substack{\langle tqr\rangle \\ t=p}} \hat{Z}_{tq}\hat{Z}_{qr}\hat{Z}_{tr} \prod_{\langle st\rangle \ni p} \hat{X}_{st} \tag{4.34}$$

and modulo the relations $\hat{G}_p = 1$ for all p.[4] Thus we may think of $\mathcal{A}_{\text{bos}}$ as the algebra of operators generated by the subset of local operators which are gauge invariant with respect to the modified Gauss's law $\hat{G}_p = 1$.

We now identify two sets of local, modified Gauss's law invariant operators which generate all of $\mathcal{A}_{\text{bos}}$ [15]. The first is $\hat{W}_{pqr} = \hat{Z}_{pq}\hat{Z}_{qr}\hat{Z}_{pr}$. The second is $\hat{U}_{pq}$, defined as:

$$\hat{U}_{pq} \equiv \hat{X}_{pq}\hat{K}_{L_{pq}}\hat{K}_{R_{pq}}, \tag{4.35}$$

with $\hat{K}_{R_{pq}}$ and $\hat{K}_{L_{pq}}$ defined as follows. The action of $\hat{K}_{R_{pq}}$ is dependent upon the triangle R_{pq} to the right of $\langle pq\rangle$. If the triangle to the right of $\langle pq\rangle$ has vertex ordering $\langle rpq\rangle$, with p and q being the second and third vertices, respectively, then $\hat{K}_{R_{pq}}$ acts as $\hat{Z}_{rp}$. Otherwise, $\hat{K}_{R_{pq}} = 1$. The action of $\hat{K}_{L_{pq}}$ is defined similarly but with 'right' replaced with 'left'. Some examples of the action of $\hat{U}_{pq}$ are depicted in FIG. 4.8. Intuition for this seemingly contrived definition can be obtained by recalling that the modified Gauss's law is a constraint that binds a $\mathbb{Z}_2$ flux on a triangle to a $\mathbb{Z}_2$ charge at the first vertex of that triangle. The operator $\hat{U}_{pq}$ then hops a $\mathbb{Z}_2$ flux across the link $\langle pq\rangle$, and also rearranges the $\mathbb{Z}_2$ charges in such a way that the modified Gauss's law remains enforced.

As shown in Ref. [15], the only nontrivial relations among the $\hat{U}_{pq}$ and $\hat{W}_{pqr}$ operators

[4] Note that on manifolds M with nontrivial $H_1(M)$ global relations need to be specified to ensure that the duality is consistent. These additional relations can be seen as coming from operator identities on the fermionic side of the duality - certain products of fermionic 'hopping' operators and parity operators along nontrivial 1-cycles are equivalent to the identity.

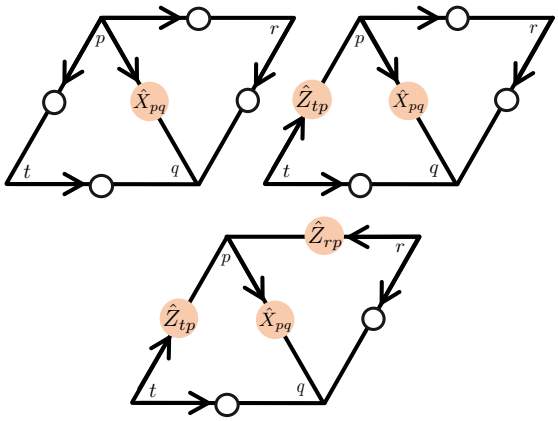

Figure 4.8: The action of $\hat{U}_{pq}$ on link $\langle pq \rangle$ depends on the branching structure of the neighboring triangles. $\hat{X}_{pq}$ is always applied to $\langle pq \rangle$, but a Pauli $\hat{Z}$ acts on the link connecting the first and second vertex of the neighboring triangle if and only if $\langle pq \rangle$ is the link connecting the second and third vertices of that triangle.

are captured in the following operator identity. For any vertex p,

$$\prod_{\substack{\langle tq \rangle \\ t=p}} \hat{U}_{tq} \prod_{\substack{\langle qt \rangle \\ t=p}} \hat{U}_{qt} = \hat{G}_p \prod_{\substack{\langle tqr \rangle \\ t=p}} \hat{W}_{tqr} \prod_{\substack{\langle qrt \rangle \\ t=p}} \hat{W}_{qrt}. \tag{4.36}$$

Note that in the first product on the left hand side all the links are oriented away from p, while in the second product all the links are oriented towards p.

4.3.2 Fermionic operator algebra $\mathcal{A}_{fer}$

On the fermionic side, the degrees of freedom are complex fermions - one at the center of each triangle $\langle pqr \rangle$. We use the pair of Majorana operators γ_{pqr} and $\bar{\gamma}_{pqr}$ to represent the operator algebra for this complex fermion. The fermion parity at triangle $\langle pqr \rangle$ is measured by

$$(-1)^{\hat{F}_{pqr}} \equiv -i\gamma_{pqr}\bar{\gamma}_{pqr}, \tag{4.37}$$

and an operator is fermion parity even if it commutes with $\prod_{\langle pqr\rangle}(-1)^{\hat{F}_{pqr}}$. The algebra $\mathcal{A}_{\text{fer}}$ of fermion parity even operators is generated by the $(-1)^{\hat{F}_{pqr}}$ and a certain set of 'hopping operators', which transfer fermion parity across a link $\langle pq\rangle$. Specifically, we define the hopping operator

$$\hat{S}'_{pq} \equiv i\gamma_{L_{pq}}\bar{\gamma}_{R_{pq}}, \tag{4.38}$$

where we have again denoted the triangles to the left and right of $\langle pq\rangle$ by L_{pq} and R_{pq}, respectively.

The $(-1)^{\hat{F}_{pqr}}$ and $\hat{S}'_{pq}$ satisfy nearly the same algebraic relations with each other as do the bosonic operators $\hat{W}_{pqr}$ and $\hat{U}_{pq}$. The only difference is that $(-1)^{\hat{F}_{pqr}}$ and $\hat{S}'_{pq}$ satisfy an algebraic relation that is similar to but not exactly the same as (4.36) [15]:

$$\prod_{\substack{\langle tq\rangle \\ t=p}} \hat{S}'_{tq} \prod_{\substack{\langle qt\rangle \\ t=p}} \hat{S}'_{qt} = c(p) \prod_{\substack{\langle tqr\rangle \\ t=p}} (-1)^{\hat{F}_{tqr}} \prod_{\substack{\langle qrt\rangle \\ t=p}} (-1)^{\hat{F}_{qrt}}. \tag{4.39}$$

In (4.39), $c(p)$ is a sign factor determined solely by the branching structure near p. We prove (4.39) in Appendix 4.C, where we also derive the following graphical method for explicitly calculating $c(p)$. First, we interpolate the branching structure to the interiors of the triangles to give a continuous non-vanishing vector field [125] $\mathcal{V}$ (see FIG. 4.9). Singularities in this vector field can occur only at vertices, and $c(p) = -1$ if the vertex p has a singularity with odd winding number and $c(p) = 1$ otherwise.

4.3.3 Spin structure dependent duality between $\mathcal{A}_{bos}$ and $\mathcal{A}_{fer}$

The geometric interpretation of the sign $c(p)$ in (4.39) as counting the singularities of a vector field $\mathcal{V}$ immediately points to a possible modification of the operators generating $\mathcal{A}_{\text{fer}}$ that makes $\mathcal{A}_{\text{fer}}$ manifestly isomorphic to $\mathcal{A}_{\text{bos}}$. To make this modification, first note that there

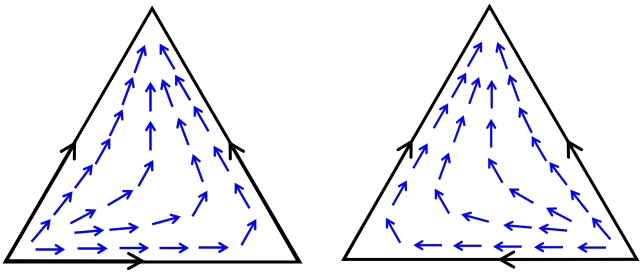

Figure 4.9: The interpolating vector field lies parallel to the branching structure for both $o_{pqr} = +1$ and $o_{pqr} = -1$ triangles. There are no singularities of the vector field away from the vertices.

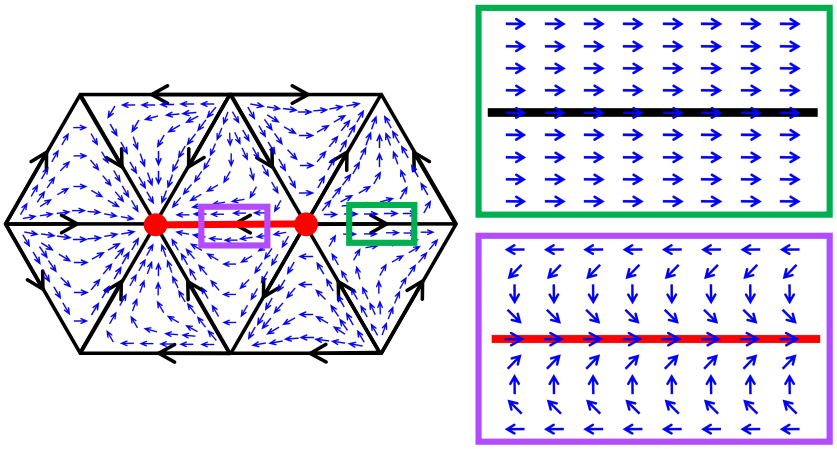

Figure 4.10: The red vertices mark singularities of the interpolating vector field with odd winding numbers, and the red link gives a choice of $\mathcal{E}$. The green inset shows the interpolating vector field near a link not belonging to $\mathcal{E}$, while the purple inset shows the 2π twist of the vector field near a link in $\mathcal{E}$.

are an even number of vertices with $c(p) = -1$. [5] Thus, we can find a set $\mathcal{E}$ of links such that the vertices in the boundary of $\mathcal{E}$ (the boundary being defined as the set of vertices which are endpoints of an odd number of links in $\mathcal{E}$) are precisely the vertices with $c(p) = -1$. Then, we can modify the vector field $\mathcal{V}$ by giving it an extra 2π winding as it crosses a link in $\mathcal{E}$ (see FIG. 4.10). The result is a new vector field with even singularities only. It is known that in 2 dimensions a vector field with only even singularities defines a spin structure [119]. Hence, a choice of $\mathcal{E}$ corresponds to a choice of spin structure.

Having made a choice of $\mathcal{E}$, we now define modified hopping operators

$$\hat{S}_{pq} \equiv (-1)^{\mathcal{E}_{pq}} \hat{S}'_{pq} \tag{4.40}$$

where $\mathcal{E}_{pq} = 0, 1$ is the indicator function for $\mathcal{E}$, i.e. $\mathcal{E}_{pq} = 1$ if $\langle pq \rangle \in \mathcal{E}$ and $\mathcal{E}_{pq} = 0$ otherwise. These modified operators then satisfy

$$\prod_{\substack{\langle tq \rangle \\ t=p}} \hat{S}_{tq} \prod_{\substack{\langle qt \rangle \\ t=p}} \hat{S}_{qt} = \prod_{\substack{\langle tqr \rangle \\ t=p}} (-1)^{\hat{F}_{tqr}} \prod_{\substack{\langle qrt \rangle \\ t=p}} (-1)^{\hat{F}_{qrt}}. \tag{4.41}$$

Now, comparing with (4.36), we see that the correspondence given by

$$\begin{aligned} \hat{W}_{pqr} &\longleftrightarrow (-1)^{F_{pqr}} \\ \hat{U}_{pq} &\longleftrightarrow \hat{S}_{pq} \end{aligned} \tag{4.42}$$

defines an explicit isomorphism of operator algebras between $\mathcal{A}_{\text{bos}}$ and $\mathcal{A}_{\text{fer}}$. We emphasize that this correspondence depends on a choice of spin structure, via the choice of $\mathcal{E}$.

The fermionization duality reviewed here admits an intuitive description in terms of a 'condensation of fermions'. We elaborate on this point in Appendix 4.D.

---

[5] The fact that the number of vertices p with $c(p) = -1$ is even is just a consequence of the fact that the winding number of singularities is additive: a contour that encloses several singularities has a winding number equal to the sum of the winding numbers of those singularities. On a compact manifold, a small contour enclosing no singularities can equivalently be thought of as a large contour enclosing all the singularities (by exchanging the notion of 'inside' and 'outside' the contour).

4.3.4 Fermionic SPT Hamiltonian

Let us now use the dictionary given in (4.42) to rewrite each local term in the shadow model Hamiltonian

$$\hat{H}_{\mathrm{b}} = \hat{U}_{\mathrm{b}} \hat{H}^0_{\mathrm{b}} \hat{U}^\dagger_{\mathrm{b}}, \tag{4.43}$$

defined in (4.25), in terms of local fermionic operators. This can be carried out by fermionizing $\hat{H}^0_{\mathrm{b}}$, defined in (4.19), and $\hat{U}_b$, defined in (4.22), independently. To fermionize $\hat{H}^0_{\mathrm{b}}$, we first use the definition of $\hat{G}_p$ to rewrite it as

$$\hat{H}^0_{\mathrm{b}} = -\sum_p \hat{P}^{\mathrm{sym}}_p - \sum_p \left(\hat{G}_p \prod_{\substack{\langle tqr \rangle \\ t=p}} \hat{W}_{tqr} \right) - \sum_{\langle pqr \rangle} \hat{W}_{pqr}. \tag{4.44}$$

Then, according to the dictionary in (4.42), $\hat{H}^0_{\mathrm{b}}$ fermionizes to

$$\hat{H}^0_{\mathrm{f}} = -\sum_p \hat{P}^{\mathrm{sym}}_p - \sum_{\langle pqr \rangle} (-1)^{\hat{F}_{pqr}}, \tag{4.45}$$

after using the gapped and unfrustrated property of the Hamiltonian to remove the fermionization of the second term in (4.44). This Hamiltonian describes a trivial atomic insulator, and the unique ground state $|\Psi^0_{\mathrm{f}}\rangle$ is a product state of symmetrized states at the vertices and zero fermion occupancy on the triangles.

To fermionize $\hat{U}_{\mathrm{b}}$, we note that the product

$$\prod_{\langle pqr \rangle} \hat{Z}^{\hat{n}_{qr}}_{pq} \prod_{\langle pq \rangle} \hat{X}^{\hat{n}_{pq}}_{pq} \tag{4.46}$$

in (4.22) can be rearranged into

$$\hat{\kappa} \prod_{\langle pq \rangle} \hat{U}^{\hat{n}_{pq}}_{pq}. \tag{4.47}$$

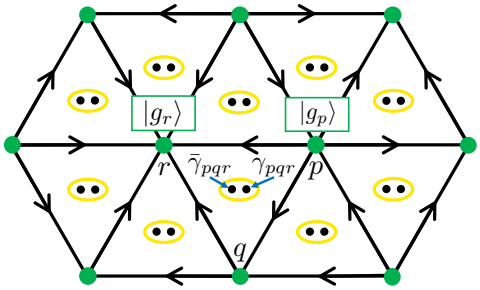

Figure 4.11: The fermionic SPT Hamiltonian acts on a Hilbert space with generalized G-spin degrees of freedom on vertices and a single complex fermion degree of freedom for each triangle. Explicitly, the total Hilbert space is $\left(\bigotimes_p \mathbb{C}_p^{|G|}\right) \otimes^{\mathbb{Z}_2} \left(\bigotimes^{\mathbb{Z}_2}_{\langle pqr\rangle} \mathbb{C}^{1|1}_{pqr}\right)$, where $\bigotimes^{\mathbb{Z}_2}$ is a $\mathbb{Z}_2$ graded tensor product. We use γ_{pqr} and $\bar{\gamma}_{pqr}$ as a basis for the operator algebra of the complex fermion at $\langle pqr\rangle$.

where $\hat{\kappa}$ is a certain diagonal operator in the $\{g_p\}$ configuration basis with eigenvalues ± 1. The eigenvalue is locally determined, in that it is a product of signs, each of which is dependent upon only the G-configuration within a disk of finite radius around some point. These signs result from commuting $\hat{Z}_{pq}$ past $\hat{X}_{pq}$ and hence the eigenvalues are dependent on the choice of ordering of the $\hat{U}_{pq}$ operators in (4.47). Although the operator $\hat{\kappa}$ is complicated to write out for general G, we note that the locality property above makes it a finite depth circuit of local unitaries. Furthermore, we will see below that in the example $G = \mathbb{Z}_2$ the situation simplifies considerably: $\hat{\kappa}$ is trivial in that case, and all of the terms in the product in (4.47) commute. Also, in Appendix 4.E we present another way of circumventing the issue posed by the unwieldy form of $\hat{\kappa}$, by introducing ancillary spin-$\frac{1}{2}$ degrees of freedom on the triangles. This allows for a more canonical finite depth circuit that does not require an arbitrary choice of ordering.

We now use (4.42) to map (4.47) to fermionic operators. The result of fermionizing $\hat{U}_{\mathrm{b}}$ is the finite depth circuit of local unitaries

$$\hat{U}_{\mathrm{f}} = \hat{\kappa} \prod_{\langle pqr\rangle} \hat{\nu}_{pqr}^{o_{pqr}} \prod_{\langle pq\rangle} \hat{S}_{pq}^{\hat{n}_{pq}} \prod_{\langle pqr\rangle} \left((-1)^{\hat{F}_{pqr}}\right)^{\hat{n}_{pr}} . \tag{4.48}$$

Therefore, fermionization turns $\hat{H}_{\mathrm{b}}$ into

$$\hat{H}_{\mathrm{f}} = \hat{U}_{\mathrm{f}} \hat{H}_{\mathrm{f}}^{0} \hat{U}_{\mathrm{f}}^{\dagger}. \tag{4.49}$$

$\hat{H}_{\mathrm{f}}$ is comprised of two types of terms. First, we have the conjugates of the terms in the second sum in (4.45), namely:

$$-\hat{U}_{\mathrm{f}} (-1)^{\hat{F}_{pqr}} \hat{U}_{\mathrm{f}}^{\dagger} = -(-1)^{\hat{n}_{pqr}} (-1)^{\hat{F}_{pqr}}. \tag{4.50}$$

These energetically enforce fermions to occupy the triangles $\langle pqr \rangle$ with nontrivial $n(g_p, g_q, g_r)$. Second, we have the conjugates of the terms in the first sum in (4.45):

$$-\hat{U}_{\mathrm{f}} \hat{P}_{p}^{\mathrm{sym}} \hat{U}_{\mathrm{f}}^{\dagger}. \tag{4.51}$$

These fluctuate the G-configuration at vertex p and move the neighboring fermions so that the fermion occupancy conforms to the first term. We will see the action of $\hat{H}_{\mathrm{f}}$ more explicitly below when we treat the case $G = \mathbb{Z}_2$.

$\hat{H}_{\mathrm{f}}$ describes a fermionic SPT phase because (1) it is gapped (2) it has a unique, SRE ground state, and (3) it is symmetric. It is gapped because it is an unfrustrated commuting projector Hamiltonian. The unique ground state is $\hat{U}_{\mathrm{f}} |\Psi_{\mathrm{f}}^{0}\rangle$, and since $\hat{U}_{\mathrm{f}}$ is a finite depth circuit of local unitaries, the ground state is SRE. Lastly, it is G-symmetric because $\hat{H}_b$ is G-symmetric, and the fermionization procedure commutes with the global action of G.

4.3.5 Example: $G = \mathbb{Z}_2$

Recall that in the $G = \mathbb{Z}_2$ case, (4.31) is

$$\hat{U}_{\mathrm{b}}^{\pm} = \prod_{\langle pqr \rangle} (\pm i)^{o_{pqr} \hat{s}_p (1-\hat{s}_q) \hat{s}_r} \hat{Z}_{pq}^{(1-\hat{s}_q)\hat{s}_r} \prod_{\langle pq \rangle} \hat{X}_{pq}^{(1-\hat{s}_p)\hat{s}_q} \prod_{\langle pqr \rangle} \hat{W}_{pqr}^{(1-\hat{s}_p)\hat{s}_r}. \tag{4.52}$$

To avoid confusion, we will for the remainder of this section focus on the case $\hat{U}_{\mathrm{b}}^{+}$ and drop the + superscript; the case $\hat{U}_{\mathrm{b}}^{-}$ can be treated similarly.

To fermionize $\hat{U}_{\mathrm{b}}$, we first recognize that it may be written in terms of the local operators $\hat{U}_{pq}$ of section 4.3. The product

$$\prod_{\langle pqr\rangle} \hat{Z}_{pq}^{(1-\hat{s}_q)\hat{s}_r} \prod_{\langle pq\rangle} \hat{X}_{pq}^{(1-\hat{s}_p)\hat{s}_q} \tag{4.53}$$

in (4.52) is exactly equal to

$$\prod_{\langle pq\rangle} \hat{U}_{pq}^{(1-\hat{s}_p)\hat{s}_q} \tag{4.54}$$

without any additional factor of $\hat{\kappa}$. This is due to the fact that $(1-s_q)s_r$ and $(1-s_p)s_q$ cannot simultaneously be 1, so that we never have to move anti-commuting operators past each other to go from one expression to the other. Therefore, the fermionization duality applied to $\hat{U}_{\mathrm{b}}$ yields

$$\hat{U}_{\mathrm{f}} = \prod_{\langle pqr\rangle} i^{o_{pqr}\hat{s}_p(1-\hat{s}_q)\hat{s}_r} \prod_{\langle pq\rangle} \hat{S}_{pq}^{(1-\hat{s}_p)\hat{s}_q} \prod_{\langle pqr\rangle} \left((-1)^{\hat{F}_{pqr}}\right)^{(1-\hat{s}_p)\hat{s}_r} \tag{4.55}$$

with $\hat{S}_{pq}$ and $(-1)^{\hat{F}_{pqr}}$ defined in section 4.3. Hence, $\hat{H}_{\mathrm{b}}$ explicitly fermionizes to

$$\hat{H}_{\mathrm{f}} = \hat{U}_{\mathrm{f}} \hat{H}_{\mathrm{f}}^{0} \hat{U}_{\mathrm{f}}, \tag{4.56}$$

where

$$\hat{H}_{\mathrm{f}}^{0} = -\sum_{p} \hat{P}_{p}^{\mathrm{sym}} - \sum_{\langle pqr\rangle} (-1)^{\hat{F}_{pqr}}. \tag{4.57}$$

We have thus constructed a $\mathbb{Z}_2$-symmetric fermionic SPT Hamiltonian for the supercohomology data specified in (4.26) and (4.27).

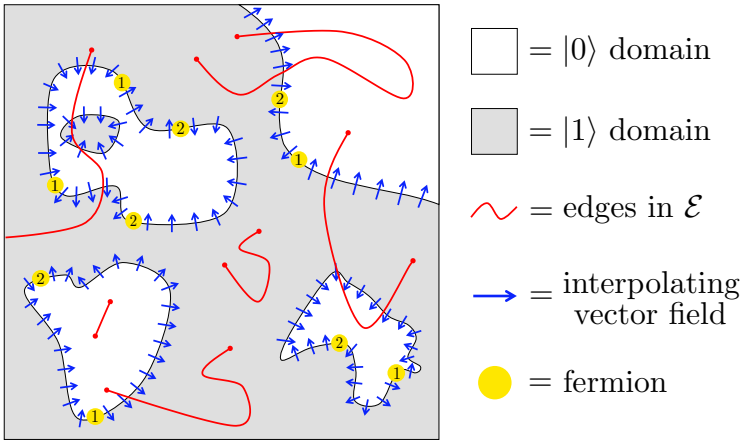

Figure 4.12: Pictured here is the effect of $\prod_{\langle pq\rangle} \hat{S}_{pq}^{(1-\hat{s}_p)\hat{s}_q}$ on a domain wall configuration. For clarity the lattice is suppressed and we have only drawn the interpolating vector field along the domain walls. The edges of $\mathcal{E}$, introduced in section 4.3, are shown to illustrate their affect on the ordering of the fermions in the figure.

Picture of the ground state: The finite depth circuit of local unitaries $\hat{U}_{\rm f}$ in (4.55) allows us to explicitly construct the ground state $|\Psi_{\rm f}\rangle$ of $\hat{H}_{\rm f}$. This is accomplished by applying $\hat{U}_{\rm f}$ to $|\Psi_{\rm f}^0\rangle$, the ground state of $\hat{H}_{\rm f}^0$. $|\Psi_{\rm f}^0\rangle$ is a product state with the $\mathbb{Z}_2$-symmetric state $\frac{1}{\sqrt{2}}(|0\rangle+|1\rangle)$ at each vertex p and zero fermion occupancy at every triangle $\langle pqr\rangle$. Expressed in the configuration basis, $|\Psi_{\rm f}^0\rangle$ is an equal amplitude superposition of domain configurations – domains containing states $|0\rangle$ or $|1\rangle$ at vertices. Note that the domain walls between the $|0\rangle$ and $|1\rangle$ domains run along the edges of the dual lattice. The ground state of $\hat{H}_{\rm f}$ is

$$|\Psi_{\rm f}\rangle = \hat{U}_{\rm f}|\Psi_{\rm f}^0\rangle = \sum_{\text{configs}} \hat{U}_{\rm f} \Big|$$ 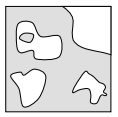 $$\Big\rangle . \tag{4.58}$$

The above sum is over all $\mathbb{Z}_2$-spin domain configurations tensored with the empty fermionic state. The operator $\hat{U}_{\rm f}$ decorates fermions onto each such domain configuration and multiplies by a configuration-dependent phase, but it does not alter the shape of the domains.

We can break the action of $\hat{U}_{\rm f}$ on a domain configuration up into three steps. In the first

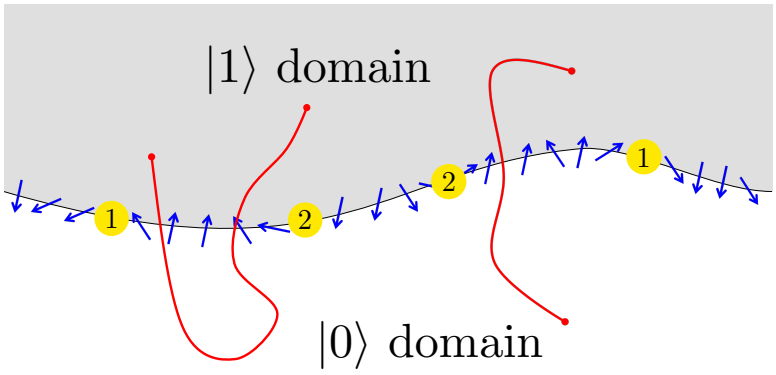

Figure 4.13: The order in which the fermions are created along the domain wall is based on the spin structure. Fermions are created in pairs – one on either side of the regions for which the interpolating vector field points from $|0\rangle$ (white) to $|1\rangle$ (gray). These fermions are created left to right if there are an even number of edges in $\mathcal{E}$ (pictured in red) between them and created right to left order otherwise. The ordering is labeled above. Note that equivalently, the fermions can be ordered from left to right across every $|0\rangle$ to $|1\rangle$ pointing region as long as a -1 sign is picked up for each edge in $\mathcal{E}$ oriented from $|0\rangle$ to $|1\rangle$.

step, we apply

$$\prod_{\langle pqr\rangle} \left((-1)^{\hat{F}_{pqr}}\right)^{(1-\hat{s}_p)\hat{s}_r}. \tag{4.59}$$

As the domain configurations in $|\Psi_{\mathrm{f}}^0\rangle$ have no fermions, they are $+1$ eigenvectors of the fermion parity operators in (4.59). Thus, this term does not affect the state.

In the second step, we act on the domain configuration with

$$\prod_{\langle pq\rangle} \hat{S}_{pq}^{(1-\hat{s}_p)\hat{s}_q}. \tag{4.60}$$

The exponent in (4.60) is 1 precisely when the link $\langle pq\rangle$ points from a $|0\rangle$ domain to a $|1\rangle$ domain. As a result, Majorana operators are applied to the two triangles on either side of the link $\langle pq\rangle$, and in this way, fermions are only created along the domain wall. The result is a pair of fermions at the two endpoints of each portion of the domain wall where the

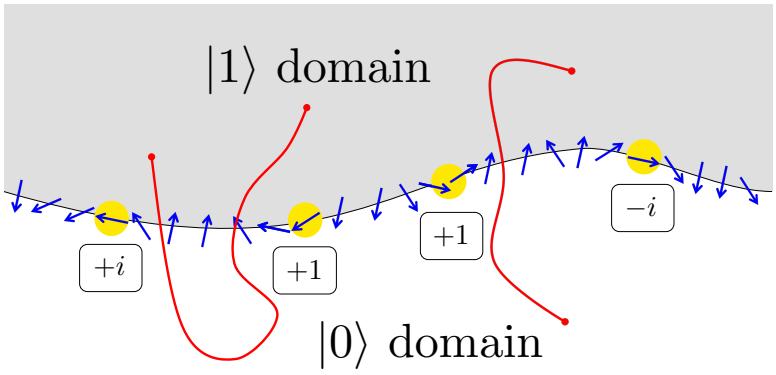

Figure 4.14: In the figure above, as we move left to right along the domain wall, the interpolating vector field (blue arrows) rotates. When it rotates clockwise from pointing towards the $|0\rangle$ domain (white) to pointing towards the $|1\rangle$ domain (gray), we get a phase of $+i$. When it rotates clockwise from pointing towards the $|1\rangle$ domain to pointing towards the $|0\rangle$ domain, we obtain a phase of $-i$. Counterclockwise rotations of the vector field along the domain wall give a trivial phase. The twist of the vector field near an edge in $\mathcal{E}$ (red edges), as displayed in FIG. 4.10, does not affect the calculation of this phase.

interpolating vector field points from the $|0\rangle$ to the $|1\rangle$ domain (see FIG. 4.12 and 4.13). The order in which these two fermions are created depends on the spin structure $\mathcal{E}$ as follows. First, we locally orient the domain wall so that it runs horizontally with the $|0\rangle$ domain below and the $|1\rangle$ domain above, as illustrated in FIG. 4.13. If there are an even number of edges in $\mathcal{E}$ crossing the $|0\rangle$ to $|1\rangle$ pointing portion of the domain wall, then we create the fermion on the left endpoint first, followed by the fermion on the right endpoint. When there are an odd number of edges in $\mathcal{E}$ crossing the region, the fermions are created in the opposite order (FIG. (4.13)). Since the difference between these two procedures is just a minus sign, we can alternatively always create the fermions from left to right, and at the end multiply by -1 for every edge of $\mathcal{E}$ that points from the $|0\rangle$ to the $|1\rangle$ domain.

Lastly, we act with

$$\prod_{\langle pqr\rangle} i^{o_{pqr}\hat{s}_p(1-\hat{s}_q)\hat{s}_r}. \tag{4.61}$$

This term assigns a phase to each configuration, which can be thought of as a product of contributions associated to points of tangency of the vector field with the domain wall, or, equivalently, associated to the fermions. These contributions can be determined as follows. Moving from left to right along a domain wall with the $|0\rangle$ domain below and the $|1\rangle$ domain above, we track the interpolating vector field. If the interpolating vector field rotates clockwise, from initially pointing in the direction of the $|0\rangle$ domain to finally pointing in the direction of the $|1\rangle$ domain, then we accrue a phase of i. If the interpolating vector field rotates clockwise from initially pointing towards the $|1\rangle$ domain to finally pointing towards the $|0\rangle$ domain, then a phase of $-i$ is picked up (see FIG. 4.14). For the two other possible rotations, no phase is picked up.

We would like to emphasize that the ground state constructed according to this prescription admits a continuum interpretation. Namely, in the continuum we can think of the spin structure being encoded in a smooth vector field together with a set of smooth segments $\mathcal{E}$ connecting the odd singularities of this vector field. The ground state is a superposition over smooth domain wall configurations decorated with fermions. The fermions appear precisely at the locations where the vector field is tangent to a domain wall, and the above prescription gives a specific ordering of fermion creation operators used to create this fermionic state from the empty fermionic state. Finally, the amplitude for each decorated domain wall is multiplied by products of $\pm i$ as determined by the rotation of the vector field at the points of tangency, as detailed above.

4.4 Classification

Thus far, we have used a choice of supercohomology data (n, ν) together with a spin structure on a 2d triangulated spatial manifold with branching structure to construct a zero correlation length fermionic SPT Hamiltonian. The strategy was to first construct a bosonic shadow

model using the group supercohomology data. This led us to a finite depth circuit $\hat{U}_{\mathrm{b}}$ (4.22):

$$\hat{U}_{\mathrm{b}} = \prod_{\langle pqr \rangle} \left(\hat{\nu}_{pqr}^{o_{pqr}} \hat{Z}_{pq}^{\hat{n}_{qr}} \right) \prod_{\langle pq \rangle} \hat{X}_{pq}^{\hat{n}_{pq}} \prod_{\langle pqr \rangle} \hat{W}_{pqr}^{\hat{n}_{pr}}, \tag{4.62}$$

which, when applied to an ordinary toric code ground state, produced the ground state of the bosonic shadow model. Furthermore, the fermionization of $\hat{U}_{\mathrm{b}}$ yielded $\hat{U}_{\mathrm{f}}$ (defined in (4.48)) - a fermionic finite depth circuit that builds a fermionic SPT ground state from a trivial product state.

In this section, we show that the composition of these circuits gives insight into the group structure of fermionic SPT phases. First, we clarify the physical meaning behind composing finite depth circuits. Then, we give a physically motivated definition of equivalence for sets of supercohomology data. Lastly, we use this notion of equivalence to establish group supercohomology classes as topological invariants for lattice fermionic SPT Hamiltonians.

4.4.1 Stacking as composition of circuits

The additive group structure on the set of SPT phases is given by stacking. To stack two SPT Hamiltonians, let us imagine that they are defined on identical lattices extending in the x, y directions, and let us put one lattice directly over the other, i.e. separated in the z direction. Then, grouping pairs of vertically separated sites with the same x, y-coordinates into supersites, the sum of the two decoupled SPT Hamiltonians for the two layers defines another 2d gapped SPT Hamiltonian. This stacking operation respects the notion of phase equivalence and thus defines an additive structure on the set of SPT phases.

We can reinterpret the stacking operation as composition of finite depth circuits of local unitaries that create the corresponding SPT ground states from a product state. To see this, suppose that $\hat{U}$ and $\hat{U}'$ are two such circuits that act on identical Hilbert spaces made out of sites which form identical G-representations. The ground state of the stacked system is

$$\left(\hat{U} \otimes \hat{U}' \right) \left(|0\rangle \otimes |0\rangle' \right) = \left(\hat{U}|0\rangle \right) \otimes \left(\hat{U}'|0\rangle' \right). \tag{4.63}$$

Now let $\hat{V}$ be the unitary operator which exchanges the two layers. Note that $\hat{V}$ can be defined as a tensor product of finite dimensional unitaries acting on the individual supersites, where they just swap the two sites in each supersite. $\hat{V}$ clearly commutes with the action of the global symmetry, and we have

$$\hat{V}\left(\hat{U}\otimes 1\right)\hat{V}^{\dagger}\left(1\otimes\hat{U}'\right)\left(|0\rangle\otimes|0\rangle'\right)=\left(1\otimes\hat{U}\hat{U}'\right)\left(|0\rangle\otimes|0\rangle'\right)=|0\rangle\otimes\left(\hat{U}\hat{U}'|0\rangle'\right). \quad (4.64)$$

Hence (4.64) is equivalent to the state obtained by composing the two circuits. Notice, $\hat{V}$ can be continuously connected to the identity via a path in the space of symmetric finite depth circuits. To construct such a path, one just needs to find a path connecting the swap unitary to the identity for a single supersite and tensor these over all the supersites. For a single supersite, the problem is straightforward. This is because, in a finite dimensional Hilbert space, any symmetric unitary is connected to the identity through a path in the space of symmetric unitaries, as can be seen by breaking up the Hilbert space into irreducible representations of G and applying Schur's lemma.

We now use this equivalence between stacking and composing circuits to derive the stacking rule for our supercohomology SPT models. In particular, this will show that the supercohomology SPT phases form a closed subgroup under stacking.

4.4.2 Computation of stacking rules by composing circuits

Let (n,ν) and (n',ν') be two sets of supercohomology data. Further, denote the bosonic finite depth circuits obtained from (n,ν) and (n',ν') via our construction by $\hat{U}_{\mathrm{b}}^{n\nu}$ and $\hat{U}_{\mathrm{b}}^{n'\nu'}$, respectively. The composition of $\hat{U}_{\mathrm{b}}^{n\nu}$ with $\hat{U}_{\mathrm{b}}^{n'\nu'}$ yields a finite depth circuit corresponding to yet another set of supercohomology data. This can be seen by explicit computation. The product of $\hat{U}_{\mathrm{b}}^{n\nu}$ with $\hat{U}_{\mathrm{b}}^{n'\nu'}$ is

$$\hat{U}_{\mathrm{b}}^{n\nu}\hat{U}_{\mathrm{b}}^{n'\nu'}=\prod_{\langle pqr\rangle}\left(\hat{\nu}_{pqr}^{o_{pqr}}\hat{Z}_{pq}^{\hat{n}_{qr}}\right)\prod_{\langle pq\rangle}\hat{X}_{pq}^{\hat{n}_{pq}}\prod_{\langle pqr\rangle}\hat{W}_{pqr}^{\hat{n}_{pr}}\prod_{\langle pqr\rangle}\left(\hat{\nu}'^{o_{pqr}}_{pqr}\hat{Z}_{pq}^{\hat{n}'_{qr}}\right)\prod_{\langle pq\rangle}\hat{X}_{pq}^{\hat{n}'_{pq}}\prod_{\langle pqr\rangle}\hat{W}_{pqr}^{\hat{n}'_{pr}}. \quad (4.65)$$

To obtain an expression in the same form as $\hat{U}_{\rm b}$, and thus reveal the group structure of the fermionic circuits, we group similar terms. In doing so, the only non-trivial signs arise when we move

$$\prod_{\langle pqr\rangle} \hat{W}_{pqr}^{\hat{n}_{pr}} \text{ past } \prod_{\langle pq\rangle} \hat{X}_{pq}^{\hat{n}'_{pq}} \tag{4.66}$$

and

$$\prod_{\langle pqr\rangle} \hat{X}_{pq}^{\hat{n}_{pq}} \text{ past } \prod_{\langle pq\rangle} \hat{Z}_{pq}^{\hat{n}'_{qr}}. \tag{4.67}$$

Using $\delta n = 0$, we can write the resulting sign as:

$$\prod_{\langle pqr\rangle} (-1)^{\hat{n}_{pr}\hat{n}'_{pqr}+\hat{n}_{pq}\hat{n}'_{qr}}. \tag{4.68}$$

We then have

$$\hat{U}_{\rm b}^{n\nu}\hat{U}_{\rm b}^{n'\nu'} = \prod_{\langle pqr\rangle} \hat{\nu}_{pqr}^{o_{pqr}} \hat{\nu}'^{o_{pqr}}_{pqr} (-1)^{\hat{n}_{pr}\hat{n}'_{pqr}+\hat{n}_{pq}\hat{n}'_{qr}} \prod_{\langle pqr\rangle} \hat{Z}_{pq}^{\hat{n}_{qr}+\hat{n}'_{qr}} \prod_{\langle pq\rangle} \hat{X}_{pq}^{\hat{n}_{pq}+\hat{n}'_{pq}} \prod_{\langle pqr\rangle} \hat{W}_{pqr}^{\hat{n}_{pr}+\hat{n}'_{pr}}. \tag{4.69}$$

This is precisely the circuit $\hat{U}_{\rm b}$ formed from the input supercohomology data $(n + n', \nu\nu'(-1)^{n\cup_1 n'})$, where[6]

$$(n \cup_1 n')(g_p, g_q, g_r, 1) = n(g_p, g_r, 1)n'(g_p, g_q, g_r) + n(g_p, g_q, 1)n'(g_q, g_r, 1) \tag{4.72}$$

---

[6] As a reminder, the cup product $\cup$ between homogeneous functions $f : G^{\ell+1} \to A$ and $h : G^{k+1} \to A$ (for abelian group A) is

$$(f \cup h)(g_0, ..., g_{\ell+k-1}) = f(g_0, ..., g_\ell)h(g_\ell, ..., g_{\ell+k-1}). \tag{4.70}$$

The $\cup_1$ product of f and h is

$$(f \cup_1 h)(g_0, ..., g_{\ell+k-1}) = \sum_{i=0}^{\ell-1} f(g_0, ..., g_i, g_{k+i}, g_{\ell+k-1})h(g_i, ..., g_{k+i}). \tag{4.71}$$

agrees with the sign in (4.68) and (4.69).

Therefore, stacking the fermionic SPT phases corresponding to (n, ν) and (n', ν') results in the fermionic SPT phase corresponding to $(n + n', \nu\nu'(-1)^{n \cup_1 n'})$, or

$$(n, \nu) * (n', \nu') = (n + n', \nu\nu'(-1)^{n \cup_1 n'}) \tag{4.73}$$

with $*$ denoting the stacking operation. This is in accord with the supercohomology data group law found in Ref. [124] through continuum space-time methods.

4.4.3 Equivalence relation on supercohomology data

The stacking rules allow us to define a physically motivated notion of equivalence between two sets of supercohomology data, which agrees with the mathematical one given in e.g. Ref. [133]. We will say that two sets of supercohomology data are equivalent if the corresponding fermionic SPT Hamiltonians $\hat{H}_{\mathrm{f}}$, constructed in section 4.3.4, are in the same phase.

Consider the supercohomology data[7]

$$(n_0, \nu_0) = (\delta\beta, (-1)^{\beta \cup \delta\beta}\delta\omega), \tag{4.74}$$

where $\beta : G \times G \to \mathbb{Z}_2$ and $\omega : G \times G \times G \to U(1)$ are both homogeneous. We claim that this set of data gives a finite depth circuit $\hat{U}_{\mathrm{b}}^{n_0\nu_0}$ built from symmetric local unitaries (up to factors of $\hat{G}_p$), i.e. the fermionic SPT phase corresponding to this set of data is trivial [1]. In Appendix 4.F, we compute $\hat{U}_{\mathrm{b}}^{n_0\nu_0}$ in detail, and we simply state the result here:

$$\hat{U}_{\mathrm{b}}^{n_0\nu_0} = \prod_{\langle pqr \rangle} \hat{\omega}_{pqr}^{-o_{pqr}} (-1)^{\hat{\beta}_{pq}\hat{\beta}_{qr}} \prod_{\langle pqr \rangle} \hat{Z}_{pq}^{\hat{\beta}_{qr}} \prod_{\langle pq \rangle} \hat{X}_{pq}^{\hat{\beta}_{pq}} \prod_{\langle pqr \rangle} \hat{W}_{pqr}^{\hat{\beta}_{pr}} \prod_{p} \hat{G}_p^{\hat{\beta}_p}. \tag{4.75}$$

[7] See Appendix 5.A for the definition of the cup product $\cup$.

Above, $\hat{\omega}_{pqr}$, $\hat{\beta}_{pq}$, and $\hat{\beta}_p$ are defined by

$$\hat{\omega}_{pqr}|\{g_t\}\rangle = \omega(g_p, g_q, g_r)|\{g_t\}\rangle \tag{4.76}$$

$$\hat{\beta}_{pq}|\{g_t\}\rangle = \beta(g_p, g_q)|\{g_t\}\rangle \tag{4.77}$$

$$\hat{\beta}_{p}|\{g_t\}\rangle = \beta(g_p, 1)|\{g_t\}\rangle. \tag{4.78}$$

The local unitary operators in $\hat{U}_{\mathrm{b}}^{n_0\nu_0}$ (besides $\hat{G}_p^{\hat{\beta}_p}$) are then manifestly symmetric due to the homogeneity properties of β and ω. Fermionization maps $\hat{G}_p^{\hat{\beta}_p}$ to the identity, so the finite depth circuit $\hat{U}_{\mathrm{f}}^{n_0\nu_0}$ obtained from fermionization is indeed built from symmetric local unitaries. Hence, $\hat{U}_{\mathrm{f}}^{n_0\nu_0}$ applied to a trivial product state gives us a trivial SPT.

Stacking a trivial SPT phase leaves the system in the same phase. Therefore, composition of $\hat{U}_{\mathrm{b}}^{n_0\nu_0}$ with $\hat{U}_{\mathrm{b}}^{n\nu}$ should give us a circuit corresponding to some supercohomology data that is equivalent to (n, ν). According to the composition rules (4.73) in the previous subsection, the product $\hat{U}_{\mathrm{b}}^{n_0\nu_0}\hat{U}_{\mathrm{b}}^{n\nu}$ is the circuit corresponding to the supercohomology data[8]

$$\left(n + \delta\beta, \nu(-1)^{\beta\cup\delta\beta + n\cup\beta + \beta\cup n}\delta\left[\omega(-1)^{n\cup_1\beta}\right]\right). \tag{4.80}$$

$\omega(-1)^{n\cup_1\beta}$ in (4.80) is some homogeneous function, which we will denote as η, from $G\times G\times G$ to $U(1)$. Therefore, two sets of supercohomology data (n, ν) and (n', ν') are equivalent if there exists a homogeneous function $\beta : G \times G \to \mathbb{Z}_2$ and homogeneous function $\eta : G \times G \times G \to U(1)$ such that

$$\begin{aligned} n' &= n + \delta\beta \\ \nu' &= \nu(-1)^{\beta\cup\delta\beta + n\cup\beta + \beta\cup n}\delta\eta. \end{aligned} \tag{4.81}$$

---

[8]Here we use the definition of $\cup_1$ (see Appendix A of [133]) to write

$$n \cup_1 \delta\beta = n\cup\beta + \beta\cup n + \delta(n\cup_1\beta). \tag{4.79}$$

It can be checked that this is a symmetric and transitive relation, and hence defines an equivalence relation. In what follows, we will show that two sets of group supercohomology data that are inequivalent with respect to this relation necessarily give rise to distinct SPT phases.

4.4.4 Quantized invariants for fermionic SPT phases

We are now in a position to establish group supercohomology data as quantized invariants for fermionic SPT phases at the level of gapped lattice Hamiltonians. In the previous subsection, two sets of supercohomology data were said to be equivalent if they correspond to the same fermionic SPT phase. Therefore, we need only argue that inequivalent sets of supercohomology data necessarily correspond to distinct fermionic SPT phases.

Suppose (n', ν') and (n'', ν'') are inequivalent choices of group supercohomology data with respect to the equivalence relation (4.81). We will show that the corresponding models are in distinct SPT phases. First, we stack the phase corresponding to (n', ν') with the inverse of the phase corresponding to (n'', ν''). Then, using the fact that SPT phases form an abelian group under stacking, the two phases will be distinct if and only if

$$(n, \nu) \equiv (n', \nu') * (n'', \nu'')^{-1} \tag{4.82}$$

gives rise to a nontrivial fermionic SPT phase. In other words, we need to demonstrate that (n, ν) corresponds to a nontrivial phase whenever it is not of the form (4.74).

To show that the phase corresponding to (n, ν) is nontrivial, we bosonize it, i.e. reverse the fermionization procedure described above. This should simply return our bosonic shadow model. However, because the bosonization dictionary is many-to-one, in the sense that all the $\hat{G}_p$ operators map to the identity on the fermionic side, we have to define our bosonization procedure carefully to avoid ambiguities. We do this by dressing each local term on the bosonic side with a projector onto the $\hat{G}_p = 1$ Hilbert space everywhere in the vicinity of that term and by adding a term $-\sum_p \hat{G}_p$ to ensure that the ground state is in the $\hat{G}_p = 1$

subspace. It is important to note that this bosonization can be performed for any gapped fermionic Hamiltonian defined on our Hilbert space, not just on our specific fixed point model. Now, having mapped the fermionic SPT Hamiltonian corresponding to (n, ν) to a bosonic symmetry enriched toric code Hamiltonian, we look for quantized invariants of the symmetry enriched model that can then be pulled back to give fermionic SPT invariants.

If (n, ν) is nontrivial, i.e. not of the form (4.74), then there are two cases. The first is that n cannot be written in the form $n = \delta\beta$ for any choice of β (β defined below (4.74)). The second is that n can be written as $\delta\beta$, but ν is nontrivial (clarified below). We treat these cases in turn.

Case 1: Assume that n cannot be written as $\delta\beta$. Then, after bosonizing, we will show that the fermion parity flux excitations (e or m excitations of the bosonic shadow model) carry the nontrivial fractionalization class $n \in H^2(G, \mathbb{Z}_2)$. Starting with the ground state of the bosonic shadow model $|\Psi_{\mathrm{b}}\rangle$, we can create a pair of e excitations at some well separated vertices a and b by applying a string operator. From this state, a low energy Hilbert space $\mathcal{H}_{\mathrm{L}}$ is obtained by projecting onto fixed values of the G-spins g_a and g_b at vertices a and b, respectively. $\mathcal{H}_{\mathrm{L}}$ has dimension $|G|^2$, with a natural basis $\{|\Psi^{ee}_{\mathrm{b}}; g_a, g_b\rangle\}$. Explicitly,

$$|\Psi^{ee}_{\mathrm{b}}; g_a, g_b\rangle = \hat{U}^{n\nu}_{\mathrm{b}} |\Psi^{ee}_{\mathrm{t.c.}}; g_a, g_b\rangle, \tag{4.83}$$

where $|\Psi^{ee}_{\mathrm{t.c.}}; g_a, g_b\rangle$ is the toric code state consisting of two e excitations at a and b respectively, tensored with a trivial G-spin paramagnet on all vertices $p \neq a, b$ and G-spins at a and b fixed to g_a and g_b, respectively.

Letting $\hat{V}(g)$ be the global on-site symmetry operator corresponding to the group element g, we now compute $\hat{V}(g)|\Psi^{ee}_{\mathrm{b}}; g_a, g_b\rangle$:

$$\hat{V}(g)|\Psi^{ee}_{\mathrm{b}}; g_a, g_b\rangle = \hat{V}(g)\hat{U}^{n\nu}_{\mathrm{b}} |\Psi^{ee}_{\mathrm{t.c.}}; g_a, g_b\rangle. \tag{4.84}$$

Using the fact (proved in Appendix 4.B) that $\hat{U}_{\mathrm{b}}^{n\nu}$ is symmetric up to factors of $\hat{G}_p$:

$$\hat{V}(g)\hat{U}_{\mathrm{b}}^{n\nu} = \hat{U}_{\mathrm{b}}^{n\nu}\prod_p \hat{G}_p^{\hat{n}_p^g}\hat{V}(g), \tag{4.85}$$

where $\hat{n}_p^g$ is defined by

$$\hat{n}_p^g|\{g_t\}\rangle = n(g_p, 1, g)|\{g_t\}\rangle, \tag{4.86}$$

we have

$$\begin{aligned}\hat{V}(g)|\Psi_{\mathrm{b}}^{ee}; g_a, g_b\rangle = \hat{U}_{\mathrm{b}}^{n\nu}\prod_p \hat{G}_p^{\hat{n}_p^g}|\Psi_{\mathrm{t.c.}}^{ee}; gg_a, gg_b\rangle = \hat{U}_{\mathrm{b}}^{n\nu}(-1)^{\hat{n}_a^g}(-1)^{\hat{n}_b^g}|\Psi_{\mathrm{t.c.}}^{ee}; gg_a, gg_b\rangle \\ = (-1)^{n(gg_a,1,g)+n(gg_b,1,g)}|\Psi_{\mathrm{b}}^{ee}; gg_a, gg_b\rangle.\end{aligned} \tag{4.87}$$

Focusing on just the a vertex, we see from (4.87) that the local effective action of $\hat{V}(g)$ near a is given by the operator:

$$\hat{V}_a(g)|\Psi_{\mathrm{b}}^{ee}; g_a, g_b\rangle = (-1)^{n(gg_a,1,g)}|\Psi_{\mathrm{b}}^{ee}; gg_a, g_b\rangle. \tag{4.88}$$

With $\hat{V}_b(g)$ defined analogously, we recover $\hat{V}_a(g)\hat{V}_b(g) = \hat{V}(g)$, as required. Note that there is a g dependent sign ambiguity in the definition of this local effective action. (A possible phase ambiguity is restricted to just an ambiguity in sign by the $\mathbb{Z}_2$ fusion rules of the e excitations [130, 136].)

The fractionalization class captures the failure of the symmetry group law to be satisfied by the effective symmetry action on a single anyon. To compute this fractionalization class, we therefore compute the phase difference between $\hat{V}_a(g)\hat{V}_a(h)$ and $\hat{V}_a(gh)$. For $\hat{V}_a(g)\hat{V}_a(h)$, we have

$$\begin{aligned}\hat{V}_a(g)\hat{V}_a(h)|\Psi_{\mathrm{b}}^{ee}; g_a, g_b\rangle &= \hat{V}_a(g)(-1)^{n(hg_a,1,h)}|\Psi_{\mathrm{b}}^{ee}; hg_a, g_b\rangle \\ &= (-1)^{n(ghg_a,1,g)+n(hg_a,1,h)}|\Psi_{\mathrm{b}}^{ee}; ghg_a, g_b\rangle,\end{aligned} \tag{4.89}$$

while for $\hat{V}_a(gh)$, we have

$$\hat{V}_a(gh)|\Psi_{\mathrm{b}}^{ee}; g_a, g_b\rangle = (-1)^{n(ghg_a,1,gh)}|\Psi_{\mathrm{b}}^{ee}; ghg_a, g_b\rangle. \tag{4.90}$$

Using $\delta n = 0$ and the homogeneity of n, we see that the difference in sign between the far right hand side of (4.89) and the right hand side of (4.90) is precisely $(-1)^{n(1,g,gh)}$. Thus, the fractionalization class of the local symmetry action is indeed given by n. Accounting for the g dependent sign ambiguity in the local symmetry action noted just below (4.88), one can show [46, 130, 136] that the symmetry fractionalization is well defined with $n \in H^2(G, \mathbb{Z}_2)$.

The nontrivial symmetry action on the fermion parity fluxes indicates that the bosonic shadow model corresponding to (n, ν) is in a nontrivial symmetry enriched phase [128, 136]. Pulling back via bosonization, this implies that the fermionic SPT corresponding to (n, ν) is nontrivial. Hence, the fermionic SPT phases given by (n', ν') and (n'', ν'') are distinct.

Alternatively, the nontrivial symmetry fractionalization can be seen more informally by recalling that the shadow model comes from gauging the $\mathbb{Z}_2$ subgroup of $\tilde{G}$, with $\tilde{G}$ the $\mathbb{Z}_2$-extension of G determined by n. Therefore, the G group law relations close only modulo a $\mathbb{Z}_2$ gauge transformation, and the fermion parity flux, being charged under this gauged $\mathbb{Z}_2$, acquires minus signs corresponding to the fractionalization class n when acted on by global G symmetry.

Case 2: Now, suppose instead that n is trivial, i.e. $n = \delta\beta$. Then using the equivalence relation (4.81), we can 'gauge' n away entirely, so that the supercohomology data (n, ν) is equivalent to $(0, \tilde{\nu})$, with $\delta\tilde{\nu} = 0$. For $(0, \tilde{\nu})$ to be nontrivial, it must be that there does not exist an ω (as defined below (4.74)) such that $\delta\omega = \tilde{\nu}$. That is to say, $\tilde{\nu}$ must be nontrivial in $H^3(G, U(1))$.

The fixed point fermionic circuit $\hat{U}_{\mathrm{f}}^{0\tilde{\nu}}$ corresponding to $(0, \tilde{\nu})$ acts trivially on the fermionic degrees of freedom, whereas the portion of it that acts on the bosonic G-spin degrees of freedom is precisely the circuit that constructs a group cohomology SPT ground state from a trivial product state [49]. To see that this system is nontrivial as a fermionic SPT, we

bosonize the system. The result is a trivial toric code phase stacked with the bosonic group cohomology phase corresponding to $\tilde{\nu}$. This symmetry enriched toric code is precisely what one obtains from gauging the $\mathbb{Z}_2$ subgroup of $G \times \mathbb{Z}_2$ in the ordinary bosonic SPT of $G \times \mathbb{Z}_2$ with cocycle $\tilde{\nu} \otimes 1$. $\tilde{\nu} \otimes 1$ is nontrivial in $H^3(G \times \mathbb{Z}_2, U(1))$ by Künneth's theorem [150] and the assumption that $\tilde{\nu}$ is nontrivial.

We have thus shown that (4.81) generates the maximal possible set of equivalence relations on supercohomology data, with inequivalent data necessarily giving rise to distinct phases. A subtle point is that the fermionic phases corresponding to inequivalent sets of supercohomology data (n', ν') and (n'', ν'') might still bosonize into the same symmetry enriched toric code phase [128]. Hence, it was important in the above argument to bosonize the model corresponding to $(n', \nu') * (n'', \nu'')^{-1}$, rather than bosonizing those corresponding to (n', ν') and (n'', ν'') individually. This subtlety arises in the the $G = \mathbb{Z}_2$ example, which we discuss below.

4.4.5 Example: $G = \mathbb{Z}_2$

For $G = \mathbb{Z}_2$, we have

$$\hat{U}^{\pm}_{\mathrm{b}} = \prod_{\langle pqr \rangle} (\pm i)^{o_{pqr} \hat{s}_p (1-\hat{s}_q) \hat{s}_r} \hat{Z}_{pq}^{(1-\hat{s}_q)\hat{s}_r} \prod_{\langle pq \rangle} \hat{X}_{pq}^{(1-\hat{s}_p)\hat{s}_q} \prod_{\langle pqr \rangle} \hat{W}_{pqr}^{(1-\hat{s}_p)\hat{s}_r}. \tag{4.91}$$

Let us square this circuit. Then the sign in (4.68) is just $+1$, so that, according to (4.69), we get

$$\left(\hat{U}^{\pm}_{\mathrm{b}}\right)^2 = \prod_{\langle pqr \rangle} \hat{\nu}^2_{pqr}. \tag{4.92}$$

But $\hat{\nu}^2_{pqr} = (-1)^{\hat{s}_p(1-\hat{s}_q)\hat{s}_r}$ is just the nontrivial cocycle in $H^3(\mathbb{Z}_2, U(1))$ evaluated on $(s_p, s_q, s_r, 0)$. Therefore the circuit $\left(\hat{U}^{\pm}_{\mathrm{b}}\right)^2$ builds the nontrivial bosonic $\mathbb{Z}_2$ SPT [49, 71]. Thus, stacking two identical copies of either the $+$ or $-$ group supercohomology phase results in the nontrivial bosonic $\mathbb{Z}_2$ SPT phase, and in this sense, these group supercohomology

phases are 'square roots' of the bosonic phase.

Note that bosonizing the + and − phases actually results in the same symmetry enriched topological order. Indeed, after gauging the $\mathbb{Z}_2$ global symmetry, the resulting twisted $\mathbb{Z}_4$ topological orders are the same. This can be seen from the fact that both can be obtained by gauging $\mathbb{Z}_4$ in the corresponding auxiliary $\mathbb{Z}_4$ bosonic SPTs, and the 3-cocycles defining these SPTs differ by the generator of $H^3(\mathbb{Z}_2, U(1))$ pulled back to $H^3(\mathbb{Z}_4, U(1))$, which is trivial. Thus, the + and − phases cannot be distinguished in this simple way; nevertheless, we know they correspond to distinct fermionic SPT phases by the argument in the previous section.

4.5 Discussion

We have shown how to use group supercohomology data (n, ν), together with a choice of spin structure on a 2d oriented manifold M, to construct a corresponding lattice fermionic SPT Hamiltonian on M. Our procedure cleanly disentangles the roles of the supercohomology data and spin structure. The former is used to build a bosonic 'shadow' model, and the latter to fermionize this model. Another advantage of our procedure is that it explicitly builds the finite depth circuit of local unitaries $\hat{U}_{\mathrm{f}}$ that creates the desired fermionic SPT ground state from a product state. Our SPT Hamiltonian is then

$$\hat{H}_{\mathrm{f}} = \hat{U}_{\mathrm{f}} \hat{H}^0_{\mathrm{f}} \hat{U}^\dagger_{\mathrm{f}}, \tag{4.93}$$

where $\hat{H}^0_{\mathrm{f}}$ is the trivial fermionic Hamiltonian - an atomic insulator tensored with a trivial G-spin paramagnet whose ground state is a product state with zero fermion occupancy. Key to this approach is the fact that the circuit $\hat{U}_{\mathrm{f}}$ is G-symmetric. This is the case despite the fact that the individual local unitaries that make up the circuit cannot all be G-symmetric, for otherwise the fermionic SPT would be trivial. Note that while we have assumed that the global action of G is unitary, we expect our construction to generalize to anti-unitary symmetries with only minor modifications.

Our commuting projector Hamiltonians suffice to show that the supercohomology phases protected by abelian groups [151] can be many-body localized. The couplings in the Hamiltonian[9] $\hat{H}_{\mathrm{f}}^{0}$ can be disordered (or made quasi-periodic), leading to a many-body localized Hamiltonian [141–145], or at least one that has a long thermalization time scale. Since $\hat{H}_{\mathrm{f}}$ is just the conjugate of $\hat{H}_{\mathrm{f}}^{0}$ by a finite depth circuit, the same is true of $\hat{H}_{\mathrm{f}}$.

The fermionization duality that was used to construct our zero correlation length lattice models can also be reversed and used to bosonize fermionic SPT Hamiltonians. This, together with a reinterpretation of the stacking structure of SPT phases in terms of composition of the corresponding finite depth circuits, allows well established invariants of the bosonic symmetry enriched toric code to be pulled back to these fermionic SPT Hamiltonians. The result is a classification of fermionic supercohomology SPT phases, with inequivalent supercohomology data necessarily defining distinct phases.

One may ask whether a similar construction is possible for the so-called beyond supercohomology phases [124, 127–129, 133, 152] in $2+1$D. That is, for these phases, can an exactly solvable model be obtained by conjugating a trivial fermionic Hamiltonian by a symmetric finite depth circuit of local unitaries? We argue that, in contrast to the supercohomology phases, the answer is no. In particular, we claim that the ground states of beyond supercohomology phases cannot be constructed from a trivial product state by applying a globally symmetric finite depth circuit of local unitaries. See Appendix 4.G for further discussion.

It is worth discussing the relation of our work to previous work. Supercohomology models were introduced in the pioneering work of Ref. [126], where wave functions for these models were written from a lattice path integral. However, the wave functions were only explicitly constructed on a specific planar lattice and required seemingly arbitrary choices to account for a spin structure. In Ref. [132], a related wave function, for the so-called fermionic toric code, was written down; this is the topological order that would result from gauging the global $\mathbb{Z}_2$ in our $G = \mathbb{Z}_2$ models. The ground states were defined by graphical rules, but

[9] Strictly speaking, the argument holds for a slightly modified $\hat{H}_{\mathrm{f}}^{0}$ (see appendix A of Ref. [145]).

again, the spin structure was encoded in these rules in a non-manifest way. The roles of the spin structure and group supercohomology data were disentangled in Ref. [125], but only in a lattice spacetime formalism. Ref. [124] extended this to beyond-supercohomology models, and also made the connection between the supercohomology data and the algebraic data defining the shadow models. Insofar as lattice Hamiltonians, Refs. [152], [131] clarified the role of spin structure in beyond-supercohomology models, and Ref. [129] extended this to include supercohomology models; however, Ref. [129] did not write down explicit Hamiltonians, but rather defined the ground states implicitly using certain self-consistent lattice-deforming local rules. The present work builds on these developments by constructing explicit Hamiltonians, as well as building the ground states explicitly using finite depth circuits, on oriented $2d$ manifolds of any topology. It uses in an essential way the 2+1D bosonization duality introduced in Ref. [15].

There are many possible avenues for future work. One would be to extend this formalism to group supercohomology models in three spatial dimensions. Another avenue is to extend the present formalism to more complicated groups than $G \times \mathbb{Z}_2^{\mathrm{f}}$, such as ones where the fermion parity symmetry forms a nontrivial subgroup of the overall symmetry. Yet another possibility is to extend the quantum circuit formalism to beyond-supercohomology models, both in two and three spatial dimensions. It may also be fruitful to understand our work in terms of tensor network states and operators. Indeed, preliminary investigations suggest that the bosonization duality can naturally be interpreted as a tensor network operator. It would then be nice to understand the relation between the present work and the fermionic models written down in Ref. [116]. Futher, our finite depth circuits could be used to study the edge theories of these fermionic SPT phases. Finally, it would be interesting to study the classification of symmetry enriched phases using finite depth circuits applied to the ground states of fixed point Hamiltonians. The circuits $\hat{U}_{\mathrm{b}}$, introduced in section 4.2.4, construct ground states of symmetry enriched toric code phases from a trivial toric code state, and thus provide a nontrivial realization of such a construction.

Appendices

4.A Derivation of the bosonic shadow theory ground state

In this appendix, we provide a derivation of the bosonic shadow theory ground state Ψ_{b} introduced in section 4.2.3. Recall that the first step of the construction is to form an auxiliary $\tilde{G}$ bosonic SPT from a choice of normalized supercohomology data (n,ν), where $\tilde{G}$ is a $\mathbb{Z}_2$ extension of G by n. The next step is to 'gauge' the $\mathbb{Z}_2$ subgroup of $\tilde{G}$ in the standard way by minimally coupling the SPT Hamiltonian to a $\mathbb{Z}_2$ gauge field. We will implement this procedure explicitly and argue that the symmetry enriched Hamiltonian obtained from this procedure - which we refer to as the 'standard' symmetry enriched Hamiltonian - can in principle be fermionized since it commutes with the modified Gauss's law $\hat{G}_p$ for all p.

4.A.1 Gauging the $\mathbb{Z}_2 \subset \tilde{G}$

As stated in (4.12), the auxiliary $\tilde{G}$ SPT ground state wave function in the configuration basis is

$$\Psi_{\mathrm{SPT}}\left(\left\{g_p^{(m_p)}\right\}\right) = \prod_{\langle pqr\rangle} \alpha\left(g_p^{(m_p)}, g_q^{(m_q)}, g_r^{(m_r)}, 1\right)^{o_{pqr}}. \tag{4.94}$$

(Recall that α can be expressed in terms of n, ν, and ϵ using (4.13).) A simple Hamiltonian $\hat{H}_{SPT}$ with this ground state is

$$\hat{H}_{SPT} = -\hat{U}_{\mathrm{SPT}} \left(\sum_p \hat{\tilde{P}}_p^{\mathrm{sym}}\right) \hat{U}_{\mathrm{SPT}}^{\dagger} \tag{4.95}$$

where $\hat{U}_{\mathrm{SPT}}$ is the finite depth circuit of local unitaries defined by matrix elements

$$\left\langle \left\{h_p^{(\ell_p)}\right\} \middle| \hat{U}_{\mathrm{SPT}} \middle| \left\{g_p^{(m_p)}\right\}\right\rangle = \delta_{\left\{h_p^{(\ell_p)}\right\},\left\{g_p^{(m_p)}\right\}} \prod_{\langle pqr\rangle} \alpha\left(g_p^{(m_p)}, g_q^{(m_q)}, g_r^{(m_r)}, 1\right)^{o_{pqr}}, \tag{4.96}$$

and $\hat{\tilde{P}}_p^{\text{sym}}$ is the projector onto the symmetric state at vertex p

$$\frac{1}{\sqrt{|\tilde{G}|}} \sum_{g_p^{(m_p)} \in \tilde{G}} \left| g_p^{(m_p)} \right\rangle \tag{4.97}$$

tensored with the identity on the remaining sites.

We gauge the $\mathbb{Z}_2$ subgroup of $\tilde{G}$ using the usual algorithm as described in Ref. [71] and Ref. [153]. First, we introduce at each link $\langle pq \rangle$ a spin-$\frac{1}{2}$ Hilbert space with Pauli operators μ_{pq}^x and μ_{pq}^z, and at all sites p, impose the gauge constraint

$$\prod_{\langle st \rangle \ni p} \hat{\mu}_{st}^x = \hat{e}_p^{\mathbb{Z}_2}. \tag{4.98}$$

Here, the product runs over all links starting or ending on p, and $\hat{e}_p^{\mathbb{Z}_2}$ is the operator that on vertex p takes

$$\left| g_p^{(m_p)} \right\rangle \to \left| g_p^{(m_p+1)} \right\rangle \tag{4.99}$$

and acts as the identity on all other sites. In other words, the action of $\hat{e}_p^{\mathbb{Z}_2}$ in the configuration basis is multiplication by the generator of the $\mathbb{Z}_2$ subgroup, $1^{(1)}$, with the assumption that n is normalized.

Second, we minimally couple each term in (4.95) to the $\mathbb{Z}_2$ gauge field degrees of freedom. In order to make this gauging procedure unambiguous, we multiply each term by a projector onto trivial $\mathbb{Z}_2$ flux on triangles in the vicinity of that term, and add the term

$$-J \sum_{\langle pqr \rangle} \hat{\mu}_{pq}^z \hat{\mu}_{qr}^z \hat{\mu}_{pr}^z \tag{4.100}$$

with J large enough to ensure that the ground state is in the trivial $\mathbb{Z}_2$ flux sector. The result is a Hamiltonian $\hat{H}_{\text{gauged}}$ which is invariant under the gauge constraints in (4.98).

A ground state of $\hat{H}_{\text{gauged}}$ can be written as

$$\Psi_{\text{gauged}}\left(\{g_p^{(m_p)}\},\{\mu^z_{pq}\}\right) = \prod_{\langle pqr\rangle} \nu(g_p,g_q,g_r,1)^{o_{pqr}} \left(\mu^z_{pq}(-1)^{\epsilon\left(\left(g_p^{(m_p)}\right)^{-1} g_q^{(m_q)}\right)}\right)^{n(g_q,g_r,1)} \times \left(\prod_{\langle pqr\rangle} \delta_{W'_{pqr},1}\right) h(\{\mu^z_{pq}\}). \quad (4.101)$$

The function h determines the holonomy of the particular ground state. The ground state with trivial holonomy, for example, is obtained with the choice of h:

$$h(\{\mu^z_{pq}\}) = \begin{cases} 1 & \text{if } \{\mu^z_{pq}\} \sim \{\mu^z_{pq} = +1\} \\ 0 & \text{otherwise} \end{cases} \quad (4.102)$$

where $\sim$ means 'gauge equivalent to'. For the ground states with nontrivial holonomy, h is defined similarly.

The δ function in (4.101) is a consequence of the flux penalizing term in the gauging procedure. The μ^z-flux is

$$W'_{pqr} = \mu^z_{pq}\mu^z_{qr}\mu^z_{pr}, \quad (4.103)$$

so the delta function

$$\delta_{W'_{pqr},1} = \begin{cases} 1 & \text{if } W'_{pqr} = 1 \\ 0 & \text{otherwise} \end{cases} \quad (4.104)$$

ensures that all configurations in the ground states have trivial μ^z-flux.

In going from (4.94) to (4.101), we have also multiplied $(-1)^{\epsilon\left(\left(g_p^{(m_p)}\right)^{-1} g_q^{(m_q)}\right)}$ by μ^z_{pq}. This guarantees that Ψ_{gauged} is gauge invariant and reduces to Ψ_{SPT} when all $\mu^z_{pq} = +1$.

4.A.2 Mapping to unconstrained variables

To obtain Ψ_{b} as expressed in section 4.2.3, we must rewrite the system in terms of unconstrained variables. To this end, we define an isomorphism of operator algebras below. This isomorphism will allow us to convert $\hat{H}_{\text{gauged}}$ into $\hat{H}'_{\mathrm{b}}$, a Hamiltonian acting on an unconstrained Hilbert space with ground state Ψ_{b}. On one side of the isomorphism, we have the algebra $\mathcal{A}_{\text{constrained}}$ appearing in the previous subsection and consisting of gauge invariant operators, modulo the Gauss's law relation. On the other side of the isomorphism, we have $\mathcal{A}_{\text{unconstrained}}$, an operator algebra naturally represented on a tensor product Hilbert space with degrees of freedom matching those of the bosonic shadow theory. We now define $\mathcal{A}_{\text{constrained}}$ and $\mathcal{A}_{\text{unconstrained}}$ more carefully and write an explicit isomorphism between the two algebras.

Algebra of constrained operators $\mathcal{A}_{constrained}$

$\mathcal{A}_{\text{constrained}}$ admits a representation on the Hilbert space discussed in the previous subsection, i.e. $\tilde{G}$ degrees of freedom on vertices and spin-$\frac{1}{2}$ degrees of freedom on links. It can generated by $\hat{e}_p^{\mathbb{Z}_2}$, $\hat{g}_p^{(0)}$, $\hat{\tilde{P}}_p^g$, $\hat{\mu}_{pq}^x$, and $(-1)^{\hat{\epsilon}_{pq}}\hat{\mu}_{pq}^z$ obeying the relation

$$\prod_{\langle st\rangle \ni p} \hat{\mu}_{st}^x = \hat{e}_p^{\mathbb{Z}_2} \tag{4.105}$$

for all p. Here, $\hat{g}_p^{(0)}$ and $\hat{\tilde{P}}_p^g$ are the defined by their action on a configuration state:

$$\hat{g}_p^{(0)} \left| h_p^{(\ell_p)} \right\rangle = \left| (gh)_p^{(\ell_p)} \right\rangle \tag{4.106}$$

and

$$\hat{\tilde{P}}_p^g \left| \left\{ h_q^{(\ell_q)} \right\} \right\rangle = \delta_{g_p, h_p} \left| \left\{ h_q^{(\ell_q)} \right\} \right\rangle. \tag{4.107}$$

In words, $\hat{g}_p^{(0)}$ is the operator that multiplies by $g^{(0)}$ at vertex p and acts as the identity elsewhere, while $\hat{\hat{P}}_p^g$ is the projector onto the subspace spanned by states with configuration $g^{(0)}$ or $g^{(1)}$ at vertex p.

Finally, $\hat{\epsilon}_{pq}$, appearing in the generator $(-1)^{\hat{\epsilon}_{pq}}\hat{\mu}_{pq}^z$, is given by

$$\hat{\epsilon}_{pq}\big|\{g_r^{(m_r)}\}\big\rangle = \epsilon\big(\big(g_p^{(m_p)}\big)^{-1} g_q^{(m_q)}\big)\big|\{g_r^{(m_r)}\}\big\rangle. \tag{4.108}$$

It can be checked that products of $\hat{g}_p^{(0)}$, $\hat{\hat{P}}_p^g$ $\hat{\mu}_{pq}^x$, and $(-1)^{\hat{\epsilon}_{pq}}\hat{\mu}_{pq}^z$ span all gauge invariant operators.

Algebra of unconstrained operators $\mathcal{A}_{unconstrained}$

We will represent $\mathcal{A}_{\text{unconstrained}}$ on a tensor product Hilbert space comprised of G degrees of freedom $|g_p\rangle$ on vertices and spin-$\frac{1}{2}$ degrees of freedom on links. The generators of this operator algebra acting on vertex Hilbert spaces are $\hat{g}_p$ and $\hat{P}_p^g$ defined by

$$\hat{g}_p|h_p\rangle = |(gh)_p\rangle \tag{4.109}$$

and

$$\hat{P}_p^g|\{h_q\}\rangle = \delta_{g_p,h_p}|\{h_q\}\rangle. \tag{4.110}$$

We take generators acting on the link Hilbert spaces to be the Pauli operators $\hat{X}_{pq}$ and $\hat{Z}_{pq}$.

Isomorphism of $\mathcal{A}_{constrained}$ with $\mathcal{A}_{unconstrained}$

An isomorphism of $\mathcal{A}_{\text{constrained}}$ with $\mathcal{A}_{\text{unconstrained}}$ is given by the map of generators:

$$\begin{aligned}
\hat{e}_p^{\mathbb{Z}_2} &\longleftrightarrow \prod_{\langle st\rangle \ni p} \hat{X}_{st} \\
\hat{g}_p^{(0)} &\longleftrightarrow \hat{g}_p \prod_{\substack{\langle tq\rangle \\ t=p}} \hat{X}_{tq}^{\hat{\xi}_{tq}^{g_p}} \prod_{\substack{\langle qt\rangle \\ t=p}} \hat{X}_{qt}^{\hat{\xi}_{qt}^{g_p}} \\
\hat{\hat{P}}_p^g &\longleftrightarrow \hat{P}_p^g \\
\hat{\mu}_{pq}^x &\longleftrightarrow \hat{X}_{pq} \\
(-1)^{\hat{\epsilon}_{pq}} \hat{\mu}_{pq}^z &\longleftrightarrow \hat{Z}_{pq}
\end{aligned} \tag{4.111}$$

where $\hat{\xi}_{pq}^{g_p}$ and $\hat{\xi}_{qp}^{g_p}$ are defined by

$$\hat{g}_p^{(0)}(-1)^{\hat{\epsilon}_{pq}} = (-1)^{\hat{\xi}_{pq}^{g_p}}(-1)^{\hat{\epsilon}_{pq}}\hat{g}_p^{(0)} \tag{4.112}$$

and

$$\hat{g}_p^{(0)}(-1)^{\hat{\epsilon}_{qp}} = (-1)^{\hat{\xi}_{qp}^{g_p}}(-1)^{\hat{\epsilon}_{qp}}\hat{g}_p^{(0)}. \tag{4.113}$$

Explicitly, $\hat{\xi}_{pq}^{g_p}$ and $\hat{\xi}_{qp}^{g_p}$ act on configuration states as

$$\hat{\xi}_{pq}^{g_p}|\{h_t\}\rangle = (n(1, h_p, h_q) + n(1, g_p, g_p h_p) + n(1, g_p h_p, h_q))|\{h_t\}\rangle \tag{4.114}$$

and

$$\hat{\xi}_{qp}^{g_p}|\{h_t\}\rangle = (n(1, h_q, h_p) + n(1, g_p, g_p h_p) + n(1, h_q, g_p h_p))|\{h_t\}\rangle. \tag{4.115}$$

$\hat{\xi}_{pq}^{g_p}$ and $\hat{\xi}_{qp}^{g_p}$ defined in this way ensure that the commutation relations exhibited by $\hat{g}_p^{(0)}$ and $(-1)^{\hat{\epsilon}_{pq}}\hat{\mu}_{pq}^z$ are mirrored on the right hand side of the mapping (4.111). Note that the

isomorphism is well defined since, for all p, the relation

$$\prod_{\langle st\rangle \ni p} \hat{\mu}^x_{st} = \hat{e}^{\mathbb{Z}_2}_p \tag{4.116}$$

is mapped to the identity.

Now, given a system described in terms of the operators in $\mathcal{A}_{\text{constrained}}$, one can rewrite it as a system in terms of the operators belonging to $\mathcal{A}_{\text{unconstrained}}$. In particular, we can apply this isomorphism to $\hat{H}_{\text{gauged}}$ to obtain $\hat{H}'_{\text{b}}$ acting on an unconstrained Hilbert space. $\hat{H}'_{\text{b}}$ has the ground state

$$\Psi_{\text{b}}(\{g_p\},\{Z_{pq}\}) = \prod_{\langle pqr\rangle} \nu^{o_{pqr}}(g_p,g_q,g_r,1) Z_{pq}^{n(g_q,g_r,1)} \times \left(\prod_{\langle pqr\rangle} \delta_{W_{pqr},(-1)^{n(g_p,g_q,g_r)}}\right) h(\{Z_{pq}(-1)^{n(1,g_p,g_q)}\}), \tag{4.117}$$

which is precisely the ground state of the bosonic shadow theory identified in section 4.2.3.

4.A.3 Fermionizability of 'standard' Hamiltonian

To conclude this appendix, we prove that $\hat{H}'_{\text{b}}$ is fermionizable, i.e. $\hat{H}'_{\text{b}}$ commutes with the modified Gauss's law $\hat{G}_p$ for all sites p. To do this, we first note that $\hat{H}_{\text{SPT}}$ in (4.95) commutes with

$$\hat{U}_{\text{SPT}} \hat{e}^{\mathbb{Z}_2}_p \hat{U}^\dagger_{\text{SPT}} \tag{4.118}$$

which follows simply from the fact that $\hat{e}^{\mathbb{Z}_2}_p$ commutes with $\hat{P}^{\text{sym}}_p$. After gauging the $\mathbb{Z}_2$ subgroup of $\tilde{G}$, $\hat{H}'_{\text{b}}$ must commute with the gauged version of (4.118), which, using the

definition of α along with $\delta n = 0$ we find to be equal to

$$\prod_{\substack{\langle tqr\rangle \\ t=p}} (-1)^{\hat{n}_{pqr}} \prod_{\langle st\rangle \ni p} \hat{X}_{st}. \tag{4.119}$$

Next, we see that (4.100), the term penalizing μ^z-flux in triangle $\langle pqr\rangle$, turns into

$$J(-1)^{\hat{n}_{pqr}} \hat{Z}_{pq}\hat{Z}_{qr}\hat{Z}_{pr}. \tag{4.120}$$

when written in terms of the unconstrained variables (here we used the definition of the group law of $\tilde{G}$ to simplify the expression).

Then, multiplying the operator in (4.119) by the product of the terms in (4.120) over all triangles whose first vertex is p yields an operator proportional to

$$\prod_{\substack{\langle tqr\rangle \\ t=p}} \hat{W}_{tqr} \prod_{\langle st\rangle \ni p} \hat{X}_{st}, \tag{4.121}$$

which is just $\hat{G}_p$, as defined in (4.3). Since the Hamiltonian $\hat{H}'_{\mathrm{b}}$ commutes with both (4.120) and (4.119), it must commute with $\hat{G}_p$ as well. Thus $\hat{H}'_{\mathrm{b}}$ is fermionizable. However, explicitly fermionizing it is unwieldy in general, as we do not have an explicit expression for it in terms of the modified Gauss's law invariant operators $\hat{W}_{pqr}$ and $\hat{U}_{pq}$. For this reason, we constructed and worked with the parent Hamiltonian $\hat{H}_{\mathrm{b}}$ in section 4.2.4 instead.

4.B Symmetry of the shadow model Hamiltonian

In this appendix we prove that $\hat{H}_{\mathrm{b}}$ is G-symmetric, as claimed in section 4.2.4. It follows that the fermionic SPT Hamiltonian $\hat{H}_{\mathrm{f}}$ constructed in section 4.3.4 is also G-symmetric, since the fermionization procedure commutes with the global G-symmetry action. Concretely, letting

$\hat{V}(g)$ be the global symmetry operator representing $g \in G$ and acting as

$$|g_p\rangle \to |g g_p\rangle \tag{4.122}$$

on every vertex degree of freedom, we will show that $\hat{V}(g)$ commutes with $\hat{H}_{\rm b}$.

Recall that

$$\hat{H}_{\rm b} = \hat{U}_{\rm b} \hat{H}^0_{\rm b} \hat{U}^\dagger_{\rm b} \tag{4.123}$$

so that

$$\hat{V}(g) \hat{H}_{\rm b} \hat{V}^\dagger(g) = \left(\hat{V}(g) \hat{U}_{\rm b} \hat{V}^\dagger(g) \right) \hat{H}^0_{\rm b} \left(\hat{V}(g) \hat{U}^\dagger_{\rm b} \hat{V}^\dagger(g) \right) \tag{4.124}$$

where we have used that $\hat{H}^0_{\rm b}$ is symmetric.

Let us now compute $\hat{V}(g) \hat{U}_{\rm b} \hat{V}^\dagger(g)$. In (4.22), $\hat{U}_{\rm b}$ was defined as

$$\hat{U}_{\rm b} = \prod_{\langle pqr \rangle} \left(\hat{\nu}^{o_{pqr}}_{pqr} \hat{Z}^{\hat{n}_{qr}}_{pq} \right) \prod_{\langle pq \rangle} \hat{X}^{\hat{n}_{pq}}_{pq} \prod_{\langle pqr \rangle} \hat{W}^{\hat{n}_{pr}}_{pqr}, \tag{4.125}$$

with the operators $\hat{\nu}^{o_{pqr}}_{pqr}$ and $\hat{n}_{pr}$ defined just below (4.22). To proceed, it is useful to first re-express $\hat{U}_{\rm b}$ in terms of the generators of the bosonic algebra $\mathcal{A}_{\rm bos}$. Following (4.47), the result is

$$\hat{U}_{\rm b} = \hat{\kappa} \prod_{\langle pq \rangle} \hat{U}^{\hat{n}_{pq}}_{pq} \prod_{\langle pqr \rangle} \hat{W}^{\hat{n}_{pr}}_{pqr}. \tag{4.126}$$

Here, κ is a unitary operator that acts as multiplication by a $\{|g_p\rangle\}$-dependent eigenvalue and whose explicit form will not be required.

Conjugating by $\hat{V}(g)$ gives

$$\hat{V}(g)\hat{U}_{\rm b}\hat{V}^{\dagger}(g) = \hat{\phi}\hat{\kappa}\prod_{\langle pq\rangle}\hat{U}_{pq}^{\hat{n}^g_{pq}}\prod_{\langle pqr\rangle}\hat{W}_{pqr}^{\hat{n}^g_{pr}}. \tag{4.127}$$

Here $\hat{\phi}$ and $\hat{n}^g_{pq}$ are operators that act as multiplication by a $\{|g_p\rangle\}$-dependent eigenvalue. $\hat{\phi}$ is unitary and its explicit form will again not be required, whereas the eigenvalue of $\hat{n}^g_{pq}$ is $n(g^{-1}g_p, g^{-1}g_q, 1) = n(g_p, g_q, g)$. The cocycle condition $\delta n = 0$ gives

$$n(g_p, g_q, g) = n(g_p, 1, g) + n(g_q, 1, g) + n(g_p, g_q, 1). \tag{4.128}$$

Thus, $\hat{n}^g_{pq}$ decomposes into three diagonal operators corresponding to the terms in (4.128), i.e.

$$\hat{n}^g_{pq} = \hat{n}^g_p + \hat{n}^g_q + \hat{n}_{pq}. \tag{4.129}$$

If we substitute for $\hat{n}^g_{pq}$ and do some rearranging, the right hand side of (4.127) becomes

$$\hat{\phi}'\hat{U}_{\rm b}\prod_{\langle pq\rangle}\hat{U}_{pq}^{\hat{n}^g_p+\hat{n}^g_q}\prod_{\langle pqr\rangle}\hat{W}_{pqr}^{\hat{n}^g_p+\hat{n}^g_r} \tag{4.130}$$

where, again, $\hat{\phi}'$ multiplies by a $\{|g_p\rangle\}$-dependent eigenvalue whose precise form will not be required. It is a combination of $\hat{\phi}$ and a phase picked up in commuting the $\hat{U}_{pq}$ operators.

Next, the product of $\hat{U}_{pq}$ in (4.130) can be re-organized so that (4.130) is

$$\hat{\phi}''\hat{U}_{\rm b}\prod_{p}\left(\prod_{\substack{\langle tq\rangle\\ t=p}}\hat{U}_{tq}\prod_{\substack{\langle qt\rangle\\ t=p}}\hat{U}_{qt}\right)^{\hat{n}^g_p}\prod_{\langle pqr\rangle}\hat{W}_{pqr}^{\hat{n}^g_p+\hat{n}^g_r}. \tag{4.131}$$

$\hat{\phi}''$ is yet another diagonal operator in the configuration basis. Employing the identity (4.36),

we thus find that $\hat{V}(g)\hat{U}_{\rm b}\hat{V}^\dagger(g)$ is equal to

$$\hat{\phi}''\hat{U}_{\rm b}\prod_p\left(\hat{G}_p\prod_{\substack{\langle tqr\rangle\\ t=p}}\hat{W}_{tqr}\prod_{\substack{\langle qrt\rangle\\ t=p}}\hat{W}_{qrt}\right)^{\hat{n}_p^g}\prod_{\langle pqr\rangle}\hat{W}_{pqr}^{\hat{n}_p^g+\hat{n}_r^g}. \tag{4.132}$$

The flux operators $\hat{W}_{pqr}$ in (4.132) cancel, so we conclude

$$\hat{V}(g)\hat{U}_{\rm b}\hat{V}^\dagger(g)=\hat{\phi}''(\{g_p\})\hat{U}_{\rm b}\prod_p\hat{G}_p^{\hat{n}_p^g}. \tag{4.133}$$

Next, we show that $\hat{\phi}''$ in (4.133) must be 1. Let us denote the ground state of $\hat{H}_{\rm b}^0$ with trivial holonomy by $|\Psi_{\rm b}^0\rangle$. It is a tensor product of trivial symmetric states

$$\frac{1}{|G|}\sum_{g_p}|g_p\rangle \tag{4.134}$$

at vertices p with the trivial holonomy toric code ground state for the Z_{pq} degrees of freedom. The latter is just a superposition of all trivial holonomy Z_{pq} configurations with trivial $\mathbb{Z}_2$-flux W_{pqr} at every triangle. We then have the following chain of equalities

$$\begin{aligned}|\Psi_{\rm b}^0\rangle&=\hat{V}(g)|\Psi_{\rm b}^0\rangle\\&=\hat{V}(g)\hat{U}_{\rm b}{}^\dagger\hat{U}_{\rm b}|\Psi_{\rm b}^0\rangle\\&=\hat{V}(g)\hat{U}_{\rm b}{}^\dagger\hat{V}^\dagger(g)\hat{U}_{\rm b}|\Psi_{\rm b}^0\rangle\\&=\hat{\phi}''^*\hat{U}_{\rm b}{}^\dagger\hat{U}_{\rm b}|\Psi_{\rm b}^0\rangle\\&=\hat{\phi}''^*|\Psi_{\rm b}^0\rangle.\end{aligned} \tag{4.135}$$

In the first equality we used that $|\Psi_{\rm b}^0\rangle$ is symmetric, and in the third equality we used that $\hat{U}_{\rm b}|\Psi_{\rm b}^0\rangle$ is symmetric. The fourth equality uses (4.133) and the fact that $\hat{U}_{\rm b}|\Psi_{\rm b}^0\rangle$ belongs to the $\hat{G}_p=1$ eigenspace for all p.

Now, comparing the far left hand side and the far right hand side of (4.135), we can

see that $\hat{\phi}''$ is trivial as follows. $\hat{\phi}''$ is a diagonal operator in the configuration basis, while $|\Psi_{\rm b}^0\rangle$ contains an equal amplitude superposition over all G configurations at vertices. For the equality to hold, it must be that $\hat{\phi}''$ has eigenvalue 1 on all configurations. Hence, $\hat{\phi}'' = 1$. Looking back at (4.133), we therefore have

$$\hat{V}(g)\hat{U}_{\rm b}\hat{V}^\dagger(g) = \hat{U}_{\rm b}\prod_p \hat{G}_p^{\hat{n}_p^g}. \tag{4.136}$$

Substituting (4.136) into (4.124) and using the fact that $\hat{H}_{\rm b}^0$ commutes with $\hat{G}_p$ to cancel the factors of $\hat{G}_p$, we find

$$\hat{V}(g)\hat{H}_{\rm b}\hat{V}^\dagger(g) = \hat{H}_{\rm b}. \tag{4.137}$$

Therefore, $\hat{H}_{\rm b}$ is symmetric, and $\hat{H}_{\rm f}$ is symmetric since fermionization commutes with the global G symmetry.

4.C Graphical interpretation of spin structure dependent relation

Here we prove that $c(p)$, as defined in (4.39) and restated here for convenience:

$$\prod_{\substack{\langle tq\rangle\\ t=p}}\hat{S}'_{tq}\prod_{\substack{\langle qt\rangle\\ t=p}}\hat{S}'_{qt} = c(p)\prod_{\substack{\langle tqr\rangle\\ t=p}}(-1)^{\hat{F}_{tqr}}\prod_{\substack{\langle qrt\rangle\\ t=p}}(-1)^{\hat{F}_{qrt}}, \tag{4.138}$$

is proportional to the identity operator, and equal to ± 1 depending on whether the interpolating vector field $\mathcal{V}$, illustrated in FIG.4.9 has an even or odd winding number about p. To see this, we first examine the two types of links around p. There are links that are oriented towards p and links that are oriented away from p. These two types of links form domains as seen in FIG. 4.15. Domains of outward pointing links are separated from domains of inward pointing links by a triangle $\langle qpr\rangle$ where p is the second vertex in the ordering. There are necessarily an even number of triangles around p for which p is the second vertex. We will call these types of triangles $\langle qpr\rangle$-triangles, and we will think of them in pairs – the

two $\langle qpr\rangle$-triangles on either side of an inward pointing domain forming a pair. Moving counter-clockwise around p, we see that each pair results in a 2π clockwise rotation of the vector field $\mathcal{V}$, relative to the outward normal. Without any $\langle qpr\rangle$-triangles, all the links are oriented towards p or they are all oriented away from p, and the vector field rotates by 2π. Therefore, the winding number of the interpolating vector field around p is, modulo 2, equal to $1 - \frac{N_{qpr}}{2}$, where N_{qpr} is the (even) number of triangles for which p is the second vertex in the ordering.

We will now show that $c(p)$ is $-(-1)^{\frac{N_{qpr}}{2}}$. In terms of Majorana operators, the equation for $c(p)$ is

$$c(p) = \left(\prod_{\substack{\langle tq\rangle \\ t=p}} i\gamma_{L_{tq}}\bar{\gamma}_{R_{tq}}\right)\left(\prod_{\substack{\langle qt\rangle \\ t=p}} i\gamma_{L_{qt}}\bar{\gamma}_{R_{qt}}\right)\left(\prod_{\substack{\langle tqr\rangle \\ t=p}} -i\gamma_{tqr}\bar{\gamma}_{tqr}\right)\left(\prod_{\substack{\langle qrt\rangle \\ t=p}} -i\gamma_{qrt}\bar{\gamma}_{qrt}\right). \tag{4.139}$$

Each term in the products over links (the first two products on the right hand side of (4.139)) has a factor of i. The number of such factors of i is equivalent to the total number of triangles having p as a vertex. We can thus assign each of these factors of i to a different triangle having p as a vertex. Each term in the product over $\langle pqr\rangle$-triangles and $\langle qrp\rangle$-triangles (the last two products on the right hand side of (4.139)) contains a factor of $-i$. After multiplying out all of the factors of i and $-i$ we are thus left only with an i for each $\langle qpr\rangle$-triangle. Since these come in pairs we have

$$c(p) = (-1)^{\frac{N_{qpr}}{2}}\left(\prod_{\substack{\langle tq\rangle \\ t=p}} \gamma_{L_{tq}}\bar{\gamma}_{R_{tq}}\right)\left(\prod_{\substack{\langle qt\rangle \\ t=p}} \gamma_{L_{qt}}\bar{\gamma}_{R_{qt}}\right)\left(\prod_{\substack{\langle tqr\rangle \\ t=p}} \gamma_{tqr}\bar{\gamma}_{tqr}\right)\left(\prod_{\substack{\langle qrt\rangle \\ t=p}} \gamma_{qrt}\bar{\gamma}_{qrt}\right). \tag{4.140}$$

Next, we notice that the terms in the product over inward pointing links all commute with each other. Likewise, the terms in the product over outward pointing links all commute with each other. Therefore, we may choose any ordering of the terms within each product. We choose to have the inward pointing link terms to be ordered counter-clockwise around

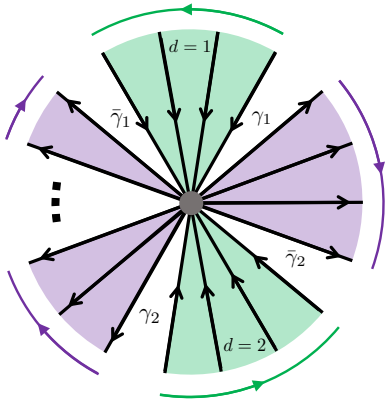

Figure 4.15: The inward oriented domains consisting of $\langle qrp\rangle$-triangles are shaded in green, and the outward oriented domains consisting of $\langle pqr\rangle$-triangles are shaded in purple. The green (purple) arrows show the ordering of the product over inward (outward) oriented links in (4.140). We have also shown one of the two Majorana operators associated with each $\langle qpr\rangle$-triangle, and re-labeled it with the subscript d that labels inward pointing domains in order to make subsequent notation convenient. The reason for only showing one of the two Majorana operators is that the one we have shown is the only one that enters into the computation of $c(p)$.

p and for the outward pointing link terms to be ordered clockwise as in FIG. 4.15. With this ordering, the two Majorana operators corresponding to each $\langle pqr\rangle$ triangle end up being positioned next to each other in the product over outward pointing links. Similarly, the two Majorana operators corresponding to each $\langle qrp\rangle$ triangle end up positioned next to each other in the product over inward pointing links. This accounts for all but two of the Majorana operators in each such product. The remaining two Majorana operators appearing at the beginning and end of each product are located respectively on the two $\langle qpr\rangle$-triangles bordering each domain. Numbering the inward oriented domains by a domain index $d = 1, \ldots, D$, we then (by a slight abuse of notation) re-label these $\langle qpr\rangle$-triangle Majorana operators by γ_d, $\bar{\gamma}_d$, as illustrated in figure 4.15. Note that this labeling scheme accounts for only one Majorana operator located on each $\langle qpr\rangle$-triangles; the other one does not appear in the expression for $c(p)$ and hence plays no role in the following. Moving the $\bar{\gamma}_d$ operators past the (even number of) other terms in each product, we obtain

$$c(p) = (-1)^{\frac{N_{qpr}}{2}} \left(\prod_{d=1}^{D} \bar{\gamma}_{d+1}\gamma_d\right) \left(\prod_{\substack{\langle tqr\rangle \\ t=p}} \bar{\gamma}_{tqr}\gamma_{tqr}\right) \left(\prod_{d=1}^{D} \bar{\gamma}_d\gamma_d\right) \left(\prod_{\substack{\langle qrt\rangle \\ t=p}} \bar{\gamma}_{qrt}\gamma_{qrt}\right) \times \left(\prod_{\substack{\langle tqr\rangle \\ t=p}} \gamma_{tqr}\bar{\gamma}_{tqr}\right) \left(\prod_{\substack{\langle qrt\rangle \\ t=p}} \gamma_{qrt}\bar{\gamma}_{qrt}\right) \quad (4.141)$$

where the subscript $D+1$ is meant to be read as 1.

After canceling the Majorana bilinears corresponding to $\langle pqr\rangle$-triangles and $\langle qrp\rangle$-triangles (last line in the product above), we find

$$\begin{aligned} c(p) &= (-1)^{\frac{N_{qpr}}{2}} \left(\prod_{d=1}^{D} \bar{\gamma}_{d+1}\gamma_d\right) \left(\prod_{d=1}^{D} \bar{\gamma}_d\gamma_d\right) \quad (4.142) \\ &= -(-1)^{\frac{N_{qpr}}{2}} \gamma_D \left(\prod_{d=1}^{D-1} \bar{\gamma}_{d+1}\gamma_d\right) \bar{\gamma}_1 \left(\prod_{d=1}^{D} \bar{\gamma}_d\gamma_d\right) \end{aligned}$$

$$= -(-1)^{\frac{N_{qpr}}{2}} \left(\prod_{d=1}^{D} \gamma_d \bar{\gamma}_d \right) \left(\prod_{d=1}^{D} \bar{\gamma}_d \gamma_d \right)$$
$$= -(-1)^{\frac{N_{qpr}}{2}}.$$

As we argued at the beginning of this appendix, $-(-1)^{\frac{N_{qpr}}{2}}$ is precisely -1 raised to the power of the winding number of the interpolating vector field $\mathcal{V}$. Thus, we have proved the claim: $c(p)$ is -1 when the interpolating vector field has an odd winding number at p and $c(p)$ is 1 otherwise.

4.D Fermion condensation and fermionization

In this appendix, we will illustrate that the fermionization duality outlined in section 4.3 and first described in Ref. [154], can be interpreted as a fermion condensation procedure for certain lattice Hamiltonians.

Fermion condensation has been thouroughly studied using a spacetime formulation [111] and admits the following intuitive picture. We begin with a bosonic system with emergent fermions and introduce a system with bonafide physical fermions. Next, we pair each emergent fermion with a physical fermion and the composite excitation, having bosonic statistics, is then condensed. This results in a fermionic theory in which all particles braiding with the emergent fermion have been confined. As argued in Ref. [124], it outputs a supercohomology SPT phase when applied to the corresponding bosonic shadow theory.

To see the relation with the fermionization duality described in the main text, we must first develop fermion condensation at the lattice Hamiltonian level. To do so, we consider Hamiltonians defined on a Hilbert space consisting of spin-$\frac{1}{2}$ degrees of freedom on links, the same as that of the bosonic shadow models defined in section 4.2, and we assume that the Hamiltonians commute with $\hat{G}_p$, for all vertices p. The restriction to Hamiltonians that commute with $\hat{G}_p$ can be motivated by interpreting $\hat{G}_p$ as a short closed emergent fermion string operator around the vertex p. Thus, the Hamiltonians considered here have a particular emergent fermion string operator, which we describe in detail below. We note that

this particular string operator creates emergent fermion excitations in the bosonic shadow models constructed in section 4.2, since those models commute with $\hat{G}_p$.

We define the emergent fermion string operator $\hat{\tilde{U}}_\Gamma$ by

$$\hat{\tilde{U}}_\Gamma \equiv \prod_{\langle pq \rangle \in \Gamma} \hat{\tilde{U}}_{pq}, \tag{4.143}$$

where Γ is a path in the dual lattice and $\hat{\tilde{U}}_{pq}$ is

$$\hat{\tilde{U}}_{pq} \equiv \hat{X}_{pq} \hat{\tilde{K}}_{L_{pq}} \hat{\tilde{K}}_{R_{pq}}. \tag{4.144}$$

The action of $\hat{\tilde{K}}_{R_{pq}}$ is dependent upon the triangle R_{pq} to the right of $\langle pq \rangle$. If the triangle to the right of $\langle pq \rangle$ has vertex ordering $\langle pqr \rangle$, with p and q being the first and second vertices, respectively, then $\hat{K}_{R_{pq}}$ acts as $\hat{Z}_{qr}$. Otherwise, $\hat{K}_{R_{pq}} = 1$. The action of $\hat{K}_{L_{pq}}$ is defined similarly but with 'right' replaced with 'left'. Intuitively, $\hat{\tilde{U}}_{pq}$ creates a pair of $\mathbb{Z}_2$ fluxes and moves $\mathbb{Z}_2$ charges so that they are bound to the fluxes at the third vertex in the vertex ordering. Letting Γ be a path in the dual lattice around the vertex p, we find that $\hat{\tilde{U}}_\Gamma$ is equal to $\hat{G}_p$ up to an inconsequential sign.

We may now describe the fermion condensation procedure for a Hamiltonian $\hat{H}$ which commutes with $\hat{G}_p$. First, as $\hat{U}_{pq}$ and $\hat{W}_{pqr}$ generate all the local operators that commute with $\hat{G}_p$, $\hat{H}$ can be expressed in terms of $\hat{U}_{pq}$ and $\hat{W}_{pqr}$. To make this explicit, we write $\hat{H}$ as $\hat{H}(\hat{U}_{pq}, \hat{W}_{pqr})$. Next, we introduce fermionic degrees of freedom into our system by adding a complex fermion degree of freedom to each triangle. The fermion parity even operators are generated by fermion parity $(-1)^{\hat{F}_{pqr}}$ and hopping operators $\hat{S}_{pq}$. Here, $\hat{S}_{pq}$ includes the spin structure related sign for edges in $\mathcal{E}$, as described in section 4.3.3.

The next step in fermion condensation is to bind physical fermions to emergent fermion excitations and to condense the composite particles. The binding of physical fermions to

emergent fermion excitations is accomplished by replacing $\hat{W}_{pqr}$ with $\hat{W}_{pqr}(-1)^{\hat{F}_{pqr}}$ so that

$$\hat{H}(\hat{U}_{pq}, \hat{W}_{pqr}) \longrightarrow \hat{H}(\hat{U}_{pq}, \hat{W}_{pqr}(-1)^{\hat{F}_{pqr}}). \tag{4.145}$$

In the resulting system, a pair of emergent fermions can be created for free as long as there is a physical fermion attached to each emergent fermion. As a consequence, the Hamiltonian becomes highly degenerate. This degeneracy, however, is eliminated by adding a term that proliferates emergent fermion-physical fermion pairs. A pair of composite excitations is created by the operator $\hat{\tilde{U}}_{pq}\hat{S}_{pq}$, so the term

$$-J\sum_{\langle pq\rangle}\hat{\tilde{U}}_{pq}\hat{S}_{pq}, \quad J>0 \tag{4.146}$$

energetically prefers states where the composite excitations have been proliferated. Adding the term in 4.146 to the Hamiltonian, we have

$$\hat{H}(\hat{U}_{pq}, \hat{W}_{pqr}(-1)^{\hat{F}_{pqr}}) \longrightarrow \hat{H}(\hat{U}_{pq}, \hat{W}_{pqr}(-1)^{\hat{F}_{pqr}}) - J\sum_{\langle pq\rangle}\hat{\tilde{U}}_{pq}\hat{S}_{pq}. \tag{4.147}$$

One may be concerned that the J-term will not proliferate the composite excitations as promised due to possible competition with $\hat{H}(\hat{U}_{pq}, \hat{W}_{pqr}(-1)^{\hat{F}_{pqr}})$. However, it can be shown that $\hat{U}_{pq}$ commutes with $\hat{\tilde{U}}_{st}$ for every $\langle st\rangle$ and $\hat{W}_{pqr}(-1)^{\hat{F}_{pqr}}$ commutes with $\hat{\tilde{U}}_{st}\hat{S}_{st}$ for every $\langle st\rangle$. Therefore, $\hat{H}(\hat{U}_{pq}, \hat{W}_{pqr}(-1)^{\hat{F}_{pqr}})$ commutes with $-J\sum_{\langle pq\rangle}\hat{\tilde{U}}_{pq}\hat{S}_{pq}$ and the J-term is indeed minimized in the ground state.

Finally, we drive the system deep into the fermion condensed regime and consider the limit as $J\to\infty$. In the resulting effective Hilbert space, $\hat{\tilde{U}}_{pq}\hat{S}_{pq}=1$ for all $\langle pq\rangle$. Thus, in this effective Hilbert space, the Hamiltonian acts as

$$\hat{H}(\hat{U}_{pq}\hat{\tilde{U}}_{pq}\hat{S}_{pq}, \hat{W}_{pqr}(-1)^{\hat{F}_{pqr}}), \tag{4.148}$$

where we have inserted $\hat{\tilde{U}}_{pq}\hat{S}_{pq}=1$ and removed the J-term. Relabeling $\hat{W}_{pqr}(-1)^{\hat{F}_{pqr}}$ as

$(-1)^{\hat{\tilde{F}}_{pqr}}$ (note the tilde above F) and $\hat{U}_{pq}\hat{\tilde{U}}_{pq}\hat{S}_{pq}$ as $\hat{\tilde{S}}_{pq}$, we have

$$\hat{H}(\hat{\tilde{S}}_{pq}, (-1)^{\hat{\tilde{F}}_{pqr}}). \tag{4.149}$$

$(-1)^{\hat{\tilde{F}}_{pqr}}$ and $\hat{\tilde{S}}_{pq}$ satisfy the same commutation relations as fermion parity operators $(-1)^{\hat{F}_{pqr}}$ and hopping operators $\hat{S}_{pq}$, respectively, and it can be checked that they satisfy a relation analogous to (4.41).

Functionally, our prescription for fermion condensation maps a Hamiltonian $\hat{H}(\hat{U}_{pq}, \hat{W}_{pqr})$ to $\hat{H}(\hat{\tilde{S}}, (-1)^{\hat{\tilde{F}}_{pqr}})$. In effect, we have replaced $\hat{U}_{pq}$ with $\hat{\tilde{S}}_{pq}$ and $\hat{W}_{pqr}$ with $(-1)^{\hat{\tilde{F}}_{pqr}}$, which is precisely the result of applying the fermionization duality. Hence, we have shown that, for Hamiltonians that commute with $\hat{G}_p$, fermionization agrees with fermion condensation.

We expect that the steps described above can be generalized to a wider class of emergent fermion string operators. This may yield new fermionization dualities and further extend our understanding of fermion condensation at the lattice level.

4.E Adding ancillary spin-$\frac{1}{2}$ degrees of freedom

In section 4.3.4, we presented the construction of a fermionic SPT Hamiltonian obtained by conjugating a trivial fermionic Hamiltonian by $\hat{U}_{\mathrm{f}}$. However, $\hat{U}_{\mathrm{f}}$ was written with an unspecified locally determined configuration dependent sign $\hat{\kappa}$. $\hat{\kappa}$ is dependent upon the triangulation of the manifold as well as an ordering of operators. Here we discuss a work around to calculating $\hat{\kappa}$ applicable to arbitrary triangulations.

Recall that $\hat{\kappa}$ is a consequence of rearranging terms in

$$\hat{U}_{\mathrm{b}} = \prod_{\langle pqr\rangle} \left(\hat{\nu}_{pqr}^{o_{pqr}} \hat{Z}_{pq}^{\hat{n}_{qr}}\right) \prod_{\langle pq\rangle} \hat{X}_{pq}^{\hat{n}_{pq}} \prod_{\langle pqr\rangle} \hat{W}_{pqr}^{\hat{n}_{pr}}, \tag{4.150}$$

to make it manifestly fermionizable. We will show that by adding ancillary spin-$\frac{1}{2}$ degrees of freedom on triangles and composing $\hat{U}_{\mathrm{b}}$ with a certain trivial circuit, we can reorganize the expression into a fermionizable operator without accruing a sign.

To this end, let us add a spin-$\frac{1}{2}$ degree of freedom to each triangle so that in total we have G degrees of freedom at vertices, a spin-$\frac{1}{2}$ degree of freedom at every link, and a spin-$\frac{1}{2}$ at each triangle. The Pauli X and Pauli Z operators acting on the spin-$\frac{1}{2}$ at $\langle pqr\rangle$ will be denoted as $\hat{\tau}^x_{pqr}$ and $\hat{\tau}^z_{pqr}$, respectively.

Next, we compose the operator in (4.150) with a circuit that acts trivially on the triangle spin-$\frac{1}{2}$ degrees of freedom. Namely, we compose with

$$1 = \left(\prod_{\langle pqr\rangle} \left(\hat{\tau}^z_{pqr}\right)^{\hat{n}_{qr}} \prod_{\langle pqr\rangle} \left(\hat{\tau}^x_{pqr}\right)^{\hat{n}_{pq}}\right)\left(\prod_{\langle pqr\rangle} \left(\hat{\tau}^x_{pqr}\right)^{\hat{n}_{pq}} \prod_{\langle pqr\rangle} \left(\hat{\tau}^z_{pqr}\right)^{\hat{n}_{qr}}\right) \tag{4.151}$$

to obtain

$$\begin{aligned}\hat{U}^{\tau}_{\mathrm{b}} \equiv \prod_{\langle pqr\rangle}\left(\hat{\nu}^{o_{pqr}}_{pqr}\hat{Z}^{\hat{n}_{qr}}_{pq}\right)\prod_{\langle pq\rangle}\hat{X}^{\hat{n}_{pq}}_{pq}\prod_{\langle pqr\rangle}\hat{W}^{\hat{n}_{pr}}_{pqr} \\ \times\left(\prod_{\langle pqr\rangle} \left(\hat{\tau}^z_{pqr}\right)^{\hat{n}_{qr}} \prod_{\langle pqr\rangle} \left(\hat{\tau}^x_{pqr}\right)^{\hat{n}_{pq}}\right)\left(\prod_{\langle pqr\rangle} \left(\hat{\tau}^x_{pqr}\right)^{\hat{n}_{pq}} \prod_{\langle pqr\rangle} \left(\hat{\tau}^z_{pqr}\right)^{\hat{n}_{qr}}\right).\end{aligned} \tag{4.152}$$

The circuit in (4.151) is equal to the identity, and as such, stacking it with $\hat{U}_{\mathrm{b}}$ certainly does not affect the phase of our system. However, we can use the anti-commutativity of $\hat{\tau}^z_{pqr}$ and $\hat{\tau}^x_{pqr}$ to make up for the anti-commutivity of $\hat{Z}_{pq}$ and $\hat{X}_{pq}$. In particular, we arrange the $\hat{\tau}^z_{pqr}$ and $\hat{\tau}^x_{pqr}$ so as to 'dress' the $\hat{Z}_{pq}$ and $\hat{X}_{pq}$ and avoid incurring the sign $\hat{\kappa}$.

First, we move $\hat{\tau}^z_{pqr}$ operators next to the $\hat{Z}_{pq}$ operators:

$$\begin{aligned}\hat{U}^{\tau}_{\mathrm{b}} = \prod_{\langle pqr\rangle}\left(\hat{\nu}^{o_{pqr}}_{pqr}\left(\hat{Z}_{pq}\hat{\tau}^z_{pqr}\right)^{\hat{n}_{qr}}\right)\prod_{\langle pq\rangle}\hat{X}^{\hat{n}_{pq}}_{pq}\prod_{\langle pqr\rangle}\hat{W}^{\hat{n}_{pr}}_{pqr} \\ \times\prod_{\langle pqr\rangle}\left(\hat{\tau}^x_{pqr}\right)^{\hat{n}_{pq}}\left(\prod_{\langle pqr\rangle} \left(\hat{\tau}^x_{pqr}\right)^{\hat{n}_{pq}} \prod_{\langle pqr\rangle} \left(\hat{\tau}^z_{pqr}\right)^{\hat{n}_{qr}}\right).\end{aligned}$$

Next, we rewrite the product $\prod_{\langle pqr\rangle}\left(\hat{\tau}^x_{pqr}\right)^{\hat{n}_{pq}}$ as a product over edges. This will allow us to dress the $\hat{X}_{pq}$ terms appearing in a product over edges. To the $\langle pq\rangle$ edge of triangle $\langle pqr\rangle$

we associate the the operator $\hat{\tau}^x_{pqr}$. This gives

$$\prod_{\langle pqr\rangle} \left(\hat{\tau}^x_{pqr}\right)^{\hat{n}_{pq}} = \prod_{\langle pq\rangle} \left(\hat{A}_{L_{pq}} \hat{A}_{R_{pq}}\right)^{\hat{n}_{pq}}, \tag{4.153}$$

where the action of $\hat{A}_{R_{pq}}$, appearing in the formula above, is determined as follows. If the triangle to the right of $\langle pq\rangle$ is $\langle pqr\rangle$, where p and q are the first and second vertices, respectively, then $\hat{A}_{R_{pq}}$ acts as $\hat{\tau}^x_{pqr}$. Otherwise, $\hat{A}_{R_{pq}} = 1$. The action of $\hat{A}_{L_{pq}}$ is defined analogously but we look at the triangle to the left of $\langle pq\rangle$ instead.

Now we write

$$\hat{U}^\tau_{\mathrm{b}} = \prod_{\langle pqr\rangle} \hat{\nu}^{o_{pqr}}_{pqr} \left(\hat{Z}_{pq}\hat{\tau}^z_{pqr}\right)^{\hat{n}_{qr}} \prod_{\langle pq\rangle} \left(\hat{X}_{pq}\hat{A}_{L_{pq}}\hat{A}_{R_{pq}}\right)^{\hat{n}_{pq}} \prod_{\langle pqr\rangle} \hat{W}^{\hat{n}_{pr}}_{pqr} \times \prod_{\langle pqr\rangle} \left(\hat{\tau}^x_{pqr}\right)^{\hat{n}_{pq}} \prod_{\langle pqr\rangle} \left(\hat{\tau}^z_{pqr}\right)^{\hat{n}_{qr}}. \tag{4.154}$$

One can check that $\hat{Z}_{pq}\hat{\tau}^z_{pqr}$ and $\hat{X}_{pq}\hat{A}_{L_{pq}}\hat{A}_{R_{pq}}$ commute. Therefore, we are free to rearrange the $\hat{Z}_{pq}\hat{\tau}^z_{pqr}$ and $\hat{X}_{pq}\hat{A}_{L_{pq}}\hat{A}_{R_{pq}}$ operators to form a product of $\hat{U}_{pq}$ (defined in (4.35)) without picking up the sign $\hat{\kappa}$.

Explicitly, rearranging yields

$$\hat{U}^\tau_{\mathrm{b}} = \prod_{\langle pqr\rangle} \hat{\nu}^{o_{pqr}}_{pqr} \prod_{\langle pq\rangle} \left(\hat{U}_{pq}\hat{B}_{L_{pq}}\hat{B}_{R_{pq}}\hat{A}_{L_{pq}}\hat{A}_{R_{pq}}\right)^{\hat{n}_{pq}} \prod_{\langle pqr\rangle} \hat{W}^{\hat{n}_{pr}}_{pqr} \prod_{\langle pqr\rangle} \left(\hat{\tau}^x_{pqr}\right)^{\hat{n}_{pq}} \prod_{\langle pqr\rangle} \left(\hat{\tau}^z_{pqr}\right)^{\hat{n}_{qr}}, \tag{4.155}$$

where we have introduced $\hat{B}_{L_{pq}}$ and $\hat{B}_{R_{pq}}$. $\hat{B}_{R_{pq}}$ is $\hat{\tau}^z_{rpq}$ when the triangle to the right is of the form $\langle rpq\rangle$, i.e. p is the second vertex in the ordering and q is the third vertex in the ordering. $\hat{B}_{R_{pq}}$ is 1 otherwise. $\hat{B}_{L_{pq}}$ is defined analogously, but for the triangle to the left of $\langle pq\rangle$.

With a choice of spin structure to define the duality, $\hat{U}^\tau_{\mathrm{b}}$ can be fermionized straightfor-

wardly. If we let $\hat{S}^{\tau}_{pq}$ be $\hat{S}_{pq}\hat{B}_{L_{pq}}\hat{B}_{R_{pq}}\hat{A}_{L_{pq}}\hat{A}_{R_{pq}}$, then

$$\hat{U}^{\tau}_{\mathrm{f}} = \prod_{\langle pqr\rangle} \hat{\nu}_{pqr}^{o_{pqr}} \prod_{\langle pq\rangle} \left(\hat{S}^{\tau}_{pq}\right)^{\hat{n}_{pq}} \prod_{\langle pqr\rangle} \left((-1)^{\hat{F}_{pqr}}\right)^{\hat{n}_{pr}} \prod_{\langle pqr\rangle} \left(\hat{\tau}^{x}_{pqr}\right)^{\hat{n}_{pq}} \prod_{\langle pqr\rangle} \left(\hat{\tau}^{z}_{pqr}\right)^{\hat{n}_{qr}} . \tag{4.156}$$

A fermionic SPT Hamiltonian $\hat{H}^{\tau}_{\mathrm{f}}$ can be formed by conjugating the trivial fermionic Hamiltonian

$$-\sum_{p} \hat{P}^{\mathrm{sym}}_{p} - \sum_{\langle pqr\rangle} (-1)^{\hat{F}_{pqr}} - \sum_{\langle pqr\rangle} \hat{\tau}^{x}_{pqr} \tag{4.157}$$

by $\hat{U}^{\tau}_{\mathrm{f}}$. $\hat{H}^{\tau}_{\mathrm{f}}$ acts identically to $\hat{H}_{\mathrm{f}}$ on the vertex and complex fermion degrees of freedom. We have simply encoded the sign $\hat{\kappa}$ appearing in $\hat{H}_{\mathrm{f}}$ in the ordering of the Pauli operators of $\hat{H}^{\tau}_{\mathrm{f}}$. Indeed, if one were to cancel the triangle Pauli operators in (4.156), one would obtain the sign $\hat{\kappa}$. In the end, we have arrived at an explicit form for a Hamiltonian in the same phase as $\hat{H}_{\mathrm{f}}$ for an arbitrary triangulation of a 2+1D manifold with spin structure.

4.F Trivial fermionic finite-depth circuit

In section 4.4.3, we claimed that the supercohomology data $(n_0, \nu_0) = \left(\delta\beta, (-1)^{\beta\cup\delta\beta}\delta\omega\right)$ corresponds to a trivial fermionic SPT phase. We prove this claim here by showing that the finite depth circuit $\hat{U}^{n_0\nu_0}_{\mathrm{b}}$ can be written in terms of symmetric local unitaries, up to factors of $\hat{G}_p$. This implies that the fermionized circuit $\hat{U}^{n_0\nu_0}_{\mathrm{f}}$ constructs a trivial SPT ground state from a trivial product state because fermionization respects the G-symmetry and maps $\hat{G}_p$ to the identity.

Plugging the data (n_0, ν_0) into the expression for $\hat{U}_{\mathrm{b}}$ (4.22) we obtain

$$\hat{U}^{n_0\nu_0}_{\mathrm{b}} = \prod_{\langle pqr\rangle} (-1)^{\hat{\beta}_{pq}\delta\hat{\beta}_{qr}} (\delta\hat{\omega}_{pqr})^{o_{pqr}} \prod_{\langle pqr\rangle} \hat{Z}^{\delta\hat{\beta}_{qr}}_{pq} \prod_{\langle pq\rangle} \hat{X}^{\delta\hat{\beta}_{pq}}_{pq} \prod_{\langle pqr\rangle} \hat{W}^{\delta\beta_{pr}}_{pqr}, \tag{4.158}$$

with $\delta\hat{\beta}_{pq}$ and $\delta\hat{\omega}_{pqr}$ defined by

$$\delta\hat{\beta}_{pq}|\{g_t\}\rangle = \delta\beta(g_p, g_q, 1)|\{g_t\}\rangle \tag{4.159}$$

$$\delta\hat{\omega}_{pqr}|\{g_t\}\rangle = \delta\omega(g_p, g_q, g_r, 1)|\{g_t\}\rangle. \tag{4.160}$$

Now we notice

$$\prod_{\langle pqr\rangle}(\delta\omega(g_p,g_q,g_r,1))^{o_{pqr}} == \prod_{\langle pqr\rangle}\left(\frac{\omega(g_q,g_r,1)\omega(g_p,g_q,1)}{\omega(g_p,g_r,1)\omega(g_p,g_q,g_r)}\right)^{o_{pqr}} = \prod_{\langle pqr\rangle}\omega(g_p,g_q,g_r)^{-o_{pqr}}. \tag{4.161}$$

The last equality follows from treating $\omega(g_s, g_t, 1)$ as corresponding to the edge $\langle st\rangle$ and canceling factors of $\omega(g_s, g_t, 1)$ from neighboring triangles. Therefore,

$$\prod_{\langle pqr\rangle}(\delta\hat{\omega}_{pqr})^{o_{pqr}} = \prod_{\langle pqr\rangle}\hat{\omega}_{pqr}^{-o_{pqr}} \tag{4.162}$$

for $\hat{\omega}_{pqr}$:

$$\hat{\omega}_{pqr}|\{g_t\}\rangle = \omega(g_p, g_q, g_r)|\{g_t\}\rangle. \tag{4.163}$$

Using $\delta\hat{\beta}_{pq} = \hat{\beta}_{pq} + \hat{\beta}_p + \hat{\beta}_q$ (with $\hat{\beta}_{pq}$ and $\hat{\beta}_p$ defined in (4.77) and (4.78)) as well as the equality in (4.162), $\hat{U}_{\rm b}^{n_0\nu_0}$ becomes

$$\hat{U}_{\rm b}^{n_0\nu_0} = \prod_{\langle pqr\rangle}\hat{\omega}_{pqr}^{-o_{pqr}}\prod_{\langle pqr\rangle}(-1)^{\hat{\beta}_{pq}(\hat{\beta}_{qr}+\hat{\beta}_q+\hat{\beta}_r)}\prod_{\langle pqr\rangle}\hat{Z}_{pq}^{\hat{\beta}_{qr}+\hat{\beta}_q+\hat{\beta}_r}\prod_{\langle pq\rangle}\hat{X}_{pq}^{\hat{\beta}_{pq}+\hat{\beta}_p+\hat{\beta}_q}\prod_{\langle pqr\rangle}\hat{W}_{pqr}^{\hat{\beta}_{pr}+\hat{\beta}_p+\hat{\beta}_r}, \tag{4.164}$$

Rearranging and keeping track of the resulting sign we have

$$\hat{U}_{\rm b}^{n_0\nu_0} = \prod_{\langle pqr\rangle}\hat{\omega}_{pqr}^{-o_{pqr}}\prod_{\langle pqr\rangle}(-1)^{\hat{\beta}_{pq}(\hat{\beta}_{qr}+\hat{\beta}_q+\hat{\beta}_r)}\prod_{\langle pqr\rangle}(-1)^{\hat{\beta}_q\hat{\beta}_{pq}+\hat{\beta}_r\hat{\beta}_{pq}}$$

$$\times \prod_{\langle pqr\rangle} \hat{Z}_{pq}^{\hat{\beta}_{qr}} \prod_{\langle pq\rangle} \hat{X}_{pq}^{\hat{\beta}_{pq}} \prod_{\langle pqr\rangle} \hat{W}_{pqr}^{\hat{\beta}_{pr}} \prod_{\langle pqr\rangle} \hat{Z}_{pq}^{\hat{\beta}_q+\hat{\beta}_r} \prod_{\langle pq\rangle} \hat{X}_{pq}^{\hat{\beta}_p+\hat{\beta}_q} \prod_{\langle pqr\rangle} \hat{W}_{pqr}^{\hat{\beta}_p+\hat{\beta}_r}. \quad (4.165)$$

Next we write $\prod_{\langle pq\rangle} \hat{X}_{pq}^{\hat{\beta}_p+\hat{\beta}_q}$ in (4.165) as a product over vertices:

$$\prod_{\langle pq\rangle} \hat{X}_{pq}^{\hat{\beta}_p+\hat{\beta}_q} = \prod_p \left(\prod_{\langle st\rangle \ni p} \hat{X}_{st}^{\hat{\beta}_p} \right). \quad (4.166)$$

Further, one can check that

$$\left[\prod_p \left(\prod_{\langle st\rangle \ni p} \hat{X}_{st}^{\hat{\beta}_p} \right) \right] \prod_{\langle pqr\rangle} \hat{W}_{pqr}^{\hat{\beta}_p} = \prod_p \hat{G}_p^{\hat{\beta}_p}. \quad (4.167)$$

Hence, substituting (4.167) in (4.165) and canceling signs we are left with

$$\hat{U}_{\mathrm{b}}^{n_0\nu_0} = \prod_{\langle pqr\rangle} \hat{\omega}_{pqr}^{-o_{pqr}} \prod_{\langle pqr\rangle} (-1)^{\hat{\beta}_{pq}\hat{\beta}_{qr}} \prod_{\langle pqr\rangle} \hat{Z}_{pq}^{\hat{\beta}_{qr}} \prod_{\langle pq\rangle} \hat{X}_{pq}^{\hat{\beta}_{pq}} \prod_{\langle pqr\rangle} \hat{W}_{pqr}^{\hat{\beta}_{pr}} \prod_{\langle pqr\rangle} \hat{Z}_{pq}^{\hat{\beta}_q+\hat{\beta}_r} \prod_{\langle pqr\rangle} \hat{W}_{pqr}^{\hat{\beta}_r} \prod_p \hat{G}_p^{\hat{\beta}_p}. \quad (4.168)$$

The product $\prod_{\langle pqr\rangle} \hat{Z}_{pq}^{\hat{\beta}_q+\hat{\beta}_r} \prod_{\langle pqr\rangle} \hat{W}_{pqr}^{\hat{\beta}_r}$ above expressed in terms of $\hat{Z}_{pq}$ operators is

$$\prod_{\langle pqr\rangle} \hat{Z}_{pq}^{\hat{\beta}_q+\hat{\beta}_r} \hat{Z}_{pq}^{\hat{\beta}_r} \hat{Z}_{qr}^{\hat{\beta}_r} \hat{Z}_{pr}^{\hat{\beta}_r} = \prod_{\langle pqr\rangle} \hat{Z}_{pq}^{\hat{\beta}_q} \hat{Z}_{qr}^{\hat{\beta}_r} \hat{Z}_{pr}^{\hat{\beta}_r} = \prod_{\langle pq\rangle} \hat{Z}_{pq}^{\hat{\beta}_q} \hat{Z}_{pq}^{\hat{\beta}_q} = 1. \quad (4.169)$$

With (4.169) we finally have that

$$\hat{U}_{\mathrm{b}}^{n_0\nu_0} = \prod_{\langle pqr\rangle} \hat{\omega}_{pqr}^{-o_{pqr}} \prod_{\langle pqr\rangle} (-1)^{\hat{\beta}_{pq}\hat{\beta}_{qr}} \prod_{\langle pqr\rangle} \hat{Z}_{pq}^{\hat{\beta}_{qr}} \prod_{\langle pq\rangle} \hat{X}_{pq}^{\hat{\beta}_{pq}} \prod_{\langle pqr\rangle} \hat{W}_{pqr}^{\hat{\beta}_{pr}} \prod_p \hat{G}_p^{\hat{\beta}_p}, \quad (4.170)$$

as claimed in section 4.4.3.

The homogeneity of ω and β guarantees that the local unitaries (not including $\prod_p \hat{G}_p^{\hat{\beta}_p}$) in (4.170) are symmetric. Fermionization commutes with the global symmetry operator and it takes $\prod_p \hat{G}_p^{\hat{\beta}_p}$ to 1. Therefore, the resulting circuit $\hat{U}_{\mathrm{f}}^{n_0\nu_0}$ is a finite depth circuit built from

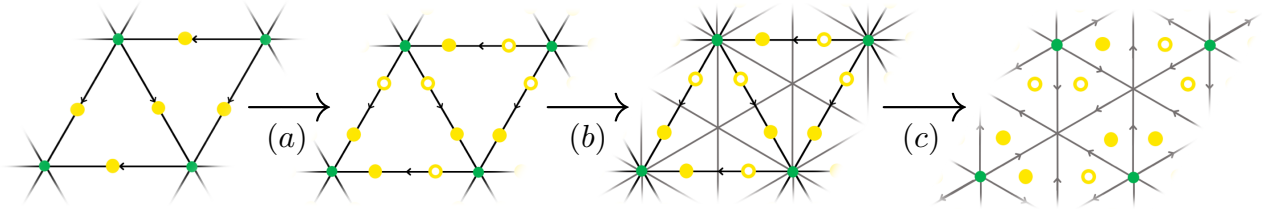

Figure 4.16: (Far left) The beyond supercohomology models in Ref. [152] have G degrees of freedom (green dots) at vertices and a single complex fermion degree of freedom (yellow dots) at each link. (a) We add an additional complex fermion degree of freedom (hollow yellow circle) to each link and modify the Hamiltonian by adding a term that enforces zero fermion occupancy at each of these additional sites. (b) We add links to the lattice to form the barycentric subdivision of our original triangulation. (c) The links of the original lattice are removed in the bulk and we associate one complex fermion to each triangle of the resulting lattice. The branching structure is determined by the branching structure of the original lattice. Importantly, the final Hilbert space has a single complex fermion degree of freedom for each triangle. Note that the G degrees of freedom remain in place.

symmetric local unitaries, and consequently, creates a trivial fermionic SPT from a trivial product state.

4.G Symmetric quantum circuits for beyond supercohomology phases

Here, we present an argument that the ground states of the beyond supercohomology phases cannot be constructed from a trivial product state using a globally symmetric finite depth quantum circuit. It has been shown, using a spacetime formulation, that the shadow models for beyond supercohomology phases are symmetry enriched toric code phases with the property that certain global symmetries transform e excitations into m excitations and vice-versa [124, 155]. We begin by giving an independent argument that this property has to hold for the lattice Hamiltonian shadow models associated to a beyond supercohomology SPT. We also show how existing lattice Hamiltonian models for beyond supercohomology phases, namely those of Ref. [152], can be slightly modified so as to be amenable to our bosonization

procedure. This argument can be generalized to show that any lattice Hamiltonian SPT model can be modified so as to be bosonizable via our procedure. We then demonstrate that this property of a global symmetry operator exchanging e and m in the shadow model, together with the assumption of the existence of a globally symmetric finite depth circuit disentangling the ground state of the original fermionic SPT, lead to a contradiction.

The beyond supercohomology models constructed in Ref. [152] are not immediately bosonizable, because the fermionic degrees of freedom live on the links instead of at the centers of triangles. This can be remedied as follows. First, we introduce a second complex fermion degree of freedom at each link and add a term to the Hamiltonian that energetically favors zero fermion occupancy at each of the new complex fermion degrees of freedom. Functionally, we have stacked an atomic insulator onto the original system, so it remains in the same phase. Then, we perform a barycentric subdivision of the lattice, remove the original lattice, and associate the two complex fermions per link to different triangles. This procedure is illustrated in FIG. 4.16. In this process, we have not changed the dynamics of the system, and in the end, we have a beyond supercohomology model which lives in the same Hilbert space as the supercohomology models constructed in this chapter, and hence is readily bosonizable.

Now we argue that bosonizing these beyond supercohomology models gives symmetry enriched toric code models in which global symmetries convert e excitations into m excitations. Key to this argument is the following property of the symmetry action in beyond supercohomology models with symmetry defects. For beyond supercohomology phases with symmetry G, there is an additional piece of data relative to supercohomology phases - a homomorphism $\sigma : G \to \mathbb{Z}_2$. According to Refs. [151, 152, 155], the effective symmetry action near a fermion parity defect is fermion parity odd when acting with on-site symmetry operator $\hat{V}(g)$ representing $g \in G$ for which $\sigma(g)$ is non-trivial.

We analyze this effect in our beyond supercohomology models by inserting a pair of fermion parity defects at well separated vertices a and b. Loosely, we create the pair of fermion parity defects by choosing a path Γ connecting a and b and modifying hopping

operators in the Hamiltonian corresponding to links in Γ. Heuristically, the modification of the Hamiltonian makes it so that when a fermion moves around one of the fermion parity defects, it picks up an extra -1 sign.

To include fermion parity defects, we first write the beyond supercohomology model $\hat{H}^{\text{b.s.}}$ as a sum of local terms

$$\hat{H}^{\text{b.s.}} = \sum_j \hat{h}_j^{\text{b.s.}}, \tag{4.171}$$

with each $\hat{h}_j^{\text{b.s.}}$ supported on the spatially bounded region R_j. Now, we define

$$\hat{\mathcal{P}}_p = \frac{1}{2}\left(1 + \prod_{\substack{\langle tq\rangle \\ t=p}} \hat{S}_{tq} \prod_{\substack{\langle qt\rangle \\ t=p}} \hat{S}_{qt} \prod_{\substack{\langle tqr\rangle \\ t=p}} (-1)^{\hat{F}_{tqr}} \prod_{\substack{\langle qrt\rangle \\ t=p}} (-1)^{\hat{F}_{qrt}}\right) \tag{4.172}$$

and

$$\hat{\mathcal{P}}_{R_j} = \prod_{p \subset R_j} \hat{\mathcal{P}}_p, \tag{4.173}$$

and write

$$\hat{H'}^{\text{b.s.}} = \sum_j \hat{\mathcal{P}}_{R_j} \hat{h}_j^{\text{b.s.}} \hat{\mathcal{P}}_{R_j} - \sum_p \hat{\mathcal{P}}_p. \tag{4.174}$$

$\hat{\mathcal{P}}_p$ is identically equal to 1, so $\hat{H'}^{\text{b.s.}}$ is equivalent to $\hat{H}^{\text{b.s.}}$.

Next, let us modify this Hamiltonian to insert a pair of defects at two well separated vertices a and b. Let Γ be a path of links connecting a and b, and let Γ_{pq} be the indicator function

$$\Gamma_{pq} = \begin{cases} 1 & \text{if } \langle pq\rangle \in \Gamma \\ 0 & \text{otherwise.} \end{cases} \tag{4.175}$$

Now we write each local term $\hat{h}_j^{\text{b.s.}}$ explicitly as a linear combination of products of $\hat{S}_{pq}$ and $(-1)^{\hat{F}_{pqr}}$, and we make the replacement:

$$\hat{h}_j^{\text{b.s.}}(\hat{S}_{pq}, (-1)^{\hat{F}_{pqr}}) \longrightarrow \hat{h}_{j,\Gamma}^{\text{b.s.}} \equiv \hat{h}_j^{\text{b.s.}}((-1)^{\Gamma_{pq}}\hat{S}_{pq}, (-1)^{\hat{F}_{pqr}}). \tag{4.176}$$

Making the same replacement in $\hat{\mathcal{P}}_j$ yields a new Hamiltonian $\hat{H}_\Gamma^{\text{b.s.}}$.

Notice that replacing $\hat{S}_{pq}$ with $(-1)^{\Gamma_{pq}}\hat{S}_{pq}$ in the expression defining $\hat{\mathcal{P}}_R$ yields 0 if a or b is contained in the region R. As a consequence, Hamiltonian terms whose support contains the defects are removed from the Hamiltonian.

Now we bosonize $\hat{H}^{\text{b.s.}}$ and $\hat{H}_\Gamma^{\text{b.s.}}$. This yields

$$\hat{H}_{\text{b}}^{\text{b.s.}} \equiv \hat{H'}^{\text{b.s.}}(\hat{U}_{pq}, \hat{W}_{pqr}) \tag{4.177}$$

and

$$\hat{H}_{\text{b},\Gamma}^{\text{b.s.}} \equiv \hat{H'}^{\text{b.s.}}((-1)^{\Gamma_{pq}}\hat{U}_{pq}, \hat{W}_{pqr}). \tag{4.178}$$

The operators $\hat{\mathcal{P}}_R$ become projectors onto the $\hat{G}_p = 1$ subspace for all $p \subset R$. As a consequence, the ground states of $\hat{H}_{\text{b}}^{\text{b.s.}}$ are in the $\hat{G}_p = 1$ subspace, and away from the defects, the ground states of $\hat{H}_{\text{b},\Gamma}^{\text{b.s.}}$ are in the $\hat{G}_p = 1$ subspace. We also note that, by construction, the bosonized Hamiltonians commute with $\hat{G}_p$ for all p, and thus, $\hat{G}_p$ can be interpreted as a small loop of an emergent fermion string operator around the vertex p.

We can obtain a ground state of $\hat{H}_{\text{b},\Gamma}^{\text{b.s.}}$ by applying a certain string operator to a ground state of $\hat{H}_{\text{b}}^{\text{b.s.}}$. In particular, the string operator $\hat{U}_\Gamma = \prod_{\langle pq\rangle\in\Gamma}\hat{Z}_{pq}$ does the job. Explicitly,

$$\hat{H}_{\text{b},\Gamma}^{\text{b.s.}}\hat{U}_\Gamma|\Psi_{\text{b}}^{\text{b.s.}}\rangle = \hat{U}_\Gamma\hat{H}_{\text{b}}^{\text{b.s.}}|\Psi_{\text{b}}^{\text{b.s.}}\rangle = E_{\min}\hat{U}_\Gamma|\Psi_{\text{b}}^{\text{b.s.}}\rangle, \tag{4.179}$$

where in the first equality, we used that $\hat{U}_\Gamma$ anticommutes with $\hat{U}_{pq}$ for $\langle pq\rangle \in \Gamma$. Applying

$\hat{G}_p$ to this ground state at either endpoint of Γ, we find that moving an emergent fermion around the endpoint produces a minus sign:

$$\hat{G}_{a/b}\hat{U}_\Gamma|\Psi_{\mathrm{b}}^{\mathrm{b.s.}}\rangle = -\hat{U}_\Gamma|\Psi_{\mathrm{b}}^{\mathrm{b.s.}}\rangle. \tag{4.180}$$

Hence, $\hat{U}_\Gamma$ creates either e excitations or m excitations at its endpoints.

Since ground states of $\hat{H}_{\mathrm{b},\Gamma}^{\mathrm{b.s.}}$ have a pair of e or m excitations relative to ground states of $\hat{H}_{\mathrm{b}}^{\mathrm{b.s.}}$, we can determine the effective symmetry action on a pair of e or m excitations at a and b by bosonizing the effective symmetry action on the fermionic state with fermion parity defects at a and b. For g such that $\sigma(g)$ is non-trivial, the effective symmetry action on the state with fermion parity defects splits into a fermion parity odd operator associated to each defect. Expressing the symmetry action in terms of local fermion parity even operators, so that it may be bosonized, requires a string of hopping operators and fermion parity operators connecting the two fermion parity odd operators. Hence, bosonization yields an effective symmetry action that includes an em string connecting a and b. This em string converts an e (m) string into an m (e) string, and we have recovered the expected effective symmetry action in the bosonic shadow theory of a beyond supercohomology phase at the lattice level.

Finally, to demonstrate that beyond supercohomology SPT ground states cannot be constructed by applying a symmetric finite depth quantum circuit to a trivial product state, we assume that this is indeed possible and derive a contradiction. If such a circuit $\hat{U}^{\mathrm{b.s.}}$ exists, then in bosonizing the circuit we obtain a circuit $\hat{U}_{\mathrm{b}}^{\mathrm{b.s.}}$ which is globally symmetric up to factors of $\hat{G}_p$. (The $\hat{G}_p$ generate the kernel of the fermionization duality.) Explicitly,

$$\hat{V}(g)\hat{U}_{\mathrm{b}}^{\mathrm{b.s.}} = \hat{U}_{\mathrm{b}}^{\mathrm{b.s.}} f_g(\hat{G}_p)\hat{V}(g) \tag{4.181}$$

for some g dependent function f_g of the $\hat{G}_p$. In what follows, let us assume that $\hat{U}_\Gamma$ creates a pair of e excitations. An analogous argument can be made if $\hat{U}_\Gamma$ instead creates m excitations.

Writing a ground state of the toric code with a pair of e excitations as $|\Psi^{ee}_{\text{t.c.}}\rangle$, the ground state of $\hat{H}^{\text{b.s.}}_{\text{b}}$ with e excitations is $\hat{U}^{\text{b.s.}}_{\text{b}}|\Psi^{ee}_{\text{t.c.}}\rangle$. We then compute the effective symmetry action on a pair of e excitations:

$$\begin{aligned}\hat{V}(g)\hat{U}^{\text{b.s.}}_{\text{b}}|\Psi^{ee}_{\text{t.c.}}\rangle &= \hat{U}^{\text{b.s.}}_{\text{b}} f_g(\hat{G}_p)\hat{V}(g)|\Psi^{ee}_{\text{t.c.}}\rangle \\ &= \hat{U}^{\text{b.s.}}_{\text{b}} f_g(\hat{G}_p)|\Psi^{ee}_{\text{t.c.}}\rangle. \end{aligned} \tag{4.182}$$

As we have argued (at least for the anyons created by $\hat{U}_\Gamma$), the effective symmetry action should convert the e excitations into m excitations. However, f_g is a function of small emergent fermion loop operators. Loops of em string are unable to transform e excitation into m excitations. This contradicts the expected affect of global symmetry action in the bosonic shadow model for beyond supercohomology phases.

We have now shown that the ground state of a specific beyond supercohomology model cannot be constructed by applying a symmetric quantum circuit to a trivial product state. This is sufficient to argue that no ground state of any supercohomology model can by constructed from a trivial product state with a symmetric quantum circuit. This is because, by definition, ground states of two beyond supercohomology phases can be related by a quantum circuit built of symmetric local unitaries.

While we have shown that a symmetric quantum circuit is incapable of building the ground state of a beyond supercohomology phase from a trivial product state, it would be interesting to identify a quantum circuit, albeit not symmetric, which is capable of creating the ground state of a beyond supercohomology SPT from a trivial product state. We leave this for future work.

Chapter 5

DISENTANGLING INTERACTING FERMIONIC SPT PHASES IN THREE DIMENSIONS

This chapter is based on:
Yu-An Chen, Tyler D. Ellison, and Nathanan Tantivasadakarn. Disentangling supercohomology symmetry-protected topological phases in three spatial dimensions. Phys. Rev. Research, 3:013056, Jan 2021.

We build exactly solvable lattice Hamiltonians for fermionic symmetry-protected topological (SPT) phases in $(3+1)$D classified by group supercohomology. A central benefit of our construction is that it produces an explicit finite-depth quantum circuit (FDQC) that prepares the ground state from an unentangled symmetric state. The FDQC allows us to clearly demonstrate the characteristic properties of supercohomology phases - namely, symmetry fractionalization on fermion parity flux loops – predicted by continuum formulations. By composing the corresponding FDQCs, we also recover the stacking relations of supercohomology phases. Furthermore, we derive topologically ordered gapped boundaries for the supercohomology models by extending the protecting symmetries, analogous to the construction of topologically ordered boundaries for bosonic SPT phases. Our approach relies heavily on dualities that relate certain bosonic 2-group SPT phases with supercohomology SPT phases. We develop physical motivation for the dualities in terms of explicit lattice prescriptions for gauging a 1-form symmetry and for condensing emergent fermions. We also comment on generalizations to supercohomology phases in higher dimensions and to fermionic SPT phases outside of the supercohomology framework.

5.1 Introduction

Symmetry-protected topological (SPT) phases of matter are classified by quantized invariants that capture a characteristic response to probing with symmetry defects [46, 50, 71, 127, 134, 156–164]. SPT phases built from fermionic degrees of freedom (d.o.f.) must conserve fermion parity, and the associated fermion parity symmetry defects can be used to probe the system. Consequently, the classification of fermionic SPT (fSPT) phases, where the constituent d.o.f. may be fermions, is notably distinct from the classification of bosonic SPT (bSPT) phases, composed of only bosonic d.o.f.. In particular, in three spatial dimensions and with unitary internal symmetries, the bSPT phases are believed to be classified by group cohomology, while the fSPT phases are only *partially* classified by the more rich, group supercohomology theory [46, 49, 50, 126, 129].

The algebraic data of group cohomology can be used to construct an exactly solvable model belonging to a bSPT phase [49]. The celebrated group cohomology models yield a transparent connection between the quantized invariant - namely, a group cocycle ν - and a lattice Hamiltonian. Another feature of these models is that a finite-depth quantum circuit (FDQC) [1] that prepares the ground state from a tensor product state can be written expressly in terms of ν. Further, in Ref. [165], it was shown that the group cohomology data could be used to identify symmetric topologically ordered gapped boundaries for the group cohomology models, by enlarging the protecting symmetry group on the boundary.

In this chapter, we construct exactly solvable models for $(3+1)$D fSPT phases directly from the group supercohomology data that characterizes the phases. The resulting supercohomology models describe fSPT phases protected by finite unitary internal symmetries of the form $G_f = G \times \mathbb{Z}_2^f$, where $\mathbb{Z}_2^f$ denotes the fermion parity symmetry. The supercohomology data can be written as a certain pair of G-dependent functions (ρ, ν), where heuristically, ν corresponds to the data that characterizes the bSPT phases, while ρ captures a response that is intrinsic to fSPT phases [163, 164]. With this, our principal contributions can be stated as follows. For any choice of supercohomology data (ρ, ν) characterizing a $(3+1)$D

fSPT phase:

(i) We construct a representative fSPT Hamiltonian with mutually commuting unfrustrated terms and verify that the quantized responses of the model correspond to the data (ρ, ν) - by explicitly computing the G-symmetry fractionalization on fermion parity fluxes.

(ii) We identify a FDQC that prepares the ground state from a symmetric product state and determine the stacking rules for supercohomology phases from the composition of the FDQCs.

(iii) We use an extension of the symmetry to build symmetric topologically ordered gapped boundaries for the supercohomology model.

Our strategy is largely motivated by the spacetime formulation in Ref. [133], wherein fSPT phases are related to particular 2-group bSPT phases through a process of bosonization. More specifically, our construction can be broken down into the three succinct steps outlined below, and shown schematically in Fig. 5.1.

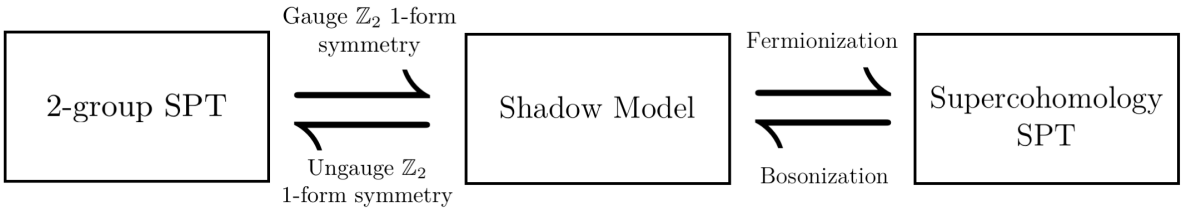

Figure 5.1: To construct a $G_f = G \times \mathbb{Z}_2^f$ supercohomology SPT model we start with a model for a particular 2-group SPT phase determined by the supercohomology data (ρ, ν). Next, we gauge the $\mathbb{Z}_2$ 1-form symmetry of the 2-group to build the shadow model. We then condense the fermion in the shadow model, or apply the fermionization duality, to obtain a model for the supercohomology SPT phase corresponding to (ρ, ν).

(1) Starting with a choice of supercohomology data (ρ, ν), we first build an auxiliary bSPT model with a 2-group symmetry. The 2-group symmetry contains a $\mathbb{Z}_2$ 1-form symmetry as a subgroup.

(2) We gauge the $\mathbb{Z}_2$ 1-form subgroup by minimally coupling the model to a 2-form gauge field. This produces a symmetry-enriched $\mathbb{Z}_2$ gauge theory with an emergent fermion, referred to as the 'shadow model' [124].

(3) Finally, we pair the emergent fermion with a physical fermion and condense the composite excitation: the $\mathbb{Z}_2$ gauge theory is dual to a fermionic theory [166]. The result is a model for a fSPT phase characterized by the supercohomology data (ρ, ν).

Relation to previous work

Our work can be viewed as a generalization of the exactly solvable supercohomology models in $(2+1)$D, described in Refs. [124, 146, 167]. Similarly, the first step is to construct an auxiliary bSPT model from the supercohomology data. In the case discussed here, however, the auxiliary bSPT phase is protected by a higher-form symmetry.

In the pioneering work of Ref. [126], representative wave functions for supercohomology phases were identified by studying re-triangulation invariant non-linear σ models on a discrete spacetime manifold. Later, Ref. [129] provided a comprehensive classification of fSPT phases on a spatial lattice, by solving for consistent domain wall decorations. Our work builds on these results by constructing an explicit parent Hamiltonian for their fixed point wave functions along with FDQCs that prepare the ground states from a product state. Within our framework, we are also able to demonstrate that the supercohomology models indeed exhibit the universal responses to symmetry fluxes captured by the supercohomology data (ρ, ν).

Our strategy for constructing the supercohomology models mirrors the methods employed at the level of spacetime partition functions in Refs. [133, 168, 169]. In particular, Ref. [168]

studies supercohomology phases by constructing a Lagrangian for the associated shadow model. However, we go beyond studying the shadow model and explicitly implement the fermionization duality to establish supercohomology data as quantized invariants of lattice Hamiltonians. In recent work, Ref. [169] constructed gapped boundaries for spacetime models of supercohomology phases using a symmetry extension (see also Ref. [170]). We employ a similar symmetry extension to construct the supercohomology Hamiltonians on a manifold with boundary.

We note that many of the models constructed in this chapter describe intrinsically interacting fSPT phases [127, 134]. That is, there are neither interacting bosonic counterparts nor free-fermionic representations of the phases. Hence, in particular, our work falls outside of the scope of Refs. [10, 11, 171].

Structure of the chapter

In Section 5.2, we define the quantized invariants of supercohomology phases and present our supercohomology models in terms of the associated data. Subsequently, we describe the derivation of the bulk supercohomology models in Sections 5.3 and 5.4. In Section 5.3, we give an example of our construction, for the case where the protecting symmetry is simply $G_f = \mathbb{Z}_2^f$. We use the opportunity to introduce the notation of cohomology on a manifold M, which is used throughout the text. Furthermore, in Section 5.3.2 and Section 5.3.3, we detail a lattice prescription for gauging a 1-form symmetry and condensing an emergent fermion, respectively. Section 5.4 describes the construction of the supercohomology models more generally, where the protecting symmetry is $G_f = G \times \mathbb{Z}_2^f$. We show that the lattice Hamiltonians are indeed characterized by the supercohomology data and recover the additive group structure of supercohomology phases under the operation of stacking by composing the corresponding FDQCs in Section 5.4.4. Section 5.5 presents the symmetry extension method for constructing symmetric gapped boundaries for the supercohomology models; we leave the detailed derivation to Appendix L of Ref. [76]. In Appendix 5.A, we compile the notation used in the chapter. We discuss spin structure and the bosonization duality

of Ref. [166] in Appendix 5.E. The remaining appendices provide the technical details and explicit calculations used in the derivation of our models.

5.2 Supercohomology models

Before discussing the construction of the supercohomology models in Sections 5.3 and 5.4, we give a concise description of the models themselves. We begin with a definition for the supercohomology data (ρ, ν), and we assume familiarity with group cohomology. The group cohomology notation used here is summarized in Appendix 5.A.1. In Section 5.2.2, we then review the group cohomology models of Ref. [49]. We finish with Section 5.2.3, where we define the more general supercohomology models and describe the stacking rules for the supercohomology phases, derived from the composition of FDQCs.

5.2.1 Supercohomology data

The supercohomology data gives quantized invariants for $(3+1)$D fSPT phases protected by a finite onsite[1] unitary $G_f = G \times \mathbb{Z}_2^f$ symmetry. To streamline the discussion, we refer to Appendix 5.A.1 for a review of the notation from group cohomology. We freely use the notion of group cochains, the coboundary operator δ, and the cup-n products $\cup_n$ with $n \in \{0, 1, 2\}$ in the discussion below.

For a finite group G, the supercohomology data is given by a pair of group cochains (ρ, ν) belonging to:

$$(\rho, \nu) \in C^3(G, \mathbb{Z}_2) \times C^4(G, \mathbb{R}/\mathbb{Z}). \tag{5.1}$$

Furthermore, ρ and ν satisfy the relations [126]:

$$\delta\rho = 0, \quad \delta\nu = \frac{1}{2}\rho \cup_1 \rho. \tag{5.2}$$

[1] An onsite representation of a 0-form G symmetry is a representation of G in which, for all $g \in G$ the representation $V(g)$ is a tensor product of linear representations of G on each site.

Note that if $\rho = 0$, then ν is a group cocycle ($\delta\nu = 0$). In this case, the supercohomology data reduces to the data that characterizes bSPT phases within the group cohomology framework [49].

The supercohomology data is further organized into equivalence classes. Two sets of supercohomology data (ρ, ν) and (ρ', ν') are considered equivalent if there exists:

$$\beta \in C^2(G, \mathbb{Z}_2), \quad \eta \in C^3(G, \mathbb{R}/\mathbb{Z}), \tag{5.3}$$

such that:

$$\begin{aligned} \rho' &= \rho + \delta\beta \\ \nu' &= \nu + \delta\eta + \frac{1}{2}\beta \cup \beta + \frac{1}{2}\beta \cup_1 \delta\beta + \frac{1}{2}\rho \cup_2 \delta\beta. \end{aligned} \tag{5.4}$$

In Section 5.4.4, we give physical motivation for the equivalence relation and show that if (ρ, ν) and (ρ', ν') are equivalent, then the corresponding supercohomology models belong to the same fSPT phase.

Throughout the text, we use the convention that group cochains are homogeneous. Therefore, in what follows, we take ρ and ν to be functions:

$$\begin{aligned} \rho &: G^4 \to \mathbb{Z}_2 = \{0, 1\}, \\ \nu &: G^5 \to \mathbb{R}/\mathbb{Z} = [0, 1), \end{aligned} \tag{5.5}$$

which are homogeneous, i.e., for any $h \in G$:

$$\begin{aligned} \rho(g_0, g_1, g_2, g_3) &= \rho(hg_0, hg_1, hg_2, hg_3), \\ \nu(g_0, g_1, g_2, g_3, g_4) &= \nu(hg_0, hg_1, hg_2, hg_3, hg_4). \end{aligned} \tag{5.6}$$

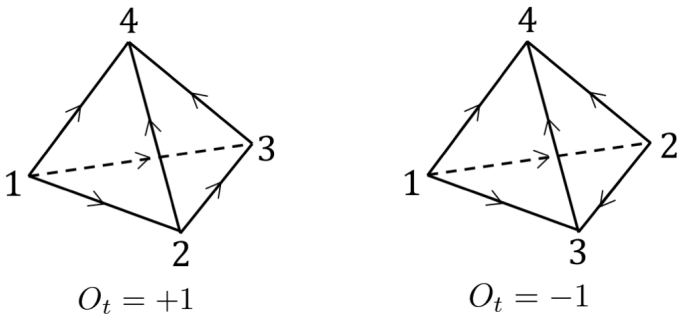

Figure 5.2: A branching structure determines an ordering of the vertices of a tetrahedron. The vertices are ordered by the number of edges oriented towards the vertex. The branching structure also gives an orientation of each tetrahedron relative to the orientation of M. We use the convention that the tetrahedron pictured on the left is positively oriented ($O_t = +1$), and the tetrahedron to the right is negatively oriented ($O_t = -1$).

5.2.2 Review of group cohomology models

When ρ is zero, the supercohomology data is equivalent to the familiar group cohomology data, which characterizes $(3+1)$D bSPT phases with a finite onsite unitary G symmetry. As a consequence, the corresponding group cohomology models are a special case of the supercohomology models. We build up to the supercohomology models in Section 5.2.3 by first reviewing the group cohomology models of Ref. [49].

The group cohomology models are defined on an arbitrary triangulation of an orientable closed 3-manifold M. The triangulation of M gives a decomposition of M into vertices, edges, faces, and tetrahedra. We further require that the triangulation is equipped with a branching structure – an assignment of an orientation to each edge in such a way that there are no cycles around any of the faces. A branching structure yields both an ordering of the vertices of each tetrahedron as well as an orientation $O_t \in \{-1, +1\}$ of any tetrahedron t relative to the orientation of M (see Fig. 5.2).

The Hilbert spaces for the group cohomology models are formed by placing a G d.o.f. on each vertex of M (Fig. 5.3). A basis for the $|G|$ dimensional Hilbert space at vertex v is given by states $|g_v\rangle$ labeled by elements of G. Furthermore, a basis for the full Hilbert

space is given by product states of the form $|\{g_v\}\rangle$, in which, the state at vertex v is $|g_v\rangle$. The G symmetry is represented using the regular representation, i.e., for any $h \in G$, h is represented by:

$$V(h) \equiv \sum_{\{g_v\}} |\{hg_v\}\rangle\langle\{g_v\}|. \tag{5.7}$$

The group cohomology models can be built from a G-paramagnet Hamiltonian – a Hamiltonian belonging to the trivial SPT phase. The G-paramagnet Hamiltonian is given by:

$$H^G \equiv -\sum_v \mathcal{P}_v, \tag{5.8}$$

where the sum is over vertices in M, and $\mathcal{P}_v$ is a projector onto a symmetric state at the vertex v, i.e.:

$$\mathcal{P}_v \equiv \frac{1}{|G|}\left(\sum_{g_v} |g_v\rangle\right)\left(\sum_{g_v}\langle g_v|\right). \tag{5.9}$$

The ground state $|\Psi^G\rangle$ of the G-paramagnet Hamiltonian is a tensor product of a symmetric state at each vertex. This can be written as an equal amplitude superposition over all $\{g_v\}$ configurations:

$$|\Psi^G\rangle \equiv \sum_{\{g_v\}} |\{g_v\}\rangle. \tag{5.10}$$

Here, as elsewhere in the chapter, we omit the normalization of the state for notational convenience.

We build the group cohomology model corresponding to the group cocycle ν by conjugating H^G by a FDQC $\mathcal{U}_b$. $\mathcal{U}_b$ is defined in terms of the data ν as [49]:

$$\mathcal{U}_b \equiv \sum_{\{g_v\}} \prod_{t=\langle 1234\rangle} e^{2\pi i O_t \nu(1,g_1,g_2,g_3,g_4)} |\{g_v\}\rangle\langle\{g_v\}|, \tag{5.11}$$

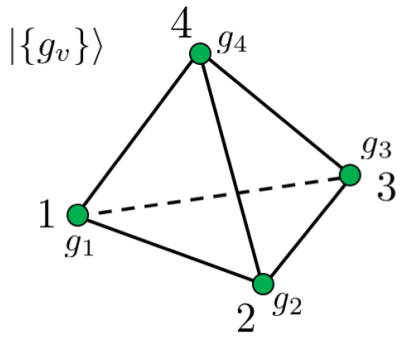

Figure 5.3: The group cohomology models are defined on a Hilbert space consisting of a G d.o.f. on every vertex. The configuration states $|\{g_v\}\rangle$ form a basis for the Hilbert space.

where the product is over all tetrahedra in M, the vertices specifying the tetrahedron $\langle 1234\rangle$ are ordered according to the branching structure, and 1, in the argument of ν, denotes the identity in G. To simplify the notation, we introduce an operator $\hat{\boldsymbol{\nu}}(\langle 1234\rangle)$, for each tetrahedron $\langle 1234\rangle$ in M:

$$\hat{\boldsymbol{\nu}}(\langle 1234\rangle) \equiv \sum_{\{g_v\}} \nu(1, g_1, g_2, g_3, g_4)|\{g_v\}\rangle\langle\{g_v\}|. \tag{5.12}$$

With this, $\mathcal{U}_b$ can be written more compactly as:

$$\mathcal{U}_b = \prod_t e^{2\pi i O_t \hat{\boldsymbol{\nu}}(t)}. \tag{5.13}$$

The Hamiltonian for the group cohomology model is then:

$$H_b \equiv \mathcal{U}_b H^G \mathcal{U}_b^\dagger, \tag{5.14}$$

with the unique ground state:

$$|\Psi_b\rangle \equiv \mathcal{U}_b|\Psi^G\rangle = \sum_{\{g_v\}} \prod_{t=\langle 1234\rangle} e^{2\pi i O_t \nu(1,g_1,g_2,g_3,g_4)}|\{g_v\}\rangle. \tag{5.15}$$

The Hamiltonian H_b indeed describes a bSPT phase. This is because the Hamiltonian is both symmetric and has a unique short-range entangled (SRE) ground state. The symmetry of the Hamiltonian follows from the fact that $\mathcal{U}_b$ is symmetric, which can be shown using the property $\delta\nu = 0$. The ground state is SRE, since it can be prepared from a product state by the FDQC $\mathcal{U}_b$.[2] Furthermore, the group cohomology models exhibit the characteristic responses encoded by ν, as can be checked by introducing symmetry defects or gauging the G symmetry and analyzing the properties of the symmetry fluxes [46, 160].

5.2.3 Definition of supercohomology models

We now generalize the discussion to supercohomology models, which describe fSPT phases. We leave the explicit derivation of the models from a choice of supercohomology data (ρ, ν) to Sections 5.3 and 5.4. Similarly to the group cohomology models, the supercohomology models are prepared from a Hamiltonian in a trivial SPT phase by conjugation with a FDQC. Further, the FDQCs for (ρ, ν) and (ρ', ν') can be used to recover the stacking laws for supercohomology phases, discussed at the end of this section.

The supercohomology models are defined on a Hilbert space with G d.o.f. at the vertices of M, as in the previous section, along with a fermionic d.o.f. at each tetrahedron.[3] Specifically, we place a single spinless complex fermion at the center of each tetrahedron and label the two Majorana operators at the tetrahedron t by γ_t and γ'_t (see Fig. 5.4). The fermion parity at t is then given by:

$$P_t \equiv -i\gamma_t\gamma'_t, \tag{5.16}$$

and we also introduce a "hopping" operator S_f that changes the fermion parity on either

[2] We note that, although $\mathcal{U}_b$ is symmetric, this does not imply that the state $|\Psi_b\rangle$ in Eq. (5.15) belongs to the trivial SPT phase. This is only the case if $\mathcal{U}_b$ can additionally be expressed as a FDQC composed of symmetric local unitaries.

[3] We note that the manifold admits a spin structure. This is always true for orientable 3-manifolds.

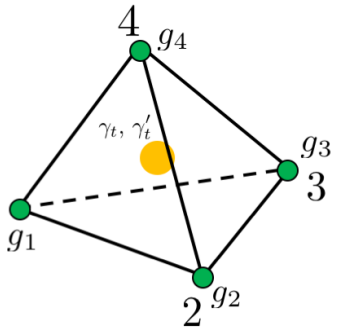

Figure 5.4: Our model for a fSPT phase is defined on a Hilbert space with G d.o.f. on the vertices of a triangulation of M and a single spinless complex fermion at the center of each tetrahedron.

side of the face f:

$$S_f \equiv (-1)^{\boldsymbol{f}(E)} i\gamma_{L(f)}\gamma'_{R(f)}. \tag{5.17}$$

Here, $L(f)$ and $R(f)$ are the tetrahedra neighboring f such that the orientation of f points out of the tetrahedron $L(f)$ and into the tetrahedron $R(f)$ (see Fig. 5.5). $\boldsymbol{f}(E) \in \{0,1\}$ corresponds to a choice of spin-structure and is determined by the branching structure of the triangulation of M. We refer to Appendix 5.E and Ref. [172] for the explicit form of $\boldsymbol{f}(E)$. As before, the G symmetry is represented with the regular representation, and here the global fermion parity symmetry is generated by $\prod_t P_t$.

The supercohomology models are built from a Hamiltonian belonging to a trivial fSPT phase - namely, an atomic insulator with a decoupled G-paramagnet. The trivial fSPT Hamiltonian is explicitly:

$$H^G_{\mathrm{AI}} \equiv -\sum_t P_t - \sum_v \mathcal{P}_v. \tag{5.18}$$

The ground state $|\Psi^G_{\mathrm{AI}}\rangle$ of H^G_{AI} is a product state with zero fermion occupancy at each

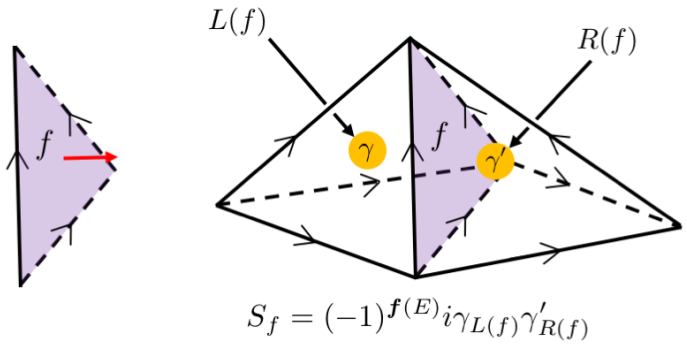

Figure 5.5: The orientation of a face f (red vector) is determined by the branching structure. The orientation of f points out of the tetrahedron $L(f)$ and into the tetrahedron $R(f)$. The hopping operator S_f acts with γ on the complex fermion Hilbert space at $L(f)$ and γ' on the site at $R(f)$.

tetrahedron and a symmetric state at each vertex.

Given a choice of supercohomology data (ρ, ν), we prepare the supercohomology model from H^G_{AI} by conjugation with the FDQC $\mathcal{U}_f$:

$$\mathcal{U}_f \equiv \prod_t e^{2\pi i O_t \hat{\boldsymbol{\nu}}(t)} \xi_{\bar{\rho}}(M) \prod_f S_f^{\hat{\boldsymbol{\rho}}(f)} \prod_t P_t^{\int \hat{\boldsymbol{\rho}} \cup_2 \boldsymbol{t}}. \tag{5.19}$$

Let us unpack the notation used in the definition of $\mathcal{U}_f$. First of all, the $\hat{\boldsymbol{\nu}}(t)$ term is analogous to the FDQC $\mathcal{U}_b$ in Section 5.2.2, tensored with the identity on the fermionic d.o.f.. Second, the product over hopping operators in Eq. (5.19) depends on a choice of ordering for the faces $f \in M$, since not all hopping operators commute. However, $\xi_{\bar{\rho}}(M)$ is an order dependent sign that compensates for the choice of ordering. Therefore, in the end, the FDQC is independent of the choice of ordering for the faces in M. We give the explicit

form of $\xi_{\bar{\rho}}(M)$ in Section 5.4.4.[4] $\hat{\bar{\boldsymbol{\rho}}}(f)$ is the ρ-dependent operator:

$$\hat{\bar{\boldsymbol{\rho}}}(\langle 123\rangle) \equiv \sum_{\{g_v\}} \rho(1, g_1, g_2, g_3) |\{g_v\}\rangle\langle\{g_v\}|, \tag{5.20}$$

for an arbitrary face $\langle 123\rangle$ and implicitly tensored with the identity on the fermionic d.o.f.. Finally, for a tetrahedron $t = \langle 1234\rangle$, $\int \hat{\bar{\boldsymbol{\rho}}} \cup_2 \boldsymbol{t}$ is shorthand for:

$$\int \hat{\bar{\boldsymbol{\rho}}} \cup_2 \boldsymbol{t} = \hat{\bar{\boldsymbol{\rho}}}(\langle 123\rangle) + \hat{\bar{\boldsymbol{\rho}}}(\langle 134\rangle). \tag{5.21}$$

The exactly-solvable fermionic Hamiltonian produced by conjugating H^G_{AI} by $\mathcal{U}_f$ is thus:

$$H_f \equiv \mathcal{U}_f H^G_{\text{AI}} \mathcal{U}_f^\dagger, \tag{5.22}$$

which has the unique ground state $|\Psi_f\rangle$:

$$|\Psi_f\rangle \equiv \mathcal{U}_f |\Psi^G_{\text{AI}}\rangle. \tag{5.23}$$

H_f describes a system in a $G \times \mathbb{Z}_2^f$ fermionic SPT phase, because (i) H_f is symmetric and (ii) it has a unique, SRE ground state [Eq. (5.23)]. The Hamiltonian in Eq. (5.22) is symmetric, since both H^G_{AI} and $\mathcal{U}_f$ are invariant under the symmetry – we argue that $\mathcal{U}_f$ is symmetric in Section 5.4.4.[5] The ground state is unique and SRE, because H_f is unitarily equivalent to a trivial fSPT Hamiltonian with a unique ground state and the unitary is a FDQC.

Most importantly, H_f belongs to the fSPT phase characterized by the corresponding supercohomology data (ρ, ν). We show this in Section 5.4.4, by gauging the fermion parity symmetry of H_f. This results in a G-symmetry-enriched $\mathbb{Z}_2$ gauge theory, where the G sym-

[4] We note that while $\xi_{\bar{\rho}}(M)$ depends on a global ordering of the faces in M, it can nonetheless be implemented by a FDQC. This can be seen from the derivation of $\xi_{\bar{\rho}}(M)$ in Appendix 5.G.2.

[5] Although $\mathcal{U}_f$ is symmetric, it cannot be decomposed into a FDQC comprised of symmetric local unitaries.

metry fractionalizes on the fermion parity flux loops, as determined by ρ. The appropriate responses to G-symmetry defects follow from the bosonic, group cohomology case.

We can gain intuition for the fSPT Hamiltonian by inserting the right hand side of Eq (5.18) into the expression for H_f:

$$H_f = -\sum_t \left(\mathcal{U}_f P_t \mathcal{U}_f^\dagger\right) - \sum_v \left(\mathcal{U}_f \mathcal{P}_v \mathcal{U}_f^\dagger\right). \tag{5.24}$$

By commuting the hopping operators of $\mathcal{U}_f$ past the parity operator P_t and using that $\delta\rho = 0$, the tetrahedron terms become:

$$-\sum_t \left(\mathcal{U}_f P_t \mathcal{U}_f^\dagger\right) = -\sum_{t=\langle 1234\rangle} (-1)^{\rho(g_1,g_2,g_3,g_4)} P_t. \tag{5.25}$$

In the ground state, the fermion occupancy depends on the $\{g_v\}$-configuration. For a $\{g_v\}$-configuration $|\{g_v\}\rangle$, it is energetically preferable for the fermion occupancy at the tetrahedron $\langle 1234\rangle$ to be equal to $\rho(g_1, g_2, g_3, g_4)$. In this way, complex fermions are bound to junctions of symmetry domains. The vertex terms of H_f, on the other hand:

$$-\sum_v \left(\mathcal{U}_f \mathcal{P}_v \mathcal{U}_f^\dagger\right), \tag{5.26}$$

are more difficult to compute, in general. Heuristically, they fluctuate the G d.o.f. and create, move, and annihilate fermions without affecting the tetrahedron terms in Eq. (5.25). The ground state is thus a weighted superposition of $\{g_v\}$-configurations with the fermion occupancy at each tetrahedron $\langle 1234\rangle$ equal to $\rho(g_1, g_2, g_3, g_4)$. This is in agreement with the fixed point wave functions in Ref. [129].

Stacking rules for supercohomology phases

Having defined the models, we can now deduce the stacking rules for supercohomology phases. We recall that two states can be stacked by taking the tensor product. Given two

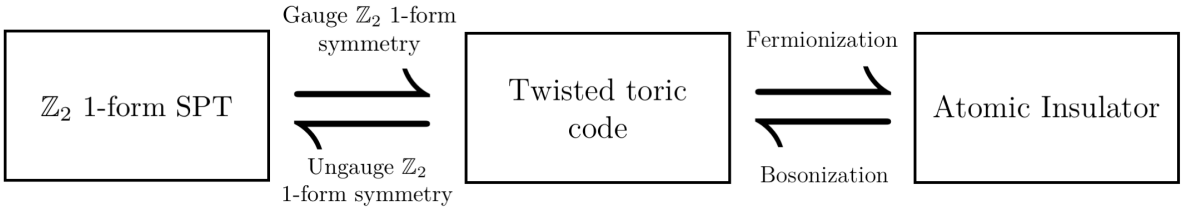

Figure 5.6: In the case of $G_f = \mathbb{Z}_2^f$, the construction of a fermionic model starts with a model for a certain $\mathbb{Z}_2$ 1-form SPT phase. We then gauge the $\mathbb{Z}_2$ 1-form symmetry to obtain a twisted toric code. Lastly, we fermionize the twisted toric code, and the result is a model for an atomic insulator.

G-SPT states $|\Psi_{\text{SPT}_1}\rangle$ and $|\Psi_{\text{SPT}_2}\rangle$, the stacked state $|\Psi_{\text{SPT}_1}\rangle \otimes |\Psi_{\text{SPT}_2}\rangle$ also belongs to a G-SPT phase. Thus, the stacking of G-SPT states induces an operation $\boxtimes$ at the level of the SPT phases.

In Ref. [167], it was argued that the stacking operation $\boxtimes$ on SPT phases can be determined from the composition of FDQCs. To state the result from Ref. [167], we define $\mathcal{U}_{\text{SPT}_1}$ and $\mathcal{U}_{\text{SPT}_2}$ to be symmetric FDQCs that prepare the G-SPT states $|\Psi_{\text{SPT}_1}\rangle$ and $|\Psi_{\text{SPT}_2}\rangle$, respectively, from a symmetric product state. According to Ref. [167], if $|\Psi_{\text{SPT}_1}\rangle$ and $|\Psi_{\text{SPT}_2}\rangle$ belong to the same Hilbert space, then the composition of the FDQCs $\mathcal{U}_{\text{SPT}_1}$ and $\mathcal{U}_{\text{SPT}_2}$ prepares a state belonging to the same G-SPT phase as $|\Psi_{\text{SPT}_1}\rangle \otimes |\Psi_{\text{SPT}_2}\rangle$.

With this, we determine the group law under stacking for $(3+1)$D supercohomology phases by composing the FDQCs $\mathcal{U}_f$ defined in Eq. (5.19). Given two sets of supercohomology data (ρ, ν) and (ρ', ν') both characterizing fSPT phases with a $G \times \mathbb{Z}_2^f$ symmetry, we consider stacking the ground states of the corresponding supercohomology models, denoted by $|\Psi_f^{\rho\nu}\rangle$ and $|\Psi_f^{\rho'\nu'}\rangle$, respectively. The result from Ref. [167] tells us that the stacked state $|\Psi_f^{\rho\nu}\rangle \otimes |\Psi_f^{\rho'\nu'}\rangle$ belongs to the same phase as the state prepared by applying $\mathcal{U}_f^{\rho'\nu'}\mathcal{U}_f^{\rho\nu}$ to a symmetric product state. Here, $\mathcal{U}_f^{\rho\nu}$ and $\mathcal{U}_f^{\rho'\nu'}$ are the FDQCs from Eq. (5.19) that prepare $|\Psi_f^{\rho\nu}\rangle$ and $|\Psi_f^{\rho'\nu'}\rangle$ from an unentangled symmetric state, respectively. In Appendix 5.G.3, we show that the composition $\mathcal{U}_f^{\rho'\nu'}\mathcal{U}_f^{\rho\nu}$ is equivalent to a FDQC $\mathcal{U}_f^{\rho''\nu''}$ corresponding to a set of

supercohomology data (ρ'', ν''):

$$(\rho'', \nu'') = (\rho + \rho', \nu + \nu' + \frac{1}{2}\rho \cup_2 \rho'). \tag{5.27}$$

Therefore, at the level of the supercohomology data, the stacking operation $\boxtimes$ is:

$$(\rho, \nu) \boxtimes (\rho', \nu') = (\rho + \rho', \nu + \nu' + \frac{1}{2}\rho \cup_2 \rho'), \tag{5.28}$$

in agreement with Ref. [126].

5.3 *Bulk construction:* $G_f = \mathbb{Z}_2^f$

We begin by illustrating our construction of exactly-solvable models for fSPT phases in the simplest possible case – for fSPT phases protected by only fermion parity symmetry $\mathbb{Z}_2^f$. While the resulting fSPT model is trivial (an atomic insulator), we nonetheless find this example instructive in demonstrating the general strategy. Moreover, we use this as an opportunity to introduce notation used throughout the chapter.

To start, we describe a model for a certain bosonic SPT phase protected by a $\mathbb{Z}_2$ 1-form symmetry in (3+1)D. The special property of this bosonic SPT is that, upon gauging the $\mathbb{Z}_2$ 1-form symmetry, we obtain a $\mathbb{Z}_2$ gauge theory with an emergent fermion. We refer to this $\mathbb{Z}_2$ gauge theory as the *twisted* toric code. In the final step, we employ the fermionization duality of Ref. [15] to map the twisted toric code to a model with a fundamental fermion. The construction is shown schematically in Fig. 5.6, for the case of $G_f = \mathbb{Z}_2^f$.

5.3.1 1-*form SPT and notation*

SPT phases protected by higher form symmetries, including 1-form symmetries, were first introduced in Ref. [173]. Subsequently, fixed point Hamiltonians for 1-form SPT phases were described in detail in Refs. [74] and [79]. We note that the Hamiltonian discussed in this section agrees with the model in Ref. [79] and is closely related to the $\mathbb{Z}_2 \times \mathbb{Z}_2$ 1-form SPT

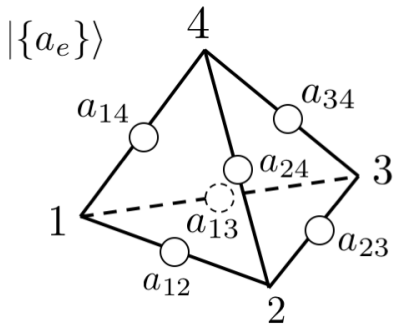

Figure 5.7: The 1-form SPT model is defined on a triangulation where each edge hosts a $\mathbb{Z}_2$ d.o.f. (represented by a circle). A state in the configuration basis is given by a value $a_e \in \{0, 1\}$ chosen for each edge e. We have suppressed the branching structure for clarity.

model of Ref. [74].[6]

Our model for a nontrivial $\mathbb{Z}_2$ 1-form SPT phase can be defined on an arbitrary triangulation of an oriented closed 3-manifold M equipped with a branching structure, as described in Section 5.2.2. We define a Hilbert space on M using the triangulation of the manifold – at each edge of the triangulation, we place a single $\mathbb{Z}_2$ degree of freedom. Correspondingly, a basis for the Hilbert space at edge e is given by states $|a_e\rangle$ with a_e valued in $\{0, 1\}$. The Pauli Z and Pauli X operators at each e act as:

$$Z_e|a_e\rangle = (-1)^{a_e}|a_e\rangle, \quad X_e|a_e\rangle = |a_e + 1\rangle, \tag{5.29}$$

where addition is taken modulo 2. A basis for the total Hilbert space consists of states $|\{a_e\}\rangle$ labeled by configurations $\{a_e\}$ (Fig. 5.7). Here, the state $|\{a_e\}\rangle$ denotes a product state with the d.o.f. at edge e in the state $|a_e\rangle$.

The $\mathbb{Z}_2$ 1-form symmetry acts on closed codimension-1 submanifolds of the dual lattice. In particular, we represent the symmetry action on a closed surface Σ of the dual lattice

[6]Specifically, our model is equivalent to the model in Ref. [74] on a four-colorable triangulation and upon restricting to the diagonal $\mathbb{Z}_2$ of the $\mathbb{Z}_2 \times \mathbb{Z}_2$ symmetry.

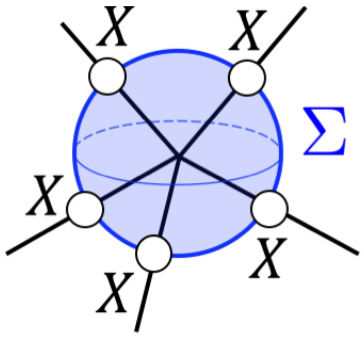

Figure 5.8: The 1-form symmetry operators act on closed surfaces in the dual lattice. Pauli X operators are applied to each edge intersected by the surface. The figure shows a surface Σ (blue) that encloses a single vertex.

with the operator:

$$A_\Sigma \equiv \prod_{e \perp \Sigma} X_e, \tag{5.30}$$

where the product is over edges intersected by the surface Σ (see Fig. 5.8).

We construct our model for the nontrivial SPT phase starting with a Hamiltonian for a $\mathbb{Z}_2$ 1-form paramagnet. The Hamiltonian for the 1-form paramagnet is given by:

$$H_0 = -\sum_e X_e. \tag{5.31}$$

H_0 is certainly symmetric, as it commutes with A_Σ for every surface Σ of the dual lattice. Further, the unique ground state of H_0 is a product state with the $+1$ eigenstate of X_e at each edge e. This state can be expressed in the configuration basis as:

$$|\Psi_0\rangle \equiv \sum_{\{a_e\}} |\{a_e\}\rangle, \tag{5.32}$$

with the sum over all configurations $\{a_e\}$.

Now, our model for the nontrivial $\mathbb{Z}_2$ 1-form SPT phase is built from the 1-form param-

agnet in Eq. (5.31) by conjugation with the FDQC:

$$\mathcal{U}_1 \equiv \sum_{\{a_e\}} \prod_{t=\langle 1234\rangle} (-1)^{a_{12}(a_{23}+a_{34}+a_{24})} |\{a_e\}\rangle\langle\{a_e\}|. \tag{5.33}$$

Specifically, the Hamiltonian of the nontrivial $\mathbb{Z}_2$ 1-form SPT model is:

$$H_1 \equiv \mathcal{U}_1 H_0 \mathcal{U}_1^\dagger = -\sum_e \mathcal{U}_1 X_e \mathcal{U}_1^\dagger. \tag{5.34}$$

Indeed, H_1 describes a *nontrivial* $\mathbb{Z}_2$ 1-form SPT phase. In the next section, we show this by gauging the 1-form symmetry. The 1-form paramagnet H_0 is mapped to a $\mathbb{Z}_2$ gauge theory with an emergent boson - the usual 3D toric code, while H_1 is mapped to a $\mathbb{Z}_2$ gauge theory with an emergent fermion - a "twisted toric code".

For now, we note that the model in Eq. (5.34) is symmetric and exactly solvable. In Appendix 5.B, we show that $\mathcal{U}_1$ is symmetric under the $\mathbb{Z}_2$ 1-form symmetry. Consequently, H_1 is also symmetric. Furthermore, the model is exactly solvable, since by construction, the terms in H_1 are mutually commuting and unfrustrated. The unique ground state is then expressly:

$$|\Psi_1\rangle \equiv \mathcal{U}_1|\Psi_0\rangle = \sum_{\{a_e\}} \prod_{t=\langle 1234\rangle} (-1)^{a_{12}(a_{23}+a_{34}+a_{24})} |\{a_e\}\rangle. \tag{5.35}$$

To further motivate this model, we recount the spacetime construction of the $\mathbb{Z}_2$ 1-form SPT phase in Ref. [79]. We consider a partition function for the SPT phase on the cone of M, denoted CM, which is the (3+1)D spacetime formed by connecting a single spacetime vertex to each vertex of the closed manifold M as shown in Fig. 5.9. This produces a manifold with a boundary equal to M. We refer to the edges connected to the additional spacetime point as "time-like" edges and extend the branching structure so that the time-like edges have an orientation pointing away from the additional spacetime vertex. Then, the partition

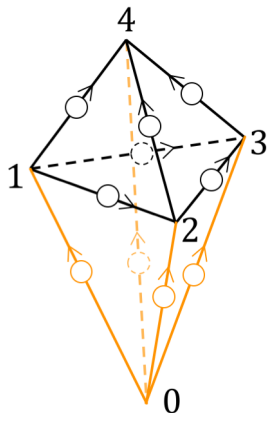

Figure 5.9: The cone of M is constructed by connecting the vertices of M to an additional spacetime point labeled by 0. A tetrahedron of the spatial manifold M is shown in black. The time-like edges (orange) are oriented away from the 0 vertex. The 1-form SPT partition function is defined on CM with $\mathbb{Z}_2$ d.o.f. on the time-like edges (orange circles). Due to the re-triangulation invariance of the partition function, a_{01}, a_{02}, and a_{03} can be set to 0.

function for the 1-form SPT model is [79]:[7]

$$\mathcal{Z}_1 = \sum_{\{a_e\}} \prod_{\langle 01234\rangle} (-1)^{(a_{01}+a_{12}+a_{02})(a_{23}+a_{34}+a_{24})}, \tag{5.36}$$

with the product over spacetime 4-simplices. The amplitude for a fixed configuration $\{a_e\}$:

$$\Psi_1(\{a_e\}) \equiv \prod_{\langle 01234\rangle} (-1)^{(a_{01}+a_{12}+a_{02})(a_{23}+a_{34}+a_{24})}, \tag{5.37}$$

is topological in the sense that it is invariant under re-triangulations of the spacetime manifold. Through re-triangulations, it can be seen that the values of a_e on the time-like edges do not affect the amplitude. Therefore, we may set their value to 0, for simplicity. As a

[7] Using notation introduced later in the chapter, the expression:

$$(a_{01} + a_{12} + a_{02})(a_{23} + a_{34} + a_{24}),$$

can be written as $\delta \boldsymbol{a}_e \cup \delta \boldsymbol{a}_e(\langle 01234\rangle)$. $\delta \boldsymbol{a}_e \cup \delta \boldsymbol{a}_e$ is a nontrivial $\mathbb{Z}_2$ 1-form cocycle that has been pulled back to CM.

result, the amplitude for a configuration $\{a_e\}$ on M reduces to:

$$\Psi_1(\{a_e\}) \equiv \prod_{t=\langle 1234\rangle} (-1)^{a_{12}(a_{23}+a_{34}+a_{24})}, \tag{5.38}$$

where the product is over tetrahedra $t = \langle 1234\rangle$ on the boundary of CM. This gives the amplitude $\Psi_1(\{a_e\})$ for a wave function on M with the configuration $\{a_e\}$, as in Eq. (5.35). We remark that this construction parallels the approach for building 0-form SPT Hamiltonians in Ref. [49].

$\mathbb{Z}_2$ cohomology on M

At this point, we find it convenient to introduce the language of $\mathbb{Z}_2$ cohomology on M. The cohomology notation allows for compact expressions and, in our opinion, more transparent calculations. Here, we only describe the necessary ingredients, and we leave a more thorough summary to Appendix 5.A.2. In the process of introducing concepts from $\mathbb{Z}_2$ cohomology on M, we re-express the 1-form SPT model using the corresponding notation. In particular, we aim to write H_1 in an explicit form.

To begin, we define a p-cochain as a linear, $\mathbb{Z}_2$-valued function of p-simplices in M. For example, we can consider the 1-cochain $\boldsymbol{e}$ defined by:

$$\boldsymbol{e}(e') = \begin{cases} 1 & e' = e \\ 0 & \text{otherwise.} \end{cases} \tag{5.39}$$

In words, $\boldsymbol{e}$ evaluates to 1 on the edge e and 0 on all other edges. More general 1-cochains can be formed from linear combinations of 1-cochains of the form in Eq. (5.39). Specifically, for each configuration $\{a_e\}$ we can define a corresponding 1-cochain $\boldsymbol{a}_e$ as:

$$\boldsymbol{a}_e \equiv \sum_{\boldsymbol{e}} a_e \boldsymbol{e}. \tag{5.40}$$

Evaluating $\boldsymbol{a}_e$ on an edge e' gives:

$$\boldsymbol{a}_e(e') = \sum_{\boldsymbol{e}} a_e \boldsymbol{e}(e') = a_{e'}. \tag{5.41}$$

Given the correspondence between 1-cochains and configurations $\{a_e\}$ in Eq. (5.40), we can label a configuration state $|\{a_e\}\rangle$ by the 1-cochain $\boldsymbol{a}_e$:

$$|\{a_e\}\rangle \to |\boldsymbol{a}_e\rangle. \tag{5.42}$$

In this notation, a Pauli Z operator at edge e' acts on the state $|\boldsymbol{a}_e\rangle$ as:

$$Z_{e'}|\boldsymbol{a}_e\rangle = (-1)^{\boldsymbol{a}_e(e')}|\boldsymbol{a}_e\rangle, \tag{5.43}$$

and an $X_{e'}$ operator acts as:

$$X_{e'}|\boldsymbol{a}_e\rangle = |\boldsymbol{a}_e + \boldsymbol{e}'\rangle. \tag{5.44}$$

Moreover, the action of the 1-form symmetry operator A_Σ on a configuration state is:

$$A_\Sigma|\boldsymbol{a}_e\rangle = \prod_{e\perp\Sigma} X_e|\boldsymbol{a}_e\rangle = |\boldsymbol{a}_e + \sum_{e\perp\Sigma} \boldsymbol{e}\rangle = |\boldsymbol{a}_e + \boldsymbol{\Sigma}\rangle, \tag{5.45}$$

where we have defined the 1-cochain $\boldsymbol{\Sigma}$ as:

$$\boldsymbol{\Sigma} \equiv \sum_{e\perp\Sigma} \boldsymbol{e}. \tag{5.46}$$

Next, we introduce the coboundary operator δ, which is a linear map taking p-cochains to $(p+1)$-cochains. Specifically, it maps a p-cochain $\boldsymbol{c}$ to the $(p+1)$-cochain $\delta\boldsymbol{c}$ for which:

$$\delta\boldsymbol{c}(s) = \boldsymbol{c}(\partial s), \tag{5.47}$$

where s is any $(p+1)$-simplex and ∂s denotes a formal sum of p-simplices in the boundary of s. Simply put, the $(p+1)$-cochain $\delta \boldsymbol{c}$ is evaluated on a $(p+1)$-simplex s by evaluating $\boldsymbol{c}$ on the boundary components of s. The coboundary of $\boldsymbol{a}_e$, for example, is a 2-cochain satisfying:

$$\begin{aligned} \delta \boldsymbol{a}_e(\langle 123\rangle) &= \boldsymbol{a}_e(\langle 12\rangle + \langle 23\rangle + \langle 13\rangle) \\ &= \boldsymbol{a}_e(\langle 12\rangle) + \boldsymbol{a}_e(\langle 23\rangle) + \boldsymbol{a}_e(\langle 13\rangle) \\ &= a_{12} + a_{23} + a_{13}, \end{aligned} \tag{5.48}$$

for a face $\langle 123\rangle$.

If the coboundary of a p-cochain is 0, we call the p-cochain closed. The 1-cochain $\boldsymbol{\Sigma}$ in Eq. (5.46) is closed, i.e.:

$$\delta \boldsymbol{\Sigma} = 0. \tag{5.49}$$

This is because Σ is a closed surface of the dual lattice. As such, for any face f, the boundary of f contains an even number of edges intersected by Σ.

Further, we define the cup product $\cup$. The cup product maps a p-cochain $\boldsymbol{c}$ and a q-cochain $\boldsymbol{d}$ to a $(p+q)$-cochain $\boldsymbol{c} \cup \boldsymbol{d}$. Specifically, $\boldsymbol{c} \cup \boldsymbol{d}$ evaluated on a $(p+q)$-simplex $\langle 0, \ldots, p+q\rangle$ is:

$$\boldsymbol{c} \cup \boldsymbol{d}(\langle 0, \ldots, p+q\rangle) = \boldsymbol{c}(\langle 0, \ldots, p\rangle)\boldsymbol{d}(\langle p, \ldots, p+q\rangle). \tag{5.50}$$

$\boldsymbol{c}$ is evaluated on the p-simplex formed by the first $p+1$ vertices, while $\boldsymbol{d}$ is evaluated on q-simplex formed by the last $q+1$ vertices.

A suggestive example of the cup product comes from considering $\boldsymbol{a}_e \cup \delta \boldsymbol{a}_e$. $\boldsymbol{a}_e \cup \delta \boldsymbol{a}_e$ evaluated on a tetrahedron $\langle 1234\rangle$ gives:

$$\boldsymbol{a}_e \cup \delta \boldsymbol{a}_e(\langle 1234\rangle) = \boldsymbol{a}_e(\langle 12\rangle)\delta \boldsymbol{a}_e(\langle 234\rangle) = a_{12}(a_{23} + a_{34} + a_{24}). \tag{5.51}$$

Referring to Eq. (5.33), we see that the FDQC $\mathcal{U}_1$ can be written as:

$$\mathcal{U}_1 = \sum_{\boldsymbol{a}_e} \prod_t (-1)^{\boldsymbol{a}_e \cup \delta \boldsymbol{a}_e(t)} |\boldsymbol{a}_e\rangle\langle \boldsymbol{a}_e|, \tag{5.52}$$

with the sum over all 1-cochains.

To simplify the notation, we use the shorthand:

$$\int_N \boldsymbol{c} \equiv \sum_{s \in N} \boldsymbol{c}(s), \tag{5.53}$$

where $\boldsymbol{c}$ is a p-cochain, N is a p-dimensional manifold, and the sum is over p-simplices s in N. Throughout the text, unless specified otherwise, it should be assumed that the integral is over the manifold M. In particular, we can make the replacement:

$$\int \boldsymbol{a}_e \cup \delta \boldsymbol{a}_e = \sum_{t \in M} \boldsymbol{a}_e \cup \delta \boldsymbol{a}_e(t). \tag{5.54}$$

With this, the circuit $\mathcal{U}_1$ is:

$$\mathcal{U}_1 = \sum_{\boldsymbol{a}_e} (-1)^{\int \boldsymbol{a}_e \cup \delta \boldsymbol{a}_e} |\boldsymbol{a}_e\rangle\langle \boldsymbol{a}_e|, \tag{5.55}$$

and the ground state in Eq. (5.35) is:

$$|\Psi_1\rangle = \sum_{\boldsymbol{a}_e} (-1)^{\int \boldsymbol{a}_e \cup \delta \boldsymbol{a}_e} |\boldsymbol{a}_e\rangle. \tag{5.56}$$

Lastly, we introduce the cup-1 product $\cup_1$. Although abstract, the cup-1 product allows for a convenient form of the Hamiltonian H_1 and is key to our analysis of the twisted toric code in the subsequent section. The cup-1 product takes a p-cochain $\boldsymbol{c}$ and a q-cochain $\boldsymbol{d}$ to a $(p+q-1)$-cochain $\boldsymbol{c} \cup_1 \boldsymbol{d}$. Explicitly, $\boldsymbol{c} \cup_1 \boldsymbol{d}$ evaluated on a $(p+q-1)$-simplex $\langle 0, \ldots, p+q-1 \rangle$

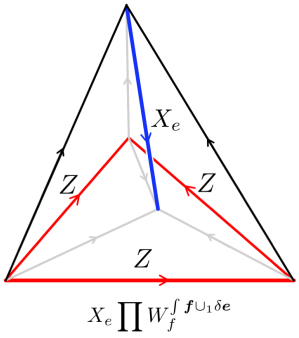

Figure 5.10: Pictured above is an example of a term in H_1 associated to an edge e with three tetrahedra meeting at e. The operator acts with X_e on e (blue) and with Pauli Z operators on edges nearby (shown in red). The placement of the Pauli Z operators depends on the branching structure through the exponent $\int \boldsymbol{f} \cup_1 \delta \boldsymbol{e}$.

is:

$$\boldsymbol{c} \cup_1 \boldsymbol{d}(\langle 0, \ldots, p+q-1 \rangle) = \sum_{i=0}^{p-1} \boldsymbol{c}(\langle 0, \ldots, i, q+i, \ldots, p+q-1 \rangle) \boldsymbol{d}(\langle i, ..., q+i \rangle). \tag{5.57}$$

A useful example, relevant to our expression for H_1, is the cup-1 product of $\boldsymbol{f}$ and $\delta \boldsymbol{e}$. Here, $\boldsymbol{f}$ is the 2-cochain that evaluates to 1 on the face f and 0 for all other faces:

$$\boldsymbol{f}(f') = \begin{cases} 1 & f' = f \\ 0 & \text{otherwise.} \end{cases} \tag{5.58}$$

The 3-cochain $\boldsymbol{f} \cup_1 \delta \boldsymbol{e}$ evaluated on a tetrahedron $\langle 1234 \rangle$ is [using Eq. (5.57)]:

$$\boldsymbol{f} \cup_1 \delta \boldsymbol{e}(\langle 1234 \rangle) = \boldsymbol{f}(\langle 134 \rangle) \delta \boldsymbol{e}(\langle 123 \rangle) + \boldsymbol{f}(\langle 124 \rangle) \delta \boldsymbol{e}(\langle 234 \rangle). \tag{5.59}$$

Now, with the notation from $\mathbb{Z}_2$ cohomology on M, we can express H_1 in Eq. (5.34) in a

compact form. In Appendix 5.B, we show that:

$$H_1 = -\sum_e \left(X_e \prod_f W_f^{\int \boldsymbol{f} \cup_1 \delta \boldsymbol{e}} \right). \tag{5.60}$$

Above, we have used W_f to denote the product of Z_e around the face f:

$$W_f \equiv \prod_{e \subset f} Z_e. \tag{5.61}$$

While the product in Eq. (5.60) is over all faces in M, the Hamiltonian is indeed local. This is because $\boldsymbol{f} \cup_1 \delta \boldsymbol{e}(t) = 0$, if the face f and edge e do not both belong to the tetrahedron t. Heuristically, X_e is "dressed" with loops of Pauli Z operators around certain faces near e [Fig. 5.10].

5.3.2 Twisted toric code

The twisted toric code is constructed from H_1 in Eq. (5.60) by gauging the $\mathbb{Z}_2$ 1-form symmetry. In this section, we provide a physical description of the gauging procedure following the steps outlined in Ref. [71]. After gauging the 1-form symmetry of H_1, we show that the resulting twisted toric code admits localized excitations with fermionic statistics.

The prescription for gauging a $\mathbb{Z}_2$ 0-form symmetry in Ref. [71] naturally generalizes to gauging a $\mathbb{Z}_2$ 1-form symmetry. In particular, the 1-form symmetry is gauged according to the following steps.

1. We introduce $\mathbb{Z}_2$ d.o.f. on faces corresponding to 2-form gauge fields. We denote the Pauli Z and Pauli X operators at the face f by Z_f and X_f, respectively.

2. We impose a gauge constraint at each edge e:

$$X_e \prod_{f \supset e} X_f = 1, \tag{5.62}$$

where the product is over faces containing e. This constraint can be interpreted as a 1-form Gauss law. We note that the operator $X_e \prod_{f \supset e} X_f$ defines a local action of the 1-form symmetry. That is, a product of $X_e \prod_{f \supset e} X_f$ over edges intersected by a closed surface Σ in the dual lattice yields the 1-form symmetry operator A_Σ.

3. To make coupling to the gauge field in the subsequent step unambiguous, we energetically enforce a "no flux condition". The point-like 1-form gauge flux can be detected by the operator W_t, where W_t is a product of Z_f operators around a tetrahedron t:

$$W_t \equiv \prod_{f \subset t} Z_f. \tag{5.63}$$

Therefore, the no flux condition is enforced by adding to the Hamiltonian the term:

$$-\sum_t W_t. \tag{5.64}$$

In addition, we conjugate each Hamiltonian term by a local projector onto the zero flux subspace in the vicinity of the term. That is, for a Hamiltonian term whose support[8] is contained in the bounded region R, we conjugate by a projector:

$$\mathcal{P}_R^{\text{0-flux}} \equiv \prod_{t \in R} \frac{(1 + W_t)}{2}, \tag{5.65}$$

where the product is over tetrahedra in R.

4. We then minimally couple the $\mathbb{Z}_2$ 1-form symmetric model to the gauge fields, so as to make the model invariant under the gauge constraint. In particular, W_f is coupled to the gauge field as:

$$W_f \to W_f Z_f. \tag{5.66}$$

[8]The support of an operator is the set of sites on which the operator acts non-identically.

5. We fix a gauge by mapping gauge invariant states to representative states in which the eigenvalue of Z_e is 1 at every edge e[9]. This gauge fixed Hilbert space is equivalent to a Hilbert space with only the gauge field d.o.f. on the faces. The action of X_e on gauge invariant states is replaced by $\prod_{f\supset e} X_f$ after fixing the gauge, and $W_f Z_f$ in Eq. (5.66) becomes equivalent to Z_f in the gauge fixed Hilbert space. Therefore, the gauge invariant operators X_e and $W_f Z_f$ are mapped according to:

$$X_e \to \prod_{f\supset e} X_f, \quad W_f Z_f \to Z_f. \tag{5.68}$$

We remark that, operationally, the gauging procedure is equivalent to a certain operator duality. In particular, the duality maps the 1-form symmetric operators X_e and W_f according to:

$$X_e \to \prod_{f\supset e} X_f, \quad W_f \to Z_f. \tag{5.69}$$

We have summarized the corresponding operator duality in Table 5.1.

As a result of applying steps 1-5 above to our model for the nontrivial 1-form SPT phase, we obtain the twisted toric code. The twisted toric code is defined on a Hilbert space composed of $\mathbb{Z}_2$ d.o.f. attached to each face of the triangulation of M (Fig. 5.11). Further, a basis for the Hilbert space is given by the product states $|\{a_f\}\rangle$, where the state at the face f is $|a_f\rangle$ (with $a_f \in \{0,1\}$). In analogy to Eq. (5.42), a configuration state $|\{a_f\}\rangle$ can

[9]More precisely, we can form an over-complete basis for the gauge invariant Hilbert space by projecting configuration basis states to the gauge invariant subspace with the operator:

$$\prod_e \left(1 + X_e \prod_{f\supset e} X_f\right). \tag{5.67}$$

Each gauge invariant state in this (over-complete) basis is a superposition of configuration states and includes exactly one state for which the eigenvalue of Z_e is 1 at every edge. By gauge fixing, we mean that the over-complete basis states are mapped to the "representative" state with the eigenvalue of Z_e equal to 1 at each edge. The representative states form a basis for the gauge fixed Hilbert space.

Model with $\mathbb{Z}_2$ 1-form symmetry	Model with dual $\mathbb{Z}_2$ 1-form symmetry
X_e	$\prod_{f \supset e} X_f$
$W_f = \prod_{e \subset f} Z_e$	Z_f
$A_\Sigma = \prod_{e \perp \Sigma} X_e,\ \delta \mathbf{\Sigma} = 0$	1
1	$M_\sigma = \prod_{f \subset \sigma} Z_f,\ \partial \sigma = 0$

Table 5.1: In the process of gauging the 1-form symmetry, the generators of local, 1-form symmetric operators are mapped according to the duality above. The symmetry operators A_Σ are mapped to the identity in the dual theory. The system on the right-hand side has a $\mathbb{Z}_2$ 1-form symmetry, generated by membrane operators M_σ, where σ is a closed 2D surface on the direct lattice.

be labeled by a 2-cochain $\boldsymbol{a}_f$:

$$\boldsymbol{a}_f \equiv \sum_f a_f \boldsymbol{f}. \tag{5.70}$$

With this notation, the Pauli Z and Pauli X operators acting on the face f' can be written as:

$$Z_{f'}|\boldsymbol{a}_f\rangle = (-1)^{\boldsymbol{a}_f(f')}|\boldsymbol{a}_f\rangle, \quad X_{f'}|\boldsymbol{a}_f\rangle = |\boldsymbol{a}_f + \boldsymbol{f}'\rangle. \tag{5.71}$$

By gauging the 1-form symmetry of H_1 [Eq. (5.60)], we find the twisted toric code Hamiltonian:

$$H_{\text{ttc}} \equiv -\sum_e \bar{G}_e - \sum_t W_t, \tag{5.72}$$

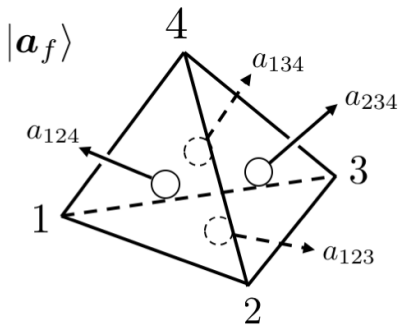

Figure 5.11: We define the twisted toric code on a triangulation with $\mathbb{Z}_2$ d.o.f. at each face (represented by a circle). A configuration state is given by a value $a_f \in \{0, 1\}$ chosen for each face f.

where $\bar{G}_e$ is:

$$\bar{G}_e \equiv \prod_{f \supset e} X_f \prod_f Z_f^{\int \boldsymbol{f} \cup_1 \delta \boldsymbol{e}}. \tag{5.73}$$

An example of the term $\bar{G}_e$ is shown in Fig 5.12. For simplicity, we have omitted the local projectors from step 3 of the gauging procedure. They do not affect the discussion in this section. The terms of H_{ttc} are all mutually commuting, since the gauging procedure preserves the commutation relations. We show in Appendix 5.C that a ground state of the model is:

$$|\Psi_{\text{ttc}}\rangle \equiv \sum_{\boldsymbol{a}_e} (-1)^{\int \boldsymbol{a}_e \cup \delta \boldsymbol{a}_e} |\delta \boldsymbol{a}_e\rangle. \tag{5.74}$$

Note that while the expression for $|\Psi_{\text{ttc}}\rangle$ has a sum over 1-cochains $\boldsymbol{a}_e$, there are no d.o.f. on the edges. Rather, by summing over 1-cochains $\boldsymbol{a}_e$, $|\Psi_{\text{ttc}}\rangle$ is a ground state of H_{ttc} with trivial holonomy.

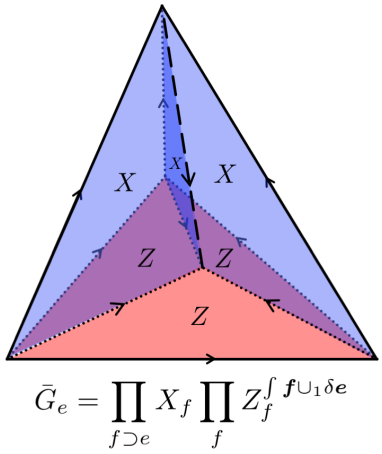

Figure 5.12: An example of $\bar{G}_e$ for the edge e (dashed line) is shown above. Pauli X operators act on the faces (shaded blue) adjoined at e and Pauli Z operators (shaded red) act on nearby faces according to $\int \boldsymbol{f} \cup_1 \delta \boldsymbol{e}$.

Excitations in the twisted toric code

There are two types of excitations of the twisted toric code. The first, is a line-like $\mathbb{Z}_2$ 1-form gauge charge corresponding to violations of the edge terms $\bar{G}_e$. A small loop of gauge charge around the face f is created by acting with the face operator Z_f. A larger loop of gauge charge can be created by acting with Z_f on all faces contained in a 2D membrane σ of the direct lattice:

$$M_\sigma \equiv \prod_{f \subset \sigma} Z_f. \tag{5.75}$$

We think of the gauge charge as lying along the boundary of σ, since the membrane operator M_σ anti-commutes with the edge terms $\bar{G}_e$ for which e is in the boundary of σ.

The second type of excitation of H_{ttc} is a point-like $\mathbb{Z}_2$ 1-form gauge flux corresponding to a violation of a W_t term. A pair of gauge fluxes can be created at neighboring tetrahedra

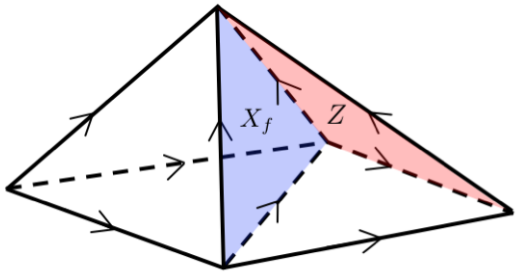

$$\bar{U}_f = X_f \prod_{f'} Z_{f'}^{\int \boldsymbol{f} \cup_1 \boldsymbol{f}'}$$

Figure 5.13: The operator $\bar{U}_f$ applies a Pauli X operator at f (blue) and Pauli Z operators on certain faces of the neighboring tetrahedra (red). For a tetrahedron $t = \langle 1234 \rangle$, the cup-1 product of $\boldsymbol{f}$ and $\boldsymbol{f}'$ evaluates to $\boldsymbol{f} \cup_1 \boldsymbol{f}'(t) = \boldsymbol{f}(\langle 134 \rangle)\boldsymbol{f}'(\langle 123 \rangle) + \boldsymbol{f}(\langle 124 \rangle)\boldsymbol{f}'(\langle 234 \rangle)$. In the figure above, f is the $\langle 124 \rangle$ face of the tetrahedron $\langle 1234 \rangle$ on the right. Thus, $\bar{U}_f$ applies a Pauli Z to $f' = \langle 234 \rangle$.

by the short string operator:[10]

$$\bar{U}_f \equiv X_f \prod_{f'} Z_{\boldsymbol{f}'}^{\int \boldsymbol{f} \cup_1 \boldsymbol{f}'}, \tag{5.76}$$

pictured in Fig. 5.13. $\bar{U}_f$ anticommutes with the tetrahedron terms W_t on either side of the face f. Thus, we interpret the gauge fluxes as living at the centers of tetrahedra. The Pauli Z operators in Eq. (5.76) ensure that for any f and any e, $\bar{U}_f$ commutes with $\bar{G}_e$. The short string operators satisfy the commutation relations [166]:

$$\bar{U}_f \bar{U}_{f'} = (-1)^{\int (\boldsymbol{f}' \cup_1 \boldsymbol{f} + \boldsymbol{f} \cup_1 \boldsymbol{f}')} \bar{U}_{f'} \bar{U}_f, \tag{5.77}$$

for any faces f and f'.

Longer string operators can be formed by composing the short string operators in

[10] To avoid confusion with the operator $U_f \equiv X_f \prod_{f'} Z_{\boldsymbol{f}'}^{\int \boldsymbol{f}' \cup_1 \boldsymbol{f}}$ in Ref. [166], we use $\bar{U}_f$.

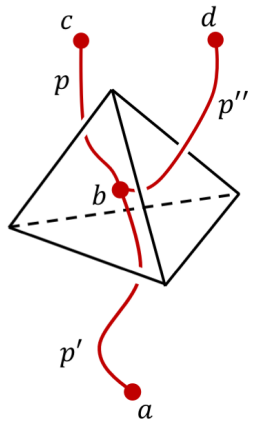

Figure 5.14: The paths p, p', and p'' share a single common endpoint b inside of a tetrahedron t. Furthermore, the paths intersect distinct faces of t. Other details of the paths are unimportant in the computation of the statistics of the gauge fluxes.

Eq. (5.76). However, a simple product of $\bar{U}_f$ operators along a path p in the dual lattice is ambiguous. This is because, given the commutation relations in Eq. (5.77), a product of $\bar{U}_f$ operators is generically order dependent. To remove the ambiguity, we define the following notation. For any set F of faces, we define an order independent product of $\bar{U}_f$ by:

$$\overline{\prod_{f\in F}}\bar{U}_f \equiv \prod_{f\in F}\left(\prod_{f'} Z_{\boldsymbol{f}'}^{\int \boldsymbol{f}\cup_1 \boldsymbol{f}'}\right)\prod_{f\in F} X_f. \tag{5.78}$$

Here, all of the Pauli Z operators from the definition of $\bar{U}_f$ appear to the left of the Pauli X operators. We can then unambiguously define a gauge flux string operator $\mathcal{S}_p$ along a path p in the dual lattice by:

$$\mathcal{S}_p \equiv \overline{\prod_{f\in F_{\perp p}}}\bar{U}_f, \tag{5.79}$$

where $F_{\perp p}$ denotes the set of faces intersected by p.

Remarkably, the gauge fluxes are emergent fermions. To see this, we use the methods

developed in Refs. [135] and [174] for computing the statistics of anyons from microscopic models. We consider three paths p, p', and p'' along the dual lattice sharing a common endpoint, as in Fig. 5.14. The statistics of the gauge fluxes can be deduced by comparing the product $\mathcal{S}_p\mathcal{S}_{p'}\mathcal{S}_{p''}$ to $\mathcal{S}_{p''}\mathcal{S}_{p'}\mathcal{S}_p$.

To gain intuition for this comparison, we imagine gauge fluxes at a and b in Fig. 5.14. In the first process $\mathcal{S}_p\mathcal{S}_{p'}\mathcal{S}_{p''}$, the gauge flux at b is moved to c and the gauge flux at a is moved to d. Whereas, in the second process $\mathcal{S}_{p''}\mathcal{S}_{p'}\mathcal{S}_p$, the gauge flux at b is moved to d and the gauge flux at a is moved to c. The final configurations of the gauge fluxes differ by an interchange of the position of the gauge fluxes. Consequently, the difference between $\mathcal{S}_p\mathcal{S}_{p'}\mathcal{S}_{p''}$ and $\mathcal{S}_{p''}\mathcal{S}_{p'}\mathcal{S}_p$ determines the statistics of the gauge fluxes.

It can be shown that the gauge flux string operator satisfies:

$$\mathcal{S}_p\mathcal{S}_{p'}\mathcal{S}_{p''} = -\mathcal{S}_{p''}\mathcal{S}_{p'}\mathcal{S}_p. \tag{5.80}$$

This follows from an explicit computation using the commutation relations of the operators $\bar{U}_f$ in Eq. (5.77).[11] Therefore, the gauge fluxes are emergent fermions. We note that this is equivalent to saying that the twisted toric code has an anomalous $\mathbb{Z}_2$ 2-form symmetry [133, 166]. The 2-form symmetry, which, by definition, acts on closed codimension-2 subspaces, is generated by loops of the emergent fermion string operator. It is called anomalous, simply because the gauge fluxes have fermionic statistics.

Before leveraging our understanding of the twisted toric code to construct a model of physical fermions, we would like to point out that the emergent fermion string operator is not unique. In fact, we can define an alternative emergent fermion string operator built from the short segments:

$$\tilde{U}_f \equiv \bar{U}_f W_{R(f)}, \tag{5.81}$$

[11] More precisely, this can be checked by explicitly computing the sign for each possible intersection at a tetrahedron. The sign for only four of the possible orientations of the tetrahedron needs to be verified, as the others follow from symmetries of the calculation.

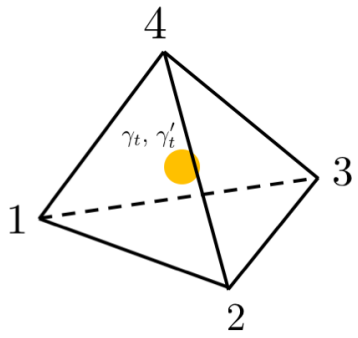

Figure 5.15: The atomic insulator is defined on a Hilbert space with a single complex fermion d.o.f. (yellow circle) at each tetrahedron. The operator algebra at the tetrahedron $t = \langle 1234 \rangle$ is generated by the Majorana operators γ_t and γ'_t.

with $R(f)$ denoting the tetrahedron neighboring f in the direction of the orientation of f (see Fig. 5.5). The corresponding string operator along a path p in the dual lattice is:

$$\tilde{\mathcal{S}}_p \equiv \overline{\prod_{f \in F_{\perp p}}} \bar{U}_f \prod_{f \in F_{\perp p}} W_{R(f)}. \tag{5.82}$$

An important observation moving forward is that $\bar{G}_e$ is equivalent to a small loop of $\tilde{\mathcal{S}}_p$ string around the edge e (see Appendix 5.D):

$$\bar{G}_e = \tilde{\mathcal{S}}_{p_e}, \tag{5.83}$$

where the path p_e intersects only the faces adjoined at e. Therefore, the $\bar{G}_e$ operators are local generators of an anomalous $\mathbb{Z}_2$ 2-form symmetry. Since $\bar{G}_e$ commutes with H_{ttc}, we see explicitly that the twisted toric code has an anomalous 2-form symmetry.

5.3.3 Atomic insulator

The last step of our $G = \mathbb{Z}_2^f$ example is to convert the twisted toric code into a model with physical fermions. This can be accomplished by applying the $(3+1)$D fermionization duality

introduced in Ref. [166], reviewed in Appendix 5.E. In this section, we instead opt to describe the fermionization process in terms of fermion condensation [111, 167]. That is, we construct the fermionic model by pairing emergent fermions with physical fermions and condensing the composite bosonic excitations. The fermion condensation procedure, described below, can be interpreted as a generalization of Refs. [71] and [175] to gauging an anomalous 2-form symmetry. Although an anomalous symmetry typically implies an obstruction to gauging the symmetry, we bypass the obstruction by employing fermionic d.o.f. for the gauge fields.

Our prescription for fermion condensation starts by introducing a spinless complex fermion d.o.f. at the center of each tetrahedron (Fig. 5.15). Thus, to prepare for the discussion of fermion condensation, we recall the notation for the operators on the fermionic Hilbert space, defined in Section 5.2.3. The fermion parity operator at t is:

$$P_t = -i\gamma_t\gamma'_t, \tag{5.84}$$

and the hopping operator S_f across the face f is:

$$S_f = (-1)^{\boldsymbol{f}(E)} i\gamma_{L(f)}\gamma'_{R(f)}. \tag{5.85}$$

$L(f)$ and $R(f)$ are defined below Eq. (5.17), and E is a formal sum of 2-simplices that amounts to a choice of spin-structure; see Appendix 5.E for the explicit form of E.[12] The hopping operators satisfy the commutation relations:

$$S_f S_{f'} = (-1)^{\int (\boldsymbol{f}'\cup_1 \boldsymbol{f} + \boldsymbol{f}\cup_1 \boldsymbol{f}')} S_{f'} S_f, \tag{5.86}$$

which we note matches the commutation relations of $\bar{U}_f$ in Eq. (5.77). Lastly, we define an alternative hopping operator $\tilde{S}_f$, instrumental for the fermion condensation prescription

[12] Note that every orientable 3-manifold admits a spin structure, so a choice of E is guaranteed.

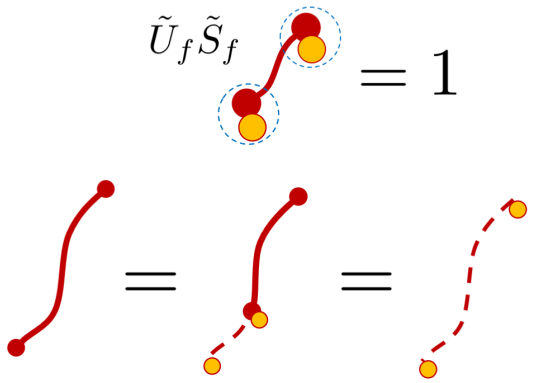

Figure 5.16: To condense the emergent fermion, we impose the gauge constraint $\tilde{U}_f \tilde{S}_f = 1$. Acting on the vacuum, $\tilde{U}_f$ creates a pair of emergent fermions (red) and $\tilde{S}_f$ creates a pair of physical fermions (yellow). The composite excitation (dashed blue circle) has bosonic statistics, so it may be condensed. Heuristically, emergent fermions can be replaced with physical fermions in the constrained Hilbert space.

below:

$$\tilde{S}_f \equiv P_{L(f)} S_f. \tag{5.87}$$

With notation for the fermionic d.o.f. defined, we can describe the fermion condensation procedure. Our procedure applies to any Hamiltonian with an emergent fermion created by the string operator $\tilde{\mathcal{S}}_p$ in Eq. (5.82). In other words, the fermion condensation procedure applies to any Hamiltonian with an anomalous $\mathbb{Z}_2$ 2-form symmetry locally represented by the operators $\bar{G}_e$. Fermion condensation then proceeds as follows.

1. We introduce a spinless complex fermion d.o.f. at each tetrahedron. In terms of gauging the 2-form symmetry, the anomalous nature requires that the "3-form gauge fields" are fermionic d.o.f..

2. We impose a gauge constraint:

$$\tilde{U}_f \tilde{S}_f = 1, \tag{5.88}$$

for each face f. This constraint enforces a proliferation (or condensation) of composite excitations composed of an emergent fermion and a physical fermion. This is because $\tilde{U}_f$ is a short segment of emergent fermion string operator [Eq. (5.82)], which creates emergent fermions at the tetrahedra on either side of f, while $\tilde{S}_f$ creates physical fermions at the corresponding tetrahedra (Fig. 5.16). Importantly, the constraints at different faces commute, due to the matching commutation relations of $\tilde{U}_f$ and $\tilde{S}_f$ (see Appendix 5.D). We note that the gauge constraint in Eq. (5.88) is a local action of the $\mathbb{Z}_2$ anomalous 2-form symmetry, in the sense that the product of $\tilde{U}_f\tilde{S}_f$ around an edge returns $\bar{G}_e$; this is guaranteed by the spin structure dependent sign in the definition of the hopping operator.

3. To make the Hamiltonian gauge invariant, i.e., commute with the constraints in Eq. (5.88), we couple the Hamiltonian to the fermionic d.o.f.. Since the Hamiltonian commutes with $\bar{G}_e$, it can be expressed in terms of $\bar{U}_f$ and W_t operators [166]. We couple $\bar{U}_f$ operators and W_t operators to the gauge fields as:

$$\bar{U}_f \to \bar{U}_f P_{L(f)}, \quad W_t \to W_t P_t. \tag{5.89}$$

To avoid possible ambiguity, we require that the coupling preserves the locality of the Hamiltonian. Any local, gauge invariant operators can be expressed in terms of the operators $\bar{U}_f P_{L(f)}$ and $W_t P_t$.

4. We fix a gauge in which the eigenvalue of Z_f is 1 at each face f. The action of $\bar{U}_f P_{L(f)}$ on the constrained space is replaced by S_f in the gauge fixed Hilbert space.[13] Further, the gauge invariant operator $W_t P_t$ becomes P_t after fixing the gauge. The generators

[13] This can be seen by multiplying $\bar{U}_f P_{L(f)}$ by $\tilde{U}_f\tilde{S}_f = 1$. We obtain:

$$\bar{U}_f P_{L(f)} = \bar{U}_f P_{L(f)} \tilde{U}_f \tilde{S}_f = \bar{U}_f P_{L(f)} \bar{U}_f W_{R(f)} P_{L(f)} S_f = W_{R(f)} S_f.$$

$W_{R(f)}$ acts as the identity in the fixed gauge.

Model with emergent fermions	Model with even fermion parity
$\bar{U}_f$	S_f
$W_t = \prod_{f \subset t} Z_f$	P_t
$\bar{G}_e$	1
1	$\prod_t P_t$

Table 5.2: Fermion condensation implements an operator duality, wherein operators describing a model with an emergent fermion (commute with $\bar{G}_e$) are mapped to operators that act on a fermionic Hilbert space and have even fermion parity (commute with $\prod_t P_t$). For simplicity, we have only listed the local generators $\bar{G}_e$ of the anomalous 2-form symmetry.

of local, gauge invariant operators are thus mapped according to:

$$\bar{U}_f P_{L(f)} \to S_f, \quad W_t P_t \to P_t. \tag{5.90}$$

The mapping in Eq. (5.90) produces a fermionic Hamiltonian defined on a Hilbert space with a single spinless complex fermion d.o.f. at each tetrahedron, as depicted in Fig. 5.15.

By condensing the emergent fermion in the twisted toric code, we obtain a model for an atomic insulator. More specifically, applying the fermion condensation procedure to H_{ttc} yields the atomic insulator Hamiltonian (Appendix 5.D):

$$H_{\text{AI}} \equiv -\sum_t P_t. \tag{5.91}$$

This Hamiltonian has a unique ground state $|\Psi_{\text{AI}}\rangle$, a product state with zero fermion occupancy at each tetrahedron. Excitations are physical fermions, where P_t has eigenvalue -1.

The process of gauging a non-anomalous symmetry, such as the 1-form symmetry in Sec-

tion 5.3.2, can be stated as an operator duality [71]. Likewise, the fermion condensation procedure can be implemented by a mapping of operators. We summarize the corresponding duality in Table 5.2 and provide more details in Appendix 5.E. Notably, the duality corresponding to fermion condensation maps:

$$\bar{U}_f \to S_f, \quad W_t \to P_t. \tag{5.92}$$

Combining Eqs. (5.89) and (5.90), we see that the duality is functionally the same as the fermion condensation procedure outlined above.

5.4 *Bulk construction:* $G_f = G \times \mathbb{Z}_2^f$

We now generalize the discussion of Section 5.3 to construct fSPT models protected by a $G_f = G \times \mathbb{Z}_2^f$ symmetry. In this case, we require a choice of supercohomology data (ρ, ν). Therefore, before outlining the construction of the fSPT models, we first review the supercohomology data (ρ, ν), and introduce corresponding cochains on the manifold M. Then, we use the supercohomology data to build a 2-group SPT model, which, loosely speaking is protected by an interdependent 1-form and 0-form symmetry. Next, we gauge the 1-form symmetry of the 2-group to obtain the so-called shadow model – a symmetry-enriched twisted toric code. The shadow model is such that fermion condensation produces a model for the fSPT phase corresponding to the supercohomology data (ρ, ν). The construction is shown schematically in Fig. 5.1.

5.4.1 Supercohomology data on M

In Section 5.2.1, we introduced the supercohomology data (ρ, ν) as homogeneous functions:

$$\rho : G^4 \to \mathbb{Z}_2, \quad \nu : G^5 \to \mathbb{R}/\mathbb{Z}, \tag{5.93}$$

which, as group cochains, satisfy the relations:

$$\delta\rho = 0, \quad \delta\nu = \frac{1}{2}\rho \cup_1 \rho. \tag{5.94}$$

In what follows, we find it convenient to work with cochains on M – functions of simplices in the triangulation of M. Therefore, in this section, we describe how functions of G variables, can be pulled back to cochains on M.

We use the functions $\bar{\rho}$, $\bar{\rho}^h$, and $\bar{\nu}$ as examples for describing the pull back of functions to cochains on M. $\bar{\rho}$, $\bar{\rho}^h$, and $\bar{\nu}$ are defined by:

$$\bar{\rho}(g_1, g_2, g_3) \equiv \rho(1, g_1, g_2, g_3), \tag{5.95}$$

$$\bar{\rho}^h(g_1, g_2) \equiv \rho(1, h^{-1}, g_1, g_2), \tag{5.96}$$

$$\bar{\nu}(g_1, g_2, g_3, g_4) \equiv \nu(1, g_1, g_2, g_3, g_4), \tag{5.97}$$

with 1 denoting the identity in G. The pull backs of these functions play an important role in the construction of the supercohomology models below. We note that the functions are not group cochains, since they fail to be homogeneous.

To define cochains on M, corresponding to $\bar{\rho}$, $\bar{\rho}^h$, and $\bar{\nu}$, we assign an element of G to each vertex in the triangulation of M. We refer to the set of G labels $\{g_v\}$ as a $\{g_v\}$-configuration. With G labels on the vertices of M, functions of G^p can be pulled back to p-cochains on M. For each $\{g_v\}$-configuration, we define the cochains $\overline{\boldsymbol{\rho}}_{\{g_v\}}$, $\overline{\boldsymbol{\rho}}^h_{\{g_v\}}$, and $\overline{\boldsymbol{\nu}}_{\{g_v\}}$ on M satisfying:

$$\overline{\boldsymbol{\rho}}_{\{g_v\}}(\langle 123\rangle) \equiv \bar{\rho}(g_1, g_2, g_3), \tag{5.98}$$

$$\overline{\boldsymbol{\rho}}^h_{\{g_v\}}(\langle 12\rangle) \equiv \bar{\rho}^h(g_1, g_2), \tag{5.99}$$

$$\overline{\boldsymbol{\nu}}_{\{g_v\}}(\langle 1234\rangle) \equiv \bar{\nu}(g_1, g_2, g_3, g_4), \tag{5.100}$$

for an arbitrary face $\langle 123\rangle$, edge $\langle 12\rangle$, and tetrahedron $\langle 1234\rangle$.

The Hamiltonians discussed below are defined on triangulated manifolds with a G d.o.f.

at every vertex, such as in Figs. 5.3 and 5.4, and a set of basis states can be labeled by $\{g_v\}$-configurations. Hence, to simplify the notation in the construction of the supercohomology models, we introduce diagonal operators for each $\{g_v\}$-dependent cochain on M. The operator associated to the $\{g_v\}$-dependent p-cochain $\boldsymbol{c}_{\{g_v\}}$ and a p-simplex s is defined as:

$$\hat{\boldsymbol{c}}(s) \equiv \sum_{\{g_v\}} \boldsymbol{c}_{\{g_v\}}(s)|\{g_v\}\rangle\langle\{g_v\}|. \tag{5.101}$$

The operators associated to $\overline{\boldsymbol{\rho}}_{\{g_v\}}$, $\overline{\boldsymbol{\rho}}^h_{\{g_v\}}$, and $\overline{\boldsymbol{\nu}}_{\{g_v\}}$ are thus:

$$\hat{\overline{\boldsymbol{\rho}}}(f) \equiv \sum_{\{g_v\}} \overline{\boldsymbol{\rho}}_{\{g_v\}}(f)|\{g_v\}\rangle\langle\{g_v\}| \tag{5.102}$$

$$\hat{\overline{\boldsymbol{\rho}}}^h(e) \equiv \sum_{\{g_v\}} \overline{\boldsymbol{\rho}}^h_{\{g_v\}}(e)|\{g_v\}\rangle\langle\{g_v\}| \tag{5.103}$$

$$\hat{\overline{\boldsymbol{\nu}}}(t) \equiv \sum_{\{g_v\}} \overline{\boldsymbol{\nu}}_{\{g_v\}}(t)|\{g_v\}\rangle\langle\{g_v\}| \tag{5.104}$$

for a choice of face f, edge e, and tetrahedron t. Unless otherwise stated, it should be assumed that the operators are tensored with the identity on any other d.o.f. in the model.

The coboundary operator and cup products can naturally be extended to the operators at the cochain level. For example, the coboundary of $\hat{\overline{\boldsymbol{\rho}}}$ is the operator:[14]

$$\delta\hat{\overline{\boldsymbol{\rho}}}(t) = \sum_{\{g_v\}} \delta\overline{\boldsymbol{\rho}}_{\{g_v\}}(t)|\{g_v\}\rangle\langle\{g_v\}|, \tag{5.105}$$

where t is an arbitrary tetrahedron. Similarly, the cup-1 product $\hat{\overline{\boldsymbol{\rho}}} \cup_1 \boldsymbol{f}(t)$ should be inter-

[14]In fact, $\delta\hat{\overline{\boldsymbol{\rho}}}$ is equivalent to the operator $\hat{\boldsymbol{\rho}}$, corresponding to the cochain $\boldsymbol{\rho}_{\{g_v\}}$ and the function ρ in the natural way. This follows from the coboundary relation in Eq. (5.94). We note that, although $\delta\overline{\boldsymbol{\rho}}_{\{g_v\}}$ is indeed equal to $\boldsymbol{\rho}_{\{g_v\}}$, this does not imply that ρ is a group coboundary. The equality holds for cochains on M. Lacking homogeneity, $\bar{\rho}$ is not a group cochain.

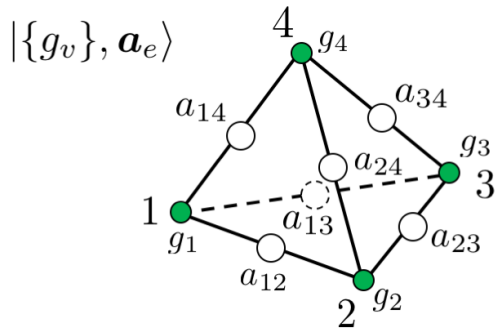

Figure 5.17: The Hilbert space for the 2-group SPT model has G d.o.f. on vertices and $\mathbb{Z}_2$ d.o.f. on edges. We have labeled the states at the edges by the value of $\boldsymbol{a}_e(e) = a_e$.

preted as:

$$\hat{\overline{\boldsymbol{\rho}}} \cup_1 \boldsymbol{f} = \sum_{\{g_v\}} \overline{\boldsymbol{\rho}}_{\{g_v\}} \cup_1 \boldsymbol{f}(t) |\{g_v\}\rangle\langle\{g_v\}|. \tag{5.106}$$

Using these operators we now build a Hamiltonian describing a certain 2-group SPT phase.

5.4.2 2-group SPT

In this section, we construct a model for a 2-group SPT phase, given a set of supercohomology data (ρ, ν). The particular 2-group symmetry is dependent upon G and the group cochain ρ. For simplicity, we describe the relevant 2-group symmetry in terms of its representation on a lattice. More details on 2-groups including a formal definition can be found in Appendix K of Ref. [76]. Our model for the 2-group SPT phase is based on a Euclidean spacetime picture presented in Ref. [133], and we elaborate on the connection to this perspective at the end of this section.

The model for the 2-group SPT phase is defined on a Hilbert space consisting of a $\mathbb{Z}_2$ d.o.f. at each edge and a G d.o.f. at each vertex of a triangulation of M (see Fig. 5.17). As described in the previous section, a basis for the G d.o.f. is given by configuration states

$|\{g_v\}\rangle$, and as in section 5.3.1, a basis for the edge d.o.f. can be formed by states $|\boldsymbol{a}_e\rangle$ labeled by $\mathbb{Z}_2$ 1-cochains $\boldsymbol{a}_e$. Thus, we use the collection of states of the form $|\{g_v\}, \boldsymbol{a}_e\rangle$ as a basis for the total Hilbert space.

The 2-group symmetry has both a $\mathbb{Z}_2$ 1-form symmetry and a certain 0-form symmetry parameterized by elements of G. Similar to Section 5.3.1, we represent the 1-form symmetry using the operators:

$$A_\Sigma = \prod_{e \perp \Sigma} X_e, \tag{5.107}$$

where the product is over edges intersected by the closed surface Σ on the dual lattice. The action of the 1-form symmetry operator on a basis state is explicitly:

$$A_\Sigma |\{g_v\}, \boldsymbol{a}_e\rangle = |\{g_v\}, \boldsymbol{a}_e + \boldsymbol{\Sigma}\rangle, \tag{5.108}$$

for a closed 1-cochain $\boldsymbol{\Sigma}$ corresponding to Σ [see Eq. (5.45)].

We represent the 0-form symmetry action associated to $h \in G$ as:

$$V_\rho(h) \equiv V(h) \prod_e X_e^{\hat{\overline{\boldsymbol{\rho}}}^h(e)}. \tag{5.109}$$

Here, $V(h)$ acts by (left) group multiplication of h on the vertex d.o.f.:

$$V(h) \equiv \sum_{\{g_v\}, \boldsymbol{a}_e} |\{hg_v\}, \boldsymbol{a}_e\rangle\langle\{g_v\}, \boldsymbol{a}_e|. \tag{5.110}$$

Therefore, the action of the 0-form symmetry operator $V_\rho(h)$ on a basis state is:

$$V_\rho(h) |\{g_v\}, \boldsymbol{a}_e\rangle = |\{hg_v\}, \boldsymbol{a}_e + \overline{\boldsymbol{\rho}}^h_{\{g_v\}}\rangle. \tag{5.111}$$

We now construct a model for an SPT phase protected by the 2-group symmetry generated by the operators in Eqs. (5.107) and (5.109). We start with the 1-form paramagnet

Hamiltonian H_0 in Section 5.3.1 and the decoupled G paramagnet H^G from Section 5.2.2:

$$H_0^G \equiv H_0 + H^G. \tag{5.112}$$

The 2-group SPT Hamiltonian is prepared from H_0^G by conjugation with the FDQC $\mathcal{U}_2$, which is a composition of two FDQC:

$$\mathcal{U}_2 = \mathcal{U}_2' \mathcal{U}_1. \tag{5.113}$$

$\mathcal{U}_1$ is the FDQC from Section 5.3.1 – it prepares a 1-form SPT model from a 1-form paramagnet:

$$\mathcal{U}_1 = \sum_{\{g_v\}, \boldsymbol{a}_e} (-1)^{\int \boldsymbol{a}_e \cup \delta \boldsymbol{a}_e} |\{g_v\}, \boldsymbol{a}_e\rangle\langle\{g_v\}, \boldsymbol{a}_e|. \tag{5.114}$$

$\mathcal{U}_2'$ is a FDQC that couples the vertex d.o.f. to the edge d.o.f. and ensures that the model is 2-group symmetric. Explicitly, $\mathcal{U}_2'$ is:

$$\mathcal{U}_2' \equiv \prod_t \left[e^{2\pi i O_t \left[\hat{\boldsymbol{\nu}}(t) + \frac{1}{2}\hat{\boldsymbol{\rho}} \cup_1 \hat{\boldsymbol{\rho}}(t)\right]} \prod_{f \subset t} W_f^{\hat{\boldsymbol{\rho}} \cup_1 \boldsymbol{f}(t)} \right]. \tag{5.115}$$

Here, the O_t is the orientation of each tetrahedron, defined in Fig. 5.2, the second product is over the faces in the boundary of t, and W_f is given in Eq. (5.61) . The 2-group SPT Hamiltonian H_2 is thus:

$$H_2 \equiv \mathcal{U}_2 H_0^G \mathcal{U}_2^\dagger. \tag{5.116}$$

In Appendix 5.F, we prove that H_2 is indeed invariant under the 2-group symmetry operators in Eqs. (5.107) and (5.109).

The important property of this 2-group SPT Hamiltonian is revealed after gauging the 1-form symmetry of the total 2-group symmetry. In the next section, we show that the re-

maining 0-form G symmetry "fractionalizes" on the loop-like 1-form gauge charges according to the group cochain ρ. This property is key to characterizing the fSPT phase that results from this construction.

Before gauging the 1-form symmetry, however, we motivate the 2-group SPT model from the spacetime construction in Ref. [133]. The spacetime model is defined on CM, the cone of the closed 3-manifold M. We orient the time-like edges, those connected to the additional spacetime point, towards the vertices of M (Fig. 5.9). We also place a G d.o.f. on the additional spacetime point of CM as well as a $\mathbb{Z}_2$ d.o.f. on each time-like edge. The partition function for the 2-group SPT phase is taken to be:

$$\mathcal{Z}_2 \equiv \sum_{\{g_v\},\boldsymbol{a}_e} \prod_{\Delta_4} e^{2\pi i O_{\Delta_4} \boldsymbol{\alpha}_{\{g_v\}}(\Delta_4)}, \tag{5.117}$$

where the product is over 4-simplices Δ_4, and $\boldsymbol{\alpha}_{\{g_v\}}$ is a certain $\{g_v\}$-dependent $\mathbb{R}/\mathbb{Z}$ valued cochain on M. In particular, $\boldsymbol{\alpha}_{\{g_v\}}$ is defined in terms of the supercohomology data (ρ, ν) as:

$$\boldsymbol{\alpha}_{\{g_v\}} \equiv \boldsymbol{\nu}_{\{g_v\}} + \frac{1}{2}\boldsymbol{\rho}_{\{g_v\}} \cup_1 \boldsymbol{\epsilon}_{\{g_v\}} + \frac{1}{2}\boldsymbol{\epsilon}_{\{g_v\}} \cup \boldsymbol{\epsilon}_{\{g_v\}}. \tag{5.118}$$

To define $\boldsymbol{\alpha}_{\{g_v\}}$, we have introduced the cochains $\boldsymbol{\rho}_{\{g_v\}}$, $\boldsymbol{\nu}_{\{g_v\}}$, and $\boldsymbol{\epsilon}_{\{g_v\}}$. $\boldsymbol{\rho}_{\{g_v\}}$ is the $\mathbb{Z}_2$ 3-cochain given by:

$$\boldsymbol{\rho}_{\{g_v\}}(\langle 0123\rangle) \equiv \rho(g_0, g_1, g_2, g_3), \tag{5.119}$$

for any 3-simplex $\langle 0123\rangle$, and $\boldsymbol{\nu}_{\{g_v\}}$ is the $\mathbb{R}/\mathbb{Z}$ valued 4-cochain:

$$\boldsymbol{\nu}_{\{g_v\}}(\langle 01234\rangle) \equiv \nu(g_0, g_1, g_2, g_3, g_4), \tag{5.120}$$

where $\langle 01234\rangle$ is an arbitrary 4-simplex. Lastly, $\boldsymbol{\epsilon}_{\{g_v\}}$ denotes the 2-cochain:

$$\boldsymbol{\epsilon}_{\{g_v\}} \equiv \overline{\boldsymbol{\rho}}_{\{g_v\}} + \delta \boldsymbol{a}_e. \tag{5.121}$$

As elaborated on in Appendix K of Ref. [76], $\boldsymbol{\alpha}_{\{g_v\}}$ is the pullback of a 2-group cocycle [133]:

$$\alpha \equiv \nu + \frac{1}{2}\rho \cup_1 \epsilon + \frac{1}{2}\epsilon \cup \epsilon, \tag{5.122}$$

which acts on the 2-group classifying space.

To write down the SPT state, we consider the amplitude for a fixed configuration:

$$\Psi_2\left(\{g_v\}, \boldsymbol{a}_e\right) \equiv \prod_{\Delta_4} e^{2\pi i O_{\Delta_4} \boldsymbol{\alpha}_{\{g_v\}}(\Delta_4)}. \tag{5.123}$$

The amplitude is invariant under re-triangulations of CM, so by a series of re-triangulations, we can remove both the dependence on the G d.o.f. at the additional spacetime point and the dependence on the $\mathbb{Z}_2$ d.o.f. at the time-like edges. Therefore, without affecting the amplitude, the additional d.o.f. can be set to the identity state. It can be checked that the resulting amplitude gives precisely the wave function for the ground state of the 2-group SPT Hamiltonian H_2.

5.4.3 Shadow model

The next step in our construction is to build the shadow model. We start by gauging the $\mathbb{Z}_2$ 1-form symmetry of the 2-group SPT Hamiltonian H_2. Then, we perform a change of basis to ensure that the remaining 0-form symmetry forms an onsite representation of G. The result is the shadow model – a G-symmetry-enriched twisted toric code, where the G symmetry fractionalizes on the loop-like 1-form gauge charges. We compute the symmetry fractionalization on the loop-like excitations explicitly, and show that the fractionalization is governed by the group cochain ρ in the supercohomology data (ρ, ν). In the subsequent section, we condense the emergent fermion in the shadow model to complete the construction of the $G \times \mathbb{Z}_2^f$ fSPT model corresponding to the supercohomology data (ρ, ν).

We gauge the 1-form symmetry of H_2 following the discussion in Section 5.3.2. As described earlier in the chapter, the procedure for gauging the 1-form symmetry is functionally

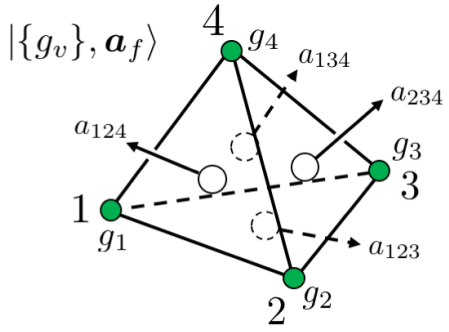

Figure 5.18: The Hilbert space for the shadow model consists of G d.o.f. on vertices and $\mathbb{Z}_2$ d.o.f. on faces. In the state $|\{g_v\}, \boldsymbol{a}_f\rangle$, the values of the $\mathbb{Z}_2$ d.o.f. at the faces are given by $\boldsymbol{a}_f(f) = a_f$.

equivalent to applying a duality that maps the 1-form symmetric operators X_e and W_f according to:

$$X_e \to \prod_{f \supset e} X_f, \quad W_f \to Z_f. \tag{5.124}$$

For the 2-group SPT model, the gauging procedure maps to a Hilbert space composed of $\mathbb{Z}_2$ d.o.f. on faces and G d.o.f. on vertices (Fig. 5.18). A basis for this Hilbert space is given by states of the form $|\{g_v\}, \boldsymbol{a}_f\rangle$, where we have used notation from Section 5.3.2 to label a configuration of the face d.o.f. with a 2-cochain $\boldsymbol{a}_f$.

To apply the operator duality in Eq. (5.124) to H_2, we rewrite H_2 as:

$$H_2 = \mathcal{U}_2' \left(\mathcal{U}_1 H_0^G \mathcal{U}_1^\dagger \right) \mathcal{U}_2'^\dagger, \tag{5.125}$$

and map $\mathcal{U}_1 H_0^G \mathcal{U}_1^\dagger$ and $\mathcal{U}_2'$ independently. $\mathcal{U}_1$ prepares the 1-form SPT model in Section 5.3.1 from H_0^G, so gauging the 1-form symmetry of $\mathcal{U}_1 H_0^G \mathcal{U}_1^\dagger$ yields H_{ttc}^G, a twisted toric code with

a decoupled G paramagnet:

$$H^G_{\text{ttc}} \equiv H_{\text{ttc}} + H^0_G. \tag{5.126}$$

Importantly, we retain the local projectors $\mathcal{P}_R^{0\text{-flux}}$ in Eq. (5.65) from the gauging procedure (for appropriate choices of regions R). They are needed to ensure that the shadow model is G symmetric.[15]

We next apply the duality to $\mathcal{U}_2'$. Before doing so, however, we multiply $\mathcal{U}_2'$ by the identity:[16]

$$1 = \prod_t \Big(\prod_{f \subset t} W_f \Big)^{\int \hat{\boldsymbol{\rho}} \cup_2 \boldsymbol{t}}. \tag{5.127}$$

Here, we have used the cup-2 product $\cup_2$, defined in Appendix 5.A.2. The $\cup_2$ product of $\hat{\boldsymbol{\rho}}$ and $\boldsymbol{t}$ evaluated on the tetrahedron $\langle 1234 \rangle$ is:

$$\hat{\boldsymbol{\rho}} \cup_2 \boldsymbol{t}(\langle 1234 \rangle) = \big[\hat{\boldsymbol{\rho}}(\langle 123 \rangle) + \hat{\boldsymbol{\rho}}(\langle 134 \rangle) \big] \, \boldsymbol{t}(\langle 1234 \rangle). \tag{5.128}$$

After multiplying by the operator in Eq. (5.127), $\mathcal{U}_2'$ becomes:

$$\mathcal{U}_2' \equiv \prod_t \Big[e^{2\pi i O_t \left[\hat{\boldsymbol{\nu}}(t) + \frac{1}{2} \hat{\boldsymbol{\rho}} \cup_1 \hat{\boldsymbol{\rho}}(t) \right]} \prod_{f \subset t} W_f^{\hat{\boldsymbol{\rho}} \cup_1 \boldsymbol{f}(t)} \Big] \prod_t \Big(\prod_{f \subset t} W_f \Big)^{\int \hat{\boldsymbol{\rho}} \cup_2 \boldsymbol{t}}. \tag{5.129}$$

While the modification to $\mathcal{U}_2'$ has no affect on the ground state subspace of the shadow model, it is crucial to the symmetry of the FDQC in Section 5.4.4 that prepares the fSPT ground state (see Appendix 5.G.1 for details). After the modification, $\mathcal{U}_2'$ maps to the FDQC $\mathcal{U}_s'$:

$$\mathcal{U}_s' \equiv \prod_t \Big[e^{2\pi i O_t \left[\hat{\boldsymbol{\nu}}(t) + \frac{1}{2} \hat{\boldsymbol{\rho}} \cup_1 \hat{\boldsymbol{\rho}}(t) \right]} \prod_{f \subset t} Z_f^{\hat{\boldsymbol{\rho}} \cup_1 \boldsymbol{f}(t)} \Big] prod_t W_t^{\int \hat{\boldsymbol{\rho}} \cup_2 \boldsymbol{t}}. \tag{5.130}$$

[15] Without the projectors, the shadow model is only guaranteed to be G symmetric up to factors of W_t.

[16] The operator $\prod_{f \subset t} W_f$ is identically 1, since: $\prod_{f \subset t} W_f = \prod_{f \subset t} \prod_{e \subset f} Z_e = \prod_{e \subset t} Z_e^2 = 1$, where the last product is over edges e in t.

The gauging procedure produces the Hamiltonian:

$$H'_s \equiv \mathcal{U}'_s H^G_{\text{ttc}} \mathcal{U}'^{\dagger}_s. \tag{5.131}$$

H'_s is invariant under a 0-form G symmetry given by applying the gauging duality to the 0-form symmetry of the 2-group [Eq. (5.109)]. The 0-form symmetry operator corresponding to $h \in G$ is mapped to:

$$V'_\rho(h) \equiv V(h) \prod_{f=\langle 123\rangle} X_f^{\hat{\overline{\boldsymbol{\rho}}}^h(\langle 23\rangle)+\hat{\overline{\boldsymbol{\rho}}}^h(\langle 13\rangle)+\hat{\overline{\boldsymbol{\rho}}}^h(\langle 12\rangle)} = \sum_{\{g_v\},\boldsymbol{a}_f} |\{hg_v\}, \boldsymbol{a}_f + \delta\overline{\boldsymbol{\rho}}^h_{\{g_v\}}\rangle\langle\{g_v\}, \boldsymbol{a}_f|. \tag{5.132}$$

We notice that the resulting symmetry $V'_\rho(h)$ is not necessarily onsite. This is because the term $\delta\overline{\boldsymbol{\rho}}^h_{\{g_v\}}(f)$ in the second line of Eq. (5.132) depends on the $\{g_v\}$-configuration at the vertices of f, in general.

To obtain the shadow model, we make a local change of basis – implemented by a FDQC, which makes the remaining 0-form G symmetry onsite. We implement the change of basis with the unitary operator:

$$\mathcal{R} \equiv \prod_f X_f^{\hat{\overline{\boldsymbol{\rho}}}(f)}. \tag{5.133}$$

Every state $|\Psi\rangle$ and operator $\mathcal{O}$ is transformed as:

$$|\Psi\rangle \to \mathcal{R}|\Psi\rangle, \quad \mathcal{O} \to \mathcal{R}\mathcal{O}\mathcal{R}^\dagger. \tag{5.134}$$

Under the transformation above, $V'_\rho(h)$ becomes:

$$\sum_{\{g_v\},\boldsymbol{a}_f} |\{hg_v\}, \boldsymbol{a}_f + \overline{\boldsymbol{\rho}}_{\{hg_v\}} + \delta\overline{\boldsymbol{\rho}}^h_{\{g_v\}}\rangle\langle\{g_v\}, \boldsymbol{a}_f + \overline{\boldsymbol{\rho}}_{\{g_v\}}|. \tag{5.135}$$

It can be shown, using that ρ is a cocycle [Eq. (5.94)], that $\overline{\boldsymbol{\rho}}_{\{g_v\}}$ and $\overline{\boldsymbol{\rho}}^h_{\{g_v\}}$ are related by:

$$\overline{\boldsymbol{\rho}}_{\{hg_v\}} + \delta\overline{\boldsymbol{\rho}}^h_{\{g_v\}} = \overline{\boldsymbol{\rho}}_{\{g_v\}}. \tag{5.136}$$

Thus, the operator in Eq. (5.135) is equivalent to the onsite symmetry action:

$$V(h) \equiv \sum_{\{g_v\},\boldsymbol{a}_f} |\{hg_v\},\boldsymbol{a}_f\rangle\langle\{g_v\},\boldsymbol{a}_f|. \tag{5.137}$$

We apply the basis transformation $\mathcal{R}$ to H'_s by conjugation. This produces the shadow model:

$$H_s \equiv \mathcal{R}H'_s\mathcal{R}^\dagger = \mathcal{R}\left(\mathcal{U}'_s H^G_{\text{ttc}}\mathcal{U}'_s\right)\mathcal{R}^\dagger = \mathcal{U}_s H^G_{\text{ttc}}\mathcal{U}_s^\dagger, \tag{5.138}$$

where, in the last line, we have introduced $\mathcal{U}_s$:

$$\mathcal{U}_s \equiv \mathcal{R}\mathcal{U}'_s. \tag{5.139}$$

The FDQC $\mathcal{U}_s$ is explicitly:

$$\mathcal{U}_s = \prod_f X_f^{\hat{\overline{\boldsymbol{\rho}}}(f)} \prod_t \left[e^{2\pi i O_t\left[\hat{\overline{\boldsymbol{\nu}}}(t)+\frac{1}{2}\hat{\overline{\boldsymbol{\rho}}}\cup_1\hat{\overline{\boldsymbol{\rho}}}(t)\right]} \prod_{f\subset t} Z_f^{\hat{\overline{\boldsymbol{\rho}}}\cup_1\boldsymbol{f}(t)}\right] \prod_t W_t^{\int\hat{\overline{\boldsymbol{\rho}}}\cup_2\boldsymbol{t}}. \tag{5.140}$$

The Hamiltonian H_s describes a symmetry-enriched twisted toric code. This is because it is both G symmetric and can be constructed from H^G_{ttc} using the FDQC $\mathcal{U}_s$. The symmetry of H_s follows from the symmetry of the 2-group SPT Hamiltonian H_2 (Appendix 5.F).

Similar to the twisted toric code, H_s admits loop-like excitations as well as point-like excitations with fermionic statistics. In the twisted toric code, the loop-like excitations are created at the boundary of a surface σ using the membrane operator M_σ, defined in Eq. (5.75). Therefore, the loop-like excitations can be created in the shadow model with the

operator:

$$M_\sigma^s \equiv \mathcal{U}_s M_\sigma \mathcal{U}_s^\dagger = \prod_{f\subset\sigma} \left[(-1)^{\hat{\tilde{\rho}}(f)} Z_f\right], \tag{5.141}$$

where in the second equality we have commuted $\mathcal{U}_s$ past the Pauli Z operators in M_σ. Likewise, emergent fermion string operators in the shadow model can be formed by conjugating the twisted toric code string operators $\mathcal{S}_p$ and $\tilde{\mathcal{S}}_p$ by $\mathcal{U}_s$:

$$\mathcal{S}_p^s \equiv \mathcal{U}_s \mathcal{S}_p \mathcal{U}_s^\dagger, \quad \tilde{\mathcal{S}}_p^s \equiv \mathcal{U}_s \tilde{\mathcal{S}}_p \mathcal{U}_s^\dagger. \tag{5.142}$$

For certain choices of supercohomology data (ρ, ν), the corresponding shadow model describes a *nontrivial*, symmetry-enriched twisted toric code. In particular, the group cochain ρ determines the fractionalization (defined below) of the G symmetry on the loop-like 1-form gauge charges. This symmetry fractionalization partially characterizes the G-symmetry-enriched twisted toric code phase [163].

Symmetry fractionalization on loop-like excitations

In what follows, we compute the symmetry fractionalization on the loop-like excitations of the shadow model, explicitly. We do so by considering an excited state of H_s obtained by applying M_σ^s to a ground state $|\Psi_s\rangle$ of H_s. The resulting state $M_\sigma^s|\Psi_s\rangle$ has a single loop of 1-form gauge charge along $\partial\sigma$, the boundary of σ. We study the effect of the G-symmetry action on this state to determine the fractionalization of the symmetry on the loop-like excitation.

To set up the computation and make the discussion more precise, we introduce an effective Hilbert space in the vicinity of the 1-form gauge charge. We define the state $|\psi_{\text{ttc}}, \{g_v\}_{\partial\sigma}\rangle$ to be the ground state of the twisted toric code Hamiltonian H_{ttc}^G with fixed G configuration $\{g_v\}_{\partial\sigma}$ at vertices v contained in $\partial\sigma$. The set of states $\left\{|\Psi_{\text{ttc}}, \{g_v\}_{\partial\sigma}\rangle\right\}$ spans a Hilbert space with dimension $|G|^N$, where N is the number of vertices in $\partial\sigma$. The effective Hilbert space

is then formed by the states $\{|\Psi_s^{\partial\sigma}, \{g_v\}_{\partial\sigma}\rangle\}$, where $|\Psi_s^{\partial\sigma}, \{g_v\}_{\partial\sigma}\rangle$ is defined by:

$$|\Psi_s^{\partial\sigma}, \{g_v\}_{\partial\sigma}\rangle \equiv M_\sigma^s \mathcal{U}_s |\Psi_{\text{ttc}}, \{g_v\}_{\partial\sigma}\rangle. \tag{5.143}$$

We note that, in particular, the state $M_\sigma^s|\Psi_s\rangle$ belongs to the effective Hilbert space:

$$M_\sigma^s|\Psi_s\rangle = \sum_{\{g_v\}_{\partial\sigma}} |\Psi_s^{\partial\sigma}, \{g_v\}_{\partial\sigma}\rangle. \tag{5.144}$$

Heuristically, a state $|\Psi_s^{\partial\sigma}, \{g_v\}_{\partial\sigma}\rangle$ in the effective Hilbert space resembles the ground state $|\Psi_s\rangle$ far away from $\partial\sigma$.[17] Since $|\Psi_s\rangle$ is symmetric, we expect the symmetry to act as the identity on $|\Psi_s^{\partial\sigma}, \{g_v\}_{\partial\sigma}\rangle$ away from $\partial\sigma$. However, the symmetry may act non-identically on the states in the effective Hilbert space, and we define the projection of the symmetry action to the effective Hilbert space to be the *effective* symmetry action on a 1-form gauge charge. The fractionalization of the G-symmetry action is an obstruction to realizing the effective symmetry action onsite.

We next determine the effective symmetry action on the loop-like excitation by acting on an arbitrary state $|\Psi_s^{\partial\sigma}, \{g_v\}_{\partial\sigma}\rangle$ in the effective Hilbert space with the symmetry operator $V(h)$:

$$V(h)|\Psi_s^{\partial\sigma}, \{g_v\}_{\partial\sigma}\rangle = V(h) M_\sigma^s \mathcal{U}_s |\Psi_{\text{ttc}}, \{g_v\}_{\partial\sigma}\rangle. \tag{5.145}$$

The expression on the right hand side of Eq. (5.145) can be evaluated further by commuting $V(h)$ past M_σ^s and $\mathcal{U}_s$. Using the relation in Eq. (5.136), we find:

$$V(h) M_\sigma^s = \Big[\prod_{e \subset \partial\sigma} (-1)^{\hat{\tilde{\rho}}^{h^{-1}}(e)} \Big] M_\sigma^s V(h), \tag{5.146}$$

[17] More concretely, any reduced density matrix of the state $|\Psi_s^{\partial\sigma}, \{g_v\}_{\partial\sigma}\rangle\langle\Psi_s^{\partial\sigma}, \{g_v\}_{\partial\sigma}|$ will agree with the reduced density matrix of $|\Psi_s\rangle\langle\Psi_s|$ on regions far from $\partial\sigma$.

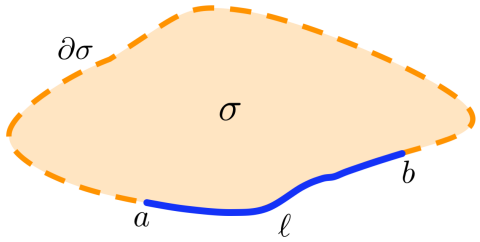

Figure 5.19: A loop-like excitation is created at $\partial\sigma$ (dashed orange line) by applying the operator M_σ^s on the surface σ of the direct lattice. ℓ (thick blue line) is a connected submanifold of $\partial\sigma$ used to determine the fractionalization of the symmetry on the gauge charge. a and b label the end points of ℓ.

and as shown in Appendix 5.G.1, $V(h)$ commutes with $\mathcal{U}_s$ up to factors of $\bar{G}_e$:

$$V(h)\mathcal{U}_s = \mathcal{U}_s\Big[\prod_e \bar{G}_e^{\hat{\bar{\rho}}^{h^{-1}}(e)}\Big]V(h). \tag{5.147}$$

Therefore, the action of $V(h)$ on a state in the effective Hilbert space is:

$$V(h)|\Psi_s^{\partial\sigma},\{g_v\}_{\partial\sigma}\rangle = \prod_{e\subset\partial\sigma}(-1)^{\hat{\bar{\rho}}^{h^{-1}}(e)}|\Psi_s^{\partial\sigma},\{hg_v\}_{\partial\sigma}\rangle, \tag{5.148}$$

where we have used that $|\Psi_{\text{ttc}},\{hg_v\}_{\partial\sigma}\rangle$ is a $+1$ eigenstate of $\bar{G}_e$. The effective symmetry action for $h\in G$ is explicitly:

$$\mathcal{V}_{\partial\sigma}(h) \equiv \sum_{\{g_v\}_{\partial\sigma}}\prod_{e\subset\partial\sigma}(-1)^{\hat{\bar{\rho}}^{h^{-1}}(e)}|\Psi_s^{\partial\sigma},\{hg_v\}_{\partial\sigma}\rangle\langle\Psi_s^{\partial\sigma},\{g_v\}_{\partial\sigma}|. \tag{5.149}$$

We identify the fractionalization of the symmetry, or an obstruction to an onsite representation, by considering the effective symmetry action restricted to a connected submanifold ℓ

of $\partial\sigma$ (Fig. 5.19):[18]

$$\mathcal{V}_\ell(h) \equiv \sum_{\{g_v\}_\ell} \prod_{e\subset\ell} (-1)^{\hat{\bar{\rho}}^{h^{-1}}(e)} |\Psi_s^{\partial\sigma}, \{hg_v\}_\ell\rangle\langle\Psi_s^{\partial\sigma}, \{g_v\}_\ell|, \tag{5.150}$$

with $\mathcal{V}_\ell(h)$ acting as the identity on sites in $\partial\sigma$ not contained in ℓ. While $\mathcal{V}_{\partial\sigma}(h)$ satisfies the group law:

$$\mathcal{V}_{\partial\sigma}(h_1)\mathcal{V}_{\partial\sigma}(h_2) = \mathcal{V}_{\partial\sigma}(h_1h_2), \tag{5.151}$$

$\mathcal{V}_\ell(h)$ only satisfies the group law up to an operator $\Omega(h_1, h_2)$:

$$\mathcal{V}_\ell(h_1)\mathcal{V}_\ell(h_2) = \Omega(h_1, h_2)\mathcal{V}_\ell(h_1h_2). \tag{5.152}$$

For $\mathcal{V}_\ell(h)$ given in Eq. (5.150), we find:

$$\Omega(h_1, h_2) = \sum_{g_a, g_b} \left[(-1)^{\rho(1,h_1,h_1h_2,g_a)+\rho(1,h_1,h_1h_2,g_b)} |\Psi_s^{\partial\sigma}, g_a, g_b\rangle\langle\Psi_s^{\partial\sigma}, g_a, g_b|\right], \tag{5.153}$$

where we have labeled the endpoints of ℓ as a and b, and $\Omega(h_1, h_2)$ acts as the identity on all other sites in $\partial\sigma$. $\Omega(h_1, h_2)$ acts non-trivially only near the endpoints of ℓ. Hence, we can split $\Omega(h_1, h_2)$ into an operator $\Omega_a(h_1, h_2)$ acting at a and an operator $\Omega_b(h_1, h_2)$ acting at b. The decomposition is unique up to a sign,[19] which may depend on h_1 and h_2. For example, we may write:

$$\Omega_a(h_1, h_2) = \sum_{g_a} (-1)^{\rho(1,h_1,h_1h_2,g_a)} |\Psi_b^{\partial\sigma}, g_a\rangle\langle\Psi_b^{\partial\sigma}, g_a|, \tag{5.154}$$

which acts as the identity away from the endpoint a. Alternatively, we could modify both

[18] There is some ambiguity in defining the restriction near the boundaries of ℓ. In fact, the calculation is unaffected by the particular choice. For more details, we refer to Ref. [46].

[19] The $\mathbb{Z}_2$ fusion rules of 1-form gauge charges reduce the ambiguity from a general phase to a sign [163].

$\Omega_a(h_1,h_2)$ and $\Omega_b(h_1,h_2)$ by a sign $(-1)^{\beta(1,h_1,h_1h_2)}$, where β is an arbitrary group cochain in $C^2(G,\mathbb{Z}_2)$.

The symmetry fractionalization can be shown by analyzing the associativity of the restricted group action. The associativity of the $\mathcal{V}_\ell(h)$ operators implies (see Ref. [46]):

$$\Omega(h_1,h_2)\Omega(h_1h_2,h_3) = \mathcal{V}_\ell(h_1)\Omega(h_2,h_3)\mathcal{V}_\ell^\dagger(h_1)\Omega(h_1,h_2h_3). \tag{5.155}$$

If the effective symmetry action can be written as onsite, then Eq. (5.155) is satisfied independently at endpoints a and b for some choice of β. (This follows from Appendix B of Ref. [46].) On the other hand, if Eq. (5.155) is not satisfied independently at the endpoints for any choice of β, then there is an obstruction to realizing the effective symmetry action onsite.

For Ω_a in Eq. (5.154), Eq. (5.155) only holds up to a G-dependent sign at the endpoint a:

$$\Omega_a(h_1,h_2)\Omega_a(h_1h_2,h_3) = (-1)^{\rho(1,h_1,h_1h_2,h_1h_2h_3)}\mathcal{V}_\ell(h_1)\Omega_a(h_2,h_3)\mathcal{V}_\ell^\dagger(h_1)\Omega_a(h_1,h_2h_3). \tag{5.156}$$

The sign $(-1)^{\rho(1,h_1,h_1h_2,h_1h_2h_3)}$ in Eq. (5.156) captures the symmetry fractionalization on the 1-form gauge charge. Taking into account the ambiguity in defining Ω_a, we see that ρ is well defined up to a group coboundary $\delta\beta$, with β an arbitrary element of $C^2(G,\mathbb{Z}_2)$. In other words, the symmetry fractionalization on the loop-like excitation is described by an element of the group cohomology $H^3(G,\mathbb{Z}_2)$. Therefore, when ρ represents a nontrivial class in $H^3(G,\mathbb{Z}_2)$, there is a nontrivial symmetry fractionalization on the 1-form gauge charges of the shadow model.

The group cohomology class represented by ρ defines a quantized invariant of the symmetry-enriched twisted toric code phase. To make this explicit, we note that any state belonging to the same symmetry-enriched phase can be constructed (approximately) from $|\Psi_s\rangle$ by applying a FDQC built of symmetric local unitaries. If we modify $\mathcal{U}_s$ by a FDQC

built of symmetric local unitaries, the calculation above is unchanged. Thus, the symmetry fractionalization on a gauge charge is given by the same group cohomology class for any state in the symmetry-enriched phase.

In the next section, we see that this quantized invariant may be pushed forward to characterize the corresponding fSPT obtained from condensing the emergent fermion in the shadow model.

5.4.4 Fermionic SPT

Finally, we condense the emergent fermion in the shadow model to construct a fSPT Hamiltonian corresponding to the supercohomology data (ρ, ν). In the process, we find a FDQC $\mathcal{U}_f$ that prepares the fSPT ground state from a product state. We argue that our models exhibit the expected responses to probing with fermion parity defects, by referring to the properties of the shadow models. Lastly, we interpret the equivalence relation on supercohomology data in Ref. [126] using the stacking rules.

Fermion condensation, described in Section 5.3.3, can be readily applied to any Hamiltonian expressed in terms of the operators $\bar{G}_e$, $\bar{U}_f$, and W_t. The fermion is then condensed by mapping the operators according to:

$$\bar{G}_e \to 1, \quad \bar{U}_f \to S_f, \quad W_t \to P_t. \tag{5.157}$$

The result is a model defined on a Hilbert space with a single spinless complex fermion at each tetrahedron. We emphasize again that this mapping requires the spatial manifold to admit a spin structure.

To apply the fermion condensation duality in Eq. (5.157) to the shadow model:

$$H_s = \mathcal{U}_s H^G_{\text{ttc}} \mathcal{U}_s^\dagger, \tag{5.158}$$

we write H^G_{ttc} and $\mathcal{U}_s$ in terms of $\bar{G}_e$, $\bar{U}_f$, and W_t operators. By definition, H^G_{ttc} can be written

using $\bar{G}_e$ and W_t. As for $\mathcal{U}_s$, the Pauli X and Pauli Z operators can be commuted to write (see Appendix 5.G.2 for a derivation):

$$\mathcal{U}_s = \prod_t e^{2\pi i O_t \hat{\bar{\boldsymbol{\nu}}}(t)} \xi_{\bar{\rho}}(M) \prod_f \bar{U}_f^{\hat{\bar{\boldsymbol{\rho}}}(f)} \prod_t W_t^{\int \hat{\bar{\boldsymbol{\rho}}} \cup_2 \boldsymbol{t}}. \tag{5.159}$$

Here, we have defined an arbitrary ordering of faces on M:

$$\{f_1, \ldots, f_i, \ldots\}, \quad (f_1 < \cdots < f_i < \cdots), \tag{5.160}$$

and the product of $\bar{U}_f$ operators is determined by the order of faces in M:

$$\prod_f \bar{U}_f^{\hat{\bar{\boldsymbol{\rho}}}(f)} = \left(\cdots \bar{U}_{f_i}^{\hat{\bar{\boldsymbol{\rho}}}(f_i)} \cdots \bar{U}_{f_1}^{\hat{\bar{\boldsymbol{\rho}}}(f_1)} \right). \tag{5.161}$$

$\xi_{\bar{\rho}}(M)$ in Eq. (5.159) is a sign that compensates for the order dependence of the product of $\bar{U}_f$ operators, so that $\mathcal{U}_s$ is independent of the choice of ordering. Specifically, $\xi_{\bar{\rho}}(M)$ is given by (Appendix 5.G.2):

$$\xi_{\bar{\rho}}(M) \equiv \prod_{i,i'|i'<i} (-1)^{\hat{\bar{\boldsymbol{\rho}}}(f_{i'}) \hat{\bar{\boldsymbol{\rho}}}(f_i) \int \boldsymbol{f}_{i'} \cup_1 \boldsymbol{f}_i}. \tag{5.162}$$

We emphasize that, although $\xi_{\bar{\rho}}(M)$ and the product of $\bar{U}_f$ operators depend on a choice of ordering of the faces in M, the FDQC $\mathcal{U}_s$ does *not* depend on the choice of ordering.[20]

With this, we apply the mapping of operators in Eq. (5.157) to H_s to condense the emergent fermion. First, H^G_{ttc} is mapped to an atomic insulator and a decoupled G paramagnet (Appendix 5.D):

$$H^G_{\text{AI}} \equiv -\sum_t P_t - \sum_v \mathcal{P}_v. \tag{5.163}$$

[20]The independence on the ordering can be derived from the commutation relations: $\bar{U}_f \bar{U}_{f'} = (-1)^{\int (\boldsymbol{f}' \cup_1 \boldsymbol{f} + \boldsymbol{f} \cup_1 \boldsymbol{f}')} \bar{U}_{f'} \bar{U}_f$, as described in Appendix 5.G.2.

Second, $\mathcal{U}_s$ is mapped to a FDQC $\mathcal{U}_f$:

$$\mathcal{U}_f \equiv \prod_t e^{2\pi i O_t \hat{\tilde{\nu}}(t)} \xi_{\bar{\rho}}(M) \prod_f S_f^{\hat{\tilde{\rho}}(f)} \prod_t P_t^{\int \hat{\tilde{\rho}} \cup_2 \boldsymbol{t}}. \tag{5.164}$$

Thus, fermion condensation leads to the exactly-solvable fermionic Hamiltonian:

$$H_f \equiv \mathcal{U}_f H_{\mathrm{AI}}^G \mathcal{U}_f^\dagger. \tag{5.165}$$

This is precisely the Hamiltonian described in Section 5.2.3.

We note that H_f is symmetric due to the symmetry of both H_{AI}^G and $\mathcal{U}_f$. To see that $\mathcal{U}_f$ is symmetric, we consider the bosonic FDQC $\mathcal{U}_s$. $\mathcal{U}_s$ commutes with the symmetry up to factors of $\bar{G}_e$ (see Appendix 5.G.1), and since $\bar{G}_e$ maps to the identity under fermion condensation, $\mathcal{U}_f$ must commute with the symmetry.

Equivalence relation on supercohomology data

For each set of supercohomology data, we can now construct a fSPT Hamiltonian H_f. However, the Hamiltonians constructed from two *a priori* different sets of supercohomology data, say (ρ, ν) and (ρ', ν'), may be within the same phase. This motivates imposing an equivalence relation on the supercohomology data, so that two sets of supercohomology data are equivalent if and only if they describe the same characteristic response of the SPT phase. Ref. [126] used spacetime methods to argue that the appropriate equivalence relation $\sim$ on the supercohomology data is:

$$(\rho, \nu) \sim (\rho + \delta\beta, \nu + \delta\eta + \frac{1}{2}\beta \cup \beta + \frac{1}{2}\beta \cup_1 \delta\beta + \frac{1}{2}\rho \cup_2 \delta\beta). \tag{5.166}$$

Here, β and η are arbitrary group cochains:

$$\beta \in C^2(G, \mathbb{Z}_2), \quad \eta \in C^3(G, \mathbb{R}/\mathbb{Z}), \tag{5.167}$$

and the group cup products can be written explicitly using the general formulas in Appendix 5.A.1.

We point out that the equivalence relation can be phrased in terms of the operation $\boxtimes$ induced by stacking. As discussed in Section 5.2.3, the stacking operation can be determined by composing FDQCs. The stacking operation applied to (ρ, ν) and (ρ', ν') gives:

$$(\rho, \nu) \boxtimes (\rho', \nu') = (\rho + \rho', \nu + \nu' + \frac{1}{2}\rho \cup_2 \rho'). \tag{5.168}$$

With this, we see that any two equivalent sets of supercohomology data can be related by stacking a "trivial" set of supercohomology data:

$$(\rho_0, \nu_0) \equiv (\delta\beta, \delta\eta + \frac{1}{2}\beta \cup \beta + \frac{1}{2}\beta \cup_1 \delta\beta), \tag{5.169}$$

for some choice of β in $C^2(G, \mathbb{Z}_2)$ and η belonging to $C^3(G, \mathbb{R}/\mathbb{Z})$. Explicitly, stacking (ρ_0, ν_0) with an arbitrary set of supercohomology data (ρ, ν) yields:

$$(\rho, \nu) \boxtimes (\delta\beta, \delta\eta + \frac{1}{2}\beta \cup \beta + \frac{1}{2}\beta \cup_1 \delta\beta) = (\rho + \delta\beta, \nu + \delta\eta + \frac{1}{2}\beta \cup \beta + \frac{1}{2}\beta \cup_1 \delta\beta + \frac{1}{2}\rho \cup_2 \delta\beta), \tag{5.170}$$

which is equivalent to (ρ, ν) according to Eq. (5.166).

The equivalence relation given in Eq. (5.166) can be motivated in terms of our supercohomology models. We show this by arguing that (i) equivalent sets of supercohomology data lead to Hamiltonians in the same phase and (ii) inequivalent sets of supercohomology data give rise to Hamiltonians in distinct phases (up to stacking bosonic SPT phases).

To see that supercohomology models built from equivalent sets of supercohomology data belong to the same phase, we consider the ground state $|\Psi_f^{\rho_0\nu_0}\rangle$ of the Hamiltonian corresponding to a set of trivial data (ρ_0, ν_0). In Appendix 5.H, we show that $|\Psi_f^{\rho_0\nu_0}\rangle$ can be

written as:

$$|\Psi_f^{\rho_0\nu_0}\rangle = \prod_t e^{2\pi i O_t \hat{\boldsymbol{\eta}}(t)} \xi_\beta(M) \prod_f S_f^{\hat{\boldsymbol{\beta}}(f)} \sum_{\{g_v\}} |\{g_v\}, \text{vac}\rangle, \tag{5.171}$$

where $\xi_\beta(M)$ is defined as in Eq. (5.162). Due to the homogeneity of η and β, we see that $|\Psi_f^{\rho_0\nu_0}\rangle$ can be prepared from a product state by a FDQC composed of symmetric local unitaries. This implies that $|\Psi_f^{\rho_0\nu_0}\rangle$ belongs to a trivial fSPT phase. Therefore, the ground state of the Hamiltonian constructed from (ρ, ν) belongs to the same phase as the ground state of the Hamiltonian built from the equivalent set of data $(\rho, \nu) \boxtimes (\rho_0, \nu_0)$ (see the discussion of the stacking rule in Section 5.2.3).

We note that in the special case that β and η in Eq. (5.169) are closed, the trivial data (ρ_0, ν_0) is equal to $(0, \frac{1}{2}\beta \cup \beta)$. This corresponds to the data of a bosonic SPT phase, which according to the equivalence relation, must be trivial when considered as a fermionic SPT phase.[21] Although $\frac{1}{2}\beta \cup \beta$ may be a nontrivial cocycle, the bosonic SPT model can nonetheless be disentangled by a FDQC composed of local symmetric unitaries if fermionic hopping operators are used.

Next, we argue that supercohomology models constructed using inequivalent sets of supercohomology data belong to distinct fSPT phases. To make this precise, suppose (ρ, ν) and (ρ', ν') are inequivalent, or in other words, the stack:

$$(\tilde{\rho}, \tilde{\nu}) \equiv (\rho, \nu) \boxtimes (\rho', \nu')^{-1} \tag{5.172}$$

is not equal to (ρ_0, ν_0), for any choice of (ρ_0, ν_0) in Eq. (5.169). There are then two possibilities for $(\tilde{\rho}, \tilde{\nu})$ to be nontrivial. The first possibility, which is the focus of our discussion, is that $\tilde{\rho}$ is a nontrivial element of $H^3(G, \mathbb{Z}_2)$, so it cannot be written as $\delta\beta$ for any choice of group cochain $\beta \in C^2(G, \mathbb{Z}_2)$. The second possibility is that $\tilde{\rho}$ is trivial (i.e., $\tilde{\rho} = \delta\beta$), but $\tilde{\nu}$ is

[21] An example (though for an anti-unitary symmetry) was given in Ref. [126], where it was observed that the in-cohomology (3+1)D bosonic SPT phase protected by time-reversal symmetry is trivial in the presence of fermions.

nontrivial [i.e., $\tilde{\nu}$ is not equal to $\delta\eta + \frac{1}{2}\beta \cup \beta + \frac{1}{2}\beta \cup_1 \delta\beta$ for any choice of $\eta \in C^3(G, \mathbb{R}/\mathbb{Z})$]. In this case, $(\tilde{\rho}, \tilde{\nu})$ is equivalent to a set of supercohomology data of the form $(0, \tilde{\nu}')$, for some $\tilde{\nu}'$. Hence, (ρ, ν) and (ρ', ν') differ by a bosonic group cohomology SPT phase with a G symmetry. To show that (ρ, ν) and (ρ', ν') belong to different fSPT phases, one needs to determine whether the bosonic SPT phase is trivialized in the presence of fermions. Below, we address only the first possibility and leave the question of the trivialization of bosonic SPT phases in the presence of fermions for future studies.

Considering the first possibility, if $\tilde{\rho}$ represents a nontrivial class in $H^3(G, \mathbb{Z}_2)$, then we can use the symmetry fractionalization properties of the shadow model to argue that $(\tilde{\rho}, \tilde{\nu})$ must correspond to a nontrivial fSPT phase. To derive a contradiction, suppose that the Hamiltonian $H_f^{\tilde{\rho}\tilde{\nu}}$ built using $(\tilde{\rho}, \tilde{\nu})$ is in a trivial fSPT phase. Then, we can find a path of symmetric gapped Hamiltonians connecting $H_f^{\tilde{\rho}\tilde{\nu}}$ to the atomic insulator Hamiltonian H_{AI}^G. For each Hamiltonian in this path, we can gauge the fermion parity symmetry – or "ungauge" the anomalous 2-form symmetry. More precisely, we can map the fermionic operators to bosonic operators according to the duality in Table 5.2. To avoid ambiguity in this ungauging process, we conjugate the bosonic operators by local projectors onto the $\bar{G}_e = 1$ subspace and add a term $-\sum_e \bar{G}_e$ to enforce the $\bar{G}_e = 1$ constraint. The result of ungauging the anomalous 2-form symmetry is a symmetric gapped path of Hamiltonians connecting the shadow model corresponding to $(\tilde{\rho}, \tilde{\nu})$ to the twisted toric code Hamiltonian H_{ttc}^G. This is a contradiction, because the shadow model describes a nontrivial symmetry-enriched twisted toric code when $\tilde{\rho}$ is nontrivial in $H^3(G, \mathbb{Z}_2)$, while H_{ttc}^G is in a trivial symmetry-enriched phase. Therefore, $H_f^{\tilde{\rho}\tilde{\nu}}$ is in a nontrivial SPT phase, and (ρ, ν) and (ρ', ν') must correspond to distinct fSPT phases.

We note that the procedure for ungauging an anomalous 2-form symmetry, briefly described here, can be applied to any fermionic model. We emphasize that it is equivalent to gauging the fermion parity symmetry – the point-like 1-form fluxes in the shadow model correspond to fermion parity gauge charges and the loop-like 1-form gauge charges correspond to fermion parity gauge fluxes.

5.5 Gapped boundaries through symmetry extension

The supercohomology models, described in Sections 5.3 and 5.4, characterize the bulk of the SPT phase, i.e., the Hamiltonians are defined on manifolds without boundary. In this section, we consider models on manifolds with boundary. In particular, we describe supercohomology models that feature gapped, topologically ordered boundaries. To get started, we review gapped boundaries for group cohomology models, constructed via a symmetry extension [165]. We then generalize the symmetry extension construction to supercohomology models. Our generalization relies on the connection between 2-group SPT phases and supercohomology phases. The details of the construction, starting from a 2-group SPT model, are provided in Appendix L of Ref. [76].

5.5.1 *Review of gapped boundary construction of group cohomology models*

As shown in Ref. [165], symmetric gapped boundaries for group cohomology models can be constructed by first enlarging the symmetry at the boundary. One can then partially gauge the extended symmetry to produce a symmetric, topologically ordered boundary. To illustrate the construction, we consider a $(3+1)$D group cohomology model corresponding to the group cocycle $\nu \in H^4(G, \mathbb{R}/\mathbb{Z})$ with a unitary G symmetry.

We motivate the gapped boundary construction by reviewing the proof that the ground state of the group cohomology model is symmetric on a manifold without boundary. Recall that the ground state of the group cohomology model is:

$$|\Psi_b\rangle = \sum_{\{g_v\}} \Psi_b(\{g_v\})|\{g_v\}\rangle, \tag{5.173}$$

with the amplitude $\Psi_b(\{g_v\})$ given by:

$$\Psi_b(\{g_v\}) \equiv \prod_{t=\langle 1234\rangle} e^{2\pi i O_t \nu(1,g_1,g_2,g_3,g_4)}. \tag{5.174}$$

Applying the symmetry action $V(h)$, for $h \in G$, to $|\Psi_b\rangle$ yields:

$$V(h)|\Psi_b\rangle = \sum_{\{g_v\}} \tilde{\Psi}_b(\{g_v\})|\{g_v\}\rangle. \tag{5.175}$$

Here, we have shifted the indices and used the homogeneity of ν to define:

$$\tilde{\Psi}_b(\{g_v\}) \equiv \prod_{t=\langle 1234\rangle} e^{2\pi i O_t \nu(h,g_1,g_2,g_3,g_4)}. \tag{5.176}$$

We evaluate Eq. (5.176) further by using the cocycle property of ν, which tells us:

$$\begin{aligned} \nu(h,g_1,g_2,g_3,g_4) &= \nu(1,g_1,g_2,g_3,g_4) - \nu(1,h,g_2,g_3,g_4) \\ +\nu(1,h,g_1,g_3,g_4) &- \nu(1,h,g_1,g_2,g_4) + \nu(1,h,g_1,g_2,g_3). \end{aligned} \tag{5.177}$$

The last four terms in Eq. (5.177) each correspond to a face of the tetrahedron $\langle 1234\rangle$. Therefore, in substituting Eq. (5.177) into Eq. (5.176), the terms associated to faces cancel in pairs. We are left with: $\tilde{\Psi}_b(\{g_v\}) = \Psi_b(\{g_v\})$, which implies that $|\Psi_b\rangle$ is symmetric.

The cancellation of the face terms in the calculation above relies crucially on the fact that the manifold has no boundary. The wave function in Eq. (5.173) is not guaranteed to be symmetric on a manifold M with boundary ∂M, since the terms associated with faces fail to cancel at the boundary. In this case, the symmetry action $V(h)$ on $|\Psi_b\rangle$ leaves a residual phase factor $\mathcal{V}_h(\{g_v\})$ on the boundary of M, i.e.:

$$\tilde{\Psi}_b(\{g_v\}) = \mathcal{V}_h(\{g_v\})\Psi_b(\{g_v\}), \tag{5.178}$$

where $\mathcal{V}_h(\{g_v\})$ is the phase:

$$\mathcal{V}_h(\{g_v\}) \equiv \prod_{f_\partial = \langle 123\rangle} e^{2\pi i O_{f_\partial} \nu(1,h,g_1,g_2,g_3)}. \tag{5.179}$$

Here, the product is over faces f_∂ in the boundary of M and $O_{f_\partial} \in \{-1,+1\}$ is -1 if the

orientation of f_∂ points out of M and $+1$ otherwise. The residual phase factor is indicative of the anomalous symmetry action at the boundary of the SPT phase [46]. To find a gapped boundary, we search for a modification of $|\Psi_b\rangle$ near the boundary to "saturate" the anomaly.

The key observation, made in Refs. [165] and [176], is that the anomaly can be saturated by enlarging the symmetry at the boundary. To make this precise, we define L to be a central extension of G by a group K,[22] giving the short exact sequence:

$$1 \to K \to L \xrightarrow{\pi} G \to 1. \tag{5.180}$$

The group cocycle ν can then be pulled back by π to form a cocycle $\nu^* \in H^4(L, \mathbb{R}/\mathbb{Z})$:

$$\nu^*(\ell_0, \ell_1, \ell_2, \ell_3, \ell_4) \equiv \nu\big(\pi(\ell_0), \pi(\ell_1), \pi(\ell_2), \pi(\ell_3), \pi(\ell_4)\big), \tag{5.181}$$

with $\ell_0, \ell_1, \ell_2, \ell_3$, and ℓ_4 in L. According to Refs. [165] and [177], one can always find an extension L such that ν^* is a coboundary, i.e.:

$$\nu^* = \delta\eta, \tag{5.182}$$

for some η in $C^4(L, \mathbb{R}/\mathbb{Z})$. As described below, the cochain η can be used to absorb the residual phase factor in Eq. (5.178).

To build a symmetric wave function using η, we extend the global symmetry of the group cohomology model to L by replacing each G d.o.f. on the boundary with an L d.o.f. (see Fig. 5.20). We denote a configuration of the L and G d.o.f. by $\{\ell_w, g_v\}$, where ℓ_w is an element of L labeling the boundary vertex $w \in \partial M$ and g_v belongs to G and labels a vertex v in the bulk $v \in M \setminus \partial M$. For $h \in L$, the global L symmetry is then represented by:

$$V(\ell) \equiv \sum_{\{\ell_w, g_v\}} |\{\ell\ell_w, \pi(\ell)g_v\}\rangle\langle\{\ell_w, g_v\}|. \tag{5.183}$$

[22] By a central extension, we mean that K belongs in the center of L.

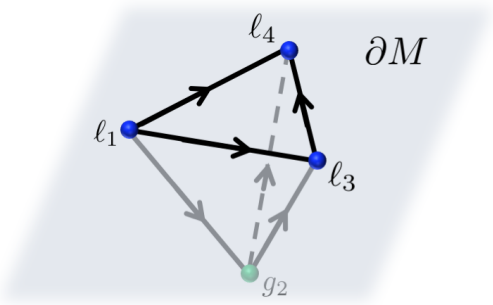

Figure 5.20: The L symmetric state $|\Psi_b^L\rangle$ is defined on a Hilbert space with L d.o.f. (blue) on the boundary of M. The vertices on the interior of M host G d.o.f. (green), as in Fig. 5.3.

Heuristically, the symmetry acts as L on the boundary sites and G on the bulk sites.

Now, we consider a modified state built using both ν and η and show that it is invariant under the L symmetry in Eq. (5.183). In particular, we consider the state $|\Psi_b^L\rangle$ defined as:

$$|\Psi_b^L\rangle \equiv \sum_{\{\ell_w, g_v\}} \Psi_\eta(\{\ell_w\})\Psi_b(\{\pi(\ell_w), g_v\})|\{\ell_w, g_v\}\rangle. \tag{5.184}$$

Here, $\Psi_\eta(\{\ell_w\})$ is a product of η dependent phase factors corresponding to faces in ∂M:

$$\Psi_\eta(\{\ell_w\}) \equiv \prod_{f_\partial = \langle 123\rangle} e^{-2\pi i O_{f_\partial} \eta(1,\ell_1,\ell_2,\ell_3)}. \tag{5.185}$$

To see that $|\Psi_b^L\rangle$ is invariant under the L symmetry, we act on the state with $V(\ell)$ in Eq. (5.183). After shifting the indices and using the homogeneity of ν and η, we find:

$$V(\ell)|\Psi_b^L\rangle = \sum_{\{\ell_w, g_v\}} \tilde{\Psi}_\eta(\{\ell_w\})\tilde{\Psi}_b(\{\pi(\ell_w), g_v\})|\{\ell_w, g_v\}\rangle, \tag{5.186}$$

where $\tilde{\Psi}_\eta(\{\ell_w\})$ is the phase:

$$\tilde{\Psi}_\eta(\{\ell_w\}) \equiv \prod_{f_\partial = \langle 123 \rangle} e^{-2\pi i O_{f_\partial} \eta(\ell, \ell_1, \ell_2, \ell_3)}. \tag{5.187}$$

The phase factors $\tilde{\Psi}_\eta(\{\ell_w\})$ and $\tilde{\Psi}_b(\{\pi(\ell_w), g_v\})$ can be simplified by using the coboundary relations for ν and η. Similar to Eq. (5.178), the coboundary relation for ν leads to a residual phase factor:

$$\tilde{\Psi}_b(\{\pi(\ell_w), g_v\}) = \mathcal{V}_\ell(\{\ell_w, g_v\}) \Psi_b(\{\pi(\ell_w), g_v\}), \tag{5.188}$$

with $\mathcal{V}_\ell(\{\ell_w, g_v\})$ given by:

$$\mathcal{V}_\ell(\{\ell_w, g_v\}) \equiv \prod_{f_\partial = \langle 123 \rangle} e^{2\pi i O_{f_\partial} \nu^*(1, \ell, \ell_1, \ell_2, \ell_3)}. \tag{5.189}$$

As for η, the coboundary relation in Eq. (5.182) tells us:

$$\begin{aligned} &\eta(\ell, \ell_1, \ell_2, \ell_3) = \nu^*(1, \ell, \ell_1, \ell_2, \ell_3) + \eta(1, \ell_1, \ell_2, \ell_3) \\ &- \eta(1, \ell, \ell_2, \ell_3) + \eta(1, \ell, \ell_1, \ell_3) - \eta(1, \ell, \ell_1, \ell_2). \end{aligned} \tag{5.190}$$

The last three terms correspond to edges in ∂M and cancel pairwise, when substituted into Eq. (5.187). The ν^* term in the coboundary relation of η produces a phase that precisely cancels the excess phase factor in Eq. (5.189):

$$\tilde{\Psi}_\eta(\{\ell_w\}) = \mathcal{V}_\ell^{-1}(\{\ell_w, g_v\}) \Psi_\eta(\{\ell_w\}). \tag{5.191}$$

Inserting Eqs. (5.188) and (5.191) into the expression for $V(\ell)|\Psi_b^L\rangle$, we see that $|\Psi_b^L\rangle$ is symmetric under the L symmetry. The η-dependent phase factors at the boundary compensates for the failure of the bulk wave function to be symmetric. (We note the similarity with anomalous SPT states introduced in Ref. [178].)

The state $|\Psi_b^L\rangle$ can be prepared from the product state:

$$|\Psi^L\rangle \equiv \sum_{\{\ell_w, g_v\}} |\{\ell_w, g_v\}\rangle \tag{5.192}$$

by the FDQC $\mathcal{U}_b^L$:

$$\mathcal{U}_b^L \equiv \prod_{f_\partial} e^{-2\pi i O_{f_\partial} \hat{\overline{\boldsymbol{\eta}}}(f_\partial)} \prod_t e^{2\pi i O_t \hat{\overline{\boldsymbol{\nu}}}(t)}. \tag{5.193}$$

Here, $\hat{\overline{\boldsymbol{\eta}}}(f_\partial)$ is the operator given by:

$$\hat{\overline{\boldsymbol{\eta}}}(\langle 123\rangle) \equiv \sum_{\{\ell_w, g_v\}} \eta(1, \ell_1, \ell_2, \ell_3) |\{\ell_w, g_v\}\rangle\langle\{\ell_w, g_v\}|, \tag{5.194}$$

and $\hat{\overline{\boldsymbol{\nu}}}(t)$ is explicitly:

$$\hat{\overline{\boldsymbol{\nu}}}(t) = \sum_{\{\ell_w, g_v\}} \overline{\boldsymbol{\nu}}_{\{\pi(\ell_w), g_v\}} |\{\ell_w, g_v\}\rangle\langle\{\ell_w, g_v\}|, \tag{5.195}$$

with $\overline{\boldsymbol{\nu}}_{\{\pi(\ell_w), g_v\}}$ defined in Eq. (5.98). $\mathcal{U}_b^L$ can be used to create a gapped parent Hamiltonian for $|\Psi_b^L\rangle$ by conjugating a certain paramagnet Hamiltonian whose ground state is $|\Psi^L\rangle$.

To recover the G symmetry, we can gauge the K subgroup of the L symmetry. This results in a G symmetric system with a K gauge theory at the boundary. The K gauge theory lives only on the boundary d.o.f., because the K subgroup acts as the identity on the bulk sites. We have thus constructed a group cohomology model with a symmetric, topologically ordered gapped boundary.

5.5.2 Gapped boundary construction for supercohomology models

We now generalize the construction of gapped boundaries for group cohomology models to build gapped boundaries for $(3+1)$D supercohomology models. The first step of the construction for group cohomology models is to find an extension of the G symmetry to

'trivialize' the cocycle ν. That is, to find an extension L such that the pull back of ν is a coboundary. Similarly, for supercohomology models, we first identify an extension of the G symmetry to an L symmetry that trivializes the supercohomology data (ρ, ν). Here, we say the supercohomology data is trivialized if the pull back (ρ^*, ν^*) is of the form:

$$(\rho^*, \nu^*) = (\delta\beta, \delta\eta + \frac{1}{2}\beta \cup \beta + \frac{1}{2}\beta \cup_1 \delta\beta), \tag{5.196}$$

for some $\beta \in C^2(L, \mathbb{Z}_2)$ and $\eta \in C^3(L, \mathbb{R}/\mathbb{Z})$. (The trivial supercohomology data in Eq. (5.196) was identified in Section 5.4.4.) We then use the data (β, η) to build a symmetric, topologically ordered gapped boundary for the supercohomology model. The detailed derivation from a 2-group SPT model is given in Appendix L of Ref. [76].

Before defining the supercohomology models on a manifold with boundary using (β, η), we argue that there exists a central extension of G for which the supercohomology data is trivialized, as in Eq. (5.196). To show that such an extension exists, we make two consecutive extensions of G. The first is given by the short exact sequence:

$$1 \to K_1 \to L' \xrightarrow{\pi_1} G \to 1, \tag{5.197}$$

and is chosen to trivialize ρ. We denote the pull backs of ρ and ν to L' by ρ' and ν', respectively. By the definition of this extension, ρ' can be written as: $\rho' = \delta\beta'$, for some $\beta' \in C^2(L', \mathbb{Z}_2)$. Using ν' and β', we then construct a cocycle:

$$\nu' + \frac{1}{2}\beta' \cup \beta' + \frac{1}{2}\beta' \cup_1 \delta\beta'. \tag{5.198}$$

The second extension is defined to trivialize the cocycle in Eq. (5.198) and corresponds to the short exact sequence:

$$1 \to K_2 \to L \xrightarrow{\pi_2} L' \to 1. \tag{5.199}$$

Consequently, there exists $\eta \in C^3(L, \mathbb{R}/\mathbb{Z})$ such that:

$$\delta\eta = \nu^* + \frac{1}{2}\beta \cup \beta + \frac{1}{2}\beta \cup_1 \delta\beta, \tag{5.200}$$

where ν^* and β are the pull backs of ν' and β' by π_2. The extensions in Eqs. (5.197) and (5.199) are guaranteed to exist by the arguments presented in Ref. [177]. Since the composition of two central extensions is itself a central extension, there exists an extension:

$$1 \to K \to L \xrightarrow{\pi} G \to 1, \tag{5.201}$$

which trivializes the supercohomology data (ρ, ν) such that the pull back (ρ^*, ν^*) is:

$$(\rho^*, \nu^*) = (\delta\beta, \delta\eta + \frac{1}{2}\beta \cup \beta + \frac{1}{2}\beta \cup_1 \delta\beta), \tag{5.202}$$

for $\beta \in C^2(L, \mathbb{Z}_2)$ and $\eta \in C^3(L, \mathbb{R}/\mathbb{Z})$. In Appendix M of Ref. [76], an example is given of the trivialization of supercohomology data by extending a $G = \mathbb{Z}_2 \times \mathbb{Z}_4$ symmetry. We also note that the two consecutive extensions above were used in Ref. [169] to construct gapped boundaries for supercohomology models using a spacetime formalism.

We now use an extension L of G, given in Eq. (5.201), and the data (β, η), satisfying Eq. (5.202), to define supercohomology models with a topologically ordered gapped boundary. To this end, we first build a gapped Hamiltonian H_f^L with an L symmetry and bulk terms that are equivalent to those of a supercohomology model with a G symmetry. The K subgroup of the L symmetry can then be gauged to obtain a G symmetric supercohomology model hosting a K gauge theory at the boundary.

The Hilbert space for the L symmetric Hamiltonian H_f^L can be constructed from the Hilbert space of the bulk supercohomology models. We recall that the supercohomology models on a manifold without boundary are defined on a Hilbert space with a G d.o.f. at each vertex and a single complex fermion on each tetrahedron, as in Fig. 5.4. For H_f^L on a manifold M with boundary ∂M, we replace the G d.o.f. on the boundary with L d.o.f.

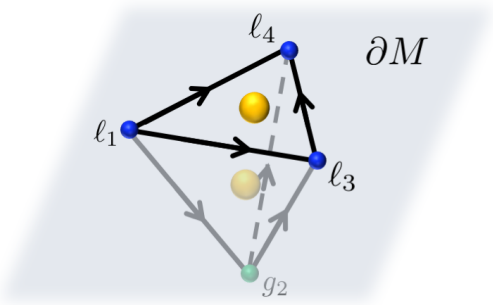

Figure 5.21: The Hamiltonian H_f^L acts on a Hilbert space with an L d.o.f. (blue) on each boundary vertex and a spinless complex fermion (yellow) on every face of ∂M. The d.o.f. in the bulk, a G-valued spin (green) at every vertex and a spinless complex fermion on each tetrahedron, are the same as the d.o.f. in Fig. 5.4.

and introduce a single spinless complex fermion on each face in ∂M (see Fig. 5.21). To define the hopping operators on this Hilbert space, we imagine extending the manifold to $\overline{M}$ by connecting all of the boundary vertices to an additional "artificial" vertex. Each fermionic d.o.f. on a boundary face can then be associated to a tetrahedron connected to the artificial vertex, and every boundary edge e_∂ can be assigned a face $f(e_\partial)$ containing the artificial vertex, as pictured in Fig. 5.22. The trick of adding a vertex allows one to unambiguously determine the spin structure dependent sign in the definition of the hopping operator, discussed in Appendix 5.E. We use S_{e_∂} to denote the hopping operator $S_{f(e_\partial)}$ between ferminionic d.o.f. at boundary faces:

$$S_{e_\partial} \equiv S_{f(e_\partial)}. \tag{5.203}$$

Similar to Eq. (5.183), the L symmetry is represented by:

$$V(\ell) = \sum_{\{\ell_w, g_v\}} |\{\ell\ell_w, \pi(\ell)g_v\}\rangle\langle\{\ell_w, g_v\}|, \tag{5.204}$$

tensored with the identity on the fermionic d.o.f..

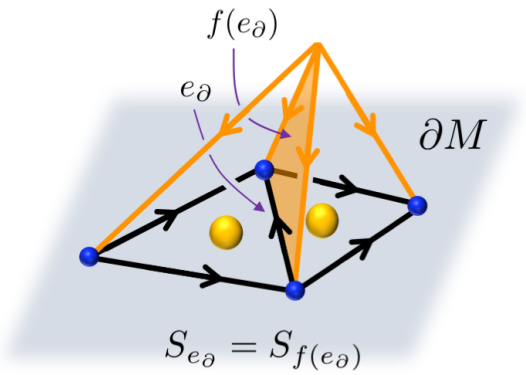

Figure 5.22: The hopping operator S_{e_∂} on the boundary is defined by connecting the vertices in the boundary to an artificial vertex. The edges connecting to the artificial vertex are shown in orange and are oriented away from the additional point. The boundary edge e_∂ is associated to the artificial face $f(e_\partial)$ (shaded orange). For clarity the bulk d.o.f. are not pictured.

The Hamiltonian H_f^L is formed from a trivial Hamiltonian - with a product state ground state - by conjugation with a FDQC. The trivial Hamiltonian H_{AI}^L is an atomic insulator with a decoupled L-paramagnet, defined as:

$$H_{\text{AI}}^L \equiv -\sum_{v\notin\partial M} \mathcal{P}_v^G - \sum_{w\in\partial M} \mathcal{P}_w^L - \sum_{f_\partial\in\partial M} P_{f_\partial} - \sum_{t\in M} P_t. \tag{5.205}$$

Here, $\mathcal{P}_v^G$ and $\mathcal{P}_w^L$ are projectors onto the symmetric state at the bulk vertex v and boundary vertex w, respectively, and P_{f_∂} is the fermion parity operator at a face f_∂ in ∂M.

We prepare H_f^L from H_{AI}^L by conjugation with the FDQC $\mathcal{U}_f^L$:

$$\begin{aligned}\mathcal{U}_f^L \equiv &\prod_{f_\partial} e^{-2\pi i O_{f_\partial}\hat{\bar{\boldsymbol{\eta}}}(f_\partial)}\chi_\beta(\partial M)\prod_{e_\partial} S_{e_\partial}^{\hat{\bar{\boldsymbol{\beta}}}(e_\partial)}\prod_{f_\partial} P_{f_\partial}^{\int_{\partial M}\boldsymbol{f_\partial}\cup_1\hat{\bar{\boldsymbol{\beta}}}}\\ &\times\prod_t e^{2\pi i O_t\hat{\bar{\boldsymbol{\nu}}}(t)}\xi_{\bar{\rho}}(M)\prod_f S_f^{\hat{\bar{\boldsymbol{\rho}}}(f)}\prod_t P_t^{\int_M\hat{\bar{\boldsymbol{\rho}}}\cup_2\boldsymbol{t}}.\end{aligned} \tag{5.206}$$

The first line of Eq. (5.206) is a FDQC supported on the boundary sites, while the second line is the FDQC that prepares the bulk supercohomology model (composed with the projector

π on the boundary vertices). The $\hat{\overline{\boldsymbol{\eta}}}$ term in Eq. (5.206) is the analog of the $\hat{\overline{\boldsymbol{\eta}}}$ term in Eq. (5.193) for the group cohomology models. In the configuration basis, $\chi_\beta(\partial M)$ is a sign that depends on an ordering of the faces in ∂M and makes up for the order dependence of the product of S_{e_∂} hopping operators; the explicit form of $\chi_\beta(\partial M)$ is given in Eq, L41 in Appendix L of Ref. [76]. Furthermore, $\hat{\overline{\boldsymbol{\beta}}}(e_\partial)$ is the diagonal operator:

$$\hat{\overline{\boldsymbol{\beta}}}(\langle 12\rangle) \equiv \sum_{\{\ell_w, g_v\}} \beta(1,\ell_1,\ell_2)|\{\ell_w, g_v\}\rangle\langle\{\ell_w, g_v\}|, \tag{5.207}$$

defined for an arbitrary edge e_∂ in the boundary of M. With this, H_f^L is the Hamiltonian:

$$H_f^L \equiv \mathcal{U}_f^L H_{\mathrm{AI}}^L \mathcal{U}_f^{L\dagger}. \tag{5.208}$$

The derivation of the model above largely follows the construction of the bulk models, in that, we first build a model for a 2-group SPT phase, then subsequently gauge the 1-form symmetry and apply the fermionization duality. However, special care is needed at the boundary, and the full detail can be found in in Appendix L of Ref. [76]. As a consistency check, notice that when ρ and β are zero, the FDQC $\mathcal{U}_f^L$ reduces to the FDQC $\mathcal{U}_b^L$ for the group cohomology case in Section 5.5.1. We also note that H_f^L agrees with the G-symmetric bulk supercohomology model on the interior of M. This is because, away from the boundary of M, the action of $\mathcal{U}_f^L$ is equivalent to that of the bulk circuit $\mathcal{U}_f$.

H_f^L has a global L symmetry, so to recover a supercohomology model with a G symmetry, one can gauge the K subgroup of L. Due to the peculiar L symmetry in Eq. (5.204), the K gauge fields live only on the boundary of M. Therefore, after gauging the K symmetry, we obtain a G-symmetric supercohomology model with a gapped boundary, hosting a K gauge theory.

5.6 Discussion

We have constructed exactly solvable lattice Hamiltonians for supercohomology fermionic SPT (fSPT) phases in $(3+1)$D. Moreover, we have identified finite-depth quantum circuits (FDQCs) that prepare the SPT ground states from symmetric product states. The Hamiltonians are of the simple form:

$$H_f = \mathcal{U}_f H^G_{\mathrm{AI}} \mathcal{U}_f^\dagger, \tag{5.209}$$

where $\mathcal{U}_f$ is the FDQC that prepares the ground state and H^G_{AI} has a unique unentangled symmetric ground state. With our models, we are able to explicitly compute the supercohomology invariants by gauging the fermion parity symmetry and calculating the symmetry fractionalization on the flux loops. We also generalized the gapped boundary construction for group cohomology models in Ref. [165] to construct gapped boundaries for the supercohomology models through a symmetry extension.

Our construction is based on the correspondence between certain bosonic 2-group SPT phases and the supercohomology fSPT phases, first recognized in Refs. [124] and [173]. By gauging the $\mathbb{Z}_2$ 1-form symmetry of the 2-group SPT phase, we obtain the shadow model – a $\mathbb{Z}_2$ gauge theory with an emergent fermion. The emergent fermion can be interpreted as the gauge charge of an fSPT phase after gauging fermion parity. The supercohomology model results from condensing the emergent fermion, or equivalently, applying the fermionization duality of Ref. [166].

We would like to point out that by adding a disordered or quasi-periodic onsite potential to the Hamiltonian in Eq. (5.209), the abelian supercohomology models can in principle exhibit many-body localization, or at least a long-lived pre-thermal regime [140–144,151,179]. This is because each eigenstate of the disordered H_f is short-range entangled and can be viewed as a representative ground state of the supercohomology SPT phase.

We also comment further on the relation between our models and the Lagrangian formu-

lation of Ref. [168]. In Ref. [168], it was shown that the shadow theory can be thought of as a G-symmetry-enriched $\mathbb{Z}_2$ gauge theory with a Steenrod square topological term in the action, which transmutes the statistics of the point-like gauge charge. In our case, we built the 2-group SPT model from a 2-group cocycle $\alpha = \nu + \frac{1}{2}\rho \cup_1 \epsilon + \frac{1}{2}\epsilon \cup \epsilon$, described in Section 5.4.2 and Appendix K of Ref. [76]. The cocycle α is cohomologous to $\alpha' \equiv \nu + \frac{1}{2}\epsilon \cup_1 \rho + \frac{1}{2}\epsilon \cup \epsilon$, which can be expressed in terms of the Steenrod square Sq^2 as $\alpha' = \nu + \frac{1}{2}Sq^2\epsilon$. α' is in the same form as the action in Ref. [168], and accordingly, our shadow model Hamiltonians can be understood as the Hamiltonian formulation of the Lagrangians in Ref. [168], for a unitary $G_f = G \times \mathbb{Z}_2^f$.

There are many interesting potential generalizations of our models and avenues for future work. We briefly comment on them below.

Supercohomology models in higher dimensions: We conjecture that supercohomology models in $(n+1)$D can be constructed using a similar approach. In general, the supercohomology data (ρ, ν) belongs to $Z^n(G, \mathbb{Z}_2) \times C^{n+1}(G, \mathbb{R}/\mathbb{Z})$ and satisfies the constraints:

$$\delta\rho = 0, \quad \delta\nu = \frac{1}{2}\rho \cup_{n-2} \rho. \tag{5.210}$$

Using ρ and ν one can first build an auxiliary bosonic SPT model with an $(n-1)$-group symmetry with the $(n-1)$-group cocycle:

$$\alpha = \nu + \frac{1}{2}\rho \cup_{n-2} \epsilon_{n-1} + \frac{1}{2}\epsilon_{n-1} \cup_{n-3} \epsilon_{n-1}. \tag{5.211}$$

Here, ϵ_{n-1} can be pulled back to M to give a cochain $\boldsymbol{\epsilon}_{n-1} \in C^{n-1}(M, \mathbb{Z}_2)$ satisfying $\delta\boldsymbol{\epsilon}_{n-1} = \boldsymbol{\rho}$.[23] In principle, one can gauge an $(n-2)$-form $\mathbb{Z}_2$ subgroup to build the shadow model and then apply the fermionization duality of Ref. [172] to construct the fSPT model. We therefore, see no obstruction to finding symmetric FDQCs that prepare the ground states

[23] For simplicity, we have suppressed the configuration dependence in the subscript used in Section 5.4.1.

from a symmetric product state, unlike the beyond cohomology model in Ref. [83] and the beyond supercohomology model in Appendix G of Ref. [167].

Time-reversal and nontrivial extensions by fermion parity: Our supercohomology models are protected by unitary symmetries of the form $G_f = G \times \mathbb{Z}_2^f$. An important generalization is to symmetries which may include anti-unitary symmetries, such as time-reversal, and for which G_f is a nontrivial central extension of G by fermion parity. These cases are outside of the supercohomology framework, however, we expect some of our results to apply more broadly.

To include time-reversal symmetries, we can modify ν as in Refs. [49] and [126] so that the homogeneity of ν is replaced with:

$$(-1)^{s(h)}\nu(g_0, g_1, g_2, g_3, g_4) = \nu(hg_0, hg_1, hg_2, hg_3, hg_4), \tag{5.212}$$

where $s(h) \in \{0, 1\}$ is 1 if h includes time-reversal. We expect that, with this modification, the FDQC $\mathcal{U}_f$ will prepare the ground state of the corresponding fSPT model – the symmetry fractionalization on fermion parity flux loops can be generalized to anti-unitary symmetries as described in Appendix B of Ref. [163]. However, the equivalence relation in Eq. (5.166) relies on the assumption that G is unitary. In fact, the models with time-reversal can be "trivialized" by accounting for the beyond supercohomology data as described in Refs. [129] and [178].

More generally, G_f can take the form $G_f = G \times_\psi \mathbb{Z}_2^f$, where G_f is a nontrivial central extension of G by $\mathbb{Z}_2^f$, specified by a 2-cocycle $\psi \in H^2(G, \mathbb{Z}_2)$. Each element of G_f can be written as $g\Pi^m$, with $g \in G$, $m \in \mathbb{Z}_2$ and Π denoting global fermion parity. The group laws in G_f are defined by:

$$(g\Pi^m)\,(h\Pi^n) = (gh)\Pi^{m+n+\psi(1,g,gh)}. \tag{5.213}$$

The supercohomology data (ρ, ν) is modified to satisfy [129]:

$$\delta\rho = 0, \quad \delta\nu = \frac{1}{2}\rho \cup_1 \rho + \frac{1}{2}\psi \cup \rho. \tag{5.214}$$

We can define a model for the fSPT protected by $G_f = G \times_\psi \mathbb{Z}_2^f$ corresponding to (ρ, ν) in Eq. (5.214). To do so, we first describe the representation of the symmetry on a Hilbert space with G d.o.f. on vertices and a spinless complex fermion on each tetrahedron. For any $g\Pi^m$ in G_f, the G_f symmetry acts as:

$$\mathbb{V}(g\Pi^m) \equiv \prod_v \mathbb{V}_v(g\Pi^m), \tag{5.215}$$

with the product over vertices and $\mathbb{V}_v(g\Pi^m)$ the symmetry action associated to v. Here, $\mathbb{V}_v(g\Pi^m)$ is defined as:

$$\mathbb{V}_v(g\Pi^m) \equiv V_v(g) \prod_{t=\langle 1234\rangle | v=\langle 1\rangle} P_t^m, \tag{5.216}$$

where $V_v(g)$ is the regular representation of g at v, and we have associated the fermionic d.o.f. at the tetrahedra $t = \langle 1234\rangle$ to the vertex $\langle 1\rangle$.

It can be checked that $\mathcal{U}_f$ built with the modified (ρ, ν) is symmetric under the representation of G_f in Eq. (5.215), so we can define a Hamiltonian H_f as in Eq. (5.209). Furthermore, it can be shown that the symmetry fractionalizes on the fermion parity flux loops according to ρ as in Section 5.4.3. Finally, using a similar argument as in Ref. [167], it can be verified that the symmetry fractionalization on the fermion parity gauge charges is determined by ψ, in accordance with Ref. [134]. However, in this case, more work is needed to understand both the equivalence relations and the corresponding auxiliary bosonic SPT phases.

Beyond supercohomology models: We showed in Section 5.2.3 that the ground states of the supercohomology models have $(0+1)$D junctions of symmetry domain walls decorated by complex fermions. The domain wall decoration picture can be extended to the beyond

supercohomology phases, where the fixed point wave functions feature $(1+1)$D and $(2+1)$D junctions of symmetry domains decorated by Majorana wires and $p+ip$ superconductors, respectively [129]. Although exactly-solvable models for beyond supercohomology phases have been constructed in Refs. [124, 133, 152, 173, 180–184], it would be interesting to search for models of the form in Eq. (5.209) – related to a trivial SPT Hamiltonian by conjugation with a locality preserving unitary. Such a construction might have implications for the classification of fermionic quantum cellular automata, analogous to the beyond group cohomology models in Ref. [83]. It would also be interesting to study the boundaries of the beyond supercohomology models in $(3+1)$D using exactly-solvable models, similar to Ref. [185].

Appendices

5.A Terminology from cohomology

Here, we compile the cohomology notation used in this chapter. This includes the group cohomology notation used to define the supercohomology data as well as the simplicial cohomology notation employed to describe the construction of the supercohomology models. For both, we define group cochains, the coboundary operator, and cup products.

5.A.1 Group cohomology

For our purposes, a p-cochain is a homogeneous function from G^{p+1} to A, where G is a finite group and A is either $\mathbb{Z}_2 = \{0, 1\}$ or $\mathbb{R}/\mathbb{Z} = [0, 1)$. By a homogeneous function, we mean that the p-cochain c satisfies:

$$c(g_0, \ldots, g_p) = c(hg_0, \ldots, hg_p), \quad \forall h \in G. \tag{5.217}$$

The collection of p-cochains is denoted as $C^p(G, A)$.

The coboundary operator δ maps a p-cochain to a $(p+1)$-cochain. Explicitly, the cobound-

ary operator maps c to the $(p+1)$-cochain δc, defined as:

$$\delta c(g_0, \ldots, g_{p+1}) \equiv \sum_{i=0}^{p+1} (-1)^i c(g_0, \ldots, \widehat{g_i}, \ldots, g_{p+1}), \tag{5.218}$$

where $\widehat{g_i}$ indicates that g_i has been omitted. When $A = \mathbb{Z}_2$, the sign in Eq. (5.218) can be ignored. A p-cochain c satisfying $\delta c = 0$ is called a p-cocycle, and we use $Z^p(G, A)$ to denote the set of p-cocycles.

We can impose an equivalence relation on $Z^p(G, A)$ to define the p^{th} group cohomology. We call the p-cocycles c and c' equivalent if there exists a $(p-1)$-cochain $d \in C^{p-1}(G, A)$ such that:

$$c' = c + \delta d. \tag{5.219}$$

The set of equivalence classes under the equivalence relation above defines the p^{th} group cohomology, denoted $H^p(G, A)$.

Throughout our calculations, we assume that the cocycles are normalized. That is, the p-cocycle c satisfies:

$$c(1, 1, g_2, \ldots, g_p) = 0, \quad \forall g_i,\ i \in \{2, \ldots, p\}, \tag{5.220}$$

where 1 is the identity in G. This assumption is justified by the fact that every group cohomology equivalence class has a normalized representative.

Lastly, for $A = \mathbb{Z}_2$, we define the cup-n products $\cup_n$ with $n \in \{0, 1, 2\}$. The cup-n product maps a p-cochain c and a q-cochain d to a $(p+q-n)$-cochain $c \cup_n d$. We note that the cup-0 product is referred to as simply the cup product and is denoted by $\cup$. The cup product of the homogeneous group cochains $c \in C^p(G, \mathbb{Z}_2)$ and $d \in C^q(G, \mathbb{Z}_2)$ is the $(p+q)$-cochain given by:

$$c \cup d(g_0, \ldots, g_{p+q}) \equiv c(g_0, \ldots, g_p) d(g_p, \ldots, g_{p+q}). \tag{5.221}$$

The cup-1 product of a p-cochain c and a q-cochain d is the $(p+q-1)$-cochain defined by:

$$c \cup_1 d(g_0, \ldots, g_{p+q}) = \sum_{i=0}^{p-1} c(g_0, \ldots, g_i, g_{q+i}, \ldots, g_{p+q-1}) d(g_i, \ldots, g_{q+i}). \tag{5.222}$$

We refer to Ref. [172] for the general formula for the cup-2 product. In the main text, we only ever use the cup-2 product between two group 3-cochains. Hence, we give the explicit cup-2 product of c and d with $c, d \in C^3(G, \mathbb{Z}_2)$:

$$\begin{aligned} c \cup_2 d(g_1, g_2, g_3, g_4, g_5) \equiv\ & c(g_1, g_2, g_3, g_4) d(g_1, g_2, g_4, g_5) + c(g_1, g_3, g_4, g_5) d(g_1, g_2, g_3, g_5) \\ & + c(g_1, g_2, g_3, g_4) d(g_2, g_3, g_4, g_5) + c(g_1, g_2, g_4, g_5) d(g_2, g_3, g_4, g_5). \end{aligned} \tag{5.223}$$

5.A.2 Simplicial cohomology

Simplicial cohomology on M with coefficients in $\mathbb{Z}_2$ was introduced in Section 5.3.1 in the context of the 1-form SPT model. Here, we summarize the terminology from Section 5.3.1 and give the cup product relations that are used in the appendices.

Given a triangulation of a manifold M, we denote the vertices, edges, faces, and tetrahedra by v, e, f, and t, respectively. We often denote a p-simplex by its $p+1$ vertices, i.e., $\langle 0, \ldots, p \rangle$. (Elsewhere in the chapter, we omit the commas between vertices for simplicity.) We define a p-chain as a formal sum (mod 2) of p-simplices in the manifold M.

A p-cochain on M is a linear, $\mathbb{Z}_2$-valued function of p-chains. The set of p-cochains on M is denoted by $C^p(M, \mathbb{Z}_2)$. We use a bold font for cochains on M, e.g., $\boldsymbol{c} \in C^p(M, \mathbb{Z}_2)$.

A cochain labeled by a p-simplex is a p-cochain that evaluates to 1 on the corresponding p-simplex and 0 otherwise. For example, $\boldsymbol{v}$ denotes the 0-cochain dual to the vertex v, i.e.:

$$\boldsymbol{v}(v') = \begin{cases} 1 & v' = v \\ 0 & \text{otherwise.} \end{cases} \tag{5.224}$$

Likewise, for an edge e, we have:

$$\boldsymbol{e}(e') = \begin{cases} 1 & e' = e \\ 0 & \text{otherwise,} \end{cases} \tag{5.225}$$

and for a face f:

$$\boldsymbol{f}(f') = \begin{cases} 1 & f' = f \\ 0 & \text{otherwise.} \end{cases} \tag{5.226}$$

The coboundary operator δ is a linear map from p-cochains to $(p+1)$-cochains:

$$\delta : C^p(M, \mathbb{Z}_2) \to C^{p+1}(M, \mathbb{Z}_2). \tag{5.227}$$

The coboundary of a p-cochain $\boldsymbol{c}$ is defined as the $(p+1)$-cochain $\delta\boldsymbol{c}$ such that:

$$\delta\boldsymbol{c}(s) = \boldsymbol{c}(\partial s), \tag{5.228}$$

for an arbitrary $(p+1)$-simplex s and ∂s its boundary. Explicitly, ∂s is an equally weighted sum of the p-simplices in s.

A p-cochain $\boldsymbol{c}$ is called closed, if $\delta\boldsymbol{c} = 0$. We denote the collection of closed p-cochains on M as $Z^p(M, \mathbb{Z}_2)$. We also note that $\delta\delta = 0$, which follows from Eq. (5.228) and the fact that $\partial\partial = 0$. Therefore, $\delta\boldsymbol{d}$ is a closed p-cochain for any $\boldsymbol{d} \in C^{p-1}(M, \mathbb{Z}_2)$.

The cup product $\cup$ maps a p-cochain and a q-cochain to a $(p+q)$-cochain:

$$\cup : C^p(M, \mathbb{Z}_2) \times C^q(M, \mathbb{Z}_2) \to C^{p+q}(M, \mathbb{Z}_2). \tag{5.229}$$

The cup product of $\boldsymbol{c} \in C^p(M, \mathbb{Z}_2)$ and $\boldsymbol{d} \in C^q(M, \mathbb{Z}_2)$ evaluated on a $(p+q)$-simplex

$\langle 0 \dots p+q \rangle$ is:

$$\boldsymbol{c} \cup \boldsymbol{d}(\langle 0 \dots p+q \rangle) = \boldsymbol{c}(\langle 0 \dots p \rangle)\boldsymbol{d}(\langle p \dots p+q \rangle). \tag{5.230}$$

The coboundary operator is a derivation, meaning it satisfies:

$$\delta\left(\boldsymbol{c} \cup \boldsymbol{d}\right) = \delta\boldsymbol{c} \cup \boldsymbol{d} + \boldsymbol{c} \cup \delta\boldsymbol{d}. \tag{5.231}$$

The cup-1 product $\cup_1$ produces a $(p+q-1)$-cochain from a p-cochain and a q-cochain:

$$\cup_1 : C^p(M, \mathbb{Z}_2) \times C^q(M, \mathbb{Z}_2) \to C^{p+q-1}(M, \mathbb{Z}_2). \tag{5.232}$$

For $\boldsymbol{c} \in C^p(M, \mathbb{Z}_2)$ and $\boldsymbol{d} \in C^q(M, \mathbb{Z}_2)$ the cup-1 product $\boldsymbol{c} \cup_1 \boldsymbol{d}$ evaluated on the $(p+q-1)$-simplex $\langle 0, \dots, p+q-1 \rangle$ is:

$$\boldsymbol{c} \cup_1 \boldsymbol{d}(\langle 0, \dots, p+q-1 \rangle) = \sum_{i=0}^{p-1} \boldsymbol{c}(\langle 0, \dots, i, q+i, \dots, p+q-1 \rangle)\boldsymbol{d}(\langle i, \dots, q+i \rangle). \tag{5.233}$$

Furthermore, the cup-1 product satisfies [186]:

$$\delta(\boldsymbol{c} \cup_1 \boldsymbol{d}) = \delta\boldsymbol{c} \cup_1 \boldsymbol{d} + \boldsymbol{c} \cup_1 \delta\boldsymbol{d} + \boldsymbol{c} \cup \boldsymbol{d} + \boldsymbol{d} \cup \boldsymbol{c}. \tag{5.234}$$

Finally, we introduce the cup-2 product

$$\cup_2 : C^p(M, \mathbb{Z}_2) \times C^q(M, \mathbb{Z}_2) \to C^{p+q-2}(M, \mathbb{Z}_2). \tag{5.235}$$

The general formula for the cup-2 product is given in Ref. [172]. We provide the explicit formula for the cup-2 product of a 3-cochains $\boldsymbol{c} \in C^3(M, \mathbb{Z}_2)$ and a 4-cochain $\boldsymbol{d} \in C^4(M, \mathbb{Z}_2)$:

$$\boldsymbol{c} \cup_2 d(\langle 1234\rangle) \equiv \boldsymbol{c}(\langle 123\rangle)\boldsymbol{d}(\langle 1234\rangle) + \boldsymbol{c}(\langle 134\rangle)\boldsymbol{d}(\langle 1234\rangle), \tag{5.236}$$

for an arbitrary tetrahedron $\langle 1234\rangle$. The cup-2 product satisfies:

$$\delta(\boldsymbol{c} \cup_2 \boldsymbol{d}) = \delta\boldsymbol{c} \cup_2 \boldsymbol{d} + \boldsymbol{c} \cup_2 \delta\boldsymbol{d} + \boldsymbol{c} \cup_1 \boldsymbol{d} + \boldsymbol{d} \cup_1 \boldsymbol{c}. \tag{5.237}$$

To simplify the expressions in the chapter, we also introduce the notation $\int_N \boldsymbol{c}$ as shorthand for the sum:

$$\int_N \boldsymbol{c} = \sum_s \boldsymbol{c}(s). \tag{5.238}$$

Here, N is a p-dimensional manifold, $\boldsymbol{c}$ is a p-cochain, and the sum is over all p-simplices in N. If unspecified, it should be assumed that the integral is over the manifold M.

5.B Explicit 1-form SPT Hamiltonian

In this appendix, we derive the 1-form SPT Hamiltonian H_1 in Eq. (5.60), i.e.:

$$H_1 = -\sum_e \left(X_e \prod_f W_f^{\int \delta \boldsymbol{e} \cup_1 \boldsymbol{f}} \right), \tag{5.239}$$

and demonstrate that it is indeed symmetric under the 1-form symmetry in Eq. (5.30). We begin with H_1 defined in Eq. (5.34) as:

$$H_1 = -\sum_e \mathcal{U}_1 X_e \mathcal{U}_1^\dagger, \tag{5.240}$$

with $\mathcal{U}_1$ given by:

$$\mathcal{U}_1 = \sum_{\boldsymbol{a}_e} \prod_t (-1)^{\boldsymbol{a}_e \cup \delta \boldsymbol{a}_e(t)} |\boldsymbol{a}_e\rangle\langle \boldsymbol{a}_e|. \tag{5.241}$$

To compute $\mathcal{U}_1 X_e \mathcal{U}_1^\dagger$ in Eq. (5.240) explicitly, we first evaluate $\mathcal{U}_1 X_e$. We find:

$$\begin{aligned} \mathcal{U}_1 X_e &= \sum_{\boldsymbol{a}_e} \prod_t (-1)^{\boldsymbol{a}_e \cup \delta \boldsymbol{a}_e(t)} |\boldsymbol{a}_e\rangle\langle \boldsymbol{a}_e| \sum_{\boldsymbol{a}'_e} |\boldsymbol{a}'_e + \boldsymbol{e}\rangle\langle \boldsymbol{a}'_e| \\ &= \sum_{\boldsymbol{a}_e} \prod_t (-1)^{(\boldsymbol{a}_e+\boldsymbol{e}) \cup \delta(\boldsymbol{a}_e+\boldsymbol{e})(t)} |\boldsymbol{a}_e + \boldsymbol{e}\rangle\langle \boldsymbol{a}_e| \\ &= X_e \sum_{\boldsymbol{a}_e} \prod_t (-1)^{(\boldsymbol{a}_e+\boldsymbol{e}) \cup \delta(\boldsymbol{a}_e+\boldsymbol{e})(t)} |\boldsymbol{a}_e\rangle\langle \boldsymbol{a}_e| \end{aligned} \tag{5.242}$$

Expanding the cup product in the last line of Eq. (5.242), we obtain:

$$\mathcal{U}_1 X_e = X_e \sum_{\boldsymbol{a}_e} \prod_t (-1)^{(\boldsymbol{e} \cup \delta \boldsymbol{a}_e + \boldsymbol{a}_e \cup \delta \boldsymbol{e} + \boldsymbol{e} \cup \delta \boldsymbol{e})(t)} |\boldsymbol{a}_e\rangle\langle \boldsymbol{a}_e| \mathcal{U}_1 \tag{5.243}$$

$\boldsymbol{e} \cup \delta \boldsymbol{e}(t)$, in the expression above [Eq. (5.243)], is zero for all tetrahedra t. This can be seen by evaluating $\boldsymbol{e} \cup \delta \boldsymbol{e}$ on an arbitrary tetrahedron $\langle 1234 \rangle$:

$$\boldsymbol{e} \cup \delta \boldsymbol{e}(\langle 1234 \rangle) = \boldsymbol{e}(\langle 12 \rangle) \left[\boldsymbol{e}(\langle 23 \rangle) + \boldsymbol{e}(\langle 34 \rangle) + \boldsymbol{e}(\langle 24 \rangle) \right]. \tag{5.244}$$

The right hand side is zero if $e \neq \langle 12 \rangle$. However, if $e = \langle 12 \rangle$, then the term in square brackets must be zero. Hence, we see that $\boldsymbol{e} \cup \delta \boldsymbol{e}(t) = 0$. We then have:

$$\mathcal{U}_1 X_e = X_e \sum_{\boldsymbol{a}_e} \prod_t (-1)^{(\boldsymbol{e} \cup \delta \boldsymbol{a}_e + \boldsymbol{a}_e \cup \delta \boldsymbol{e})(t)} |\boldsymbol{a}_e\rangle\langle \boldsymbol{a}_e| \mathcal{U}_1. \tag{5.245}$$

We simplify the right hand side of Eq. (5.245) further by employing the identities in

Eqs. (5.231) and (5.234). An application of Eq. (5.231) gives us:

$$\mathcal{U}_1 X_e = X_e \sum_{\boldsymbol{a}_e} \prod_t (-1)^{(\delta \boldsymbol{e} \cup \boldsymbol{a}_e + \boldsymbol{a}_e \cup \delta \boldsymbol{e})(t)} |\boldsymbol{a}_e\rangle\langle \boldsymbol{a}_e| \mathcal{U}_1, \tag{5.246}$$

where we have also used that M is closed. Then, using Eq. (5.234), we see:

$$\mathcal{U}_1 X_e = X_e \sum_{\boldsymbol{a}_e} \prod_t (-1)^{\delta \boldsymbol{a}_e \cup_1 \delta \boldsymbol{e}(t)} |\boldsymbol{a}_e\rangle\langle \boldsymbol{a}_e| \mathcal{U}_1, \tag{5.247}$$

where again we have used that M is closed.

We can express the term:

$$\sum_{\boldsymbol{a}_e} \prod_t (-1)^{\delta \boldsymbol{a}_e \cup_1 \delta \boldsymbol{e}(t)} |\boldsymbol{a}_e\rangle\langle \boldsymbol{a}_e| \tag{5.248}$$

in Eq. (5.247) using Pauli Z operators. To do so, we notice that, for any face $f = \langle 123 \rangle$:

$$\sum_{\boldsymbol{a}_e} (-1)^{\delta \boldsymbol{a}_e(f)} |\boldsymbol{a}_e\rangle\langle \boldsymbol{a}_e| = \sum_{\boldsymbol{a}_e} (-1)^{a_{12}+a_{23}+a_{13}} |\boldsymbol{a}_e\rangle\langle \boldsymbol{a}_e| = W_f, \tag{5.249}$$

where in the last equality we have defined:

$$W_f \equiv \prod_{e \subset f} Z_e. \tag{5.250}$$

Therefore, Eq. (5.248) can be written as:

$$\sum_{\boldsymbol{a}_e} \prod_t (-1)^{\delta \boldsymbol{a}_e \cup_1 \delta \boldsymbol{e}(t)} |\boldsymbol{a}_e\rangle\langle \boldsymbol{a}_e| = \prod_t \prod_f W_f^{\boldsymbol{f} \cup_1 \delta \boldsymbol{e}(t)}, \tag{5.251}$$

with $\prod_f$ a product over all faces in M. Exchanging the product over tetrahedra for a sum,

we see that:

$$\sum_{\boldsymbol{a}_e} \prod_t (-1)^{\delta \boldsymbol{a}_e \cup_1 \delta \boldsymbol{e}(t)} |\boldsymbol{a}_e\rangle\langle \boldsymbol{a}_e| = \prod_f W_f^{\int \boldsymbol{f} \cup_1 \delta \boldsymbol{e}}. \tag{5.252}$$

Then, plugging Eq. (5.252) into Eq. (5.247), we arrive at:

$$\mathcal{U}_1 X_e = X_e \prod_f W_f^{\int \boldsymbol{f} \cup_1 \delta \boldsymbol{e}} \mathcal{U}_1. \tag{5.253}$$

Finally, we can compute $\mathcal{U}_1 X_e \mathcal{U}_1{}^\dagger$. From Eq. (5.253), we have:

$$\mathcal{U}_1 X_e \mathcal{U}_1{}^\dagger = \left(X_e \prod_f W_f^{\int \boldsymbol{f} \cup_1 \delta \boldsymbol{e}} \mathcal{U}_1 \right) \mathcal{U}_1{}^\dagger = X_e \prod_f W_f^{\int \boldsymbol{f} \cup_1 \delta \boldsymbol{e}}. \tag{5.254}$$

The 1-form SPT Hamiltonian is then:

$$H_1 = -\sum_e \left(X_e \prod_f W_f^{\int \boldsymbol{f} \cup_1 \delta \boldsymbol{e}} \right), \tag{5.255}$$

as claimed.

Next, we show that H_1 is symmetric under the $\mathbb{Z}_2$ 1-form symmetry. Recall that the symmetry is generated by operators of the form [Eq. (5.30)]:

$$A_\Sigma \equiv \prod_{e \perp \Sigma} X_e, \tag{5.256}$$

for a closed surface Σ of the dual lattice. We prove that H_1 is symmetric by showing that $\mathcal{U}_1$ is symmetric, i.e.:

$$A_\Sigma \mathcal{U}_1 A_\Sigma = \mathcal{U}_1, \tag{5.257}$$

for all choices of Σ.

Conjugation of $\mathcal{U}_1$ by an arbitrary generator of the 1-form symmetry A_Σ gives:

$$A_\Sigma \mathcal{U}_1 A_\Sigma = \sum_{\boldsymbol{a}_e} \prod_t (-1)^{\boldsymbol{a}_e \cup \delta \boldsymbol{a}_e(t)} |\boldsymbol{a}_e + \boldsymbol{\Sigma}\rangle\langle \boldsymbol{a}_e + \boldsymbol{\Sigma}|. \tag{5.258}$$

Redefining the summation, we have:

$$A_\Sigma \mathcal{U}_1 A_\Sigma = \sum_{\boldsymbol{a}_e} \prod_t (-1)^{(\boldsymbol{a}_e + \boldsymbol{\Sigma}) \cup \delta(\boldsymbol{a}_e + \boldsymbol{\Sigma})(t)} |\boldsymbol{a}_e\rangle\langle \boldsymbol{a}_e|. \tag{5.259}$$

Then we expand the exponent and use that $\delta \boldsymbol{\Sigma} = 0$ to obtain:

$$A_\Sigma \mathcal{U}_1 A_\Sigma = \sum_{\boldsymbol{a}_e} \prod_t (-1)^{\boldsymbol{a}_e \cup \delta \boldsymbol{a}_e(t) + \boldsymbol{\Sigma} \cup \delta \boldsymbol{a}_e(t)} |\boldsymbol{a}_e\rangle\langle \boldsymbol{a}_e|. \tag{5.260}$$

Finally, we employ the identity in Eq. (5.231) and use that M is closed to arrive at:

$$A_\Sigma \mathcal{U}_1 A_\Sigma = \sum_{\boldsymbol{a}_e} \prod_t (-1)^{\boldsymbol{a}_e \cup \delta \boldsymbol{a}_e(t) + \delta(\Sigma \cup \boldsymbol{a}_e)(t)} |\boldsymbol{a}_e\rangle\langle \boldsymbol{a}_e| = \sum_{\boldsymbol{a}_e} \prod_t (-1)^{\boldsymbol{a}_e \cup \delta \boldsymbol{a}_e(t)} |\boldsymbol{a}_e\rangle\langle \boldsymbol{a}_e| = \mathcal{U}_1. \tag{5.261}$$

Thus, $\mathcal{U}_1$ is symmetric.

5.C A ground state of the twisted toric code

Here, we give a direct proof that the state $|\Psi_{\text{ttc}}\rangle$, defined in Eq. (5.74) as:

$$|\Psi_{\text{ttc}}\rangle \equiv \sum_{\boldsymbol{a}_e} \prod_t (-1)^{\boldsymbol{a}_e \cup \delta \boldsymbol{a}_e(t)} |\delta \boldsymbol{a}_e\rangle, \tag{5.262}$$

is a ground state of the twisted toric code Hamiltonian:

$$H_{\text{ttc}} = \sum_e \bar{G}_e - \sum_t W_t. \tag{5.263}$$

In particular, we show that $|\Psi_{\text{ttc}}\rangle$ is a $+1$ eigenstate of both W_t and $\bar{G}_e$. This implies that $|\Psi_{\text{ttc}}\rangle$ is a ground state of H_{ttc}, since W_t and $\bar{G}_e$ have eigenvalues ± 1.[24]

Let us compute $W_t|\Psi_{\text{ttc}}\rangle$ and $\bar{G}_e|\Psi_{\text{ttc}}\rangle$ explicitly. For $W_t|\Psi_{\text{ttc}}\rangle$, we have:

$$W_t|\Psi_{\text{ttc}}\rangle = W_t \sum_{\boldsymbol{a}_e} \prod_t (-1)^{\boldsymbol{a}_e \cup \delta \boldsymbol{a}_e(t)} |\delta \boldsymbol{a}_e\rangle = \sum_{\boldsymbol{a}_e} (-1)^{\delta \boldsymbol{a}_e(\partial t)} \prod_t (-1)^{\boldsymbol{a}_e \cup \delta \boldsymbol{a}_e(t)} |\delta \boldsymbol{a}_e\rangle$$
$$= \sum_{\boldsymbol{a}_e} (-1)^{\boldsymbol{a}_e(\partial \partial t)} \prod_t (-1)^{\boldsymbol{a}_e \cup \delta \boldsymbol{a}_e(t)} |\delta \boldsymbol{a}_e\rangle = |\Psi_{\text{ttc}}\rangle. \quad (5.264)$$

While for $\bar{G}_e|\Psi_{\text{ttc}}\rangle$, we find:

$$\bar{G}_e|\Psi_{\text{ttc}}\rangle = \bar{G}_e \sum_{\boldsymbol{a}_e} \prod_t (-1)^{\boldsymbol{a}_e \cup \delta \boldsymbol{a}_e(t)} |\delta \boldsymbol{a}_e\rangle = \sum_{\boldsymbol{a}_e} \prod_t (-1)^{\boldsymbol{a}_e \cup \delta \boldsymbol{a}_e(t) + \delta \boldsymbol{a}_e \cup_1 \delta \boldsymbol{e}(t)} |\delta \boldsymbol{a}_e + \delta \boldsymbol{e}\rangle. \quad (5.265)$$

To evaluate this further, we focus on the sign:

$$\prod_t (-1)^{\boldsymbol{a}_e \cup \delta \boldsymbol{a}_e(t) + \delta \boldsymbol{e} \cup_1 \delta \boldsymbol{a}_e(t)}. \quad (5.266)$$

Using Eqs. (5.234), (5.231) and that M is closed, we can write the sign as:

$$\prod_t (-1)^{(\boldsymbol{a}_e + \boldsymbol{e}) \cup \delta(\boldsymbol{a}_e + \boldsymbol{e})(t)}. \quad (5.267)$$

Now, we plug this sign into the expression for $\bar{G}_e|\Psi_{\text{ttc}}\rangle$ in Eq. (5.265):

$$\bar{G}_e|\Psi_{\text{ttc}}\rangle = \sum_{\boldsymbol{a}_e} \prod_t (-1)^{(\boldsymbol{a}_e + \boldsymbol{e}) \cup \delta(\boldsymbol{a}_e + \boldsymbol{e})(t)} |\delta \boldsymbol{a}_e + \delta \boldsymbol{e}\rangle = \sum_{\boldsymbol{a}_e} \prod_t (-1)^{\boldsymbol{a}_e \cup \delta \boldsymbol{a}_e(t)} |\delta \boldsymbol{a}_e\rangle = |\Psi_{\text{ttc}}\rangle. \quad (5.268)$$

Therefore, $|\Psi_{\text{ttc}}\rangle$ is a $+1$ eigenstate of W_t and $\bar{G}_e$ for all t and e, respectively.

[24] This follows from the observation that W_t and $\bar{G}_e$ square to the identity

5.D *Fermion condensation of the twisted toric code*

Here, we elaborate on the fermion condensation procedure for the twisted toric code:

$$H_{\text{ttc}} = -\sum_e \bar{G}_e - \sum_t W_t. \tag{5.269}$$

We begin by showing that the operators $\bar{G}_e$ are local generators of an anomalous $\mathbb{Z}_2$ 2-form symmetry of the twisted toric code. Then, we apply the prescription for fermion condensation in Section 5.3.3 to the twisted toric code.

Anomalous 2-form symmetry of the twisted toric code

We prove the identity in Eq. (5.83) – for a path p_e intersecting the faces meeting at the edge e:

$$\bar{G}_e = \tilde{\mathcal{S}}_{p_e}, \tag{5.270}$$

where for reference, $\bar{G}_e$ is defined as:

$$\bar{G}_e = \prod_{f \supset e} X_f \prod_f Z_f^{\int \boldsymbol{f} \cup_1 \delta \boldsymbol{e}}. \tag{5.271}$$

Eq. (5.270) says that $\bar{G}_e$ is equal to a small loop of emergent fermion string operator, i.e., it is a local generator of a $\mathbb{Z}_2$ anomalous 2-form symmetry. We prove the equality in Eq. (5.270) as follows. First, by definition, $\tilde{\mathcal{S}}_{p_e}$ is:

$$\tilde{\mathcal{S}}_{p_e} \equiv \overline{\prod_{f \in F_{\perp p_e}} \bar{U}_f} \prod_{f \in F_{\perp p_e}} W_{R(f)}. \tag{5.272}$$

We simplify the W_t term and $\bar{U}_f$ term independently and then show that their product is $\bar{G}_e$.

To simplify the W_t term, we note that the product $\prod_{f \in F_{\perp p_e}} W_{R(f)}$ can be rewritten as:

$$\prod_t W_t^{\boldsymbol{t} \cup_1 \boldsymbol{e}(t) + \boldsymbol{e} \cup_1 \boldsymbol{t}(t)}. \tag{5.273}$$

For $t = \langle 1234 \rangle$, the cochain $\boldsymbol{t} \cup_1 \boldsymbol{e}(t) + \boldsymbol{e} \cup_1 \boldsymbol{t}(t)$ evaluates to:

$$\boldsymbol{e}(\langle 12 \rangle) + \boldsymbol{e}(\langle 23 \rangle) + \boldsymbol{e}(\langle 34 \rangle) + \boldsymbol{e}(\langle 14 \rangle). \tag{5.274}$$

The edges $\langle 12 \rangle$, $\langle 23 \rangle$, $\langle 34 \rangle$, and $\langle 14 \rangle$ above are precisely the edges e of t such that, for the two faces of t meeting at e, the orientation of one is towards the center of t, while the orientation of the other is away from the center of t. Therefore, for exactly one of these faces, we have $R(f) = t$. Using the higher cup product relations in Appendix 5.A.2, we can re-express Eq. (5.273) in terms of a product over faces as:

$$\prod_t W_t^{\boldsymbol{t} \cup_1 \boldsymbol{e}(t) + \boldsymbol{e} \cup_1 \boldsymbol{t}(t)} = \prod_f Z_f^{\int (\boldsymbol{f} \cup_1 \delta \boldsymbol{e} + \delta \boldsymbol{e} \cup_1 \boldsymbol{f})}. \tag{5.275}$$

For the $\bar{U}_f$ term of Eq. (5.272), we have:

$$\overline{\prod_{f \in F_{\perp p_e}}} \bar{U}_f = \prod_f Z_f^{\int \delta \boldsymbol{e} \cup_1 \boldsymbol{f}} \prod_{f \supset e} X_f. \tag{5.276}$$

By commuting the Pauli Z operators to the right of the Pauli X operators, we find:

$$\overline{\prod_{f \in F_{\perp p_e}}} \bar{U}_f = (-1)^{\int \delta \boldsymbol{e} \cup_1 \delta \boldsymbol{e}} \prod_{f \supset e} X_f \prod_f Z_f^{\delta \boldsymbol{e} \cup_1 \boldsymbol{f}(t)}. \tag{5.277}$$

Using the cup product relations in Appendix 5.A.2, it can be shown that $\int \delta \boldsymbol{e} \cup_1 \delta \boldsymbol{e} = 0$. Therefore, the product in Eq. (5.272) is:

$$\tilde{\mathcal{S}}_{p_e} = \prod_{f \supset e} X_f \prod_f Z_f^{\delta \boldsymbol{e} \cup_1 \boldsymbol{f}(t)} \prod_f Z_f^{\int (\boldsymbol{f} \cup_1 \delta \boldsymbol{e} + \delta \boldsymbol{e} \cup_1 \boldsymbol{f})} = \prod_{f \supset e} X_f \prod_f Z_f^{\int \boldsymbol{f} \cup_1 \delta \boldsymbol{e}}. \tag{5.278}$$

This is exactly $\bar{G}_e$ in Eq. (5.270).

Fermion condensation procedure

Following the steps outlined in Section 5.3.3, we first introduce a fermionic d.o.f. at the center of each tetrahedron and impose the gauge constraint:

$$\tilde{U}_f \tilde{S}_f = 1, \tag{5.279}$$

at each face f. As noted in the main text, the product of $\tilde{U}_f \tilde{S}_f$ over faces adjoined to the edge e is precisely $\bar{G}_e$. Therefore, in the constrained space and after a shift of energy, H_{ttc} becomes:

$$H'_{\text{ttc}} = -\sum_t W_t. \tag{5.280}$$

Next, we couple H_{ttc} to the fermionic d.o.f. to make the Hamiltonian gauge invariant. We do so by replacing W_t with $W_t P_t$:

$$H''_{\text{ttc}} \equiv -\sum_t W_t P_t. \tag{5.281}$$

The last step is to fix a gauge in which the eigenvalue of each Z_f is $+1$. Starting with H''_{ttc}, this gives us the atomic insulator Hamiltonian:

$$H_{\text{AI}} = -\sum_t P_t. \tag{5.282}$$

Thus, fermion condensation produces the atomic insulator from the twisted toric code Hamiltonian.

For completeness, let us show here that the gauge constraints in Eq. (5.279) are all mutually commuting. Using the definition $P_{L(f)} \tilde{S}_f = S_f$ and Eq. (5.86), the commutation

relations between $\tilde{S}_f$ and $\tilde{S}_{f'}$ are:

$$\tilde{S}_f \tilde{S}_{f'} = (-1)^{\int (f' \cup_1 f + f \cup_1 f')} (-1)^{\delta \boldsymbol{f}'(L(f)) + \delta \boldsymbol{f}(L(f'))} \tilde{S}_{f'} \tilde{S}_f.$$

The expression $\delta \boldsymbol{f}'(L(f)) + \delta \boldsymbol{f}(L(f'))$ is 1 when both f and f' share a tetrahedron t and the orientation of only one of the faces points towards the center of t. Otherwise, the expression is 0. This is also true of $\delta \boldsymbol{f}'(R(f)) + \delta \boldsymbol{f}(R(f'))$, so we may write:

$$\tilde{S}_f \tilde{S}_{f'} = (-1)^{\int (f' \cup_1 f + f \cup_1 f')} (-1)^{\delta \boldsymbol{f}'(R(f)) + \delta \boldsymbol{f}(R(f'))} \tilde{S}_{f'} \tilde{S}_f.$$

Given the commutation relations between $\bar{U}_f$ and $\bar{U}_{f'}$ in Eq. (5.77), for $\tilde{U}_f$ and $\tilde{U}_{f'}$, we have:

$$\tilde{U}_f \tilde{U}_{f'} = (-1)^{\int (f' \cup_1 f + f \cup_1 f')} (-1)^{\delta \boldsymbol{f}'(R(f)) + \delta \boldsymbol{f}(R(f'))} \tilde{U}_{f'} \tilde{U}_f.$$

Therefore, for all faces f and f':

$$\left(\tilde{U}_f \tilde{S}_f\right) \left(\tilde{U}_{f'} \tilde{S}_{f'}\right) = \left(\tilde{U}_{f'} \tilde{S}_{f'}\right) \left(\tilde{U}_f \tilde{S}_f\right).$$

5.E Bosonization duality in $(3+1)$D and spin structure

In this appendix, we review the operator-level duality between a fermionic theory and a $\mathbb{Z}_2$ lattice gauge theory in three spatial dimensions [166]. The fermion condensation duality in Section 5.3.3 is functionally equivalent to applying the duality described here. We also elaborate on the spin structure dependent sign in the definition of the hopping operator. We note that the boson-fermion duality in $(2+1)$D is described in Ref. [15], and the duality in arbitrary dimensions is worked out in Ref. [172].

The duality is defined for fermionic systems where each tetrahedron t of the triangulated 3-manifold M hosts a single spinless complex fermion with an operator algebra generated by the Majorana operators γ_t, γ_t'. The fermion parity even algebra is generated by the site

fermion parity:

$$P_t = -i\gamma_t\gamma'_t, \tag{5.283}$$

and the fermionic hopping operator:

$$S_f = (-1)^{\boldsymbol{f}(E)} i\gamma_{L(f)}\gamma'_{R(f)}. \tag{5.284}$$

In the definition of S_f, $L(f)$ and $R(f)$ are the tetrahedra on either side of f, with the orientation of f pointing out of $L(f)$ and into $R(f)$ (Fig. 5.5). We discuss the spin structure dependent sign $(-1)^{\boldsymbol{f}(E)}$ of S_f in detail below.

The 2-chain $E \in C_2(M, \mathbb{Z}_2)$ in Eq. (5.284), is a formal sum of faces, corresponding to a choice of spin structure. E is chosen such that the boundary of E is equal to $w_2 \in C_1(M, \mathbb{Z}_2)$, a representative of the Poincaré dual of the second Stiefel-Whitney cohomology class $\boldsymbol{w}_2(TM)$. For a triangulated 3D manifold, a representative w_2 is given by [98, 129, 172, 187]:

$$w_2 = \sum_e [1 + N^+_{13}(e) + N^-_{02}(e)]_{\mathbf{2}} \cdot e, \tag{5.285}$$

where $[\cdots]_{\mathbf{2}}$ denotes that the coefficient of e is taken modulo 2, $N^+_{13}(e)$ is the number of positively oriented tetrahedra $\langle 0123\rangle$ such that $\langle 13\rangle = e$, and $N^-_{02}(e)$ is the number of negatively oriented tetrahedra $\langle 0123\rangle$ such that $\langle 02\rangle = e$.

The set of edges with coefficient 1 in w_2 admits a graphical interpretation, which generalizes the graphical interpretation in Refs. [167] and [188] for a spin structure in 2D. To see this, we use the branching structure of M to define a section of the frame bundle on M - an assignment of a coordinate frame to each point in M. Similar to the 2D case, we first interpolate the branching structure to a vector field on the interior of a tetrahedron of M, as depicted in Fig. 5.23. These vectors form the x-axes of the coordinate frames. The y-axes are then formed by interpolating the orientations of the faces to a vector field on the interior of the tetrahedron. Finally, the z-axes are determined by the orientation of M. The edges

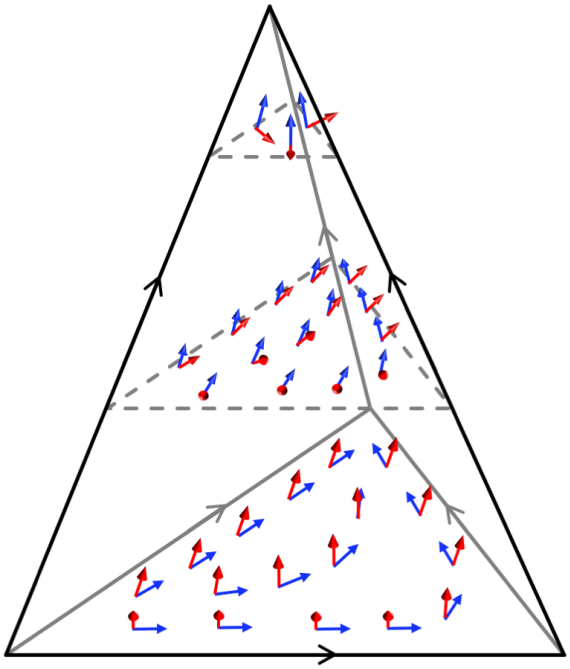

Figure 5.23: A coordinate frame field can be constructed from the branching structure. We show cross sections of the frame field above. The x-axes (blue vectors) are given by an interpolation of the edge orientations into the interior of the tetrahedron. The y-axes (red vectors) are an interpolation of the face orientations into the interior of the tetrahedron. The z-axes (not pictured) are chosen with respect to the orientation of the manifold.

forming w_2 give precisely the singular edges of the frame field, i.e., for any path that encloses an odd number of edges in w_2, the frames along the path rotate by an odd multiple of 2π. Heuristically, a fermion that is moved around a singular edge is rotated by an odd multiple of 2π, and the sign in Eq. (5.284) compensates for the rotation via the spin-statistics of fermions (see Fig. 5.24).

To describe the bosonization duality, it is convenient to define a product of hopping operators corresponding to a 2-cochain. For a 2-cochain $\boldsymbol{\lambda}$, we define S_λ to be:

$$S_\lambda = \prod_{i,i'|i<i'} (-1)^{\boldsymbol{\lambda}(f_i)\boldsymbol{\lambda}(f_{i'}) \int \boldsymbol{f}_i \cup_1 \boldsymbol{f}_{i'}} \prod_f S_f^{\boldsymbol{\lambda}(f)}, \tag{5.286}$$

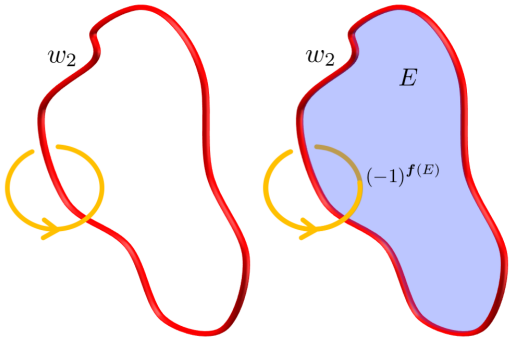

Figure 5.24: The frames along a path (yellow) rotate by an odd multiple of 2π when linked with the 1-chain w_2 (red). The 2-chain E (blue) satisfies $\partial E = w_2$. The hopping operators are modified with the sign $(-1)^{\boldsymbol{f}(E)}$ to account for the twisting of the framed path by an odd multiple of 2π.

where the faces are arbitrarily ordered $\{f_1, f_2, f_3, \cdots\}$ and the product is $\prod_{f\in\{f_1,f_2,\cdots,f_n\}} S_f = S_{f_n}\cdots S_{f_2}S_{f_1}$. The order dependent sign ensures that the definition of S_λ is independent of the choice of ordering. This follows from the commutation relations of the hopping operators:

$$S_f S_{f'} = (-1)^{\int (\boldsymbol{f}\cup_1 \boldsymbol{f}' + \boldsymbol{f}'\cup_1 \boldsymbol{f})} S_f S_{f'}. \tag{5.287}$$

Given a pair of 2-cochains $\boldsymbol{\lambda}$ and $\boldsymbol{\lambda}'$, we have the identity:

$$S_{\lambda+\lambda'} \equiv (-1)^{\int \boldsymbol{\lambda}\cup_1 \boldsymbol{\lambda}'} S_{\lambda'} S_\lambda. \tag{5.288}$$

The two generators P_t and S_f satisfy the following constraint at each edge e [172]:

$$S_{\delta \boldsymbol{e}} \prod_t P_t^{\int \boldsymbol{e}\cup_1 \boldsymbol{t} + \boldsymbol{t}\cup_1 \boldsymbol{e}} = 1 \tag{5.289}$$

The physical meaning of this identity is that moving a fermion along a small loop around a edge e is an identity operator. We note that the spin structure dependent sign in the

definition of the hopping operator guarantees that the product in Eq. (5.289) is 1.

The bosonic dual of this system has $\mathbb{Z}_2$-valued spins on the faces of the triangulation, with an operator algebra generated by X, Z Pauli operators. For every tetrahedron t, we define the flux operator:

$$W_t = \prod_{f \subset t} Z_f, \tag{5.290}$$

and for every face f, we define a bosonic hopping operator:

$$\bar{U}_f = \prod_{f'} Z_{f'}^{\int \boldsymbol{f} \cup_1 \boldsymbol{f}'} X_f. \tag{5.291}$$

Similar to the fermionic hopping operator, we define a product of $\bar{U}_f$ for any 2-cochain $\boldsymbol{\lambda}$. In this case, $\bar{U}_\lambda$ is defined as:

$$\bar{U}_\lambda = \prod_{f'} Z_{f'}^{\int \boldsymbol{\lambda} \cup_1 \boldsymbol{f}'} \prod_f X_f^{\boldsymbol{\lambda}(f)}. \tag{5.292}$$

To define a consistent duality between the even fermionic operator algebra and the algebra generated by W_t and $\bar{U}_f$ operators, we also define $\bar{G}_e$, given by:

$$\bar{G}_e = \prod_{f \supset e} X_f \prod_{f'} Z_{f'}^{\int \boldsymbol{f}' \cup_1 \delta \boldsymbol{e}}. \tag{5.293}$$

The duality in Ref. [15], is an isomorphism of the C^* algebras $\mathcal{F}$ and $\mathcal{B}$, where $\mathcal{F}$ is the algebra of even fermion parity operators and $\mathcal{B}$ is the algebra generated by W_t and $\bar{U}_f$ with the constraint $\bar{G}_e = 1$. The mapping of operators is:

$$W_t \leftrightarrow P_t, \quad \bar{U}_f \leftrightarrow S_f. \tag{5.294}$$

We note the correspondence above is well-defined since the nontrivial relations map to con-

straints on the algebra, i.e.:

$$\begin{aligned} \bar{G}_e \leftrightarrow S_{\delta \boldsymbol{e}} \prod_t P_t^{\int \boldsymbol{e} \cup_1 \boldsymbol{t} + \boldsymbol{t} \cup_1 \boldsymbol{e}} = 1 \\ \prod_t W_t = 1 \leftrightarrow \prod_t P_t. \end{aligned} \tag{5.295}$$

Also, the operators $\bar{U}_\lambda$ and S_λ are defined so that the duality in Eq. (5.294) maps:

$$\bar{U}_\lambda \leftrightarrow S_\lambda, \tag{5.296}$$

for any 2-cochain $\boldsymbol{\lambda}$. This is because the Pauli X and Pauli Z operators in $\bar{U}_\lambda$ can be commuted past one another to obtain (see Appendix 5.G.2):

$$\bar{U}_\lambda = \prod_{i,i'|i<i'} (-1)^{\boldsymbol{\lambda}(f_i)\boldsymbol{\lambda}(f_{i'}) \int \boldsymbol{f}_i \cup_1 \boldsymbol{f}_{i'}} \prod_f \bar{U}_f^{\boldsymbol{\lambda}(f)}. \tag{5.297}$$

5.F *Symmetry of the 2-group SPT Hamiltonian*

We use this Appendix to prove that the 2-group Hamiltonian $H_2 = \mathcal{U}_2 H_0^G \mathcal{U}_2^\dagger$ in Section 5.4.2 is symmetric. Given that H_0^G is invariant under the 2-group symmetry, it suffices to show that $\mathcal{U}_2$ is symmetric. For convenience, we re-write $\mathcal{U}_2$ here as:

$$\mathcal{U}_2 = \sum_{\{g_v\}, \boldsymbol{a}_e} \prod_t e^{2\pi i O_t \overline{\boldsymbol{\alpha}}_{\{g_v\}}(t)} |\{g_v\}, \boldsymbol{a}_e\rangle\langle\{g_v\}, \boldsymbol{a}_e|, \tag{5.298}$$

where the 3-cochain $\overline{\boldsymbol{\alpha}}_{\{g_v\}}$ is:

$$\overline{\boldsymbol{\alpha}}_{\{g_v\}} = \overline{\boldsymbol{\nu}}_{\{g_v\}} + \frac{1}{2}\overline{\boldsymbol{\rho}}_{\{g_v\}} \cup_1 \overline{\boldsymbol{\rho}}_{\{g_v\}} + \frac{1}{2}\overline{\boldsymbol{\rho}}_{\{g_v\}} \cup_1 \delta \boldsymbol{a}_e + \frac{1}{2}\boldsymbol{a}_e \cup \delta \boldsymbol{a}_e. \tag{5.299}$$

We note that we have expressed the W_f term of $\mathcal{U}_2$ in terms of $\delta \boldsymbol{a}_e$.

First of all, the FDQC $\mathcal{U}_2$ is symmetric under the 1-form symmetry in Eq. (5.107). The 1-form symmetry only affects the last two terms of $\overline{\boldsymbol{\alpha}}_{\{g_v\}}$, those with $\boldsymbol{a}_e$. The $\frac{1}{2}\boldsymbol{a}_e \cup \delta \boldsymbol{a}_e$ term

is invariant, as shown in Appendix 5.B. The $\frac{1}{2}\overline{\boldsymbol{\rho}}_{\{g_v\}} \cup_1 \delta \boldsymbol{a}_e$ term is also symmetric, since it can be written in terms of the 1-form symmetric operators W_f, as in Eq. (5.115).

Second, we show that $\mathcal{U}_2$ commutes with the 0-form symmetry operator $V_\rho(h)$, for all $h \in G$:

$$V_\rho(h) = V(h) \prod_e X_e^{\hat{\overline{\boldsymbol{\rho}}}^h(e)}. \tag{5.300}$$

Specifically, we compute:

$$V_\rho(h)\mathcal{U}_2 V_\rho^\dagger(h). \tag{5.301}$$

First, in moving the product of Pauli X operators in Eq. (5.300) past $\mathcal{U}_2$, we find:

$$V_\rho(h)\mathcal{U}_2 V_\rho^\dagger(h) = V(h) \sum_{\{g_v\},\boldsymbol{a}_e} \prod_t e^{2\pi i O_t \overline{\boldsymbol{\alpha}}'_{\{g_v\}}(t)} |\{g_v\}, \boldsymbol{a}_e\rangle\langle\{g_v\}, \boldsymbol{a}_e| V^\dagger(h), \tag{5.302}$$

where $\overline{\boldsymbol{\alpha}}'_{\{g_v\}}$ is:

$$\overline{\boldsymbol{\alpha}}'_{\{g_v\}} = \overline{\boldsymbol{\nu}}_{\{g_v\}} + \frac{1}{2}\overline{\boldsymbol{\rho}}_{\{g_v\}} \cup_1 \overline{\boldsymbol{\rho}}_{\{g_v\}} + \frac{1}{2}\overline{\boldsymbol{\rho}}_{\{g_v\}} \cup_1 \delta(\boldsymbol{a}_e + \overline{\boldsymbol{\rho}}^h_{\{g_v\}}) + \frac{1}{2}(\boldsymbol{a}_e + \overline{\boldsymbol{\rho}}^h_{\{g_v\}}) \cup \delta(\boldsymbol{a}_e + \overline{\boldsymbol{\rho}}^h_{\{g_v\}}).$$

Then, conjugation by $V(h)$ on the right hand side of Eq. (5.302) produces:

$$V_\rho(h)\mathcal{U}_2 V_\rho^\dagger(h) = \sum_{\{g_v\},\boldsymbol{a}_e} \prod_t e^{2\pi i O_t \overline{\boldsymbol{\alpha}}'_{\{h^{-1}g_v\}}(t)} |\{g_v\}, \boldsymbol{a}_e\rangle\langle\{g_v\}, \boldsymbol{a}_e|, \tag{5.303}$$

with $\overline{\boldsymbol{\alpha}}'_{\{h^{-1}g_v\}}$ given explicitly by:

$$\begin{aligned}\overline{\boldsymbol{\alpha}}'_{\{h^{-1}g_v\}} = \overline{\boldsymbol{\nu}}_{\{h^{-1}g_v\}} &+ \frac{1}{2}\overline{\boldsymbol{\rho}}_{\{h^{-1}g_v\}} \cup_1 \overline{\boldsymbol{\rho}}_{\{h^{-1}g_v\}} \\ &+ \frac{1}{2}\overline{\boldsymbol{\rho}}_{\{h^{-1}g_v\}} \cup_1 \delta(\boldsymbol{a}_e + \overline{\boldsymbol{\rho}}^h_{\{h^{-1}g_v\}}) + \frac{1}{2}(\boldsymbol{a}_e + \overline{\boldsymbol{\rho}}^h_{\{h^{-1}g_v\}}) \cup \delta(\boldsymbol{a}_e + \overline{\boldsymbol{\rho}}^h_{\{h^{-1}g_v\}}).\end{aligned} \tag{5.304}$$

We now simplify the expression for $\overline{\boldsymbol{\alpha}}'_{\{h^{-1}g_v\}}$ in Eq. (5.304). To do so, we make use of the

cochain $\widetilde{\boldsymbol{\rho}}^{h}_{\{g_v\}}$, defined on an arbitrary edge $\langle 12\rangle$ as:

$$\widetilde{\boldsymbol{\rho}}^{h}_{\{g_v\}}(\langle 12\rangle) = \rho(h, 1, g_1, g_2). \tag{5.305}$$

It is also useful to introduce $\widetilde{\boldsymbol{\nu}}^{h}_{\{g_v\}}$:

$$\widetilde{\boldsymbol{\nu}}^{h}_{\{g_v\}}(\langle 123\rangle) \equiv \nu(h, 1, g_1, g_2, g_3), \tag{5.306}$$

for an arbitrary face $\langle 123\rangle$. We then employ the following identities:

$$\overline{\boldsymbol{\nu}}_{\{h^{-1}g_v\}} = \overline{\boldsymbol{\nu}}_{\{g_v\}} + \delta\widetilde{\boldsymbol{\nu}}^{h}_{\{g_v\}} + \frac{1}{2}\delta\widetilde{\boldsymbol{\rho}}^{h}_{\{g_v\}} \cup_1 \overline{\boldsymbol{\rho}}_{\{g_v\}} + \frac{1}{2}\widetilde{\boldsymbol{\rho}}^{h}_{\{g_v\}} \cup \delta\widetilde{\boldsymbol{\rho}}^{h}_{\{g_v\}} + \delta(\widetilde{\boldsymbol{\rho}}^{h}_{\{g_v\}} \cup_1 \overline{\boldsymbol{\rho}}_{\{g_v\}}), \tag{5.307}$$

$$\overline{\boldsymbol{\rho}}_{\{h^{-1}g_v\}} = \overline{\boldsymbol{\rho}}_{\{g_v\}} + \delta\widetilde{\boldsymbol{\rho}}^{h}_{\{g_v\}}, \tag{5.308}$$

$$\overline{\boldsymbol{\rho}}^{h}_{\{h^{-1}g_v\}} = \widetilde{\boldsymbol{\rho}}^{h}_{\{g_v\}}. \tag{5.309}$$

The first relation, in Eq. (5.307), can be derived using the coboundary relation of ν [Eq. (5.2)], the homogeneity of ν [Eq. (5.6)], and the cup product relations in Appendix 5.A.2. The second identity, [Eq. (5.308)], follows from the fact that ρ is closed [Eq. (5.2)] as well as the homogeneity of ρ [Eq. (5.6)]. The final relation, [Eq. (5.309)], is a result of the homogeneity of ρ. Plugging Eqs. (5.307), (5.308), and (5.309) into the right hand side of Eq. (5.304) and using the cup product relations, we find:

$$\overline{\boldsymbol{\alpha}}'_{\{h^{-1}g_v\}} = \overline{\boldsymbol{\alpha}}_{\{g_v\}} \tag{5.310}$$

$$+\frac{1}{2}\delta\left[\widetilde{\boldsymbol{\nu}}^{h}_{\{g_v\}} + \widetilde{\boldsymbol{\rho}}^{h}_{\{g_v\}} \cup_1 (\overline{\boldsymbol{\rho}}_{\{g_v\}} + \delta\boldsymbol{a}_e) + \boldsymbol{a}_e \cup \widetilde{\boldsymbol{\rho}}^{h}_{\{g_v\}}\right]. \tag{5.311}$$

On a closed manifold, the coboundary term in Eq. (5.310) vanishes after taking the product over all tetrahedron in Eq. (5.298), by Stokes' theorem. Therefore, for arbitrary

$h \in G$:

$$V_\rho(h)\mathcal{U}_2 V_\rho^\dagger(h) = \mathcal{U}_2. \tag{5.312}$$

Since $\mathcal{U}_2$ commutes with the symmetry, H_2 must be symmetric under the 2-group symmetry.

5.G Properties of $\mathcal{U}_s$

The goal of this Appendix is to establish the properties of the FDQC $\mathcal{U}_s$ employed in the main text. We first show that $\mathcal{U}_s$ is symmetric up to factors of $\bar{G}_e$. This is used to compute the fractionalization of the G symmetry on the loop-like excitations of the shadow model (see Section 5.4.3). Next, we express $\mathcal{U}_s$ in terms of $\bar{U}_f$ and W_t, as required in Section 5.4.4. As such, $\mathcal{U}_s$ can be straightforwardly fermionized using the fermion condensation duality in Section 5.3.2. Lastly, we derive the algebraic composition laws of the FDQCs for different sets of supercohomology data. With this, we determine the stacking laws of the corresponding fSPT phases in Section 5.4.4.

To start, we make a minor simplification to $\mathcal{U}_s$:

$$\mathcal{U}_s = \prod_f X_f^{\hat{\boldsymbol{\rho}}(f)} \prod_t \left[e^{2\pi i O_t \left[\hat{\boldsymbol{\nu}}(t) + \frac{1}{2}\hat{\boldsymbol{\rho}} \cup_1 \hat{\boldsymbol{\rho}}(t)\right]} \prod_{f \subset t} Z_f^{\hat{\boldsymbol{\rho}} \cup_1 \boldsymbol{f}(t)} \right] \prod_t W_t^{\int \hat{\boldsymbol{\rho}} \cup_2 \boldsymbol{t}}. \tag{5.313}$$

We commute the product of X_f operators past the product of Z_f operators. This cancels the sign from $\frac{1}{2}\hat{\boldsymbol{\rho}} \cup_1 \hat{\boldsymbol{\rho}}(t)$, and we are left with:

$$\mathcal{U}_s = \prod_t e^{2\pi i O_t \hat{\boldsymbol{\nu}}(t)} \prod_f Z_f^{\int \hat{\boldsymbol{\rho}} \cup_1 \boldsymbol{f}} \prod_f X_f^{\hat{\boldsymbol{\rho}}(f)} \prod_t W_t^{\int \hat{\boldsymbol{\rho}} \cup_2 \boldsymbol{t}}. \tag{5.314}$$

We have also changed the product of Z_f operators to a product over all faces in M. Since the $\cup_1$ product vanishes if f is not contained in the boundary of t, the change of bounds does not affect $\mathcal{U}_s$. We use the form of $\mathcal{U}_s$ in Eq. (5.314) for the calculations below.

5.G.1 Symmetry variation

Our goal is to show the identity:

$$V(h)\mathcal{U}_s = \mathcal{U}_s \Big[\prod_e \bar{G}_e^{\hat{\boldsymbol{\rho}}^{h^{-1}}(e)} \Big] V(h), \tag{5.315}$$

for an arbitrary $h \in G$, used in Section 5.4.3 [Eq. (5.147)]. We compute the action of the symmetry on $\mathcal{U}_s$, i.e., $V(h)\mathcal{U}_s V^\dagger(h)$ by conjugating terms in $\mathcal{U}_s$ one at a time.

First, conjugation of the $\hat{\boldsymbol{\nu}}$ term by $V(h)$ produces:

$$V(h) \prod_t e^{2\pi i O_t \hat{\boldsymbol{\nu}}(t)} V^\dagger(h) = \phi(h, \{g_v\}) \prod_t e^{2\pi i O_t \hat{\boldsymbol{\nu}}(t)}. \tag{5.316}$$

$\phi(h, \{g_v\})$ is a phase factor that depends on h and the $\{g_v\}$-configuration. We put constraints on the phase factors that appear during the calculation at the end by using the symmetry of the ground state(s) of H_s.

Next, we conjugate the Pauli X and Pauli Z terms:

$$\prod_f Z_f^{\int \hat{\boldsymbol{\rho}} \cup_1 \boldsymbol{f}} \prod_f X_f^{\hat{\boldsymbol{\rho}}(f)}. \tag{5.317}$$

After conjugation by the symmetry, $\hat{\boldsymbol{\rho}}$ becomes:

$$\hat{\boldsymbol{\rho}} \to \hat{\boldsymbol{\rho}} + \delta \hat{\boldsymbol{\rho}}^{h^{-1}}. \tag{5.318}$$

Therefore, up to a phase factor $\phi_1'(h, \{g_v\})$, the Pauli X and Z terms of $\mathcal{U}_s$ are mapped by the symmetry action to:

$$\prod_f Z_f^{\int \hat{\boldsymbol{\rho}} \cup_1 \boldsymbol{f}} \prod_f X_f^{\hat{\boldsymbol{\rho}}(f)} \phi_1'(h, \{g_v\}) \prod_f X_f^{\delta \hat{\boldsymbol{\rho}}^{h^{-1}}(f)} \prod_f Z_f^{\int \delta \hat{\boldsymbol{\rho}}^{h^{-1}} \cup_1 \boldsymbol{f}} \tag{5.319}$$

Rearranging the last two products in Eq. (5.319), we find:

$$\prod_f Z_f^{\int \hat{\bar{\boldsymbol{\rho}}} \cup_1 \boldsymbol{f}} \prod_f X_f^{\hat{\bar{\boldsymbol{\rho}}}(f)} \tag{5.320}$$

$$\times \phi_2'(h, \{g_v\}) \prod_e \left(\prod_{f \supset e} X_f \prod_f Z_f^{\int \delta \boldsymbol{e} \cup_1 \boldsymbol{f}} \right)^{\hat{\bar{\boldsymbol{\rho}}}^{g^{-1}}(e)}, \tag{5.321}$$

for another phase factor $\phi_2'(h, \{g_v\})$. The term in parentheses in Eq. (5.320) is equal to:

$$\prod_{f \supset e} X_f \prod_f Z_f^{\int \delta \boldsymbol{e} \cup_1 \boldsymbol{f}} = \bar{G}_e \prod_t W_t^{\int \delta \boldsymbol{e} \cup_2 \boldsymbol{t}}, \tag{5.322}$$

after using a cup product relation from Appendix 5.A.2. Thus, the symmetry action on the Pauli X and Pauli Z terms yields:

$$\prod_f Z_f^{\int \hat{\bar{\boldsymbol{\rho}}} \cup_1 \boldsymbol{f}} \prod_f X_f^{\hat{\bar{\boldsymbol{\rho}}}(f)} \phi_2'(h, \{g_v\}) \prod_e \bar{G}_e^{\hat{\bar{\boldsymbol{\rho}}}^{g^{-1}}(e)} \prod_t W_t^{\int \delta \hat{\bar{\boldsymbol{\rho}}}^{h^{-1}} \cup_2 \boldsymbol{t}}. \tag{5.323}$$

Lastly, we compute the symmetry action on the W_t term of $\mathcal{U}_s$:

$$\prod_t W_t^{\int \hat{\bar{\boldsymbol{\rho}}} \cup_2 \boldsymbol{t}}. \tag{5.324}$$

$\hat{\bar{\boldsymbol{\rho}}}$ is transformed as in Eq. (5.318), so we obtain:

$$\prod_t W_t^{\int \hat{\bar{\boldsymbol{\rho}}} \cup_2 \boldsymbol{t}} \prod_t W_t^{\int \delta \hat{\bar{\boldsymbol{\rho}}}^{h^{-1}} \cup_2 \boldsymbol{t}}. \tag{5.325}$$

Putting Eqs. (5.316), (5.323), and (5.325) together, we have:

$$V(h) \mathcal{U}_s V^\dagger(h) = \phi''(h, \{g_v\}) \mathcal{U}_s \prod_e \bar{G}_e^{\hat{\bar{\boldsymbol{\rho}}}^{h^{-1}}}, \tag{5.326}$$

where $\phi''(h, \{g_v\})$ is some yet undetermined phase factor. We note that the equality above

differs from Eq. (5.315) by precisely $\phi''(h, \{g_v\})$. In what follows, we use the symmetry of the ground state(s) of H_s to argue that $\phi''(h, \{g_v\})$ is indeed 1.

A ground state of the shadow model is given by applying $\mathcal{U}_s$ to a ground state of H^G_{ttc}:

$$|\Psi_s\rangle \equiv \mathcal{U}_s \sum_{\{g_v\},\{\boldsymbol{a}_e\}} (-1)^{\sum_t \boldsymbol{a}_e \cup \delta \boldsymbol{a}_e(t)} |\{g_v\}, \{\delta \boldsymbol{a}_e\}\rangle. \tag{5.327}$$

Furthermore, the state $|\Psi_s\rangle$ is invariant under the G symmetry, i.e.:

$$V(g)|\Psi_s\rangle = |\Psi_s\rangle. \tag{5.328}$$

The symmetry of $|\Psi_s\rangle$ follows from the symmetry of H_s and the fact that it can be prepared from a ground state of H^G_{ttc} by a FDQC.

With this, we argue that the phase factor $\phi''(h, \{g_v\})$ is 1. We apply $V(h)$ to $|\Psi_s\rangle$ to find:

$$\begin{aligned} V(h)|\Psi_s\rangle &= V(h)\mathcal{U}_s \sum_{\{g_v\},\{\boldsymbol{a}_e\}} (-1)^{\sum_t \boldsymbol{a}_e \cup \delta \boldsymbol{a}_e(t)} |\{g_v\}, \{\delta \boldsymbol{a}_e\}\rangle. \\ &= \mathcal{U}_s \sum_{\{g_v\},\{\boldsymbol{a}_e\}} \phi(h, \{g_v\})(-1)^{\sum_t \boldsymbol{a}_e \cup \delta \boldsymbol{a}_e(t)} |\{g_v\}, \{\delta \boldsymbol{a}_e\}\rangle, \end{aligned} \tag{5.329}$$

where we have used both Eq. (5.326) and that the ground state(s) of H^G_{ttc} are $+1$ eigenstates of $\bar{G}_e$. Now, in comparing Eq. (5.328) and the last line of Eq. (5.329), we see that $\phi''(h, \{g_v\})$ must be 1 for every $\{g_v\}$. This implies that:

$$V(h)\mathcal{U}_s = \mathcal{U}_s \prod_e \bar{G}_e^{\hat{\rho}^{h^{-1}}} V(h), \tag{5.330}$$

as claimed.

5.G.2 Fermionizability

Here, we show that the FDQC $\mathcal{U}_s$ in Eq. (5.314) can be expressed in terms of $\bar{U}_f$ and W_t operators. The fermion condensation duality (Table 5.2) can then be immediately applied

to $\mathcal{U}_s$ to construct the FDQC $\mathcal{U}_f$.

By re-arranging the Pauli X and Pauli Z operators in Eq. (5.313):

$$\mathcal{U}_s = \prod_t e^{2\pi i O_t \hat{\boldsymbol{\nu}}(t)} \prod_f Z_f^{\int \hat{\boldsymbol{\rho}} \cup_1 \boldsymbol{f}} \prod_f X_f^{\hat{\boldsymbol{\rho}}(f)} \prod_t W_t^{\int \hat{\boldsymbol{\rho}} \cup_2 \boldsymbol{t}}, \tag{5.331}$$

we can form $\bar{U}_f$ operators. To show this, we decompose the product of Z_f operators into:

$$\prod_f Z_f^{\int \hat{\boldsymbol{\rho}} \cup_1 \boldsymbol{f}} = \prod_f \prod_{f'} Z_{f'}^{\hat{\boldsymbol{\rho}}(f) \sum_t \boldsymbol{f} \cup_1 \boldsymbol{f}'(t)}. \tag{5.332}$$

We then see that we can form a factor of $\bar{U}_f^{\hat{\boldsymbol{\rho}}(f)}$ for each face f:

$$\bar{U}_f^{\hat{\boldsymbol{\rho}}(f)} = X_f^{\hat{\boldsymbol{\rho}}(f)} \prod_{f'} Z_{f'}^{\hat{\boldsymbol{\rho}}(f) \sum_t \boldsymbol{f} \cup_1 \boldsymbol{f}'(t)}. \tag{5.333}$$

Given the commutation relations of $\bar{U}_f$ operators, the resulting product of $\bar{U}_f^{\hat{\boldsymbol{\rho}}(f)}$ operators will generically depend on a choice of ordering. Hence, we choose an arbitrary ordering of the faces $(f_1 < \cdots < f_i < \cdots)$ of the set F of faces in M. We aim to form a product of $\bar{U}_f^{\hat{\boldsymbol{\rho}}(f)}$ according to the ordering on F, i.e.:

$$\prod_{f \in F} \bar{U}_f^{\hat{\boldsymbol{\rho}}(f)} = (\cdots \bar{U}_{f_i}^{\hat{\boldsymbol{\rho}}(f_i)} \cdots \bar{U}_{f_1}^{\hat{\boldsymbol{\rho}}(f_1)}). \tag{5.334}$$

We re-order the Pauli X and Pauli Z operators of $\mathcal{U}_s$ into the product in Eq. (5.334) by first, ordering the product of Z_f operators by the ordering on F:

$$\prod_{f \in F} \prod_{f'} Z_{f'}^{\hat{\boldsymbol{\rho}}(f) \sum_t \boldsymbol{f} \cup_1 \boldsymbol{f}'(t)} = \Big[\cdots \prod_{f'} Z_{f'}^{\hat{\boldsymbol{\rho}}(f_i) \sum_t \boldsymbol{f} \cup_1 \boldsymbol{f}'(t)} \cdots \prod_{f'} Z_{f'}^{\hat{\boldsymbol{\rho}}(f_1) \sum_t \boldsymbol{f} \cup_1 \boldsymbol{f}'(t)} \Big]. \tag{5.335}$$

To form $\bar{U}_{f_i}^{\hat{\boldsymbol{\rho}}(f_i)}$, $X_{f_i}^{\hat{\boldsymbol{\rho}}(f_i)}$ in Eq. (5.331) is commuted past the Pauli Z operators of $\bar{U}_{f_{i'}}^{\hat{\boldsymbol{\rho}}(f_{i'})}$ for

each $i' < i$. This produces the sign:

$$\prod_{i'<i} (-1)^{\hat{\bar{\boldsymbol{\rho}}}(f_{i'})\hat{\bar{\boldsymbol{\rho}}}(f_i) \sum_t \boldsymbol{f}_{i'} \cup_1 \boldsymbol{f}_i(t)}. \tag{5.336}$$

In creating the product in Eq (5.334), we thus accrue the sign:

$$\xi_{\bar{\rho}}(F) = \prod_i \left[\prod_{i'<i} (-1)^{\hat{\bar{\boldsymbol{\rho}}}(f_{i'})\hat{\bar{\boldsymbol{\rho}}}(f_i) \int \boldsymbol{f}_{i'} \cup_1 \boldsymbol{f}_i} \right]. \tag{5.337}$$

In summary, we have shown that $\mathcal{U}_s$ can be written as:

$$\mathcal{U}_s = \prod_t e^{2\pi i O_t \hat{\bar{\boldsymbol{\nu}}}(t)} \xi_{\bar{\rho}}(F) \prod_{f \in F} \bar{U}_f^{\hat{\bar{\boldsymbol{\rho}}}(f)} \prod_t W_t^{\int \hat{\bar{\boldsymbol{\rho}}} \cup_2 \boldsymbol{t}}. \tag{5.338}$$

which matches the form of $\mathcal{U}_s$ in Eq. (5.159). Fermion condensation is implemented by replacing $\bar{U}_f$ with S_f and W_t with P_t. This gives the circuit $\mathcal{U}_f$ in Eq. (5.164):

$$\mathcal{U}_f \equiv \prod_t e^{2\pi i O_t \hat{\bar{\boldsymbol{\nu}}}(t)} \xi_{\bar{\rho}}(M) \prod_f S_f^{\hat{\bar{\boldsymbol{\rho}}}(f)} \prod_t P_t^{\int \hat{\bar{\boldsymbol{\rho}}} \cup_2 \boldsymbol{t}}. \tag{5.339}$$

5.G.3 Composition laws

As argued in Section 5.2.3, the stacking laws of supercohomology phases can be determined by composing the FDQCs $\mathcal{U}_f$ that prepare the supercohomology models. For convenience, we evaluate the composition of the FDQCs $\mathcal{U}_s$ that prepare the shadow model. The composition of $\mathcal{U}_f$ operators follows from this by applying the fermionization duality to the $\mathcal{U}_s$ circuits. For reference, the FDQC $\mathcal{U}_s$ corresponding to the supercohomology data (ρ, ν) is:

$$\mathcal{U}_s^{\rho\nu} = \prod_t e^{2\pi i \hat{\boldsymbol{\nu}}(t) O_t} \prod_{f'} Z_{f'}^{\int \hat{\boldsymbol{\rho}} \cup_1 \boldsymbol{f}'} \prod_f X_f^{\hat{\boldsymbol{\rho}}(f)} \prod_t W_t^{\int \hat{\boldsymbol{\rho}} \cup_2 \boldsymbol{t}}. \tag{5.340}$$

Given two sets of supercohomology data (ρ, ν) and (ρ', ν'), we calculate the product of

$\mathcal{U}_s^{\rho\nu}$ and $\mathcal{U}_s^{\rho'\nu'}$ directly:

$$\begin{aligned}\mathcal{U}_s^{\rho\nu}\mathcal{U}_s^{\rho'\nu'} &= \prod_t e^{2\pi i \hat{\boldsymbol{\nu}}(t) O_t} \prod_{f'} Z_{f'}^{\int \hat{\boldsymbol{\rho}} \cup_1 \boldsymbol{f}'} \prod_f X_f^{\hat{\boldsymbol{\rho}}(f)} \prod_t W_t^{\int \hat{\boldsymbol{\rho}} \cup_2 \boldsymbol{t}} \\ &\times \prod_t e^{2\pi i \hat{\boldsymbol{\nu}}'(t) O_t} \prod_{f'} Z_{f'}^{\int \hat{\boldsymbol{\rho}}' \cup_1 \boldsymbol{f}'} \prod_f X_f^{\hat{\boldsymbol{\rho}}'(f)} \prod_t W_t^{\int \hat{\boldsymbol{\rho}}' \cup_2 \boldsymbol{t}} \\ &= \prod_t e^{2\pi i \hat{\boldsymbol{\nu}}''(t) O_t} \prod_{f'} Z_{f'}^{\int \hat{\boldsymbol{\rho}}'' \cup_1 \boldsymbol{f}'} \prod_f X_f^{\hat{\boldsymbol{\rho}}''(f)} \prod_t W_t^{\int \hat{\boldsymbol{\rho}}'' \cup_2 \boldsymbol{t}}.\end{aligned} \tag{5.341}$$

In the last line, we have combined the Pauli Z and Pauli X operators and defined $\hat{\boldsymbol{\rho}}'' \equiv \hat{\boldsymbol{\rho}} + \hat{\boldsymbol{\rho}}'$. The operator $\hat{\boldsymbol{\nu}}''$ is a sum of $\hat{\boldsymbol{\nu}}$ and $\hat{\boldsymbol{\nu}}'$ and also incorporates the sign incurred from commuting the Pauli X and Pauli Z operators. In particular, to form the last line in Eq. (5.341), we commute the operators:

$$\begin{aligned}&\prod_{f'} \left(Z_{f'}^{\int \hat{\boldsymbol{\rho}}' \cup_1 f'} \right) \text{ past } \prod_f \left(X_f^{\hat{\boldsymbol{\rho}}(f)} \right), \\ &\prod_f \left(X_f^{\hat{\boldsymbol{\rho}}'(f)} \right) \text{ past } \prod_t \left(W_t^{\hat{\boldsymbol{\rho}} \cup_2 \boldsymbol{t}} \right).\end{aligned} \tag{5.342}$$

This produces the sign:

$$(-1)^{\int \hat{\boldsymbol{\rho}}' \cup_1 \hat{\boldsymbol{\rho}} + \hat{\boldsymbol{\rho}} \cup_2 \delta \hat{\boldsymbol{\rho}}'}, \tag{5.343}$$

so we define $\hat{\boldsymbol{\nu}}''$ as:

$$\hat{\boldsymbol{\nu}}'' \equiv \hat{\boldsymbol{\nu}} + \hat{\boldsymbol{\nu}}' + \frac{1}{2} \hat{\boldsymbol{\rho}}' \cup_1 \hat{\boldsymbol{\rho}} + \frac{1}{2} \hat{\boldsymbol{\rho}} \cup_2 \delta \hat{\boldsymbol{\rho}}'. \tag{5.344}$$

Now, we recover the supercohomology data corresponding to $\hat{\boldsymbol{\rho}}''$ and $\hat{\boldsymbol{\nu}}''$ from their diagonal matrix elements. For a face $\langle 123 \rangle$, the matrix element $\langle \{g_v\} | \hat{\boldsymbol{\rho}}''(\langle 123 \rangle) | \{g_v\} \rangle$ is:

$$\langle \{g_v\} | \hat{\boldsymbol{\rho}}''(\langle 123 \rangle) | \{g_v\} \rangle = \rho(1, g_1, g_2, g_3) + \rho'(1, g_1, g_2, g_3). \tag{5.345}$$

Therefore, $\hat{\overline{\boldsymbol{\rho}}}''$ corresponds to the function $\rho'' = \rho + \rho'$. For $\hat{\overline{\boldsymbol{\nu}}}''$, we compute the matrix element $\langle\{g_v\}|\hat{\overline{\boldsymbol{\nu}}}''(\langle 1234\rangle)|\{g_v\}\rangle$, with an arbitrary tetrahedron $\langle 1234\rangle$:

$$\begin{aligned}\langle\{g_v\}|\hat{\overline{\boldsymbol{\nu}}}''(\langle 1234\rangle)|\{g_v\}\rangle = {}& \nu(1,g_1,g_2,g_3,g_4) + \nu'(1,g_1,g_2,g_3,g_4) \\ & + \frac{1}{2}\rho(1,g_1,g_2,g_3)\rho'(1,g_1,g_3,g_4) + \frac{1}{2}\rho(1,g_2,g_3,g_4)\rho'(1,g_1,g_2,g_4) \\ & + \frac{1}{2}\rho(1,g_1,g_2,g_3)\rho'(g_1,g_2,g_3,g_4) + \frac{1}{2}\rho(1,g_1,g_3,g_4)\rho'(g_1,g_2,g_3,g_4).\end{aligned} \tag{5.346}$$

To obtain the right-hand side of Eq. (5.346), we have used the explicit formulas for cup products in Appendix 5.A.2. The sum of ρ and ρ' terms can be further simplified to $\frac{1}{2}\rho \cup_2 \rho'(1,g_1,g_2,g_3,g_4)$ with Eq. (5.223). Thus, $\hat{\overline{\boldsymbol{\nu}}}''$ corresponds to the function $\nu'' \equiv \nu + \nu'' + \frac{1}{2}\rho \cup_2 \rho'$.

In summary, we have found $\mathcal{U}_s^{\rho\nu}\mathcal{U}_s^{\rho'\nu'} = \mathcal{U}_s^{\rho''\nu''}$, where (ρ'', ν'') is:

$$(\rho'', \nu'') = (\rho + \rho', \nu + \nu'' + \frac{1}{2}\rho \cup_2 \rho'). \tag{5.347}$$

Since the composition rules are preserved under fermionization, we have that $\mathcal{U}_f^{\rho\nu}\mathcal{U}_f^{\rho'\nu'} = \mathcal{U}_f^{\rho''\nu''}$. Hence, the stacking rules for supercohomology phases is given by:

$$(\rho, \nu) \boxtimes (\rho', \nu') = (\rho + \rho', \nu + \nu' + \frac{1}{2}\rho \cup_2 \rho'). \tag{5.348}$$

5.H SPT state built from trivial supercohomology data

In this appendix, we show that the fSPT state $|\Psi_f^{\rho_0\nu_0}\rangle$ corresponding to the trivial supercohomology data:

$$(\rho_0, \nu_0) = (\delta\beta, \delta\eta + \frac{1}{2}\beta \cup \beta + \frac{1}{2}\beta \cup_1 \delta\beta), \tag{5.349}$$

can be constructed from a product state by a FDQC composed of local symmetric unitaries. According to the definition of fSPT phases, $|\Psi_f^{\rho_0\nu_0}\rangle$ must belong to the trivial fSPT phase. This verifies the claim made in the main text that the supercohomology data (ρ_0, ν_0) corresponds to the trivial phase. As a warmup, we consider the case in which β and η are closed. We then derive the more general statement for an arbitrary choice of (ρ_0, ν_0).

Assuming β and η are closed

In this case, (ρ_0, ν_0) is equal to $(0, \frac{1}{2}\beta \cup \beta)$. Note that ν_0 is given by the group cocycle $\frac{1}{2}\beta \cup \beta$, which can be used to construct a group cohomology model following the discussion in Section 5.2.2. If $\frac{1}{2}\beta \cup \beta$ is a nontrivial cocycle, then the model describes a nontrivial bosonic SPT phase. However, after introducing fermions [either emergent (in the twisted toric code) or physical (in the fSPT model)], the phase factor associated to $\frac{1}{2}\beta \cup \beta$ can be produced by a FDQC comprised of local symmetric unitaries, as we show below.

For convenience, we consider the shadow model. A ground state of the shadow model corresponding to the supercohomology data $(0, \frac{1}{2}\beta \cup \beta)$ is:

$$|\Psi_s^{\rho_0\nu_0}\rangle = \sum_{\{g_v\}, \boldsymbol{a}_e} (-1)^{\int \hat{\overline{\boldsymbol{\beta}}} \cup \hat{\boldsymbol{\beta}} + \boldsymbol{a}_e \cup \delta \boldsymbol{a}_e} |\{g_v\}, \delta \boldsymbol{a}_e\rangle, \tag{5.350}$$

where we have introduced the notation:

$$\begin{aligned} \hat{\boldsymbol{\beta}}(\langle 123\rangle)|\{g_v\}, \delta \boldsymbol{a}_e\rangle &= \beta(g_1, g_2, g_3)|\{g_v\}, \delta \boldsymbol{a}_e\rangle, \\ \hat{\overline{\boldsymbol{\beta}}}(\langle 12\rangle)|\{g_v\}, \delta \boldsymbol{a}_e\rangle &= \beta(1, g_1, g_2)|\{g_v\}, \delta \boldsymbol{a}_e\rangle. \end{aligned} \tag{5.351}$$

Since β is a cocycle, we have $\delta\hat{\overline{\boldsymbol{\beta}}} = \hat{\boldsymbol{\beta}}$. Using the cup product relations in Appendix 5.A.2, the exponent in Eq. (5.350) can be written as:

$$\int \hat{\overline{\boldsymbol{\beta}}} \cup \delta\hat{\overline{\boldsymbol{\beta}}} + \boldsymbol{a}_e \cup \delta \boldsymbol{a}_e = \int (\boldsymbol{a}_e + \hat{\overline{\boldsymbol{\beta}}}) \cup \delta(\boldsymbol{a}_e + \hat{\overline{\boldsymbol{\beta}}}) + \hat{\boldsymbol{\beta}} \cup_1 \delta \boldsymbol{a}_e. \tag{5.352}$$

By defining $\boldsymbol{a}'_e \equiv \boldsymbol{a}_e + \hat{\overline{\boldsymbol{\beta}}}$, the ground state of the shadow model in Eq. (5.350) becomes:

$$\begin{aligned}|\Psi_s^{\rho_0\nu_0}\rangle &= \sum_{\{g_v\},\boldsymbol{a}_e} (-1)^{\int \hat{\boldsymbol{\beta}}\cup_1(\delta\boldsymbol{a}'_e+\hat{\boldsymbol{\beta}})+\boldsymbol{a}'_e\cup\delta\boldsymbol{a}'_e} \prod_f X_f^{\hat{\boldsymbol{\beta}}(f)}|\{g_v\},\delta\boldsymbol{a}'_e\rangle \\ &= \sum_{\{g_v\},\boldsymbol{a}'_e} \prod_{f'} Z_{f'}^{\int \hat{\boldsymbol{\beta}}\cup_1 \boldsymbol{f}'} \prod_f X_f^{\hat{\boldsymbol{\beta}}(f)} (-1)^{\int \boldsymbol{a}'_e\cup\delta\boldsymbol{a}'_e}|\{g_v\},\delta\boldsymbol{a}'_e\rangle \\ &= \sum_{\{g_v\},\boldsymbol{a}'_e} \bar{U}_\beta (-1)^{\int \boldsymbol{a}'_e\cup\delta\boldsymbol{a}'_e}|\{g_v\},\delta\boldsymbol{a}'_e\rangle.\end{aligned} \tag{5.353}$$

According to the fermionization duality reviewed in Appendix 5.E $|\Psi_s^{\rho_0\nu_0}\rangle$ maps to the fermionic state:

$$|\Psi_f^{\rho_0\nu_0}\rangle = \sum_{\{g_v\}} S_\beta|\{g_v\},\mathrm{vac}\rangle. \tag{5.354}$$

Here, S_β is the FDQC built from the product of hopping operators:

$$S_\beta \equiv \xi_\beta(M)\prod_f S_f^{\hat{\boldsymbol{\beta}}(f)}, \tag{5.355}$$

with $\xi_\beta(M)$ given by:

$$\xi_\beta(M) \equiv \prod_{i,i'|i'<i} (-1)^{\hat{\boldsymbol{\beta}}(f_{i'})\hat{\boldsymbol{\beta}}(f_i)\int \boldsymbol{f}_{i'}\cup_1\boldsymbol{f}_i}. \tag{5.356}$$

The FDQC S_β is composed of local symmetric unitaries due to the homogeneity of β. Therefore, $|\Psi_f^{\rho_0\nu_0}\rangle$ belongs to the trivial fSPT phase.

General trivial supercohomology data

We now consider the more general case where (ρ_0,ν_0) takes the form in Eq. (5.349) for any $\eta \in C^3(G,\mathbb{R}/\mathbb{Z})$ and $\beta \in C^2(G,\mathbb{Z}_2)$. A ground state of the shadow model (after the basis

transformation introduced in Eq. (5.133)) is:

$$|\Psi_s^{\rho_0\nu_0}\rangle = \sum_{\{g_v\},\boldsymbol{a}_e} \prod_t e^{2\pi i O_t \hat{\tilde{\boldsymbol{\nu}}}(t)} (-1)^{\int \hat{\tilde{\boldsymbol{\rho}}} \cup_1 (\delta \boldsymbol{a}_e + \hat{\tilde{\boldsymbol{\rho}}})} (-1)^{\int \boldsymbol{a}_e \cup \delta \boldsymbol{a}_e} \prod_f X_f^{\hat{\tilde{\boldsymbol{\rho}}}(f)} |\{g_v\}, \delta \boldsymbol{a}_e\rangle. \tag{5.357}$$

The $\hat{\tilde{\boldsymbol{\nu}}}$ term can be decomposed into:

$$\prod_t e^{2\pi i O_t \hat{\boldsymbol{\eta}}(t)} (-1)^{\int \hat{\tilde{\boldsymbol{\beta}}} \cup \hat{\boldsymbol{\beta}} + \hat{\tilde{\boldsymbol{\rho}}} \cup \hat{\tilde{\boldsymbol{\beta}}} + \hat{\tilde{\boldsymbol{\beta}}} \cup_1 \hat{\boldsymbol{\rho}}}, \tag{5.358}$$

where $\hat{\boldsymbol{\rho}}$ and $\hat{\tilde{\boldsymbol{\rho}}}$ are defined by:

$$\begin{aligned} \hat{\boldsymbol{\rho}}(\langle 1234 \rangle) |\{g_v\}, \delta \boldsymbol{a}_e\rangle &= \rho(g_1, g_2, g_3, g_4) |\{g_v\}, \delta \boldsymbol{a}_e\rangle, \\ \hat{\tilde{\boldsymbol{\rho}}}(\langle 123 \rangle) |\{g_v\}, \delta \boldsymbol{a}_e\rangle &= \rho(1, g_1, g_2, g_3) |\{g_v\}, \delta \boldsymbol{a}_e\rangle. \end{aligned} \tag{5.359}$$

To obtain Eq. (5.358), we have used $\hat{\boldsymbol{\rho}} = \delta \hat{\boldsymbol{\beta}}$ and the explicit $\cup_1$ product:

$$\begin{aligned} \hat{\boldsymbol{\beta}} \cup_1 \delta \hat{\boldsymbol{\beta}}(\langle 01234 \rangle) =& \hat{\boldsymbol{\beta}}(\langle 034 \rangle) \delta \hat{\boldsymbol{\beta}}(\langle 0123 \rangle) + \hat{\boldsymbol{\beta}}(\langle 014 \rangle) \delta \hat{\boldsymbol{\beta}}(\langle 1234 \rangle) \\ =& \hat{\tilde{\boldsymbol{\rho}}}(\langle 123 \rangle) \hat{\tilde{\boldsymbol{\beta}}}(\langle 34 \rangle) + \hat{\tilde{\boldsymbol{\beta}}}(\langle 14 \rangle) \hat{\boldsymbol{\rho}}(\langle 1234 \rangle) \\ =& [\hat{\tilde{\boldsymbol{\rho}}} \cup \hat{\tilde{\boldsymbol{\beta}}} + \hat{\tilde{\boldsymbol{\beta}}} \cup_1 \hat{\boldsymbol{\rho}}](\langle 1234 \rangle). \end{aligned} \tag{5.360}$$

Now, using the identity $\hat{\tilde{\boldsymbol{\rho}}} = \hat{\boldsymbol{\beta}} + \delta \hat{\tilde{\boldsymbol{\beta}}}$ and defining the new variables $\boldsymbol{a}'_e \equiv \boldsymbol{a}_e + \hat{\tilde{\boldsymbol{\beta}}}$, the ground state of the shadow model can be organized into:

$$\begin{aligned} |\Psi_s^{\rho_0\nu_0}\rangle &= \sum_{\{g_v\},\boldsymbol{a}'_e} \prod_t e^{2\pi i O_t \hat{\boldsymbol{\eta}}(t)} (-1)^{\int \hat{\boldsymbol{\beta}} \cup_1 (\delta \boldsymbol{a}'_e + \hat{\boldsymbol{\beta}})} (-1)^{\int \boldsymbol{a}'_e \cup \delta \boldsymbol{a}'_e} \prod_f X_f^{\hat{\tilde{\boldsymbol{\rho}}}(f)} X_f^{\delta \hat{\tilde{\boldsymbol{\beta}}}(f)} |\{g_v\}, \delta \boldsymbol{a}'_e\rangle \\ &= \sum_{\{g_v\},\boldsymbol{a}'_e} \prod_t e^{2\pi i O_t \hat{\boldsymbol{\eta}}(t)} \prod_{f'} Z_{f'}^{\int \hat{\boldsymbol{\beta}} \cup_1 \boldsymbol{f}'} \prod_f X_f^{\hat{\boldsymbol{\beta}}(f)} (-1)^{\int \boldsymbol{a}'_e \cup \delta \boldsymbol{a}'_e} |\{g_v\}, \delta \boldsymbol{a}'_e\rangle \\ &= \sum_{\{g_v\},\boldsymbol{a}'_e} \prod_t e^{2\pi i O_t \hat{\boldsymbol{\eta}}(t)} \bar{U}_\beta (-1)^{\int \boldsymbol{a}'_e \cup \delta \boldsymbol{a}'_e} |\{g_v\}, \delta \boldsymbol{a}'_e\rangle \end{aligned} \tag{5.361}$$

This fermionizes to the fermionic state:

$$|\Psi_f^{\rho_0\nu_0}\rangle = \sum_{\{g_v\}} \prod_t e^{2\pi i O_t \hat{\boldsymbol{\eta}}(t)} S_\beta |\{g_v\}, \text{vac}\rangle = \prod_t e^{2\pi i O_t \hat{\boldsymbol{\eta}}(t)} S_\beta \sum_{\{g_v\}} |\{g_v\}, \text{vac}\rangle, \tag{5.362}$$

which is constructed from a product state by a FDQC composed of local symmetric unitaries.

BIBLIOGRAPHY

[1] Dominic J. Williamson, Nick Bultinck, Michael Mariën, Mehmet B. Şahinoğlu, Jutho Haegeman, and Frank Verstraete. Matrix product operators for symmetry-protected topological phases: Gauging and edge theories. *Phys. Rev. B*, 94:205150, Nov 2016.

[2] Dominic V. Else, Ilai Schwarz, Stephen D. Bartlett, and Andrew C. Doherty. Symmetry-protected phases for measurement-based quantum computation. *Phys. Rev. Lett.*, 108:240505, Jun 2012.

[3] Nicolas Tarantino and Lukasz Fidkowski. Discrete spin structures and commuting projector models for two-dimensional fermionic symmetry-protected topological phases. *Phys. Rev. B*, 94:115115, Sep 2016.

[4] Xie Chen, Zheng-Cheng Gu, and Xiao-Gang Wen. Local unitary transformation, long-range quantum entanglement, wave function renormalization, and topological order. *Phys. Rev. B*, 82:155138, Oct 2010.

[5] Liang Fu and C. L. Kane. Josephson current and noise at a superconductor/quantum-spin-hall-insulator/superconductor junction. *Phys. Rev. B*, 79:161408, Apr 2009.

[6] Robert Raussendorf and Hans J. Briegel. A one-way quantum computer. *Phys. Rev. Lett.*, 86:5188–5191, May 2001.

[7] M. B. Hastings. How quantum are non-negative wavefunctions? *Journal of Mathematical Physics*, 57(1):015210, 2016.

[8] Sergey Bravyi and Alexei Kitaev. Universal quantum computation with ideal clifford gates and noisy ancillas. *Phys. Rev. A*, 71:022316, Feb 2005.

[9] Norbert Schuch, David Pérez-García, and Ignacio Cirac. Classifying quantum phases using matrix product states and projected entangled pair states. *Phys. Rev. B*, 84:165139, Oct 2011.

[10] Katharine Hyatt and E. M. Stoudenmire. Dmrg approach to optimizing two-dimensional tensor networks, 2020.

[11] G. Scarpa, A. Molnár, Y. Ge, J. J. García-Ripoll, N. Schuch, D. Pérez-García, and S. Iblisdir. Projected entangled pair states: Fundamental analytical and numerical limitations. *Phys. Rev. Lett.*, 125:210504, Nov 2020.

[12] Michael P. Zaletel and Frank Pollmann. Isometric tensor network states in two dimensions. *Phys. Rev. Lett.*, 124:037201, Jan 2020.

[13] Alexei Kitaev. Periodic table for topological insulators and superconductors. *AIP Conference Proceedings*, 1134(1):22–30, 2009.

[14] Shinsei Ryu, Andreas P Schnyder, Akira Furusaki, and Andreas W W Ludwig. Topological insulators and superconductors: tenfold way and dimensional hierarchy. *New Journal of Physics*, 12(6):065010, jun 2010.

[15] Adam Smith, Omri Golan, and Zohar Ringel. Intrinsic sign problems in topological quantum field theories. *Phys. Rev. Research*, 2:033515, Sep 2020.

[16] Sergey B. Bravyi and Alexei Yu. Kitaev. Fermionic quantum computation. *Annals of Physics*, 298(1):210–226, 2002.

[17] M. B. Hastings and Xiao-Gang Wen. Quasiadiabatic continuation of quantum states: The stability of topological ground-state degeneracy and emergent gauge invariance. *Phys. Rev. B*, 72:045141, Jul 2005.

[18] Yu-An Chen, Anton Kapustin, and Djordje Radicevic. Exact bosonization in two spatial dimensions and a new class of lattice gauge theories. *Annals of Physics*, 393:234 – 253, 2018.

[19] Victor Veitch, S A Hamed Mousavian, Daniel Gottesman, and Joseph Emerson. The resource theory of stabilizer quantum computation. *New Journal of Physics*, 16(1):013009, jan 2014.

[20] Daniel Gottesman. The Heisenberg Representation of Quantum Computers. *Group22: Proceedings of the XXII International Colloquium on Group Theoretical Methods in Physics, eds. S. P. Corney, R. Delbourgo, and P. D. Jarvis, pp. 32-43 (Cambridge, MA, International Press, 1999).*

[21] Tarun Grover and Matthew P. A. Fisher. Entanglement and the sign structure of quantum states. *Phys. Rev. A*, 92:042308, Oct 2015.

[22] Giacomo Torlai, Juan Carrasquilla, Matthew T. Fishman, Roger G. Melko, and Matthew P. A. Fisher. Wave-function positivization via automatic differentiation. *Phys. Rev. Research*, 2:032060, Sep 2020.

[23] Matthias Troyer and Uwe-Jens Wiese. Computational complexity and fundamental limitations to fermionic quantum monte carlo simulations. *Phys. Rev. Lett.*, 94:170201, May 2005.

[24] Milad Marvian, Daniel A. Lidar, and Itay Hen. On the computational complexity of curing non-stoquastic hamiltonians. *Nature Communications*, 10(1):1571, Apr 2019.

[25] Joel Klassen, Milad Marvian, Stephen Piddock, Marios Ioannou, Itay Hen, and Barbara Terhal. Hardness and ease of curing the sign problem for two-local qubit hamiltonians. *arXiv:1906.08800*, 2020.

[26] Joel Klassen and Barbara M. Terhal. Two-local qubit Hamiltonians: when are they stoquastic? *Quantum*, 3:139, May 2019.

[27] Ryan Levy and Bryan K. Clark. Mitigating the sign problem through basis rotations. *arXiv:1907.02076*, 2019.

[28] Zhou-Quan Wan, Shi-Xin Zhang, and Hong Yao. Mitigating sign problem by automatic differentiation. *arXiv:2010.01141*, October 2020.

[29] Dominik Hangleiter, Ingo Roth, Daniel Nagaj, and Jens Eisert. Easing the monte carlo sign problem. *Science Advances*, 6(33), 2020.

[30] Christopher David White, ChunJun Cao, and Brian Swingle. Conformal field theories are magical. *arXiv:2007.01303*, July 2020.

[31] S Sarkar, C Mukhopadhyay, and A Bayat. Characterization of an operational quantum resource in a critical many-body system. *New Journal of Physics*, 22(8):083077, aug 2020.

[32] Zi-Wen Liu and Andreas Winter. Many-body quantum magic. *arXiv:2010.13817*, October 2020.

[33] Zohar Ringel and Dmitry L. Kovrizhin. Quantized gravitational responses, the sign problem, and quantum complexity. *Science Advances*, 3(9), 2017.

[34] Omri Golan, Adam Smith, and Zohar Ringel. Intrinsic sign problem in fermionic and bosonic chiral topological matter. *Phys. Rev. Research*, 2:043032, Oct 2020.

[35] Maxime Dupont, Snir Gazit, and Thomas Scaffidi. Evidence for deconfined U(1) gauge theory at the transition between toric code and double semion. *arXiv:2008.06509*, 2020.

[36] Maxime Dupont, Snir Gazit, and Thomas Scaffidi. From trivial to topological paramagnets: The case of $\mathbb{Z}_2$ and $\mathbb{Z}_2^3$ symmetries in two dimensions. *arXiv:2008.11206*, 2020.

[37] C. L. Kane and E. J. Mele. Z_2 topological order and the quantum spin hall effect. *Phys. Rev. Lett.*, 95:146802, Sep 2005.

[38] C. L. Kane and E. J. Mele. Quantum spin hall effect in graphene. *Phys. Rev. Lett.*, 95:226801, Nov 2005.

[39] Robert Raussendorf and Hans J. Briegel. A one-way quantum computer. *Phys. Rev. Lett.*, 86:5188–5191, May 2001.

[40] Robert Raussendorf, Dong-Sheng Wang, Abhishodh Prakash, Tzu-Chieh Wei, and David T. Stephen. Symmetry-protected topological phases with uniform computational power in one dimension. *Phys. Rev. A*, 96:012302, Jul 2017.

[41] Robert Raussendorf, Cihan Okay, Dong-Sheng Wang, David T. Stephen, and Hendrik Poulsen Nautrup. Computationally universal phase of quantum matter. *Phys. Rev. Lett.*, 122:090501, Mar 2019.

[42] David T. Stephen, Hendrik Poulsen Nautrup, Juani Bermejo-Vega, Jens Eisert, and Robert Raussendorf. Subsystem symmetries, quantum cellular automata, and computational phases of quantum matter. *Quantum*, 3:142, May 2019.

[43] Austin K. Daniel, Rafael N. Alexander, and Akimasa Miyake. Computational universality of symmetry-protected topologically ordered cluster phases on 2D Archimedean lattices. *Quantum*, 4:228, February 2020.

[44] Trithep Devakul and Dominic J. Williamson. Universal quantum computation using fractal symmetry-protected cluster phases. *Phys. Rev. A*, 98:022332, Aug 2018.

[45] Akimasa Miyake. Quantum computation on the edge of a symmetry-protected topological order. *Phys. Rev. Lett.*, 105:040501, Jul 2010.

[46] Jacob Miller and Akimasa Miyake. Hierarchy of universal entanglement in 2D measurement-based quantum computation. *npj Quantum Information*, 2(9):16036, 2016.

[47] Jacob Miller and Akimasa Miyake. Latent computational complexity of symmetry-protected topological order with fractional symmetry. *Phys. Rev. Lett.*, 120:170503, Apr 2018.

[48] Beni Yoshida. Gapped boundaries, group cohomology and fault-tolerant logical gates. *Annals of Physics*, 377:387 – 413, 2017.

[49] Dominic V. Else and Chetan Nayak. Classifying symmetry-protected topological phases through the anomalous action of the symmetry on the edge. *Phys. Rev. B*, 90:235137, Dec 2014.

[50] Sergey Bravyi, Matthew B Hastings, and Spyridon Michalakis. Topological quantum order: stability under local perturbations. *Journal of mathematical physics*, 51(9):093512, 2010.

[51] Sergey Bravyi and Matthew B Hastings. A short proof of stability of topological order under local perturbations. *Communications in mathematical physics*, 307(3):609, 2011.

[52] Xie Chen, Zheng-Cheng Gu, Zheng-Xin Liu, and Xiao-Gang Wen. Symmetry protected topological orders and the group cohomology of their symmetry group. *Phys. Rev. B*, 87:155114, Apr 2013.

[53] Davide Gaiotto and Theo Johnson-Freyd. Symmetry protected topological phases and generalized cohomology. *Journal of High Energy Physics*, 2019(5):7, 2019.

[54] Anton Kapustin. Symmetry Protected Topological Phases, Anomalies, and Cobordisms: Beyond Group Cohomology. *arXiv:1403.1467*, March 2014.

[55] Kazuya Yonekura. On the cobordism classification of symmetry protected topological phases. *Communications in Mathematical Physics*, 368:1121–1173, Jun 2019.

[56] Ling-Yan Hung and Xiao-Gang Wen. Quantized topological terms in weak-coupling gauge theories with a global symmetry and their connection to symmetry-enriched topological phases. *Phys. Rev. B*, 87:165107, Apr 2013.

[57] Xie Chen, Yuan-Ming Lu, and Ashvin Vishwanath. Symmetry-protected topological phases from decorated domain walls. *Nature communications*, 5(1):1–11, 2014.

[58] Xie Chen, Zheng-Xin Liu, and Xiao-Gang Wen. Two-dimensional symmetry-protected topological orders and their protected gapless edge excitations. *Phys. Rev. B*, 84:235141, Dec 2011.

[59] R. Shankar and Ashvin Vishwanath. Equality of bulk wave functions and edge correlations in some topological superconductors: A spacetime derivation. *Phys. Rev. Lett.*, 107:106803, Sep 2011.

[60] Yi-Zhuang You, Zhen Bi, Alex Rasmussen, Kevin Slagle, and Cenke Xu. Wave function and strange correlator of short-range entangled states. *Phys. Rev. Lett.*, 112:247202, Jun 2014.

[61] Robijn Vanhove, Matthias Bal, Dominic J. Williamson, Nick Bultinck, Jutho Haegeman, and Frank Verstraete. Mapping topological to conformal field theories through strange correlators. *Phys. Rev. Lett.*, 121:177203, Oct 2018.

[62] Nick Bultinck, Robijn Vanhove, Jutho Haegeman, and Frank Verstraete. Global anomaly detection in two-dimensional symmetry-protected topological phases. *Phys. Rev. Lett.*, 120:156601, Apr 2018.

[63] Xie Chen, Zheng-Cheng Gu, and Xiao-Gang Wen. Classification of gapped symmetric phases in one-dimensional spin systems. *Phys. Rev. B*, 83:035107, Jan 2011.

[64] Lukasz Fidkowski and Alexei Kitaev. Topological phases of fermions in one dimension. *Phys. Rev. B*, 83:075103, Feb 2011.

[65] Michael A. Nielsen and Isaac L. Chuang. *Quantum Computation and Quantum Information: 10th Anniversary Edition*. Cambridge University Press, 2010.

[66] Daniel Gottesman. *Stabilizer codes and quantum error correction*. PhD thesis, California Institute of Technology, January 1997.

[67] Héctor J. García, Igor L. Markov, and Andrew W. Cross. On the geometry of stabilizer states. *Quantum Info. Comput.*, 14(7 & 8):683720, May 2014.

[68] Victor Veitch, Christopher Ferrie, David Gross, and Joseph Emerson. Negative quasi-probability as a resource for quantum computation. *New Journal of Physics*, 14(11):113011, nov 2012.

[69] Mark Howard and Earl Campbell. Application of a resource theory for magic states to fault-tolerant quantum computing. *Phys. Rev. Lett.*, 118:090501, Mar 2017.

[70] Sergey Bravyi, Dan Browne, Padraic Calpin, Earl Campbell, David Gosset, and Mark Howard. Simulation of quantum circuits by low-rank stabilizer decompositions. *Quantum*, 3:181, September 2019.

[71] Zi-Wen Liu, Kaifeng Bu, and Ryuji Takagi. One-shot operational quantum resource theory. *Phys. Rev. Lett.*, 123:020401, Jul 2019.

[72] Xin Wang, Mark M. Wilde, and Yuan Su. Efficiently computable bounds for magic state distillation. *Phys. Rev. Lett.*, 124:090505, Mar 2020.

[73] Michael Levin and Zheng-Cheng Gu. Braiding statistics approach to symmetry-protected topological phases. *Phys. Rev. B*, 86:115109, Sep 2012.

[74] Trithep Devakul, Dominic J. Williamson, and Yizhi You. Classification of subsystem symmetry-protected topological phases. *Phys. Rev. B*, 98:235121, Dec 2018.

[75] Yizhi You, Trithep Devakul, F. J. Burnell, and S. L. Sondhi. Subsystem symmetry protected topological order. *Phys. Rev. B*, 98:035112, Jul 2018.

[76] Beni Yoshida. Topological phases with generalized global symmetries. *Phys. Rev. B*, 93:155131, Apr 2016.

[77] Robert Raussendorf, Sergey Bravyi, and Jim Harrington. Long-range quantum entanglement in noisy cluster states. *Phys. Rev. A*, 71:062313, Jun 2005.

[78] Yu-An Chen, Tyler D. Ellison, and Nathanan Tantivasadakarn. Disentangling supercohomology symmetry-protected topological phases in three spatial dimensions. *Phys. Rev. Research*, 3:013056, Jan 2021.

[79] Sam Roberts, Beni Yoshida, Aleksander Kubica, and Stephen D. Bartlett. Symmetry-protected topological order at nonzero temperature. *Phys. Rev. A*, 96:022306, Aug 2017.

[80] Sam Roberts and Stephen D. Bartlett. Symmetry-protected self-correcting quantum memories. *Phys. Rev. X*, 10:031041, Aug 2020.

[81] Lokman Tsui and Xiao-Gang Wen. Lattice models that realize $\mathbb{Z}_n$-1 symmetry-protected topological states for even n. *Phys. Rev. B*, 101:035101, Jan 2020.

[82] Juven C. Wang, Zheng-Cheng Gu, and Xiao-Gang Wen. Field-theory representation of gauge-gravity symmetry-protected topological invariants, group cohomology, and beyond. *Phys. Rev. Lett.*, 114:031601, Jan 2015.

[83] F. J. Burnell, Xie Chen, Lukasz Fidkowski, and Ashvin Vishwanath. Exactly soluble model of a three-dimensional symmetry-protected topological phase of bosons with surface topological order. *Phys. Rev. B*, 90:245122, Dec 2014.

[84] Lukasz Fidkowski, Jeongwan Haah, and Matthew B. Hastings. Exactly solvable model for a $4+1$D beyond-cohomology symmetry-protected topological phase. *Phys. Rev. B*, 101:155124, Apr 2020.

[85] Jeongwan Haah, Lukasz Fidkowski, and Matthew B. Hastings. Nontrivial Quantum Cellular Automata in Higher Dimensions. *arXiv e-prints*, page arXiv:1812.01625, December 2018.

[86] Sergey Bravyi, David P. Divincenzo, Roberto Oliveira, and Barbara M. Terhal. The complexity of stoquastic local hamiltonian problems. *Quantum Info. Comput.*, 8(5):361385, May 2008.

[87] Lalit Gupta and Itay Hen. Elucidating the interplay between non-stoquasticity and the sign problem. *Advanced Quantum Technologies*, 3(1):1900108, 2020.

[88] Luiz H. Santos. Rokhsar-kivelson models of bosonic symmetry-protected topological states. *Phys. Rev. B*, 91:155150, Apr 2015.

[89] Zohar Ringel and Steven H. Simon. Hidden order and flux attachment in symmetry-protected topological phases: A laughlin-like approach. *Phys. Rev. B*, 91:195117, May 2015.

[90] Thomas Scaffidi and Zohar Ringel. Wave functions of symmetry-protected topological phases from conformal field theories. *Phys. Rev. B*, 93:115105, Mar 2016.

[91] Iman Marvian. Symmetry-protected topological entanglement. *Phys. Rev. B*, 95:045111, Jan 2017.

[92] J.I. Cirac, D. Prez-Garca, N. Schuch, and F. Verstraete. Matrix product density operators: Renormalization fixed points and boundary theories. *Annals of Physics*, 378:100149, Mar 2017.

[93] Sergey Bravyi, Alexander Kliesch, Robert Koenig, and Eugene Tang. Obstacles to State Preparation and Variational Optimization from Symmetry Protection. *arXiv:1910.08980*, October 2019.

[94] William K Wootters. A wigner-function formulation of finite-state quantum mechanics. *Annals of Physics*, 176(1):1 – 21, 1987.

[95] D. Gross. Hudsons theorem for finite-dimensional quantum systems. *Journal of Mathematical Physics*, 47(12):122107, 2006.

[96] Hakop Pashayan, Joel J. Wallman, and Stephen D. Bartlett. Estimating outcome probabilities of quantum circuits using quasiprobabilities. *Phys. Rev. Lett.*, 115:070501, Aug 2015.

[97] Jeongwan Haah. Classification of translation invariant topological Pauli stabilizer codes for prime dimensional qudits on two-dimensional lattices. *arXiv:1812.11193*, December 2018.

[98] M. Popp, F. Verstraete, M. A. Martín-Delgado, and J. I. Cirac. Localizable entanglement. *Phys. Rev. A*, 71:042306, Apr 2005.

[99] Nathanan Tantivasadakarn. Dimensional reduction and topological invariants of symmetry-protected topological phases. *Phys. Rev. B*, 96:195101, Nov 2017.

[100] Maissam Barkeshli, Parsa Bonderson, Meng Cheng, and Zhenghan Wang. Symmetry fractionalization, defects, and gauging of topological phases. *Phys. Rev. B*, 100:115147, Sep 2019.

[101] David Fattal, Toby S. Cubitt, Yoshihisa Yamamoto, Sergey Bravyi, and Isaac L. Chuang. Entanglement in the stabilizer formalism. *arXiv:quant-ph/0406168*, June 2004.

[102] Noah Linden, Frantisek Matus, Mary Beth Ruskai, and Andreas Winter. The Quantum Entropy Cone of Stabiliser States. In Simone Severini and Fernando Brandao, editors, *8th Conference on the Theory of Quantum Computation, Communication and Cryptography (TQC 2013)*, volume 22 of *Leibniz International Proceedings in Informatics (LIPIcs)*, pages 270–284, Dagstuhl, Germany, 2013. Schloss Dagstuhl–Leibniz-Zentrum fuer Informatik.

[103] P. Jordan and E. Wigner. Über das paulische äquivalenzverbot. *Zeitschrift für Physik*, 47(9):631–651, Sep 1928.

[104] R. C. Ball. Fermions without fermion fields. *Phys. Rev. Lett.*, 95:176407, Oct 2005.

[105] F Verstraete and J I Cirac. Mapping local hamiltonians of fermions to local hamiltonians of spins. *Journal of Statistical Mechanics: Theory and Experiment*, 2005(09):P09012–P09012, Sep 2005.

[106] Alexei Kitaev. Anyons in an exactly solved model and beyond. *Annals of Physics*, 321(1):2–111, January 2006.

[107] J. v. Neumann. Die eindeutigkeit der schrödingerschen operatoren. *Mathematische Annalen*, 104(1):570–578, Dec 1931.

[108] Jutho Haegeman, Karel Van Acoleyen, Norbert Schuch, J. Ignacio Cirac, and Frank Verstraete. Gauging quantum states: From global to local symmetries in many-body systems. *Phys. Rev. X*, 5:011024, Feb 2015.

[109] Erez Zohar. Gauss law, Minimal Coupling and Fermionic PEPS for Lattice Gauge Theories. *arXiv e-prints*, page arXiv:1807.01294, Jul 2018.

[110] Tyler D. Ellison and Lukasz Fidkowski. Disentangling interacting symmetry-protected phases of fermions in two dimensions. *Phys. Rev. X*, 9:011016, Jan 2019.

[111] Dominic J. Williamson, Nick Bultinck, and Frank Verstraete. Symmetry-enriched topological order in tensor networks: Defects, gauging and anyon condensation. *arXiv e-prints*, page arXiv:1711.07982, Nov 2017.

[112] David Aasen, Ethan Lake, and Kevin Walker. Fermion condensation and super pivotal categories. *arXiv:1709.01941*, Sep 2017.

[113] Philippe Corboz and Guifré Vidal. Fermionic multiscale entanglement renormalization ansatz. *Phys. Rev. B*, 80:165129, Oct 2009.

[114] Philippe Corboz, Román Orús, Bela Bauer, and Guifré Vidal. Simulation of strongly correlated fermions in two spatial dimensions with fermionic projected entangled-pair states. *Phys. Rev. B*, 81:165104, Apr 2010.

[115] Christina V. Kraus, Norbert Schuch, Frank Verstraete, and J. Ignacio Cirac. Fermionic projected entangled pair states. *Phys. Rev. A*, 81:052338, May 2010.

[116] Nick Bultinck, Dominic J. Williamson, Jutho Haegeman, and Frank Verstraete. Fermionic matrix product states and one-dimensional topological phases. *Phys. Rev. B*, 95:075108, Feb 2017.

[117] Nick Bultinck, Dominic J Williamson, Jutho Haegeman, and Frank Verstraete. Fermionic projected entangled-pair states and topological phases. *Journal of Physics A: Mathematical and Theoretical*, 51(2):025202, dec 2017.

[118] Djordje Radicevic. Spin Structures and Exact Dualities in Low Dimensions. *arXiv e-prints*, page arXiv:1809.07757, Sep 2018.

[119] Davide Gaiotto and Anton Kapustin. Spin TQFTs and fermionic phases of matter. *International Journal of Modern Physics A*, 31:1645044–184, Oct 2016.

[120] David Cimasoni and Nicolai Reshetikhin. Dimers on surface graphs and spin structures. i. *Communications in Mathematical Physics*, 275(1):187–208, Oct 2007.

[121] Yu-An Chen and Anton Kapustin. Bosonization in three spatial dimensions and a 2-form gauge theory. *arXiv e-prints*, page arXiv:1807.07081, Jul 2018.

[122] Wilbur Shirley, Kevin Slagle, and Xie Chen. Foliated fracton order from gauging subsystem symmetries. *SciPost Phys.*, 6:41, 2019.

[123] Aleksander Kubica and Beni Yoshida. Ungauging quantum error-correcting codes. *arXiv e-prints*, page arXiv:1805.01836, May 2018.

[124] Alexei Kitaev and Chris Laumann. Topological phases and quantum computation. *arXiv e-prints*, page arXiv:0904.2771, Apr 2009.

[125] Lakshya Bhardwaj, Davide Gaiotto, and Anton Kapustin. State sum constructions of spin-tfts and string net constructions of fermionic phases of matter. *Journal of High Energy Physics*, 2017(4):96, 2017.

[126] Davide Gaiotto and Anton Kapustin. Spin tqfts and fermionic phases of matter. *Int. J. Mod. Phys. A*, 31:1645044, 2016.

[127] Zheng-Cheng Gu and Xiao-Gang Wen. Symmetry-protected topological orders for interacting fermions: Fermionic topological nonlinear σ models and a special group supercohomology theory. *Phys. Rev. B*, 90:115141, Sep 2014.

[128] Chenjie Wang, Chien-Hung Lin, and Zheng-Cheng Gu. Interacting fermionic symmetry-protected topological phases in two dimensions. *Phys. Rev. B*, 95:195147, May 2017.

[129] Meng Cheng, Zhen Bi, Yi-Zhuang You, and Zheng-Cheng Gu. Classification of symmetry-protected phases for interacting fermions in two dimensions. *Phys. Rev. B*, 97:205109, May 2018.

[130] Qing-Rui Wang and Zheng-Cheng Gu. Towards a complete classification of symmetry-protected topological phases for interacting fermions in three dimensions and a general group supercohomology theory. *Phys. Rev. X*, 8:011055, Mar 2018.

[131] N. Tarantino, N. Lindner, and L. Fidkowski. Symmetry fractionalization and twist defects. *New Journal of Physics*, 18:035006, 2016.

[132] Brayden Ware, Jun Ho Son, Meng Cheng, Ryan V. Mishmash, Jason Alicea, and Bela Bauer. Ising anyons in frustration-free majorana-dimer models. *Phys. Rev. B*, 94:115127, Sep 2016.

[133] Zheng-Cheng Gu, Zhenghan Wang, and Xiao-Gang Wen. Lattice model for fermionic toric code. *Phys. Rev. B*, 90:085140, Aug 2014.

[134] Anton Kapustin and Ryan Thorngren. Fermionic spt phases in higher dimensions and bosonization. *Journal of High Energy Physics*, 2017(10):80, Oct 2017.

[135] Meng Cheng, Nathanan Tantivasadakarn, and Chenjie Wang. Loop braiding statistics and interacting fermionic symmetry-protected topological phases in three dimensions. *Phys. Rev. X*, 8:011054, Mar 2018.

[136] Michael Levin and Xiao-Gang Wen. Fermions, strings, and gauge fields in lattice spin models. *Phys. Rev. B*, 67:245316, Jun 2003.

[137] M. Barkeshli, P. Bonderson, M. Cheng, and Z. Wang. Symmetry, Defects, and Gauging of Topological Phases. *arXiv:1410.4540*, October 2014.

[138] J. C. Y. Teo, T. L. Hughes, and E. Fradkin. Theory of Twist Liquids: Gauging an Anyonic Symmetry. *Annals of Physics*, 360:349, 2015.

[139] A. C. Potter, A. Vishwanath, and L. Fidkowski. An infinite family of 3d Floquet topological paramagnets. *arXiv:1706.01888*, June 2017.

[140] D. M. Basko, I. L. Aleiner, and B. L. Altshuler. On the problem of many-body localization. *arXiv:cond-mat/0602510*, February 2006.

[141] Arijeet Pal and David A. Huse. Many-body localization phase transition. *Phys. Rev. B*, 82:174411, Nov 2010.

[142] David A. Huse, Rahul Nandkishore, Vadim Oganesyan, Arijeet Pal, and S. L. Sondhi. Localization-protected quantum order. *Phys. Rev. B*, 88:014206, Jul 2013.

[143] Yasaman Bahri, Ronen Vosk, Ehud Altman, and Ashvin Vishwanath. Localization and topology protected quantum coherence at the edge of hot matter. *Nat. Commun.*, 6, 2015.

[144] Anushya Chandran, Vedika Khemani, C. R. Laumann, and S. L. Sondhi. Many-body localization and symmetry-protected topological order. *Phys. Rev. B*, 89:144201, Apr 2014.

[145] Bela Bauer and Chetan Nayak. Area laws in a many-body localized state and its implications for topological order. *Journal of Statistical Mechanics: Theory and Experiment*, 2013(09):P09005, 2013.

[146] A. C. Potter and A. Vishwanath. Protection of topological order by symmetry and many-body localization. *arXiv:1506.00592*, June 2015.

[147] Nathanan Tantivasadakarn and Ashvin Vishwanath. Full commuting projector hamiltonians of interacting symmetry-protected topological phases of fermions. *Phys. Rev. B*, 98:165104, Oct 2018.

[148] X.-L. Qi. A new class of (2 + 1)-dimensional topological superconductors with $\mathbb{Z}_8$ topological classification. *New Journal of Physics*, 15(6):065002, June 2013.

[149] Shinsei Ryu and Shou-Cheng Zhang. Interacting topological phases and modular invariance. *Phys. Rev. B*, 85:245132, Jun 2012.

[150] Zheng-Cheng Gu and Michael Levin. Effect of interactions on two-dimensional fermionic symmetry-protected topological phases with Z_2 symmetry. *Phys. Rev. B*, 89:201113, May 2014.

[151] James R. Munkres. *Elements of algebraic topology*. Addison-Wesley, 1984.

[152] Andrew C. Potter and Romain Vasseur. Symmetry constraints on many-body localization. *Phys. Rev. B*, 94:224206, Dec 2016.

[153] X. Chen. Symmetry Fractionalization in Two Dimensional Topological Phases. *arXiv:1606.07569*, June 2016.

[154] Yu-An Chen, Anton Kapustin, and Djordje Radicevic. Exact bosonization in two spatial dimensions and a new class of lattice gauge theories. *arXiv:1711.00515*, November 2017.

[155] Meng Cheng, Michael Zaletel, Maissam Barkeshli, Ashvin Vishwanath, and Parsa Bonderson. Translational symmetry and microscopic constraints on symmetry-enriched topological phases: A view from the surface. *Phys. Rev. X*, 6:041068, Dec 2016.

[156] Anton Kapustin. Bosonic topological insulators and paramagnets: a view from cobordisms, 2014.

[157] Anton Kapustin, Ryan Thorngren, Alex Turzillo, and Zitao Wang. Fermionic symmetry protected topological phases and cobordisms. *Journal of High Energy Physics*, 2015(12):1–21, 2015.

[158] Xiao-Gang Wen. Construction of bosonic symmetry-protected-trivial states and their topological invariants via $G \times SO(\infty)$ nonlinear σ models. *Phys. Rev. B*, 91:205101, May 2015.

[159] Charles Zhaoxi Xiong. Minimalist approach to the classification of symmetry protected topological phases. *Journal of Physics A: Mathematical and Theoretical*, 51(44):445001, 2018.

[160] Chenjie Wang and Michael Levin. Topological invariants for gauge theories and symmetry-protected topological phases. *Phys. Rev. B*, 91:165119, Apr 2015.

[161] Chenjie Wang. Braiding statistics and classification of two-dimensional charge-$2m$ superconductors. *Phys. Rev. B*, 94:085130, Aug 2016.

[162] Jing-Ren Zhou, Qing-Rui Wang, Chenjie Wang, and Zheng-Cheng Gu. Non-Abelian Three-Loop Braiding Statistics for 3D Fermionic Topological Phases. *arXiv e-prints*, page arXiv:1912.13505, December 2019.

[163] Meng Cheng. Symmetry Fractionalization in Three-Dimensional $\mathbb{Z}_2$ Topological Order and Fermionic Symmetry-Protected Phases. *arXiv e-prints*, page arXiv:1511.02563, November 2015.

[164] Lukasz Fidkowski and Ashvin Vishwanath. Realizing anomalous anyonic symmetries at the surfaces of three-dimensional gauge theories. *Phys. Rev. B*, 96:045131, Jul 2017.

[165] Juven Wang, Xiao-Gang Wen, and Edward Witten. Symmetric gapped interfaces of spt and set states: Systematic constructions. *Phys. Rev. X*, 8:031048, Aug 2018.

[166] Yu-An Chen and Anton Kapustin. Bosonization in three spatial dimensions and a 2-form gauge theory. *Phys. Rev. B*, 100:245127, Dec 2019.

[167] Tyler D. Ellison and Lukasz Fidkowski. Disentangling interacting symmetry-protected phases of fermions in two dimensions. *Phys. Rev. X*, 9:011016, Jan 2019.

[168] Tian Lan, Chenchang Zhu, and Xiao-Gang Wen. Fermion decoration construction of symmetry-protected trivial order for fermion systems with any symmetry and in any dimension. *Phys. Rev. B*, 100:235141, Dec 2019.

[169] Ryohei Kobayashi, Kantaro Ohmori, and Yuji Tachikawa. On gapped boundaries for spt phases beyond group cohomology. *Journal of High Energy Physics*, 2019(11):131, 2019.

[170] Meng Guo, Kantaro Ohmori, Pavel Putrov, Zheyan Wan, and Juven Wang. Fermionic finite-group gauge theories and interacting symmetric/crystalline orders via cobordisms. *Communications in Mathematical Physics*, pages 1–82, 2020.

[171] Andreas P Schnyder, Shinsei Ryu, Akira Furusaki, and Andreas WW Ludwig. Classification of topological insulators and superconductors in three spatial dimensions. *Physical Review B*, 78(19):195125, 2008.

[172] Yu-An Chen. Exact bosonization in arbitrary dimensions. *Phys. Rev. Research*, 2:033527, Sep 2020.

[173] Anton Kapustin and Ryan Thorngren. *Higher Symmetry and Gapped Phases of Gauge Theories*, pages 177–202. Springer International Publishing, Cham, 2017.

[174] Kyle Kawagoe and Michael Levin. Microscopic definitions of anyon data. *Phys. Rev. B*, 101:115113, Mar 2020.

[175] Chris Heinrich, Fiona Burnell, Lukasz Fidkowski, and Michael Levin. Symmetry-enriched string nets: Exactly solvable models for set phases. *Phys. Rev. B*, 94:235136, Dec 2016.

[176] Abhishodh Prakash, Juven Wang, and Tzu-Chieh Wei. Unwinding short-range entanglement. *Phys. Rev. B*, 98(12):125108, September 2018.

[177] Yuji Tachikawa. On gauging finite subgroups. *SciPost Phys.*, 8:15, 2020.

[178] Qing-Rui Wang, Yang Qi, and Zheng-Cheng Gu. Anomalous Symmetry Protected Topological States in Interacting Fermion Systems. *Phys. Rev. Lett.*, 123(20):207003, November 2019.

[179] Dominic V. Else, Bela Bauer, and Chetan Nayak. Prethermal phases of matter protected by time-translation symmetry. *Phys. Rev. X*, 7:011026, Mar 2017.

[180] Lukasz Fidkowski, Xie Chen, and Ashvin Vishwanath. Non-abelian topological order on the surface of a 3d topological superconductor from an exactly solved model. *Phys. Rev. X*, 3:041016, Nov 2013.

[181] Zitao Wang, Shang-Qiang Ning, and Xie Chen. Exactly solvable model for two-dimensional topological superconductors. *Phys. Rev. B*, 98:094502, Sep 2018.

[182] Qing-Rui Wang and Zheng-Cheng Gu. Construction and classification of symmetry-protected topological phases in interacting fermion systems. *Phys. Rev. X*, 10:031055, Sep 2020.

[183] Jun Ho Son and Jason Alicea. Commuting-projector hamiltonians for two-dimensional topological insulators: Edge physics and many-body invariants. *Phys. Rev. B*, 100:155107, Oct 2019.

[184] Ryohei Kobayashi. Commuting projector models for $(3 + 1)$-dimensional topological superconductors via a string net of $(1 + 1)$-dimensional topological superconductors. *Phys. Rev. B*, 102:075135, Aug 2020.

[185] Max A Metlitski. A 1d lattice model for the boundary of the quantum spin-hall insulator. *arXiv preprint arXiv:1908.08958*, 2019.

[186] N. E. Steenrod. Products of cocycles and extensions of mappings. *Annals of Mathematics*, 48(2):290–320, 1947.

[187] Richard Z Goldstein and Edward C Turner. A formula for stiefel-whitney homology classes. *Proceedings of the American Mathematical Society*, 58(1):339–342, 1976.

[188] Davide Gaiotto and Anton Kapustin. Spin tqfts and fermionic phases of matter. *International Journal of Modern Physics A*, 31(28n29):1645044, 2016.